

A Thesis Submitted for the Degree of PhD at the University of Warwick

Permanent WRAP URL:

<http://wrap.warwick.ac.uk/162468>

Copyright and reuse:

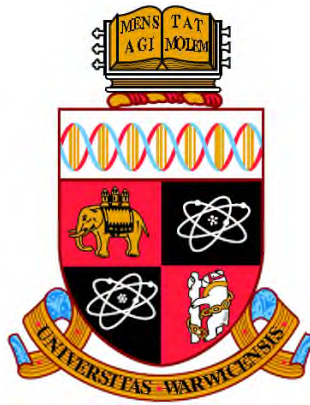
This thesis is made available online and is protected by original copyright.

Please scroll down to view the document itself.

Please refer to the repository record for this item for information to help you to cite it.

Our policy information is available from the repository home page.

For more information, please contact the WRAP Team at: wrap@warwick.ac.uk



Pro-/Anti-inflammatory Signalling Pathways in Brown and White Adipocytes

By
Farah Omran

A thesis submitted in partial fulfilment of the requirements for
the degree of
Doctor of Philosophy in Medicine

Division of Biomedical Sciences
Warwick Medical School
The University of Warwick

June 2021

This thesis is dedicated to the greatest two people in my life. Without their endless love and unconditional support, I would not be what I am today. To my mother who is bravely fighting cancer today and to my patient father who has been supporting her in this brutal fight. To my inspiring parents

Najah & Hashem

Table of Contents

List of Figures.....	I
List of Tables	V
Acknowledgements.....	VI
Declaration	VIII
Published Abstracts.....	IX
Publications Including Submitted Papers	X
ABSTRACT	XI
Abbreviations	XII
Chapter 1. Introduction and Aims	1
1.1 Adipose Tissue: BAT, WAT and Beige	2
1.1.1 Overview	2
1.1.2 BAT, WAT and Beige Adipose	2
1.1.2.1 Origin and Location.....	2
1.1.2.2 Histology and Morphology	6
1.1.2.3 Function and Regulation	7
1.1.2.4 Brown Adipocyte Differentiation <i>in vitro</i>	20
1.2 BAT Dysfunction in Obesity and Type 2 Diabetes.....	22
1.2.1 Angiogenesis.....	23
1.2.2 Extracellular Matrix (ECM)	26
1.3 Insulin Resistance in Thermogenic Tissue	28
1.4 Inflammatory Signalling and Adipose Tissue Biology	30
1.4.1 BAT Is an Active Inflammatory Secretory Tissue	34
1.4.2 LPS-TLR4 Activation Pathway Relevance to Activation of Inflammation in Brown and White Adipose Tissue	37
1.5 Adipose Mitochondrial Function in the Pathophysiology of Metabolic Disease	41
1.6 Anti-Inflammatory Pathways and BAT Function	45
1.6.1 G Protein-Coupled Receptor 120 (GPR120)	46
1.7 Hypothesis, Aims and Objectives	49
Chapter 2. Materials and Methods	51
2.1 Cell Culture and Differentiation	52
2.1.1 Mouse Cell Lines.....	52
2.1.2 White Adipocyte Culture, Differentiation and Treatment	52
2.1.3 Immortalized Brown Adipocyte Culture, Differentiation and Treatment	53

2.1.4	Primary Brown and White Adipocyte Isolation, Culture, Differentiation and Treatment	53
2.1.5	Spheroid Brown Adipocyte Culture, Differentiation and Treatment	54
2.1.6	Cell Culture Treatments	55
2.2	RNA-Isolation, Quantification and qRT-PCR.....	55
2.2.1	RNA Extraction	55
2.2.2	RNA Quantification.....	56
2.2.3	DNAase Treatment	56
2.2.4	cDNA Synthesis.....	57
2.2.5	Primer Design	57
2.2.6	Quantitative Real Time PCR (qRT-PCR).....	58
2.3	Protein Isolation, Quantification and Immunoblotting	59
2.3.1	Determination of Protein Concentration (Bradford Protein Assay)	59
2.3.2	Preparation of SDS-polyacrylamide Gel and Required Solutions	60
2.3.3	SDS-polyacrylamide Gel Electrophoresis and Immunoblotting (Western blotting)	61
2.3.4	Oxygen Consumption and Seahorse Cell Mito-Stress Test.....	63
2.3.5	2-Deoxyglucose Uptake.....	67
2.4	Enzyme-linked Immunosorbent Assay (ELISA)	69
2.4.1	C-X-C Motif Chemokine Ligand 5 (CXCL5/ LIX) and B-Cell Activating Factor (BAFF/ BLyS/ TNFSF13B).....	69
2.4.2	Matrix Metalloprotease (MMP3)	70
2.4.3	C-X-C Motif Chemokine Ligand 16 (CXCL16)	70
2.4.4	Calculation of ELISA Results.....	71
2.5	Oil Red-O Staining	71
2.6	Immunohistochemistry (IHC)	72
2.6.1	Haematoxylin and Eosin (H&E) Stain.....	72
2.6.2	UCP1-Staining	73
2.7	Determination of Mitochondrial Membrane Potential Through Confocal Microscopy	74
2.8	Statistical Analysis.....	74
Chapter 3. Lipopolysaccharide Mediates Biological Alteration in Brown		
Adipocytes	76
3.1	Introduction.....	77
3.2	Methods	80
3.2.1	Glycerol Assay	80
3.2.2	Triglyceride Assay	81
3.2.3	Nile Red Staining of Lipid Droplets and Fluorescence Microscopy	81

3.3	Results.....	82
3.3.1	Characterization of a Mouse TLR4-knockout Brown Adipocyte (TLR4ko.BAT) Cell Line.....	82
3.3.2	Wild Type Brown Adipocyte Differentiation in 2D and 3D Culture	84
3.3.3	LPS Administration to Brown Adipocytes Directly Induced Insulin Resistance	88
3.3.4	LPS Increased Inflammatory Gene Expression	90
3.3.5	LPS Reduced UCP1, the Main Brown Fat Marker, in Brown Adipocytes.....	92
3.3.6	LPS Reduced UCP1 Expression in Other Wild Type Brown Adipocytes Models	99
3.3.7	LPS Reduced Expression of Key Brown Fat Genes.....	103
3.3.8	LPS Impaired Lipid Metabolism	104
3.4	Discussion.....	108
Chapter 4. The Effect of Lipopolysaccharide (LPS) on Brown Adipocyte Whole Transcriptome and Cytokine Secretion through TLR4..... 113		
4.1	Introduction.....	114
4.1.1	Brown Adipose Tissue (BAT) Is a Secretory Organ	114
4.1.2	Thermogenesis; Regulation and Role of Secreted Factors.....	114
4.1.3	Extracellular Matrix (ECM) and Thermogenesis	117
4.1.4	Additional Effects of LPS on Brown Adipocyte Activity	118
4.1.5	The Importance of Identifying Novel Factors Secreted from Brown Adipocytes and the Wide Influence of LPS on Brown Adipocytes	118
4.2	Methods	120
4.2.1	Mouse Adipocyte Cell Lines Differentiation	120
4.2.2	RNA Isolation, Purification and Quantification.....	120
4.2.3	Quality Control Measurements and Sequencing	120
4.2.4	Cell Culture Supernatant Collection	121
4.2.5	Array Determination of Secreted Mouse Cytokines.....	121
4.2.6	RNA Sequence Analysis	121
4.3	Results.....	124
	RNA-Sequencing results.....	124
4.3.1	Principal Component Analysis.....	124
4.3.2	Differential Gene Expression Profiling Was Impacted by LPS	125
4.3.3	LPS Influenced Metabolism and Immunity Related Gene Ontology (GO) Term Enrichment Analysis of DEGs of Brown Adipocytes.....	131
4.3.4	TLR4 Mediates LPS Potent Actions on KEGG Enrichment of DEGs.....	149
4.3.5	Thermogenesis	154
4.3.6	Extracellular Matrix (ECM)-Receptor Interaction.....	163

LPS-Induced Cytokine Secretion by Brown Adipocytes	167
4.3.7 LPS Activates Secretion of Multiple Cytokines in wt.BAT Cells	167
4.4 Discussion.....	176
Chapter 5. Lipopolysaccharide Mediates Mitochondrial Alteration in Brown	
Adipocytes	182
5.1 Introduction.....	183
5.2 Methods	186
5.2.1 Mitochondrial DNA (mt-DNA) Copy Number Evaluation	186
5.2.2 Reactive Oxygen Species (ROS) Assay	187
5.2.3 Endogenous Antioxidant Activity Assays (SOD Assay & Catalase Assay)	187
5.2.4 ATP Assay	188
5.3 Results.....	189
5.3.1 LPS Administration Up-Regulated Oxidative Stress.....	189
5.3.2 LPS Administration Resulted in Alteration in Mitochondrial Proteostasis	191
5.3.3 LPS Administration Resulted in Deterioration in Mitochondrial Dynamics	193
5.3.4 LPS Administration Resulted in Alteration in Expression of Genes Associated with Mitochondrial Biogenesis and Oxidative Phosphorylation and Other Important Functions....	196
5.3.5 Effect of LPS on Mitochondrial Bioenergetics	199
5.3.6 Effect of LPS on Global Mitochondrial Transcriptome through TLR4.....	203
5.4 Discussion.....	213
Chapter 6. Lipopolysaccharide Reduces the Browning Process in Human	
Adipocytes	216
6.1 Introduction.....	217
6.2 Methods	220
6.2.1 Ethics and Study Design.....	220
6.2.2 Blood Biochemistry and Anthropometry	220
6.2.3 Primary Human Pre-Adipocyte Isolation	220
6.2.4 Primary Human Pre-Adipocyte Differentiation and Treatment	221
6.2.5 RNA Isolation	222
6.2.6 Statistical Analysis	222
6.3 Results.....	224
6.3.1 Anthropometric and Metabolic Variables for Study Participants	224
6.3.2 BMI Correlation with BAT Genes.....	224
6.3.3 Inflammatory Markers and the Relation with BMI	226
6.3.4 Inflammatory Genes Correlate with Reduced BAT Genes.....	227
6.3.5 BAT Genes Correlation with Mitochondrial Dynamic and Biogenesis Genes.....	228

6.3.6	Inflammatory Genes Correlate with Mitochondrial Genes	231
6.3.7	LPS Induces Inflammation in Mouse Adipocytes and Primary Human Adipocytes....	234
6.3.8	LPS Effects on Adipocyte Browning	240
6.3.9	LPS Effects on Thermogenesis-Associated Genes in Beige Cells	243
6.3.10	LPS Effect on Mitochondrial Function of Mouse Beige Adipocytes.....	246
6.3.11	LPS Effect on Expression of Genes Associated with Mitochondrial Dynamics	248
6.3.12	LPS Effect on the Expression of Mitochondrial Biogenesis Genes.....	251
6.3.13	LPS Effect on Other Important Mitochondrial Genes.....	254
6.3.14	Is Serum LPS Negatively Correlated with BAT and Mitochondrial Dynamic/Biogenesis Genes?.....	259
6.4	Discussion.....	261
Chapter 7.	<i>TUG-891 Reverses Lipopolysaccharide Mediated Biological and Mitochondrial Alterations in Brown Adipocytes.....</i>	265
7.1	Introduction.....	266
7.2	Methods	268
7.3	Results.....	269
7.3.1	GPR120 is Expressed in Human Brown/Beige Adipocytes	269
7.3.2	Brown Adipocyte Differentiation in the Presence of TUG-891 and/or LPS.....	271
7.3.3	TUG-891 Administration to Brown Adipocytes Reduces LPS-Induced Insulin Resistance	274
7.3.4	TUG-891 Administration to Brown Adipocytes Reduces LPS-Induced Inflammation	276
7.3.5	TUG-891 Administration to Brown Adipocytes Enhances UCP1 Expression	279
7.3.6	TUG-891 Administration to Brown Adipocytes Enhances Brown Fat Gene Expression	282
7.3.7	Effect of TUG-891 Administration to Brown Adipocytes on Reactive Oxygen Species Clearance	285
7.3.8	Effect of TUG-891 Administration on the Expression of Genes Involved in Mitochondrial Biogenesis, and Protein Depletion.....	287
7.3.9	Effect of TUG-891 Administration on Mitochondrial Dynamics.....	291
7.3.10	Effect of TUG-891 Administration on Other Mitochondrial Functions.....	294
7.3.11	TUG-891 Administration Prevented the Inhibitory Action of LPS	297
7.3.12	LPS-Induced Secretion of Cytokines by Brown Adipocytes is Inhibited by TUG-891	303
7.4	Discussion.....	310
Chapter 8.	<i>Final Conclusions</i>	314
Appendix.....		322
	Supplementary Table 2.1 Primer Sequences.....	322

Supplementary Table 4.1: RNA Integrity Number (RIN) and 28s/18s rRNA Ratio of the Samples Used in RNA-sequence Analysis	327
Supplementary Table 4.2 wt.BAT Top 50 Up-Regulated and Down-Regulated Genes in Response to LPS	328
Supplementary Table 4.3 TLR4ko.BAT Top 50 Up-Regulated and Down-Regulated Genes in Response to LPS	332
Supplementary Table 4.4 GO Enrichment Analyses Summarized Using REVIGO Derived from Up-Regulated Genes in wt.BAT.....	336
Supplementary Table 4.5 GO Enrichment Analyses Summarized Using REVIGO Derived from Down-Regulated Genes in wt.BAT	338
Supplementary Table 4.6 GO Enrichment Analyses Summarized Using REVIGO Derived from Up-Regulated Genes in TLR4ko.BAT.....	339
Supplementary Table 4.7 GO Enrichment Analyses Summarized Using REVIGO Derived from Down-Regulated Genes in TLR4ko.BAT	340
Supplementary Table 4.8 Significantly Enriched KEGG Pathways Associated with Top Up-Regulated Genes and Corresponding P-values in wt.BAT.....	341
Supplementary Table 4.9 Significantly Enriched KEGG Pathways Associated with Top Down-Regulated Genes and Corresponding P-values in wt.BAT	343
Supplementary Table 4.10 Significantly Enriched KEGG Pathways Associated with Top Up-regulated Genes and Corresponding P-values in TLR4ko.BAT	345
Supplementary Table 4.11 Significantly Enriched KEGG Pathways Associated with Top Down-Regulated Genes and Corresponding P-values in TLR4ko.BAT	346
<i>References</i>	347

List of Figures

<i>Figure 1.1.2.1.1 White, Beige and Brown Adipocytes Are Derived from Distinct Precursor Cells and Have Distinct Morphological Characteristics.</i>	4
<i>Figure 1.1.2.1.2 Distribution of Adipose Tissue in Mice and Humans.</i>	6
<i>Figure 1.1.2.3.1 Summary of Thermogenesis Control.</i>	11
<i>Figure 1.1.2.3.2 Transcriptional Regulators of UCP1 Expression.</i>	15
<i>Figure 1.4.2.1 Schematic Representation of TLR4-Mediated Signalling Pathways.</i>	39
<i>Figure 2.3.4.1 Seahorse XF Analyzer in the Measuring (left) Phases and the Resting (right).</i>	64
<i>Figure 2.3.4.2 Mitochondrial Functions Determination by the Seahorse XF Cell Mito-Stress.</i>	66
<i>Figure 3.3.1.1 TLR4 Knockout Brown Adipocyte Cell Line Differentiation.</i>	83
<i>Figure 3.3.1.2 Expression of Adipocyte-Associated Genes in TLR4 Knockout Brown Adipocyte Cell Line.</i>	84
<i>Figure 3.3.2.1 Wild-Type Brown Adipocyte Differentiation.</i>	86-87
<i>Figure 3.3.3.1 Effect of LPS on Brown Adipocyte Insulin Sensitivity.</i>	89
<i>Figure 3.3.4.1 Effect of LPS on Inflammation of Brown Adipocyte Cell-Line.</i>	91
<i>Figure 3.3.4.2 Effect of LPS on Primaries and Spheroids Brown Adipocyte Inflammation.</i>	92
<i>Figure 3.3.5.1 Effect of LPS on UCP1 Gene Expression.</i>	93
<i>Figure 3.3.5.2 αP2 in Brown Adipocyte.</i>	95
<i>Figure 3.3.5.3 Mature Brown Adipocyte Differentiation Pictures Under LPS Treatment.</i>	95
<i>Figure 3.3.5.4 LPS-Activated TLR4 Suppresses UCP1 Protein Expression.</i>	96
<i>Figure 3.3.5.5 LPS-Activated TLR4 Suppresses both Basal and CL-Induced UCP1 Protein Expression.</i>	97
<i>Figure 3.3.5.6 Effect of LPS on PGC-1 Gene Expression.</i>	98
<i>Figure 3.3.5.7 Effect of LPS on RIP140 Gene Expression.</i>	99
<i>Figure 3.3.6.1 Differentiation of LPS-Treated Wild Type Primary Brown Adipocytes and Spheroids.</i>	100
<i>Figure 3.3.6.2 Effect of LPS on UCP1 and PGC1α Gene Expression.</i>	101
<i>Figure 3.3.6.3 UCP1 Staining, in Murine Brown Adipocyte Spheroids by Immunohistochemistry.</i>	102
<i>Figure 3.3.6.4 UCP1 Staining Quantification, in Murine Brown Adipocytes Spheroids by Immunohistochemistry.</i>	102
<i>Figure 3.3.7.1 Effect of LPS on Key Brown Fat Gene Expression.</i>	103
<i>Figure 3.3.8.1 LPS Effects on Lipid Metabolism in Brown Adipocytes.</i>	104
<i>Figure 3.3.8.2 Confocal Microscopies of Brown Adipocytes Treated with or without LPS 100 ng/mL or LPS 1000 ng/mL.</i>	106
<i>Figure 3.3.8.3 Effect of LPS on Lipid Droplets (LD).</i>	107
<i>Figure 3.4.1 Schematic of Investigated LPS Actions in Brown Adipocytes.</i>	112
<i>Figure 4.3.1.1 PCA Plots of mRNA Sequencing Analysis.</i>	125
<i>Figure 4.3.2.1 Genes Differentially Expressed between Control and LPS-Treated Brown Adipocytes (A,B: wt Brown Adipocytes), (C,D: TLR4 Ko Brown Adipocytes).</i>	126

Figure 4.3.2.2 Venn Diagram.....	127
Figure 4.3.2.3 The Most 50 Regulated Genes in wt.BAT.	129
Figure 4.3.2.4 The Most 50 Regulated Genes in TLR4ko.BAT.....	130
Figure 4.3.3.1 GO Enrichment Analyses Summarized and Visualized Using REVIGO Derived from Upregulated Genes in wt.BAT.	133-136
Figure 4.3.3.2 GO Enrichment Analyses Summarized and Visualized Using REVIGO Derived from Downregulated Genes in wt.BAT.....	137-140
Figure 4.3.3.3 GO Enrichment Analyses Summarized and Visualized Using REVIGO Derived from Upregulated Genes in TLR4ko.BAT Cells.....	141-144
Figure 4.3.3.4 GO Enrichment Analyses Summarized and Visualized Using REVIGO Derived from Downregulated Genes in TLR4ko.BAT Cells.....	145-148
Figure 4.3.4.1 KEGG Pathways Hierarchical Clustering Tree.....	151
Figure 4.3.5.1 The Thermogenesis Pathway in KEGG Pathway Analysis in (A) wt.BAT, (B) TLR4ko.BAT.	156
Figure 4.3.5.2 Heatmap of DEGS of Brown Fat Genes upon LPS-Induction in (A) wt.BAT, (B) TLR4ko.BAT.....	158-159
Figure 4.3.5.3 Toll-Like Receptor Pathway in KEGG Pathway Analysis in (A) wt.BAT, (B) TLR4ko.BAT.	162
Figure 4.3.6.1 Heatmap of DEGS of Extracellular Matrix (ECM)-Receptor Interaction upon LPS-Induction in wt.BAT.	164
Figure 4.3.6.2 Heatmap of DEGS of Extracellular matrix (ECM)-Receptor Interaction upon LPS-Induction in TLR4ko.BAT.....	165
Figure 4.3.6.3 Extracellular Matrix (ECM)-Receptor Interaction Pathway in KEGG Pathway Analysis in (A) wt.BAT, (B) TLR4ko.BAT.	166
Figure 4.3.7.1 Media Cytokine Array for wt.brown Adipocytes (both 1.imBAT and 2.Primary Cultures), and 3.TLR4ko.BAT.	169
Figure 4.3.7.2 Testing Control vs LPS Treatment in Media by ELISA for Novel Cytokines.....	172
Figure 4.3.7.3 Cytokines Heatmaps from RNA-Sequencing and q-RT PCR to confirm RNA-sequencing results for Selected Novel Cytokines.....	174-175
Figure 5.3.1.1 Effect of LPS on Brown Adipocyte Oxidative Stress.	190
Figure 5.3.1.2 Effect of LPS on Brown Adipocyte Antioxidants Enzymes.....	191
Figure 5.3.2.1 Mitochondrial Protein Abundance (Denoted by Mitochondrial MT-CO1 to Nuclear SDHA Protein Ratio) in imBAT following Differentiation with/without LPS (100 ng/mL, 1000 ng/mL).	193
Figure 5.3.3.1 Effect of LPS on Genes Involved in Mitochondrial Dynamics in Brown Adipocytes.	194
Figure 5.3.3.2 Effect of LPS on Proteins Involved in Mitochondrial Dynamics in imBAT.	195
Figure 5.3.4.1 Effect of LPS on Genes Involved in Mitochondrial Biogenesis in Brown Adipocytes....	197

<i>Figure 5.3.4.2 Effect of LPS on Genes Involved in Mitochondrial Oxidative Phosphorylation in Brown Adipocytes.</i>	198
<i>Figure 5.3.4.3 Effect of LPS on Genes Involved in Other Mitochondrial Function in Brown Adipocytes.</i>	199
<i>Figure 5.3.5.1 Effect of LPS on Basal Mitochondrial Bioenergetics in Brown Adipocytes.</i>	201-202
<i>Figure 5.3.6.1 Heatmaps from RNA-Sequencing for Genes Associated with Mitochondrial Respiratory Function in wt.BAT cells (left panel) and TLR4ko.BAT cells (right panel).</i>	206
<i>Figure 5.3.6.2 Heatmaps from RNA-Sequencing for Genes Associated with Mitochondrial Biological Processes in wt.BAT cells (left panel) and TLR4ko.BAT cells (right panel).</i>	207
<i>Figure 5.3.6.3 Heatmaps from RNA-Sequencing for Genes Associated with Mitochondrial Membrane Function in wt.BAT cells (left panel) and TLR4ko.BAT cells (right panel).</i>	209
<i>Figure 5.3.6.4 Changes in Oxidative Phosphorylation Gene Expression under LPS Treatment in wt.BAT.</i>	210
<i>Figure 5.3.6.5 Changes in Oxidative Phosphorylation Gene Expression under LPS Treatment in TLR4ko.BAT.</i>	211
<i>Figure 6.3.2.1 BMI Correlates with Reduced Brown Adipose Tissue Genes.</i>	225
<i>Figure 6.3.2.2 Key Brown Fat Genes are Decreased with BMI.</i>	226
<i>Figure 6.3.3.1 Inflammatory Markers Are Increased with BMI.</i>	227
<i>Figure 6.3.7.1 Effect of Inflammatory and Adipocyte Browning Treatments on Mouse Adipocyte Differentiation.</i>	235
<i>Figure 6.3.7.2 Effect of Inflammatory and Adipocyte Browning Treatments on Primary Human Adipocyte Differentiation.</i>	236
<i>Figure 6.3.7.3 Effect of Inflammatory and Adipocyte Browning Treatments on Mouse Adipocyte Inflammation.</i>	238
<i>Figure 6.3.7.4 Effect of Inflammatory and Adipocyte Browning Treatments on Primary Human Adipocyte Inflammation.</i>	239
<i>Figure 6.3.8.1 Impact of LPS on Mouse Adipocyte Browning.</i>	241
<i>Figure 6.3.8.2 Impact of LPS on Human Primary Adipocyte Browning.</i>	242
<i>Figure 6.3.9.1 Impact of LPS on Beige Mouse Adipocyte Function.</i>	244
<i>Figure 6.3.9.2 Impact of LPS on Beige Adipocyte Function.</i>	245
<i>Figure 6.3.10.1 Effect of LPS on Aerobic Capacity Under Stress or Adrenergic Stimulus.</i>	247
<i>Figure 6.3.11.1 Impact of LPS on the Expression of Genes Associated with Mitochondrial Dynamics in Mouse Adipocytes.</i>	249
<i>Figure 6.3.11.2 Impact of LPS on the Expression of Genes Associated with Mitochondrial Dynamics in Human Adipocytes.</i>	250
<i>Figure 6.3.12.1 The Impact of LPS on the Expression of Mitochondrial Biogenesis Genes in Mouse Adipocytes.</i>	252
<i>Figure 6.3.12.2 The Impact of LPS on the Expression of Mitochondrial Biogenesis Gene Expression.</i>	253

<i>Figure 6.3.13.1 The Impact of LPS on Important Mitochondrial Genes in Mouse Cells.....</i>	<i>255</i>
<i>Figure 6.3.13.2 The Impact of LPS on Important Mitochondrial Genes in Human Cells.....</i>	<i>256</i>
<i>Figure 6.3.13.3 The Impact of LPS on Reactive Oxygen Species Clearance Genes in Mouse White Adipocytes.....</i>	<i>258</i>
<i>Figure 6.3.13.4 The Impact of LPS on Reactive Oxygen Species Clearance Genes in Human Cells.....</i>	<i>259</i>
<i>Figure 7.3.1.1 Impact of LPS on GPR120 Gene Expression in Beige Mouse Adipocyte.....</i>	<i>270</i>
<i>Figure 7.3.1.2 Impact of LPS on GPR120 Gene Expression of Human Primary Adipocytes.</i>	<i>271</i>
<i>Figure 7.3.2.1 aP2 Expression in Brown Adipocytes.</i>	<i>272</i>
<i>Figure 7.3.2.2 Morphology of Brown Adipocytes Differentiated in the Absence and Presence of TUG-891 and/or LPS.</i>	<i>273</i>
<i>Figure 7.3.3.1 Effect of TUG-891 (891) on Brown Adipocyte Insulin Sensitivity.</i>	<i>276</i>
<i>Figure 7.3.4.1 Anti-Inflammatory Effects of TUG-891 (891) on Brown Adipocytes.....</i>	<i>278</i>
<i>Figure 7.3.5.1 Effects of TUG-891 (891) on UCP1 in Brown Adipocytes.</i>	<i>279</i>
<i>Figure 7.3.5.2 Effects of TUG-891 (891) on UCP1 Gene Expression in LPS-Treated Brown Adipocyte.</i>	<i>280</i>
<i>Figure 7.3.5.3 UCP1 Staining, in Murine Brown Adipocyte Spheroids by Immunohistochemistry.</i>	<i>281</i>
<i>Figure 7.3.5.4 UCP1 Staining Quantification, in Mouse Brown Adipocytes Spheroids By Immunohistochemistry.....</i>	<i>282</i>
<i>Figure 7.3.6.1 Effect of TUG-891 (891) on Brown Fat Genes in Brown Adipocytes.</i>	<i>284</i>
<i>Figure 7.3.6.2 Effect of TUG-891 (891) on GPR120 Gene Expression in Brown Adipocytes.</i>	<i>285</i>
<i>Figure 7.3.7.1 Effect of TUG-891 (891) on Catalase (CAT) and Superoxide Dismutase 2 (SOD2) in Brown Adipocytes.....</i>	<i>286</i>
<i>Figure 7.3.8.1 Effect of TUG-891 (891) on Genes Involved in Mitochondrial Biogenesis in Brown Adipocytes.....</i>	<i>288</i>
<i>Figure 7.3.8.2 Mitochondrial Protein Abundance.</i>	<i>290</i>
<i>Figure 7.3.9.1 Effect of TUG-891 (891) on Genes Involved in Mitochondrial Dynamics in Brown Adipocytes.....</i>	<i>292</i>
<i>Figure 7.3.9.2 Effect of TUG-891 (891) on Protein Involved in Mitochondrial Dynamics in imBAT Cells.</i>	<i>293</i>
<i>Figure 7.3.10.1 Effect of TUG-891 (891) on Genes Involved in Key Mitochondrial Functions in Brown Adipocytes.....</i>	<i>296</i>
<i>Figure 7.3.11.1 Effect of TUG-891 on Aerobic Capacity under Stress and Mitochondrial Bioenergetics.</i>	<i>299-300</i>
<i>Figure 7.3.11.2 Confocal Microscopies of Differentiated imBAT Cells.....</i>	<i>301</i>
<i>Figure 7.3.12.1 Media Cytokine Array for Brown Adipocytes (both 1.imBAT cells and 2.primaries)..</i>	<i>304</i>
<i>Figure 7.3.12.2 Selected Cytokines Measured by ELISA in Media of imBAT Cells.....</i>	<i>306</i>
<i>Figure 7.3.12.3 Selected Cytokines Gene Expression in imBAT Cells.</i>	<i>308</i>

List of Tables

<i>Table 1.2.1 The International Classification of Underweight, Overweight and Obesity According to BMI.</i>	22
<i>Table 2.3.3.1 Primary and Secondary Antibodies Used for Western Blotting.</i>	63
<i>Table 4.3.4.1 Comparison between KEGG Functional Category Associated with Upregulated DEGs (A.) or Downregulated DEGs (B.) in wt.BAT and TLR4ko.BAT</i>	153
<i>Table 4.3.7.1 Cytokines Secreted by wt. Mature Brown Adipocytes with References for the Previously Reported Ones and No Reports for the Novel Ones.</i>	168
<i>Table 5.3.5.1 Summary of Mitochondrial Characteristics following LPS Treatment.</i>	203
<i>Table 5.3.6.1 Enriched Gene Ontology Terms Associated with “Mitochondria”.</i>	204
<i>Table 6.3.1.1 Clinical Characteristics of Participants According to Group.</i>	224
<i>Table 6.3.4.1 Correlation of Inflammatory Genes with BAT Genes.</i>	228
<i>Table 6.3.5.1 Correlation of BAT Genes with Mitochondrial Dynamics Genes.</i>	229
<i>Table 6.3.5.2 Correlation of BAT Genes with Mitochondrial Biogenesis Genes.</i>	230
<i>Table 6.3.5.3 Correlation of BAT Genes with Mitochondrial Genes.</i>	231
<i>Table 6.3.6.1 Correlation of Inflammatory Genes with Mitochondrial Dynamics Genes.</i>	232
<i>Table 6.3.6.2 Correlation of Inflammatory Genes with Mitochondrial Biogenesis Genes.</i>	233
<i>Table 6.3.6.3 Correlation of Inflammatory Genes with Mitochondrial Genes.</i>	234
<i>Table 7.3.1.1 GPR120 Gene Expression Correlation with Brown Fat Genes.</i>	269
<i>Table 7.3.1.2 GPR120 Gene Expression Correlation with Inflammatory Genes.</i>	270
<i>Table 7.3.11.1 Effect of TUG-891 on Mitochondrial Function.</i>	302

Acknowledgements

This work has been carried out at the Clinical Sciences Research Laboratory, Warwick Medical School, University of Warwick. My sincere gratitude to the University of Warwick and CARA for their wellbeing and financial support. This PhD placement and thesis would not have been possible without the scholarship I was awarded by the University of Warwick. Giving me a chance to work outside the war in my home country of Syria in a safe, supportive and fun environment.

Every journey comes to an end but undertaking this PhD has been a truly life-changing experience for me and it would not have been possible to do so without the support and guidance that I received from wonderful people. I am grateful to everyone who has been there to support my journey towards finishing my thesis. I'm indebted to and grateful for all of you....

I'm not sure how to start but as I used to say "you have been my greatest help over the last few years when I was here on my own". I will never forget your constant support on academic levels. Your guidance through the scientific research has been the essence of my professional growth. Your passion for science and your willingness to teach me and always answer my many questions have provided me with an excellent role model to follow. I will always be grateful for the opportunity you gave me to undertake this research in your lab and for all your patience with me towards the very end. My brilliant supervisor Prof.

Mark Christian

I know how difficult it was for you to contribute in my supervision from off-site. I greatly appreciate all your efforts to catch up with my work. I am forever grateful that I had the opportunity to have your guidance throughout my PhD. Your kindness, spectacular support and going above and beyond to help me mean a lot. I cannot forget your patience during this thesis proof reading. I know it was a pain to get it all done in a short period. HUGE thanks go to you, my incredible supervisor Prof.

Philip McTernan

Although it was only a short period of supervision, thank you for all the help and support you gave me finishing up my research both as a supervisor and as a friend. I will always remember your open door to hear me, and all tissues I got through when crying in your office or in our monthly online meetings during particularly difficult times. Thank you very much Dr.

Andrew Blanks

I am also hugely appreciative to you; for helping me finish my analysis. I know how difficult it was to help me solve the last minute analysis. I greatly appreciate your logical support and collaboration in the bioinformatics analysis and for kindly performing the tissue histology, thank you Dr.

Nigel Dyer, Mohammad Tauqeer Alam, Peter Kimani, Claire Mitchel and Sean James

Thanks to all the staff, receptionists and technicians at the Warwick Medical School for all their assistance and help. Thanks to the study skills team for helping me learn and improve my potential and for assisting with proofreading parts of my thesis. My sincere appreciation goes out to the PGR officer for unlimited support, valuable help and advice when I needed it most, to you

Sean Barret, Francesca Meneghetti, Gerard Sharpling, James Connolly and Sue Walter

To the person who smiled at me and said 'you are welcome' when I first arrived in the UK a few years ago, leaving my war-torn country for the first time in my life; young and full of dreams, to a new country and a new continent; new culture and new weather. Those three simple words meant a lot to me and later on it became the way I summarised my whole experience at Warwick that 'I am welcome'. Without your precious support it would not have been possible to overcome the breakdown stages of my journey when the way forward seemed impossible. I gratefully acknowledge

Claire O'Leary and all members of the global engagement team

To my best aider and friend who has always encouraged me and been an enlightening guide to me, especially throughout the final steps of my PhD. I will not forget your help during my lab work and the experience that I gained through your advice. I know how hard it was to make time to read my thesis and to discuss with me your thoughts. I miss chatting to you at the end of long working days, and our Friday's online meetings so much, to you

Alice Murphy

To my secret helper and friend that I am lucky to have in my life, words cannot help me but a thank you as big as this world goes to you for all your patience and support. For listening in the hard times; for proof reading my thesis; for your unwavering enthusiasm, even when mine was lacking; and helping me to greatly broaden my knowledge and learn new skills. Your support has been priceless my enthusiastic friend,

Anne Gleinich

A heartfelt gratitude to the people who have been a family to me in the UK and gave me a safe home so far away from home from the very beginning of this journey to the very end. THANK YOU from all my heart would not be enough to say how lucky I am to have you always being there for me and for believing in me, you saved my sanity and helped me reach where I am today. Without all your love and support, it would not be possible to complete my work, and finish my thesis, to you

Christine, John, David and all MY family in Newcastle

I would like to extend my thanks to all friends and colleagues especially Mark, Lindsay, Elena, Steven, Zusa, Joe, Ruby, Russel, Christian, Lara, Habeeb, Brenden, Ibtisam, Rana, Rafeef, Hasan, Shaza, Reem, Rama, Ahmed, Hytham, Kam, Seley, Vanlata, Jinus, Laura... I am really grateful for having you all in my life. Everyone had his/her unique touch in one way or another. Thank you for bravely listening to my science talk and for reminding me that occasionally there is a life outside of the lab. For all our happy times together, thank you.

I finish with my amazing, unique family, my most basic source of life energy, the stereotype of a perfect family in many ways. Your support for my ambitions has been unconditional all these years; you have given up many things for me to be what I am today; you have cherished with me every great moment and encouraged me (even when I thought it was impossible), I would not have gotten this far without you. I love you so much and I hope one day soon we can be altogether again. To you

Mum, Dad, Raghad and Karam

Farah
June 2021

Declaration

This thesis is submitted to the University of Warwick in support of my application for the degree of Doctor of Philosophy. It has not been submitted in any previous application for any degree. I hereby declare that this thesis is my own original work and that I have fully acknowledged by name all of those individuals and organizations that have contributed to the research for this thesis. The work presented (including data generated and data analysis) was carried out by the author except in the case of transcriptomics analysis, including the creation of libraries of template molecules, the sequencing of the libraries and creating differentially expressed genes, which was carried out by Dr. Nigel Dyer and Dr. Mohammad Tauqeer Alam. However, the assessment of RNA quality, the analysis of the data, visualization and presenting of the data was carried out by the author. Acknowledgement has been made in the text and appendix to all other materials used. All figures were generated by the author and are original, unless otherwise stated. Parts of this thesis have been published as a review article, reviewed abstracts and presented as posters or oral presentations by the author and are listed in the following section.

Published Abstracts

F Omran, A Murphy, L Jackisch, J Samavat, PG Mc Ternan, M Christian. 2019. Endotoxin and adiposity as mediators of down-regulating the BRITE fat phenotype. Endocrine Abstracts 40. Brighton. **Poster Presentation**. P185.

DOI: 10.1530/endoabs.65.P185

F Omran, PG Mc Ternan, M Christian. 2019. Mitochondrial dysfunction and insulin resistance induced by endotoxin was restored by GPR120 agonist, TUG-891 in brown adipocytes. 10th World Congress on Targeting Mitochondria, Berlin. **Oral Presentation**.

F Omran, PG Mc Ternan, M Christian. 2019. Lipopolysaccharide Induces Mitochondrial Dysfunction in Brown Adipocytes through TLR4. 5th annual Wellcome-Warwick Quantitative Biomedicine Programme Symposium. Coventry. **Poster Presentation**. P10

F Omran, PG Mc Ternan, M Christian. 2019. The GPR120 agonist TUG-891 Prevents LPS-Induced Mitochondrial Dysfunction, and Insulin Resistance in Brown Adipocytes. 2nd CPH BAT International Conference. Copenhagen. **Poster Presentation**. P8

F Omran, L Jackisch, J Samavat, PG Mc Ternan, M Christian. 2019. Is Inflammation the link between obesity and down-regulating the BRITE fat phenotype in Human Adipose tissue? Warwick Medical School Symposium. Coventry. **Oral Presentation**

F Omran, PG Mc Ternan, M Christian. 2018. Lipopolysaccharide Mediates biological and Mitochondrial Alterations in Brown Adipocytes through TLR4. 44th Adipose Tissue Discussion Group. Edinburgh. **Oral Presentation**.

F Omran, PG Mc Ternan, M Christian. 2018. The impact of lipopolysaccharide on mitochondrial efficiency in brown adipocytes. Endocrine Abstracts (2018) 59. Glasgow. **Poster Presentation**. P157
DOI: 10.1530/endoabs.59.P157

F Omran, PG Mc Ternan, M Christian. 2018. Lipopolysaccharide modulates mitochondrial function in brown adipocytes. Warwick Medical School Symposium. Coventry. **Poster Presentation**. P15

2017. Warwick Medical School Symposium. Coventry.

2016. Society for Endocrinology BES. Brighton.

Publications Including Submitted Papers

F Omran, M Christian. 2020. Inflammatory Signalling and Brown Fat Activity. Front. Endocrinol.

Review Article.

DOI: 10.3389/fendo.2020.00156

ABSTRACT

Brown adipose tissue (BAT) and beige adipocytes offer an appealing prospect to combat obesity and associated metabolic diseases through its thermogenic capacity. A state of low-grade chronic inflammation is described in obesity with increasing evidence that inflammation directly alters the thermogenic activity of BAT. As such, gut-derived lipopolysaccharide (LPS) could be among the triggers of pro-inflammatory status and may contribute to BAT dysfunction in obesity as it has been previously reported to be elevated in obesity. In contrast, Activation of GPR120, a G protein-coupled receptor, by TUG-891 or other agonists mediates anti-inflammatory actions and enhances the metabolic activity of BAT, representing a potential treatment to reduce adipocyte dysfunction in obesity. Therefore, the aims of this thesis were (1) to investigate the effects of LPS on brown adipocyte biology and secretory function, (2) to identify the impact of LPS on the induction of beige adipocytes, (3) to explore GPR120 activation via TUG-891 as therapeutic potential against brown adipocyte dysfunction. With the use of cutting-edge laboratory technology, the outcome of this study elucidated that LPS is a potent inhibitor of the brown phenotype, insulin sensitivity, mitochondrial function and the browning process in white adipocytes. Additionally, the analysis of a wide spectrum of LPS effects revealed that thermogenesis and extracellular matrix (ECM)-receptor interaction are among the top downregulated pathways as well as inflammatory microenvironment results from cytokine secretion from brown adipocytes themselves. BAFF, CXCL5, CXCL16 and MMP3 were identified as novel brown adipocyte-secreted cytokines and may target thermogenic potential of brown adipocytes. Finally, TUG-891, a GPR120 agonist, showed effectiveness in reversing LPS damaging actions. In conclusion, this study provides evidence that LPS-induced inflammation directly alters the thermogenic components of brown adipocytes at transcriptional and functional levels. Targeting GPR120 via TUG-891 offers a promising strategy to protect against the detrimental effects of LPS. Ultimately, combating the effects of inflammation in BAT could help in reducing obesity and its consequences.

Abbreviations

Abbreviation	Definition
ABHD5	α - β -hydrolase domain-containing protein 5
AC	Adenylyl cyclase
ACC	Acetyl-CoA carboxylase
ACSL1	Acyl-CoA synthase 1
ADAM	A disintegrin and metalloproteinase domain-containing protein
AKT	Protein Kinase B
Ang 2	Angiogenin, ribonuclease A family, member 2
ANT	Adenine nucleotide translocase
aP2	Adipocyte protein 2/ fatty acid binding protein 4
AT	Adipose tissue
ATF 2	Activating transcription factor 2
ATGL	Adipose triglyceride lipase
ATP	Adenosine triphosphate
BAFF/BLyS/TNFSF13B	B-cell activating factor
BAT	Brown adipose tissue
BMI	Body mass index
C/EBP α	CCAAT-enhancer binding protein alpha
C/EBP β	CCAAT/enhancer binding protein beta
C/EBP δ	CCAAT-enhancer binding protein delta
CACT	Carnitine/acylcarnitine translocase
cAMP	Cyclic adenosine monophosphate
CCAAT	Cytosine-cytosine-adenosine-adenosine-thymidine/enhancer-binding protein
CD137	TNF receptor superfamily member 9 (TNFRSF9)
CD36	Cluster of differentiation 36
CIDEA	Cell death-inducing DFFA-like effector A
CL	CL-316,243
CLS	Crown-like structure
CM	Chylomicron
COL5	Collagen V
CPT	Carnitine palmitoyl transferase
CREB	cAMP response element binding protein 1
CXCL5/ LIX	C-X-C motif chemokine ligand 5
CXCL16	C-X-C motif chemokine ligand 16
DAMPs	Damage-associated molecular patterns
DIO2	Iodothyronine deiodinase 2
DNA	Deoxyribonucleic acid
DRP1	Dynamin related protein 1
ECM	Extracellular matrix
ELISA	Enzyme-linked immunosorbent assay

ELOVL3	Elongation of very long chain fatty acids protein 3
ERK	Extracellular Signal-Regulated Kinase
ERR α	Estrogen-related receptor alpha
ET1	Endothelin-1
ETC	Electron transport chain
FABP4	Fatty acid binding protein 4
FADH	Flavin adenine dinucleotide + H
FAO	Fatty acid oxidation
FAs	Fatty acids
FAS	Fatty acid synthase
FFAs	Free fatty acids
FGF21	Fibroblast growth factor 21
FIS1	Fission, mitochondrial 1
CX3CL1	Fractalkine/ C-X3-C Motif Chemokine Ligand 1
GDF15	Growth differentiation factor 15
GDF8	Growth differentiation factor 8
GLP-1	Glucagon-like peptide-1
GLUT1	Glucose transporter 1
GLUT4	Glucose transporter 4
GPCR	G protein-coupled receptor
GPR120	G protein-coupled receptors 120
GSK3 β	Glycogen synthase kinase-3 beta
GTP	Guanosine triphosphate
H ₂ O ₂	Hydrogen peroxide
HDL	High-density lipoprotein
HFD	High fat diet
HIF	Hypoxia-inducible factor
HSL	Hormone sensitive lipase
IBMX	Isobutylmethylxanthine
IGF-1	Insulin-Like Growth Factor-1
IKK β	Inhibitor of kappa B kinase beta
IL1 β	Interleukin 1 beta
IL6	Interleukin 6
IRF3	Interferon regulatory factor 3
IRS-2	Insulin Receptor Substrate-2
JNK	c-Jun N-terminal kinase
L19	Ribosomal Protein L19
LBP	LPS-binding protein
LCFAs	Long-chain fatty acids
L-PGDS	Prostaglandin D synthase
LPL	Lipoprotein lipase
LPS	Lipopolysaccharide
LSD1	Lysine-specific demethylase 1
MAPK	Mitogen-activated protein kinase

MCP1	Monocyte chemoattractant protein 1
MFN2	Mitofusion 2
MGL	Monoacylglycerol lipase
MMPs	Matrix metalloproteases
mRNA	Messenger ribonucleic acid
MSCs	Mesenchymal stem cells
mTORC2	Mammalian target of rapamycin complex 2
MyD88	Myeloid differentiation primary response protein 88
Myostatin	Growth differentiation factor 8
n-3PUFAs	n-3 polyunsaturated fatty acids
NAD	Nicotinamide adenine dinucleotide
NADH	Nicotinamide adenine dinucleotide + hydrogen
NFκB	Nuclear factor kappa B
NLRP3	Nucleotide-binding oligomerization domain-like receptor-3 inflammasome
NO	Nitric oxide
NODs	Nucleotide-oligomerisation domain-containing proteins
NRF1	Nuclear respiratory factor 1
Om	Omental adipose tissue
OPA1	Protein optic atrophy 1
OPN	Osteopontin
OXPHOS	Oxidative phosphorylation
p38 MAPK	p38 mitogen-activated protein kinase
PAI-1	Plasminogen activator inhibitor-1
PAMPs	Pathogen-associated molecular patterns
PCR	Polymerase chain reaction
PDGFR-α	Platelet-derived growth factor receptor-alpha
PET/CT	Positron Emission Tomography associated with Computed Tomography
PGC1α	Peroxisome proliferator-activated receptor γ coactivator-1
PGC1β	Peroxisome proliferator-activated receptor γ coactivator-1
PI3K/AKT	Phosphatidylinositol 3-kinase/ protein kinase B
PKA	Protein kinase A
PLIN5	Perilipin 5
PLINs	Perilipins
POLG	DNA polymerase gamma, catalytic subunit
PPARα	Peroxisome proliferator activated receptor alpha
PPARγ	Peroxisome proliferator activated receptor gamma
PRDM16	PR-domain zinc-finger protein 16
PRRs	Pattern recognition receptors
qRT-PCR	Quantitative real-time polymerase chain reaction
RB	Retinoblastoma protein
RBP4	Retinol-Binding Protein 4
ROS	Reactive oxygen species
RXR	Retinoid X receptor

SAT	Subcutaneous adipose tissue
SCD	Stearoyl-CoA desaturase
SIRT1	Sirtuin-1 inhibition
SLC25A7	Thermogenin
SNS	Sympathetic nervous system
SRC	Steroid receptor coactivator
SREBP-1	Sterol regulatory element binding protein-1
STAT3	Signal transducer and activator of transcription 3
T2DM	Type 2 diabetes mellitus
T3	Triiodothyronine
T4	Thyroxine
TFAM	Mitochondrial transcription factor A
TG	Triacylglycerol
THBS1	Thrombospondin 1
TIMPs	Tissue inhibitor of metalloproteinases
TLRs	Toll like receptors
TMEM26	Transmembrane protein 26
TNF α	Tumour necrosis factor alpha
TR	Thyroid receptor
TRE	Thyroid response element
TRIF	TIR domain-containing adaptor inducing interferon- β
TZD	Thiazolidinedione
UCP1	Uncoupling protein 1
VAT	Visceral adipose tissue
VCAM 1	Vascular cell adhesion molecule 1
VEGF	Vascular endothelial growth factor
VEGFR 2	VEGF receptor subtype 2
VLDL	Very low density lipoprotein
WAT	White adipose tissue
WHO	World Health Organisation
Zfp516	Zinc finger protein 516
β 3-AR	Beta3-adrenergic Receptor
β -AR	Beta-adrenergic receptor
ω 3-FAs	Omega 3 fatty acids
CTRL	Control
FC	Fold Change

Chapter 1. Introduction and Aims

1.1 Adipose Tissue: BAT, WAT and Beige

1.1.1 Overview

Adipose tissue (AT) is a dynamic endocrine organ that controls whole-body energy balance; it plays intrinsic roles in storing and unleashing calories and the regulation of metabolic homeostasis, and thermogenesis (1–4). The body's ability to accumulate lipids is an evolutionary strategy to store energy in order to sustain relatively long periods of food scarcity (5,6). AT constitutes about 20 % of the body weight and is considered the largest endocrine organ in humans (7,8). Mammals have two main classes of AT: brown AT (BAT) and white AT (WAT). These act together to maintain a balance between fat accumulation and energy expenditure (9). AT serves as an essential coordinator of glucose homeostasis (1). In addition, AT regulates cell function in many other tissues from the immune system to the liver, pancreas, hypothalamus and kidneys (10–13). As such, AT is known to impact metabolic diseases, the immune system and cancer predisposition (10–13). AT has a multifunctional nature on account of adipocyte derived factors, namely lipid derivatives and a group of secretory proteins known as adipokines. These adipokines include a set of chemokines and cytokines such as inflammatory mediators including tumour necrosis factor alpha (TNF α), interleukin 6 (IL6) as well as anti-inflammatory mediators such as adiponectin (3,14–18). It is thought that there is a link between obesity and undesirable changes in the expression of adipokines including up-regulation of TNF α , IL6 and down-regulation of adiponectin (17). With its secretion of over 100 different adipokines, cytokines, and chemokines, AT is a key endocrine organ that links metabolism and immunity (16,19). A deeper understanding of adipocyte biology is therefore crucial to understand the pathophysiological grounds of obesity and its comorbidities including metabolic diseases such as Type 2 Diabetes (T2DM). Furthermore, a targeted manipulation of adipose physiology offers a potential strategy to treat these conditions.

1.1.2 BAT, WAT and Beige Adipose

1.1.2.1 Origin and Location

During the postnatal period, between the 4th and 6th months of human life (20,21), there is a substantial growth of WAT, while the onset of functional BAT formation takes place during the prenatal stage. Functional BAT in prenatal stage is a prerequisite

for immediate protection and effective adaptation to the cold challenge of the extra-uterine environment in the majority of mammals including humans (20,22). BAT and WAT are both derived from mesenchymal stem cells (MSCs), originating in the mesoderm (23). MSCs are multipotent stem-cells which can self-renew and originate myocytes, chondrocytes, osteocytes, neurons, besides adipocytes (24). Whether the adipocytes are white or brown is determined through different developmental pathways whereby the microenvironment contributes to the generation of mature adipocytes (24–26).

White adipocytes are derived from the myogenic factor 5 (Myf5)-negative lineage in mice and humans (27). Studies have demonstrated that white adipocytes in the interscapular and retroperitoneal area can be descended from Myf5-positive progenitors (Figure 1.1.2.1.2) (28). Classical brown adipocytes develop from Myf5-positive precursors, which is in common with myocytes (25). Moreover, cells with some BAT characteristics have been found within white depots. These present a brown-like phenotype, while still keeping some classical white fat gene expression. This in turn introduced the concept of beige adipocytes (also called brite, which means brown in white) (4,29). Beige adipocytes have been demonstrated to be distinct from classic brown adipocytes, in that they are not derived from the Myf5-positive lineage in mice and humans (4,30). They arise from white adipocyte transdifferentiation which leads morphologically and histochemically to a “browning” appearance (29,31). The origins of beige cells are not entirely known although there are multiple suggestions including being derived from resident stem cells in WAT depots (32), recruitment of stem cells in WAT from other tissues (33) or transdifferentiation of mature white adipocytes (34). Beige and brown adipocytes share similar molecular expression. However, some beige markers were identified to be specific for beige adipocytes such as T-Box 1 (TBX1), Cbp/p300-Interacting Transactivator with Glu/Asp-rich Carboxy-Terminal Domain 1 (CITED1) and Transmembrane Protein 26 (TMEM26). It is noteworthy that molecular expression differences between beige and brown adipocytes are controversial (35,36). Figure 1.1.2.1.1 shows a simplified illustration of the origin of white, brown and beige adipocytes.

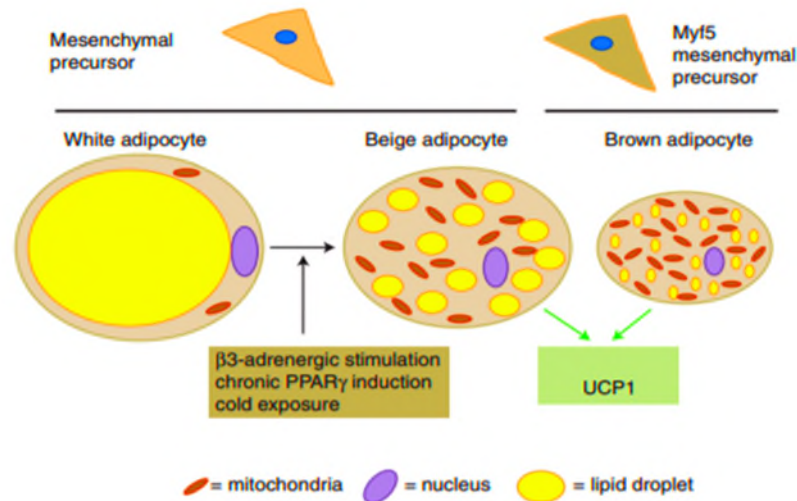


Figure 1.1.2.1.1 White, Beige and Brown Adipocytes Are Derived from Distinct Precursor Cells and Have Distinct Morphological Characteristics.

White adipocytes originated from Myf5 negative mesenchymal precursor. Beige adipocytes appear under stimulation including adrenergic activation or cold exposure. Brown adipocytes originated from Myf5 positive mesenchymal precursor. UCP1: uncoupling protein 1. PPARγ: peroxisome proliferator-activated receptor gamma. Adapted from (37).

Genetic lineage tracing has been leveraged in mice to determine the development of adipose tissue. Surprisingly, these reports demonstrated that a single adipose depot can comprise adipocytes from different lineages (28,38,39). In addition, microenvironment niches such as depot related cues impact the development of adipose tissue. This has been evidenced by transplantation of the same adipocyte precursors in different regions of mice which gave rise to functionally different adipose tissues (26). While such lineage tracing cannot be performed in humans, relevant information can nonetheless be derived from multipotent mesenchymal adipocyte progenitors present within adipose tissue (40,41). In several studies, it was observed that human adipocyte precursor cells produce multiple functional subtypes, and that the human brown/beige fat differentiation process is cell autonomous and depot related (40–42). Also, PR-domain zinc-finger protein 16 (PRDM16), together with CCAAT/enhancer binding protein β (C/EBP β) form a lineage switching transcriptional complex that enhances brown fat differentiation, whilst suppressing muscle cell differentiation from mice and humans (43,44). Recently, it has also been reported that primate-specific lncRNA, namely LINC00473, appears early in the development of human thermogenic adipocytes, affecting the fundamental aspects of thermogenic adipocyte physiology necessary for the development and function of human thermogenic adipose tissue. This is because it increases with differentiation

and is strongly induced by the activation of UCP1-expressing thermogenic adipocytes (45).

AT is distributed throughout the body and anatomical locations of BAT and WAT depots are distinct (46), and is shown in humans and rodents in Figure 1.1.2.1.2. BAT depots in rodents and human infants are primarily found in inter- and subscapular, axillary and cervical areas (11,47). For a long time, in humans, BAT was thought to be possessed only by newborn infants and that it regressed shortly after birth. However, it has now been proved that BAT exists in adult humans, although its detectable amount strongly decreases with age, body mass and season (48–55). The existence of BAT is evidenced by PET/CT-scanning (Positron Emission Tomography associated with Computed Tomography), which has revealed the presence of BAT, principally in the interscapular area and in supraclavicular, suprarenal and paravertebral regions as well as in the neck of healthy men exposed to a cold temperature. These data were later confirmed with the safer magnetic resonance imaging (MRI) technique as it does not require the use of radioisotopes (42,50–52,56,57).

WAT covers various distinct regional depots and the distribution of fat between these depots influences the risk of different metabolic disorders (58–61). The two main WAT depots are: subcutaneous (SAT) and visceral (VAT). SAT, which makes up about 85 % of all body fat in humans, is found just beneath the skin (60,61). VAT can include omental, mesenteric or peritoneal fat and it is stored deeper within the abdominal cavity and surrounds a number of internal organs, including the liver, pancreas and intestines (61). The distribution of WAT throughout the different depots seems to be more important than the total adipose tissue mass in contributing to the risk of developing obesity-associated diseases (61). VAT accumulation has a much higher association with an adverse metabolic, dyslipidemic and atherogenic obesity phenotype, whilst SAT accumulation is more benign (62). In addition to the major WAT depots, there are multiple smaller depots, with distinct functions and metabolic disease association. Among these, inter-/intramuscular adipose tissue (63), bone marrow adipose tissue (64) and pancreatic fat (65).

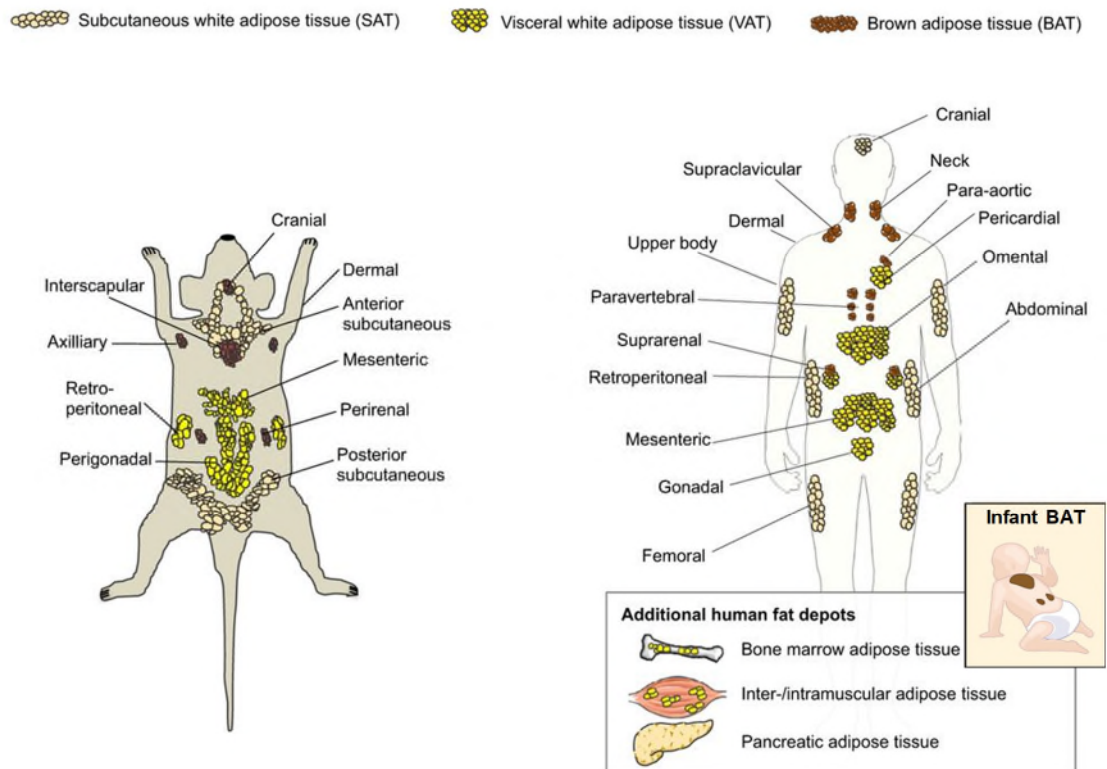


Figure 1.1.2.1.2 Distribution of Adipose Tissue in Mice and Humans.

Mammalian adipose tissue is distributed throughout the body in distinct depots. White adipose tissue depots store excess energy as triglycerides, while brown adipose tissue depots dissipate energy through the production of heat. Adapted from (61,66).

1.1.2.2 Histology and Morphology

AT is a loose connective tissue and has a heterogeneous nature. It fills spaces between other tissues and organs, helping to keep certain organs in place. Adipocytes, the lipid-filled cells, constitute the major cellular component of the AT and are held in a framework of collagen fibres. AT also consists of various other cells including stem cells, preadipocytes, endothelial cells and immune cells such as macrophages, neutrophils, lymphocytes (11,67,68). AT is innervated by the sympathetic nervous system (SNS), with BAT being more highly innervated and vascularized than WAT (69–71).

Adipocytes of white adipose tissue are spherical when isolated. When completely differentiated, a white adipocyte is large, between 50 and 150 μm in diameter, and contains a single huge droplet of triglycerides filling almost the entire cell; therefore, they are called unilocular. The periphery of the cell includes the nucleus and a few mitochondria (Figure 1.1.2.1.1) (11,70,72,73). Larger adipocytes are generally more highly metabolic and release more factors attracting immune cells (74).

In comparison, brown adipocytes are polygonal or ellipsoid cells and much smaller (15-60 µm in diameter), with their nucleus occupying a central position. The colour of BAT is due to both the large number of mitochondria (containing cytochrome pigment) dispersed among the lipid droplets, and the large number of blood capillaries in this tissue (7,11,75,76). Brown adipocytes contain many small lipid inclusions to store triglycerides, and are therefore called multilocular (7,11). This increases the surface exposed to lipases to allow easy access to lipids that can be rapidly catabolised (75).

At a morphological level, beige cells appear to be an intermediate between brown and white adipocytes. For example, they have a predominant lipid vacuole in the cytoplasm and many mitochondria (76). They express high levels of thermogenetic markers and adopt a multilocular appearance upon prolonged stimulation by cold or specific intracellular signalling pathways (36,77).

1.1.2.3 Function and Regulation

Animals such as *C. elegans*, *Drosophila* and sharks store lipids in gut cells, body fat and liver respectively (5,6,78). The development of specialised fat depots in mammals implicates a high level of coordination among these fat tissues and other organs to regulate food intake, lipid absorption and transport, fatty acid biosynthesis and oxidation in order to maintain the homeostatic balance. Adipocytes facilitate placing adipose tissue at the centre of nutritional homeostasis as they are metabolically active cells, responding to both nervous and hormonal stimuli. Also, they release hormones and various other biologically active substances called adipokines or batokines to fulfil their function (79,80).

WAT works as a storage repository for lipids from which fatty acids are easily mobilized during periods of energy restriction or increased physical activity to provide enough fuel for energy synthesis in the form of Adenosine triphosphate (ATP). Whereas VAT is packed between the organs, SAT helps shape the body surface and functions as padding for the body, and cushions regions subject to repeated mechanical stress such as the palms, heels, and toe pads. It conducts heat poorly and provides thermal insulation for the body (7). In addition, white adipocytes (including both SAT and VAT) are involved in a range of functions beyond fat storage including: secretion of cell-signalling molecules (adipokines), cytokines such as TNFα, Plasminogen

activator inhibitor 1 (PAI-1), IL6, and hormones such as leptin, adiponectin, and resistin (11,81,82).

Together with beige adipocytes, BAT, as the thermogenic tissue, is active not only in rodents and newborn humans, but also in adult humans. It uniquely specialises in expending energy as heat instead of generating ATP, playing an important role in the regulation of body temperature especially when an organism is in need of extra heat, e.g. postnatally, during entry into a febrile state, and during arousal from hibernation (75). This non-shivering thermogenic property is derived from the ability of uncoupling protein 1 (UCP1) to dissipate the mitochondrial membrane potential, leading to the uncoupling of oxidative phosphorylation from ATP synthesis.

Overall, WAT serves as storage depots for neutral fats, primarily triglycerides (long-chain fatty acyl esters of glycerol), while BAT functions to generate heat through UCP1. Different types of adipocytes work together as key regulators of the body's overall energy homeostasis. The coordination of BAT and WAT functions is a prerogative for achieving a balance between energy storage and consumption of excessive fatty acids. With obesity, this equilibrium is compromised through WAT expansion and BAT repression, which increases the risk of several metabolic disorders. With a growing epidemic of obesity and its associated health problems, including diabetes and heart disease (83,84), adipocytes and adipose tissue constitute a major area of medical research. Brown and beige adipocytes offer a promising means of tackling obesity and its consequences, and it is thus the focus of this thesis. The sections that follow outline in greater depth the main functional characteristics and regulatory pathways of thermogenic cells.

Thermogenesis

Thermogenesis is the process of dissipating energy through metabolic processes, from chemical energy to thermal energy. This process is classified into obligatory or adaptive (facultative) thermogenesis (85). Obligatory thermogenesis is the heat that results from sustaining all critical metabolic processes involved in maintaining the body in its living state (86). Adaptive thermogenesis includes shivering or non-shivering, and is a regulated process for active heat production in response to external stimuli so as to ensure survival (87,88). The shivering type occurs in muscles, while the non-shivering is mainly a function of BAT and WAT upon acquisition of brown-

like features (89,90). In this thesis, the term thermogenesis is used to describe adaptive non-shivering thermogenesis. BAT thermogenesis is facilitated by multilocular lipid stores, the exceptionally large mitochondrial content of brown adipocytes and the enriched vascular and nerve supply to this tissue. Adaptive non-shivering thermogenesis can be induced by cold or diet and requires BAT to be activated (89). In addition to the classical BAT response, white adipocyte 'browning' can occur in response to certain conditions such as chronic cold exposure and exercise (91,92). The browning process refers to the emergence of adipocytes with high thermogenic activity in WAT known as 'beige', or 'brite' adipocytes. Beige adipocytes are associated with increased energy expenditure, decreased body weight and increased insulin sensitivity (93). Humans are susceptible to browning of their WAT as it was reported that omental WAT biopsies obtained from patients affected by pheochromocytoma, a catecholamine secreting tumour, are enriched with beige cells (94).

Thermogenesis and the recruitment process in thermogenic cells are controlled by the simultaneous occurrence of lipogenesis and lipolysis or glycolysis and gluconeogenesis (75,86). The enormous energy requirements of thermogenesis imply that for the most part free fatty acids go through lipolysis as the main process of substrate production (75). Thermogenesis is regulated mainly by sympathetic control and thyroid hormone (75).

UCP1, also called thermogenin or SLC25A7, is the key factor behind thermogenesis. It is a transmembrane protein located in the inner membrane of the mitochondria of BAT and beige adipocytes (95,96). The uncoupling activity of UCP1 is due to its ability to transport protons across the inner mitochondrial membrane during cellular respiration, in particular when it binds to free fatty acids (FFAs), which are acute regulators of this transporter (97). Cellular respiration involves a series of oxidative phosphorylation (OXPHOS) processes which are coupled with ATP synthesis as a final energy product (98). However, some of the energy dissipation as heat occurs during OXPHOS (98). This partial uncoupling of respiration from ATP synthesis, also known as 'proton leak', can be mediated by UCP1 and by other mitochondrial inner membrane proteins, such as adenine nucleotide translocase (ANT) (98,99). For instance, following exposure to cold, the induction of UCP1 in BAT mediates a 'proton' leak thereby uncoupling OXPHOS from ATP generation to produce heat (75). Mechanistically, UCP1 decreases the proton gradient generated in OXPHOS by

increasing the permeability of the inner mitochondrial membrane, enabling the protons pumped into the intermembrane space to return to the mitochondrial matrix. Hence, the proton flux cannot reach the ATP synthase machinery which results in heat production instead of ATP synthesis (68,100,101). The “short circuit” in the proton gradient caused by UCP1 means less efficient OXPHOS with increased fat oxidation. It also means that fuel consumption can be accelerated and is independent of the saturating concentration of ATP (93). Hence, all of the biochemical steps of mitochondrial fuel oxidation (Krebs cycle and electron transport chain (ETC)) are accelerated, and the inherent inefficiencies in their reactions result in heat production which ultimately reduces feed efficiency (ratio of weight gain to food intake) (93,102,103). Accordingly, mice on high fat diet with deleted UCP1 rapidly increased their body mass index (BMI) as compared to the control at thermoneutrality (90). The expression and activity of UCP1 are substantially controlled by the sympathetic nervous system (SNS) via the stimulation of β 3-adrenergic Receptor (β 3-AR) (104). The family of β -adrenergic receptors (β -AR) are cell membrane receptors which belong to the superfamily of G-protein-coupled receptors (GPCRs) (105). In the absence of β -adrenergic signalling, mice are unable to maintain their core temperature (106). Figure 1.1.2.3.1 represents a simplified picture of thermogenesis function.

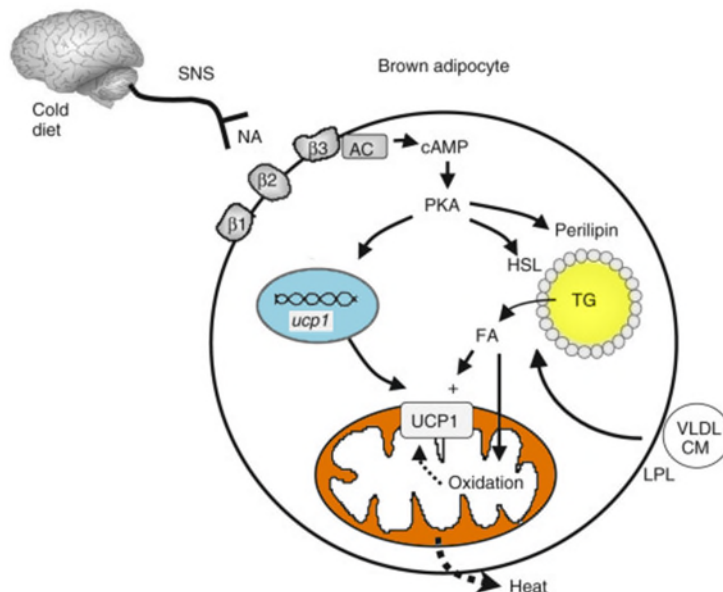


Figure 1.1.2.3.1 Summary of Thermogenesis Control.

Norepinephrine (NA) released by the activated SNS (by cold or diet) acts on adrenoceptors, primarily the β_3 , which is followed by adenylyl cyclase (AC) activation through G proteins, and thus stimulates the generation of cAMP, which in turn activates protein kinase A (PKA). PKA acts to activate different factors at transcriptional levels, which leads to increased Ucp1 gene expression. PKA also activates hormone sensitive lipase (HSL) and perilipin (the protein that covers the intra-cellular lipid droplets) triggering activation of the former and dissociation of the latter from the lipid droplets, thus activating lipolysis of triacylglycerol (TG) stored in lipid droplets. Released fatty acids (FA) are directed to the mitochondria where they eventually fuel the respiratory chain (oxidative phosphorylation (OXPHOS) processes). UCP1 dissipates the proton gradient generated by the respiratory chain, leading to a release of energy as heat (thermogenesis). CM, chylomicrons; VLDL, very low-density lipoproteins; LPL, lipoprotein lipase. Adapted from (107).

The β_3 -ARs are the adipocyte specific adrenergic receptors and are expressed in both brown and white adipocytes in rodents and in BAT in humans (108,109). They respond to epinephrine and norepinephrine induction. CL-316,243 (CL) is a selective β_3 -AR agonist. CL-treatment of rodent white adipocytes causes these cells to adopt a beige phenotype, similar to observable characteristics after cold accumulation (34,110). However, stimulating β_3 -adrenergic receptors in humans did not lead to a significant emergence of beige cells in white tissues (111). Under stimuli, such as cold temperature exposure, norepinephrine is released by the SNS, and binds to the β_3 -AR (111). This activates adenylyl cyclase via receptor coupling to the $G_{\alpha s}$ subfamily of heterotrimeric G proteins, which increases the levels of cyclic adenosine monophosphate (cAMP) and protein kinase A (PKA) activation. This pathway mediates the thermogenic signal including lipolysis, the release of lipids from the lipid droplets (109). PKA phosphorylates Hormone-Sensitive Lipase (HSL), which in turn converts triacylglycerol into free fatty acids (FFAs) (75,109). Full induction of HSL

activity requires PKA-mediated phosphorylation of perilipins (PLINs), the proteins that covers the intra-cellular lipid droplets (112). Phosphorylated perilipin is also needed to fully activate adipose triglyceride lipase (ATGL), the rate-limiting step enzyme for lipolysis (112). ATGL performs the first step of triglyceride lipolysis, the hydrolysis of triglycerides into diacylglycerides and FAs (112). Finally, monoacylglycerol lipase (MGL) culminates the lipolysis process by hydrolysing monoacylglycerol into glycerol and FFAs (112). The fatty acids are then directed to the mitochondria for combustion, activating UCP1 and thermogenesis (75). In addition to the three lipases mentioned above, β 3-AR activation of the thermogenic pathway mediates lipoprotein lipase (LPL) induction, another key enzyme that governs the release and deposition of fatty acids (75,113). Thus, synthesis and release of LPL occurs, which breaks down the triglycerides in the lipoproteins/chylomicrons in the circulation to provide further fatty acids as a fuel for combustion in the mitochondria (113). Lipids absorbed via LPL are suggested to be the main source of fatty acids in BAT (114). Additionally, glucose uptake from the circulation is stimulated via β 3-AR activation. After cytosolic conversion to pyruvate, the glucose is also combusted in the mitochondria. Glucose uptake is thus a consequence of sympathetic activity and not of thermogenesis. The increased glucose uptake during thermogenesis is due to an activation of expression of the gene for the glucose transporter GLUT1. This is, therefore, a fundamentally different process from the glucose uptake into the tissue (and in other insulin-sensitive tissues), which is stimulated by insulin and results from a transfer of the glucose transporter GLUT4 from intracellular vesicles to the plasma membrane(101).

Mitochondrial fatty acid oxidation (FAO) is the main fuel for thermogenesis. It is produced by actions of the acyl-CoA synthase 1 (ACSL1) and the carnitine palmitoyl transferase (CPT) system. ACSL converts long-chain fatty acids (LCFAs) into LCFAs-CoA which is subsequently converted into LCFAs-carnitine by CPT-1 β through a trans-esterification reaction of the fatty acyl group. Acylcarnitines are carried into the mitochondrial matrix by the carnitine/acylcarnitine translocase (CACT). CPT-2 then reverts the LCFA-acylcarnitine into LCFAs-CoA which are then moved to the mitochondrial inner membrane space and beta-oxidized. This produces nicotinamide adenine dinucleotide (NAD) + hydrogen (H) (NADH) and flavin adenine dinucleotide + H (FADH) generation. NAD and FAD transfer the electrons to the electron transport chain allowing the proton pumps to create the proton gradient for

either ATP production or thermogenesis. If thermogenesis takes place, the heat produced is rapidly distributed in the body by the blood.

Transcriptional Regulation of UCP1

Various transcriptional regulatory pathways have been reported to control thermogenic function, mainly affecting UCP1 transcription. The main pathways have been shown to be critical for both WAT and BAT, despite the fact that they arise from different origins and have opposing functions and morphological differences. They both require members of groups of transcription factors for maintaining functional characteristics of their mature adipocytes. Pathways include transcription factors such as:

- Basic-leucine zipper protein transcription factor family called CCAAT (cytosine-cytosine-adenosine-adenosine-thymidine)/enhancer-binding protein (termed C/EBP) including (C/EBP α , C/EBP β , and C/EBP δ) (93,115).
- The transcription factor Peroxisome proliferator activated receptor gamma (PPAR γ) (93,115).
- cAMP response element binding protein (CREB) (93,115).

The regulatory factors of UCP1 transcription are displayed in Figure 1.1.2.3.2. In fact, the presence of PPAR γ and C/EBPs is indispensable for brown and beige adipogenesis and their sustained expression has a fundamental effect in conserving the characteristics of mature adipocytes (46). However, PPAR γ and C/EBP α expression leads stem cells to differentiate to white adipocytes (43,116,117). Consequently, PPAR γ and C/EBPs are essential but not the exclusive factors required for the formation and maintenance of brown/beige adipocytes. Instead, brown/beige cell fate is decided by expression of PPAR γ activator 1 α (PGC-1 α) and PR domain zinc-finger protein 16 (PRDM16). PGC-1 α functions as thermogenesis regulator but it does not determine adipocytes' lineage (118,119), while PRDM16 is compulsory for both processes (25,120). The following section provides more in-depth descriptions of the function of thermogenesis regulators.

C/EBP β and C/EBP δ are induced at the early stage of adipocyte differentiation and they increase the expression of C/EBP α (121). C/EBP α is required for transcription of the β 3-AR gene during adipogenesis which plays a major role in regulating lipolysis and adaptive thermogenesis (122). Deletion of C/EBP α in mice leads to failure in

accumulating lipids in brown adipose tissue and in expressing UCP1 (75,123). Moreover, C/EBP β may compensate for C/EBP α absence in brown adipocyte development (123). Expression of C/EBP β (but not other C/EBP isoforms) is stimulated in BAT during cold accumulation and adrenergic induction (124). Additionally, increased and sustained expression of C/EBP β in white adipocytes promotes the expression of BAT characteristic genes (125). Upstream signals which lead to activation of C/EBP β gene expression involve phosphorylation of CREB (126), mitogen-activated protein kinase (MAPK) and glycogen synthase kinase-3 β (GSK3 β) (127,128).

CREB is localized in the nucleus and acts as a transcription factor, which binds to the cAMP response element (CRE) of the promoters of its target genes, upon phosphorylation by different receptor-activated protein kinases, including PKA (129). CREB phosphorylation may determine cell fate because it has collective effects on a series of genes, for example it is sufficient to induce adipogenesis in preadipocytes (126,130). In brown adipocytes, CREB mediates transcription of a series of key genes under adrenergic control which positively regulate brown adipocyte proliferation and differentiation. Also, increased levels of cAMP following adrenergic stimulation triggers the PKA-mediated CREB phosphorylation and activation along with recruitment of the transcriptional machinery at a number of thermogenesis genes including UCP1 and iodothyronine deiodinase 2 (DIO2), which contain functional CREB binding sites (127,129,130).

PPAR γ , a member of the nuclear hormone receptor superfamily, is the key transcription factor that is necessary for both white and brown adipogenesis and has a fundamental role in the maintenance of mature adipocytes (43). There are three different isoforms of PPAR γ : PPAR γ 1, 2 and 3. PPAR γ 2 is the most expressed isoform; it heterodimerizes with the retinoid X receptor (RXR), recruits cofactor proteins and unfolds the Deoxyribonucleic acid (DNA) structure in specific regions. This enables gene transcription and adipocyte differentiation (30). PPAR γ can however be regulated at multiple levels, prompting brown adipocyte-specific target gene expression (131). Studies have shown that mice with a dominant-negative mutation of PPAR γ (P465L) have defects in BAT but not WAT function (132). PPAR γ can be activated by natural ligands such as oxidized and unsaturated fatty acids, prostaglandins, or by synthetic agonists including thiazolidinedione (TZD) drugs such as rosiglitazone (133). Rosiglitazone is a known 'browning agent': It increases mRNA

and protein levels of UCP1 in murine white adipocytes causing increased mitochondrial function, norepinephrine-induced thermogenesis capacity and multilocularization of white adipocytes (30,134–136). In humans, Rosiglitazone increases UCP1 content and BAT features *in vivo* (77,137).

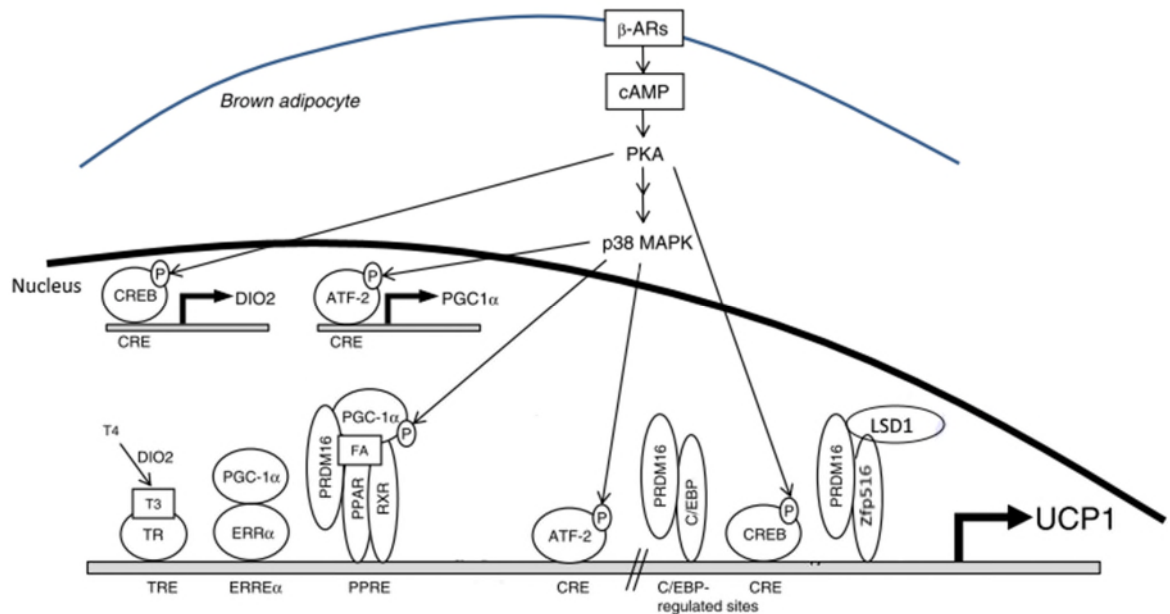


Figure 1.1.2.3.2 Transcriptional Regulators of UCP1 Expression.

The different response elements of the UCP1 gene. ATF-2 (activating transcription factor 2), β-ARs (β-adrenoceptors), cAMP (cyclic adenosine monophosphate), C/EBPβ (CCAAT-enhancer binding protein β), CRE (cAMP response element), CREB (cAMP response element binding protein), DIO2 (Iodothyronine deiodinase 2), ERRα (estrogen-related receptor α), FA (fatty acid), PGC-1α (PPAR coactivator-1α), p38 MAPK (p38 mitogen-activated protein kinase), PKA (cAMP-dependent protein kinase A), PPAR (peroxisome proliferator-activated receptor), pRB (retinoblastoma protein), PRDM16 (PRD1-BF1-RIZ1 homologous domain containing 16), RXR (retinoid X receptor), T3 (triiodothyronine), T4 (thyroxine), TR (thyroid receptor), TRE (thyroid response element), UCP1 (uncoupling protein 1). Adapted from (129).

The activity of PPARγ is coordinated by a coactivator called peroxisome proliferative activated receptor gamma coactivator 1 alpha (PGC1α). It plays a pivotal role in the regulation of energy metabolism by integrating diverse environmental and physiological cues that signal energy needs and promote thermogenesis. PGC1α is identified as a transcriptional regulator of UCP1 that acts at the UCP1 gene promoter which is specifically induced by cold and is essential for cAMP-mediated induction of UCP1 gene transcription (93). In context of the PKA–CREB pathway, activation of PGC1α during cold exposure stimulates expression of UCP1, electron transport chain genes and mitochondrial biogenesis (75,93,102,138,139). Also, PGC1α expression is directly and indirectly activated by p38 MAP kinase-mediated stimuli. p38 MAP

kinase increases upon PKA-cAMP activation. Increased PGC1 α levels are mediated through activating transcription factor 2 (ATF2), which, following phosphorylation by p38 MAPK, drives gene transcription of both UCP1 and PGC1 α itself through the cAMP-regulatory elements (129). In addition to PPAR γ , PGC1 α interacts with several nuclear hormone receptors including estrogen-related receptors (ERR α) and nuclear respiratory factors (NRFs)(127,129,140). Another level of PGC1 α regulation is represented by several steroid receptor coactivators (SRC) such as SRC-1 and SRC-2, which respectively enhances or inhibits PGC1 α - PPAR γ interactions (141). Interestingly, PGC1 α in muscle cells regulates the expression of irisin, a membrane protein that is secreted into the plasma, especially after physical exercise. In mice, released irisin, induces high thermogenic activity and beige cell formation in WAT depots (142).

PGC1 α is also a dominant regulator of other essential processes associated with determination of adipocyte fate and brown adipocyte differentiation in both mice and humans including mitochondrial biogenesis, oxidative metabolism and acquisition of an insulin-sensitive cellular status (43,77,119,127,140,143). This is a cell-autonomous requirement for PGC1 α in brown adipocytes, since immortalized brown fat cells lacking PGC1 α display a blunted induction of thermogenic genes in response to cAMP (43,119). Also, deletion of the PGC1 α gene leads to a significant decrease in capacity for cold-induced adaptive thermogenesis (118). However, many non-cAMP-dependent classical brown fat cell-selective genes are still expressed normally, and the fat differentiation program itself is unaltered in the absence of PGC1 α (43). Furthermore, the direct antagonism of PGC-1 α by receptor-interacting protein 140 (RIP140), a corepressor for nuclear receptors, leads to repression of genes involved in thermogenesis regulation (131,144). Collectively, PGC1 α is a crucial regulator of adaptive thermogenesis, however, it is not an essential determinant of brown fat identity (43,118,119).

PRDM16, a protein with seven zinc-finger domains through which it binds specific DNA regions, is a key factor enriched in classical brown fat relative to WAT (43,127). PRDM16 is required for the identity and function of brown fat phenotype *in vitro* and *in vivo*, and is sufficient to promote visceral fat browning in response to β -adrenergic induction (36). It directly promotes the complete program of brown fat differentiation, including activation of thermogenic genes (e.g. UCP1, PGC1 α , and Deiodinase2

(DO2)), mitochondrial genes, and other classical BAT genes (e.g. cell death-inducing DFFA-like effector A (CIDEA) and Elongation of very long chain fatty acids protein (ELOVL3)) (145,146). Moreover, artificially introduced PRDM16 induces UCP1-expressing brown adipocytes in WAT depots (93). Further studies demonstrated that PRDM16's main mechanism of action in adipocytes is by direct binding and coactivation of proteins such as PGC1 α , and PPAR γ (25) and together with C/EBP β , form a lineage-switching transcriptional complex that promotes brown fat differentiation and suppresses myocytes differentiation (44). PRDM16 is considered as a critical brown adipocyte lineage marker which inhibits specific white fat gene expression (such as resistin and angiotensinogen) (146,147). In mice, depletion of PRDM16 from cultured brown adipocytes leads to the expression of a myocyte phenotype in BAT, total loss of the brown fat characteristics and negatively affects thermogenic activity (25,145). Additionally, PRDM16-expressing cells show induced uncoupled cellular respiration in response to cAMP that is comparable to typical brown adipocytes. In fact, PRDM16 strongly coactivates the transcriptional activity of PGC1 α and PGC1 β , as well as PPAR α and PPAR γ , through direct physical interaction (36,145,146). PRDM16 also directly interacts with zinc finger protein-516 (Zfp516), a transcription factor which binds to the proximal region of the UCP1 gene promoter to play a role in regulating UCP1 gene expression (148). Zfp516 enhances BAT development and WAT browning while suppressing myogenesis. PRDM16 expression in brown fat is induced in response to cold exposure or adrenergic stimulation via the cAMP pathway (69). In addition, Lysine-specific demethylase 1 (LSD1) interacts with Zfp516 to promote UCP1 transcription and to function as a coactivator at other BAT-enriched genes, such as PGC1 α . LSD1 is necessary for adipogenesis of brown adipocytes as well as thermogenesis activation and its ablation has been shown to lead to whitening features of brown fat including impairments of the BAT program and BAT development, as well as reducing thermogenic activity and promoting obesity (149,150).

In addition to the response to cAMP induced kinases, which establishes a first, rapid mechanism of thermogenesis regulation, there are other layers of regulation of UCP1 transcription. Some of them have been identified to regulate both classical and beige cells in a similar way. Triiodothyronine (T3) directly activates the expression of thermogenic genes including transcription of the UCP1 gene via thyroid receptor (TR)

binding site in the enhancer region; it also functions centrally to activate BAT. The capacity of cAMP-driven signals to induce the expression of thyroxine 5'-deiodinase (T4) in brown adipocytes, and therefore to provide active intracellular production of T3, contributes to UCP1 gene transcriptional regulation (127).

Another protein involved in the thermogenic program is Fibroblast growth factor 21 (FGF21) (151) which positively regulates glucose uptake in adipocytes (152). Activation of cAMP-induced kinases including PKA and p38 MAPK, following β -adrenergic stimulation, induces brown/beige adipocytes to secrete FGF21 (153). Secreted FGF21 has endocrine and autocrine effects, which increase expression of UCP1 and other thermogenic genes in adipose tissues, at least in part, by enhancing adipose tissue PGC1 α protein levels (153,154). Additionally, deletion of FGF21 in mice impairs activation of an adequate thermogenic program after exposure to cold temperatures (154). Finally, there are other factors which have been reported to regulate adaptive thermogenesis. These include brown- and beige-fat recruiters and activators; for instance, irisin which promotes browning via an inter-organ crosstalk between skeletal muscle and WAT (142,155). Another example is Bone morphogenetic protein 8b (Bmp8b), which is produced by mature brown fat cells and functions to amplify the thermogenic response of brown adipocytes to adrenergic activators (156). Furthermore, atrial natriuretic peptide, brain-type natriuretic peptide (157), and inflammatory markers such as Interleukin 6 (IL6) and Interleukin 1 (IL1 β) (158) are factors that have been reported to regulate adaptive thermogenesis.

Lipid Handling

As highlighted above, lipids and FAs are the primary substrate for oxidation in brown adipocytes during thermogenesis. In brown adipocytes, lipids are packed into intracellular triglyceride stores, forming many lipid droplets from which FA can be released for energy metabolism. In this context, prior to FA storage in adipocytes lipids derived from nutrients are absorbed in the intestine and transported into the blood stream via lipoprotein forms such as chylomicrons to reduce hydrophobicity and regulate FA release. In the blood stream, lipoprotein lipase (LPL) catalyses the hydrolysis of the triglycerides from the chylomicrons into monoacylglycerol and free fatty acids that can be internalized by the brown adipocytes by different fatty acid transporter proteins (FATPs) and cluster of differentiation 36 (CD36) expressed on

the cytoplasmic membrane (159). In the cytoplasm, fatty acid binding proteins (FABP) such as FABP4, also known as aP2, bind to the internalized fatty acids to protect against their lipotoxicity to cellular structures (160). aP2 expression is highly induced during adipocyte differentiation and highly expressed in mature adipocytes compared to pre-adipocytes and therefore is considered a marker of differentiated adipocytes (160,161). Adipocytes can also generate lipids from glucose in a process called *de novo* lipogenesis. Glucose is taken up into the cell by the glucose transporter (GLUT4) (21,75). Via the glycolytic pathway, glucose is first converted to pyruvate and then decarboxylated by the pyruvate dehydrogenase complex, generating acetyl coenzyme A (acetyl-CoA)(21,75). *De novo* fatty acid synthesis is subsequently initiated by acetyl-CoA carboxylase (ACC), which converts acetyl-CoA, into malonyl-CoA. The enzyme fatty acid synthase (FAS) converts malonyl-CoA into palmitate, a 16 carbon saturated fatty acid (21,75,112). Fatty acid chains of palmitate molecules are extended by elongase enzymes such as elongation of very long chain fatty acids protein 3 (ELOVL3), which are located on the membrane of the endoplasmic reticulum. ELOVL3 is highly expressed in BAT and its transcription and activity increases upon cold accumulation to re-pack intracellular triacylglycerides (TG) into lipid droplets and maintain lipid homeostasis. Therefore, ELOVL3 is considered one of the markers of brown adipocytes (112,162–166).

After elongation, fatty acids are desaturated through the introduction of double bonds in determined positions of the chain by desaturase enzymes such as stearoyl-CoA desaturase (SCD). Following reduction of FAs, they can be oxidised or stored. For storage, FAs are esterified and stored in lipid droplets in the form of triacylglycerides (112). Triacylglycerides are then packaged into lipid droplets surrounded by a phospholipidic layer where specific proteins, such as Cell death-inducing DFFA (CIDEA), perilipins (e.g PLIN5) and adipose triglyceride lipase (ATGL), control lipid droplet enlargement and lipolysis.

CIDEA plays an important role in metabolism and programmed cell death (167). Its mRNA is upregulated during BAT adipogenesis and is considered a brown adipocyte marker (144,162). In mice, it has been reported to be a regulator of Ucp1 function in BAT (168), and a negative regulator of lipolysis in human white adipocytes (169,170). Mice lacking the CIDEA gene are resistant to diet induced obesity (168). Interestingly, studies showed that diet-induced obesity led to downregulation of CIDEA transcription in WAT of mice and humans (171,172). Accordingly, CIDEA gene

expression was the most highly expressed gene in WAT after weight loss (173). A polymorphism in the CIDEA gene has also been found to be associated with obesity (174).

Perilipins contribute to lipolysis regulation by phosphorylation-dependent and -independent pathways by interactions with different domains of the protein (71,112,136,175). BAT is rich in Perilipin-5 (PLIN5) and one of the upregulated genes in browning of WAT (163,176,177). It is considered to have a protective role against lipotoxicity (178). PLIN5 binds adipose-triglyceride lipase (ATGL) and the ATGL activator, α - β -hydrolase domain-containing protein 5 (ABHD5), thus providing a mechanistic link between PLIN5 and lipolysis (179). Interestingly, expression of PLIN5 can promote either triglyceride storage or fatty acid oxidation (179). As such, to promote efficient fatty acid catabolism, PLIN5 is reported as an important molecular link that couples the coordinated catecholamine activation of the PKA pathway and of lipid droplet lipolysis with transcriptional regulation via PGC1 α and eventually preventing mitochondrial dysfunction (180). On the other hand, to shift the metabolism of cells from fatty acid storage to oxidation, PLIN5 expression in adipose tissue is up-regulated by PPAR α as part of an expression program to trigger FA oxidation (181,182).

1.1.2.4 Brown Adipocyte Differentiation *in vitro*

Adipogenesis, the differentiation of pre-adipocytes into adipocytes, is a complex process characterized by changes in cell morphology, gene expression, hormone sensitivity, and secretory capacity (183), and is regulated by pathway crosstalk of transcription factors (183). The fundamental alterations in gene transcription involve changes in the two principal adipogenic factors, PPAR γ and C/EBP α (46), interacting with different corepressors and coactivators to determine adipocyte function (184). During the adipogenesis process two main stages occur: determination and differentiation. Determination is the first phase which ends with the irreversible conversion of the pluripotent stem cells into committed pre-adipocytes that have partially lost the differentiation potential (185). *In vivo*, the events occurring between these two stages remain unclear. However, proliferation of committed pre-adipocytes, which are cultured to confluence *in vitro*, is strongly reduced because of contact inhibition, even when no stimuli is applied to induce the final differentiation (123). These cells express the pre-adipocyte factor-1 (Pref-1) that prevents adipocyte

differentiation in its soluble active form (186). The re-entry in the cell cycle is then induced by hormonal stimuli, for instance: *in-vitro* culture of adipocyte differentiation requires insulin and triiodo-L-thyronine (T3) which are hormones that induce adipose-specific gene transcription (187,188). Dexamethasone, a synthetic glucocorticoid, is also added because it supports insulin actions in adipose differentiation (189,190). Similarly, a compound that increases intracellular levels of cAMP is included in the differentiation cocktail, usually a non-specific inhibitor of phosphodiesterases called 3-isobutylmethylxanthine (IBMX) (183,191). Indomethacin, cyclooxygenase-2 inhibitor, is frequently used in culture systems to enhance adipogenesis at the cost of decreasing osteoprogenitor output (192); it increases C/EBP and PPAR γ expression in a prostaglandin-independent way (192). Thiazolidinediones (TZDs) such as Rosiglitazone, the activators of PPAR γ , can also be added to stimulate adipogenesis and differentiation (193). Whilst not all brown adipocyte cell lines require Rosiglitazone for differentiation, it is needed in white adipocyte cell lines to induce differentiation. Rosiglitazone also has browning effects on white adipocytes with increased UCP1 levels and multilocularisation (30,77,134–137).

Differentiation is finally reached upon activation of a cascade of transcriptional factors where, the most important are PPAR γ and C/EBPs (123). At this stage, fully differentiated brown adipocytes display high levels of UCP1, CIDEA and multiple other characteristic BAT markers. However, beige cells show molecular signatures distinct from both white and brown adipocytes. Among beige selective genes, there are the developmental transcription factor 15 (Tbx15) and plasma membrane proteins such as transmembrane protein 26 (TMEM26) as well as markers known to be important in immune and inflammatory response pathways i.e. TNF receptor superfamily member 9 (CD137) (31,194). In addition, platelet-derived growth factor receptor- α (PDGFR- α) is a marker for white adipocyte precursor cells with the potential ability to differentiate into beige adipocytes (32). However, the substantial distinction between typical brown and inducible beige adipocytes is that the former express UCP1 at high levels without any stimulation, while beige adipocytes induce UCP1 only after cold exposure or β -adrenergic stimulation (30,93). Despite originating from two different lineages thermogenesis in both brown and beige adipocytes is triggered by the same stimuli that leads to UCP1 activation (195). *In vivo*, activation of the thermogenic program in both cells is fundamentally under the control of the SNS after being triggered by cold exposure through norepinephrine

activated β -adrenergic receptors. *In vitro*, physiological activation can be mimicked pharmacologically by using β adrenergic ligands to trigger specific genes reputed to promote the program for heat production (196,197). For instance, CL-316243, a selective β_3 adrenergic ligand, is commonly used to induce UCP1 in both classical brown and beige adipocytes. CL-316243 increases BAT lipolysis and thermogenesis, WAT browning and the metabolic rate (34,198). It was shown in studies to improve insulin sensitivity following oral administration *in vivo* in rodents (199–201).

1.2 BAT Dysfunction in Obesity and Type 2 Diabetes

Obesity is described by the World Health Organisation (WHO) as an abnormal or excessive fat accumulation that may impair health. It affects more than 1.9 billion adults worldwide and is currently considered a global epidemic (202). Body mass index (BMI) is the most accepted and used anthropometric criteria to diagnose obesity. BMI is calculated based on an individual's weight in kilograms divided by the height in meters squared. According to World Health Organisation (WHO) classifications as shown in **Table 1.2.1**, BMI can be used to classify people as underweight, overweight or obese (203)

Classification	BMI (kg/m ²)
Underweight	< 18.5
Normal range	18.5-24.9
Overweight	25.0-29.9
Obese	≥ 30.0
Class I	30.0-34.9
Class II	35.0-39.92
Class III	≥ 40.0

Table 1.2.1 The International Classification of Underweight, Overweight and Obesity According to BMI.

Morbid obesity can be defined as BMI ≥ 40.0 , or class II with significant comorbidities (203).

Obesity is associated with many disturbances in multiple organs including dysfunction of the adipose tissue which links metabolism and immunity (16,204). For instance, undesirable changes in adipokine expression are linked to obesity including up-regulation of inflammatory markers and down-regulation of adiponectin (17).

While the presence of BAT is associated with metabolic health, the amount of BAT is reduced in obesity with many studies demonstrating that obese individuals have reduced BAT compared with their lean counterparts (205–207). Further evidence has demonstrated that reduced BAT is reversible with weight-loss (208–211). Cold-induced thermogenesis is also severely impaired in BAT from obese humans and diet-induced obese mice (212,213). In addition, it has been indicated that higher BAT content is correlated with improved insulin sensitivity and protection against excess adiposity in both humans and animal models (207,214–217), with BAT glucose uptake rates highly reduced in obese individuals compared to healthy individuals (213). BAT transplantations have cemented this evidence in mice, whereby transplant models that increase BAT mass also improve glucose metabolism, increase insulin sensitivity, and reduce adiposity and body mass (218–221). BAT activation has been proposed as a potential strategy to combat obesity by converting energy from nutrients to heat through thermogenesis. As such, understanding how obesity impacts BAT and brown adipocytes function is essential to combat the obesity epidemic.

In the state of obesity, adipose tissue is remodelled. Different components contribute to the adipose tissue remodelling depending on the metabolic status, giving it striking plasticity to expand and regress through the course of its life. Adipogenesis and vascularisation are closely linked (222–224), and the plasticity feature of adipose tissues thus requires an intimate crosstalk between adipocytes and vascular endothelial cells. This cellular crosstalk is facilitated by components of the extracellular matrix (ECM), which co-ordinate adipose tissue remodelling to either develop, keep stable, or even undergo apoptosis (225). That coordination is necessary to ensure the appropriate oxygen and nutrient supply as well as the clearance of toxic waste products. The plasticity of the adipose vasculature reflects the balanced actions between pro/anti-angiogenic factors, which collectively determine expansion or regression of the vasculature (223). These coordinated and balanced functions are compromised in obesity (226).

1.2.1 Angiogenesis

Angiogenesis is a highly regulated process since the formation of new vessels requires endothelial cell proliferation triggered by pro-angiogenic stimuli, and extracellular matrix (ECM) components such as proteinases to degrade existing capillary walls

(225,226). Both WAT and BAT produce various proangiogenic factors, adipokines, and cytokines that induce neovascularization, maintenance, and remodelling of the vasculature (223).

WAT remodelling in obesity includes an increase in the number (hyperplasia) or size (hypertrophy) of adipocytes which leads to the formation of a dysfunctional adipose tissue (227–229). The hypertrophic growth of the adipose tissue is not accompanied by a similar expansion rate of angiogenesis (230). The impaired formation of new blood vessels causes an imbalanced production of overlapping angiogenic factors and inhibitors contributing to the dysfunction of the tissue. Dysfunctional WAT presents with features of necrosis and hypoxia, as well as larger adipocytes which favour expression of pro-inflammatory factors. This contributes to chronic, low-grade inflammation and fibrosis, that is present in obesity and counts as a major player in adipose tissue dysfunction which leads to insulin resistance (IR) (74,231–233). There are many factors that contribute to this chronic inflammation with hypoxia in WAT during the expansion and acute inflammatory insults. Gut-derived factors such as Lipopolysaccharide (LPS) worsen the impairment and possibly leading to insulin resistance and Type 2 diabetes mellitus (T2DM) (233–237). As such, vascularisation in adipose tissues appears as a key element in the morbidity of obesity (222,238). While WAT is associated with obesity-related morbidities, BAT is a thermogenic organ that can counteract the obese phenotype (75). BAT contains a significantly high density of vascular networks. These serve to meet the demands of the high thermogenic activity of BAT which requires a particularly high flow rate of blood to accomplish both release of heat as well as supply of oxygen and other essential substrates (232).

Chronic cold exposure leads to the remodelling of BAT and subcutaneous WAT, and is also associated with angiogenesis and an increase in vascular density, resulting in a dramatic increase in the metabolic rate, mitochondrial biogenesis, and fatty acid oxidation (223,239–241). The up-regulation of pro-angiogenic factors and down-regulation of anti-angiogenic factors are associated with cold-induced WAT browning and increased BAT activity in mice (240). Thus, brown adipocytes generate angiogenic factors such as vascular endothelial growth factor (VEGF) and nitric oxide (NO), which facilitate BAT angiogenesis and vascularisation (240,242–244). A study showed that this process is reduced in obese mice resulting in a whitening of BAT and loss of thermogenic activity (245). It is also suggested that brown adipocytes may have

a vasoprotective role that might be mediated by the secretion of hydrogen peroxide (H_2O_2), which inhibits vessel contractions in nearby vascular cells (246). The full list of angiogenic factors secreted from brown adipocytes is yet to be identified. In WAT, however, many pro-angiogenic factors are identified such as VEGFs, angiopoietins (Ang 1 and Ang 2), matrix metalloproteinases, leptin, and plasminogen activators (230).

Among known angiogenic factors, VEGF plays a crucial role in the coordination of vasculogenesis, angiogenesis, remodelling, and vascular leakage under both physiological and pathophysiological states especially in adipose tissue (247–249). During hypoxia, expression levels of VEGF are upregulated by hypoxia-inducible factor (HIF)-triggered transcription (250–252). Also, induction of VEGFA can be a result of adrenergic stimulation via PGC1 α activation (240). This PGC1 α -induced proangiogenic effect could be adipose tissue-specific because PGC1 α works through PPAR γ , upstream of PGC1 α , to have a proangiogenic effect in adipocytes, but not in endothelial cells. Indeed, activation of PPAR γ in adipocytes stimulates adipogenesis in parallel with the expression of pro-angiogenic factor VEGFA (253). This paradox indicates the complexity of the regulation of adipose tissue angiogenesis under different conditions.

Inhibition of VEGF receptor subtype 2 (VEGFR2) blocks cold-induced angiogenesis and damages thermogenic capacity in both WAT and BAT, indicating that angiogenic remodelling of BAT is one of the important processes for thermoregulation (240). Also, overexpression of VEGF in BAT of transgenic mice results in higher vascularisation and marked expansion of this adipose depot with increased UCP1 expression and higher thermogenic activity (254,255). Furthermore, when fed a high fat diet, transgenic mice with overexpression of VEGF exhibited less ectopic fat deposition, reduced inflammation, improved blood lipid profiles as well as higher glucose tolerance and insulin sensitivity compared to wild-type mice (256,257). However, overexpression of active HIF1 α triggers fibrosis and inflammation rather than an appropriate angiogenic response (258,259).

Studies have shown that a high fat diet is associated with hypoxia in adipose tissues of rodents (260,261). However, in humans, separate studies obtained inconsistent results regarding oxygen tension in adipose tissue between lean and obese subjects (262–264). One study in humans found that levels of VEGF-A expression are lower in adipose tissue (lateral from the umbilicus) from obese compared to lean (264), while

another study showed that VEGF-A expression was greater in adipose tissues (omental and subcutaneous) from insulin-sensitive obese versus both lean and insulin-resistant subjects (226). However, blood flow in obese subjects was not increased proportionally to fat mass expansion (264,265), which suggests that adipose tissue in obese humans fails to sufficiently induce adequate angiogenesis. Collectively, angiogenesis is massively affected in obesity and is mediated by secreted angiogenic factors from adipose tissue. The identification of these secreted angiogenesis factors from adipocytes represents an important aspect to study. That is particularly important in brown adipocytes because impaired angiogenesis in BAT could lead to brown adipocyte dysfunction, which has further implications in the context of obesity and associated disorders.

1.2.2 Extracellular Matrix (ECM)

The extracellular matrix (ECM) is a network of different proteins and proteoglycans that fills the spaces between cells. ECM binds cells and tissues together providing the structural support to adipocytes. It also controls essential actions in adipocytes for standard differentiation, migration, cell adhesion, repair, survival, and development, and it seems that its remodelling is required for healthy adipose tissue expansion (266). An excess of ECM components (such as collagens, elastin, and fibronectin) causes fibrosis which is a result of excessive lipid accumulation in obesity, besides immune cell infiltration and inflammation. Fibrosis in BAT may also impair thermogenesis (267) and cause local hypoxia, potentially leading to insulin resistance (268). Although the ECM is well-described in WAT, few studies focus on the BAT ECM and its remodelling in pathophysiological conditions.

ECM consists of a large variety of components. The prime components of ECM in adipose tissue are collagens (type I, II, III, IV and VI), fibronectin, and a small amount of laminin (68,269,270). However, several components, such as a disintegrin and metalloproteinase domain-containing protein (ADAMs), osteopontin (OPN), hyaluronan (HA), thrombospondins (THBS1), matrix metalloproteinases (MMPs), and tissue inhibitor of metalloproteinases (TIMPs), play an important role in the ECM remodelling and adipose tissue function (68,271).

Alterations in the expression of collagens impact the functionality of adipose tissue. For instance: collagen V (COL5) levels are increased in human obesity where it seems

to exert an antiangiogenic function (272). Also, excessive presence of collagens in the WAT was reported in obese mice and humans (273) and collagen VI has been recognized as one of the most important collagen types involved in the development of WAT fibrosis (274). The different types of collagen are encoded by specific genes. The main types of collagen in the ECM in adipose tissue are encoded by six genes: COL6A1, COL6A2, COL6A3, COL6A4, COL6A5, and COL6A6 (275). Collagen VI ablation in mouse obese models improves WAT expansion and plays a protective role against the development of a diabetic phenotype (276). In addition, collagen VI is reported to be upregulated in brown adipocytes in response to cAMP induction (277). Overexpression of COL6A3 in rodents induces BAT inflammation and fibrosis and also reduces energy expenditure (267).

Thrombospondin1 (THBS1) is another relevant component of ECM which is known to be highly induced in insulin-resistant obese mice and humans (278–281). One study in mice showed that treatment with recombinant THBS1 suppresses insulin signalling in the cultured muscle cell, which could represent crosstalk between the WAT and skeletal muscle in obesity (282). Therefore, treatments against THBS1 may be a beneficial therapy.

Adhesion of the cells as well as signalling between cells and the ECM are mediated by transmembrane receptors, called integrins. Integrins are the major tissue receptors for ECM proteins. Together with other focal adhesion proteins, they regulate cellular motility and mediate both inside-out and outside-in signalling (266). Two major families of integrins consist of α and β , which include eighteen and eight subunits, respectively, that compose different forms of integrin heterodimers (283). Although the function of integrins in adipose tissue is still not fully known, there are reports which indicate an important role. As such, abnormal integrin expression may be linked with insulin-resistance and malformed vascularisation (271). For example, deletion of $\beta 2$ integrin is associated with modulation of glucose homeostasis and attraction of neutrophils to adipose tissue in mice (284), while ablation of $\alpha 2\beta 1$ integrin induces vascularisation in the muscles of obese mice (285).

In addition, CD44 is a ubiquitously expressed cell surface transmembrane glycoprotein on adipocytes and it interacts with different components of the ECM (286). It regulates different cell functions like cell–cell and cell–matrix interactions. CD44 is involved in development of inflammation and insulin-resistance in obesity (287). CD44 deficiency or treatment with an anti-CD44 antibody leads to positive

effects on metabolism, such as amelioration of insulin resistance in a diabetic mouse model, and decreases in blood glucose levels and macrophage infiltration under high-fat diet (288).

Remodelling of the ECM is facilitated by enzymes that degrade and regulate modifications of the ECM composition (289). These include matrix metalloproteinases (MMPs) and tissue inhibitors of metalloproteinases (TIMPs). The involvement of TIMPs and MMPs in the pathogenesis of obesity was suggested by the differential pattern of their expression in two different mouse models of obesity (290). Moreover, ADAM10 (A disintegrin and metalloproteinase domain-containing protein 10) is known to inhibit angiogenesis by modulating Notch signalling (291). ADAM10 was found to be upregulated in obese mice and its silencing ameliorated insulin sensitivity (292).

In addition, obese plasmatic membrane rupture of hypertrophic adipocytes and accumulation of ECM components cause necrotic adipocyte death. The rupture leads to lipid leakage and release of molecules, that recruit macrophages, which in turn sustain inflammation and promote insulin-resistance (271,293).

Collectively, the ECM and integrins are important regulators of insulin action. They are, however, less studied in relation to brown adipocyte dysfunction. Therefore, it is important to study factors that modulate ECM physiology in BAT as these may be novel therapeutic targets to treat the underlying insulin resistance associated with as Type 2 Diabetes (T2DM).

1.3 Insulin Resistance in Thermogenic Tissue

The link between obesity and development of insulin resistance and T2DM is well established, although the detailed mechanism is still not entirely understood. It is also known that T2DM status is classically defined by insulin resistance in peripheral tissues, and the inability of pancreatic β -cells to release adequate levels of insulin into the circulation to regulate glycaemia, two features related to obesity status (294–297). However, not all obese individuals develop insulin resistance and T2DM, highlighting the great influence of various predisposing factors.

Initial onset of insulin resistance in obesity could be a result of WAT dysfunction and its inability to cope with the high demand for lipid storage, resulting in excess circulating free fatty acids and accumulation of lipotoxic metabolites such as

diacylglycerol, ceramides and long-chain fatty acyl-CoA in adipose and non-adipose tissues. This process is termed ectopic fat deposition and eventually leads to low grade inflammation and apoptosis (298–300). Lipotoxic metabolites lead to direct inhibition of insulin signalling through serine phosphorylation of insulin receptor substrate (IRS) proteins and activation of inflammatory pathways (301–303). Apoptosis is a factor that contributes to adipose tissue dysfunction by reducing WAT capacity to adequately buffer lipids. Moreover, apoptosis derived lipotoxic metabolites further trigger a local inflammatory response, which directly hinders insulin sensitivity (304). Increasing BAT thermogenesis, however, would enhance lipolysis and therefore contribute to preventing fat deposition in peripheral tissues that are non-specialized in fat storage (305). Indeed, rodents and humans with high content of brown and induced beige fat depots have higher insulin sensitivity, improved glucose homeostasis and resistance to obesity (53,57,219,306–308). In the obese state, the capacity of thermogenesis is reduced (50,213,309,310). Therefore, it is important to understand the mechanism behind this reduction as well as brown adipocyte dysfunction to enhance insulin sensitivity.

Activation of inflammatory pathways represents a good candidate for involvement in thermogenic tissue dysfunction and promoting insulin resistance since the pro-inflammatory cytokines have consistently been proved to cause insulin resistance in WAT (14,311). However, their effects are less known in BAT. Elevated inflammatory marker levels in diet-induced obese mice are suggested to be responsible for BAT insulin resistance via AKT (protein kinase B) and Extracellular Signal-Regulated Kinase (ERK) pathways (312). For instance, the TNF α mechanism to impair insulin responses involves disturbances in the activation of the MAP-kinases, Insulin Receptor Substrate-2 (IRS-2) and AKT (313–315). Mammalian target of rapamycin complex 2 (mTORC2), which activates inflammation, sustains thermogenesis via AKT-induced glucose uptake and glycolysis in BAT (316,317). These interconnections underscore the importance of metabolic signalling pathways in BAT during thermogenesis and point out the necessity of establishing mechanisms through which inflammation modifies BAT biology. This will be reviewed in more details below.

1.4 Inflammatory Signalling and Adipose Tissue Biology

Low-grade chronic inflammation in WAT, mediated by the secretion of a range of inflammatory cytokines, has long been recognised as a main feature in obesity, termed metabolic inflammation or ‘metainflammation’ (81,204,318). Many pathologies are associated with this inflamed state, including T2DM, cancer, heart disease, and neurodegenerative diseases. Additionally, inflammation has been shown to impact the thermogenic capacity of brown and beige adipocytes (313–315,319). In comparison to WAT, relatively little is known about the inflammatory status of BAT in physiology and pathophysiology and how it affects thermogenesis. However, it is known that the inflammatory microenvironment is affected by cytokines secreted from immune cells as well as by adipocytes. In fact, pro-inflammatory signals also represent an important component of the thermogenic potential of brown and beige adipocytes and could contribute to adipocyte dysfunction in obesity (320–323).

In adipose tissue of individuals categorised as ‘normal weight’ via their BMI as well as metabolically unaffected obese individuals, both BAT and WAT accommodate innate immune cells - mainly M2 macrophages - that secrete anti-inflammatory molecules (such as IL-10 and IL-4) and serve primarily an antigen presenting role (204,324,325). These molecules also participate in heat generation. For instance: IL-4, IL-33 and IL-13 are secreted by innate lymphoid cells, mast cells and eosinophils. These three cytokines are upregulated in cold-induced thermogenesis and promote UCP1 expression and browning of WAT (325–328). IL-13, which possesses anti-inflammatory traits, provokes growth differentiation factor 15 (GDF15) expression which is reported to reduce obesity by triggering thermogenesis, lipolysis, and oxidative metabolism in mice (329,330), and also averts inflammation (331). In subcutaneous WAT (scWAT), it is known that M2 macrophages are involved in adaptive thermogenesis. Throughout chronic cold exposure, adipocyte-derived adiponectin triggers M2 macrophage proliferation. In turn, depletion of macrophages or adiponectin leads to lack of adaptation by reducing cold induced browning in scWAT (332). Activated M2 macrophages also participate in the browning impacts of both adrenomedullin2 (ADM2) and meteorin-like (Metrl), causing a subsequent rise in UCP1 transcription in adipocytes (333). ADM2 is synthesized by white adipocytes, and its expression has been shown to be reduced in adipose tissues of obese mice (333).

These data provide evidence of a relationship between adaptive thermogenic reactions and anti-inflammatory transcriptional regulation in adipose tissue (334).

In the obese state, hypertrophic adipocytes in both WAT and BAT display perpetuation of their endocrine activity with increased levels of apoptosis as well as increased immune cell count, i.e. presence of macrophages, neutrophils and mast cells (212,323,335,336). In fact, inflammation due to infiltration by macrophages and other immune cells is recognised as a key contributor to WAT pathophysiology in adiposity including insulin resistance and other alterations in metabolism (337,338). Similar to WAT, it is thought that there is recruitment of immune cells in BAT as a result of elevated lipolysis and the release of fatty acids from stored TG in adiposity (339). In diet-induced obese mice, after being obese for six months, BAT showed an elevated immune response, involving infiltration with leukocytes, monocytes, M1 macrophages, and cytokine release (340–343). However, BAT shows more resistance to macrophage infiltration than WAT in diet-induced obese mice as these immune cells take longer to become evident and have a lower impact on BAT (342,343). Moreover, the transcription of inflammatory mediators is lower in BAT than WAT, regardless of diet (312,342), presenting additional evidence that BAT is typically more resistant to inflammation. Eventually, inflammatory alterations and enhanced manifestation of inflammation indicators (including TNF α and F4/80) are apparent in BAT after a persistent high calorie intake (212,312,344,345).

Recent studies have indeed identified infiltrated immune cells in BAT and inflammatory processes as contributors to BAT dysfunction. During this inflammation, macrophage populations distribute in the tissue forming crown-like structures (CLS) (346–348). These macrophages adopt an M1 phenotype which is suggested to play a crucial role in controlling adaptive thermogenesis (212,349), and together with the dysfunctional adipocytes themselves secrete pro-inflammatory molecules like IL1 β , TNF α , monocyte chemoattractant protein-1 (MCP1) and IL6. Thus recruiting and activating more immune cells which sustain the inflammatory state and contribute to insulin resistance (81,336,350–352). Inflammatory state also directly alters thermogenic activity in obesity and associated metabolic disorders by impairing the energy expenditure mechanism and glucose uptake. For instance, inflammation of BAT caused by infiltrated macrophages reduces thermogenesis and UCP1 activation (212,349). Whereas experimental depletion of pro-inflammatory

macrophages removes the repression of cold-induced up-regulation of UCP1 found in obesity (212). However, how macrophages affect thermogenesis and BAT biology is controversial (325). In addition, the increased expression of pro-inflammatory markers in BAT such as Fractalkine, TNF α and MCP1 in obese murine models co-occurs with reduced UCP1 levels and key thermogenesis indicators as well as shortage of fatty acids which act as substrates for thermogenesis (341,353,354). Also, it is reported that IL1 β reduces the cAMP-mediated induction of UCP1 expression (320), cold-induced thermogenesis in adipocytes *in vivo* via sirtuin-1 inhibition (SIRT1) (355) and WAT browning (356). Besides the direct actions of pro-inflammatory cytokines on brown adipocytes, some of these factors are thought to hinder stimulation of adrenergic receptors, activation of the sympathetic nervous system and thus regional increases of norepinephrine.

Further evidence suggests that inflammation also influences browning capacity of WAT. In this context, among the different types of WAT, subcutaneous depots are more predisposed to browning and acquisition of thermogenic characteristics (120,357,358). It can be speculated that differences in susceptibility to inflammation between different fat depots is one of the factors behind this variation since the tendency for inflammation in visceral is higher than in subcutaneous WAT (359–361). In fact, visceral WAT tissue has a higher content of innate immune cells (360,362,363) compared to subcutaneous WAT which has higher lipid handling capacity (364,365). Thus, distribution of WAT appears to be a factor that influences cardio-metabolic risk, likely because of disparity of the inflammation susceptibility. Individuals with lipodystrophic syndromes address this fact, as these individuals display a loss of femoroglutea or subcutaneous fat, and therefore increased lipid deposition in visceral WAT results in worsening metabolic and cardiovascular risk (366,367). It is indeed demonstrated that infiltrated macrophages and other immune cells in subcutaneous WAT negatively impact the ability of precursor cells to differentiate into thermogenic active beige adipocytes because of pro-inflammatory cytokine secretion and generation of an inflammatory microenvironment (368). Also, the prominence of inflammation-driven suppression of the formation of beige adipocytes in adiposity has been underscored by research of the interplay between α 4-integrin receptor on pro-inflammatory macrophages and vascular cell adhesion molecule-1 (VCAM-1) on adipocytes. These interactions decrease transcription of UCP1 via the extracellular

signal-regulated kinase (ERK) pathway. Moreover, the repression of $\alpha 4$ integrin results in augmentation of beige adipocyte formation and protects against metabolic impairment in the regulation of obese AT, which highlights a considerable contribution of ECM molecules (330). This mechanism establishes a self-sustained cycle of inflammation-driven impairment of the beige phenotype in obesity.

Heightened inflammation is proposed to act as a key player in the whitening of BAT that results after extended consumption of high-fat diet at thermoneutrality. This conversion of brown adipocytes to unilocular cells, comparable to white adipocytes, is a consequence of an incorporation of various elements that involve provoking macrophage infiltration, brown adipocyte decrease, and CLS generation. Whitened BAT display CLS formation encircling adipocytes that comprise of augmented endoplasmic reticulum, cholesterol crystals and some deteriorating mitochondria, and become encompassed by multiplied collagen fibrils. The analysis of BAT gene expression shows that whitened BAT exhibits a robust inflammatory reaction and stimulation of nucleotide-binding oligomerization domain-like receptor-3 inflammasome (NLRP3) (348). Furthermore, the multimodular adaptor protein p62 is implicated in several roles including inflammation, and it participates in controlling energy metabolism via regulating mitochondrial function in BAT, which is a further marker of the significance of inflammation and immune cell signalling pathways in BAT biology (369).

During chronic inflammation of adipose tissue in obesity, angiogenesis plays an important role and promotes immune cell infiltration (370). For instance, Ang-2, an angiogenic factor, upregulates several pro-inflammatory pathways that can lead to leukocyte recruitment through NF κ B signaling interaction (371). Immune cells in turn also communicate with endothelial cells by releasing angiogenic factors, e.g. VEGF, angiopoietins, fibroblast growth factor and transforming growth factor (TGF- β) (372,373). This indicates a close relationship between inflammation and angiogenesis in obesity (374). Also, ECM components facilitate adhesion of immune cells to the endothelium, which is one of the key steps in the inflammatory process (370). Adhesion molecules play a communication role in the inflammatory process and can have a role in immune cell infiltration, e.g. intracellular adhesion molecule (ICAM-1), vascular cellular adhesion molecule (VCAM-1), and integrins (375).

Overall, the inflammatory state including the combination of CLS, apoptotic adipocytes and circulating pro-inflammatory cytokines during obesity is strongly

associated with an escalated risk of insulin resistance complications such as T2DM and cardio-metabolic disorders (351,352,360). Also, inflammation is a modulator of insulin responses in BAT and is strongly linked to UCP1 expression and thermogenesis. Despite, BAT appearing to be less susceptible to developing inflammation than WAT (342), evidence suggests that inflammation directly alters the thermogenic activity of brown/beige fat depots by impairing its capacity of energy expenditure and glucose uptake (323,336). In fact, brown adipocytes themselves have recently being recognized to play an effective endocrine role. They can secrete multiple factors including inflammatory modulators which contribute to the systemic consequences of BAT activity (80).

1.4.1 BAT Is an Active Inflammatory Secretory Tissue

Adipocytes release a large number of hormones and cytokines, known as adipokines that communicate signals between different fat depots and distal tissues/organs (376). For instance, leptin, the satiety hormone, is secreted in response to food ingestion by white adipocytes and controls dietary intake by suppressing the appetite centre in the hypothalamus (377–379). Another adipokine released by adipocytes into the blood stream is adiponectin which is encoded by the ADIPOQ gene (376,380). It has anti-inflammatory effects and promotes lipid oxidation (381), thus enhancing insulin sensitivity and preventing obesity (381,382). Indeed, levels of circulating adiponectin are decreased in obese subjects and increase after weight loss (383). In addition, the secretory role of brown/beige adipocytes is involved in regulating the systemic influence of BAT activity. For instance, studies have shown it to be involved in the beneficial effects of BAT transplantation in rodents (214–216,218–221,384,385). Several brown/beige adipocytes-derived molecules, grouped under the name brown adipokines or batokines, that practice paracrine or autocrine effects have been identified. These factors include inflammatory modulators, which are associated with BAT recruitment when thermogenic activity is stimulated as well as actions on other tissues and organs.

Factors with documented anti-inflammatory actions that are released by brown/beige adipocytes positively influence systemic metabolism and convey the beneficial metabolic effects of BAT activation. In fact, induction of thermogenesis and/or browning of white adipocytes (e.g. by cold exposure) is associated with upregulation

of brown/beige adipocyte secretion of these factors with anti-inflammatory effects. These factors themselves stimulate thermogenesis, including: fibroblast growth factor 21 (FGF21) (151,153), follistatin (Fst) (386), c-terminal fragment of SLIT2 protein (SLIT2-C)(387), C-X-C motif chemokine ligand-14 (CXCL14) (388), vascular endothelial growth factor A (VEGFA) (240,242), lipocalin prostaglandin D synthase (L-PGDS) (389), growth and differentiation factor 15 (GDF15) (331). Other positive effects of these factors involve:

- Improving glucose metabolism and weight regulation in addition to prevention of hyperglycaemia and hyperlipidaemia by FGF21 (390,391).
- Sensitising effects in response to insulin and protection against diet-induced obesity and enhancement of adipocyte differentiation by Fst (386).
- Regulation of glucose metabolism and an increasing of M2- macrophages in BAT by CXCL14 (388,392,393).
- Protecting against obesity and increasing basal metabolic rates and lipid utilization in BAT by L-PGDS (389,394).
- Reducing food intake, body weight and adiposity, and improving glucose tolerance under normal and obesogenic diets as well as inhibition of local inflammatory pathways originating from macrophages by GDF15 (331,395,396).

Whereas pro-inflammatory factors, which are also secreted from brown adipocytes themselves under certain conditions (e.g. obesity state), contribute to impairing thermogenesis of BAT and browning capacity of WAT, they are also linked to deleterious impacts on metabolism. Examples of these pro-inflammatory cytokines include: chemerin (397), endothelin 1 (ET1) (398), retinol-binding protein 4 (RBP4) (398), growth differentiation factor (GDF8/myostatin) (399), fractalkine (CX3CL1)(353), and classic pro-inflammatory cytokines such as IL6, MCP1, TNF α and IL1 (344). Both chemerin and ET1 increase in obesity, are associated with a rise in inflammation markers, are components of the metabolic syndrome and are down regulated in response to cold exposure or during adrenergic stimulation (397,398,400–405). GDF8 and CX3CL1 inhibit WAT browning, thermogenesis and metabolic activity of BAT as well as play a role in the recruitment of immune cells and exacerbation of the inflammatory state (353,399,406–411). The increase in levels of

MCP1, TNF α and IL1 is accompanied by repression of thermogenesis genes and mitochondrial respiration in BAT (344).

There are also cytokines, which play pleiotropic roles in inflammation, reported to be released from brown adipocytes. These include IL6 and Insulin-Like Growth Factor-1 (IGF-1) which are both increased upon cold exposure or following adrenergic stimulation (412–414). IGF-1 also leads to proliferation and differentiation of preadipocytes and IGF-1 signalling integrates immune-metabolic interactions to facilitate macrophage activation status (225,412,413,415,416). IL6, classically a pro-inflammatory cytokine, leads to increased UCP1 expression and M2 macrophage polarization in BAT, and enhanced browning of WAT (417,418). However, this is in opposition to the fact that IL6 is a potent pro-inflammatory cytokine, demonstrated by elevation of plasma IL6 in obesity and diabetes, in addition to reduced levels in weight loss (419–421). Moreover, it acts as a key pro-inflammatory cytokine in obese adipose tissue, macrophage polarization, and T cell regulation via signal transducer and activator of transcription 3 (STAT3), triggering subsequent insulin resistance and aggravating diet induced obesity (422). Furthermore, as anticipated for IL6, owing to its classical function as a pro-inflammatory cytokine, its ablation leads to abolition of pro-inflammatory signalling in the obese state (421). With respect to browning induction, IL6 is involved in stimulating inguinal WAT atrophy by promoting WAT lipolysis and browning (423).

It is important to determine the role of each inflammatory cytokine in insulin resistance. Also, the identification of novel brown adipokines forms an interesting aspect of obesity research. This is explained by its ability to direct drug discovery approaches for managing obesity and its associated chronic metabolic diseases. It was therefore explored in this project.

In addition, understanding the mechanisms that lead to the dysfunction of thermogenic adipose tissue including triggers to initiate the upregulation of pro-inflammatory factors and associated consequences are essential. This is especially useful to determine the effect of such mechanisms on thermogenesis in order to identify therapeutic target strategies against obesity. This may involve the utilisation of BAT thermogenesis and conversion of white fat cells into thermogenic brown-fat-like adipocytes. Thus, inflammatory signals represent an important area to investigate in brown adipocytes. Therefore, it has been the main focus of this thesis, utilising

lipopolysaccharide (LPS)/endotoxin to activate inflammatory related pathways. Indeed, gut-derived LPS is increased in obesity because of the alterations to the gut microbial composition and the resulted leaky gut, causing endotoxemia state (448). Endotoxemia exacerbates the adipose tissue dysfunction in obesity leading to insulin resistance and T2DM (233–237). The following section discusses in further details LPS activated pathway and its relation to obesity progression and adipose tissue dysfunction.

1.4.2 LPS-TLR4 Activation Pathway Relevance to Activation of Inflammation in Brown and White Adipose Tissue

BAT interaction with immunity and inflammatory signalling components is evidenced by its expression of relevant receptors, including innate immune system receptors such as toll like receptors (TLRs), and nucleotide-oligomerisation domain-containing proteins (NODs). Free fatty acids (424), reactive oxygen species (ROS)(425), and cytokines themselves (426) are some examples of activators of immune system receptors and the subsequent pro-inflammatory cytokine synthesis and secretion. In fact, stimulation of the innate immune receptors by immune and metabolic clues conveys a negative effect of pro-inflammatory pathways on BAT thermogenesis (344). For instance, studies have shown that activation of TLR4 or TNF receptors by LPS or TNF α , respectively, diminish UCP1 in BAT of mice *in vivo* and *in vitro* studies (355,427). Moreover, stimulation of TLR4 hinders β 3-adrenergic-induced browning of WAT, whereas TLR4-ablation sustains thermogenic capacity (356). Also, the Nod-like receptor 3 (NLRP3) inflammasome multiprotein complex controls inflammation and macrophage actions by splitting IL1 β and IL-18 precursors into their active forms. Stimulation of NLRP3 in macrophages impairs UCP1 and adaptive thermogenesis stimulation of white adipocytes and mitochondrial respiration, while NLRP3 ablation protects against UCP1 decrease. The effect is mediated by IL-1 as suppressing the IL-1 receptor in adipocytes maintains thermogenesis activity (356). Some of these inflammatory inducers could cause further perturbation of WAT browning in comparison to thermogenesis in BAT. For example, depletion of the intestinal microbiota or LBP (LPS-binding protein) leads to greatly enhanced WAT browning while having only a minor effect on classical BAT (428,429). This might be a

consequence of a higher basal level of inflammation in subcutaneous WAT compared to BAT (322,323,343).

It has been reported that the innate immune system can recognise an overload of nutrient intake as a danger event in obesity through pattern recognition receptors (PRRs) in adipose tissue: PRRs initiate inflammatory and stress responses, contributing to the chronic low-grade inflammation (430). A significant body of evidence suggests that much of this association can be attributed to the TLR family. In particular, TLR4, a transmembrane receptor which belongs to a unique family of PRRs, senses excessive nutrients and their derivatives, such as saturated long-chain fatty acids, modified LDLs and ceramides (431–433). Activated TLR4 stimulates the inflammatory response and expression of pro-inflammatory cytokines via different adaptor molecules such as myeloid differentiation primary response protein 88 (MyD88) and TIR domain-containing adaptor inducing interferon- β (TRIF) (431,434) (Figure 1.4.2.1). MyD88 and TRIF are signalling adaptors that lead to activation of mitogen-activated protein kinases (MAPKs) and transcription factors such as nuclear factor kappa B (NF κ B), and subsequent induction of cytokines (431,435). Thus, activation of TLR4, upregulates signalling pathways of IKK β –NF κ B (inhibitor of nuclear factor (NF)- κ B (I κ B) kinase- β –NF- κ B) and JNK–AP1 (Jun N- terminal kinase–activator protein-1) (436,437). Activation of these pathways by different upstream stimuli inhibits PPAR γ activity via MAPKs (438,439) (Figure 1.4.2.1), suppressing the expression of adipogenic genes such as C/EBPs. Also, this activation leads to an enhanced imbalance between storage and release of fatty acid into the circulation and eventually inhibits insulin signalling leading to insulin resistance (338,436). In fact, JNK, IKK+ (I κ B kinase +) and IRF3 (interferon regulatory factor-3) are among the main inflammation regulators in obesity (81,440–442). Deletion of IKK+ or IRF3 results in a reduction of inflammatory markers in adipose tissues and enhanced WAT browning with increased UCP1 expression and energy expenditure, while there are only minor effects on BAT (440,443).

To activate TLR4, one potential stimulus is lipopolysaccharide (LPS) which binds to CD14 (cluster of differentiation 14) on the cell membrane to activate TLR4 in adipose tissue (444,445). This is facilitated by the LPS-binding protein (LBP), an acute-phase protein produced in the liver, which recognizes LPS in the bloodstream and presents it to CD14 (444). Thus, serum LBP and pro-inflammatory cytokines link the immune response of the host to LPS in systemic circulation. As highlighted above, obesity-

associated chronic inflammation is linked with reduced insulin responses in white and brown adipose tissue as well as reduced brown adipocytes function. Systemic LPS, a key activator of inflammation, is known to be increased in obesity and T2DM (446,447). As such, LPS poses an intriguing primary insult to investigate in BAT and brown adipocytes as it activates inflammation contributing to metabolic consequences in obesity through TLR4. To date, this mechanism has not been described in detail and it was therefore one of the main focuses of this thesis.

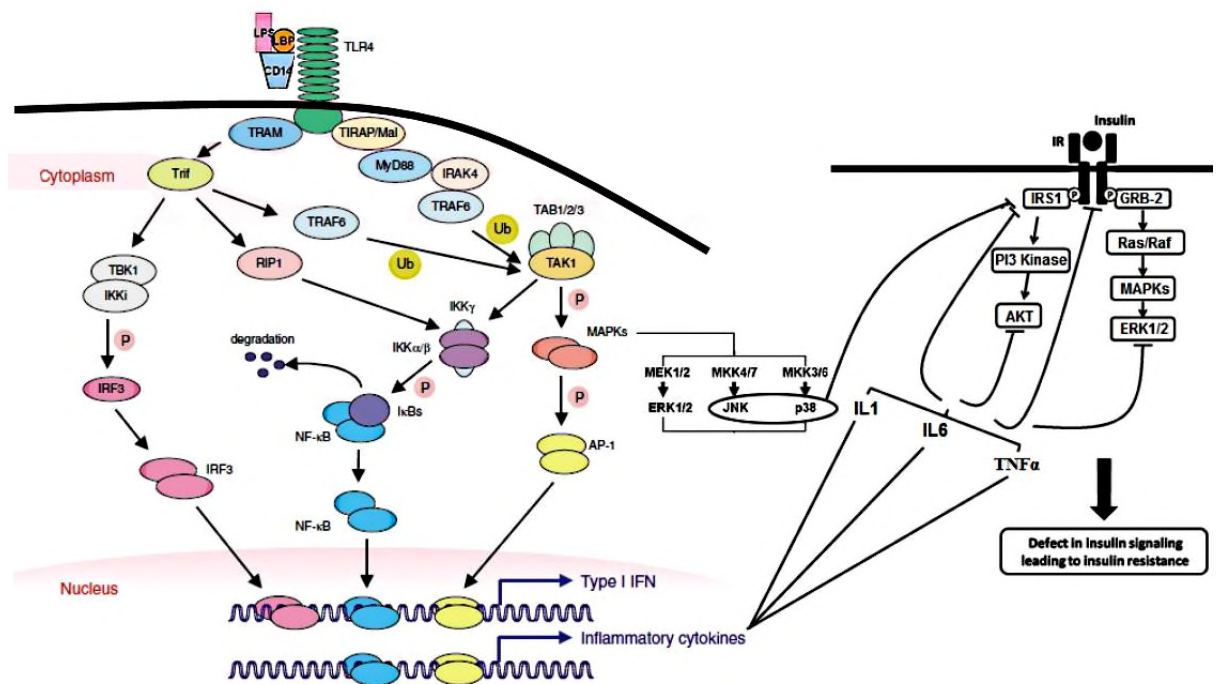


Figure 1.4.2.1 Schematic Representation of TLR4-Mediated Signalling Pathways.

TLR4 utilizes four adaptors; MyD88, TIRAP/MAL, TRIF and TRAM. The MyD88-dependent pathway controls inflammatory responses, while TRIF mainly mediates type I IFN responses. The MyD88-dependent pathway requires TIRAP/MAL to be activated and recruits IRAK4 and TRAF6 which activate TAB, leading to activated TAK1. Activated TAK1 then activates IKK β which is followed by translocation of activated- NF κ B into the nucleus. At the same time TAK1 activates MAPK which leads to the activation of AP-1. Both NF κ B and AP-1 induce pro-inflammatory cytokines transcription. The TRIF -dependent pathway requires TRAM to be activated and recruits TRAF6 and RPI1 which mediate NF κ B and AP-1 activation. In addition, TRIF interacts with TBK1, which together with IKKi mediate phosphorylation of IRF3. Then, IRF3 translocate into the nucleus and together with activated NF κ B and AP-1 induce type I IFN. Secreted inflammatory cytokines including IL6, TNF α , and IL1 combined with the activation of MAPK predispose to the insulin resistance. (Ub) ubiquitination; (P) phosphorylation, (GRB-2) growth factor receptor-bound 2; (PI3) phosphatidylinositol (adapted from (435)).

LPS is the product of gut bacteria as it is the primary component of the cell wall (outer membrane) of gram-negative bacteria (448). It is a biologically active endotoxin which may enter the bloodstream and exert crucial effects (449–455). When binding to its

receptor in adipose tissue, namely TLR4, it can stimulate an inflammatory response and therefore enhance inflammation-associated chronic disorders such as obesity (430). Indeed, it is now recognised that diet is a key player in the composition of gut microbiota constituents and systemic uptake of gut microbiota derivatives (456). Also, the development of obesity is associated with alterations in gut microbial composition and activity as well as increasing gut permeability which is called 'leaky gut'. Studies have found that the 'leaky gut' triggers a transition of numerous endogenous damage-associated molecular patterns (DAMPs) and microbiota-derived pathogen-associated molecular patterns (PAMPs) into the circulation, therefore they stimulate their corresponding PRRs like TLR4 in many tissues, including WAT and BAT (431–433). Ultimately, both DAMPs and PAMPs influence immune function and inflammatory response in obesity and related disorders (457), which in turn stimulate fat accumulation and increased insulin resistance.

Studies have identified that LPS may directly contribute to inflammation-dependent obesity and insulin resistance in both rodents and humans. Accumulating evidence indicates that LPS has an important role in the onset and progression of obesity in both rodents and humans based on the fact that plasma LPS concentration is significantly elevated in the obesity state and named 'endotoxemia' (454). Moreover, cross sectional and longitudinal data indicate elevated systemic endotoxin levels in conditions of obesity, T2DM, coronary artery disease and fatty liver disease. Furthermore, in these studies, circulating LPS is observed to be positively associated with inflammatory cytokines as well as lipids, including total cholesterol, triglycerides, and LDL-cholesterol, but negatively associated with HDL-cholesterol (446,458–462). Also, study subjects with metabolic disease, who were given a single high fat meal, were shown to not only change their systemic lipids levels substantially, but also increase their systemic levels of LPS (461). In addition, it has been demonstrated that endotoxemia may initiate hyperinsulinemia, as a direct association between increasing systemic LPS and insulin secretion (463). Hyperinsulinemia is a condition in which there are high levels of circulating insulin relative to the level of glucose. This may, therefore, lead to insulin resistance development. Correspondingly, alterations in the gut microbiota after antibiotic treatment reduces the LPS levels in both the caecal content and serum, and also results in decreased inflammation, improved glucose intolerance, as well as reduced obesity and fat accumulation (464,465). The full details of how LPS affects BAT and brown adipocyte activity and lipid-driven metabolic

diseases has not been fully addressed in the field. In addition, the role of TLR4 in these tissues has not been studied in detail. Research on the detailed role of TLR4 is important to identify new targets to combat obesity as TLR4 recognises host- derived factors as “danger” signals and has a significant impact on the pathogenesis of non-infectious, inflammatory diseases of the host such as obesity and related lipid abnormalities (466,467).

1.5 Adipose Mitochondrial Function in the Pathophysiology of Metabolic Disease

Mitochondrial function is essential for maintaining physiological cellular processes. They are the cells’ powerhouses, generating energy in the form of ATP, and possess their own DNA and protein synthesis machinery (468–470). Mitochondria are highly dynamic; varying from single structures to inter-connected networks constantly undergoing fission and fusion events (471). They are responsible for many vital activities at cellular levels such as nutrient oxidation and ATP production via oxidative phosphorylation, reactive oxygen species (ROS) synthesis and detoxification, regulation of mitochondrial matrix and calcium homeostasis, metabolite synthesis and catabolism, organelle transport and cell signalling, and some types of apoptosis (470,472,473). To perform these actions, they undergo numerous stringent mechanisms including mitochondrial dynamics, motility, protein homeostasis, biogenesis and mitophagy (471). The folds of the mitochondrial inner membrane, which are called cristae and give the characteristic wrinkled shape to the inner membrane, provide a large amount of surface area to accommodate various reactions (474).

Mitochondrial dynamics involve continuous fission and fusion of mitochondria. These dynamics facilitate the turnover of damaged mitochondria by mitophagy, exchange of matrix content and the division of organelles during mitosis; combined, these processes maintain the functionality of the mitochondrial network (475). Cells with high fusion-to-fission rates form networks of interconnected mitochondria, whereas low fusion-to-fission rates lead to the production of many fragmented mitochondria (476). In BAT, mitochondrial fission acts in synergy with fatty acid-induced uncoupling to activate heat production in response to adrenergic stimuli (477,478). Fission is operated by dynamin related protein 1 (DRP1) and mitochondrial fission 1

protein (FIS1). FIS1 recruits DRP1 to translocate to the outer mitochondrial membrane where it aggregates into rings that encircle and constrain the membranes resulting in fission (474). In contrast, the main fusion mechanism includes autosomal dominant optic atrophy-1 (OPA1) and mitofusion 2 (MFN2). MFN2 is a GTPase located in the outer mitochondrial membrane, where it facilitates tethering between adjacent mitochondria, while OPA1 controls the fusion of inner mitochondrial membranes (479). Indeed, mitochondrial dynamics change with nutritional conditions and are important to maintain healthy mitochondrial function; mitochondria under caloric excess maintain a fragmented state, whereas mitochondria under caloric restriction stay primarily in a fused state (480).

Mitochondrial biogenesis is the process of increasing the number of mitochondria through growth and division (481). It is induced in WAT as a result of imbalance between cellular energy demands and ATP production (481). Such imbalance can be a consequence of internal or external stimuli, for instance inflammation or caloric restriction. In addition, as one of the hallmarks of adaptive recruitment of thermogenic capacity during cold acclimation, expression of mitochondrial biogenesis genes is strongly increased. Also, the induction of mitochondrial biogenesis is one of the characteristics of the differentiation programme of brown adipocytes, which is fundamentally different from the adipogenesis of white adipocytes (102). The key factor that regulates mitochondrial biogenesis is PGC1 α through co-activation of nuclear respiratory factor 1 (NRF1), which in turn regulates the mitochondrial transcription factor A (TFAM) and the expression of DNA polymerase (POLG) and OXPHOS genes, necessary for mitochondrial gene expression and replication (482–484). Mitochondrial biogenesis is impaired in conditions of high oxidative stress and inflammation. This can generate mutations in the mitochondrial genome, reduce the number of mitochondria, impair oxidative capacity, further increase ROS production and adversely impact general mitochondrial function and insulin signalling (480,485). In brown adipocytes, healthy mitochondria are essential for effective thermogenesis through the inner mitochondrial membrane protein UCP1. It dissipates the energy stored in the mitochondrial electrochemical gradient as heat, “uncoupled” from ATP synthesis. The colour of brown fat reflects the high iron content of mitochondria as BAT is a mitochondria packed tissue compared to WAT (69). Another important role

for mitochondria in both BAT and WAT is the regulation of lipolysis in times of starvation or energy demands, which has been addressed above (58).

In general, mitochondrial dysfunction describes inefficient and/or insufficient ATP production since the primary role of mitochondria is energy production in the form of ATP (472,486). However, an abnormality in any mitochondrial function can be termed mitochondrial dysfunction, and has the potential to produce severe metabolic alterations and contribute to insulin resistance. Substantial evidence indicates that impairments of mitochondrial function and biogenesis are directly implicated in metabolic disorders such as obesity, T2DM and cardiac diseases. In fact, inflammation and obesity are both associated with mitochondrial dysfunction and alteration in mitochondrial mass (468,487). For instance, in WAT in obesity, reports showed reduction in the rate of mitochondrial biogenesis, oxidative metabolic pathways, and oxidative phosphorylation proteins, and a correlation with pro-inflammatory cytokines (488). Furthermore, mitochondrial efficiency is altered by pro-inflammatory cytokines which influence energy homeostasis in human white adipocytes. TNF α drastically impacts mitochondrial functions in 3T3-L1 adipocytes, whereas IL1 β and IL6 have limited effects. Also, stimulation of the macrophages-NLRP3 inflammasome lessens UCP1 activation and mitochondrial respiration in primary adipocytes potentially via IL-1, whilst the loss of NLRP3 preserves UCP1 and adaptive thermogenesis capacity in adipocytes (356,489,490). The stimulation of pattern recognition receptors in brown adipocytes, including activation of TLR4 by LPS, and the following augmented inflammation results in dysfunctional mitochondria and inhibition of mitochondrial respiration with decreased UCP1 transcription levels (344) and suppressed browning capacity of white adipocyte in response to adrenergic activation (355). The mechanism of such effects are expected to include a retardation of SIRT1 function (355). Additionally, the loss of TLR4 maintains mitochondrial function and thermogenesis in WAT (356). However, these studies do not detail the wider effects of LPS on mitochondria of different models of brown adipocytes.

Mitochondrial dysfunction in adipocytes is suggested to be a primary cause of adipose tissue inflammation, adipocyte enlargement and insulin resistance (491–495). According to this hypothesis mitochondrial dysfunction and reduced fatty acid oxidation through impaired β -oxidation in adipocytes leads to adipocyte enlargement because of triglyceride accumulation. This also increases intracellular build-up of lipotoxic molecules such as diacylglycerol and ceramides, which stimulate pro-

inflammatory signalling and directly alter insulin action (491–495). Moreover, dysfunctional mitochondria in adipocytes results in pseudo-hypoxia with substantial aggregation of hypoxia-inducible factor 1 α (HIF-1 α), which initiates inflammation and fibrosis in adipose tissue (496,497). Interestingly, there is adipose tissue depot-specific discrepancy in mitochondrial number and respiration, linking mitochondrial functionality to obesity associated complications (498). Correspondingly, changes in mitochondrial functionality in BAT could be efficiently linked with impaired thermogenesis and energy expenditure in obesity and higher vulnerability to acquire obesity induced insulin resistance. A model of chronic systemic inflammation in mice presents high levels of systematic pro-inflammatory cytokines and abnormal regulation of both innate and adaptive immune responses. Using this mouse model, mitochondrial swelling is exhibited as well as impaired cristae, in addition to decreased cold-stimulated thermogenic capacity and UCP1- reliant mitochondrial respiration (499). Moreover, low grade inflammation in BAT during obesity increases reactive oxygen species (ROS) generation and the subsequent oxidative stress, which is reported to cause mitochondrial dysfunction (500–504). Furthermore, increased levels of ROS itself directly stimulates stress kinases (505) and pro-inflammatory signalling, leading to the compromised function of insulin receptor substrate proteins by their phosphorylation at serine residues (485,506,507). Further studies in BAT ascertain the coexistence of higher levels of inflammation and ROS production in the obese state, but this is associated with the doubling of mitochondria respiration in comparison to lean mice. It is possible that if the obesogenic factors were continued for longer, mitochondria would ultimately fail to adapt to obesity stress and thermogenic function would be eventually be perturbed (341). It is worth considering that ROS generation does not always negatively impact BAT function. In this context, an intrinsic rise in mitochondrial ROS levels is reported in activated BAT thermogenesis *in vivo*. Also, pharmacological diminution of mitochondrial ROS results in hypothermia in response to cold accumulation, and suppresses UCP1-dependent induction of whole body energy expenditure (508). Dysfunctional mitochondria as a consequence of the loss of TFAM results in death of adipocytes coincident with inflammation in WAT and a whitening of BAT with reduced energy expenditure. BAT whitening in these mice is essentially elucidated by defects in mitochondrial electron transport chain function, decreased fatty acid oxidation, and excess circulating fatty acids, rather than a transformation of brown to white

adipocytes (509). These outcomes underline the link between mitochondrial function and inflammation and indicate mitochondria dysfunction resulting in increased inflammation which could eventually lead to a vicious cycle.

Collectively, the evidence set out above highlights the impact of mitochondrial alterations in BAT dysfunction with close link to inflammation and the pathogenesis of obesity, which are in turn associated with insulin resistance and cardiometabolic diseases.

1.6 Anti-Inflammatory Pathways and BAT Function

Current obesity therapies such as lifestyle modification (diet and exercise) and pharmacotherapy are important. However, their effectiveness is limited in terms of weight loss, improving metabolic profile and subsequently minimising the risk of obesity and insulin resistance, T2DM and cardiovascular diseases. Therefore, it is necessary to develop more effective therapeutic strategies by identifying novel targets to treat obesity. In fact, alleviating the inflammation state can reverse adipose tissue dysfunction in obesity, playing an essential role in developing strategies to prevent progression of metabolic diseases. Consequently, it has been demonstrated that a diminished inflammatory response can restore insulin sensitivity. Targeting inflammation in diet-induced obese mice leads to a decrease in adipocyte area, macrophage infiltration and pro-inflammatory gene expression, along with JNK and NFkB activation and increased insulin sensitivity via increased AKT phosphorylation (510–514). In addition, suppression of inflammation could offer a mechanism to enhance BAT activity, implicating the related benefits on weight loss. For instance, factors associated with the AMPK-related kinase family, which inhibit inflammation, are linked with maintaining UCP1 expression and enhanced BAT thermogenesis (515–517). Dysregulation of these anti-inflammatory kinases leads to induction of insulin resistance in BAT via impairment of the PP2A-AKT pathway (515,516). This provides evidence to support the use of an anti-inflammatory mechanism to develop anti-obesity therapies. One potential approach is dietary intervention which can have anti-inflammation activity (e.g. curcumin, epicatechin, etc), leading to enhanced insulin sensitivity as well as increased energy expenditure and body temperature in response to cold (510,518). Free fatty acids (FFAs) provide another example of dietary constituents that function as inflammation modulators. FFA actions are mediated by

cell-surface receptors G protein-coupled receptors (GPCRs) which are active stimulators for members of the rhodopsin like sub-family, including GPR40, GPR41, GPR43, GPR84, and GPR120 (519,520). Short-chain FA (less than 6 carbons) are ligands for GPR41 and GPR43, and medium-chain FAs (6-12 carbons) for GPR84. Long chain FAs (12 or more carbons) can activate GPR40 and GPR120 (519,521). GPR120 is of particular interest as it mediates actions that counteract inflammation and enhance metabolism, and as such will be discussed further in the following section.

1.6.1 G Protein-Coupled Receptor 120 (GPR120)

GPR120 positively impacts metabolic health. In enteroendocrine cells, for instance, activated GPR120 stimulates glucagon-like peptide-1 (GLP-1) secretion both *in vitro* and *in vivo*, which is followed by the elevation of insulin levels in the systemic circulation (522). In fact, activated GPR120 results in elevation of the intracellular calcium concentration, which plays a significant role in triggering GLP-1 hormone secretion from enteroendocrine cells and activation of extracellular signal-regulated kinase (ERK) and phosphatidylinositol 3-kinase/ protein kinase B (PI3K/AKT) pathways. It has been shown that the capacity of GPR120 ligands to induce AKT phosphorylation was revoked with GPR120 knockdown or by suppressing PI3 kinase (522,523). Also, in brown fat, it stimulates mitochondrial respiration via intracellular calcium release, which leads to mitochondrial depolarisation and fragmentation. This is accompanied by mitochondrial UCP1 activation, which is able to act synergistically with mitochondrial fragmentation to enhance respiration. GPR120 activation by the agonist TUG- 891 increases fat combustion in BAT thereby decreasing fat mass (524). Furthermore, in the BAT of mice lacking GPR120, UCP1 expression is reduced along with plasma FGF21 levels which contributes to defective thermogenesis (525). GPR120 deficiency diminishes expression of genes involved in nutrient metabolism and leads to obesity and metabolic disorders including glucose intolerance and hepatic steatosis in mice fed a high-fat diet (524,526). This highlights the positive role of GPR120 on stimulating metabolism.

High expression of GPR120 is found within adipocytes, therefore, it is expected to have profound effects in both BAT and WAT functions. It is more abundant in brown compared to white adipose tissue, and it is one of the genes that is increased following cold exposure in both BAT and subcutaneous WAT of mice (163). Indeed, a role for

GPR120 in BAT activation and WAT browning in response to cold via induction of FGF21 (a thermogenic promoting hormone) secretion, has also been confirmed (527). In mice on high fat diet-feeding, GPR120 is upregulated in the stromal vascular fraction (SVF) of adipose tissue (which contains macrophages) and in Kupffer cells in liver (528). Investigations in humans show that WAT of obese individuals express higher levels of GPR120 compared to lean individuals (526).

GPR120 plays a role in the process of adipogenesis as its expression levels are increased and regulated by PPAR γ during differentiation of 3T3-L1 adipocytes and human white adipocytes (528,529). Also, GPR120 expression increases during brown adipocyte differentiation (524) and the GPR120 agonist, TUG-891, has been found to promote differentiation (530). Deletion of GPR120 in mice suppresses adipogenesis which manifested by decreased adipogenic and lipogenic gene expression levels including Adipocyte Protein 2 (aP2), PPAR- γ , and sterol regulatory element binding protein 1 (SREBP-1) (526,529,531).

There is involvement of GPR120 in inflammation processes. Importantly, GPR120 mediates anti-inflammatory and insulin sensitising effects of ω 3-FAs (n-3 polyunsaturated fatty acids, n-3PUFAs) including in adipocytes and macrophages (528,532). In fact, ω 3-FAs have anti-inflammatory effects and may significantly impact chronic inflammatory diseases including obesity-related disorders (533). An ω 3-enriched diet, in non-obesogenic non-inflammatory conditions, produces oxylipins, which possess an anti-inflammatory response in both WAT and BAT with a macrophage modulation effect, but with no effect on inflammatory cytokine release (534). In addition, a non-selective synthetic GPR120-agonist GW9508 significantly inhibits the ability of LPS, the TLR4 ligand, to stimulate inflammatory responses in macrophages. Thus, GW9508 inhibits LPS-stimulated phosphorylation of IKK β and JNK, preventing I κ B degradation, and inhibits TNF α and IL6 secretion. GW9508 is a GPR120 and GPR40 agonist but is a functional GPR120-specific compound in macrophages and adipocytes because they do not express GPR40. All of these anti-inflammatory effects of GW9508 are completely abrogated by knockdown of GPR120 (528). Another effect of activation of GPR120 involves induction of VEGF-A in 3T3-L1 adipocytes through a GPR120-PPAR γ pathway. This suggests a role for GPR120 as a promoter of angiogenesis which may itself have an anti-inflammatory function in adipocytes. Angiogenesis inducers show anti-inflammatory properties given the fact that secretion of a number of inflammation-related adipokines are upregulated by

hypoxia, which in turn is the principle physiological stimulus that induces angiogenesis (535,536). Also, GPR120 knockout mice are insulin resistant with features of increased inflammation in adipose tissue, along with reduced insulin signalling. Since chronic inflammation is an important feature in the pathogenesis of insulin resistance and obesity-related disorders, the anti-inflammatory effect of GPR120 activation could enhance insulin sensitisation and prevent obesity complications. However, the role of GPR120 and its connection to inflammatory pathways in brown adipocytes is not fully understood. Specifically, the implications of GPR120 activation by TUG-891 as a strategy to combat the inflammation in brown adipocytes is not known. Therefore, one of the main aims for this thesis is to improve the understanding of the processes that mediate BAT dysfunction which may have pharmacological applications.

1.7 Hypothesis, Aims and Objectives

The hypothesis for this research is to suggest: LPS mediates metabolic dysfunction of brown adipocytes and impairs the browning process through activation of inflammatory pathways and dysregulation of mitochondrial function. Whilst this thesis has also explored whether the activation of GPR120 by TUG-891 to protect against the effects of LPS-mediated inflammation in brown adipocytes. As such, this thesis aims were to:

1. Investigate the influence of LPS through the TLR4 innate immune pathway on classical characteristics of brown adipocytes.
2. Explore the wide-spectrum effects of LPS-induced damage on brown adipocytes through TLR4.
3. Define the impact of LPS on mitochondrial function in brown adipocytes.
4. Assess the phenotype of brown fat-associated gene expression in the development of human obesity and study LPS interference during the browning process in human white adipocytes.
5. Evaluate the inflammatory modulation effects of TUG-891, a GPR120 agonist, to reduce the damaging effects of LPS on the cellular metabolism and mitochondria.

In order to ascertain the above aims, the following objectives were carried out

1. Determine how inflammatory stimuli, such as LPS, affect brown adipocyte biology, and how LPS impacts thermogenic features through TLR4 in brown adipocytes, which are currently unclear. To investigate this, wild-type brown adipocytes and TLR4 knockout brown adipocytes were cultured and treated with LPS throughout differentiation. Protein and RNA samples were collected and studied through Western Blotting and qRT-PCR, and functional assays including lipid handling profile and glucose uptake were conducted to study the LPS-mediated stress.
2. Identify the wider effects of LPS-mediated inflammation in brown adipocytes to consider novel therapeutic targets. This was investigated by culturing wild-type brown adipocytes and TLR4ko brown adipocytes with LPS throughout

differentiation. Comprehensive transcriptomic and proteomic techniques were used to study this in further detail.

3. Characterise the effects of LPS-mediated stress on mitochondrial function. As such to undertake this, immortalised brown adipocytes were exposed to an LPS stressor over the period of differentiation. Once differentiated, various important parameters of mitochondrial health were investigated such as mitochondrial encoding genes, mitochondrial respiration, mitochondrial membrane potential, production of reactive oxygen species, mitochondrial number and mitochondrial dynamics.
4. Ascertain the extent of brown fat gene expression changes in obesity and how they progress during weight gain. For this objective, adipose tissue from abdominal subcutaneous and omental depots were isolated from a large female cohort and expression evaluated. Also, to examine the effect of LPS on browning capacity, human primary white adipocytes from obese and lean subjects were differentiated with and without LPS. Following RNA isolation, genes encoding proteins involved in the browning process, inflammation and mitochondrial function, including mitochondrial biogenesis, oxidative phosphorylation, mitochondrial dynamics, and antioxidant action were assessed using qRT-PCR.
5. Lastly, to elucidate how GPR120 activation by TUG-891 impacts LPS mediated-effects on brown adipocytes, brown adipocytes cultured with the ligand TUG-891, LPS, or a combination of the two were used over the course of differentiation of brown adipocytes. As before, different parameters of brown adipocyte biology were assessed for indicators of improvement in adipocyte function. These measures include quantification of key inflammatory, brown fat and mitochondrial genes and proteins, mitochondrial respiration, dynamics, and membrane potential. This was to determine whether TUG-891 may reduce the risk of LPS-induced brown adipocyte dysfunction via different mechanisms.

Chapter 2. Materials and Methods

In this chapter, the overall methods used in this thesis are outlined. Any methods that are specific to a particular chapter are described within the chapter itself.

2.1 Cell Culture and Differentiation

2.1.1 Mouse Cell Lines

Cell lines were generated as previously described (163). In brief, isolated pre-adipocytes from murine interscapular BAT and subcutaneous WAT were immortalized by retroviral-mediated expression of temperature-sensitive SV40 large T-antigen H-2kb-tsA58. In addition, conditionally immortalised BAT TLR4^{-/-} cell lines were generated beforehand, using the same procedure but with cultures prepared from the adipose tissue of TLR knockout mice (537).

These conditionally immortalised pre-adipocyte cell lines were cultured at 33 °C in growth media containing DMEM/F12 (#D8437, Sigma-Aldrich, UK), fetal bovine serum (FBS 10 % v/v) (#10500064, Gibco, Fisher Scientific, UK) and penicillin/streptomycin (pen/strep 1 % v/v) (#15140122, Gibco, Fisher Scientific, UK). Cultured pre-adipocytes were grown in T75/T175 flasks and incubated at 33 °C, 5 % CO₂. Cells were passaged at 80 % confluence and experiments were conducted between passages 4-10.

Once cells were 80 % confluent in the flasks, they were trypsinised and plated onto 6 or 12 well plates, pre-coated with 0.01 % gelatin, and left at 33 °C, 5 % CO₂ until they reached 90 % confluence, at which point they were transferred into a 37 °C incubator for an additional 24 hours. After this, the cells were induced to differentiate using specific protocols for brown or white adipocytes. Differentiation protocols were carried out without penicillin/streptomycin to avoid any possible impact on mitochondrial function. The following sections demonstrate the protocols used to differentiate these white adipocytes and the immortalized brown AT cell lines.

2.1.2 White Adipocyte Culture, Differentiation and Treatment

Confluent pre-adipocytes of a cell line derived from murine subcutaneous white AT were differentiated according to the following protocol. The differentiation media for WAT was prepared using Advanced DMEM/F12 (#12634010, Gibco, Fisher Scientific, UK) and supplemented with FBS (10 %), insulin (1 µg/mL) (#I9278, Sigma-Aldrich, UK), T3 (0.1 nM) (#T6397 Sigma-Aldrich, UK), dexamethasone (250

nM) (#D2915, Sigma-Aldrich, UK), IBMX (0.5 mM), (#I5879, Sigma-Aldrich, UK), hydrocortisone (1 μ M) (#H0888, Sigma-Aldrich, UK) and rosiglitazone (5 μ M) (#CAYM71740-10, VWR International Ltd., UK) for 72 hours. Hereafter, cells were kept in a maintenance medium: Advanced DMEM/F12 supplemented with FBS (10 %), insulin (1 %), T3 (0.1 nM), and rosiglitazone (5 μ M) for 48 hours. Afterwards, the maintenance medium (without Rosiglitazone) was replenished every 2 days until differentiation was complete (8-12 days).

2.1.3 Immortalized Brown Adipocyte Culture, Differentiation and Treatment

Pre-adipocytes derived from immortalized brown AT cell line (imBAT) or BAT TLR4^{-/-} cell line (TLR4ko.BAT) were differentiated using an induction medium containing advanced DMEM/F12 supplemented with FBS (10 %), insulin (1 μ g/mL), T3 (1 nM), dexamethasone (250 nM), IBMX (0.5 mM) and indomethacin (30 μ M) for a total of 48 hours. Cells were then cultured in a maintenance medium: Advanced DMEM supplemented with FBS (10 %), insulin (1 μ g/mL) and T3 (1 nM) for complete differentiation (8-12 days).

2.1.4 Primary Brown and White Adipocyte Isolation, Culture, Differentiation and Treatment

Primary brown adipose tissue was obtained from mice by Prof. Mark Christian and I carried out the tissue digestion and primary brown adipocyte isolation. Briefly, as previously described (538,539), interscapular BAT and subcutaneous WAT were dissected from 4 to 10-week old mice type C57BL/6. The tissues were digested in a Krebs-Ringer bicarbonate buffer (KRB) solution (# K4002 Sigma-Aldrich, UK), containing 0.2 % collagenase Type II (#LS004177, Lorne Laboratories Ltd, UK) and 1.5 % BSA (#A9418-100G, Sigma-Aldrich, UK), and then vortexed every 10 minutes to mix. After 45 minutes, 5 mL of FBS was added for every 45 mL of digested tissue to stop the enzymatic activity of collagenase. The tissues were centrifuged at 1000 rpm for 7 minutes at RT and the supernatant was discarded. The stromal vascular fraction was re-suspended in DMEM/F12, penicillin/streptomycin 1 % and FBS 10 % (growth media), filtered through a 40 μ m strainer (#22363547, Fisher Scientific, UK) and plated in tissue culture flasks or dishes.

Growth media was refreshed every other day until cells reached 80-90 % confluence. Following trypsinisation, $4 - 5 \times 10^4$ cells per well were plated onto a gelatine-coated 12-well cell culture plate. At 100 % confluence differentiation was induced. The differentiation protocol required the addition of induction media to the cells for 3-4 days. The induction media were composed of advanced DMEM/F12 supplemented with FBS (10 %), insulin (1 $\mu\text{g/mL}$), T3 (1 nM), dexamethasone (500 nM), IBMX (250 μM), Rosiglitazone (2 μM) and indomethacin (30 μM). This induction medium was used for both white and brown adipocytes; indomethacin was omitted for white adipocyte differentiation.

Hereafter, induction medium was replaced with first maintenance media for 48 hours. First maintenance media was composed of advanced DMEM/F12 supplemented with FBS (10 %), insulin (1 $\mu\text{g/mL}$), T3 (1 nM), and Rosiglitazone (2 μM).

Cells were then switched to the second maintenance media and kept for at least 48 hours prior to experiments. The second maintenance medium was composed of advanced DMEM/F12 supplemented with FBS (10 %), insulin (1 $\mu\text{g/mL}$), T3 (1 nM).

2.1.5 Spheroid Brown Adipocyte Culture, Differentiation and Treatment

A 3D adipocyte spheroid cell culture model was used in this thesis in addition to the 2D-models of immortalised and primary brown adipocyte cells. 3D culture is expected to better represent the structural complexity and cellular environment of fat tissue. It is previously reported that 3D adipocyte spheroids express and release higher levels of adiponectin compared to 2D culture and respond to stress, either culture-related or toxin-associated, by secreting pro-inflammatory adipokines. In addition, 3D spheroids derived from brown adipose tissue (BAT) express BAT markers better than 2D cultures derived from the same tissue (539). This 3D model has not been studied in the context of brown adipocytes inflammation. Therefore, it was interesting to see whether the same response of monolayer cell culture systems could be reproduced in the 3D-cell culture model.

In brief, pre-adipocytes self-organize into spheroids in hanging drops and upon transfer to low attachment plates, were differentiated according to the imBAT differentiation protocol described above. This resulted in imBAT pre-adipocytes maturing into brown adipocytes and accumulating large lipid droplets that expanded with time. More specifically, immortalised wild type brown adipocytes were used to

form hanging droplets. Droplets consisting of 75×10^5 cells per mL of pre-adipocyte growth media mixed with 20 % of Methyl cellulose (# M0512, Sigma-Aldrich, UK) were deposited on the underside of the lid of a cell culture plate using a pipette at 20 μ L (15000 cell) per droplet. The lid was then inverted and placed on a tissue culture plate containing PBS for humidity for 48 hours, to allow spheroid formation by allowing cells to coalesce and generate an extracellular matrix within the spheroid. Following this, the spheroids were transferred to 24-well low attachment plates (#3473, Corning, Appleton Woods, UK) (5 spheroids per well) to prevent the attachment of spheroids to well surfaces. Differentiation media (induction media followed by maintenance media) was added, and the differentiation protocol outlined above was carried out as usual. Attention was taken to keep individual spheroids separated to avoid any alteration of the phenotype as a result of spheroid fusion.

2.1.6 Cell Culture Treatments

Lipopolysaccharide (LPS) from *Escherichia coli* O55:B5 (#L6529, Sigma-Aldrich, UK) was used. LPS doses of 100 ng/mL or 1000 ng/mL were in the experiments, as indicated in figure legends.

TUG-891, a GPR120 ligand, was used at a dose of 10 μ M (#4601, Tocris, BIO-TECHNE LTD, UK).

CL316243, a β 3 adrenergic receptors ligand, was used at a dose of 10 μ M (#1499, Tocris, BIO-TECHNE LTD, UK).

2.2 RNA-Isolation, Quantification and qRT-PCR

RNA processing was performed following the below protocol, unless otherwise specified.

2.2.1 RNA Extraction

Total RNA was extracted from cell culture samples using the Trizol method whereby after removing the medium, cells were washed with PBS and then Trizol® reagent (#T9424 Sigma-Aldrich, UK) was added. Samples were collected by scraping and were then homogenized and transferred into RNase-free tubes. To avoid ribonuclease (RNase) contamination RNase-free tips, tubes and DEPC-treated water were used.

Moreover, disposable gloves were worn at all times and the surfaces and pipettes were cleaned with RNase Away. Samples were then incubated at room temperature (RT) for 5 minutes to allow the complete dissociation of the nucleoprotein complex. Chloroform (#J67241.AP, VWR International Ltd., UK), (0.2 x Trizol volume) was added and samples were vigorously shaken for 15 seconds, incubated at RT for 3 minutes and centrifuged at 13,000 rpm for 30 minutes at 4 °C. The lower red phenolchloroform phase and the interphase, resulting from phase separation, were discarded. The upper aqueous phase was transferred into a new RNase-free tube and 100 % Isopropanol (#BP2618-212, Fisher Bioreagents, UK) (0.5 x Trizol volume) was added to precipitate the RNA. Samples were incubated for 10 minutes at RT and RNA was pelleted by centrifuging at 13,000 x rpm for 30 minutes at 4 °C. The supernatant was removed and the pellet was washed with 75 % ethanol (1 mL) (#10428671, Fisher Scientific, UK) before being centrifuged at 13,000 x rpm for 30 minutes at 4 °C. The supernatant was removed, and the pellet air-dried and re-suspended in 10 µL of RNase-free water (# BP561-1, Fisher Bioreagents, UK).

2.2.2 RNA Quantification

RNA quantification was performed using a spectrophotometer (Nanodrop ND-1000, Labtech, UK), measuring at an absorbance of 260 nm. The ratios between the two absorbances 260/280 nm and 260/230 nm were measured to give an estimate of RNA purity. A value between 1.8 and 2.1 for both ratios was accepted as suitable RNA purity for use.

2.2.3 DNAase Treatment

To remove DNA contamination, 1000 ng of cellular RNA was dissolved into 4 µL of RNase-free water and treated with 0.5 µL of 10x DNase I buffer (#AMP-D1 DNase I kit, Sigma-Aldrich, UK) and 0.5 µL of amplification grade DNase I (#AMP-D1 DNase I kit, Sigma-Aldrich, UK). After 15 minutes of incubation at RT, the reaction was stopped by adding 0.5 µL of stop solution (#AMP-D1 DNase I kit, Sigma-Aldrich, UK) and incubating at 65 °C for 10 minutes to inactivate the DNase I.

2.2.4 cDNA Synthesis

In the reverse transcription reaction, RNA is converted into cDNA through a reverse transcriptase enzyme (DNA polymerase RNA-dependent), in the presence of nucleotides. The reaction results in RNA-DNA hybrid products. The newly polymerized DNA will work as a template in the next amplification step through classic PCR or Quantitative Real-Time PCR reaction. The product amplified is proportional to the initial amount of RNA. In this thesis the reagents for the reverse transcription reaction were: Moloney Murine Leukemia Virus Reverse Transcriptase (M-MLV) and random hexamers for total RNA reverse transcription using SIGMA-ALDRICH mRNA reverse transcription kit (#M1302-40KU) according to the manufacturer's instructions.

Briefly, master mix was prepared to reverse transcribe for n+1 samples to reverse transcribe was prepared. For each sample, this contained: 1 μ L random hexamers (#SO142, Thermo Scientific, UK), 1 μ L dNTPs (#U1511, Promega uk ltd), and RNase-free water (4.5 μ L) up to 12 μ L final volume. Samples were then incubated at 70 °C for 10 minutes to allow random hexamer annealing to the RNA. After this, they were instantly removed into ice. The following step involved the preparation of a mix for n+1 samples containing for each sample M-MLV Buffer (2 μ L), M-MLV (1 μ L), RNase OUT (0.5 μ L) (#10777019, Invitrogen, UK), and RNase-free water up to 20 μ L final volume of reaction. Following the manufacturer's recommended protocol, reverse transcription reaction conditions were 10 minutes at 25 °C followed by 50 minutes at 37 °C, and finally 80 °C for 10 minutes. 180 μ L of RNase-free water was added to each sample to make the solution up to 200 μ L. The obtained cDNA was stored at -20 °C.

2.2.5 Primer Design

Primers for mRNAs of specific genes were designed using the Primer BLASTtool (<https://www.ncbi.nlm.nih.gov/tools/primer-blast/>), and their characteristics were evaluated through USCS Genome In-silico PCR (<http://genome.uscs.edu/cgi-bin/hgPcr>). These included: size of product between 70 and 150 nucleotides, melting temperature around 60 °C and GC content around 55 %. Primers for mRNAs of specific proteins were designed so that one was complementary to a sequence of an exon-exon junction, in order to exclude amplification of any residual contaminating

genomic DNA. Primers were synthesised by Sigma Aldrich and 100 μ M stocks were made by dissolving the nucleic acids powder in nucleic acid nuclease-free water and stored at -20 °C. The primers used are listed in supplementary table 2.1 in Appendix.

2.2.6 Quantitative Real Time PCR (qRT-PCR)

Quantitative Real-Time PCR allows DNA amplification and its simultaneous quantification is possible by using particular fluorescent systems. It is based on a classic PCR, where, during the exponential phase, the number of amplified DNA copies is proportional to the initial cDNA quantity and to the fluorescence emitted by the fluorophore. Thus, through this technique it is possible to measure the absolute or relative expression of a particular gene.

SYBR Green I fluorescence dye was used for Real-time PCR in this project (#S4438-500RXN Sigma-Aldrich, UK). This fluorophore is an asymmetrical cyanine dye able to bind the DNA. DNA-dye-complex absorbs blue light with a maximum wavelength (λ) of 497 nm and emits green light (λ_{max} = 520 nm). SYBR Green molecules preferentially bind to double stranded DNA intercalating in its minor grooves, hence, fluorescence intensity increases with PCR product accumulation at every cycle. Following the manufacturer's recommended protocol, the reaction mix was prepared in different tubes for every reference gene and gene of interest with a volume for n+1 samples. Each one contained: 7.5 μ L SYBR Green I mix, 0.15 μ L forward and reverse primer for protein-encoding genes of interest, ROX reference dye 0.02 μ L, RNase free-water up to the 15 μ L final volume. 12 μ L of this mix was added to each well along with 3 μ L of each cDNA sample (or RNA-free water as non-template control), these were mixed in a 96-well PCR plate in duplicates. These reaction components were scaled down three times when using 384-well PCR plates.

Hereafter, quantitative real-time PCR (qRT-PCR) reactions were carried out using an ABI 7500 fast sequence detection system, 96-well (Applied Biosystems, UK) or a QuantStudio™ 5 Real-Time PCR System, 384-well (Applied Biosystems, UK). These reactions were performed at 95 °C for 2 minutes followed by 40 cycles at 94 °C for 34 seconds, 60 °C for 34 seconds and a final step at 72 °C for 30 seconds at which data were obtained. Following this, a step for a melting curve was added to evaluate the presence of single or multiple products.

The expression of the gene of interest was normalised to that of the housekeeping gene L19, enabling the calculation of delta threshold cycle (ΔCt) values (where $\Delta Ct = Ct$ of L19 subtracted from Ct of gene of interest). Gene expression data was then expressed based on the following formula:

$$\text{mRNA expression} = 2^{-\Delta Ct}, \text{ where } \Delta Ct = \text{target gene} - \text{L19}.$$

2.3 Protein Isolation, Quantification and Immunoblotting

For harvesting protein, 1.2×10^6 cultured adipocytes were serum starved for 24 hours, rinsed once with ice cold PBS and lysed in 100 μL of ice-cold $\times 1$ RIPA buffer (#5872S RIPA Buffer (10X), CST, New England Biolabs LTD, UK) supplemented with $\times 1$ Protease/Phosphatase Inhibitor Cocktail (#5872 Protease/Phosphatase Inhibitor Cocktail (100X), CST, New England Biolabs LTD, UK) and 1 mM phenylmethylsulfonyl fluoride (PMSF) (#M145-5G, PMSF Proteomics Grade, VWR International Ltd, UK). Cell lysates were rotated for 10 minutes at 4 °C. Homogenates were then centrifuged (12,000 rpm, 15 minutes, 4° C) and the supernatant collected, avoiding the upper lipid layer. The protein was assayed immediately or frozen at - 80 °C.

2.3.1 Determination of Protein Concentration (Bradford Protein Assay)

Protein content of the supernatant was determined using a Coomassie Plus Protein Assay Kit (#23236 Coomassie Plus TM, Thermo Scientific, UK). This kit involves a colorimetric method for total protein quantitation based on the Bradford method. When coomassie dye binds protein, maximum absorption occurs from 465 nm to 595 nm with a concomitant colour change from brown to blue. Briefly, 10 mg/mL bovine serum albumin (BSA) (#421501J, VWR Chemicals, UK) stock solution was prepared and was used for protein standard dilutions. The BSA dilution range was between 0 - 25 $\mu\text{g/mL}$. Tested protein samples were diluted 1/400 – 5/400 (v/v) in distilled water depending on the initial protein content ensuring that colour of each sample fits within the standard curve. A protein dye reagent concentrate containing Coomassie dye was then added to the standard dilutions and to tested samples at a ratio of 1/5. Tubes were

incubated at room temperature for 15 minutes, vortex mixed and loaded in duplicates into a 96-well transparent assay plate. Plates were read at 595 nm using a nanospectrophotometer (GeneFlow, UK). Standard curves were generated from the optical density of the BSA standards and were used to calculate the protein concentration of tested samples.

2.3.2 Preparation of SDS-polyacrylamide Gel and Required Solutions

Sodium dodecyl sulfate polyacrylamide gel (SDS-polyacrylamide gel) composes of two phases: stacking gel on top and resolving (separating gel) gel on the bottom as described below. Resolving gels were added into the cassettes and overlaid with isopropanol. Once gels were set, the isopropanol was removed, stacking gels were added, and combs inserted.

Stacking gel was prepared following the recipe below to prepare 5 mL:

H ₂ O	2.975mL
Acylamide/Bis-acrylamide (30 %/0.8 % w/v) (#A3699-5X100ML, Sigma-Aldrich, Germany)	1.25mL
0.5M TRIS–HCL (PH=8.8)	50μL
Prepared by adjusting pH of Tris-Base (#10376743, Fisher Scientific, UK) with hydrochloric acid (#CHE2124, Scientific Laboratory Supplies LTD., UK)	
10 % (w/v) Sodium dodecyl sulfate (SDS) (#L3771-25G, Sigma-Aldrich, Germany) in distilled water.	670μL
10 % (w/v) ammonium persulfate (AP) (#A3678-100G, Sigma-Aldrich, Germany) in distilled water.	50μL
Tetramethylethylenediamine (TEMED) (#1610801, Bio-Rad Laboratories LTD, UK)	5μL

Resolving gel was prepared following the recipe below to prepare 10 mL of 10 % acylamide:

H ₂ O	3.8mL
Acylamide/Bis-acrylamide (30 %/0.8 % w/v) (#A3699-5X100ML, Sigma-Aldrich, Germany)	3.4mL

1.5M TRIS-HCL (PH=8.8) Prepared by adjusting pH of Tris-Base 2.6Ml (#10376743, Fisher Scientific, UK) by hydrochloric acid (#CHE2124, Scientific Laboratory Supplies LTD., UK)

10 % (w/v) SDS (#L3771-25G, Sigma-Aldrich, Germany) in distilled water. 100µL

10 % (w/v) ammonium persulfate (AP) (#A3678-100G, Sigma-Aldrich, Germany) in distilled water. 100µL

TEMED (#1610801, Bio-Rad Laboratories LTD, UK) 10µL

Running buffer was prepared by mixing 30 g Tris-Base (#10376743, Fisher Scientific, UK) with 144 g of glycerin (#G8898-1KG, Sigma-Aldrich, Germany) and 10 g of SDS (#L3771-25G, Sigma-Aldrich, Germany) in 1 litre of distilled water.

Washing buffer: 10× TBST was prepared by mixing 24.2 g Tris-Base (#10376743, Fisher Scientific, UK) with 80 g sodium chloride (S9625-1KG, Sigma-Aldrich, Germany) into 1 litre of distilled water, adjusting the pH to 7.6 and adding 10 mL of tween-20 (#P1379-500 mL, Sigma-Aldrich, Germany).

2.3.3 SDS-polyacrylamide Gel Electrophoresis and Immunoblotting (Western blotting)

After mixing the samples with ×1 loading dye (#EC-887, 5X Protein Loading Buffer, National Diagnostics, USA), and heating them (5 minutes, 95 °C) to denature the proteins, giving the antibody access to its epitope, 30 µg of protein was separated by 10 % SDS-PAGE gel along with a protein molecular weight standard ladder. The gel was run at 100 volts for about 1.5 hour until the ladder reached the bottom of the gel. Proteins were then transferred to a PVDF membrane (#1704272/#1704275 Trans-Blot® Turbo™ RTA Mini/Midi PVDF Transfer Kit, BIO-RAD Laboratories LTD, UK) using a Trans-Blot Turbo Transfer System (Bio-Rad), semi-dry turbo transfer (1.3 A for 7 minutes) after immersing the PVDF membrane and the sandwich paper layers in ×1 transfer buffer (#170-4272, BIO-RAD Laboratories LTD, UK). The assembly of the blotting sandwich in the cassette consists of paper, gel, membrane and then paper from top to bottom.

After protein transfer, membrane blots were blocked with 5 % BSA (#421501J, VWR Chemicals, UK) dissolved in TRIS-buffered saline, 0.1 % Tween 20 (TBST) for 1 hour at RT. After blocking, membranes were incubated overnight at 4 °C with protein-specific primary antibody, or as per manufacturer's instructions. This was followed by $\times 3$ washing with $\times 1$ TBST for 10 minutes each and then incubation for 1 hour at RT with horseradish peroxidase (HRP)-conjugated secondary antibodies. A further three washes with $\times 1$ TBST for 10 minutes each were then carried out. Dilutions of primary and secondary antibodies were previously optimized and dilutions are listed in Table 2.3.3.1 below. Protein bands were visualized through a chemiluminescence detection system using ECL Prime Western Blotting Detection Reagent (#RPN2236, ECL Prime, GE Healthcare, UK) using a G:Box (Syngene, Cambridge, UK). Densitometry was conducted using ImageQuant LAS 4000 Software (GE Healthcare, UK). Equal protein loading was confirmed by examining expression of a reference protein such as β -actin protein or GAPDH.

Protein	Primary antibody (Dilution)	Provider (Cat.No)	Secondary antibody (Dilution)	Provider (Cat.No)
<i>UCP1</i>	Rabbit anti-UCP1 (1:1000)	Sigma-Aldrich (#U6382)	Goat anti-Rabbit HRP (1:2000)	Dako (P0448)
pAKT	Rabbit anti- Phospho AKT (Ser 473) (1:1000)	Cell Signalling (#9271)	Goat anti-Rabbit HRP (1:2000)	Dako (P0448)
AKT	Rabbit anti-AKT (1:1000)	Cell Signalling (#9272)	Goat anti-Rabbit HRP (1:2000)	Dako (P0448)
β -Actin	Mouse anti- β -Actin HRP (1:5000)	Santa Cruz (sc-47778)	-	-
SDHA	Rabbit anti- SDHA (1:1000)	Cell Signalling (#5839)	Goat anti-Rabbit HRP (1:2000)	Dako (P0448)
<i>MT-CO1</i>	Mouse anti- MT-CO1 (1:1000)	Abcam (#Ab14705)	Goat anti-mouse HRP (1:2000)	Dako (P0447)
<i>pDRP1</i>	Rabbit anti-Phospho-DRP1 (Ser637) (1:500)	Cell Signalling (#4867S)	Goat anti-Rabbit HRP (1:1000)	Dako (P0448)
<i>DRP1</i>	Mouse Anti-Drp1 (1:500)	BD Transduction Laboratories (#611739)	Goat anti-mouse HRP (1:1000)	Dako (P0447)
<i>OPA1</i>	Mouse Anti-OPA1 (1:1000)	BD Transduction Laboratories (#612607)	Goat anti-mouse HRP (1:2000)	Dako (P0447)
<i>GAPDH</i>	Mouse anti-GAPDH (1:1000)	GeneTex (#GTX627408)	Goat anti-mouse HRP (1:2000)	Dako (P0447)
<i>c-jun</i>	Rabbit anti-Phospho-c-Jun (Ser73) Antibody (1:1000)	Cell Signalling (#9164)	Goat anti-Rabbit HRP (1:2000)	Dako (P0448)
<i>NFkB</i>	Rabbit anti-Phospho-NF- κ B p65 (Ser536) (1:500)	Cell Signalling (##3031)	Goat anti-Rabbit HRP (1:2000)	Dako (P0448)

Table 2.3.3.1 Primary and Secondary Antibodies Used for Western Blotting.

2.3.4 Oxygen Consumption and Seahorse Cell Mito-Stress Test

Cellular respiration can be either aerobic or anaerobic. Aerobic respiration occurs when oxygen is used to oxidise fatty acids for ATP and/or heat generation through

UCP1, while anaerobic respiration leads to ATP-generation via glycolysis, which produces lactic acid.

The Seahorse XF Analyzer provides a method to estimate these metabolic events by monitoring real time changes in concentrations of oxygen and protons (acidification) in the extracellular media. These concentrations are measured by two different embedded fluorophore probes in polymers at the bottom of sensor cartridges, which take place on top of each well of the cell culture plate; one probe is sensitive to oxygen and the other one to protons. Inside the instrument, the sensor is lowered to less than 3 μL of media above the cell monolayer (Figure 2.3.4.1), creating a “microenvironment”, which allows almost immediate detection in any small changes in oxygen and proton concentrations.

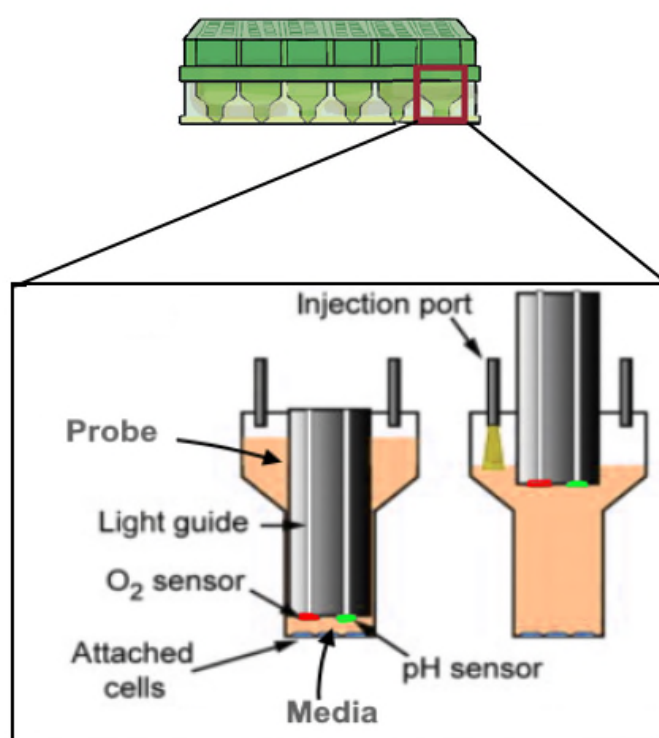


Figure 2.3.4.1 Seahorse XF Analyzer in the Measuring (left) Phases and the Resting (right).

Black box shows on a large scale the probes of the sensor cartridge (solid red box), a piston equipped with sensors for O₂ and protons enclosed in a small volume of medium over the cells. The piston is then raised, allowing O₂ to re-equilibrate and injections to be made before the cycle is repeated.

The detection, based on the decreases in the fluorescence intensity of the sensors, arises as a result of stimulation of the fluorophores by a light diffused by optic fibres that insert themselves into each sensor sleeve during the measurements. The emission of the excited fluorophores is captured back via the optical fibres. When the sensor detects a 10 % drop in oxygen or proton concentration, the instrument lifts the sensor,

allowing the media to mix, restoring the baseline and avoiding cell damage. Measurements can be repeated several times and the oxygen consumption rate (OCR) and extracellular acidification rate (ECAR) can be calculated. There are 4 ports surrounding the sensor probe sleeve in which different drugs can be preloaded and injected sequentially in the same experiment to study their effect on cell metabolism. For instance, the mito-stress test is used in this thesis to study different aspects of mitochondrial function. It consists of the successive delivery of 3 compounds which systematically shut down different components of the electron transport chain, allowing several measures of mitochondrial respiration, including basal respiration, ATP-linked respiration, proton leak respiration and spare respiratory capacity and provides information on how the cells respond to stress, as shown in Figure 2.3.4.2. The compound oligomycin inhibits ATP synthase, and the resulting OCR is used to derive ATP-linked respiration (by subtracting the oligomycin rate from baseline cellular OCR) and proton leak respiration (by subtracting non-mitochondrial respiration from oligomycin rate). Next, the ionophore Carbonyl cyanide 4-(trifluoromethoxy) phenylhydrazone (FCCP) disrupts the mitochondrial membrane potential as it collapses the inner membrane gradient, driving the electron transfer chain (ETC) function to its maximal rate, and maximal respiratory capacity is derived by subtracting non-mitochondrial respiration from the FCCP OCR. Finally, Rotenone/Antimycin A inhibits complex I action and complex III action, thereby effectively arresting all mitochondrial respiration, revealing non-mitochondrial respiration. Hence, basal respiration is derived by subtraction of non-mitochondrial respiration from baseline cellular oxygen consumption. With each additional compound, the cell must increase its reliance on glycolysis to meet ATP demand and sustain life.

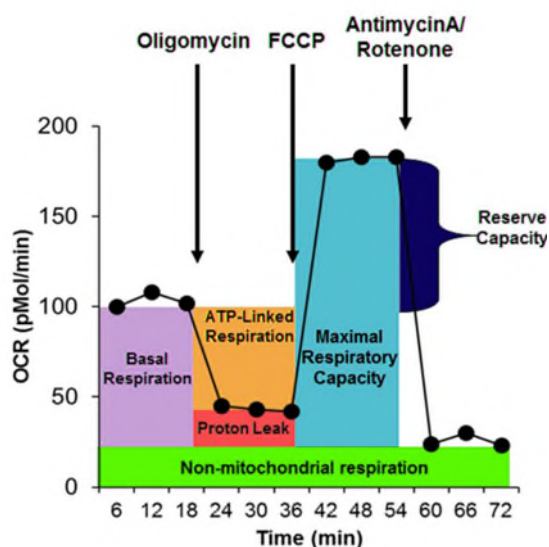


Figure 2.3.4.2 Mitochondrial Functions Determination by the Seahorse XF Cell Mito-Stress.

Test profile of the key parameters of mitochondrial respiration. Sequential injections of pharmacological inhibitors measure basal respiration, ATP production (after oligomycin injection), proton leak (after oligomycin injection), maximal respiration (after FCCP injection), Reserve capacity or spare respiratory capacity (after FCCP injection), and non-mitochondrial respiration (after Antimycin A/Rotenone injection). Figure from (<https://doi.org/10.1371/journal.pone.0177951.g001>)

Respiration rate was measured using a Seahorse XF24 Extracellular Flux Analyzer (Seahorse Bioscience). Immortalised mouse brown pre-adipocytes imBAT were seeded onto gelatine-coated 24-well V28 PS Culture Microplates (#100882-004, Agilent Technologies Ltd UK Ltd) at a density of 5,000 cells/well, grown and differentiated using the standard protocol outlined above, and treated throughout differentiation with or without LPS (100 ng/mL, E. Coli O55:B5, Sigma, #L6529), with or without TUG-891 (10 μ M, Tocris, #4601). Each experimental group consisted of at least 5 replicates, with the experiment repeated on at least 2 separate occasions. The assay was conducted in sterile, unbuffered Assay Media prepared with Seahorse base media (Seahorse Bioscience, #102365-100) at 37 °C (pH 7.4), and supplemented with Sodium Pyruvate (1 mM, Sigma, # S8636), Glucose (10 mM, Sigma, #G8769). Mature adipocytes were washed twice in this supplemented seahorse media to fully remove the maintenance media, and were then incubated for 40 minutes at 37 °C with no CO₂.

After a calibration step (30 minutes) and an equilibration step (30 minutes), the assay protocol consisted of 3 cycles of the following, previously optimized, steps: mix (5 minutes), wait (2 minutes), measure (2 minutes), which were completed before and after each injection of Oligomycin (Sigma, #O4876), FCCP (Sigma, #C2920-10MG), Antimycin A (Sigma, #A8674-25MG) and Rotenone (Sigma, #R8875-1G). Stocks of

these chemicals were prepared in Dimethyl Sulfoxide (DMSO) (Sigma, D1435-500 mL) and aliquoted and frozen at -20 °C. Freeze-thaw cycles were avoided at all times. Dilutions were prepared in the assay media and loaded into a sensor cartridge (#100850-001, Agilent Technologies Ltd UK Ltd) that is placed on top of the cell 24-well V28 PS Culture Microplates. The cartridge, pre-incubated overnight or for at least 2 hours with the calibrant solution (#100850-001, Agilent Technologies Ltd Uk Ltd) at 37 °C without CO₂ was inserted first in the instrument to allow calibration of the probes.

Reagents were injected at the appropriate volume of a ten-fold concentrated stock solution to give the following previously optimized and determined final in-well concentrations. For imBAT cells these were 1 µM Oligomycin, 0.5 µM FCCP, 0.5 µM Rotenone/Antimycin A. For primary brown adipocytes, these were 2.5 µM Oligomycin, 1 µM FCCP, 2 µM Rotenone/Antimycin A.

Prior to experiments, reagent concentrations, seeding density and the assay protocol time were optimised as per the manufacturer's recommendations.

Oxygen consumption rate (OCR) values were collected from the machine. The respiration parameters of 3 individual OCR measurements were collected. Parameters were calculated as per the following equations:

Basal Respiration = (Last rate measurement before first injection) – (Non-Mitochondrial Respiration Rate)

Proton Leak = (Minimum rate measurement after Oligomycin injection) – (Non-Mitochondrial Respiration)

Spare Respiratory Capacity = (Maximal Respiration) – (Basal Respiration)

ATP Production = (Last rate measurement before Oligomycin injection) – (Minimum rate measurement after Oligomycin injection)

Coupling Efficiency = (ATP Production Rate) / (Basal Respiration Rate) × 100

For OCR response to injection of each compound, data was normalised to the protein content (Bradford assay) or cell number of each well to account for well-to-well variability in cell number.

2.3.5 2-Deoxyglucose Uptake

Glucose uptake in differentiated imBAT adipocytes was evaluated via cellular incorporation of [³H]-2-deoxyglucose. Following differentiation and treatment on 6-

well plates, 48 hours prior to the assay, cells were incubated in serum-free low glucose media (#22320022, Gibco, Fisher Scientific) supplemented with 2 % BSA (#A9418-100G, Sigma-Aldrich, UK).

On the day of assay (day 10 of differentiation), imBAT cells were washed 3 times with warmed PBS and allowed to equilibrate in low glucose KHB buffer (containing 0.01 % BSA, 5 mmol/L glucose (#G7021, Sigma-Aldrich, UK) and 10 mM HEPES (#15630049, Fisher Scientific, UK), pH 7.4) at 37 °C for 3 hours. Adipocytes were then incubated a further 30 minutes with KRH buffer without glucose or BSA (10 mM HEPES, pH 7.4) at 37 °C in the absence (basal control) or presence of 100 µM insulin (#I9278, Sigma-Aldrich, UK) during the last 15 minutes. Immediately after, media was discarded and 1 mL of labelling mixture (consists of 1 µCi/mL of [³H]-2-deoxyglucose (PerkinElmer, NET328A001MC) and 100 nM cold 2-deoxyglucose (#D8375-1G, Sigma-Aldrich, UK) in ×1 KRH buffer, at 37 °C) was added for a further 20 minutes. To terminate the assay, cells were then washed 3 times with ice-cold PBS, lysed and harvested in 400 µL RIPA buffer with a cell scraper. Radioactivity was evaluated via scintillation counting of the lysates, 300 µL cell lysate was transferred to 4 mL of scintillation fluid (Beta-Plate Scint, PerkinElmer) and radioactivity (becquerels, Bq) was counted using a scintillation counter. Results in counts per minute (CPM) were normalised to total protein content (the remaining 100 µL cell lysate was used to quantify protein) and glucose uptake calculated in cpm/mg protein relative to the basal control.

Preparation of 5x KHB (1l)

The following reagents were added separately (each one allowed to dissolve before adding the next one) in listed order to 900 mL distilled and autoclaved water (dH₂O) in a 1 litre beaker containing a sterile magnet stir bar. The final volume was adjusted to 1000 mL with dH₂O and stored at 4 °C for later use.

Chemical	5X (mM)	5X (g/l)
NaCl	555	32.532
KCl	23.5	1.752
MgSO ₄	10	1.204
Na ₂ HPO ₄	6	0.852

2.4 Enzyme-linked Immunosorbent Assay (ELISA)

2.4.1 C-X-C Motif Chemokine Ligand 5 (CXCL5/ LIX) and B-Cell Activating Factor (BAFF/ BLyS/ TNFSF13B)

The quantitative sandwich enzyme immunoassay technique was used to perform this assay on culture supernatant (conditioned media). A monoclonal antibody specific for analyte including mouse BAFF (#MBLYS0, R&Dsystems, USA) or LIX (#MX000, R&Dsystems, USA) was pre-coated onto a microplate. Standards and samples were pipetted into the wells and any analyte present was bound by the immobilized antibody. After washing away any unbound substances, an enzyme-linked polyclonal antibody specific for the analyte was added to the wells. Following a wash to remove any unbound antibody-enzyme reagent, a substrate solution was added to the wells and colour developed in proportion to the amount of analyte bound in the initial step. The colour development was stopped and the intensity of the colour measured.

Cell culture supernatant was retrieved and centrifuged at 3000 RPM for 10 minutes at 4 °C to remove debris and assayed immediately or stored at - 80 °C until use. Six standard dilutions were prepared according to manufacturer's instruction. Cell culture supernatant samples were diluted 1/10 for LIX measurements while no dilutions were required for BAFF. Standards and supernatant samples (40 µL/well each for BAFF, 50 µL/well each for LIX) were loaded into the wells in duplicate and incubated at room temperature on a plate shaker for 2 hours at 500 rpm. Plates were washed 4 times with 400 µL Washing Buffer. 100 µL for LIX or 120 µL for BAFF of analyte conjugate was added to each well and incubated at room temperature on a plate shaker for 2 hours. Afterwards, wells were washed with 400 µL Washing Buffer and 200 µL for LIX or 120 µL for BAFF of Substrate Solution was added to each well. Plates were incubated at room temperature for 10 minutes and 100 µL Stop Solution for LIX or 120 µL for BAFF were applied to stop the reaction. A plate reader (PheraStar FS microplate reader (BMG Labtech)) was used at 450 nm with correction at 570 nm for determining the optical density. A standard curve based on the standard dilutions optical density was generated. The concentrations of analyte in the samples were calculated using the standard curve. This assay has a detection range from 1.8-7.8 pg/mL for BAFF and 15.6 - 1,000 pg/mL for LIX.

2.4.2 Matrix Metalloprotease (MMP3)

MMP3 was measured using Abcam's MMP3 SimpleStep ELISA® kit (# ab203363) which is designed for the quantitative measurement of MMP3 in cell culture supernatant.

This assay employs an affinity tag labelled capture antibody and a reporter conjugated detector antibody which immunocapture the sample analyte in solution. This entire complex (capture antibody/analyte/detector antibody) is in turn immobilized via immunoaffinity of an anti-tag antibody coating the well.

To perform the assay, cell culture supernatant was collected and centrifuged at 3000 RPM for 10 minutes at 4 °C to remove debris and assayed immediately or stored at - 80 °C until use. Eight standard dilutions were prepared according to the manufacturer's instruction. Samples were diluted 1:10. Samples or standards were added to the wells (50 µL/well), followed by the antibody cocktail (50 µL/well). After incubation for 1 hour on a plate shaker at 400 rpm, the wells were washed with 350 µL washing buffer to remove unbound material. TMB substrate was then added (100 µL) and during incubation was catalysed by HRP, generating blue colouration. This reaction was then stopped by the addition of Stop Solution (100 µL) completing any colour change from blue to yellow. Signal was generated proportionally to the amount of bound MMP3 and the intensity was measured at 450 nm using a plate reader (PheraStar FS microplate reader (BMG Labtech)). This assay has a detection range of 18.8 pg/mL - 1200 pg/mL.

2.4.3 C-X-C Motif Chemokine Ligand 16 (CXCL16)

CXCL16 in cell culture supernatant was measured using the DuoSet ELISA Development kit. To perform the assay, cell culture supernatant was collected and centrifuged at 3000 RPM for 10 minutes at 4 °C to remove debris and assayed immediately or stored at - 80 °C until use. DuoSetAncillary Reagent Kit 2 (# DY008, R&D Systems) was used as complementary kit to perform the assay. Firstly, plates were coated with diluted capture antibody (100 µL per well) to the working concentration (2 µg/mL) in PBS without carrier protein and incubated overnight at room temperature. Wells were then washed three times with Wash Buffer (400 µL). After the last wash, plates were blocked by adding 300 µL of Reagent Diluent to each well and incubated at room temperature for 1 hour. Wells were washed again and

plates were ready for sample addition. Samples were diluted 1:3 and seven standard dilutions were prepared according to manufacturer's instruction. 100 μ L of sample or standards in Reagent Diluent per well were added to each well, covered with an adhesive strip and incubated for 2 hours at room temperature. After washing each well three times with Wash Buffer (400 μ L), the Detection Antibody (100 μ L), diluted in Reagent Diluent (12.5 ng/mL), was added to each well and covered with a new adhesive strip and incubated for further 2 hours at room temperature. Washing was performed again prior to addition of Streptavidin-HRP (100 μ L) to each well and incubated for 20 minutes at room temperature in the absence of direct light. The final wash was performed before incubating 100 μ L of Substrate Solution in each well for 20 minutes at room temperature without direct light. 50 μ L of Stop Solution was added to each well and thoroughly mixed. Using a plate reader (PheraStar FS microplate reader (BMG Labtech)) at 450 nm and at 570 nm for corrections, the optical density of each well was determined immediately. This assay has a detection range of 15.6 – 1000 pg/mL.

2.4.4 Calculation of ELISA Results

The duplicate readings for each standard, control (if used), and sample were averaged and the average zero standard optical density subtracted. A standard curve was created by reducing the data using graphpad prism or ELISA analysis website (<https://elisaanalysis.com/app>) to generate a four parameter logistic (4-PL) curve-fit to produce the most precise fit possible of the data. When samples were diluted, the concentrations read from the standard curve were multiplied by the dilution factor for each analyte.

2.5 Oil Red-O Staining

Following the growth and differentiation of adipocytes, as described above, Oil Red-O (ORO) stock solution was prepared by dissolving 0.5 g of ORO powder (#O0625, Sigma-Aldrich, UK) in 200 mL absolute isopropanol in a 56 °C water bath for 1 hour, and left stirred overnight. A working ORO solution was then prepared by diluting ORO stock with 6:4 ratio in distilled water to make a 60 % solution, which was then stirred well for 10 minutes and left to stand for a further 10 minutes before being filtered through a 0.22 μ m filter.

Media were removed from each well, and cells were washed twice with PBS before being fixed with 4 % paraformaldehyde for 15 minutes at room temperature. Paraformaldehyde solution (4 %) in PBS (#sc-281692, Insight Biotechnology Ltd, UK) was removed and cells were washed twice with PBS for 5 minutes at room temperature, before being stained with working ORO solution and incubated at room temperature for 40 minutes. The ORO solution was discarded and cells were quickly washed with 60 % isopropanol in distilled water. Finally, cells were further washed with PBS until the excess dye had gone. Cells were then viewed under a light microscope to assess lipid accumulation in lipid droplets, and digital photographs were taken.

2.6 Immunohistochemistry (IHC)

For IHC preparation, spheroids were washed with PBS and immediately placed into 4 % paraformaldehyde for fixation. Spheroids were processed overnight using a routine processing cycle on a Thermo scientific Excelsior tissue processor prior to embedding. Spheroids were sectioned at 4 μ m, using a Leica RM2235 rotary microtome and Wax ribbons were transferred onto a warm water bath (43-45 °C) and spread on the microscope glass slide before drying for at least one hour at 45 °C. Haematoxylin and Eosin staining was performed in addition to UCP1 staining.

2.6.1 Haematoxylin and Eosin (H&E) Stain

Haematoxylin and eosin staining of brown spheroids to assess morphology was performed by Dr. Sean James (Arden Tissue Bank, University Hospital Coventry & Warwick). Images were taken using a light microscope connected to a digital camera (Nikon Microscope Camera Control Unit, DS-L3). To perform the haematoxylin stain, the slides were deparaffinised by bathing three times in Xylene, three times in isopropyl alcohol (sequentially: 100 %, 95 % and 80 %) for 3 minutes each and rinsed in deionized water for 5 minutes. Hereafter, the slides were stained with Mayers Haematoxylin for 3 to 10 minutes. The staining was blued by immersion of the sections by rinsing in tap water for 2-3 minutes. Staining was differentiated by repeated brief immersion of the slides up to 12 times in 0.5 % acid alcohol solution, followed by two rinses in tap water and one in deionized water, for 2 minutes each time. The slides were then stained with eosin for 30 seconds and immersed 3 times in 95 % isopropyl alcohol, 3 times in 100 % isopropyl alcohol for 5 minutes each time,

and 3 times in Xylene for 15 minutes. Spheroid sections were then cover-slipped using Permount, which was allowed to dry overnight under fume hood prior to imaging.

2.6.2 UCP1-Staining

UCP1 staining was performed by Dr. Sean James at UHCW. Briefly, the spheroid sections on the prepared slides, described above, were deparaffinised and re-hydrated via the following process. The sections were placed in a rack and washed in Xylene three times for 5 minutes, then in 100 % isopropanol for 2 minutes, followed by 70 % isopropanol for 2 minutes. Sections were rinsed for at least 2 minutes in running distilled water. Heat-induced antigen retrieval was carried out via a Pickcell Antigen retrieval unit, in which sections were immersed in sodium citrate pH 6 buffer solution for 2 hours at 90 °C. Sections were placed on a moisture chamber and rinsed with TBS-T. Novolink Polymer Detection System (#RE7140CE, Leica microsystems Ltd., UK) was employed to achieve immunohistochemically staining of the UCP1 epitope, as per the manufacturer's protocol, summarised thus: Two drops (100 µL) of peroxidase were placed onto the tissue sections to ensure coverage of the sample, for 5 minutes. Sections were then flooded with TBS-T twice for 5 minutes, before being incubated with 2 drops of Protein Block for 20 minutes to inhibit non-specific staining. Sections were washed twice with TBS-T for 5 minutes. UCP1 anti-rabbit antibody (#ab10983, Abcam, UK) was diluted (1:500 or 1:1000 vol/vol) in TBS-T for optimization of the staining. This was determined to be optimized at 1:1000. Thus, 200 µL of diluted primary antibody was placed on the slides. Sections were incubated for 2 hours at room temperature. Excess primary antibody was removed by a thorough rinse with TBS, twice, for 5 minutes. Sections were then incubated with 2 drops of post-primary block for 30 minutes, prior to being washed with TBS-T for 5 minutes each wash. Sections were then incubated with 2 drops of Polymer solution for 30 minutes. After this, sections were washed again twice with TBS-T for 5 minutes per wash. Diaminobenzidine (DAB) working solution was made by adding 50 µL of chromagen to 1 mL of Novolink DAB substrate. Approximately 2-3 drops of DAB working solution were added to the slides for 7 minutes. Sections were rinsed thoroughly in deionised water for 5 minutes, and lightly counterstained by immersion in Haematoxylin for 5 minutes, to highlight UCP1-staining. Haematoxylin staining was developed and blued in running water for 5 minutes. Sections were dehydrated

via graded isopropyl alcohol (70 %, 80 % and 3x 100 % IPA), and cleared in Xylene and mounted with coverslips. Finally, images were produced on a 3D Histech Panoramic Midi digital slide scanner; all sections were scanned using a 3D Histech Panoramic Midi digital slide scanner to produce high resolution digital scans of the tissue; these scans were performed at x40 optical resolution. Staining was not observed when the UCP1 primary antibody was omitted.

2.7 Determination of Mitochondrial Membrane Potential Through Confocal Microscopy

ImBAT cells were seeded on to gelatine-coated 35 mm glass bottom culture dishes (MatTek corporation), grown and differentiated with/without LPS (100 ng/mL), as described above. Differentiated imBAT adipocytes were incubated for 30 minutes at 37 °C with Mito-Tracker Green FM (125 nM; Thermo Fisher, #M7514 Invitrogen™) and MitoTracker Red CMXRos (250 nM; Thermo Fisher, #M7512 Invitrogen) in phenol-free media (DMEM/F-12, #11039047 Gibco) without FBS. The cells were washed three times with media and imaged in HEPES-buffered media (pH 7.35) using a spinning disk confocal microscope (PerkinElmer, UltraVIEW VoX) with x40 oil objective (Nikon, 1.30, Plan Fluor) and a 488 nm, 561 nm excitation filter. The Z system, attached to an inverted fluorescence microscope fitted with x2 Hamamatsu Orca-R2 interline CCD, was used to observe cells which were maintained at 37 °C throughout the imaging process. Live cell imaging was performed for 10 minutes to monitor mitochondrial morphology. Control cells were monitored to correct for potential photobleaching, and corrected total cell fluorescence (CTCF, integrated density - (area of selected cell × mean fluorescence of background)) of around 50 cells per condition was quantified using ImageJ.

2.8 Statistical Analysis

Statistical analyses were undertaken using SPSS or Graphpad prism. The latter being used to plot graphs. Data were reported as mean ± standard error of the mean (SEM), unless otherwise specified. Comparisons between samples were performed via two-tailed t-tests, one-way ANOVA or two-way ANOVA, followed by Tukey's multiple correction test. The specific test selected depended on the design of the experiment, the number of samples (two or more than two) involved and the assumption that the data came or did not

come from a normal distribution. $p < 0.05$ was considered to be statistically significant, with significance levels being indicated as follows: * $p < 0.05$, ** $p < 0.01$, *** $p < 0.001$, unless otherwise specified. The test used in each experiment is detailed in each figure legend. Peter Kimani, a statistician at Warwick Medical School was consulted in regards to what the appropriate tests were to perform.

Chapter 3. Lipopolysaccharide Mediates Biological Alteration in Brown Adipocytes

3.1 Introduction

Chronic inflammation in WAT at both local and systemic levels is now well recognized to be associated with obesity and its comorbidities (318,430). It is characterized by high levels of expression and secretion of pro-inflammatory cytokines/chemokines along with infiltration of immune cells, including macrophages, and is thought to contribute to obesity-associated comorbidities, such as insulin resistance and diabetes (14,15,81,540).

The underlying mechanisms of WAT inflammation in obesity have been the focus of intense research (311,430,541). Comparatively, little is known about the underlying mechanisms of BAT inflammation in the context of obesity and its contribution to brown adipocyte dysfunction and associated disorders. However, there is increasing evidence that inflammation directly alters the thermogenic activity of brown fat by impairing its capacity for energy expenditure and glucose uptake (323,336,542). Activation of pattern recognition receptors (PRRs) has not been comprehensively studied in BAT, while in WAT/adipocytes is shown to mediate white adipose inflammation (432).

PRRs are part of the innate immune system and function to detect invading pathogens and subsequently initiate a signalling cascade of distinctive inflammatory and immune responses in the host cells (466,543). PRRs can recognise dysregulations of the immune system and equally metabolism. The homeostasis of both systems is essential for survival (432,544). A role of PRR activators in this immune-metabolism relationship has been identified in several organs and cell types including WAT (545–548), liver, muscle (547,548), and pancreatic β -cells (548). Activators of PRRs include excess of (a) nutrients such as saturated fatty acids (344,549), or (b) endogenous molecules produced from metabolic stress and tissue injuries, for instance: ceramides (550), and high mobility group box 1 (551), or alteration of intestinal microbiota (454,552). Excess of these PRRs ligands occurs in obesity through multiple means leading to PRR activation.

One major family of PRRs is Toll-like receptors (TLR). TLRs are transmembrane receptors composed of extracellular leucine-rich repeat motifs and a cytoplasmic Toll/interleukin-1 receptor (TIR) homology domain (435). Ten and twelve functional TLRs

have been identified in humans and mice, respectively. The particular bacterial or viral pathogen-associated molecular patterns (PAMP) that individual TLRs detect have been characterized. Each TLR recognizes a different ligand. For example, TLR2 and TLR4 recognize lipoprotein and lipopolysaccharide (LPS), respectively (435,543). Various TLRs, including TLR4, have been detected in white and brown adipocytes (344,426,545,553). TLR2 and TLR4 expression levels are upregulated with increased BMI in obesity and type 2 diabetes mellitus (T2DM) in humans (554). Activation of TLRs, specifically TLR4 and TLR2, is involved in metabolic functions and the inflammatory response in obesity. It induces a pro-inflammatory status, resulting in white adipocyte dysfunction and disturbed homeostasis of whole body metabolism (436,545,546,548,553).

Activation and subsequent upregulation of TLR4 generates innate immune responses by inducing signalling cascades of kinases and several transcription factor activations. These cascades lead to enhanced inflammation with secretion of pro-inflammatory cytokines including IL6, MCP1 and TNF α , and phosphorylation of p65 and NF κ B (19,436,553,555,556). Deletion of TLR4 leads to beneficial metabolic effects *in vitro* with reduced inflammatory response and improved insulin sensitivity in 3T3-L1 adipocytes, and *in vivo* with observations of lower body weight, subcutaneous and visceral WAT compared to wild type mice (436,555,556).

Gut-derived LPS is a potent agonist of TLR4. It is an abundant glycolipid of the outer membrane of gram-negative bacteria and is composed of oligosaccharides and acylated-saturated fatty acids (426). Obesity influences circulating levels of LPS by altering gut microbiota growth and composition as well as gut permeability (347,557–559). Consequently, LPS is absorbed alongside dietary lipids and its levels are elevated in obesity, resulting in a low-grade chronic inflammation and insulin resistance (446,555). Little is known about the effects of LPS on brown adipocytes. However, Bae *et al.* have reported that activation of pattern recognition receptors in brown adipocytes induces inflammation through NF κ B and MAPK signalling pathways, and suppresses basal and isoproterenol-induced UCP1 expression and mitochondrial respiration (344). This will ultimately impact thermogenesis capacity, leading to metabolic dysfunction. However, this report did not completely address the

role of TLR4, the LPS receptor, in UCP1 down regulation. Also, the response to LPS in other brown adipocyte models has not been explored.

Research in this area is essential to uncover novel targets in BAT for obesity treatment and prevention. Therefore, the aim of this study was to determine the direct *in vitro* effect of LPS in brown adipocytes on the following:

- Insulin sensitivity
- TLR4-dependent inflammation
- The main biological brown characteristics, thermogenesis
- Lipid metabolism

3.2 Methods

Murine brown pre-adipocytes (imBAT cells/primary cultures/spheroids) and TLR4 knockout brown pre-adipocyte (TLR4ko.BAT) cells were differentiated into mature adipocytes over 8 days with or without LPS 100 ng/mL or 1000 ng/mL (100 ng/mL if not indicated), according to the differentiation protocol described in the methods section (Chapter 2). Hereafter, RNA and protein were harvested for qRT-PCR and Western blotting. Also, the cells were harvested to assess triglyceride levels inside the cells. Cells were analysed for glucose uptake or studied with a Seahorse XF Analyser to determine impact on mitochondrial function. Immunofluorescence cell imaging using a spinning disk confocal microscope was conducted to assess Glut4 and lipid droplets.

3.2.1 Glycerol Assay

imBAT cells were grown and differentiated until day 10 in phenol-red free DMEM/F12 (#11039-021, Gibco, The UK) with/without LPS. Cells were washed once with PBS and incubated in phenol red free DMEM/F12 without any supplementation overnight prior to treatment. Cells were washed once prior to adding media supplemented with/without CL316,243, a β 3-adrenoreceptor (β 3-AR) agonist, with/without LPS. Conditioned media were collected at 2, 4, 8, 10 and 12 hours and were assayed immediately.

Prior to the assay Free Glycerol Reagent (#F6428, Sigma, UK) was reconstituted in 40 mL of ultrapure distilled water and pre-warmed to 37 °C. A dilution series of glycerol (#G7793, sigma, UK) was prepared ranging from concentration of 4 μ g/dL to 260 μ g/dL. 100 μ L of standards or conditioned media (samples) were pipetted in duplicate into wells of a transparent 96-well plate. 150 μ L of diluted Free Glycerol Reagent was added into each well. The plate was then covered and incubated at 37 °C for 15 minutes. Finally, the absorbance was measured using PheraStar FS microplate reader (BMG Labtech); at wavelength of 540 nm. The concentration for each sample was then calculated based on interpolation of a standard curve of known glycerol concentrations.

3.2.2 Triglyceride Assay

Total cellular triglyceride levels in imBAT cells were determined with the triglyceride colorimetric assay kit (#10010303, Cayman Chemical, UK) according to the manufacturer's instructions. Briefly, ($\approx 18 \times 10^6$) cells were washed in BPS and scraped using a rubber policeman, centrifuged ($1000 \times g$ at 4°C) and resuspended in 1 mL of cold diluted standard diluent. Samples were then sonicated ($20 \times$ at one second bursts) and centrifuged at $10000 \times g$ for 10 minutes at 4°C . Supernatants were kept in ice and assayed immediately. Standard dilutions were prepared in diluted standard diluent ranging from 3.123 mg/dL to 200 mg/dL. Each sample or standard ($10 \mu\text{L}$) was added to the designated wells on a transparent 96-well plate. Diluted enzyme mixture solution ($150 \mu\text{L}$) was added to each well. The plate was then covered, placed on a shaker for five minutes to mix and incubated for 10 minutes at room temperature. Finally, the absorbance was measured using PheraStar FS microplate reader (BMG Labtech); at a wavelength of 540 nm. The concentration for each sample was then calculated based on interpolation of a standard curve of known triglyceride concentrations.

3.2.3 Nile Red Staining of Lipid Droplets and Fluorescence Microscopy

Brown adipocytes were plated on glass coverslips and differentiated as described in the methods section (Chapter 2). Cells were fixed with 4 % paraformaldehyde for 30 minutes, and lipid droplets were visualized after Nile Red staining ($1 \mu\text{g/mL}$) (#N3013, Sigma-Aldrich, UK) by spinning disk confocal microscopy (PerkinElmer, UltraVIEW VoX) with 100x oil objective (Nikon, 1.30, Plan Fluor) and a 488 nm, 405 nm excitation filter.

Briefly, fixed cells were washed with PBS before Nile Red staining solution diluted in PBS to $1 \mu\text{g/mL}$ (stock concentration: 1 mg/mL in methanol) was added to the cells (0.5 mL of staining solution per coverslip). The cells were then incubated for 15 minutes at room temperature and protected from light by covering the culture plate with foil. The staining solution was aspirated from the cells and washed three times with PBS (0.5 mL of PBS per coverslip was added and incubated for 5 minutes at room temperature with protection from light). Finally, to mount the cover slips, they were lifted out of the well and placed cell side down on a slide with a drop of mounting medium which was left to set overnight in the dark (Invitrogen™ ProLong™ Gold

Antifade Mountant with DAPI, #P36935, Fisher Scientific). (7.5 μ L of mounting medium was placed on a slide and the edge of the coverslip was touched with a tissue to remove excess PBS). The edges of the coverslip were sealed with clear nail varnish. Quantification of lipid droplet-containing cells in control and LPS-treated cells was performed in 20 cells per group using ImageJ (FIJI, (version 1.52i)). The lipid droplet parameters assessed were LD area (μ m²) and number as they were measured directly by the area measure function of ImageJ. Then, lipid content was calculated by dividing average lipid droplets area in each cell against total cell area.

3.3 Results

3.3.1 Characterization of a Mouse TLR4-knockout Brown Adipocyte (TLR4ko.BAT) Cell Line

This study examined the key LPS-TLR4 pathway in brown adipocytes biology. To investigate the specificity of TLR4 signalling in responses to LPS, experiments were performed in both wild type and TLR4 knockout brown adipocytes (TLR4ko.BAT). This required initial characterisation and validation of the TLR4ko.BAT. To investigate whether the absence of TLR4 affects adipocyte differentiation capacity, TLR4ko.BAT cells were stimulated to differentiate *in vitro*. TLR4ko.BAT cells differentiated and assumed the classical morphology of mature adipocytes (Figure 3.3.1.1).

TLR4^{ko}BAT

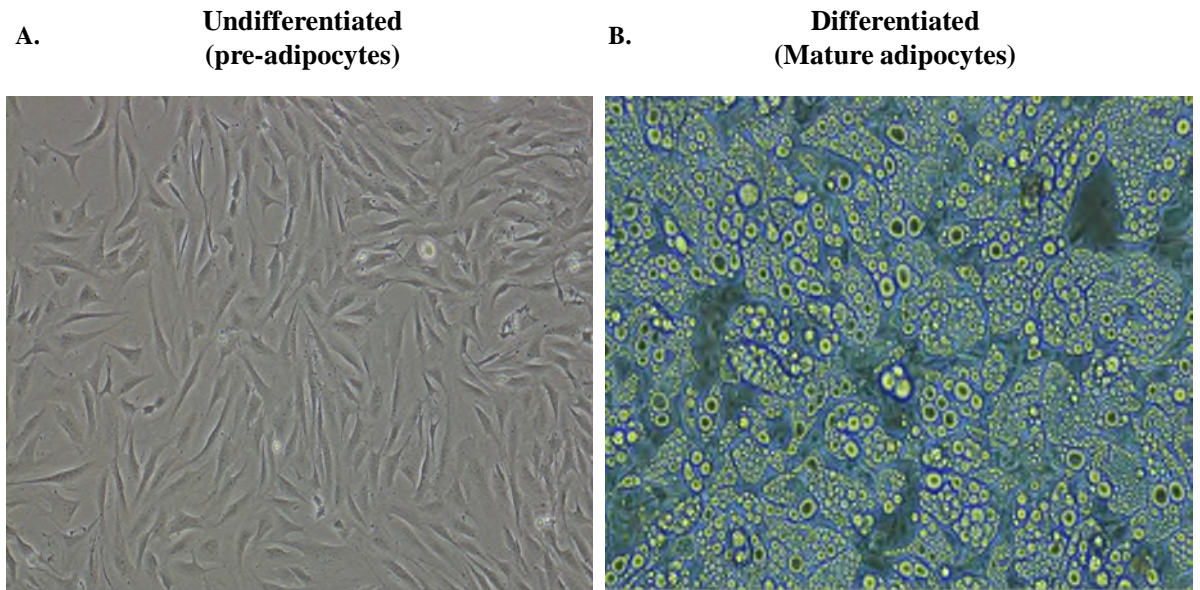


Figure 3.3.1.1 TLR4 Knockout Brown Adipocyte Cell Line Differentiation.

(A) Pre-adipocytes of mouse TLR4 ko BAT were differentiated into (B) mature TLR4 ko brown adipocytes. Photos are taken with a 20x magnification.

In addition, expression of the mature adipocyte marker fatty acid binding protein 4 (aP2) (Figure 3.3.1.2, A) was highly induced upon differentiation in all the investigated cells. Similarly, the brown AT markers uncoupling protein 1 (UCP1) and cell death inducing DFFA like effector a (CIDEA) were highly induced upon differentiation of the brown adipocytes (Figure 3.3.1.2, C, D).

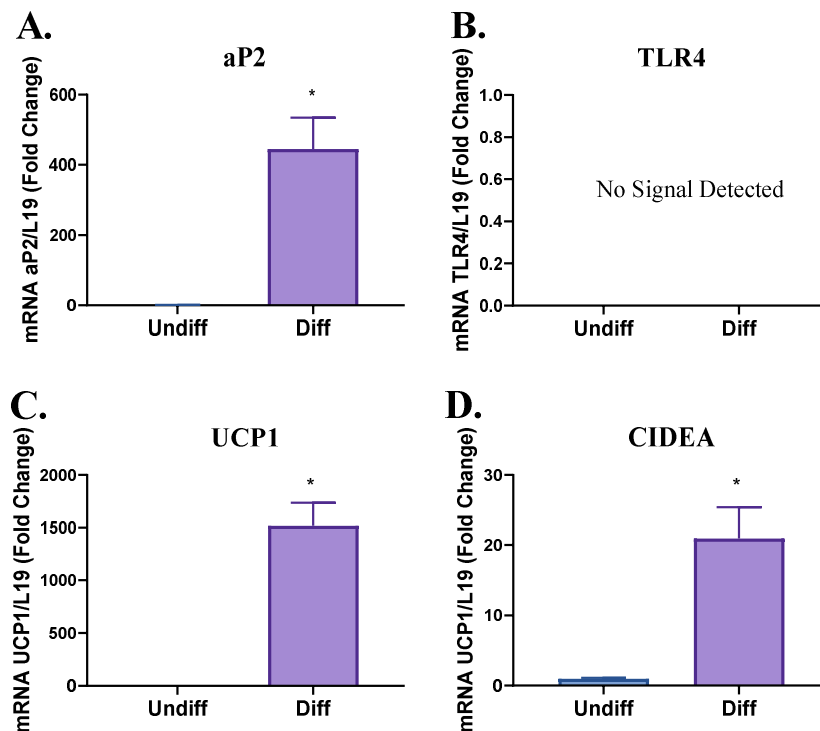


Figure 3.3.1.2 Expression of Adipocyte-Associated Genes in TLR4 Knockout Brown Adipocyte Cell Line.

TLR4 koBAT cells were grown and differentiated. The expression of (A) aP2, (B) TLR4, (C) UCP1, and (D) CIDEA, in Pre-adipocytes (Undiff) was analysed by q-RT PCR and compared with mature adipocytes (Diff). Data are presented as mean fold change \pm standard error of mean. Unpaired t test was used for comparisons. * $P \leq 0.05$. aP2; fatty acid binding protein 4. UCP1; uncoupling protein 1. CIDEA; cell death inducing DFFA like effector a. TLR4: Toll-Like Receptor 4. Undif: undifferentiated. Diff: differentiated.

3.3.2 Wild Type Brown Adipocyte Differentiation in 2D and 3D Culture

Next, wild type brown adipocyte differentiation was investigated to confirm expected morphology and other markers of mature adipocytes. In this context, on the very first day, before applying induction media, imBAT cells and primary cultures showed a flatter and more compact shape (Figure 3.3.2.1, A1, B1) while Haemotoxylin and Eosin (H & E)-stained spheroids showed no lipid droplets (Figure 3.3.2.1, C1). Around day 4 lipid droplets started to develop and became larger and more numerous with the progression of differentiation.

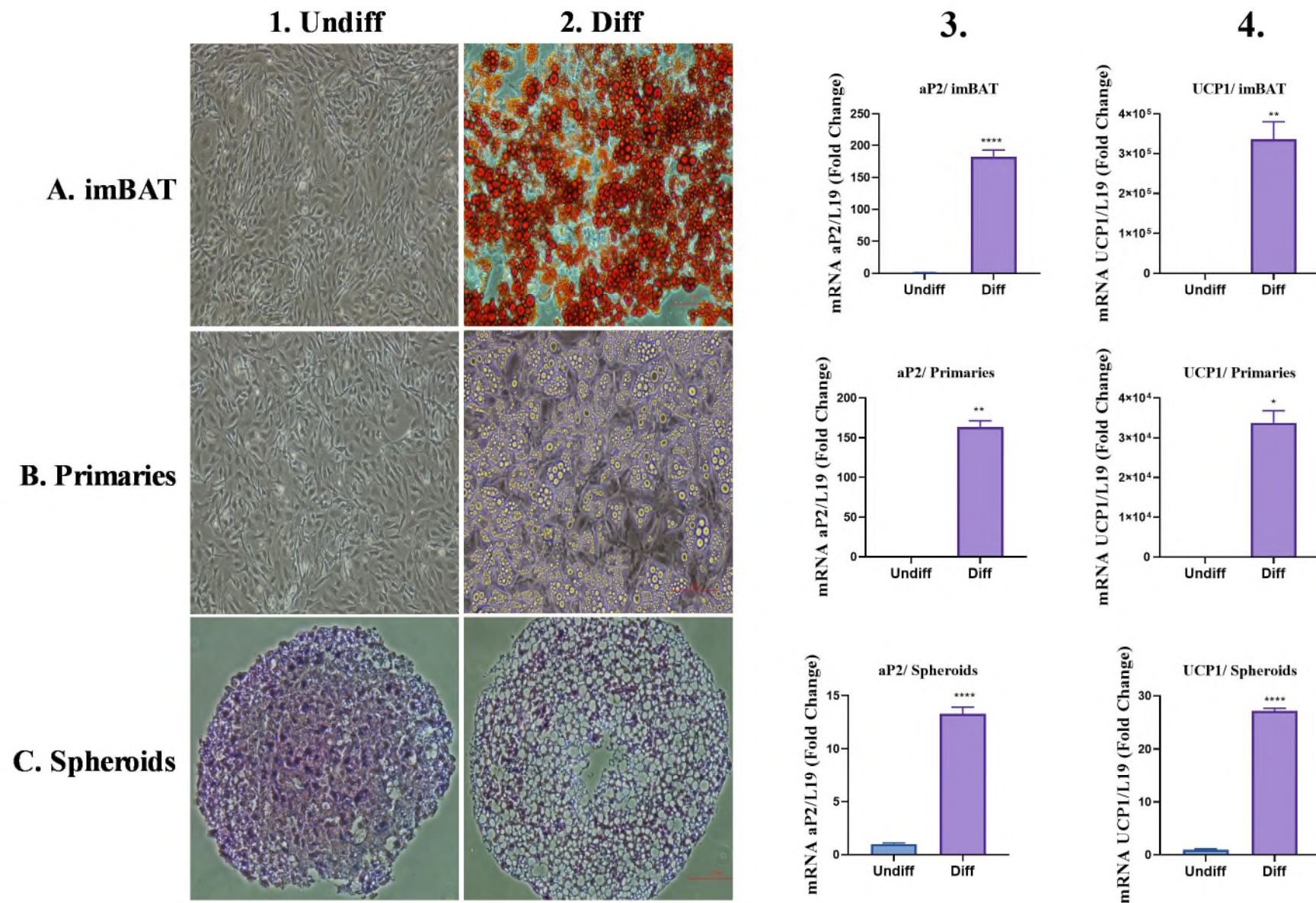
Figure 3.3.2.1, A2 below represents Oil Red O staining of imBAT cells which show successfully differentiating cells. Figure 3.3.2.1, B2 shows differentiated primary brown adipocytes. There were, however, no additional wells to perform Red O

staining. In any case, the images clearly show fully differentiated brown adipocytes. Finally, in the 3D spheroid culture model, differentiated lipid droplet-containing brown adipocytes are present in H & E stained sections Figure 3.3.2.1, C3.

Similarly, all three models showed highly induced differentiation makers of brown adipocytes including aP2 and UCP1 which confirmed that imBAT cells (Figure 3.3.2.1, A3, A4) primary cultures (Figure 3.3.2.1, B3, B4) and spheroids had efficiently differentiated (Figure 3.3.2.1, C3, C4).

Figure 3.3.2.1 Wild-Type Brown Adipocyte Differentiation.

Pictures with a 20x magnification of undifferentiated (Undiff) imBAT cells (A1), primary cultures (B1), spheroids (C1) and differentiated (Diff) imBAT cells (A2), primary cultures (B2), spheroids (C2) pictures. imBAT cells were stained with Oil Red O and pictures were taken. Spheroids were stained with H&E staining and pictures were taken. Expression of mature adipocyte-associated genes including aP2 gene expression levels in imBAT cells (A3), primary cultures (B3) and spheroids (C3), and UCP1 gene expression levels in imBAT cells (A4), primary cultures (B4) and spheroids (C4). Data are presented as mean fold change \pm standard error of mean. Unpaired t test was used for comparisons. * $P \leq 0.05$. aP2; fatty acid binding protein 4. UCP1; uncoupling protein 1.



3.3.3 LPS Administration to Brown Adipocytes Directly Induced Insulin Resistance

To test the hypothesis that LPS drives adipocyte insulin resistance in obesity and causes brown adipocyte dysfunction, the first step was to establish whether *in vitro* LPS administration could directly induce insulin resistance in brown adipocytes. Therefore, imBAT cells were treated with two different doses of LPS (100 ng/mL, 1000 ng/mL). As shown in (Figure 3.3.3.1, D), differentiating imBAT cells with both LPS doses resulted in insulin resistance, as evidenced by significant reductions in the uptake of insulin-induced radio-labelled glucose (100 nM) compared with control adipocytes (-66.03 %, $P < 0.0001$ with LPS 100 ng/mL, -66.73 %, $P < 0.0001$ with LPS 1000 ng/mL).

This functional observation of insulin resistance was accompanied by reduced phosphorylated protein expression of Serine/Threonine Kinase AKT, a key step in the insulin signalling cascade. The higher dose of LPS completely blocked insulin-stimulated AKT (Ser 473) phosphorylation. (FC=-2.63, $P < 0.05$ with LPS 100 ng/mL, Figure 3.3.3.1, E1, E2). Thus, differentiating imBAT with both LPS doses resulted in impaired insulin signalling and adipocyte glucose uptake.

In addition to the protein levels, differentiating multiple brown adipocyte cell models (imBAT cells, primary brown adipocytes, and spheroids) with LPS (100 ng/mL) reduced gene expression of GLUT4 (solute carrier family 2 (facilitated glucose transporter), member 4) (Figure 3.3.3.1, A1, B1, C1) with a maximum decrease of FC=-29.94, $P < 0.001$ with LPS 100 ng/mL in spheroids. GLUT4 is the insulin-regulated glucose transporter. In contrast, investigations of GLUT1 (Solute carrier family 2 (facilitated glucose transporter), member 1) showed that LPS treatment resulted in increased expression in spheroids and primary cultures although in imBAT cells levels were similar to the control adipocytes (Figure 3.3.3.1, A2, B2, C2). GLUT1 facilitates the basal transport of glucose across the plasma membranes of mammalian cells. The GLUT1 transporter is distributed in most tissues, whereas the GLUT4 transporter is exclusive to muscle and fat (560).

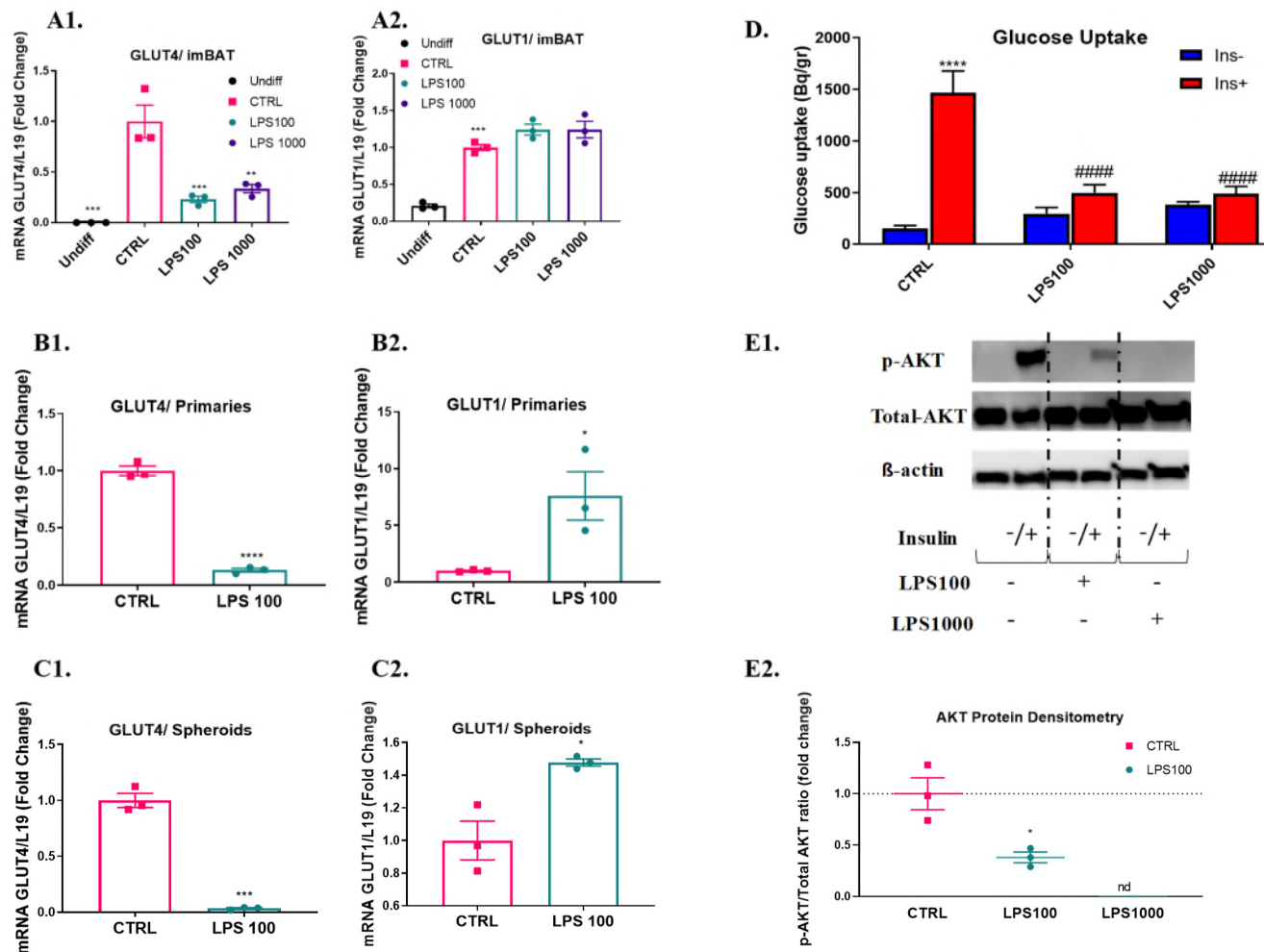


Figure 3.3.3.1 Effect of LPS on Brown Adipocyte Insulin Sensitivity.

ImBAT cells, primary cultures and spheroids were differentiated with/without LPS (100 ng/mL or 1000 ng/mL). (A1, B1, C1) GLUT4 gene expression levels in imBAT cells, primary cultures and spheroids, respectively. (A2, B2, C2) GLUT1 gene expression levels in imBAT cells, primary cultures and spheroids, respectively. (D) Glucose uptake and (E1, E2) AKT protein expression and densitometry in imBAT cells following an acute dose of insulin (100 nM). (E1) Image of AKT and loading control β -actin Western blot membranes. For protein densitometry and gene expression, results are expressed as a fold change from control cells. For glucose uptake normalised counts per minute to total protein content are shown. Bars represent mean \pm standard error of the mean. * $p < 0.05$, ** $p < 0.01$, *** $p < 0.001$, **** $p < 0.0001$ compared to CTRL. Unpaired T Test was used for comparisons. GLUT4: solute carrier family 2 (facilitated glucose transporter), member 4; AKT (Ser 473); Serine/Threonine Kinase; CTRL: control.

3.3.4 LPS Increased Inflammatory Gene Expression

The impact of LPS on inflammation was then assessed via measurement of the pro-inflammatory cytokines interleukin 6 (IL6), chemokine (C-C motif) ligand 2 (CCL2/MCP1) in wild type brown and TLR4ko.BAT adipocytes.

LPS induced IL6 mRNA by a 600-800 % increase, and MCP1 mRNA by a 400-600 % increase in LPS-treated imBAT cells relative to control (Figure 3.3.4.1, A, B). This was indeed also the case in primaries and spheroids, with LPS treatment resulting in induction of mRNA of IL6 (1000 % and 21,400 % respectively, Figure 3.3.4.2, A, C) and MCP1 (8,600 % and 5,900 % respectively, Figure 3.3.4.2, B, D).

As expected, LPS did not induce IL6 or MCP1 when differentiated TLR4ko.BAT cells were treated with LPS throughout differentiation supporting that TLR4 mediates the inflammatory actions of LPS in brown adipocytes (Figure 3.3.4.1, C, D).

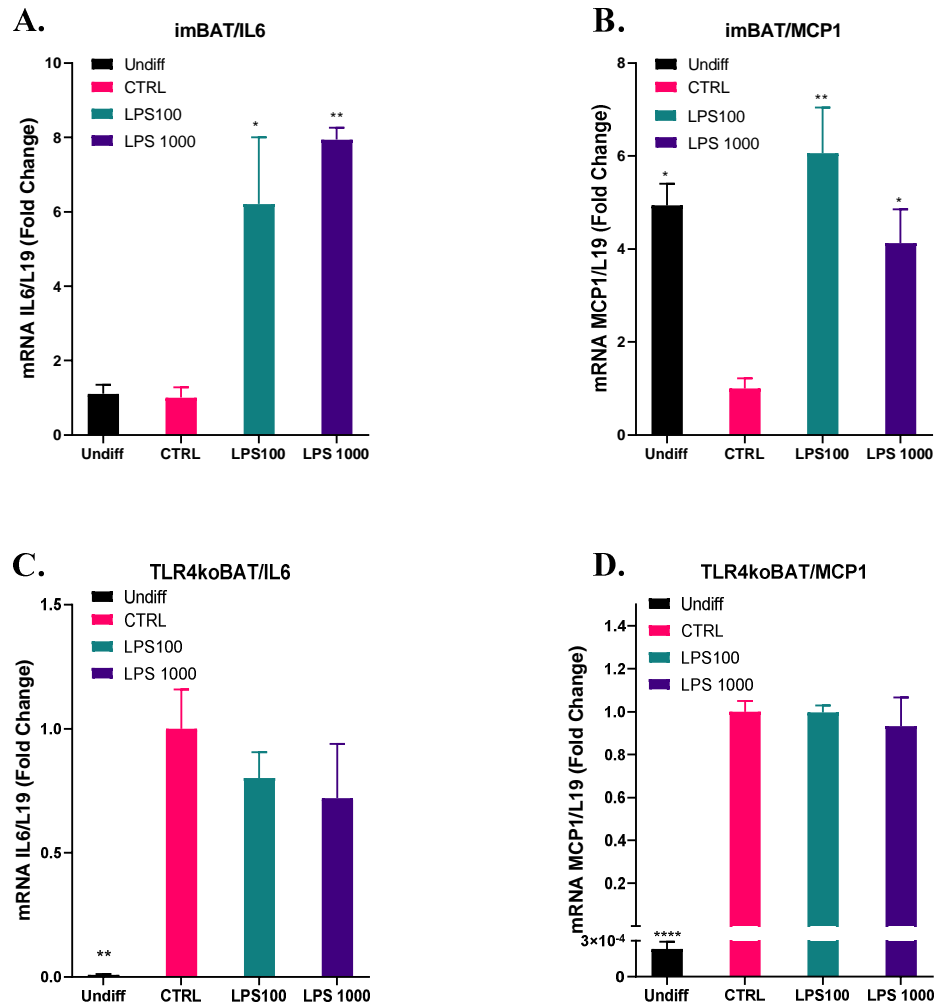


Figure 3.3.4.1 Effect of LPS on Inflammation of Brown Adipocyte Cell-Line.

ImBAT cells and TLR4ko.BAT cells were differentiated with/without LPS (100 ng/mL or 1000 ng/mL). (A, C) IL6 gene expression levels in imBAT and TLR4ko.BAT cells, respectively. (B, D) MCP1 gene expression levels in imBAT and TLR4ko.BAT cells, respectively. Data are expressed as a mean fold change from control cells \pm standard error of the mean. One-way ANOVA was used for comparisons. * $p < 0.05$, ** $p < 0.01$. CTRL; control. IL6; interleukin 6. MCP1; chemokine (C-C motif) ligand 2.

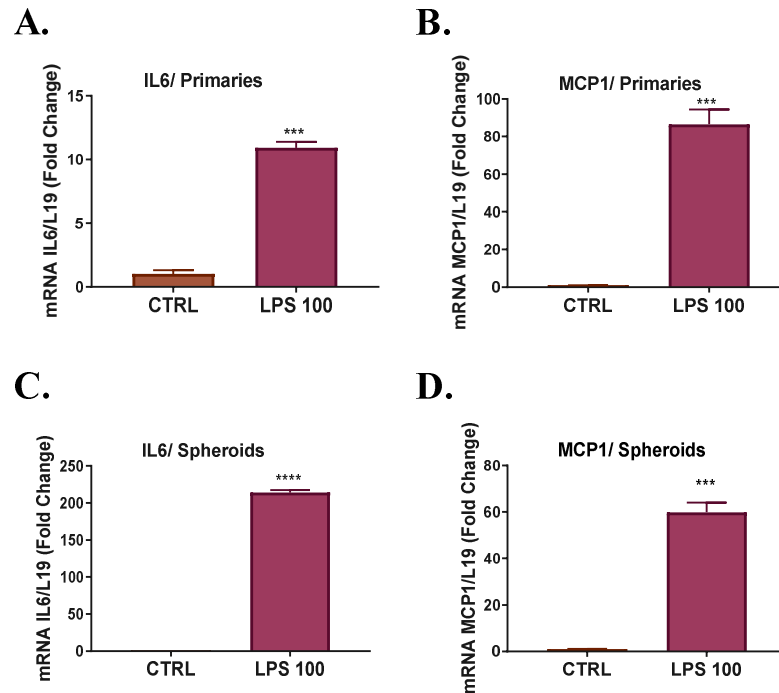


Figure 3.3.4.2 Effect of LPS on Primaries and Spheroids Brown Adipocyte Inflammation.

Primary brown adipocytes and spheroids were differentiated with/without LPS (100 ng/mL). (A, C) IL6 gene expression levels in primary cultures and spheroids, respectively. (B, D) MCP1 gene expression levels in primary cultures and spheroids, respectively. Data are expressed as a mean fold change from control cells \pm standard error of the mean. T Test was used for comparisons. *** $p<0.001$, **** $p<0.0001$. CTRL; control. IL6; interleukin 6. MCP1; chemokine (C-C motif) ligand 2.

3.3.5 LPS Reduced UCP1, the Main Brown Fat Marker, in Brown Adipocytes

Given that LPS induced inflammation and insulin resistance in wild type brown adipocytes but had no inflammatory effect on TLR4ko.BAT, and in line with previous investigation (344), the possibility of perturbing the brown adipocyte phenotype through TLR4 was investigated.

UCP1 mediates thermogenesis, the fundamental function of brown adipocytes, to uncouple oxidative phosphorylation from ATP synthesis to produce heat, and is known to be regulated at the transcriptional level (561). Therefore, it was determined whether TLR4 activation by LPS in brown adipocytes affects UCP1 mRNA expression. CL316,234, the β 3-selective adrenergic receptor agonist, was added for 5 hours before mRNA-harvesting to induce UCP1 expression. That was to study the effect of differentiating brown adipocytes with LPS on UCP1 induction through TLR4 in addition to the UCP1 basal levels. Activation of TLR4 by LPS throughout

differentiation suppressed both basal and CL-induced UCP1 mRNA expression (Figure 3.3.5.1, A, C). UCP1 suppression was apparent from day 5 of differentiation through until day 9 when harvested. (Figure 3.3.5.1, B, C).

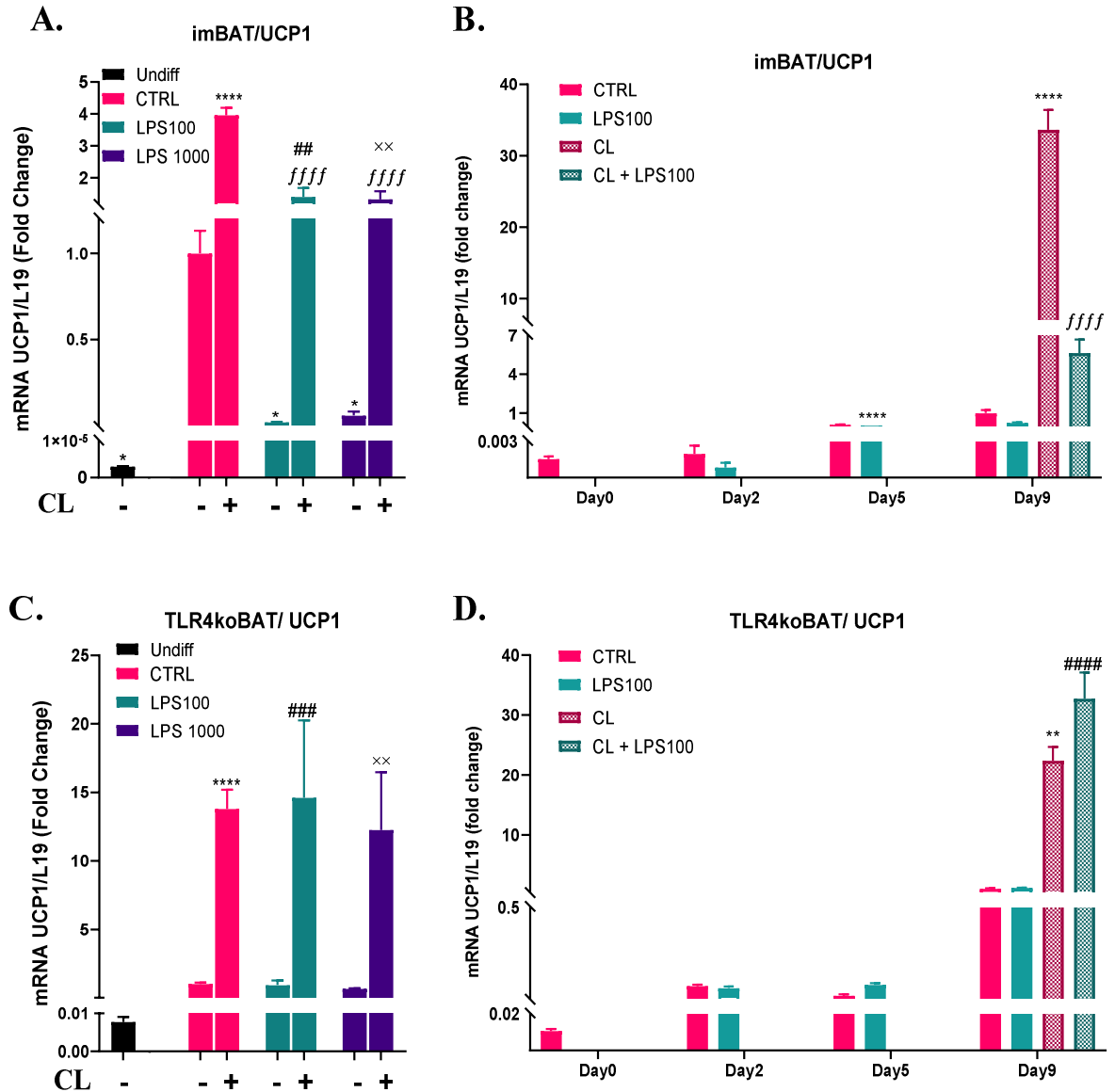


Figure 3.3.5.1 Effect of LPS on UCP1 Gene Expression.

ImBAT and TLR4ko.BAT cells were differentiated with/without LPS (100 ng/mL or 1000 ng/mL). mRNA was harvested on day 0, day 2, day 5, day 9. On day 9 mature adipocytes were treated with/without CL 316,234 (10 μ M) for 5 hours. UCP1 gene expression levels where the CL induction is shown in imBAT cells (A), TLR4ko.BAT cells (C) respectively. UCP1 gene expression levels on day 0, day 2, day 5, day 9 in imBAT cells (B), TLR4ko.BAT cells (D) respectively. Data are expressed as a mean fold change from control cells \pm standard error of the mean. One-way ANOVA was used for comparisons. * p <0.05, ** p <0.01, **** p <0.0001 Compared to CTRL in absence of CL, ffff p <0.0001 Compared to CL-treated CTRL. ## p <0.01, ### p <0.001, #### p <0.0001 Compared to LPS100 in absence of CL, xx p <0.01 Compared to LPS1000 in absence of CL. UCP1, uncoupling protein 1.

The morphology of differentiated imBAT cells and TLR4ko.BAT cells was determined and both control and LPS-treated cells showed the typical morphology of mature adipocytes with many lipid droplets and both groups looked healthy (Figure 3.3.5.3). This normal morphology was consistent with expression of the adipocyte differentiation marker aP2 which was similarly upregulated upon differentiation for both control and LPS-treated brown adipocytes (Figure 3.3.5.2). This indicates that the effect of LPS on UCP1 suppression was specific and cannot be attributed to cell death or inhibition of differentiation.

Suppression of UCP1 by LPS was further examined at the protein level. Western blot analysis and relative quantification confirmed that UCP1 protein expression was suppressed by LPS-activated-TLR4 in imBAT cells under both basal (FC=-1.74, $P<0.05$, Figure 3.3.5.4) and CL treatment (FC=-2.89, $P<0.001$, Figure 3.3.5.5).

In contrast, there were no changes in UCP1 expression in response to LPS when TLR4 was deleted. Neither dose of LPS altered basal UCP1 mRNA at any stage during differentiation (Figure 3.3.5.1) or affected CL-induced UCP1 mRNA (Figure 3.3.5.1). Similarly, UCP1 protein expression was not affected by LPS at basal (Figure 3.3.5.4) or with CL stimulus (Figure 3.3.5.5) in TLR4ko.BAT.

Taken together, these results support that LPS does not adversely affect cell morphology and viability. Stimulation of brown adipocytes with LPS suppresses both basal and CL-induced UCP1 gene and protein expression predominantly mediated through TLR4.

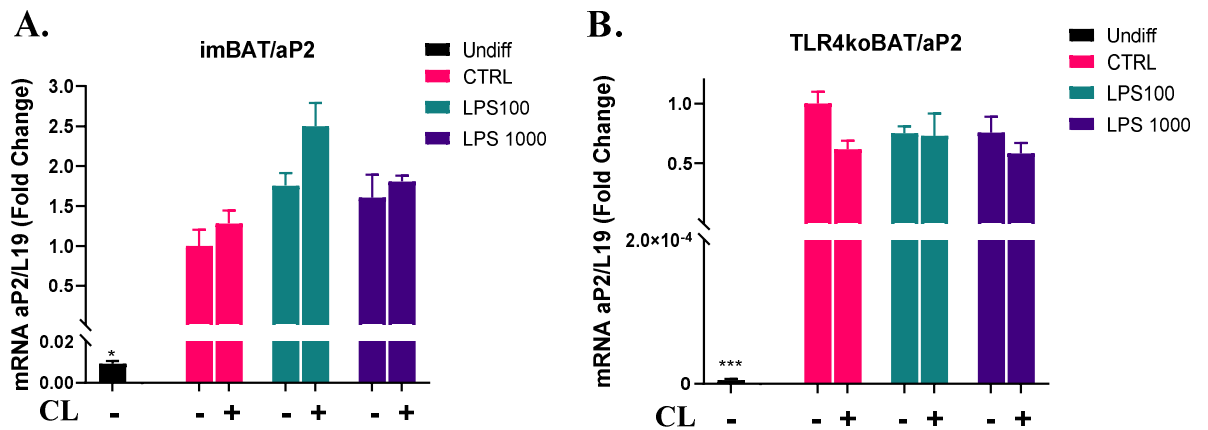


Figure 3.3.5.2 aP2 in Brown Adipocyte.

ImBAT and TLR4ko.BAT cells were differentiated with/without LPS (100 ng/mL or 1000 ng/mL). On day 9 mature adipocytes were treated with/without CL 316,234 (10 μ M) for 5 hours. (A) aP2 gene expression levels in imBAT cells. (B) aP2 gene expression levels in TLR4ko.BAT cells. Results are expressed as a mean fold change from control cells \pm standard error of the mean. One-way ANOVA was used for comparisons. CTRL; control. aP2: fatty acid binding protein 4.

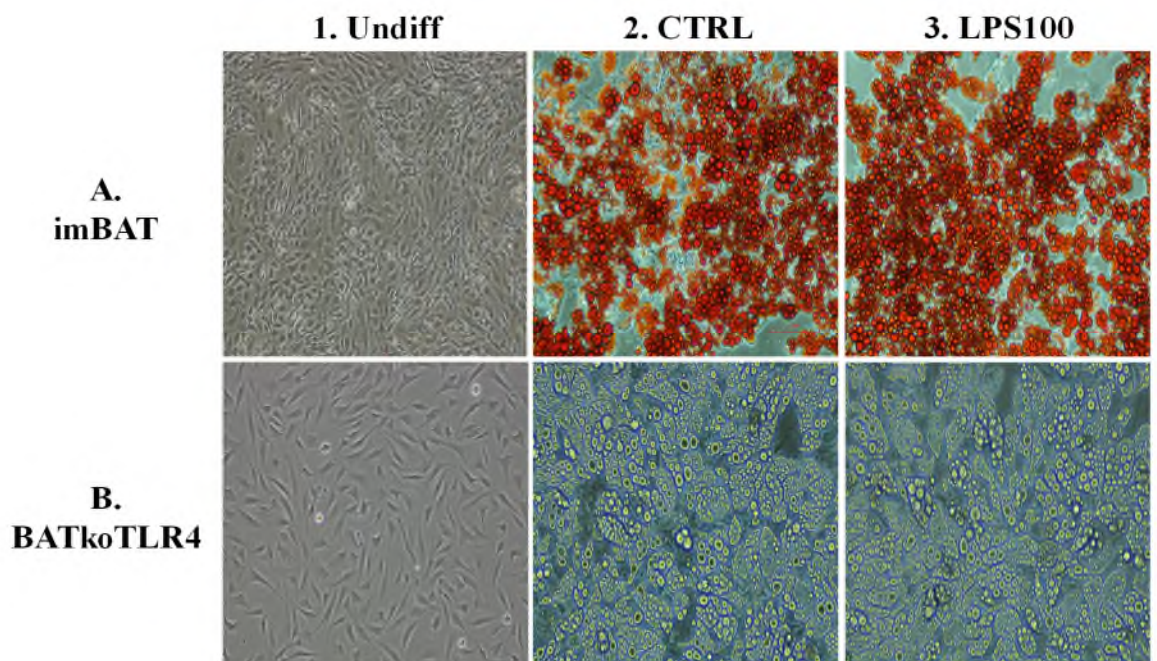


Figure 3.3.5.3 Mature Brown Adipocyte Differentiation Pictures Under LPS Treatment.

ImBAT and TLR4ko.BAT cells were differentiated with/without LPS (100 ng/mL). Pictures with a 20x magnification of undifferentiated (Undiff) imBAT cells (A1), TLR4ko.BAT cells (B1), and differentiated control (CTRL) imBAT cells (A2), TLR4ko.BAT cells (B2) pictures. LPS-treated imBAT cells (A3) and LPS-treated TLR4ko.BAT cells (B3). imBAT were stained with Oil Red O and pictures were taken.

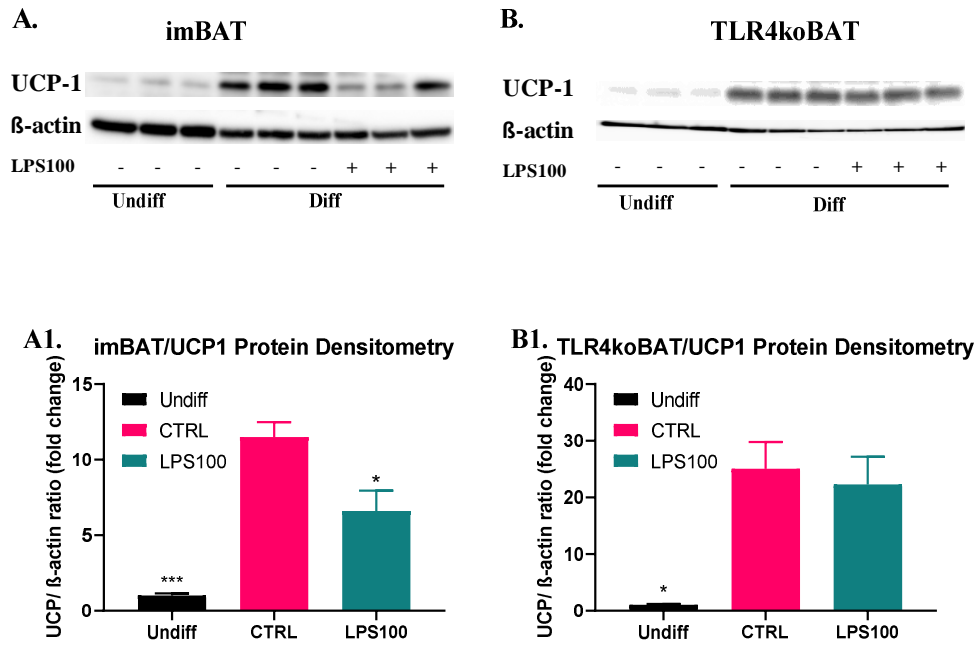


Figure 3.3.5.4 LPS-Activated TLR4 Suppresses UCP1 Protein Expression.

ImBAT and TLR4ko.BAT cells were differentiated with/without LPS (100 ng/mL or 1000 ng/mL). Brown adipocytes were serum starved for 24 hours before protein harvesting. (A) imBAT image of UCP1 and loading control β-actin Western blot membranes and (A1) densitometry. (B) TLR4ko.BAT image of UCP1 and loading control β-actin Western blot membranes and (B1) densitometry. Data are expressed as a fold change from control cells. Bars represent mean ± standard error of the mean. One-way ANOVA was used for comparisons. * $p < 0.05$, *** $p < 0.001$ compared to CTRL. CTRL; control. Undiff; undifferentiated. UCP1; uncoupling protein 1.

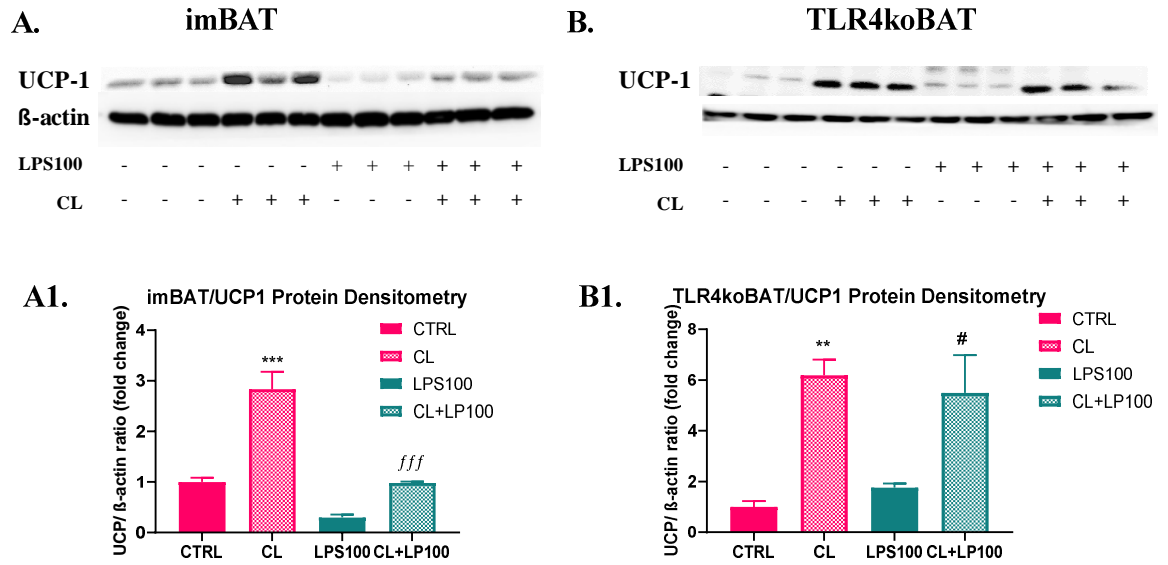


Figure 3.3.5.5 LPS-Activated TLR4 Suppresses both Basal and CL-Induced UCP1 Protein Expression.

ImBAT and TLR4ko.BAT cells were differentiated with/without LPS (100 ng/mL or 1000 ng/mL). Brown adipocytes were serum starved for 24 hours and treated with/without CL 316,234 (10 μ M) before protein harvesting. (A) imBAT image of UCP1 and loading control β -actin Western blot membranes and (A1) densitometry. (B) TLR4ko.BAT image of UCP1 and loading control β -actin Western blot membranes and (B1) densitometry. Data are expressed as a fold change from control cells. Bars represent mean \pm standard error of the mean. One-way ANOVA was used for comparisons. ** $p < 0.01$, *** $p < 0.001$ compared to CTRL. *fff* $p < 0.001$ compared to CL-treated CTRL. # $p < 0.05$ compared to LPS in absence of CL. CTRL; control. UCP1; uncoupling protein 1.

Next, because PGC1 is a master regulator of brown adipocyte thermogenesis and UCP1 gene expression, the levels of different PGC1 family member transcripts were monitored, including peroxisome proliferative activated receptor, gamma, coactivator 1 alpha (PGC1 α) and PPARG coactivator 1 beta (PGC1 β).

Similar to UCP1, activation of TLR4 by both LPS doses throughout differentiation suppressed both basal and CL-induced mRNA expression of PGC1 α and PGC1 β in wild type cells. In contrast, differentiating TLR4ko.BAT with LPS had no effect on either PGC1 α or PGC1 β gene expression (Figure 3.3.5.6, C, D). This indicates that TLR4 mediates LPS-mediated suppression actions on UCP1 levels at least in part by downregulating the upstream regulators PGC1 α and PGC1 β .

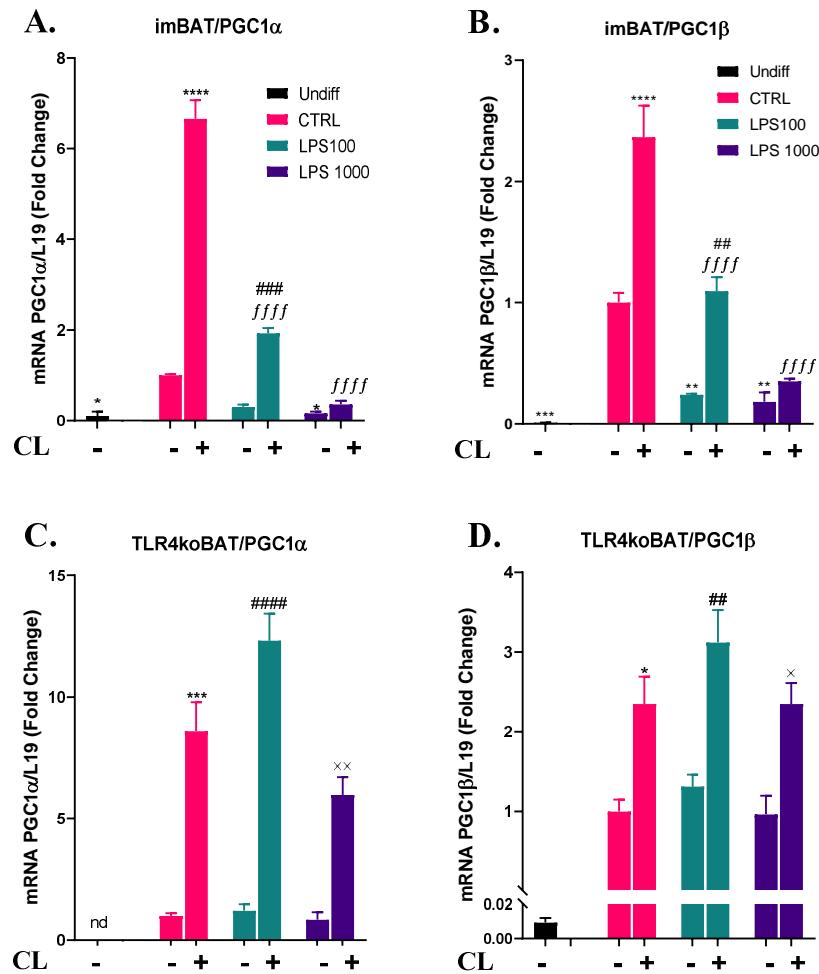


Figure 3.3.5.6 Effect of LPS on PGC-1 Gene Expression.

ImBAT and TLR4ko.BAT cells were differentiated with/without LPS (100 ng/mL or 1000 ng/mL). On day 9 mature adipocytes were treated with/without CL 316,234 (10 μ M) for 5 hours. PGC1 α gene expression levels in imBAT (A) and TLR4ko.BAT cells (C), respectively. PGC1 β gene expression levels in imBAT (B) and TLR4ko.BAT cells (D), respectively. Data are expressed as a mean fold change from control cells \pm standard error of the mean. One-way ANOVA was used for comparisons. * $p < 0.05$, *** $p < 0.001$, **** $p < 0.0001$ Compared to CTRL in absence of CL, *ffff* $p < 0.0001$ Compared to CL-treated CTRL. ## $p < 0.01$, ### $p < 0.001$, #### $p < 0.0001$ Compared to LPS100 in absence of CL, \times $p < 0.05$, $\times\times$ $p < 0.01$ Compared to LPS100 in absence of CL. UCP1, uncoupling protein 1. CTRL; control. Nd: not determined. PGC1 α ; peroxisome proliferative activated receptor, gamma, coactivator 1 alpha. PGC1 β ; PPARG coactivator 1 beta.

Finally, receptor-interacting protein 140 (RIP140) gene expression levels in imBAT cells was observed. RIP140 is known to have opposing actions to PGC1 and blocks the beiging program in WAT, preventing the expression of brown fat genes and inhibiting a triacylglycerol futile cycle, with important implications for energy homeostasis (562). Interestingly, RIP140 mRNA expression was increased when differentiating imBAT were treated with both LPS doses (FC=4.47, $P < 0.001$ with LPS100 ng/mL, FC=4.66, $P < 0.001$ with LPS1000 ng/mL, Figure 3.3.5.7). This

indicates that RIP140 could be key to the potent suppression of thermogenesis by LPS and it indicates the wide range of affected factors.

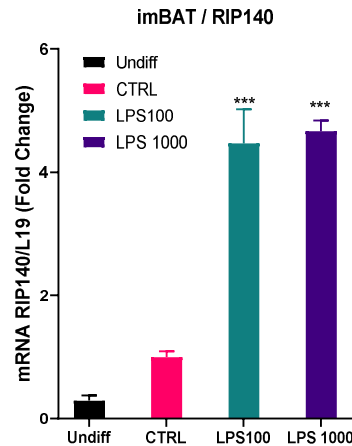


Figure 3.3.5.7 Effect of LPS on RIP140 Gene Expression.

ImBAT cells were differentiated with/without LPS (100 ng/mL or 1000 ng/mL). RIP140 gene expression levels in imBAT cells were assessed using qRT-PCR. Data are expressed as a mean fold change from control cells \pm standard error of the mean. One-way ANOVA was used for comparisons. *** $p < 0.001$ Compared to CTRL. CTRL; control. RIP140; Receptor-interacting protein 140.

3.3.6 LPS Reduced UCP1 Expression in Other Wild Type Brown Adipocytes Models

After determining the inhibitory actions of LPS on UCP1 expression in the immortalised brown adipocyte cell line, whether LPS had the same effect on other models of brown adipocytes investigated. This included primary brown adipocytes and a 3D spheroid model. These two models closely represent the physiological brown adipocyte state. Thus, both primary brown adipocytes and spheroids were differentiated with or without LPS, the TLR4 ligand.

Primary brown adipocytes showed the typical morphology of mature brown adipocytes full of lipid droplets (Figure 3.3.6.1, A) with classic aP2 induction upon differentiation (Figure 3.3.6.1, A4) in cells differentiated with or without LPS compared to undifferentiated. Similarly, H&E immunohistochemical staining of spheroids equally showed lipid droplets (Figure 3.3.6.1, B) in differentiated spheroids with or without LPS compared to undifferentiated spheroids, along with aP2 mRNA induction upon differentiation (Figure 3.3.6.1, B4)

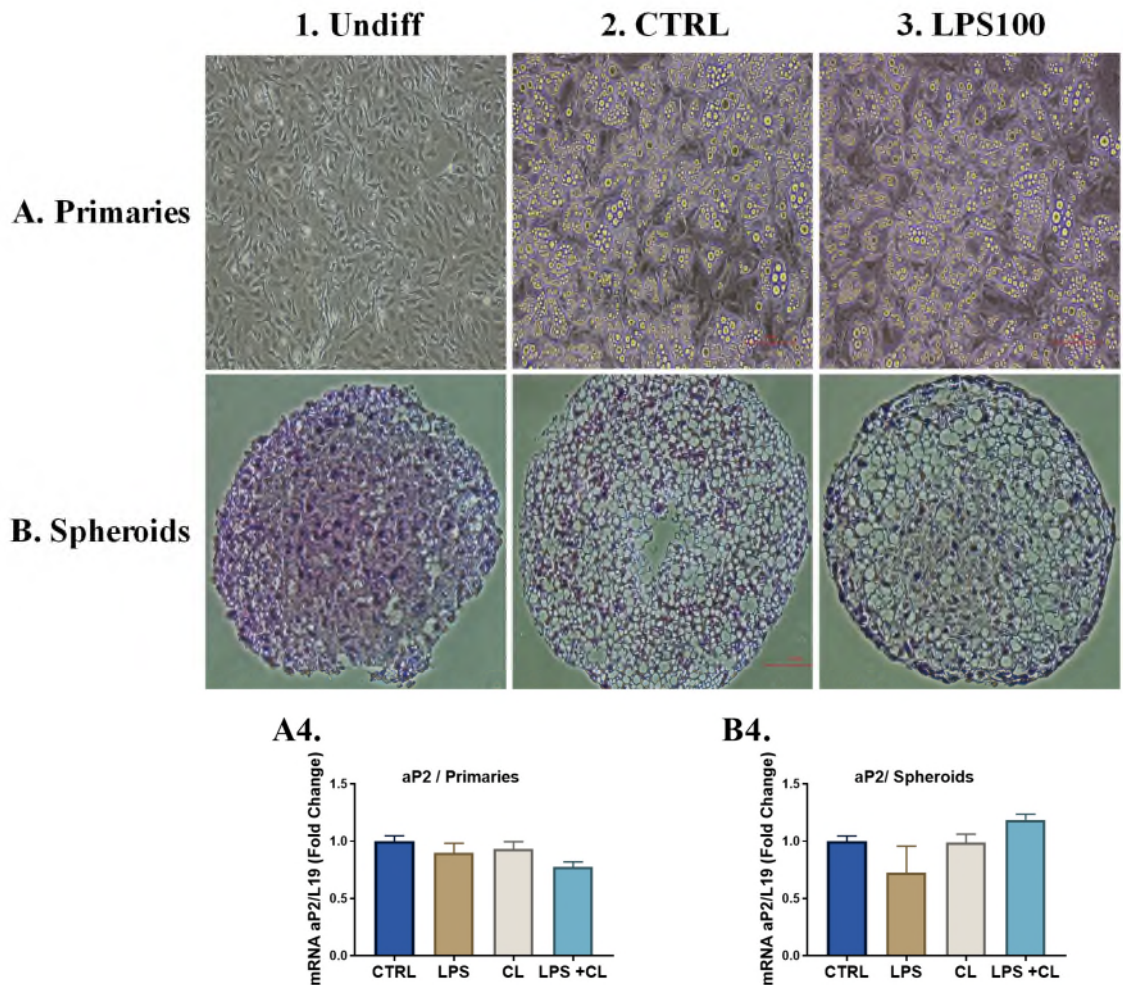


Figure 3.3.6.1 Differentiation of LPS-Treated Wild Type Primary Brown Adipocytes and Spheroids.

Pictures with a 20x magnification of undifferentiated (Undiff) primary brown adipocytes (A1), spheroids (B1) and differentiated control (CTRL) primary brown adipocytes (A2), spheroids (B2). LPS-treated primary cultures (A3) and LPS-treated spheroids (B3). Spheroids were stained with H&E staining and pictures were taken. Expression of mature adipocyte-associated genes including aP2 gene expression levels in primary cultures (A4) and spheroids (B4). Data are presented as mean fold change \pm standard error of mean. One-way ANOVA was used for comparisons. aP2; fatty acid binding protein 4.

Consistent with the findings using imBAT cells, LPS stimulation throughout differentiation greatly suppressed both basal and CL-induced mRNA expression of UCP1 and PGC1 α in both primary brown adipocytes (Figure 3.3.6.2. B) and brown adipocyte spheroids (Figure 3.3.6.2.D). Further investigations of UCP1 expression in spheroids by immunohistochemistry showed clear evidence of reduced UCP1 expression in differentiated spheroids with LPS compared to control spheroids (Figure 3.3.6.3, Figure 3.3.6.4).

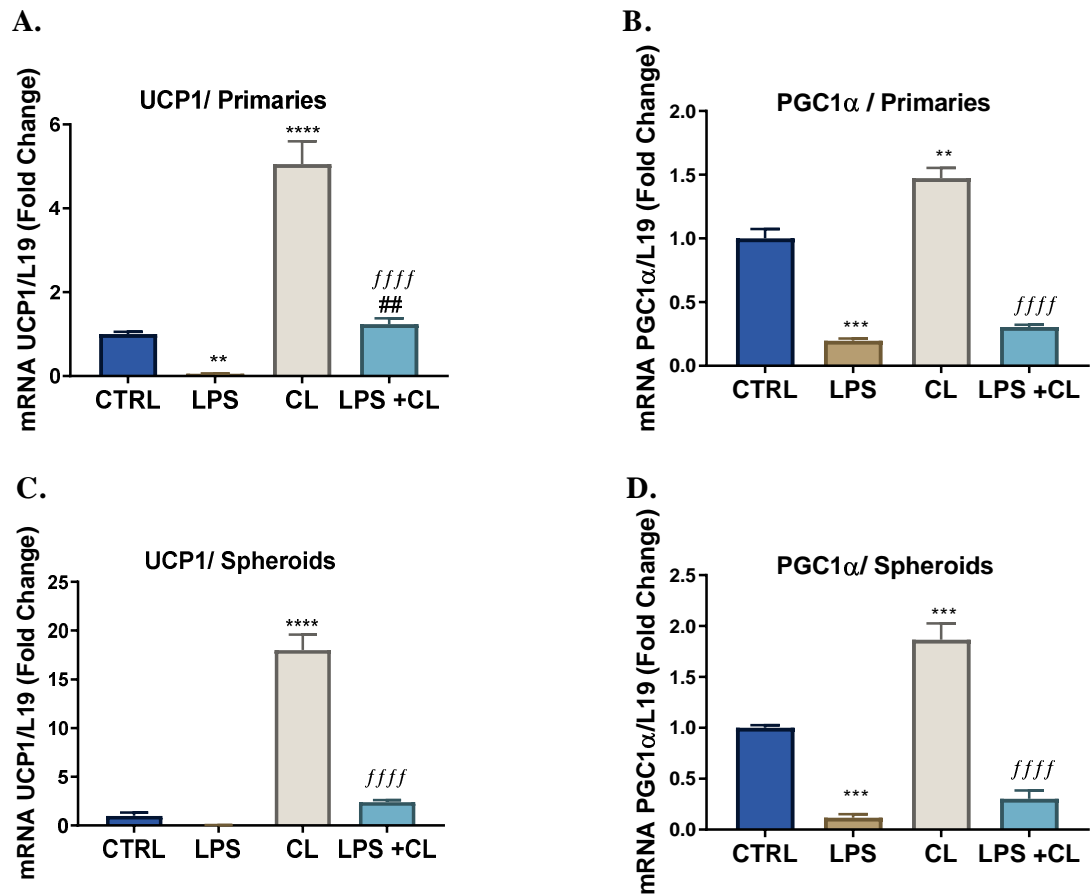


Figure 3.3.6.2 Effect of LPS on UCP1 and PGC1α Gene Expression.

Primary brown adipocytes and spheroids were differentiated with/without LPS (100 ng/mL)). On day 9 mature adipocytes of both models were treated with/without CL 316,234 (10μM) for 5-hours. UCP1 gene expression in primaries (A), spheroids (C) respectively. PGC1α gene expression in primaries (B), spheroids (D) respectively. Data are expressed as a mean fold change from control cells \pm standard error of the mean. One-way ANOVA was used for comparisons. ** $p < 0.01$, *** $p < 0.001$, **** $p < 0.0001$ Compared to CTRL in absence of CL, ffff $p < 0.0001$ Compared to CL-treated CTRL. ## $p < 0.01$ Compared to LPS in absence of CL. UCP1, uncoupling protein 1. PGC1α; peroxisome proliferative activated receptor, gamma, coactivator 1 alpha.

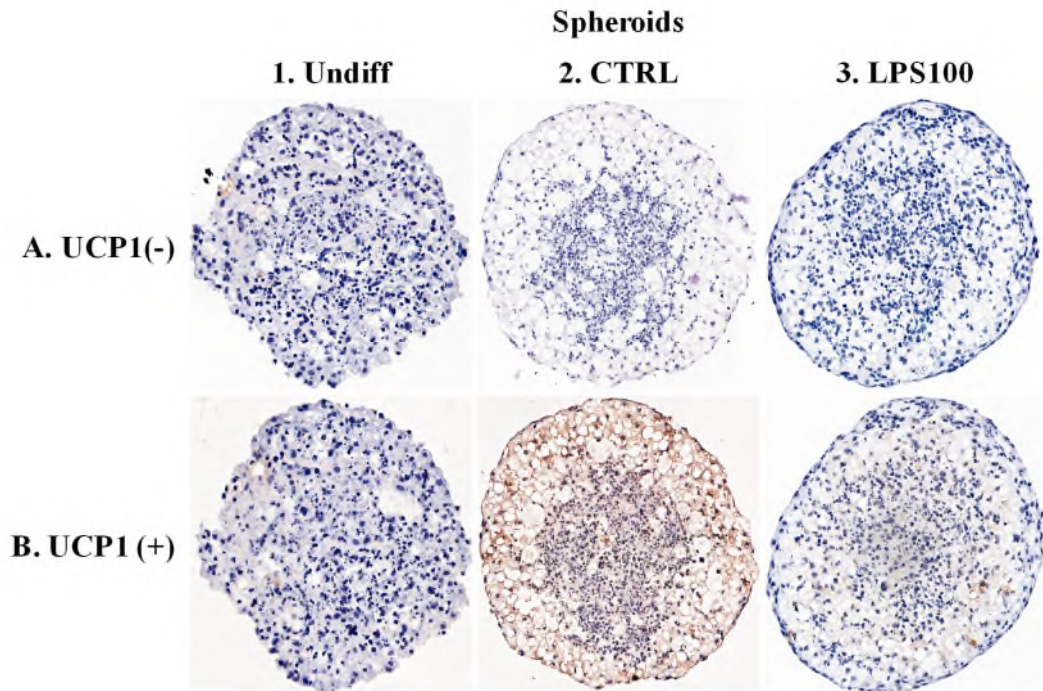


Figure 3.3.6.3 UCP1 Staining, in Murine Brown Adipocyte Spheroids by Immunohistochemistry.

Sectioned spheroids were incubated without (A1, A2, A3)/with (B1, B2, B3) UCP1 primary antibody and staining was detected using an HRP/DAB detection kit. Sections were counterstained using hematoxylin. Pictures taken with a 20x magnification. B2 appears more stained compared to B3 which indicates LPS reduced UCP1 in brown adipocytes spheroids.

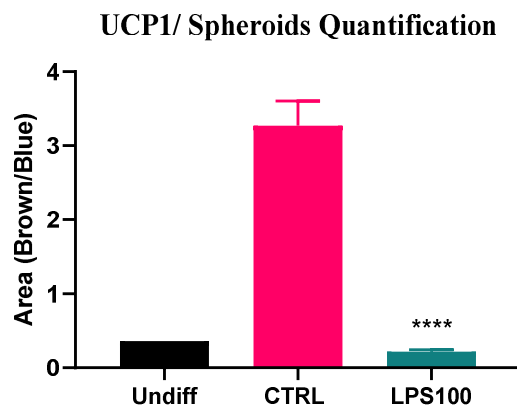


Figure 3.3.6.4 UCP1 Staining Quantification, in Murine Brown Adipocytes Spheroids by Immunohistochemistry.

At least 3 stained spheroids at dilution 1:1000 for UCP1 antibody were quantified. Data are expressed as mean \pm standard error of the mean. Unpaired t test was used for comparisons. **** $p < 0.0001$ Compared to CTRL. CTRL, control. UCP1, uncoupling protein 1.

3.3.7 LPS Reduced Expression of Key Brown Fat Genes

Similar to UCP1, when wild type brown adipocytes were treated with LPS throughout differentiation, suppression was observed for gene expression of cell death inducing DFFA like effector a (CIDEA) (FC=-14.11 with LPS 100 ng/mL, $P<0.0001$, FC=-5.49 with LPS 1000 ng/mL Figure 3.3.7.1, A), perilipin 5 (PLIN5) (FC=-4.50, $P<0.01$ with LPS 100 ng/mL, FC=-24.18, $P<0.01$ with LPS 1000 ng/mL, Figure 3.3.7.1, B), and Elongation of very long chain fatty acids protein 3 (ELOVL3) (FC=-24.84, $P<0.0001$ with LPS 100 ng/mL, FC=-13.93, $P<0.0001$ with LPS 1000 ng/mL, Figure 3.3.7.1, C). In contrast, mRNA for CIDEA, PLIN5 and ELOVL3 was not altered in TLR4ko.BAT cells by differentiating cells with LPS (Figure 3.3.7.1, D, E, F). This further supports that LPS is playing a role as an inhibitor of brown adipocyte characteristics through TLR4 and likely eventually causing a whitened brown adipocyte phenotype.

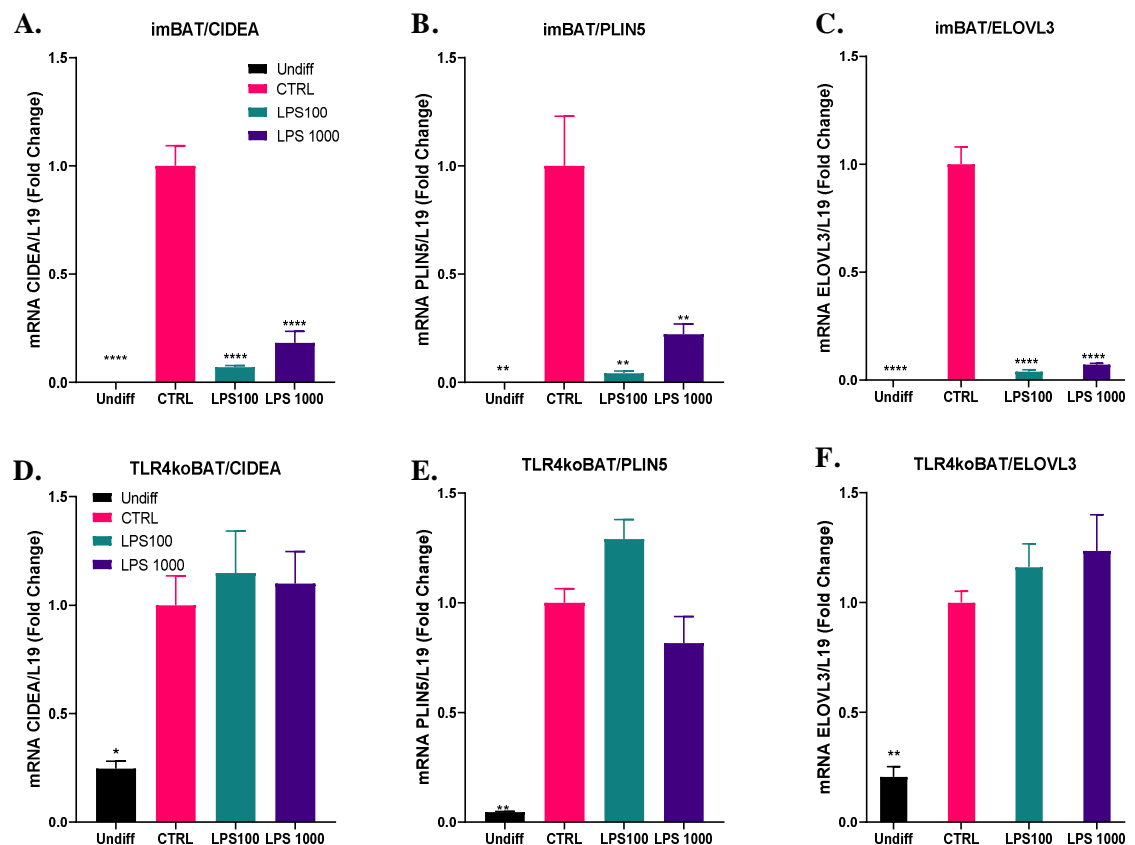


Figure 3.3.7.1 Effect of LPS on Key Brown Fat Gene Expression.

ImBAT or TLR4ko.BAT cells were differentiated with/without LPS (100 ng/mL or 1000 ng/mL). CIDEA gene expression levels in (A)imBAT. (D) TLR4ko.BAT. PLIN5 gene expression levels in (B)imBAT. (E) TLR4ko.BAT. ELOVL3 gene expression levels in (C)imBAT. (F) TLR4ko.BAT. Data are expressed as a mean fold change from control cells \pm standard error of the mean. One-way ANOVA was used for comparisons. * $p<0.05$, ** $p<0.01$, *** $p<0.001$, **** $p<0.0001$ Compared to CTRL. CTRL; control. CIDEA; cell death inducing DFFA like effector a. PLIN5; perilipin 5. ELOVL3; Elongation of Very Long Chain Fatty Acids Protein 3.

3.3.8 LPS Impaired Lipid Metabolism

Functional assays were undertaken to determine the impact of LPS on glycerol metabolism. Glycerol levels were lower in media collected from brown adipocytes differentiated with LPS when stimulated with CL for 8 hours compared to CL-stimulated control cells (Figure 3.3.8.1, A). However, the basal levels were unaffected by LPS. Furthermore, the total cellular triglyceride levels were higher in the brown adipocytes differentiated with LPS (Figure 3.3.8.1,B). Thus, LPS appears to promote triglyceride retention in brown adipocytes which could indicate elevated levels of lipogenesis rather than lipolysis being affected in the basal state.

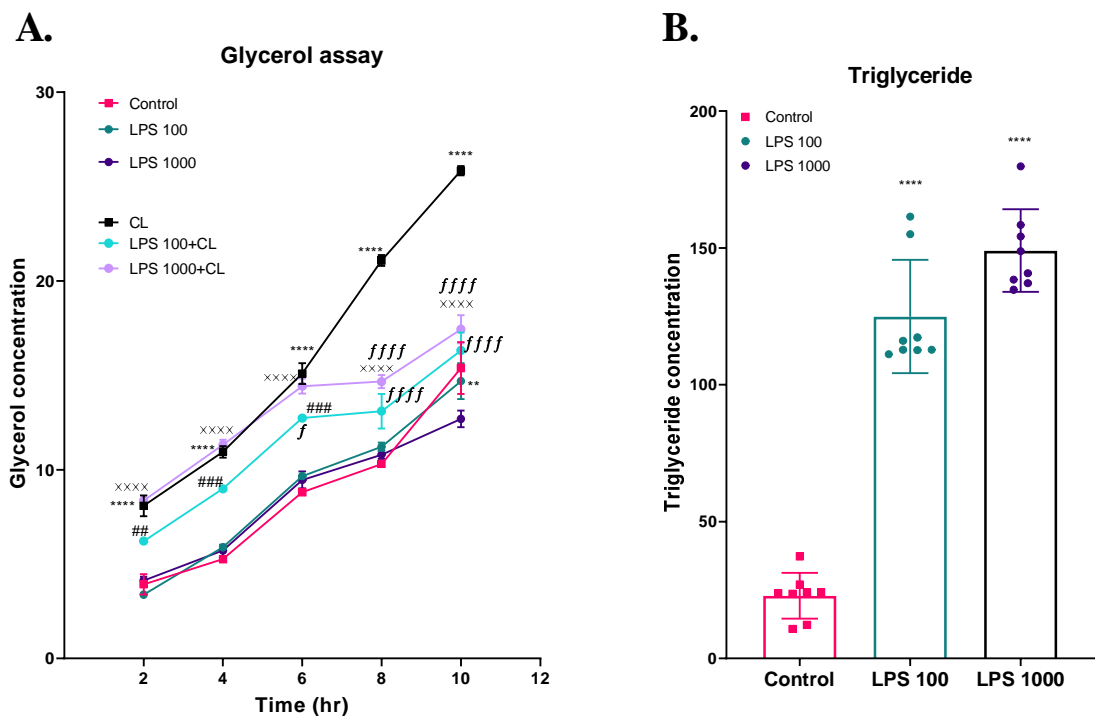


Figure 3.3.8.1 LPS Effects on Lipid Metabolism in Brown Adipocytes.

ImBAT cells were differentiated with/without LPS (100 ng/mL or 1000 ng/mL). (A) Released Glycerol into conditioned media (B) Total cellular triglyceride levels. Measurements are expressed as mean \pm standard error of the mean. One-way ANOVA was used for comparisons. **** p <0.0001 Compared to CTRL in absence of CL, $ffff$ p <0.0001 Compared to CL-treated CTRL. ## p <0.01, ### p <0.001, ##### p <0.0001 Compared to LPS100 in absence of CL, ##### p <0.0001 Compared to LPS1000 in absence of CL.

Triglycerides are stored in lipid droplets (LDs), the major cellular organelles for the storage of neutral lipids. Among cellular organelles, LDs are uniquely composed of an organic phase of neutral lipids surrounded by a phospholipid monolayer. A wide range of proteins interact with lipid droplets to regulate their size and control the storage and release of lipid. In light of LPS affecting brown adipocyte triglyceride content and the CL-induced release of glycerol, the effect of LPS on LD biology was investigated by confocal microscopy. Representative images are shown in (Figure 3.3.8.2). The analysis showed that areas occupied with LDs in LPS-treated adipocytes was significantly increased compared with controls. The ratio of area covered by LD was increased by 38 % with LPS100 and 52 % with LPS1000 treatment compared to control cells (Figure 3.3.8.3). However, the average LD area in the measured 20 control cells was comparable with LPS treated cells (Figure 3.3.8.3). In contrast, the number of LDs was significantly higher in LPS treated cells -there was 1.8 fold increase in the number of LDs in LPS-treated cells compared to control cells (Figure 3.3.8.3). Therefore, the augmentation of lipid content inside LPS-treated cells was due to increased mean LD number in these cells. Overall, LPS appears to enhance lipid storage inside brown adipocytes.

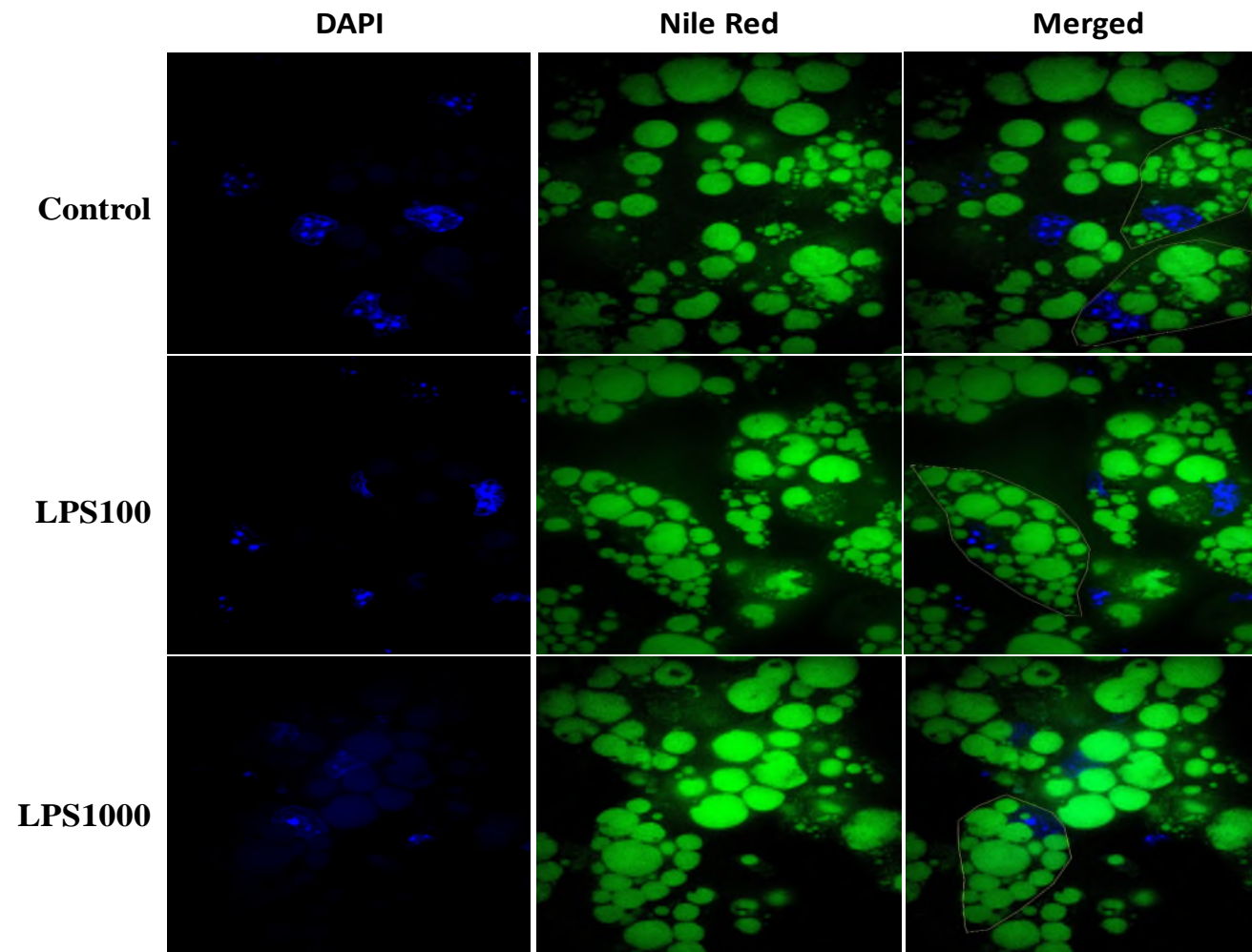


Figure 3.3.8.2 Confocal Microscopies of Brown Adipocytes Treated with or without LPS 100 ng/mL or LPS 1000 ng/mL.

Representative confocal images of control (left panel) and LPS-100 (middle panel) and LPS1000 (right panel). Images are shown at 100x magnification imBAT cells immunostained with Nile-red (green) and DAPI (blue).

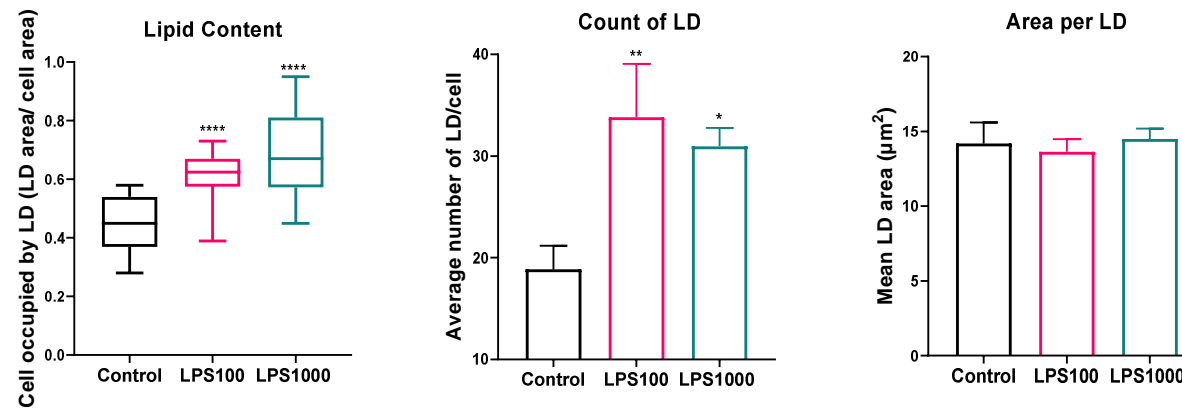


Figure 3.3.8.3 Effect of LPS on Lipid Droplets (LD).

Lipid content, number and area of LD are calculated through confocal microscopy analysis (n=20). Data are expressed as median of lipid content, and bars represent max and minimum values. Data are expressed as mean \pm SEM for number and area per LD. One-way ANOVA was performed for statistical comparison. *p<0.05, **p<0.01, ***p<0.0001

3.4 Discussion

BAT has a unique feature in energy expenditure through the process of thermogenesis and its existence was rediscovered in adult humans. Therefore, it is considered as an interesting aspect to study for obesity management and prevention and there is an intensive research on this fat depot to address its physiology and function (563). Although it is well recognized that obesity is associated with chronic inflammation both systemically and locally in WAT, chronic inflammation is less studied in BAT. Specifically, the effect of inflammatory activators on brown adipocyte activity and factors related to thermogenesis in these cells has not been studied in detail.

This chapter has explored the impact of LPS on brown adipocytes to provide insight into how gut derived LPS inflammation may induce brown adipocyte dysfunction. These studies utilised 2D models including an immortalized brown cell line (imBAT) and primary brown adipocytes, as well as a 3D model represented by spheroids, to investigate how LPS induces an inflammatory response in brown adipocytes. Furthermore, these studies identified how perturbation of prominent features of brown adipocyte function including thermogenesis regulation, represented by reduced UCP1 in the different models is impacted. The findings from these studies also identified that in brown adipocytes LPS elicits inflammatory markers along with impairing insulin sensitivity and lipid handling mechanism.

The effects of LPS on brown adipocytes appear to be mediated by TLR4, evidenced by the use of TLR4ko.BAT cells leading to compromised action of LPS of cellular dysfunction in such cells. This highlighted that TLR4Ko.BAT cells could eliminate the actions of LPS on thermogenesis UCP1, the main brown adipocytes marker, at both gene expression and protein levels.

In order to investigate the effect of LPS in brown adipose tissue, inflammatory transcription markers were measured following chronic LPS treatment through differentiation. Detected by qRT-PCR, mRNA expression of the inflammatory chemokine MCP1 and cytokine IL6 were upregulated in different models of wild type brown adipocytes (2D and 3D models). MCP1 is a chemotactic agent which plays a profound role in macrophage infiltration into the adipose tissue, and causes adipose

inflammation (564,565). IL6 is a cytokine that is associated with insulin resistance in skeletal muscle and liver (566,567). This upregulation of inflammatory markers is expected to be as a result of activation of the NF κ B and MAPK signalling pathways upon TLR4 induction by LPS, as denoted in various cell types including white adipocytes (446,448,454,568). The activation of inflammatory pathways upon LPS treatment in BAT and cultured immortalised brown adipocytes is in agreement with a previous study (344). However, LPS-induced inflammatory markers in 3D brown adipocyte spheroids has not been reported before. Prior study demonstrated that gene expression of selected PRRs including TLR4 were increased in BAT in obesity, which correlated with augmented pro-inflammatory cytokine/chemokine gene expression levels. In their study, activation of PRRs stimulated MCP1, IL6 and RANTES levels in immortalised brown adipocytes via upregulating of NF κ B and MAPK pathways as downstream of TLR4 activation by LPS. However, in previous study, immortalised brown adipocytes were only treated with LPS (1000 ng/mL) for 12-15 hours post-differentiation with no further observations of other models, and as such the chronic impact of LPS treatment during differentiation of brown adipocytes was not investigated and the LPS effect on different cell models was not addressed. Consequently, this current data enhances the evidence that LPS is a potent inflammatory stimulator of brown adipocytes and when applied chronically it profoundly inhibits brown adipocyte function including primary and 3D spheroids brown adipocyte.

In parallel with stimulation of the inflammatory response, reduction in both insulin-stimulated glucose uptake and GLUT4 mRNA expression suggested greater insulin resistance with LPS treatment. In this context, the observed reduction in insulin-stimulated AKT phosphorylation in differentiated cells with LPS indicated that LPS acted on the AKT pathway to disturb insulin signalling. Similarly, Song et al. revealed that LPS decreased phosphorylation levels of Akt/PKB and glycogen synthase kinase 3 beta (GSK3b) upon insulin stimulation in 3T3-L1 adipocytes (553). AKT is known to mediate the responses of glucose transport, glycogen synthesis, protein synthesis, and antilipolytic effects of insulin (569). Therefore, these findings suggest that LPS induces inflammation and hence triggers insulin resistance in brown adipocytes. In recent years, a relation between low-grade chronic inflammation and insulin resistance has been established in different cells and organs with activation of TLRs considered

to contribute to diet induced obesity, enhanced tissue inflammation, and insulin resistance (426,436,545,546,548,570).

It is further reported that nutritional fatty acids, other activators of TLR4 whose circulating levels also rise in obesity, signal to white adipocytes and macrophages to induce inflammation and insulin resistance (436,571). Studies have also demonstrated that lack of TLR4 activation, leads to protection against insulin resistance with reduced inflammation in endothelial cells, liver and fat; and reduced susceptibility to high-fat diet induced obesity compared with the WT control mice (426,436,571–574). Inhibition of TLR4 signalling is in tandem with both lack of inflammatory signalling in adipose cells or tissue and macrophages as well as improvements of insulin sensitivity. This is suggested to result from the blunted capacity of fatty acids but may also be affected by interruptions of LPS actions. In these prior studies *in-vivo*, inflammation in BAT was not reported. Therefore, the role of LPS-mediated actions in BAT in inflammation, insulin resistance, and altered energy expenditure in brown adipocytes was studied. Overall, it can be speculated that LPS, which increases in obesity, is a molecular link for nutrition overload and inflammation, and that the innate immune system participates in the regulation of energy balance and insulin resistance in response to changes in the nutritional environment.

The effect of LPS on the wild type brown adipocytes involved suppression of basal and CL316,243 -induced UCP1 mRNA and protein expression, to a great extent through activation of TLR4. Whilst further analysis sought to examine TLR4 in LPS-mediated down-regulation of thermogenesis markers using TLR4ko.BAT cells. The critical role of TLR4 is supported by the fact that TLR4ko.BAT cells were not affected by LPS as shown in data obtained by qRT-PCR and western-blotting investigations. In fact, the effect of LPS on basal UCP1 expression in wild type brown adipocytes was obvious as early as day 2 of differentiation at gene expression levels, whereas this was not observed in TLR4ko.BAT cells. This clearly indicates that activation of TLR4 by LPS in the brown adipocytes diminishes the main cellular characteristics and ultimately impairs their thermogenesis capability. Also, the possible mechanisms for TLR4-mediated suppression of UCP1 is through the NFκB and JNK pathway. Impairing thermogenesis capability of brown adipocytes by LPS was further observed by reduced expression of key markers of brown fat through differentiation including

CIDEA, ELOVL3 and PLIN5. In line with these findings, it was also reported in immortalised brown adipocytes that LPS reduced basal and isoproterenol-induced UCP1 mRNA and protein expression with more pronounced suppression under the isoproterenol-stimulated condition. Also, PPAR γ and PGC1 α expression was suppressed by LPS, both of which are important regulators of expression of UCP1. It was suggested that the suppression of UCP1 promoter activity mediated this LPS action.

The current studies further explored the effect of LPS on brown adipocyte cell morphology and lipid accumulation was investigated via Oil Red-O staining and fluorescence images. Both the cell morphology and lipid droplets looked healthy by Oil Red-O staining in control and LPS-treated cells. Quantification of fluorescence images of stained lipid droplets demonstrated that LPS treatment affected the cells. It was also demonstrated that LPS enhanced triglyceride accumulation inside the cells by increasing LD numbers and decreasing glycerol released by CL-stimulated lipolysis. That indeed can lead to less free fatty acids available for thermogenesis and increased risk of metabolic dysfunction as brown adipocyte cells become compromised. Also, this inhibition of glycerol by LPS release, might be downstream of PGC1 gene expression inhibition, as PPAR response elements regulate glycerol metabolism (575,576). In fact, this study's current data showed both PGC1 α and PGC1 β were reduced by LPS treatment at basal and CL-treated levels in imBAT cells. These findings demonstrate that brown adipocytes differentiated in the presence of LPS selectively suppressed UCP1, display enhanced lipid accumulation, and reduced lipid release.

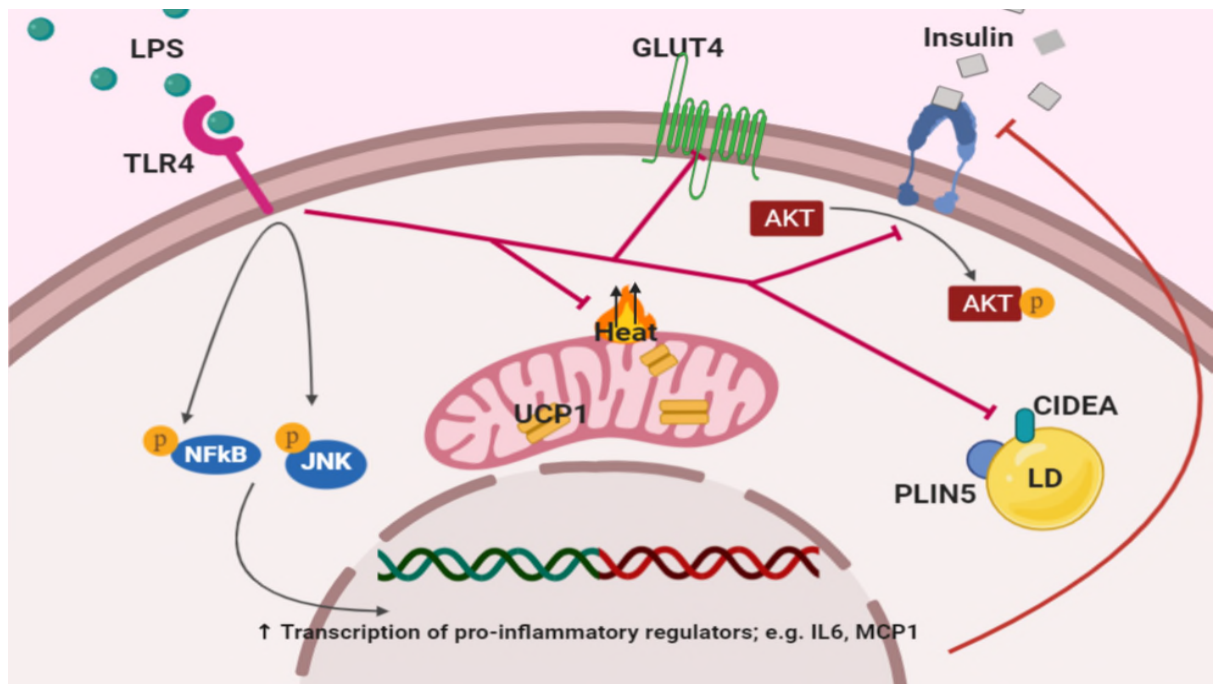


Figure 3.4.1 Schematic of Investigated LPS Actions in Brown Adipocytes.

LPS activation of TLR4 signal leads to activation of innate immune responses (including NFκB, JNK and subsequent pro-inflammatory cytokine secretion) and inhibition of insulin signal transduction, through AKT phosphorylation. Most importantly, LPS suppresses UCP1, the main thermogenic factor, and the expression of some other brown adipocyte markers (e.g., ELOVL3, PLIN5 and Cidea).

Taken together, this chapter supports findings by previous investigations which demonstrate that a role of selected PRR activation in inducing inflammation and downregulation of UCP1 expression in brown adipocytes. Here, these data were further expanded and established novel findings to indicate that activation of the LPS-TLR4 pathway induces a pro-inflammatory response via TLR4, leading to suppression of insulin sensitivity, attenuated UCP1 expression, and expression of other key markers of brown adipocytes (e.g., ELOVL3 and CIDEA) as well as increased lipid accumulation in brown adipocytes in culture. Figure 3.4.1 summarises the findings of this chapter outlining the mechanism of how LPS impacts the function of BAT cells. These results suggest that LPS-mediated inflammation in brown adipocytes may be a potential target to modulate BAT function for obesity treatment and prevention.

This chapter has highlighted that identifying the wider effect of LPS on brown adipocytes is important to design strategies that target individual cytokine/chemokines to reverse brown adipocyte cellular dysfunction. Such strategies could enhance the functions of brown adipocytes, which the next chapter explores in further detail.

**Chapter 4. The Effect of Lipopolysaccharide (LPS) on
Brown Adipocyte Whole Transcriptome and Cytokine
Secretion through TLR4**

4.1 Introduction

4.1.1 Brown Adipose Tissue (BAT) Is a Secretory Organ

The secretory role of BAT has received little attention in comparison to other functions such as the activity of mitochondria, influence of fatty acids in heat generation, as well as thermogenesis as means to transfer energy from food into heat. However, in recent years, growing evidence suggests that brown adipocytes and BAT have an active secretory role, which could contribute to improving systemic health. This reflects the capability of BAT to act as an endocrine organ by producing hormones which can communicate to distal tissues as well as mediating autocrine and paracrine effects. Additionally, experimental evidence from BAT transplantation indicates that BAT has systemic effects by secreting bioactive regulatory molecules with hormonal actions which could reverse metabolic abnormalities in high-fat diet-induced obese, insulin-resistant mice (384,577–579).

BAT can release many factors that contribute to autocrine, paracrine and endocrine functions and may be required for intercellular communications in obesity and related disorders. Most of these factors modulate hypertrophy and hyperplasia of BAT as well as innervation and angiogenesis processes that are all associated with BAT recruitment when thermogenesis is activated (80). Most reports of BAT secreted factors have focused on cells other than brown adipocytes as the source, whilst it has been identified that such cells secrete: fibroblast growth factor 21 (FGF21), neuregulin-4 (NRG4), and angiogenic factors (80,277,542); although the full specific secretory profile of brown adipocytes is yet to be identified.

4.1.2 Thermogenesis; Regulation and Role of Secreted Factors

Thermogenesis is heat production by burning calories and it is necessary for warm-blooded species (86). It also can be obligatory or adaptive to ensure normal performance in coping with different environmental conditions and challenges (86). Obligatory thermogenesis happens when heat is produced by obligate metabolic processes for the basic functioning of the organism (86). Adaptive thermogenesis can be classified as shivering (mainly in muscles) and non-shivering and is a controlled process for stimulating heat production (75). Non-shivering thermogenesis is the unique function in brown and beige adipose tissue and is mainly controlled by the

sympathetic nervous system via norepinephrine secretion in response to cold or dietary stimuli (75,89,93). The key element for non-shivering thermogenesis is the mitochondrial uncoupling protein 1 (UCP1). It is located in the inner membrane of mitochondria, particularly in brown adipocytes and beige adipocytes (75,93). Activation of UCP1 and thermogenesis in these adipocytes leads to an increase in calorie combustion and is expected to improve overweight conditions, providing a potential mechanism for treating obesity and its associated metabolic disorders (90). In activated thermogenesis, UCP1 functions to dissipate the mitochondrial membrane potential leading to uncoupling of oxidative phosphorylation from ATP synthesis. That is because it increases the proton permeability in the oxidative respiratory chain so that the protons pumped in the intermembrane area stay in the mitochondrial matrix. Therefore, the proton flux cannot reach the ATP synthase machinery leading to heat generation instead of ATP synthesis (96,100). This mechanism and therefore nutrient consumption can be protracted at a higher rate and independently of ATP saturating concentration.

On the molecular level, UCP1 is classically controlled by β -adrenergic receptors (β -ARs) which are located on the cell membrane, coupled with $G_{\alpha s}$ -proteins. The β 3-adrenergic receptors are expressed at higher levels on adipocytes and fat tissue than other type of cells and tissues (75). As the diagram in Figure 4.3.5.1 explains: under stimuli, such as cold exposure or overfeeding, norepinephrine is released by the SNS, and binds to the β -AR. This leads to a conformational change in the receptor and with a resultant activation of the coupled G protein and Adenylate Cyclase (AC); The $G_{\alpha s}$ subunit of the coupled G protein activates the AC by replacing guanosine diphosphate (GDP) with guanosine triphosphate (GTP) and dissociates from the $G\beta\gamma$ subunits. Activation of AC causes a raise in cAMP and PKA activation. PKA then stimulates lipid catabolism processes by phosphorylating both lipolysis agents on lipid droplets: protein perilipin 1A (PLIN1) and the Hormone-Sensitive Lipase (HSL), which in turn converts triacylglycerol into free fatty acids (FFAs) activating UCP1 and thermogenesis. FFAs level appears to be critical for thermogenesis which activates FFAs entry to the mitochondria. Acyl-CoA synthetase (ACS) mediates the conversion of FFAs to acyl-CoA and specifically directs them towards the mitochondrial matrix to undergo fatty acid oxidation (FAO) via the carnitine palmitoyl transferase1 (CPT1) system. FAO is thought to be a major contribution to thermogenesis. CPT-1 β is

considered to be responsible for a trans-esterification reaction of the fatty acyl CoA to form acylcarnitine in brown adipocytes. The carnitine/acylcarnitine translocase (CACT) transports the acylcarnitines into the mitochondrial matrix where CPT-2 reconverts the acyl carnitine into acyl-CoA which are then transferred into the mitochondrial inner membrane space and β -oxidized and enter the tricarboxylic acid cycle (TCA-cycle). This generates nicotinamide adenine dinucleotide (NAD) + hydrogen (H) (NADH) and flavin adenine dinucleotide + H (FADH) which transfer the electrons to the electron transport chain allowing the proton pumps to create the proton gradient for ATP production or thermogenesis (112).

In brown adipocytes, PKA phosphorylates transcription factors including cAMP response element binding protein (CREB). CREB directly activate UCP1 expression or indirectly by upregulating PR domain containing 16 (PRDM16) or zinc finger protein 516 (Zfp516) (72,580). In addition, activation of protein kinase A (PKA) following β -adrenergic stimulation, leads to p38 mitogen-activated protein kinase (MAPK) activation and induces brown adipocytes to become a source of FGF-21 through phosphorylation of activating transcription factor 2 (ATF2).

Thermogenesis in brown adipocytes is affected by environmental stimuli and regulated by multiple factors secreted by other organs or by BAT and brown adipocytes themselves. These factors can modulate different levels along the thermogenesis pathway. For instance, pro-inflammatory cytokine IL1 β reduces the cAMP-mediated induction of the UCP1 expression (320), cold-induced thermogenesis in adipocytes *in vivo* via sirtuin-1 inhibition (SIRT1) (355), and WAT browning (356). Another example is FGF21, a brown adipokine and key factor in the regulation of energy homeostasis that regulates PGC1 α and browning of white adipose tissues in adaptive thermogenesis (154).

Identification of the molecular actions of different factors on the thermogenesis pathway is important as these factors could modulate BAT activity and hence contribute to the systemic consequences. This also forms an interesting aspect of obesity research as it could lead to the identification of novel brown fat factors to direct drug discovery approaches and ultimately improve metabolic health.

4.1.3 Extracellular Matrix (ECM) and Thermogenesis

Studies suggest activity of brown adipocytes is influenced by their microenvironment, which is determined by extracellular matrix (ECM) molecules. These molecules, including collagens and fibronectin, are non-cellular components of tissues, provide mechanical support and mediate various signalling pathways (581,582). The main components of the ECM in adipose tissue are collagen (type I, IV, and VI), laminin (LN1,8), fibronectin (FN), hyaluronan, and proteoglycan (583). Also, the ECM is able to interact with transmembrane receptors such as integrins and play significant roles in many important biological processes such as adhesion, migration, cell motility, cell proliferation and differentiation, and regulation of gene expression (582).

The communication between adipocytes and their environment increases during the inflammatory responses, possibly leading to adipose tissue fibrosis. While often fibrosis is thought to occur following an injury, in adipose tissue an inflammatory cascade triggered by changes in metabolism such as in obesity initiates the maladaptive fibrotic repair process fibrosis impairs adipocyte plasticity and is closely associated with obesity and insulin resistance (271,584). Also, abnormal ECM remodelling in WAT is identified to accompany the development of obesity (585,586). ECM remodelling suppression contributes to improved systemic insulin sensitivity through the activation of AMPK and inhibition of transforming growth factor- β (TGF- β)/Smad3 signalling (587). Interestingly, microfibril-associated glycoprotein 1 (MAGP1), a component of ECM microfibrils, is protective against the effects of metabolic stress of TGF- β , and its absence predisposes to metabolic dysfunction. MAGP1 prevents TGF- β negative effects on PPAR-and PRDM-16-related activation of PGC-1 α as well as UCP1 transcription and thus on thermogenesis (588). Moreover, the overexpression of collagen VI (a cleaved fragment of the α -3 chain of collagen VI (Col6a3)), named endotrophin, in mice stimulates fibrotic collagen deposition in WAT and BAT and triggers adipose inflammation and insulin resistance, while genetic knockout mice exhibit symptoms of systemic metabolic dysfunction when fed a high-fat diet (267,276). In addition, a peptide derived from collagen alpha-1 (III) chain (CO3A1) is found to significantly increase UCP1 and PGC-1 α gene expression levels (589). Finally, the capacity to generate brown adipocytes from bone marrow-derived mesenchymal stem cells (bmMSCs) appears to be dependent on the microenvironment

which is dimensionally shaped by ECM molecules, where collagen IV mediates higher UCP1 expression and thus higher thermogenic activity (590). All these discoveries highlight the vital function of ECM in modulating metabolic homeostasis and adipose tissue functions.

4.1.4 Additional Effects of LPS on Brown Adipocyte Activity

The previous chapter identified a TLR mediated reduction of brown adipocyte function by LPS. Whilst the impact of LPS on thermogenesis, the main characteristic of the brown phenotype, is also likely to influence wider aspects of brown adipocyte biology. This may involve other brown adipocyte cellular components (*e.g.* immune, inflammatory, endothelial and other factors), whose interaction and activity could directly or indirectly affect meeting thermogenic demands. However, little is currently known about brown fat cellular responses in the inflammatory state, including the response to inflammatory stimulus such as LPS and what various released factors are modulated. There is meanwhile evidence to suggest that high-fat diet leads to upregulation of gene expression of inflammatory and immune markers in BAT (312,340). Also, current evidence demonstrates secretion of IL6, MCP1, TNF α and Rantes from brown adipocytes in response to activation of pattern recognition receptors (344). However, it is not known what other factors are affected within BAT and specifically within brown adipocytes under the inflammatory state.

4.1.5 The Importance of Identifying Novel Factors Secreted from Brown Adipocytes and the Wide Influence of LPS on Brown Adipocytes

The identification of BAT-adipokines or Batokines in addition to providing basic information regarding physiology and metabolism, might allow the discovery of circulating BAT biomarkers. Also, profiling the modulated secreted factors in response to LPS and exploring the role of TLR4 in mediating such effect might direct drug discovery approaches. That is critical for developing safe therapeutic strategy to manage obesity and its associated chronic metabolic diseases such as T2DM and/or dyslipidaemia.

Therefore, the aim of this chapter was to investigate the wider range of *in vitro* LPS effects by:

- Identifying new factors secreted by brown adipocytes
- Identifying LPS-induced changes in gene expression levels and secreted factors in brown adipocytes.
- Investigating the role of TLR4 in mediating LPS effects in brown adipocytes

Subsequently, sequencing (mRNA gene analysis) was performed to explore the differences in gene expression upon LPS treatment in differentiated (mature) brown adipocytes (wild type: wt.BAT). mRNA sequencing was also performed on TLR4 knockout brown adipocytes (TLR4ko.BAT) to investigate the TLR4 deletion effect on the LPS-response and the potential LPS effects not mediated through TLR4 receptors in brown adipocytes. Furthermore, detection of an array of secreted cytokines was also performed on brown adipocytes to explore extracellular signalling molecules that are modulated by LPS treatment and might mediate cell to cell communication and many other biological processes.

4.2 Methods

4.2.1 Mouse Adipocyte Cell Lines Differentiation

Mouse brown adipocytes WT and TLR4 KO were seeded in 6-well plates and differentiated with or without LPS as described in the method's chapter (Chapter 2).

4.2.2 RNA Isolation, Purification and Quantification

Medium was removed and cells were washed with PBS, lysed in 1 mL of TRI reagent® and transferred into RNase-free tubes. Samples were incubated at room temperature (RT) for 5 minutes to allow the complete dissociation of the nucleoprotein complex. Extraction was performed immediately or samples were stored at -80 °C. Chloroform (0.2 mL, TRI reagent®:Chloroform 5:1 v/v) was added and samples were vigorously shaken for 15 seconds, incubated at RT for 5 minutes and centrifuged at 12,000 x g for 30 minutes at 4 °C. The upper aqueous phase was transferred into a new RNase-free tube and extraction was continued using a silica column-based isolation method (ISOLATE II RNA Mini Kit #BIO-52071, Bioline) according to manufacturer's instructions. Briefly, RNA was bound to the column, then DNA was digested. Hereafter, the silica membrane was washed and dried. Finally, RNA was eluted in 20 µL RNase-free water. Samples (1 µL) were then quantified in duplicate using a spectrophotometer (Nanodrop ND-1000, labtech) at 260 nm absorbency.

4.2.3 Quality Control Measurements and Sequencing

Eluted RNA (4 µL) for each sample were sent to the Genomics Research Facility at the School of Life Sciences, The University of Warwick. At the Genomics lab, the RNA integrity of each sample was tested using Agilent 2100 Bioanalyser (RNA Nano (5-500 ng/µL)-Chip service). Samples with sharp 28S and 18S peaks, 28S/18S rRNA ratio above 0.9 and RNA Integrity Number (RIN) above 7.5 were deemed suitable to be sent for sequencing (Supplementary Table 4.1). At least 2 µg of RNA were sent to BGI Tech Solutions Co. Limited (Hong Kong) for sequencing. Sequencing was done by looking at the transcriptome (mRNA) changes, using Poly (T) oligo-attached magnetic beads to purified Poly (A)-containing mRNA molecules from total RNA. The reads were 20 M PE100, so 4 Gb data per sample.

4.2.4 Cell Culture Supernatant Collection

Differentiated adipocytes in each well of 6-well plates were incubated in 1 mL of serum-free media for 24 hours prior to the assay. Media was collected from each well and particulates were removed by centrifugation at 3,000 x g for 10 minutes at 4 °C. The assay was performed immediately or samples were aliquoted and stored at -80 °C.

4.2.5 Array Determination of Secreted Mouse Cytokines

Secreted mouse cytokines were determined using the Proteome Profiler Array, Mouse XL Cytokine Array Kit (#ARY028, R&D systems) according to manufacturer's instructions to screen for the presence of 111 different cytokines in the media of mature mice brown adipocytes treated with or without LPS. Briefly, membranes were blocked, then incubated with samples overnight at 4 °C on a rocking platform shaker. Hereafter, membranes were washed and incubated with Detection Antibody Cocktail for 1 hour at room temperature on a rocking platform shaker. Streptavidin-HRP was then added into each sample and incubated for 30 minutes at room temperature. Finally, Chemi Reagent Mix was evenly added onto each membrane for 1 minute to visualise cytokines of interest (dots) and detected using automated chemiluminescence digital imaging (Syngene's GeneSys). Densitometry was conducted using ImageQuantLAS 4000 Software (GE Healthcare, UK).

4.2.6 RNA Sequence Analysis

Data analysis was carried out with the assistance of Dr. Nigel Dyer (University of Warwick) and Dr. Mohammad Tauqeer Alam (University of Warwick).

- Principal Component Analysis (PCA) was performed prior to differential expression analysis to evaluate variation among the samples. Briefly, PCA is a method used to reduce the dimension of large data sets by considering only those variables that inflict large variance to the data. The component accounting for the largest variation is plotted along the X-axis; the second largest is plotted on the Y-axis etc. If samples present pronounced differences in terms of unique biological characteristic, for instance cell type or level of differentiation, this will be a primary component of variance. Each sample will scatter in different areas of the PCA plot corresponding to their biology eventually clustering with samples presenting similarity for that

characteristic. This method is particularly useful to assess the quality of the samples and therefore the reliability of the results that can be obtained by their analysis for a specific experiment. For instance, if RNA quality inflicts further variation to the samples, these will no longer cluster based on their biology and can be removed from the data analysis. PCA analysis was performed using 'prcomp' function in R and in the PCA plot the first two principal components (PC), capturing the maximum variation in the data, were plotted in X and Y axis respectively.

- mRNA sequencing technology targets all polyadenylated (poly-A) transcripts of the transcriptome and allows identification of either known or unknown genes and their eventual novel splicing isoforms expressed in the system analysed. For the purpose of this study we compared gene expression of total RNA between LPS treated differentiated brown adipocytes and non-treated differentiated brown adipocytes. Both WT and TLR4ko differentiated cells were used. The sequencing was performed using BGI Tech Solutions Co., Ltd.
- The raw fastq sequencing data were aligned to the mouse genome (Mus_musculus.GRCm38.84) using STAR aligner ("STAR --readFilesCommand zcat --runThreadN 16 --genomeDir Mus_musculus.GRCm38.84 --readFilesIn my_sample_1.fq.gz my_sample_2.fq.gz --outFileNamePrefix my_bamfile.bam --outSAMtype BAM SortedByCoordinate"). The aligned bam files were used to produce the readcount data using htseq-count tool ("htseq-count -f bam -s reverse -i gene_id -m intersection-nonempty my_bamfile.bam Mus_musculus.GRCm38.84.gtf >my_countfile.txt"). The read count data were further analysed with background correction and normalization by DESeq2 package in R in order to obtain the list of differentially expressed genes (DEGs) in LPS treated samples with reference to the controls for both cell lines. Wald test was used for differential expression analysis and we used adjusted p-value (padj) <0.05 as a threshold.
- Volcano plots R package was used. The base 2 log of the fold change was plotted against the adjusted p value as calculated by DESeq2 using the default "BH" option. This builds on a standard R function for adjusting P values which is documented here: <https://stat.ethz.ch/R-manual/R-devel/library/stats/html/p.adjust.html>.
- Scatter X-y plots were produced using R package. The base 2 log of the average gene expression for each gene of the control and LPS-treated samples was plotted against

each other. Points associated with genes where the adjusted p value is less than 0.05 are marked in red. p values and adjusted p values were calculated by DESeq2 as for volcano plots (see above).

- Gene ontology (GO) analysis, to perform this analysis: Top 500 up/down regulated DEGs ensemblID mRNA accession numbers with adjusted p-value < 0.05 were submitted separately to DAVID Bioinformatics Resources 6.8 (Database for Annotation, Visualization and Integrated Discovery) for separate analysis of functional classification (591). The output GO terms were used for interrelationship analysis and or visualized as a scatter plot or interactive graph using REViGO. Only GO terms with adjusted P < 0.05 were plotted (Benjamini)(592).

- Heatmaps were produced after preparing gene of interest lists. The lists were submitted with normalized gene expression values to heatmapper online tool:

<http://www2.heatmapper.ca/expression/>

Average Linkage was used as clustering Method was and Pearson as Distance Measurement Method. Rows represent the different genes and each column represents a sample. The clustering tree is shown on the left. For the relative gene expression level of each sample a different colour of the red-green scale is assigned. Red represents an expression level below the mean, green colour represents expression above the mean (593).

- KEGG Pathways analysis hierarchical clustering tree of KEGG pathways was produced by ShinyGO online tool <http://bioinformatics.sdstate.edu/go/> by separately submitting a list of up or downregulated genes with adjusted p-value < 0.05 for wt.BAT or TLR4ko.BAT (594). In this hierarchical clustering tree, related KEGG terms are grouped together based on how many genes they share. The size of the solid circle corresponds to the enrichment FDR.

KEGG Pathways analysis were visualized using Pathview online tool <https://pathview.uncc.edu/home>. Mouse was selected as the species, the pathway to be looked at was checked, and the type of gene identifier which was identified as ensemblID. The lists of up/downregulated genes with adjusted P < 0.05 were submitted (595).

4.3 Results

RNA-Sequencing results

4.3.1 Principal Component Analysis

In order to test the hypothesis that *in vitro* LPS administration directly drives a wide range of transcriptional changes in brown adipocytes through TLR4 and to identify new secreted factors by brown adipocytes, RNA-sequence was performed. For this purpose, imBAT cells were treated with LPS (100 ng/mL). The first step of the RNA analysis was to examine variation among samples. In Figure 4.3.1.1 below the Principal component analysis (PCA) plots were performed on mRNA sequencing normalized gene data for wt.BAT (Panel A) and for TLR4ko.BAT (Panel B) data.

As shown in Figure 4.3.1.1, A, in wt.BAT, where PC1 corresponds to the largest variation (91 %), the samples clustered so that untreated mature brown adipocytes (control) grouped on the left side (red dots) and the LPS-treated mature brown adipocytes (blue dots) on the right side. This is a preliminary indicator that LPS-treated wt.brown adipocytes have clearly different gene expression profiles, reflecting the biological influence of LPS treatment. PC2 reveals a 3 % variation among samples for mRNA sequencing of wt.BAT, which might be due to secondary factors such as quality of RNA. In addition, in TLR4ko.BAT, PC1 explains only 47 % of variation while PC2 explains 19 % of the variation among samples for mRNA sequencing of TLR4ko.BAT data (Figure 4.3.1.1, B). This is an early indication of differences between LPS effects on wt.BAT and TLR4ko.BAT.

In conclusion, the PCAs revealed the high quality of the data obtained by the mRNA sequencing, so that all samples were included for statistical and integrative data analysis.

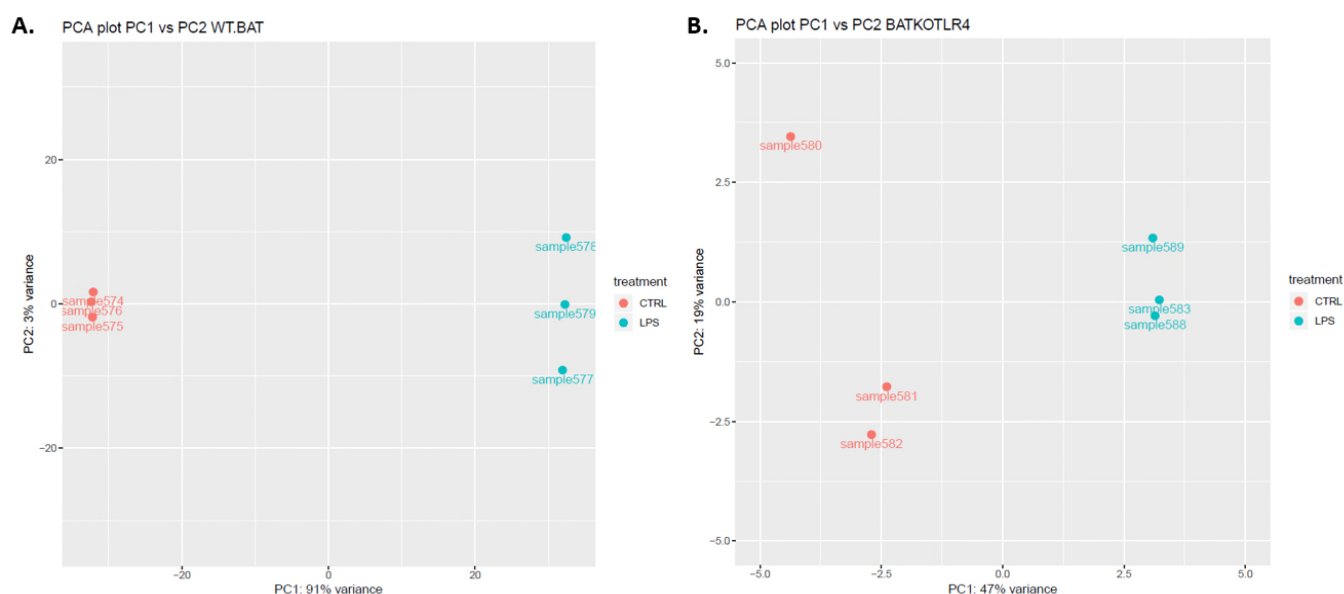


Figure 4.3.1.1 PCA Plots of mRNA Sequencing Analysis.

(A) PCA plot for wt.brown adipocytes on the basis of mRNA sequencing read count data. The PCA was performed on all samples and all expressed genes revealing the distribution of samples according to LPS-treatment (PC1) and variation among samples (PC2). PC1 explains 91 % of the variation and PC2 explains 3 % of the variation. (B) PCA plot for TLR4ko.brown adipocytes on the basis of mRNA sequencing read count data. The PCA was performed on all samples and all genes. PC1 explains 47 % of the variation and PC2 explains 19 % of the variation.

4.3.2 Differential Gene Expression Profiling Was Impacted by LPS

For the purpose of this study differentially expressed genes (DEGs) between Control and LPS-treated mature brown adipocytes were determined. The volcano plot in (Figure 4.3.2.1, A, C), shows that there are much bigger fold changes seen when wild type (wt) cells are treated with LPS than the TLR4-knockout (ko) cells. In this context, as shown in the plot (Figure 4.3.2.1, C), for TLR4 knockout cells there are no genes presenting a log2fold change lower than -1 and higher than +1 with an adjusted P-value lower or equal to 0.05. In addition, x-y plots (Figure 4.3.2.1, B, D) illustrate the magnitude of the gene expression for both control and LPS-treated adipocytes as pairs. At adjusted p value lower or equal to 0.05, there are 6911 genes with a significantly changed expression (red dots) for wt cells, while there are 684 genes with a significantly changed expression (red dots) for TLR4 knockout cells. Once more, the changes in the expression were notably higher in WT cells. As a result, both the volcano plots and the x-y plots show in different ways that upon LPS treatment, there

is a big difference in the number of genes where the change in expression is considered to be significant between wt.BAT and TLR4ko.BAT.

Finally, 3485 genes were identified as significantly upregulated upon LPS-treatment and 3127 genes are significantly downregulated upon LPS-treatment in mature wt.BAT. In addition, in mature TLR4ko.BAT upon LPS-treatment, 175 genes were significantly upregulated and 210 genes were significantly downregulated. This shows that ablating TLR4 largely blocked the LPS effect in brown adipocytes as only 4.3 % (151 genes) upregulated in wt.cells, were also upregulated in TLR4ko.cells and only 6.7 % (148 genes) were downregulated in wt.cells as well as TLR4ko.cells. (Figure 4.3.2.2)

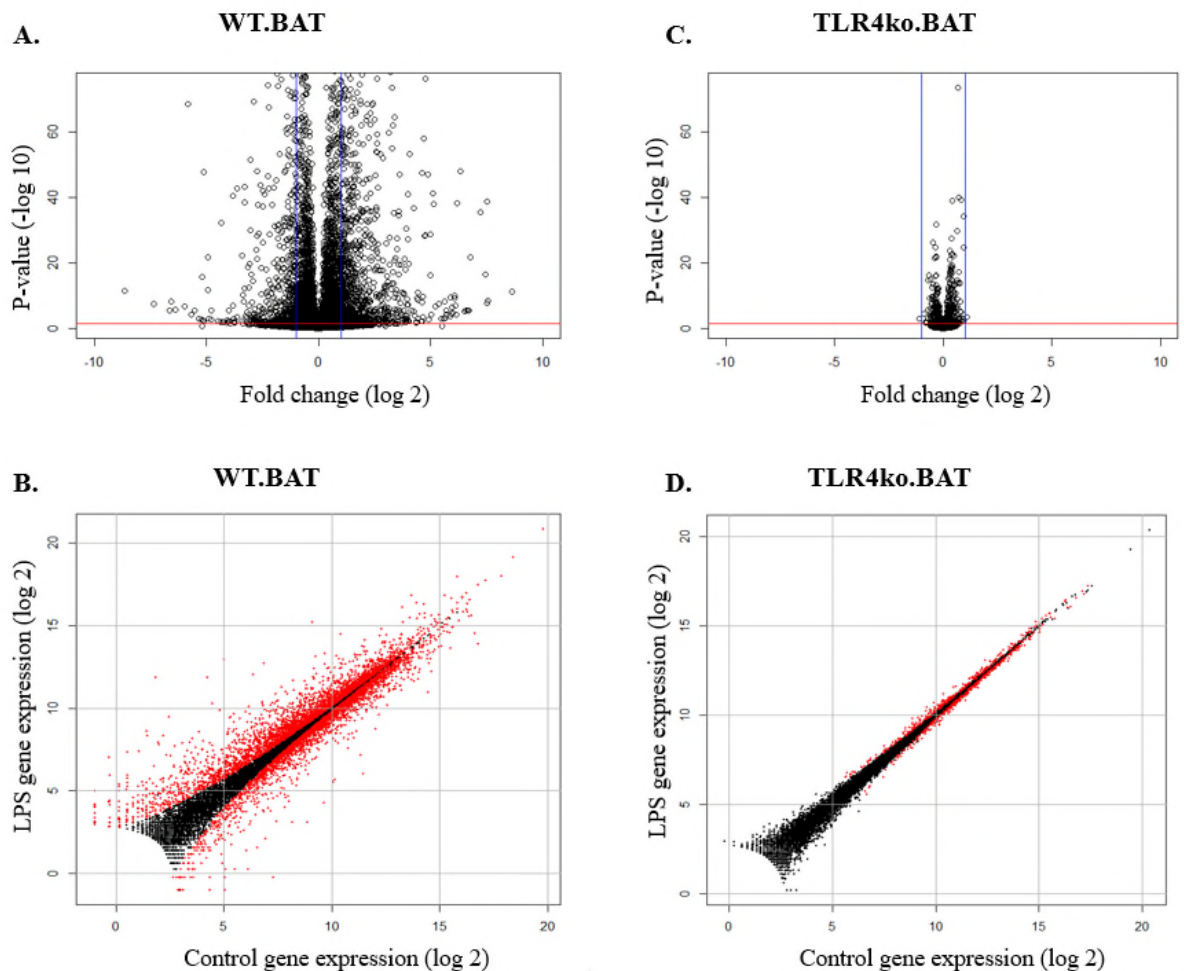


Figure 4.3.2.1 Genes Differentially Expressed between Control and LPS-Treated Brown Adipocytes (A,B: wt Brown Adipocytes), (C,D: TLR4 Ko Brown Adipocytes).

A, C: volcano plots are generated using log2 fold-change against $-\log_{10}$ (p-value) displaying the distribution of differentially expressed genes. The red line shows where $p = 0.05$ with points above the line having $p < 0.05$ and points below the line having $p > 0.05$. Vertical blue line is at fold-change equal absolute 2 ($\log_2 = 1$). B, D scatter x-y plots pairwise comparison of the gene expression levels of control vs LPS-treated brown adipocytes. The red dots are genes where the change in expression is considered significant. Both graphs are showing in different ways a confirmation of much less change in expression as a result of LPS treatment in TLR4 ko cells compared to control.

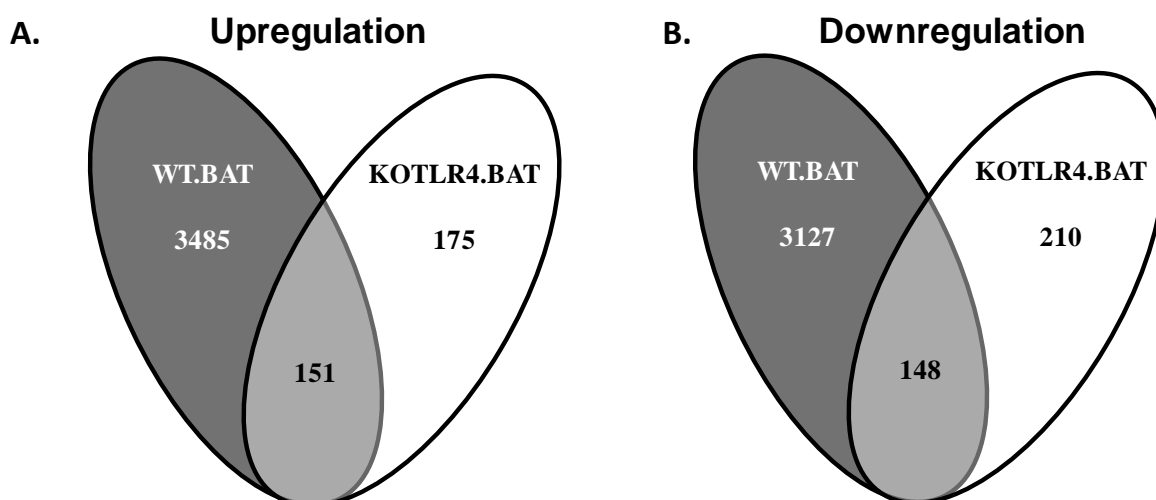


Figure 4.3.2.2 Venn Diagram.

Comparing genes being up/downregulated in LPS-treated cells compared to control cells of WT.BAT with genes being up/downregulated in LPS-treated cells compared to control cells of TLR4ko.BAT . A. Summarizing number of upregulated genes with WT.BAT and TLR4ko.BAT. B. Summarizing number of downregulated genes with WT.BAT and TLR4ko.BAT.

In order to analyse the general profiling, heatmaps (Figure 4.3.2.3, Figure 4.3.2.4) and tables in appendix (supplementary Tables 4.2, Table 4.3) of top up/down regulated genes were created to demonstrate the major changes occurring in response to LPS.

A brief examination of the most affected genes in wt.BAT (Figure 4.3.2.3) clearly shows inflammatory mediators upregulated including C-X-C motif chemokine ligand 5 (CXCL5/ LIX), TNF superfamily member 11 (Tnfsf11), decorin (Dcn) and NLR family pyrin domain containing 2 (Nlrp2). In contrast, UCP1, the key thermogenesis gene is downregulated. In addition, fatty acid metabolic process (Acot11), lipid catabolic process (Aspg) and solute carrier family 40 member 1 (Slc40a1) are among the top 50 downregulated genes in response to LPS. These genes are beige/ brown markers reported to be enriched in BAT and induced after cold acclimatization in WAT (162,163). This clearly confirms the profound changes that occur with LPS treatment in relation to the main characteristic genes of brown adipocytes and hence full pathways analysis was later performed.

In comparison with the most affected genes in TLR4ko.BAT (Figure 4.3.2.4), neither UCP1 nor any other well-characterised brown fat gene markers were identified in the down-regulated genes. Also in TLR4ko.BAT, it was observed that some of the up-regulated genes were related to negative regulation of inflammatory response such as immediate early response 3 (Ier3), 5' nucleotidase, ecto (Nt5e) and free fatty acid

receptor 4 (Ffar4), whilst top downregulated genes where related to inflammatory and immunity response such as chemokine (C-X-C motif) ligand 9 (CXCL 9), Sp110 nuclear body protein (Sp110) and interferon inducible GTPase 1 (Iigp1).

WT.BAT Top 50 up-regulated & down-regulated genes

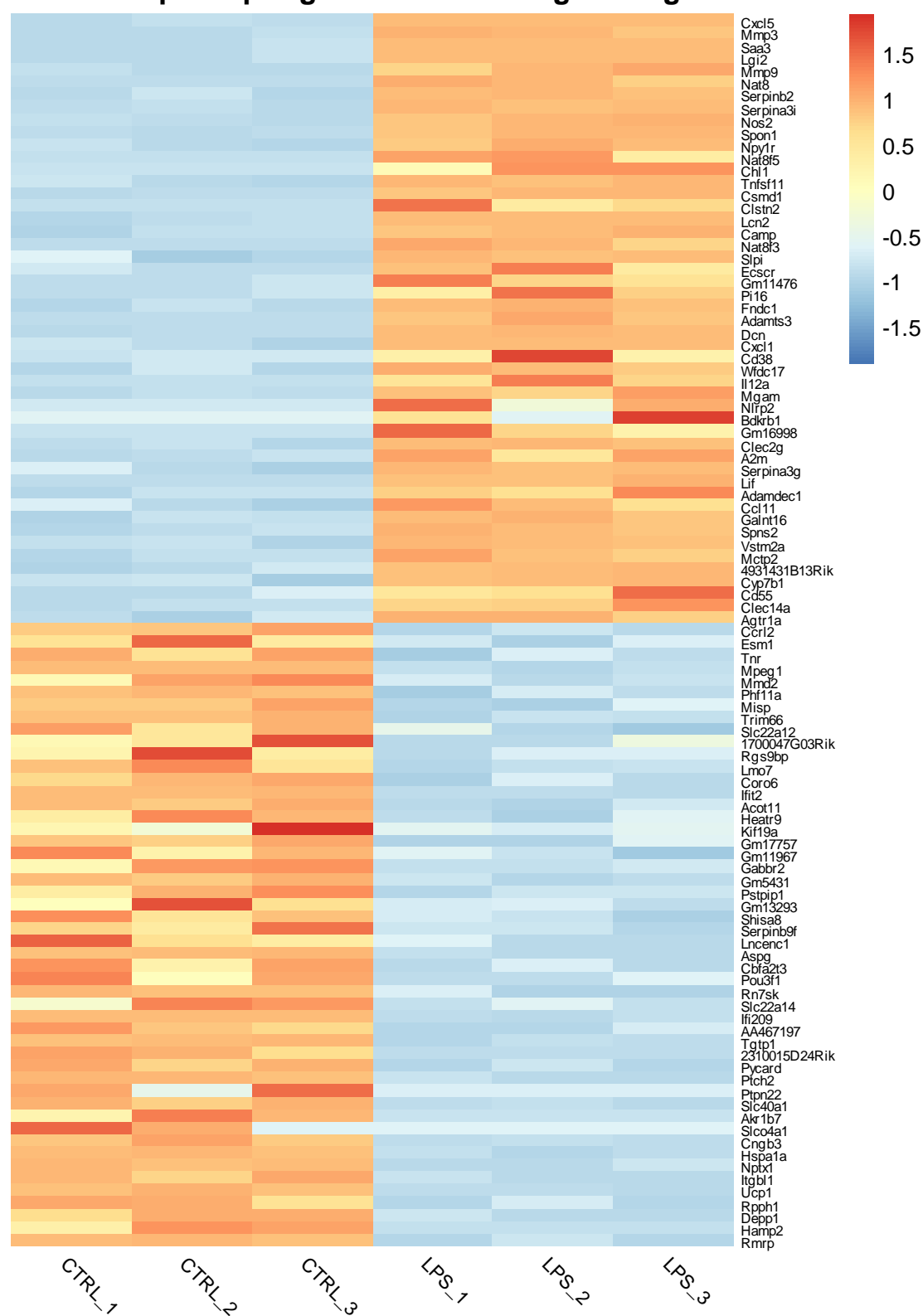


Figure 4.3.2.3 The Most 50 Regulated Genes in wt.BAT.

Rows represent the different genes and each column represents a sample. For the relative gene expression level of each sample a different colour of the red-blue scale is assigned. Red represents an expression level above the mean, blue colour represents expression below the mean

TLR4koBAT Top 50 Up-regulated & Down-regulated genes

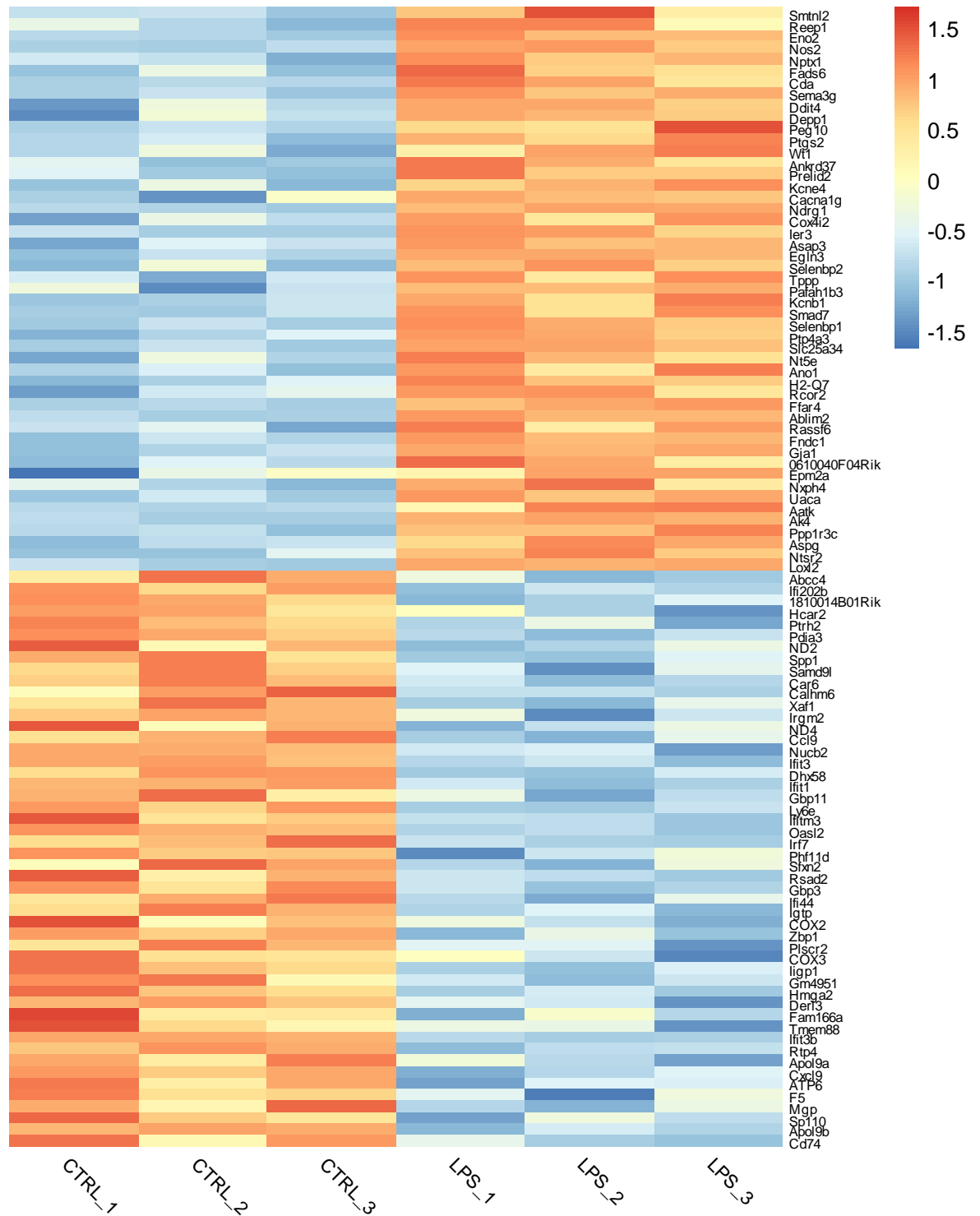


Figure 4.3.2.4 The Most 50 Regulated Genes in TLR4ko.BAT.

Rows represent the different genes and each column represents a sample. For the relative gene expression level of each sample a different colour of the red-blue scale is assigned. Red represents an expression level above the mean, blue colour represents expression below the mean.

The range of log2FoldChange was smaller compared to wt.BAT. This is a clear indication that TLR4 mediates most of the profound LPS actions in brown adipocytes.

4.3.3 LPS Influenced Metabolism and Immunity Related Gene Ontology (GO) Term Enrichment Analysis of DEGs of Brown Adipocytes

Statistically enriched terms gave insights into biological pathways that were likely to be highly active by comparing them to the frequency at which those GO terms appeared in the transcriptome. GO terms associated with the top 500 significant DEGs (upregulated/downregulated) for both wt.BAT and TLR4ko.BAT were identified. Resulting GO terms fall into three parts: BP: Biological Processes, CC: Cellular Component and MF: Molecular Function. REVIGO online tool is used to summarize GO categories. Both supplementary tables in appendix (supplementary table 4.4, supplementary table 4.5) and graphs (Figure 4.3.3.1, Figure 4.3.3.2, Figure 4.3.3.3, Figure 4.3.3.4) showed only significant GO categories ($P < 0.05$) after applying Benjamini multiple testing correction. In total, 52 GO terms are reported as statistically significant in the 'biological process' category. (supplementary table 4.4). Among the different GO terms of upregulated genes in this category, several enriched terms are compatible with the fact that LPS is an inflammatory agent. The identified biological process categories are related to molecular mechanisms associated with inflammation (response to cytokine, positive regulation of protein kinase B signalling); immune response (response to lipopolysaccharide, extracellular matrix organization), and stress response (response to hypoxia, response to mechanical stimulus). Other important biological processes mediated by upregulated genes are cell adhesion, angiogenesis and oxidation-reduction process (Figure 4.3.3.1, A). Molecular functions mediated by upregulated genes refer also to enhanced extracellular, inflammation and stress activation (Figure 4.3.3.1, B). Cellular component of the upregulated genes included various extracellular activity (Figure 4.3.3.1, C) All these GO terms are directly connected to events taking place during brown adipocyte inflammation.

GO terms associated with downregulated genes are enriched for various terms related to different categories of transcriptional regulation. Between these categories are interferon regulation, metabolic process, glucose metabolism and various mitochondrial function aspects (Figure 4.3.3.2, A, B, C). Approximately 25 GO terms

appear involved in mitochondrial activity in which genes within these categories were down-regulated.

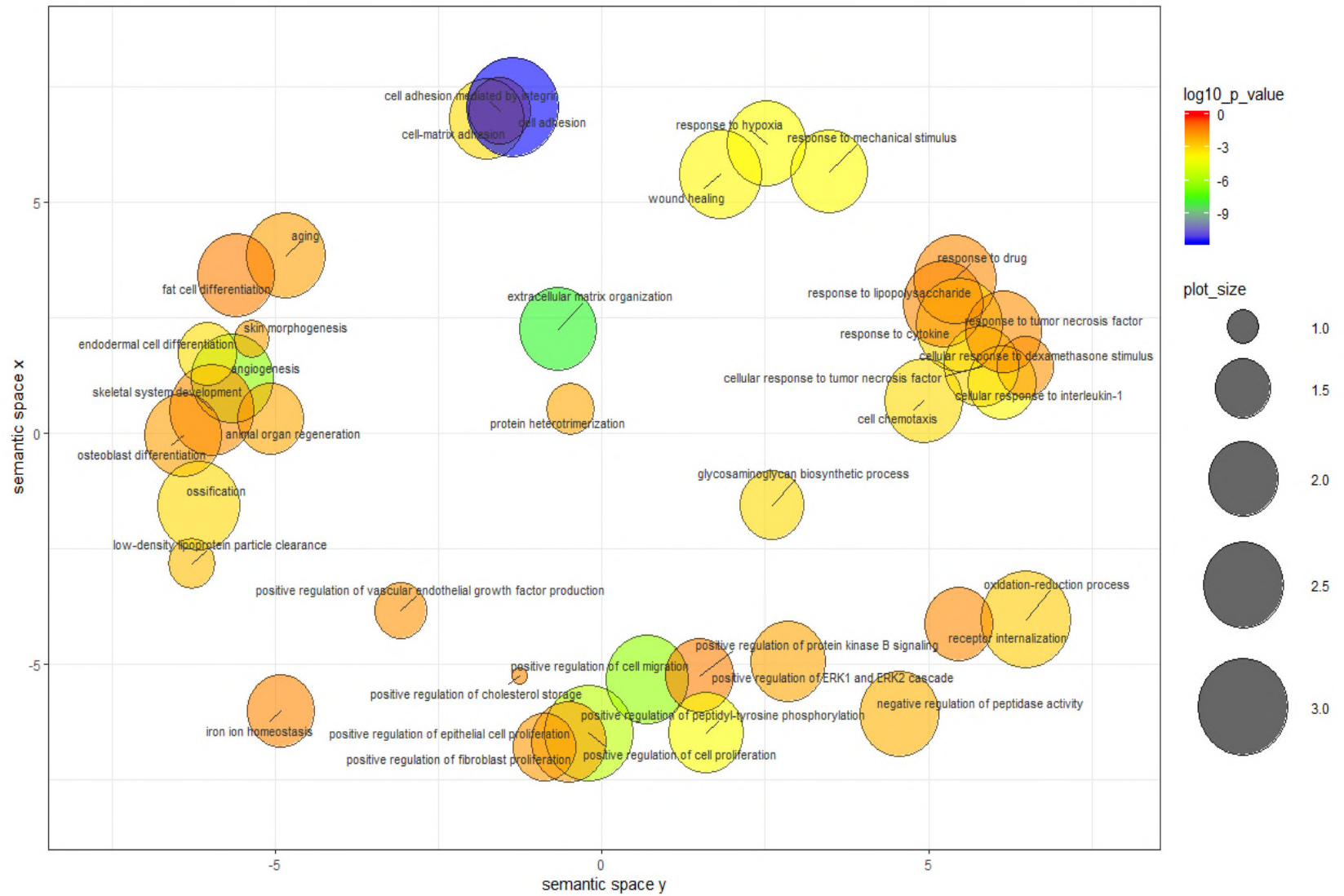
TLR4ko.BAT, when treated with LPS, was associated with upregulated genes related to GO categories of extracellular activity and down-regulated genes related to GO categories of immune response and mitochondrial function (Figure 4.3.3.3, Figure 4.3.3.4). However, this was to a much lesser extent compared to wt.BAT. This suggests that LPS exercises its effect on brown adipocytes mainly through TLR4, but it still appears to have some residual cellular effects in the absence of the TLR4 receptor.

These results indicate that the brown adipocytes when treated with LPS, differentially express genes involved in inflammation, immune response, glucose metabolism mediated by mitochondrial function and stress response related pathways. The findings are consistent with the inhibition of brown adipocytes activity by LPS treatment.

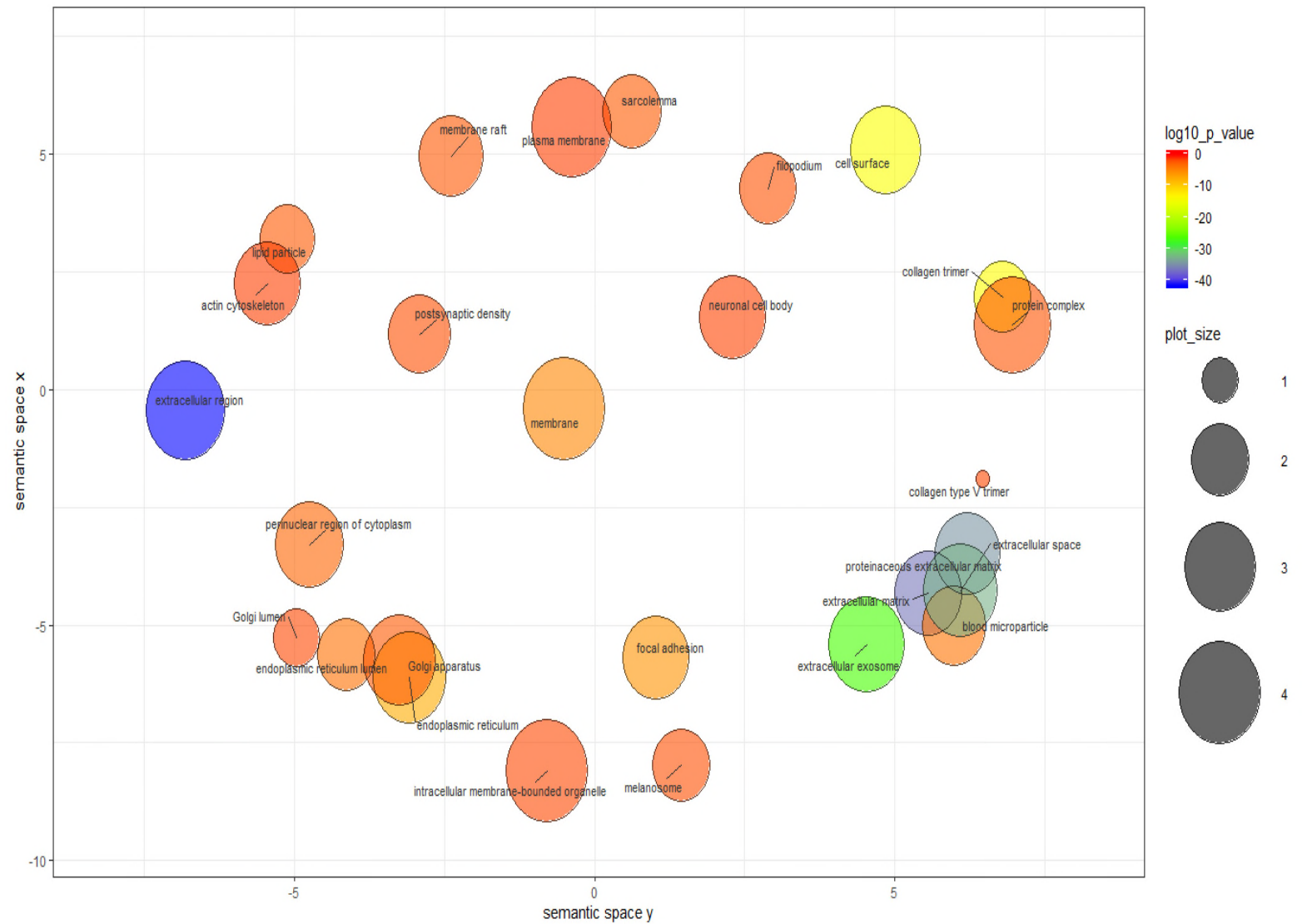
Figure 4.3.3.1 GO Enrichment Analyses Summarized and Visualized Using REVIGO Derived from Upregulated Genes in wt.BAT.

(A) Significantly enriched GO terms related to biological processes in wt.BAT vs. LPS treatment. (B) Significantly enriched GO terms related to cellular component in wt.BAT vs. LPS treatment. (C) Significantly enriched GO terms related to molecular function in wt.BAT vs. LPS treatment. GO terms are represented by circles and are clustered according to semantic similarities to other GO terms in the gene ontology (more general terms are represented by larger size circles, and adjoining circles are most closely related). Circle size indicates to the frequency of the GO term in the underlying GOA database (Barrell et al. 2009), whereas colour indicates the log10P-value for the enrichment derived from DAVID GO analysis (red higher, blue lower). Only significant GO terms with adjusted $P < 0.05$ following multiple testing correction (Benjamini) are plotted. Full data sets are available for Supplemental Table 4.4.

(A) WT.BAT Biological Process GO Associated with Top 500 Up Regulated Genes



(B) WT.BAT Cellular Component GO Associated with Top 500 Up-Regulated Genes



(C) WT.BAT Molecular Function GO Associated with Top 500 Up-Regulated Genes

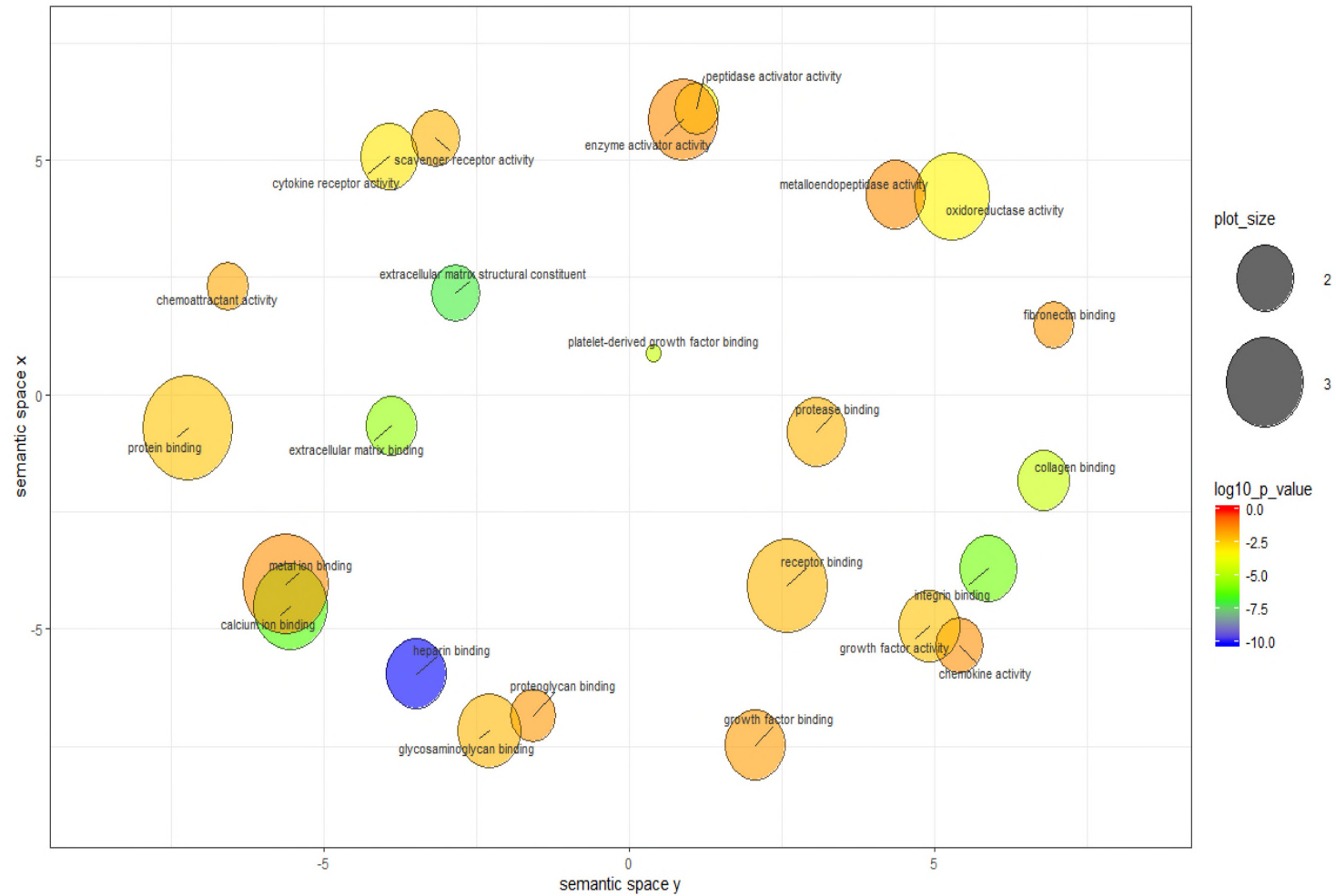
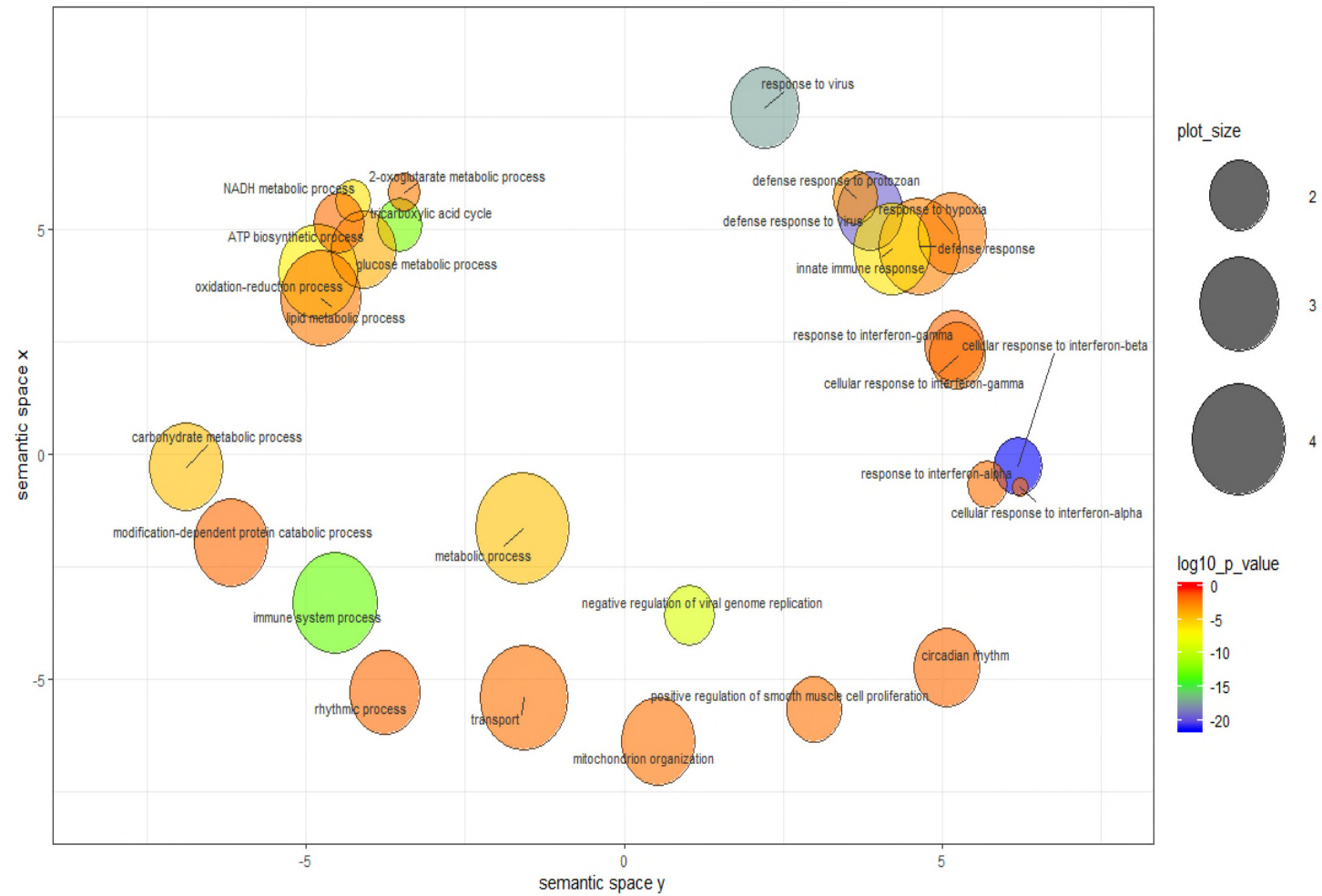


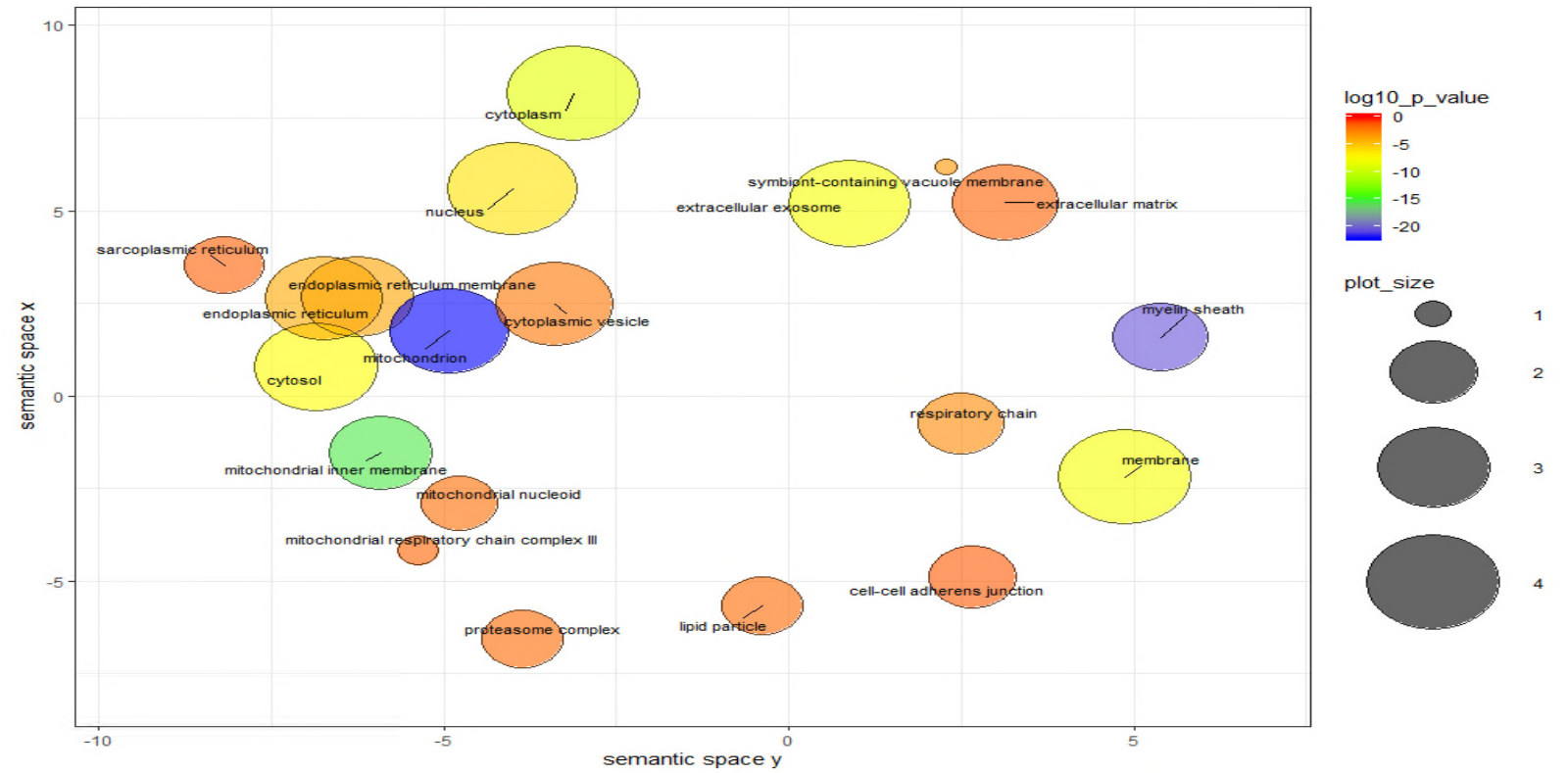
Figure 4.3.3.2 GO Enrichment Analyses Summarized and Visualized Using REVIGO Derived from Downregulated Genes in wt.BAT

(A) Significantly enriched GO terms related to biological processes in wt.BAT vs. LPS treatment. (B) Significantly enriched GO terms related to cellular component in wt.BAT vs. LPS treatment. (C) Significantly enriched GO terms related to molecular function in wt.BAT vs. LPS treatment. GO terms are represented by circles and are clustered according to semantic similarities to other GO terms in the gene ontology (more general terms are represented by larger size circles, and adjoining circles are most closely related). Circle size indicates to the frequency of the GO term in the underlying GOA database (Barrell et al. 2009), whereas colour indicates the log10P-value for the enrichment derived from DAVID GO analysis (red higher, blue lower). Only significant GO terms with adjusted $P < 0.05$ following multiple testing correction (Benjamini) are plotted. Full data sets are available for Supplemental Table 4.5

(A) WT.BAT Biological Process GO Associated with 500 down-Regulated Genes



(B) WT.BAT Cellular Component GO Associated with 500 Down-Regulated Genes



(C) WT.BAT Molecular Function GO Associated with 500 Down-Regulated Genes

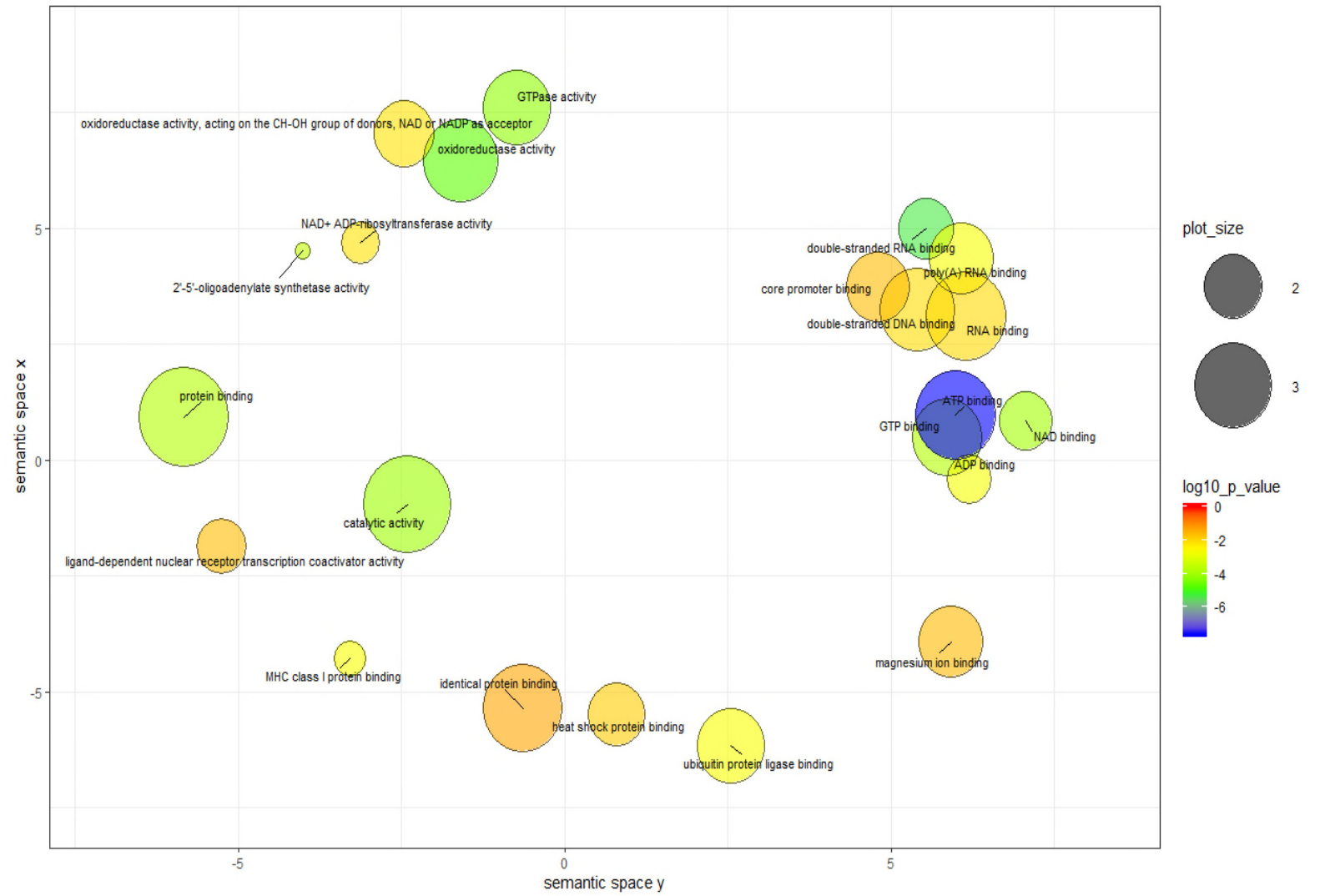
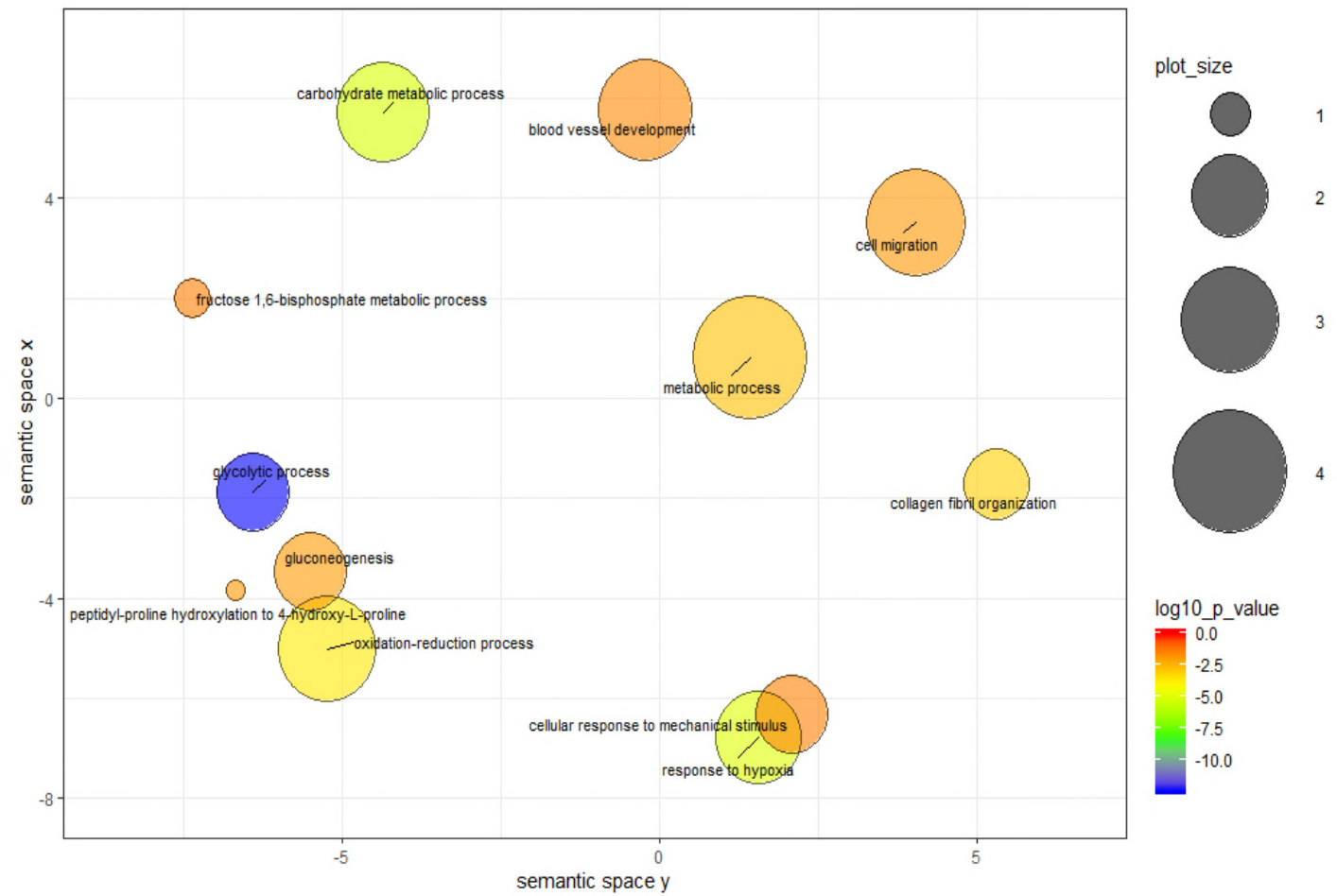


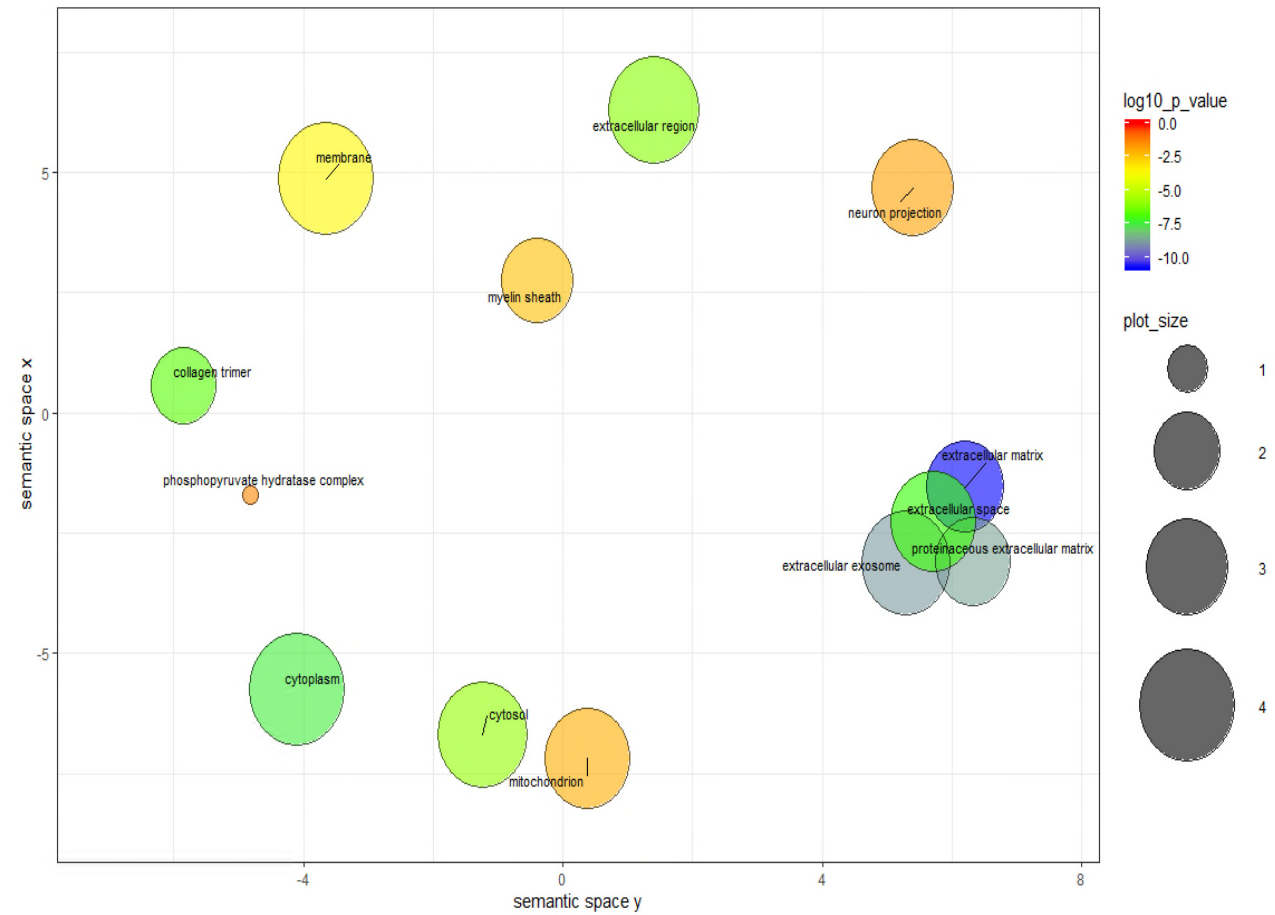
Figure 4.3.3.3 GO Enrichment Analyses Summarized and Visualized Using REVIGO Derived from Upregulated Genes in TLR4ko.BAT Cells

(A) Significantly enriched GO terms related to biological processes in TLR4ko.BAT vs. LPS –treated cells. (B) Significantly enriched GO terms related to cellular component in TLR4ko.BAT vs. LPS –treated cells. (C) Significantly enriched GO terms related to molecular function in TLR4ko.BAT vs. LPS –treated cells. GO terms are represented by circles and are clustered according to semantic similarities to other GO terms in the gene ontology (more general terms are represented by larger size circles, and adjoining circles are most closely related). Circle size indicates to the frequency of the GO term in the underlying GOA database (Barrell et al. 2009), whereas colour indicates the log₁₀P-value for the enrichment derived from DAVID GO analysis (red higher, blue lower). Only significant GO terms with adjusted P < 0.05 following multiple testing correction (Benjamini) are plotted. Full data sets are available for Supplemental Table 4.6

(A) TLR4KO.BAT BP GO Associated with 500 Up-Regulated Genes



(B) TLR4KO.BAT CC GO Associated with 500 Up-Regulated Genes



(C) TLR4KO.BAT MF GO Associated with 500 Up-Regulated Genes

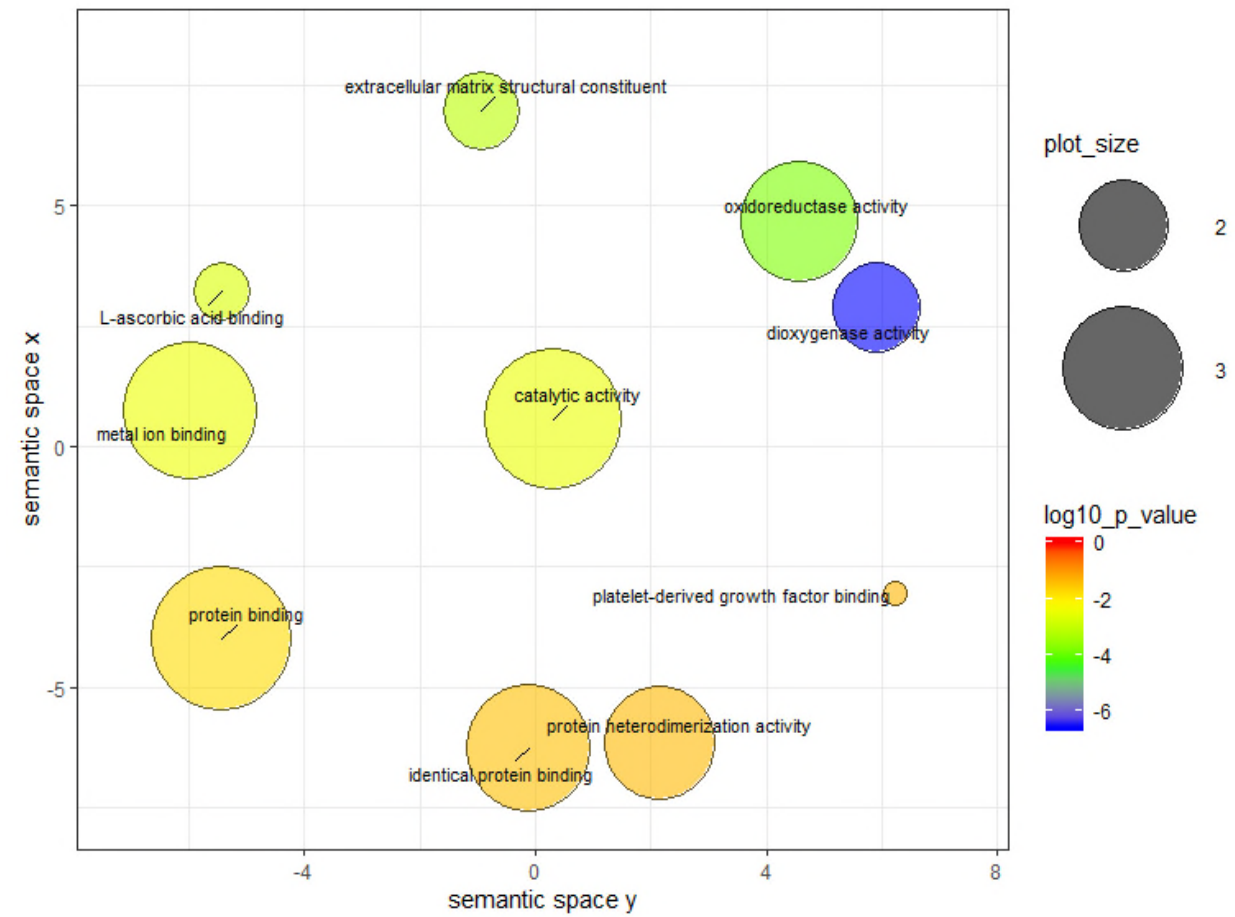
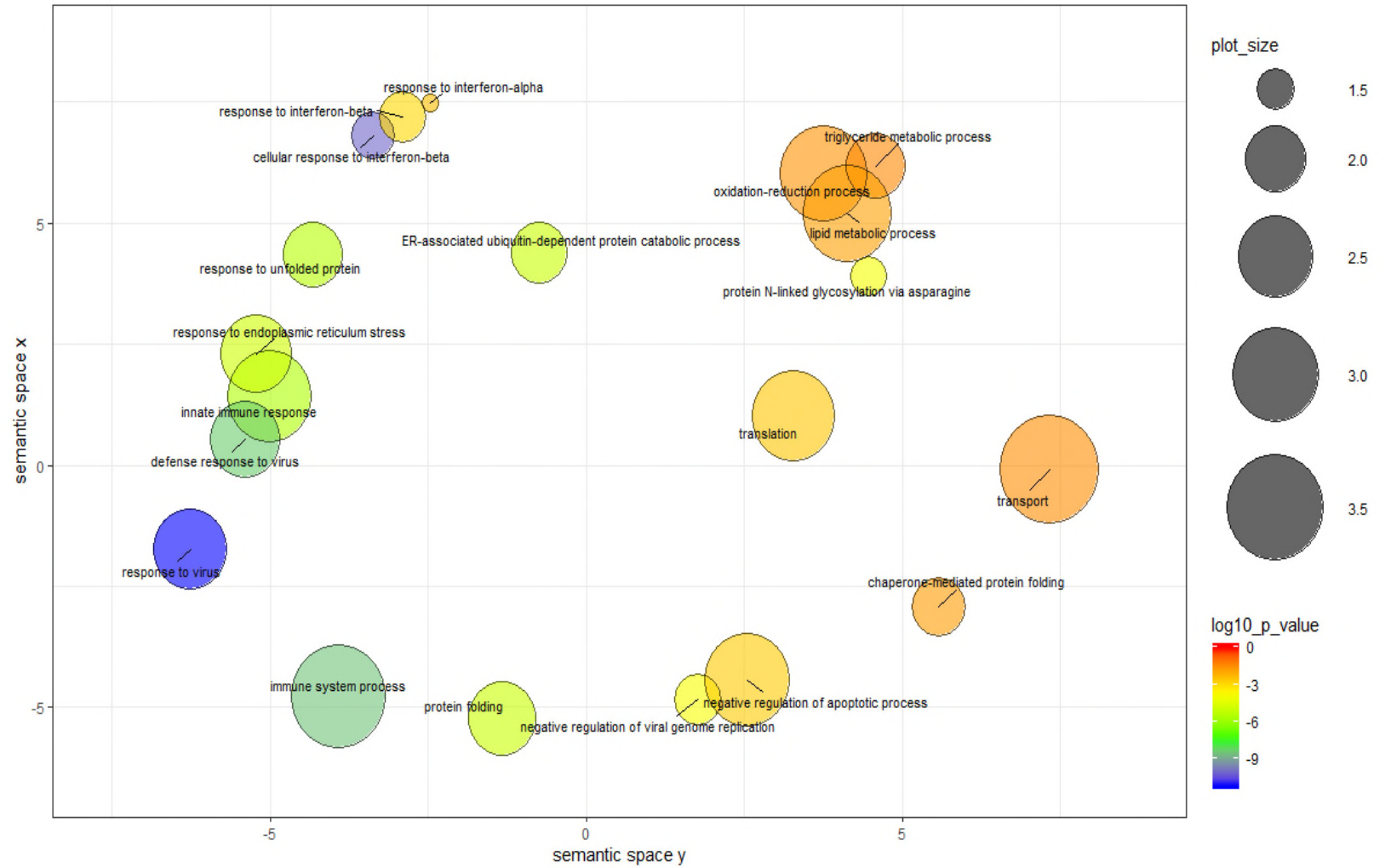


Figure 4.3.3.4 GO Enrichment Analyses Summarized and Visualized Using REVIGO Derived from Downregulated Genes in TLR4ko.BAT Cells

(A) Significantly enriched GO terms related to biological processes in TLR4ko.BAT vs. LPS –treated cells. (B) Significantly enriched GO terms related to cellular component in TLR4ko.BAT vs. LPS –treated cells (C) Significantly enriched GO terms related to molecular function in TLR4ko.BAT vs. LPS –treated cells. GO terms are represented by circles and are clustered according to semantic similarities to other GO terms in the gene ontology (more general terms are represented by larger size circles, and adjoining circles are most closely related). Circle size indicates to the frequency of the GO term in the underlying GOA database (Barrell et al. 2009), whereas colour indicates the log10P-value for the enrichment derived from DAVID GO analysis (red higher, blue lower). Only significant GO terms with adjusted $P < 0.05$ following multiple testing correction (Benjamini) are plotted. Full data sets are available for Supplemental Table 4.7

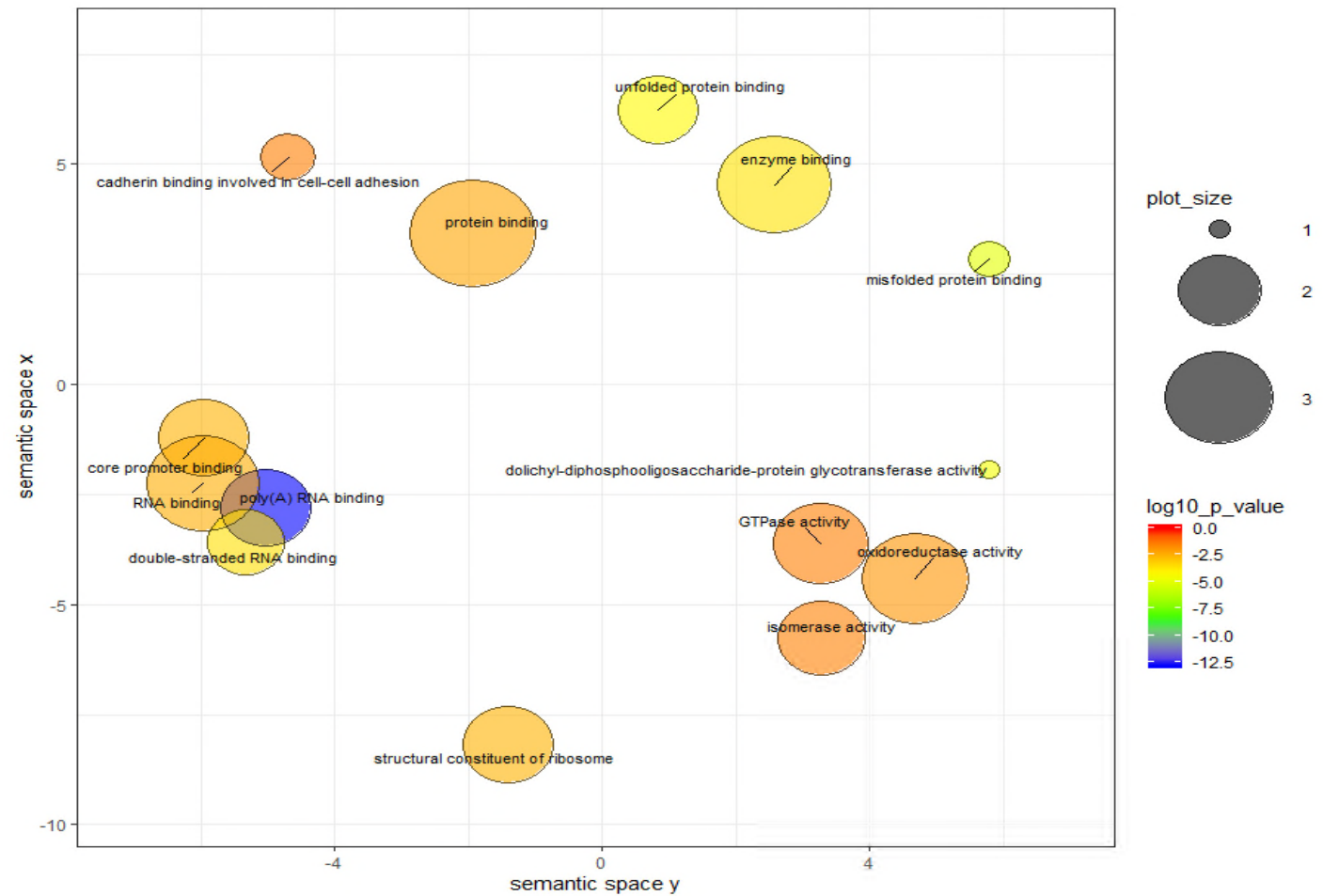
TLR4KO.BAT BP GO Associated with 500 Down-Regulated Genes



TLR4KO.BAT CC GO Associated with 500 down-Regulated Genes



TLR4KO.BAT MF GO Associated with 500 Down-Regulated Genes



4.3.4 TLR4 Mediates LPS Potent Actions on KEGG Enrichment of DEGs

ShinyGO was used to assess the statistical significance of KEGG pathways associated with differentially expressed genes as described in the methods section above. The KEGG enrichment analyses are shown as a hierarchical clustering tree in Figure 4.3.4.1. In the tree below, related KEGG pathways are grouped together based on how many genes they share. The size of the solid circle corresponds to the enrichment false discovery rate (FDR). In this figure, top 50 significant pathways (at FDR <0.05) associated upregulated/downregulated DEGs are showed for either wt.BAT or TLR4ko.BAT. This analysis of KEGG pathway classes reveal that in wt.BAT: extracellular matrix (ECM)-receptor interaction is one of the most significant pathways associated with upregulated DEGs with 42 % (35 genes) of total genes in this pathway upregulated (Figure 4.3.4.1). In addition, the most significant KEGG pathways associated with upregulated genes are:

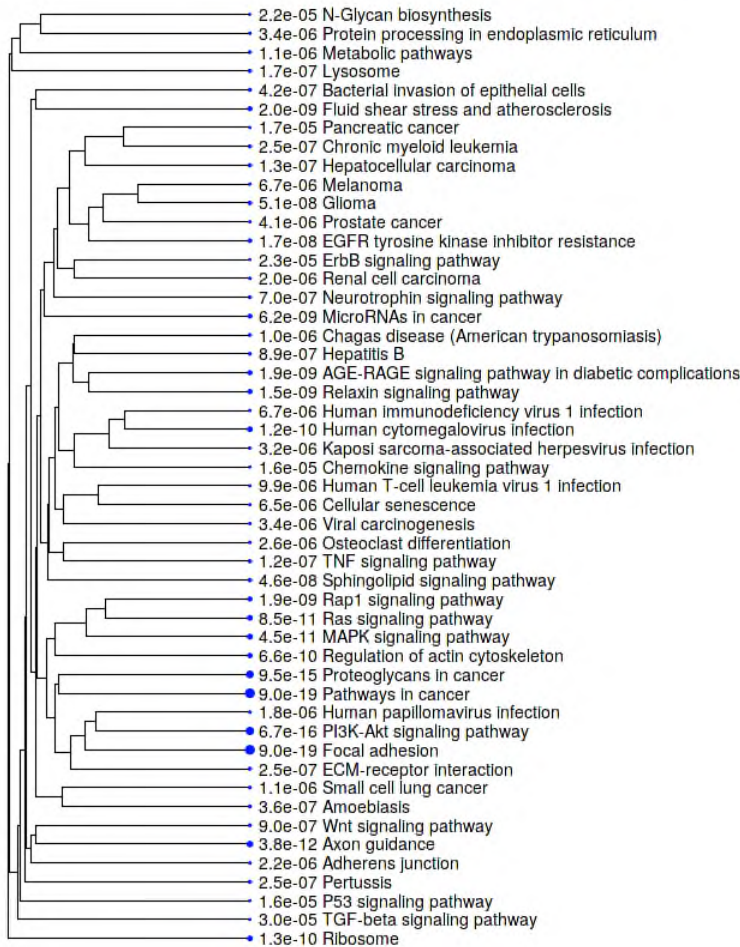
- Focal adhesion which regulate binding to the ECM
- Advanced glycation end products (AGE)- receptor for advanced glycation end products (RAGE) signalling pathway in diabetic complications. Its activation is reported to be the possible mechanism that initiates diabetic complications. That is because it leads to NF-kB activation and subsequent expression of pro-inflammatory cytokine's genes such as IL1, IL6 and TNF α and a variety of atherosclerosis-related genes, including VCAM-1, tissue factor, VEGF, and RAGE (596,597).
- TNF signalling pathway and PI3K-Akt signalling pathway.

Thermogenesis is the most significant pathway associated with downregulated DEGs with downregulation of 42 % (96 genes) of total genes involved in the thermogenesis pathway. Moreover, mitochondrial function related pathways are among the most significant downregulated pathways including Citrate cycle (TCA cycle), Oxidative phosphorylation, fatty acid metabolism, pyruvate metabolism, mitophagy and autophagy. Likewise, a significant reduction in DNA replication pathway is shown in the results. Similarly, downregulation of DEGs appears to be associated with other pathways known to be involved in the main functions that distinguishes the brown adipocytes being energy expending cells such as fatty acid degradation and PPAR signalling. Other significantly decreased pathways seem less obviously expected to be

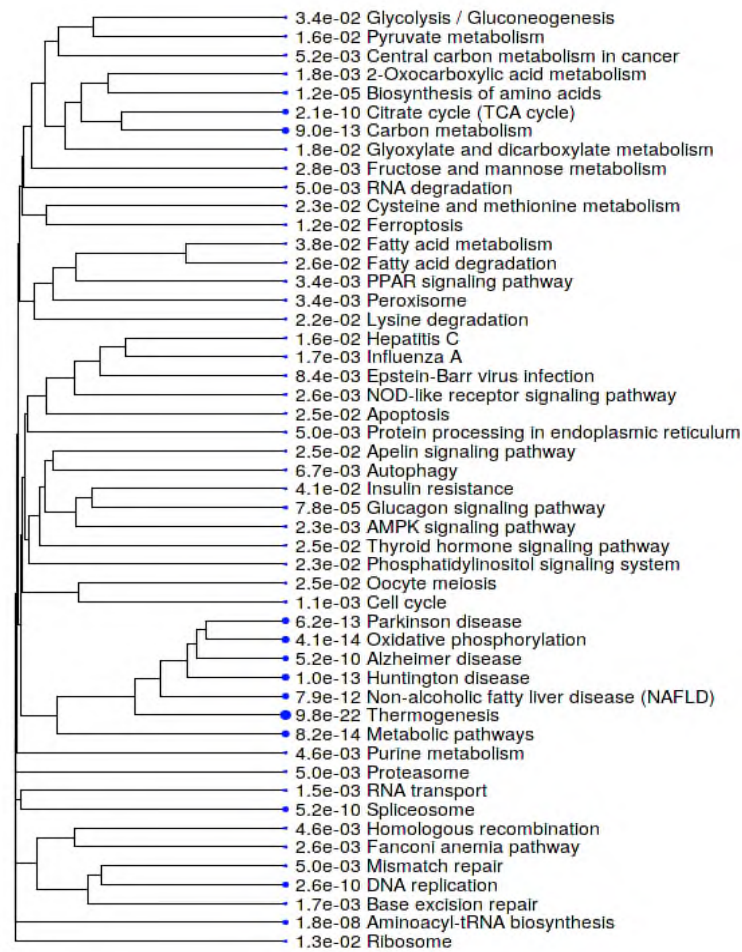
associated with reduced DEGs as Huntington disease (HD) and Parkinson's disease (PD).

To investigate the role of TLR4 in mediating the above mentioned LPS effects on KEGG related pathways, the following data was collected. In total in wt.BAT: 169 significant identified KEGG pathways are associated with upregulated genes and 57 significant pathways are associated with downregulated genes (at $FDR < 0.05$). While in TLR4ko.BAT: 38 identified pathways are associated with upregulated genes and 28 pathways are significant in downregulated genes ($FDR < 0.05$). Yet again, the effect of LPS in TLR4ko.BAT is lower compared to the LPS effect on wt.BAT. The Table 4.3.4.1 shows KEGG pathways that appeared in both cell types with the number and percentage of mapped genes in each pathway. All significantly enriched KEGG pathways and corresponding P-values are listed in appendix (Supplementary Table 4.8, Supplementary Table 4.9, Supplementary Table 4.10, Supplementary Table 4.11).

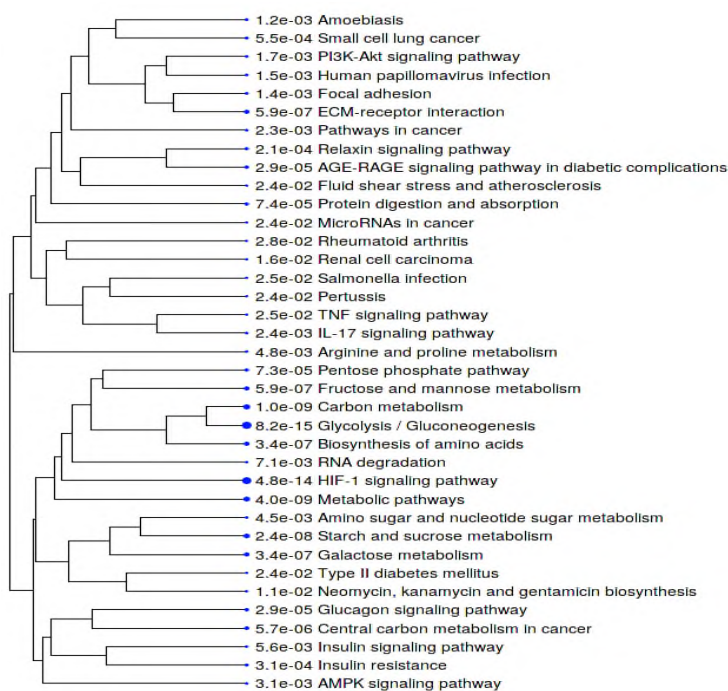
(A) wt. BAT Upregulated Genes (top 50)



(B) wt. BAT Down-Regulated Genes (top 50)



(C) TLR4ko.BAT Upregulated Genes (top 50)



(D) TLR4ko.BAT Down-Regulated Genes (top 50)

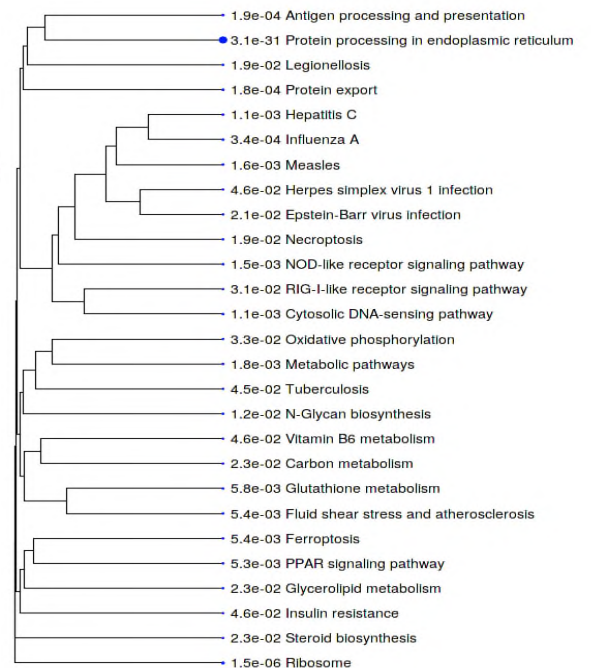


Figure 4.3.4.1 KEGG Pathways Hierarchical Clustering Tree.

In this tree related GO terms are grouped together based on how many genes they share. The size of the solid circle corresponds to the enrichment FDR. Top 50 KEGG pathways associated with (A) upregulated genes in wt.BAT, (B) downregulated genes in wt.BAT, (C) upregulated genes in TLR4ko.BAT, (D) downregulated genes in TLR4ko.BAT.

Table 4.3.4.1 below shows the comparison between wt.BAT and TLR4ko.BAT with regard to the KEGG functional category associated with upregulated genes (Table 4.3.4.1, A), and downregulated genes for reported functional category in both wt.BAT and TLR4ko.BAT. This table clearly shows the limited effects of LPS in TLR4ko.BAT. Only protein processing in the endoplasmic reticulum pathway, which is associated with downregulated DEGs, is similarly affected in both wt and TLR4.ko brown cell. This is an indication of a non TLR4-dependant mechanism mediating regulation of this pathway. Although some pathways associated with up/down-regulated DEGs are significantly enriched in TLR4ko.BAT, that is to a much lower extent than wt.BAT in terms of number of participated genes in each pathway and fold change values of each gene. This suggests that TLR4-receptor in brown adipocytes mediates almost all LPS actions.

Table A.					
Functional Category associated with upregulated genes	Total genes	Genes in wt.BAT list	%wt.BAT of total genes in the list	Genes in TLR4ko.BAT list	%TLR4ko. BAT of total genes in the list
Focal adhesion	198	88	44	11	6
AGE-RAGE signalling pathway in diabetic complications	101	44	44	10	10
Pertussis	76	33	43	5	7
Renal cell carcinoma	68	29	43	5	7
ECM-receptor interaction	83	35	42	11	13
Relaxin signalling pathway	129	52	40	10	8
Small cell lung cancer	92	36	39	8	9
TNF signalling pathway	110	43	39	6	5
Amoebiasis	103	40	39	8	8
Fluid shear stress and atherosclerosis	142	55	39	7	5
MicroRNAs in cancer	142	54	38	7	5
PI3K-Akt signalling pathway	353	123	35	15	4
Pathways in cancer	532	173	33	19	4
Human papillomavirus infection	348	94	27	15	4
Metabolic pathways	1301	281	22	51	4

Table B.					
Functional Category associated with downregulated genes	Total genes	Genes in wt.BAT list	%wt.BAT of total genes in the list	Genes in TLR4ko.BAT list	%TLR4ko.BAT of total genes in the list
Oxidative phosphorylation	131	58	44	7	5
Carbon metabolism	119	52	44	7	6
Ferroptosis	41	14	34	5	12
PPAR signalling pathway	84	25	30	7	8
Glutathione metabolism	64	17	27	6	9
Influenza A	161	42	26	12	7
Ribosome	129	32	25	14	11
Protein processing in endoplasmic reticulum	162	40	25	38	23
NOD-like receptor signalling pathway	197	48	24	12	6
Insulin resistance	109	26	24	6	6
Hepatitis C	158	37	23	11	7
Epstein-Barr virus infection	216	49	23	10	5
Metabolic pathways	1301	295	23	39	3
Measles	142	32	23	10	7
Necroptosis	176	38	22	9	5

Table 4.3.4.1 Comparison between KEGG Functional Category Associated with Upregulated DEGs (A.) or Downregulated DEGs (B.) in wt.BAT and TLR4ko.BAT

4.3.5 Thermogenesis

The thermogenesis signalling pathway was associated with the identified KEGG pathways. In fact, it was the most significantly down-regulated pathway in KEGG analysis and the Figure 4.3.5.1. presents the output thermogenesis diagram.

UCP1, the master regulator of thermogenesis, is one of the significantly down-regulated DEGs ($\log_2\text{FoldChange} = -5.8$) as it can be seen in the Figure 4.3.5.1, A and the heatmap in Figure 4.3.5.2. This seems to be accompanied by disturbances with expression levels of both oxidative respiratory chain complexes and ATPase enzymes and indicates mitochondrial dysfunction upon LPS treatment.

Upstream to UCP1, the analysis showed that LPS decreased AC (e.g. *Adcy10*: $\log_2\text{FoldChange} \approx -3$, adjusted P-value ≤ 0.0001 , Figure 4.3.5.1). Activation of AC is usually part of the first step following β_3 -ARs stimulation by cold, overfeeding or other sympathetic nervous system stimuli capable of triggering norepinephrine release (75). Thus, a decrease in AC will interrupt subsequent intracellular signal transduction to activate UCP1 transcription. In fact, the expression of a gene related to lipolysis (HSL) was also significantly decreased by LPS ($\log_2\text{FoldChange} = -0.2$, adjusted P-value ≤ 0.0001 , Figure 4.3.5.1) which is downstream to AC activation and expected to lead to reduced available FFAs to activate UCP1. Whereas LPS significantly increased the level of PKA ($\log_2\text{FoldChange} = 0.23$, adjusted P-value ≤ 0.0001), PLIN1 ($\log_2\text{FoldChange} = 0.24$, adjusted P-value ≤ 0.0001), ACS (e.g. *Acs16*: $\log_2\text{FoldChange} = 2.75$, adjusted P-value ≤ 0.0001), CPT1 (e.g. *CPT1c*: $\log_2\text{FoldChange} \approx 1$, adjusted P-value ≤ 0.0001) perhaps to compensate for the reduction of AC and HSL. Under normal conditions, activation of AC causes an increase of cAMP and PKA activation. PKA then stimulates lipid catabolism processes by phosphorylating both PLIN1 and HSL, lipolysis agents in lipid droplets, which in turn converts triacylglycerol into free fatty acids (FFAs) to activate UCP1 and thermogenesis. FFA levels are critical for thermogenesis either directly or indirectly. ACS mediates indirect FFA actions on UCP1 through the conversion of FAs to acyl-CoA and specifically directs them toward the mitochondrial matrix to undergo fatty acid oxidation (FAO) via the CPT1 system. FAO is also thought to be a major contributor to thermogenesis. CPT-1 β is responsible for a trans-esterification reaction of the fatty acyl CoA to form acylcarnitine in brown adipocytes allowing the proton pumps to create the proton gradient for ATP production or thermogenesis (112).

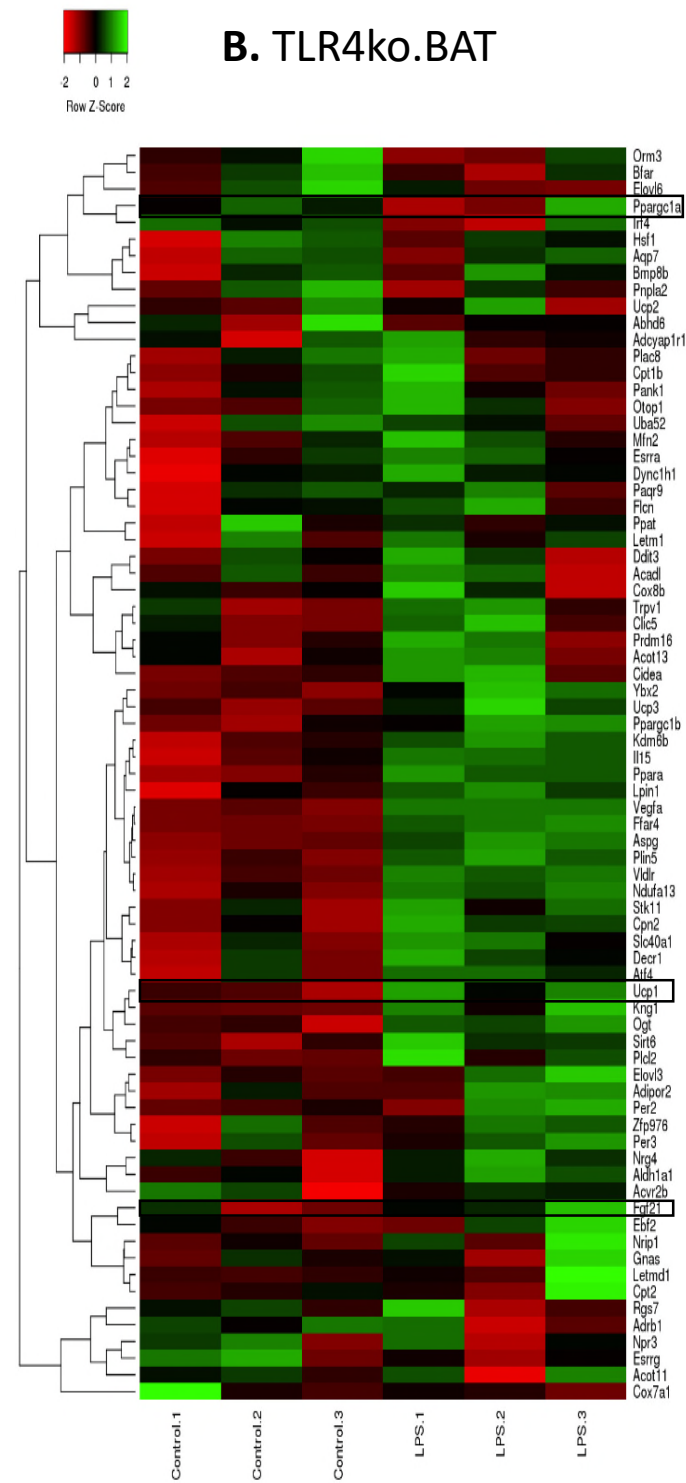
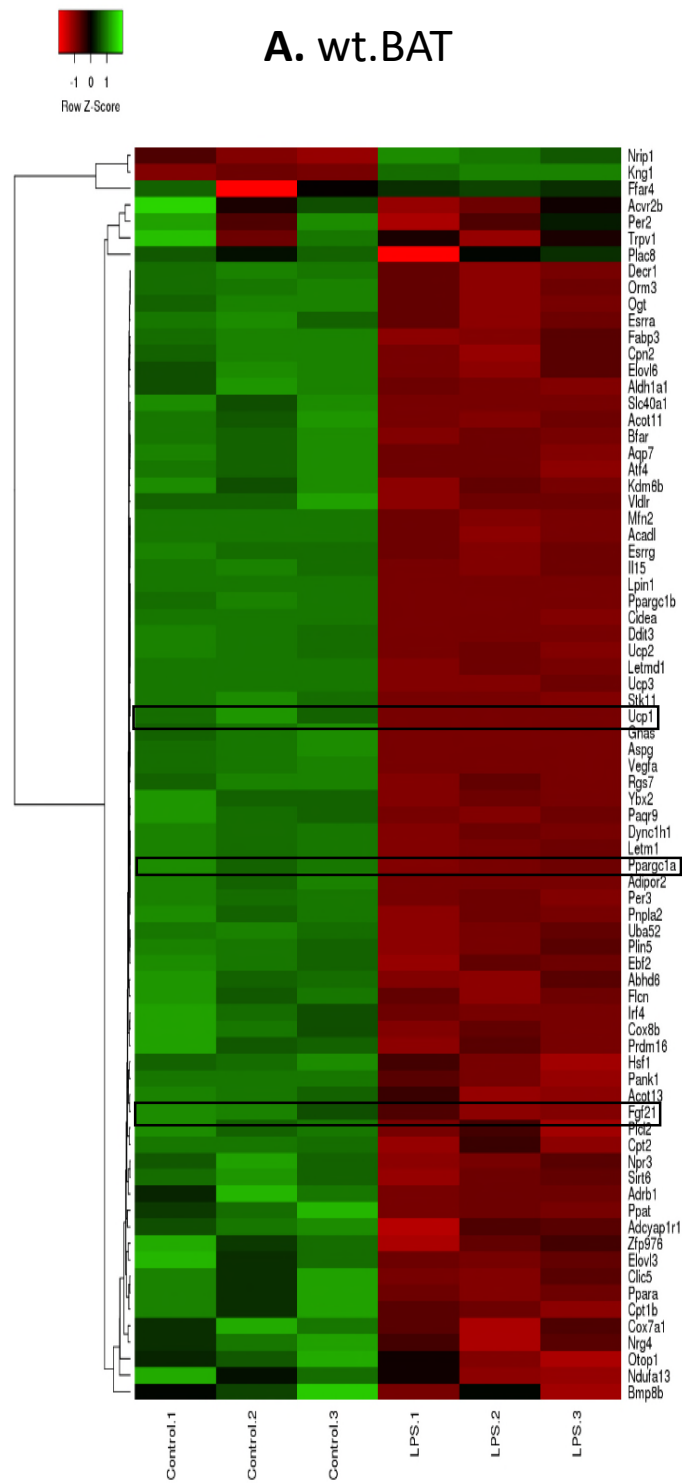
Thus, LPS-dependant upregulation of PKA, PLIN1, ACS, CPT1 has the capacity to increase the availability of FFA, but it is still not capable of compensating the dysregulation of the pathway evidenced by the reduced UCP1 levels and ultimately negatively affecting thermogenesis.

In addition, this data showed that LPS increased the level of CREB but no subsequent increase in PRDM16 was observed. Upregulated PKA typically phosphorylates CREB which then either directly activates UCP1 expression or indirectly by upregulating PRDM16 and Zfp516 (72,580). Here, PRDM16 was expectedly decreased ($\log_2\text{FoldChange} \approx -1$, adjusted P-value ≤ 0.0001). This strongly suggests that LPS induces the whitening of brown adipocytes as PRDM16 is one of core transcriptional regulators of classical BAT development and has key roles in the regulation of inducible brown fat. In one study, the reduction of PRDM16 levels has no effect on morphological differentiation of these cells, but causes an almost complete suppression of brown fat-selective genes, including UCP1 mRNA and protein, while leaving intact the expression of genes common to both white and brown fat cells such as PPAR γ and aP2 (245). This whitening effect of LPS is further supported by the fact that it also diminished expression of PPAR α ($\log_2\text{FoldChange} = -1.3$, adjusted P-value ≤ 0.0001) and PGC1 (e.g. PGC1 α $\log_2\text{FoldChange} = -1.5$, adjusted P-value ≤ 0.0001), both are brown fat selective genes that are important regulators of fatty acid oxidation (598–600). Specifically, PGC-1 α is the master regulator of brown adipocyte program (142,598). It is strongly induced by cold exposure and β -adrenergic signalling, playing a role in inducing UCP1 gene expression and co-ordinately increasing mitochondrial gene expression and function (119,599). Also, ectopic expression of PGC1 α in white adipocytes induces acquisition of BAT features, including expression of mitochondrial and fatty acid-oxidation and thermogenic genes. Therefore, decreasing PGC1 α by LPS is a clear indication of a compromised physiological commitment to the brown adipocyte lineage (77,143).

Strikingly, most selected brown fat DEGs were specifically reduced in wt.BAT cells differentiated with LPS as the heatmap below shows (Figure 4.3.5.2). For example, *Elovl3* a very long chain fatty acid elongase that is enriched in brown compared to white fat and is implicated in brown fat hyperplasia (165,601), was reduced by LPS ($\log_2\text{FoldChange} = -1.05$, adjusted P-value ≤ 0.0001). *CIDEA*, a gene predominantly expressed in brown fat where it has key roles in lipid droplet dynamics (144) was decreased by LPS ($\log_2\text{FoldChange} = -1.4$, adjusted P-value ≤ 0.0001). In addition, several other key brown fat genes were significantly reduced by LPS treatment, such as *Fgf21* ($\log_2\text{FoldChange} = -2.9$, adjusted P-value ≤ 0.0001) which has important roles in promoting a brown fat phenotype (153), and *Slc40a1* ($\log_2\text{FoldChange} = -5.1$, adjusted P-value ≤ 0.0001), an isozyme of the long-chain fatty acid-coenzyme A ligase family that has the capacity to convert free long-chain fatty acids into fatty acyl-CoA esters and also functions as a fatty acid transporter (163,602,603). LPS also reduced the mRNA levels for many genes of mitochondrial oxidative phosphorylation, that are known to be enriched in brown fat cells and tissue. In particular, *Cox8b*, a highly brown fat-selective mitochondrial gene was less expressed ($\log_2\text{FoldChange} = -0.74$, adjusted P-value ≤ 0.0001) in LPS differentiated brown adipocyte cultures. Interestingly, *Nrip1* (known as RIP140), a negative regulator of brown adipocytes that represses the “Brown-in-White” Adipocyte program (562) was increased with LPS treatment ($\log_2\text{FoldChange} \approx 0.5$, adjusted P-value ≤ 0.0001). Overall, there is a set of genes that have been altered indicating the whole brown fat program is affected in wt.BAT cells. In comparison, TLR4ko.BAT cells did not show notable alteration in brown fat genes when differentiated with LPS (Figure 4.3.5.1, Figure 4.3.5.2). This shows nearly all BAT-associated genes are down-regulated by LPS in TLR4-dependent manner.

Figure 4.3.5.2 Heatmap of DEGS of Brown Fat Genes upon LPS-Induction in (A) wt.BAT, (B) TLR4ko.BAT.

Key genes are highlighted as examples. Rows represent the different genes and each column represents a sample. For the relative gene expression level of each sample a different colour of the red-green scale is assigned. green represents an expression level above the mean, red colour represents expression below the mean.



In addition, thermogenesis pathway analysis in the present study Figure 4.3.5.3 revealed an increase in p38 expression (p38delta (p38 δ): log2FoldChange \approx 2.15, p38beta (p38 β): log2FoldChange \approx 1) appears to be accompanied by reduction of PGC1 α (log2FoldChange \approx -1.5), ATF2 (log2FoldChange \approx -0.35) and FGF21 (log2FoldChange \approx -2.9) which subsequently reduces UCP1. Physiologically, activation of PKA following β -adrenergic stimulation, leads to p38 mitogen-activated protein kinase (MAPK) activation and induces brown adipocytes to produce FGF21 through ATF-2 phosphorylation. p38 MAPK activation also increases PGC1 α which regulates mitochondria biogenesis and triggers the transcription of thermogenic genes, in particular UCP1. Activation of ATF-2 by p38 MAPK additionally play a role as the cAMP sensor that increases expression of the PGC1 α gene itself in brown adipose tissue (153,604–606). However, in the present study it is likely that the elevated p38 (p38 β and p38 δ), caused by LPS activation of TLR4, may lead to reduced thermogenesis rather than enhancing it, but would need further study at the protein level (Figure 4.3.5.3). Although this suggested role for p38 is opposite to the positive role of p38 mentioned above that has been repeatedly reported in literature (75,604,607), it is in line with an unexpected opposite role for p38 in a report by Valladares et al. Here, the authors demonstrated that TNF α inhibits the expression of UCP1 through p38 activation, and when a p38 inhibitor is used, UCP1 activity is restored (427). Also, Bae et al. provide support that activation of p38 following LPS treatment in brown adipocytes is accompanied by reduced thermogenesis and UCP1 expression, although the relationship between p38 and thermogenesis was not discussed (344). Moreover, Matesanz et al. found that. p38 α blocks BAT thermogenesis. However, the suggested mechanism, through p38 δ inhibition, is opposite to what data in the present study suggest.(608)

Deletion of TLR4 completely attenuates LPS effects on the thermogenesis pathway and the genes involved Figure 4.3.5.3, and at the same time there is no increase in p38 following LPS stimulation in TLR4ko.BAT Figure 4.3.5.3. Although there are some contradictions in the available data concerning the role of p38 there are clear indications of both pro- and anti-thermogenic actions. How these different actions affect BAT biology needs further investigation. In this context, it seems like p38 acts differently in different situations. Activation of p38 as part of innate immune system inflammatory response (TNF α , LPS) appears to negatively affect thermogenesis by a

mechanism yet to be identified, probably dependant on changes of other signals/factors under such situation.

Overall, this data suggests potential therapeutic prospects of targeting p38 β and p38 δ for treatment of obesity and increased thermogenesis. Future studies examining the effects of selective p38 β and p38 δ targeting at the protein level with *in vivo* investigations to determine what other factors are involved in p38 actions will elucidate the functional roles of these two p38MAPKs in the thermogenesis process and will guide future therapeutic strategies.

4.3.6 Extracellular Matrix (ECM)-Receptor Interaction

ECM, which contains the non-cellular components of the tissue that are found to play a role in energy homeostasis with direct influence on UCP1, was among the most upregulated pathways upon LPS treatment in brown adipocytes. Specifically, the ECM-Receptor interaction pathway in brown adipocytes is significantly enriched in the KEGG enrichment analysis in wt.BAT. There are 35 DEGs involved in the ECM interaction, which has 83 total genes mapped to KEGG pathways; as such 42 % of them are upregulated upon LPS treatment. The heatmap in figure represents these genes, which include collagen genes which were significantly up-regulated in wt.BAT when treated with LPS, for example: (Col1a1: FC=2.5, Col1a2: FC=1.93, Col6a2: FC=1.9, and COL6A3: FC≈1, $P \leq 0.001$). Similarly, the included integrins in the heatmap were significantly up-regulated (Itga2: FC=3.5, Itgb8: FC=2.5, and Itga11 FC=1.5, $P \leq 0.001$). In contrast, most laminins were down-regulated (Lama5: FC=-1.88, Lamc2 FC=-1.29, $P \leq 0.001$) and nephronectin (Npnt FC=-1.88, $P \leq 0.001$). In comparison, for TLR4ko.BAT only 13 DEGs involved in the ECM interaction (heatmap in Figure 4.3.6.1) and 13 % of total genes in ECM interaction pathway are upregulated, but to a much lower extent than wt.BAT. For example: Col1a1: FC=0.42, Col6a3: FC=0.23 ($P \leq 0.001$).

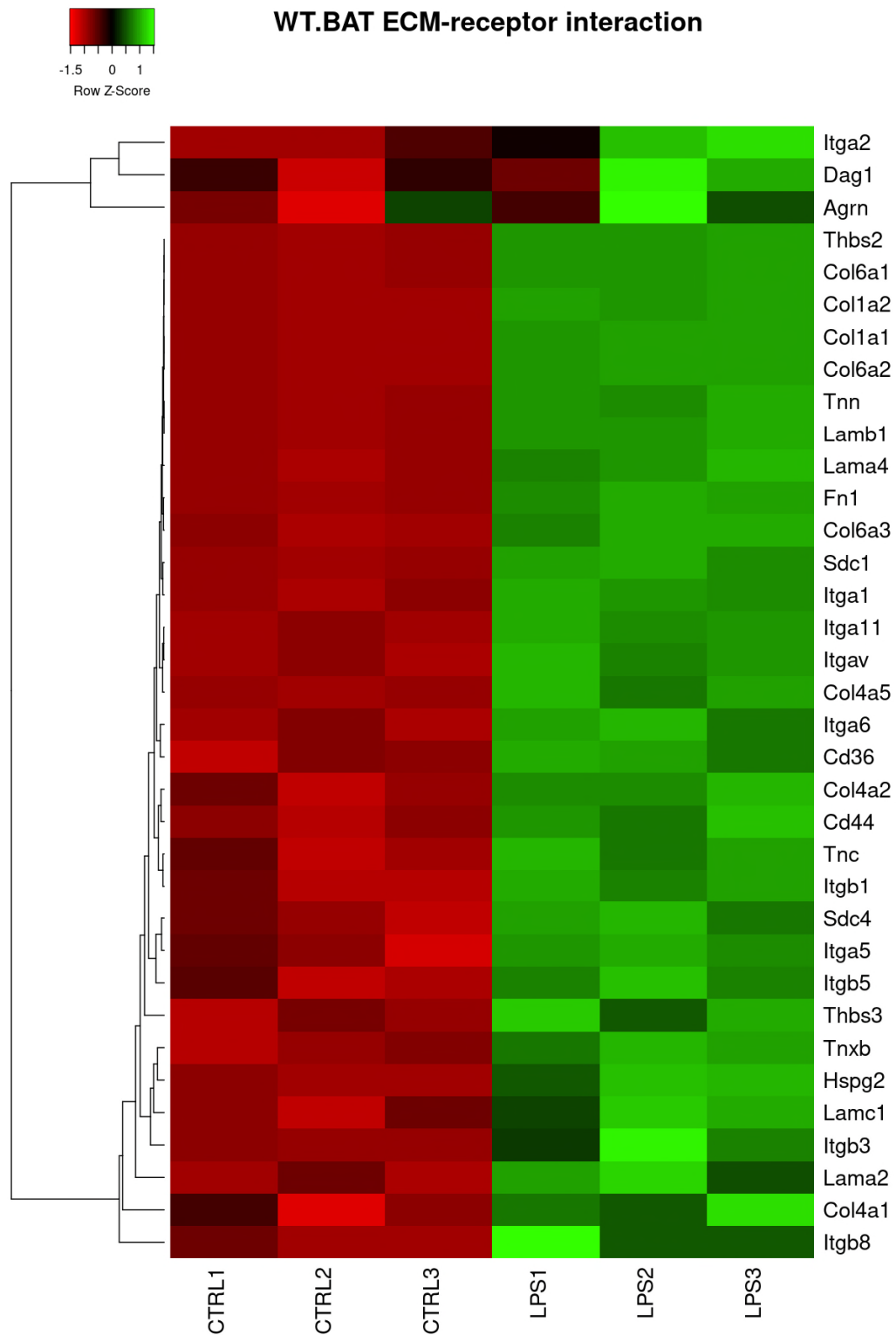


Figure 4.3.6.1 Heatmap of DEGS of Extracellular Matrix (ECM)-Receptor Interaction upon LPS-Induction in wt.BAT.

Rows represent the different genes and each column represents a sample. For the relative gene expression level of each sample a different colour of the red-green scale is assigned. Green represents an expression level above the mean, red colour represents expression below the mean.

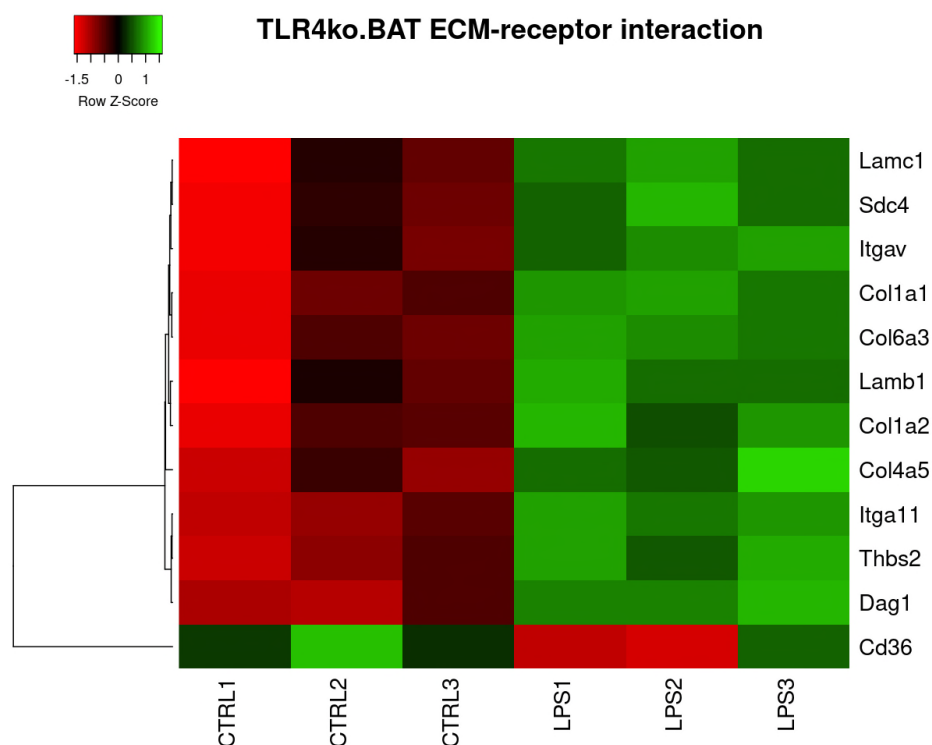


Figure 4.3.6.2 Heatmap of DEGS of Extracellular matrix (ECM)-Receptor Interaction upon LPS-Induction in TLR4ko.BAT.

Rows represent the different genes and each column represents a sample. For the relative gene expression level of each sample a different colour of the red-green scale is assigned. Green represents an expression level above the mean, red colour represents expression below the mean.

Collectively, the differentially expressed genes in this pathway were generally significantly upregulated upon LPS treatment in wt.BAT but not in TLR4ko.BAT. This can be clearly seen in the Figure 4.3.6.3 which represents the overview of affected genes along the pathway. It is clear that the interactions between ECM components and integrins were differentially regulated because of TLR4 deletion. Therefore, these results demonstrate that the communication between brown adipocytes and the extracellular matrix is enhanced with elevated LPS levels, mostly mediated by TLR4. These results provoke the hypothesis that peptides derived from ECM-related proteins are greatly altered upon LPS treatment, which possibly act as important players in impairing BAT activation and thermogenesis through TLR4.

LPS-Induced Cytokine Secretion by Brown Adipocytes

4.3.7 LPS Activates Secretion of Multiple Cytokines in wt.BAT Cells

The RNA-sequence analysis showed modulation of gene expression for a wide range of factors upon LPS-treatment which contributes to various functions. As many of the factors identified have the capacity to be secreted, a focused secretome analysis was undertaken. Proteome Cytokine Arrays were conducted on conditioned serum-free media collected after 48 hours to avoid the significant contribution of cytokines present in the serum media supplement. The cells were visibly healthy prior to media collection (conditioned media) and serum deprivation did not affect cell morphology or appearance during this time course.

A Proteome Cytokines Array analysis was used to investigate the cytokines secreted by brown adipocytes in the absence and presence of LPS treatment. The secreted cytokines and how LPS affect cytokine secretion by brown adipocytes are shown in Figure 4.3.7.1 . This investigation was undertaken using two types of wild type brown adipocytes, the imBAT cell line and primary brown adipocytes. In addition, TLR4ko.BAT conditioned media was collected to examine TLR4-dependence of LPS effects on cytokine secretion.

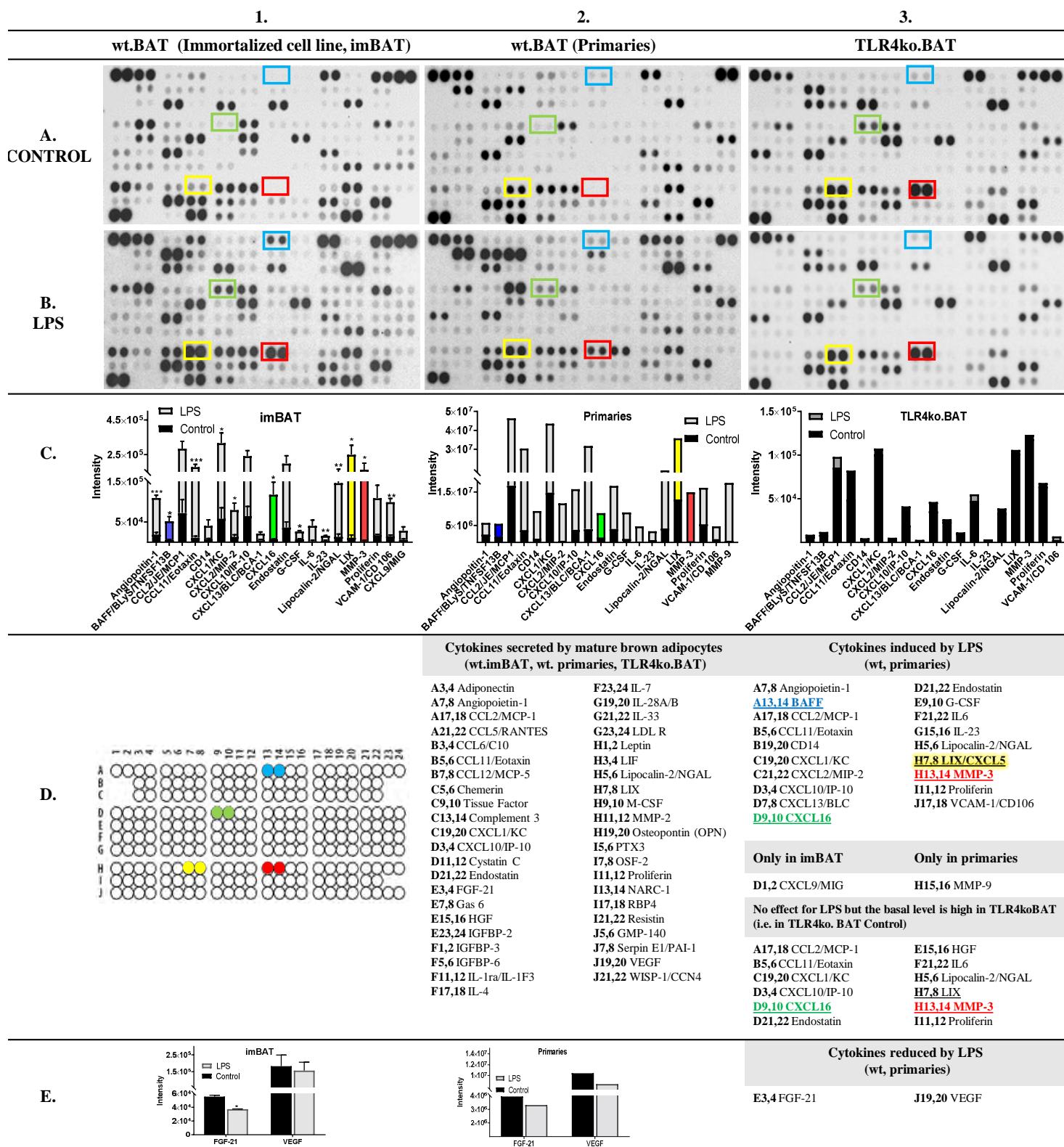
Interestingly, mature wild type brown adipocytes (both wt.imBAT and primary cultures) demonstrated the ability to secrete various cytokines with no stimulus. This is in agreement with increasing evidence that BAT performs a secretory role releasing factors such as fibroblast growth factor 21 (FGF21), and angiogenic factors that contribute to autocrine, paracrine and endocrine functions and may be required for intercellular coordination and tissue remodelling (80).

Forty-three different cytokines were identified as secreted by brown adipocytes in this study. Adiponectin, Retinol-Binding Protein 4 (RBP4), Chemerin, Tissue factor and FGF21 are some of the cytokines previously reported to be secreted from brown adipocytes, and therefore they provide validation of the data. From this study a set of cytokines are reported to be secreted from cultured brown adipocytes *in vitro* for the first time (at the time of writing my thesis) such as IL-28A/B, IGFBP-6, Complement Factor D and others shown in the table below. Table 4.3.7.1.

These novel cytokines are involved in immune and inflammatory responses including CCL6/C10, CCL12/MCP-5, IL-4, IL-7, LIF, CXCL5 (LIX), M-CSF, GMP-140/CD62P. While others belong to Insulin-like growth factor binding family such as IGFBP-6 and WISP-1. In addition, LDL R, NARC-1/PCSK9 are factors known to be involved in regulation of cholesterol homeostasis.

Cytokines secreted by wt. mature brown adipocytes			
Ref.		Ref.	
(609)	A3,4 Adiponectin	No reports	F23,24 IL-7
(610–613)	A7,8 Angiopoietin-1	No reports	G19,20 IL-28A/B
(344)	A17,18 CCL2/MCP1	(542)	G21,22 IL-33
(344)	A21,22 CCL5/RANTES	No reports	G23,24 LDL R
No reports	B3,4 CCL6/C10	(75,80)	H1,2 Leptin
(542)	B5,6 CCL11/Eotaxin	No reports	H3,4 LIF
No reports	B7,8 CCL12/MCP-5	(614,615)	H5,6 Lipocalin-2/NGAL
(397)	C5,6 Chemerin	No reports	H7,8 LIX
(18)	C9,10 Tissue Factor	No reports	H9,10 M-CSF
(75)(277)	C13,14 Adipsin	(277)	H11,12 MMP-2
(18)	C19,20 CXCL1/KC	(18)	H19,20 Osteopontin (OPN)
(18)	D3,4 CXCL10/IP-10	(18)	I5,6 PTX3
(277)	D11,12 Cystatin C	(605)	I7,8 OSF-2/ Periostin
(18)	D21,22 Endostatin	(18)	I11,12 Proliferin
(80,542)	E3,4 FGF-21	No reports	I13,14 NARC-1/PCSK9
No reports	E7,8 Gas 6	(616)	I17,18 RBP4
(18)	E15,16 HGF	(75)	I21,22 Resistin
(18)	E23,24 IGFBP-2	No reports	J5,6 GMP-140/ CD62P
(18)	F1,2 IGFBP-3	(18)	J7,8 Serpin E1/PAI-1
No reports	F5,6 IGFBP-6	(617)	J19,20 VEGF
No reports	F11,12 IL-1ra/IL-1F3	No reports	J21,22 WISP-1/CCN4
No reports	F17,18 IL-4		

Table 4.3.7.1 Cytokines Secreted by wt. Mature Brown Adipocytes with References for the Previously Reported Ones and No Reports for the Novel Ones.



In addition, differentiating cells with LPS led to induction of secretion of many cytokines by both wt.imBAT and primaries, but not TLR4ko.BAT. Nineteen cytokines were identified to be induced by LPS as shown in Figure 4.3.7.1. This is in line with significant upregulation of DEGs of most of these cytokines upon LPS treatment identified from the RNA-sequence analysis in wt.BAT (Figure 4.3.7.3). None of these cytokines have been previously reported to be elevated upon LPS treatment in cultured brown adipocytes apart from MCP1 and IL6 (344). However, many of these cytokines are angiogenesis-related factors (about 4.5 fold increase in Angiopoietin-1 and chemokine (C-X-C motif) ligand 1 (CXCL1/KC), 55 fold increase for matrix metalloproteinase 3 (MMP3), 14 fold increase for C-X-C motif chemokine ligand 16 (CXCL16), 5 fold increase for Proliferin).

In line with the RNA-sequence analysis revealing upregulation of ECM-receptor interaction partners, different members of ECM fibrous proteins and integrin signalling pathways were also upregulated by LPS treatment in the secretome analysis including vascular cell adhesion molecule-1 (VCAM-1) (5.5 fold increase), Endostatin (4.5 fold increase), and MMP3. Recently, the interaction between α 4-integrin on pro-inflammatory macrophages and VCAM-1 on adipocytes was reported as a novel mechanism through which inflammatory signalling can suppress beige adipogenesis and UCP1 gene expression (330,336). Thus, the present study provides new insight into these pathways with elevated LPS levels a candidate to trigger such effects of VCAM-1 by directly affecting brown adipocytes rather than only activating macrophages.

The upregulation of secreted angiogenesis modulators and members of ECM molecules is accompanied by the typical response to exposure to an inflammatory agent such as LPS Figure 4.3.7.1. This includes the interleukin signalling pathway with the increase of IL6 (12 fold) and IL23a (3.5 fold), and inflammation mediated by chemokine and cytokine signalling pathways with increases in Eotaxin (14 fold) and CXCL1/KC (4.5 fold), and finally Toll receptor signalling pathway with increase in secretion of CD14 (4 fold). Together these data indicate that brown adipocytes are key components in immunity and the inflammatory response of adipose tissue.

LPS treatment reduced FGF21 and VEGF release from brown adipocytes (Figure 4.3.7.1, E). This is consistent with both FGF21 and VEGF being reduced in DEGs upon LPS treatment from the RNA-sequence analysis in wt.BAT (Figure 4.3.7.1, E).

Both FGF21 and VEGF are reported to play a role in BAT thermogenesis regulation and increase UCP1 levels. In fact, compromising of VEGF actions decreases BAT activity with reduced vascular density (618–620). VEGF loss and capillary rarefaction in BAT were found to precede mitochondrial loss and the development of the whitened BAT phenotype (621). Therefore, LPS-mediated reduction of their levels provides further evidence of the negative impact of LPS on brown adipocyte activity and thermogenesis.

In TLR4ko.BAT adipocytes (Figure 4.3.7.1, B), LPS did not induce the secretion of any cytokines. However, the basal levels of LPS-induced cytokines in TLR4ko.BAT seem to be higher than wt.BAT for unknown reasons. This could be a consequence of technical issues related to differences in blot production or imaging technique as this was not accompanied by higher gene expression in RNA-sequence analysis (Figure 4.3.7.3). Equally, the higher basal levels may be due to biological reasons related to TLR4 deletion. To confirm the mechanisms involved, further experiments would need to be undertaken. Further research is necessary to identify the role of these elevated cytokines when differentiating brown adipocytes with LPS in dysfunction of BAT in obesity and associated comorbidities.

In the current study four cytokines were investigated further. They were chosen because of high secretion and expression, and large response to LPS which suggest a potential important role in brown adipocytes dysfunction. These cytokines are B-cell activating factor (BAFF/BLyS/TNFSF13B), CXCL16, CXCL5 (LIX) and MMP3. Their increase upon LPS treatment in media was confirmed by ELISA (Figure 4.3.7.2) and significant gene expression upregulation in both qRT-PCR and DEGs in RNA-sequence analysis as shown in Figure 4.3.7.3.

CXCL5 was the most highly upregulated DEG ($\log_2\text{FoldChange} = 10$, $P \leq 0.0001$) in RNA-sequence analysis and its induction was confirmed by qRT-PCR (Figure 4.3.7.3).

In addition, CXCL5 secretion massively increased in media upon LPS treatment in brown adipocytes with an increase of 21-fold change, $P < 0.05$ detected by a proteome array analysis as well as an increase of 9.8-fold change, $P < 0.001$ detected by ELISA assay (Figure 4.3.7.2). MMP3 was the second most upregulated gene with LPS treatment in the set of DEGs from RNA-sequence data ($\log_2\text{FoldChange} = 8$, $P \leq 0.0001$) and confirmed by qRT-PCR (with average of 500-fold change induction, $P < 0.01$). This was accompanied by induced MMP3 secretion into media in LPS-stimulated brown adipocytes in a proteome array (with 55-fold change, $P < 0.05$) and

ELISA measurements (50-fold change, $P < 0.001$). BAFF and CXCL16 were among the most highly upregulated DEGs in RNA-sequence analysis in wt.BAT ($\log_2\text{FoldChange} = 1.65$, $P \leq 0.001$, $\log_2\text{FoldChange} = 3.46$, $P \leq 0.001$, respectively) (Figure 4.3.7.3). Their induction was further confirmed by qRT-PCR with maximum increase of 8.28-fold change for BAFF ($P < 0.001$), and 15.22-fold change ($P < 0.001$) for CXCL16 (Figure 4.3.7.3).

In tandem with that, an increase of both BAFF and CXCL16 secretion in media upon LPS treatment in brown adipocytes was detected by proteome array with 7.3-fold change ($P < 0.05$) and 14.6 fold change ($P < 0.05$), as well as by ELISA data indicating an increase of 12.5-fold change ($P < 0.001$), 13.26-fold change ($P < 0.001$), respectively (Figure 4.3.7.2).

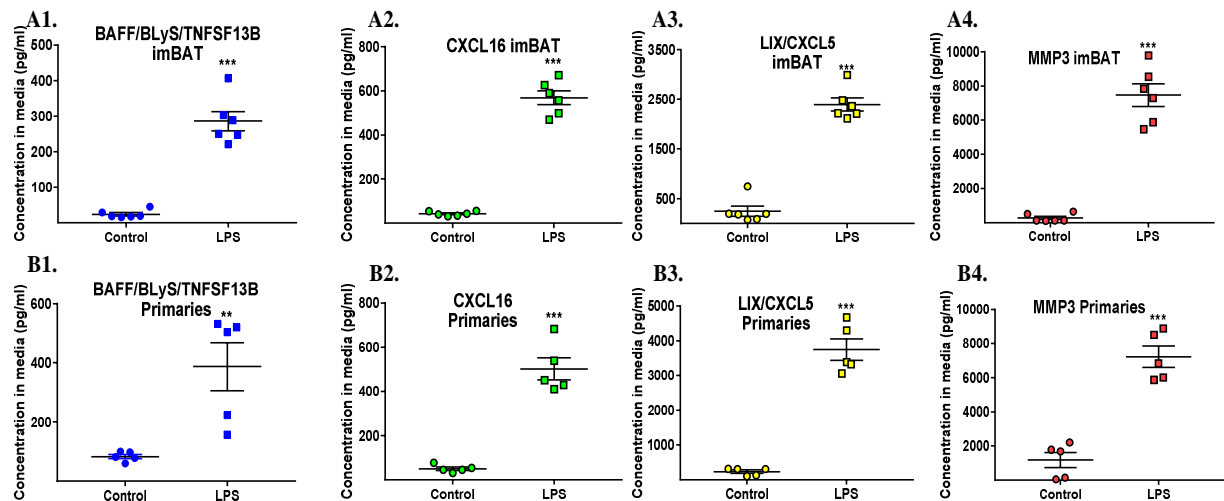


Figure 4.3.7.2 Testing Control vs LPS Treatment in Media by ELISA for Novel Cytokines.

BAFF (A1. in imBAT, B1. in primary brown adipocytes), CXCL16 (A2. in imBAT, B2. in primary brown adipocytes), LIX (A3. in imBAT, B3. in primary brown adipocytes), MMP3 (A4. in imBAT, B4. in primary brown adipocytes). ELISA imBAT, Primary brown adipocyte data represent the mean of three (total $n=6$ each treatment), two experiments (total $n=5$ each treatment), respectively \pm SEM. Two-tailed unpaired Student's t-test was performed to test significance: ** $P < 0.01$, *** $P < 0.001$ control vs. LPS

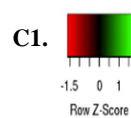
A sub-list of cytokines that were included in the proteome array were further explored at gene level by comparing with DEGs from RNA-sequence analysis; these are represented in the heatmap (Figure 4.3.7.3) highlighting the factors mentioned above. In addition, there are many other factors of interest in the context of adipocytes and metabolic diseases. For instance, upregulated genes included resistin (Retn;

log2FoldChange = 1.32, $P \leq 0.0001$) and adiponectin (Adipoq; log2FoldChange = 0.68, $P \leq 0.0001$). Both resistin and adiponectin have a well-recognized inflammatory function in white adipocytes with an anti-inflammatory role for the former and pro-inflammatory effects for the latter (15). Amphiregulin (Areg; log2FoldChange = 1.84, $P \leq 0.0001$) is reported to be downregulated in BAT compared to subcutaneous WAT at thermoneutrality and it is typically a part of immune system response as a product of IL-33/Group 2 innate lymphoid cells (ILC2s) (163,327). Interleukin 33 (IL33; log2FoldChange = 2.95, $P \leq 0.0001$) is a controversial cytokine with reports indicating that it limits the development of spontaneous obesity by increasing numbers of ILC2s and eosinophils. This coincides with being and energy expenditure in the WAT of mice but not BAT, while deletion of IL-33 leads to opposite effects (327,328,622).

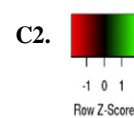
Pentraxin related gene (Ptx3; log2FoldChange = 3.03, $P \leq 0.0001$) is a pro-inflammatory adhesion molecule reported to be upregulated upon cAMP treatment of brown adipocytes (277). Also among the downregulated genes were delta like non-canonical Notch ligand 1 (Dlk1; log2FoldChange = -2.24, $P \leq 0.0001$) which is an established inhibitor of adipogenesis and reported to be one of the few genes more highly expressed in WAT compared to BAT (162). Interleukin 15 (IL15; log2FoldChange = -1.58, $P \leq 0.0001$) has a pleiotropic influence on mitochondrial function and thermoregulation with reports of activation of BAT UCP1 gene expression and thermogenesis genes, while opposing data suggested an inhibitory role of WAT browning in obesity(322). RANTES (CCL5; log2FoldChange = -1.66, $P \leq 0.0001$) is a pro-inflammatory cytokine involved in insulin resistance (542). Deletion of TLR4 clearly attenuated the LPS-mediated effect. This suggests that TLR4 facilitates most of the cellular response caused by LPS. However, the changes in this particular set of genes expression were not translated to cytokine secretion detected by proteome array. It is possible the proteome assay was not sensitive enough to detect such changes, or their transcription might be blocked by certain physiological process. More research is needed to understand the influence of these LPS-TLR4 triggered alteration in gene expression.

Figure 4.3.7.3 Cytokines Heatmaps from RNA-Sequencing and q-RT PCR to confirm RNA-sequencing results for Selected Novel Cytokines.

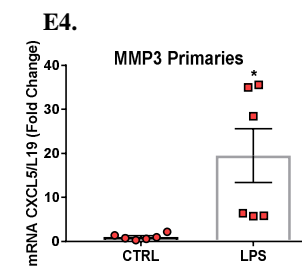
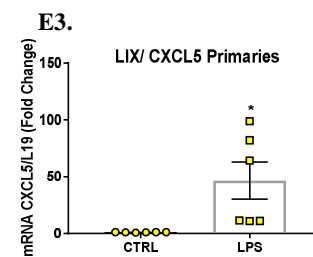
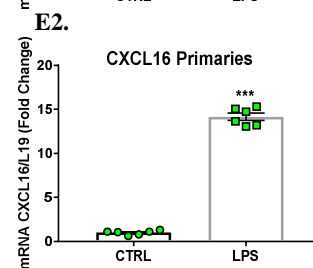
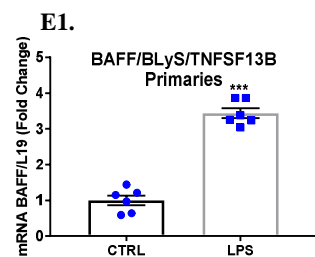
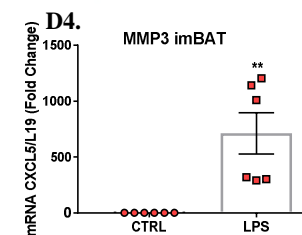
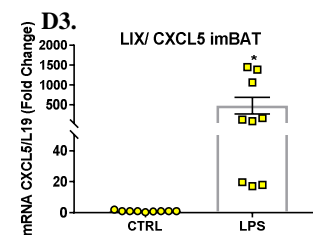
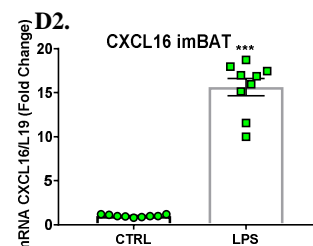
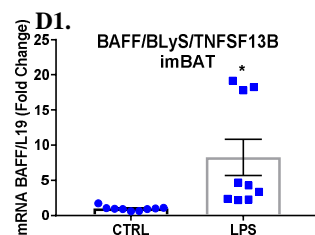
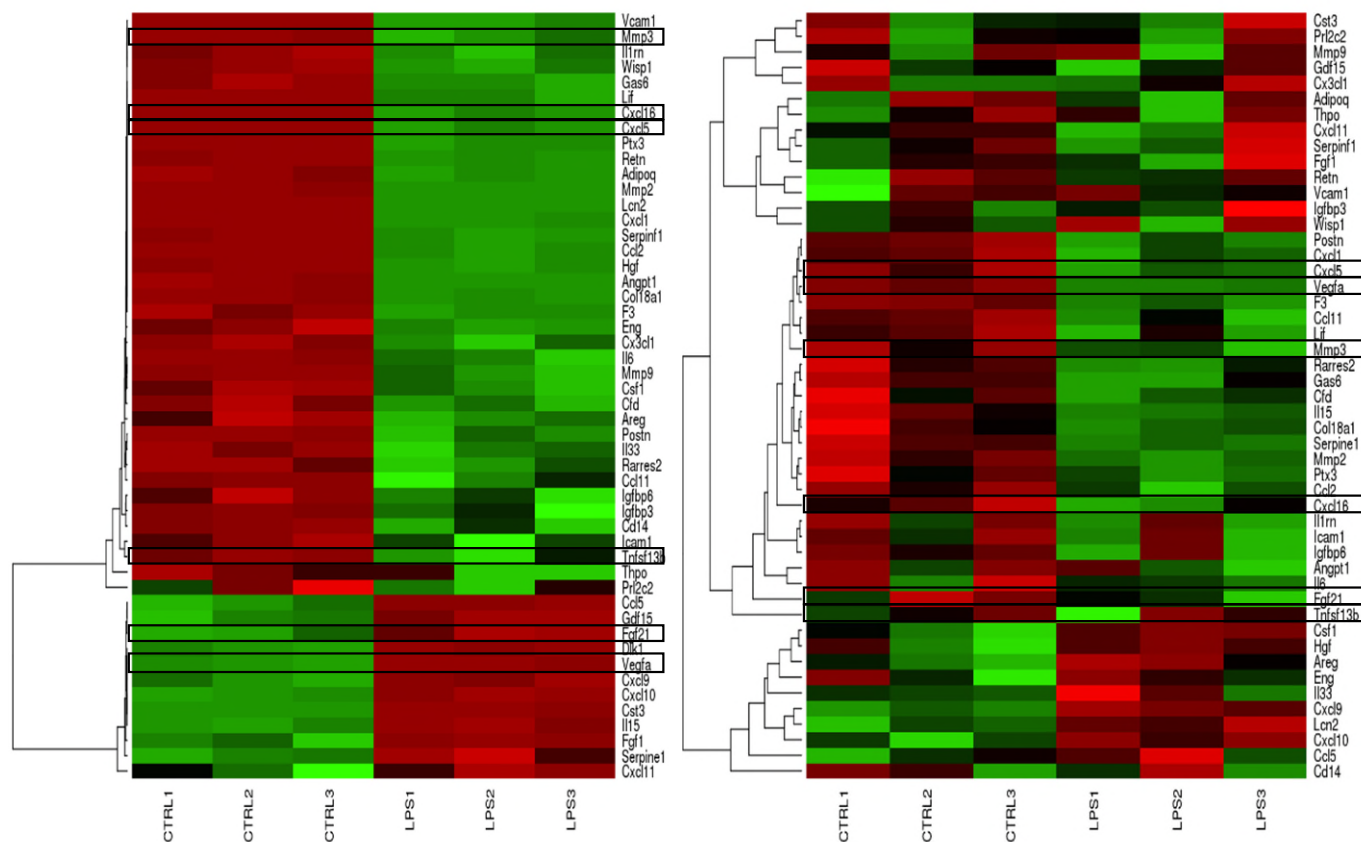
for C1. Wt.imBAT cells, C2. TLR4ko.BAT cells. q-RT PCR to confirm RNA-sequencing results for BAFF (D1. in imBAT cells, E1. in primary cultures), CXCL16 (D2. in imBAT cells, E2. in primary cultures), LIX (D3. in imBAT cells, E3. in primary cultures), MMP3 (D4. in imBAT cells, E4. in primary cultures). q-RT PCR imBAT, primary cultures data represent the mean of three (total n=9 each treatment), two experiments (total n=6 each treatment), \pm SEM. *P < 0.05, ** P < 0.01, ***P < 0.001 control vs. LPS. Two-tailed unpaired Student's t-test. Rows in heat maps represent the different genes and each column represents a sample. For the relative gene expression level of each sample a different colour of the red-green scale is assigned. Green represents an expression level above the mean, red colour represents expression below the mean



wt. imBAT



TLR4ko.BAT



4.4 Discussion

BAT presents an important target to treat obesity and related disorders. Understanding brown adipocyte physiology has great potential for treating the underlying dysfunction which occurs in the progression of obesity. As such, establishing an array of physiologically secreted factors which can be altered by inflammatory markers present in the obese state is an important aspect, and can lead to novel targets to prevent brown adipocyte dysfunction and improve metabolism. Therefore, a wide range of LPS-mediated effects was investigated at the gene expression and secreted protein levels. This was important to determine the effects of LPS beyond its role in repressing features of the thermogenesis programme (described in the previous chapter). The main outcome is LPS is a potent stimulator of a cascade of detrimental effects on brown adipocytes including upregulating pathways involved in inflammation and cancer, mainly through TLR4, but it still appears to have limited effects in the absence of the TLR4 receptor.

Differentiation of brown adipocytes with LPS led to the induction of genes related to inflammation, cancer, immune response and stress response related pathways, alongside inhibition of mitochondrial function and glucose metabolism. Alterations in gene expression were investigated by intensive RNA-sequence analysis for genes associated with gene-ontology and KEGG pathways. In fact, insulin resistance and increased predisposition to T2DM is promoted by immune response and stress response which include a transition in macrophage polarization from an alternative M2 activation state maintained by STAT6 and PPARs to a classical M1 activation state driven by NF κ B, AP1, and other signal-dependent transcription factors that play crucial roles in innate immunity (81). Interactions among adipocytes and adipose-resident immune cells enhance adipocyte lipolysis and secretion of lipids, as well as adipocyte and immune cell production of multiple pro-inflammatory factors with drops in anti-inflammatory markers. Negative effects of these alterations on peripheral target tissues can subsequently induce insulin resistance and hyperinsulinemia, hyperglycemia, hyperlipidemia, and vascular injury and cell death, all of which are associated with oxidative stress and cancer development and/or progression (13). Therefore, given the current findings LPS-mediated inflamed adipose tissue could impact the tumour microenvironment, which potentially associated with the strong

relationship between adiposity and a variety of tumours. These findings that LPS acts as an upstream modulator of such pathways are consistent with the fact that obesity is generally characterized by low-grade chronic inflammation and increases the risk of cancer as well as risk of T2DM (13,81,348).

ECM-receptor interaction was among the pathways with upregulated genes upon LPS treatment as well, with increased gene expression and secreted factors. Secretion was studied by performing a proteome array. ECM-receptor interaction pathway activation indicated the abnormal expression of extracellular matrix receptor in LPS-treated brown adipocytes, which might lead to paracrine effects *in vivo* through downstream stimulation of secretion of multiple mediators. For instance, in other cell types, the increase in collagen and fibronectin leads to increased inflammation and fibrosis through the activation of integrin receptors, and the possible downstream consequences of activation of integrin molecules can be activation of ERK, AKT, JNK (266,582). However, the role of integrin and other ECM receptors in brown adipose tissues has not been studied before. These results also showed that peptides derived from ECM-related proteins are greatly altered upon LPS treatment which could act as important players in impairing BAT activation and thermogenesis. It could also be speculated that these peptides are being upregulated to enhance supporting structural networks of brown adipocytes to form new blood vessels in an attempt to compensate for LPS-damage and meet functional thermogenic demands. Nevertheless, brown adipocytes eventually fail to deal with LPS stress due to down regulation of the main brown fat characteristics described in chapter 1, including UCP1 downregulation at basal and CL-induced level. It should be noted that this induction is not attributable to a central effect and is completely independent from the central nervous system since these brown adipocytes are cultured *in-vitro* and are not influenced by exposure to adrenergic agonists.

Differentially expressed genes (DEGs) downregulated by LPS treatment were related to the suppression of brown adipocyte activity. Thermogenesis was the most significant pathway associated with downregulated DEGs when investigating KEGG pathways. There was almost total inhibition of the brown adipocytes program as all well-established brown genes were suppressed by LPS in a TLR4-dependent manner. Interestingly, Huntington disease (HD) and Parkinson's disease (PD) related gene groups were downregulated by LPS. Both HD and PD are associated with high energy

expenditure and weight loss (623,624). WAT of HD mice presents brown-like features such as a high level of UCP1 (625) and a PD model is reported to be associated with activation of BAT-mediated thermogenesis and increased expression of UCP1 (624). This may explain why the HD and PD pathways are negatively enriched in LPS-treated brown adipocytes and provide further support of negative LPS impact on brown adipocytes and impairment of thermogenesis.

p38 appears to play an important role in LPS-mediated down regulation of thermogenesis. There is contradictory data concerning its role which is indicative of both pro- and anti-thermogenic actions. How these different actions affect BAT biology needs further investigation. In this context, p38 acts differently under different situations, with activation of p38 as part of the innate immune system inflammatory response (TNF α , LPS) appearing to negatively affect thermogenesis by a mechanism yet to be identified, probably dependant on changes in other signals/factors. Overall, the present data suggests a controversial potential therapeutic prospect by targeting p38 β and p38 δ for treatment of obesity and increasing thermogenesis. Future studies examining the effects of selective p38 β and p38 δ targeting at the protein level with *in vivo* investigations as to what other factors are involved in p38 actions will elucidate the functional roles of these two p38MAPKs in the thermogenesis process, and will guide future therapeutic strategies.

Only limited effects of LPS in TLR4ko.BAT were observed. TLR4-dependent actions of LPS are evidenced by the fact that nearly all BAT-associated genes are down-regulated by LPS in wt.BAT and when knocking out TLR4, this downregulation was eliminated. Although some pathways associated with up/down-regulated DEGs are significantly enriched in TLR4ko.BAT, it was to a much lower extent than wt.BAT in terms of number of genes in each pathway and fold change values of each gene. This suggests that the TLR4-receptor in brown adipocytes mediates almost all LPS actions and indicates that deletion of TLR4 massively attenuates the LPS effect. Following proteome array analysis, four novel cytokines were selected for further study due to their high level of secretion, expression and large response to LPS. This suggest a potential important role in brown adipocyte dysfunction, and as such these cytokines were studied further:

BAFF, TNF superfamily ligand (TNFSF13B), is a transmembrane protein from which a soluble BAFF form can be released into media. BAFF is mainly produced by cells

of the immune system including monocytes, macrophages, neutrophils, dendritic cells, and T lymphocytes, and is found to be elevated in autoimmune diseases (626,627). Interestingly, BAFF is also reported to be involved in obesity-related metabolic disorders such as insulin resistance and oxidative stress (628–630). In white adipocytes and adipose tissue, it is reported to be secreted and acts as an adipokine that regulates inflammation in obesity (631). It is secreted from white adipocytes under inflammatory stimulus such as TNF α treatment and increases their cytokine secretion (632). Deletion of BAFF results in reduced diet-induced obesity and reduced circulating inflammatory cytokines (628,631). Hence, BAFF appears to play an important role in obesity and related metabolic dysfunction. However, there is a lack of understanding regarding the cellular influence of BAFF in the development of systemic inflammation in obesity. This study is the first to show the secretion of BAFF from brown adipocytes. BAFF induction upon LPS treatment in brown adipocytes could indicate its role in brown adipocyte inflammation as well as in thermogenesis during obesity. Having confirmed the secretion of BAFF by brown adipocytes, understanding its role in brown adipose tissue and the possible mechanisms by which it could regulate BAT activity might provide therapeutic opportunities to target obesity-related chronic diseases.

CXCL16 is a transmembrane chemokine involved in leucocyte recruitment, with a role in kidney diseases, atherosclerosis, and liver injuries (633). In addition, it is an angiogenic factor that induces angiogenesis via extracellular signal-regulated kinase pathways (633). CXCL16 is found to be higher in serum of obese compared to lean mice with lower expression in WAT of lean mice. As angiogenesis accompanies adipogenesis in obesity development and almost all its related disorders (e.g T2DM, cardiovascular disorders and malignancies), it is possible that altering angiogenesis through modulating CXCL16 action may offer a novel therapeutic approach to ameliorate the development of obesity (634). In fact, angiogenesis modulators were demonstrated to reduce adipose tissue mass and prevent obesity. They also are reported to positively affect energy balance and energy expenditure (635–638). However, given that adipose tissue is one of the biggest tissues in the body, effective angiogenesis-targeted therapy would probably require systemic delivery of angiogenesis modulators, which may lead to many side effects. In addition, the metabolic state of adipose tissue must be considered. Thus, it is important to identify

and study new potential targets such as CXCL16. CXCL16 is reported to be secreted from brown adipocytes under stimulation of bone morphogenetic protein 8b (BMP8b) (18). However, this is the first time its secretion has been found to be subject to LPS stimulation. Further studies are needed to investigate the role of CXCL16 in BAT remodelling and thermogenesis in inflammatory conditions such as obesity and associated disorders.

LIX/CXCL5 is known as LPS-induced CXC chemokine (LIX). It amplifies a pro-inflammatory cytokine response and has been linked to tumour progression as it promotes breast cancer cell proliferation (639). It is reported to be secreted from WAT-resident macrophages and it is suggested to link inflammation in obesity and insulin resistance. This is because CXCL5 is dramatically increased in the serum of human obese patients with insulin resistance compared to lean subjects and it decreases with weight loss. Furthermore, neutralizing CXCL5 leads to protection against obesity-induced insulin resistance (640,641). Its secretion by brown adipocytes has not been reported previously. CXCL5 is a potential candidate for the whitening of brown adipocytes in obesity by making them less responsive to insulin. This needs further investigation to determine if CXCL5 inhibition can help in treating obesity and associated disorders.

MMP3 is a member of the Matrix Metalloproteinase family that are responsible for the degradation of ECM proteins. This family is involved in wound healing, angiogenesis, and tumour cell metastasis. MMP imbalance is associated with the pathophysiology of obesity and T2DM in humans (266) and MMP3 is upregulated in obese animals (642). MMP3 is reported to be secreted from brown adipocytes following BMP8b treatment (18). The expression and secretion of MMP3 in response to LPS could indicate an important role in modulating BAT biology and possibly reduced thermogenesis. However, further studies are needed to explore the consequence of MMP3 production by brown adipocytes in BAT function as well as obesity.

Collectively, the current study further strengthens the ideology that BAT acts as a major endocrine organ that can participate in driving systemic chronic inflammation and obesity-related metabolic diseases. In addition, the data supports that LPS is a potent player in obesity and has a negative impact on brown adipocyte activity and the vascular network regulating thermogenic demands. Furthermore, the findings indicate

that LPS-mediated inflammation and associated changes with ECM components could lead to fibrosis in BAT during the development of obesity. Thus, it raises the possibility that an increase in angiogenesis and adipogenesis in obesity can cause brown adipocyte hyperplasia and the development of inflammation can lead to fibrosis and whitening of brown adipocytes. To a large extent, these negative effects of LPS appear to be mediated by TLR4. However, further studies are needed to confirm that inhibition of the TLR4 pathway or more practically up/downstream of TLR4 pathway activation can be used as a therapeutic target. In addition, follow up investigations on the cytokines identified in this study (BAFF, LIX, CXCL16, MMP3) is warranted to explore their therapeutic potential. Overall, these results suggest LPS is a major player in inflammation induced adipocyte dysfunction, impacted by conditions of obesity and its comorbidities possibly exacerbated by induction of brown adipocyte inflammation. Hence, interventions in LPS-activated pathways harbour the potential to provide novel strategies to increase BAT activity as a therapeutic target for obesity.

Chapter 5. Lipopolysaccharide Mediates Mitochondrial Alteration in Brown Adipocytes

5.1 Introduction

Inflammation and obesity are closely linked with alteration in mitochondrial function and mass (468,487). There is a suggestion that mitochondrial dysfunction in adipocytes is a primary cause of, adipocyte enlargement and insulin resistance (497). In this context, mitochondrial dysfunction and fatty acid oxidation in adipocytes leads to adipocyte enlargement due to triglyceride accumulation (497). Furthermore, adipocyte mitochondrial dysfunction leads to pseudo-hypoxia with enhanced accumulation of the hypoxia-inducible factor 1 α (HIF-1 α), which elevates adipose tissue inflammation and fibrosis (496,497). Similarly, an alteration of mitochondrial capacity in BAT could be functionally associated with defective thermogenesis and energy expenditure in obesity and an increased risk to develop obesity-induced insulin resistance (344). That may arise as mitochondria are present in large numbers within BAT and they play an important role in BAT thermogenesis. In general terms, energy production in eukaryotic cells (primarily in the form of ATP) occurs in the mitochondrion through OXPHOS or the electron transport chain (ETC) which is comprised of several inter-membrane proteins (complex I, II, III, IV and ATP synthase) located in the inner mitochondrial membrane. In this process, reducing agents NADH and FADH₂ (generated from upstream pathways such as glycolysis, Krebs's cycle and fatty acid beta-oxidation) are oxidized to NAD and FAD by complex I/ complex II, generating electrons, which are carried over from complex I of the ETC to II and so on to IV and O₂, generating H₂O. In parallel to this, protons are pumped from the matrix through to the inter-membrane space to produce an electrochemical gradient that will become the driving force for the ATP synthase complex to produce ATP from ADP (485). UCP1 is an inter-membrane protein plays an important role in lowering this electrochemical gradient and increasing the proton leak by utilizing protons energy for thermogenesis, this is referred to as uncoupled OXPHOS. This is particularly relevant in the obesity state when there is imbalance between energy demand and supply. As such, uncoupling efficiency means fuel consumption can be accelerated and is independent of ATP saturating concentration to meet the energy demand (617).

In prior mouse models of chronic systemic inflammation, there is increased systemic inflammatory cytokine levels and abnormal regulation of both innate and adaptive immune responses. Furthermore, in this situation mitochondrial fuse is detected with

severe damage of the cristae, in addition to reduced cold-induced thermogenic capacity and UCP1-dependent mitochondrial respiration (499). Additionally, low grade BAT inflammation in obesity is noted as a contributor to excess reactive oxygen species (ROS) production and associated oxidative stress, which may cause mitochondrial dysfunction (500–504). Further investigations in BAT in obese mice has affirmed increased inflammation and ROS generation, accompanied by a doubling of mitochondria respiration compared to lean counterparts (341). It is possible to speculate that under prolonged weight gain in mice, mitochondria become increasingly dysfunctional with their thermogenic capacity ultimately compromised (341). Further evidence linking inflammation and mitochondrial dysfunction was demonstrated by deletion of the mitochondrial transcription factor A (TFAM) resulting in adipocyte cell death coincident with inflammation in WAT and a whitening of BAT with decreased energy expenditure. BAT whitening in these mice is mainly explained by impairments of mitochondrial electron transport chain function, reduced fatty acid oxidation, and increased circulating fatty acids, rather than a conversion of brown to white adipocytes (509). These alterations in mitochondria during inflammation in WAT are further demonstrated by a downregulation of mitochondrial biogenesis, oxidative metabolic pathways, and oxidative phosphorylation proteins in obesity, and a negative correlation with pro-inflammatory cytokines (488). In fact, pro-inflammatory cytokines have a significant influence on modulating mitochondrial efficiency leading to effects on energy homeostasis in human white adipocytes. For instance, TNF α dramatically alters 3T3-L1 adipocyte mitochondrial functions, whereas IL1 β and IL6 have more modest effects. In general, how inflammatory markers mediate mitochondrial dysfunction in BAT is less studied. It has, however, been demonstrated that activation of the NLRP3 inflammasome in macrophages attenuates UCP1 induction and mitochondrial respiration in cultures of primary adipocytes possibly via IL-1, while the absence of NLRP3 is protective for UCP1 and adaptive thermogenesis capacity in adipocytes (356,489,490).

The activation of pattern recognition receptors in brown adipocytes and subsequent increased inflammation leads to mitochondrial dysfunction and suppression of mitochondrial respiration with reduced UCP1 expression levels and repressed white adipocyte browning capacity in response to adrenergic stimulation (344,355,356). Moreover, deletion of TLR4 protected mitochondrial function and thermogenesis in

WAT (356). It has been proposed that the effect of LPS on brown adipocytes causes mitochondrial dysfunction (344). Therefore, this current study was to further investigate the chronic effect of LPS mitochondrial dysfunction which has not been studied in depth before.

In Chapter Three, activation of TLR4 by LPS in brown adipocytes attenuated both basal and CL-induced UCP1 levels with a reduction in key brown fat gene expression levels. The objectives of this chapter were to determine broader range of abnormalities in mitochondrial function in wild-type LPS-treated brown adipocytes cell model with a specific focus on:

- Investigation of mitochondria oxidative stress.
- Definition of mitochondria dynamics and biogenesis.
- Evaluation of mitochondria respiration and bioenergetics.

5.2 Methods

Immortalized brown pre-adipocytes (imBAT) were differentiated into mature adipocytes over 8 days with or without LPS 100 ng/mL or 1000 ng/mL; E. Coli O55:B5, Sigma, L6529 (100 ng/mL if not indicated), according to the differentiation protocol described in the methods section (Chapter 2). Hereafter, RNA and protein were harvested for qRT-PCR and Western blotting according to methods described in the methods section (Chapter 2). DNA was harvested for mitochondrial DNA-copy number assessments as described below. Also, cells were studied with a Seahorse XF Analyser to determine impact on mitochondrial function. Fluorescence live cell imaging using a spinning disk confocal microscope was conducted to assess mitochondrial membrane potential according to methods outlined in the methods section (Chapter 2). ATP measurements were performed in live cells as detailed below. Functional assays to determine reactive oxygen species (ROS), superoxide dismutase (SOD) and catalase activity were undertaken as described below after harvesting the cells.

5.2.1 Mitochondrial DNA (mt-DNA) Copy Number Evaluation

Total DNA was extracted from cell lysates containing approximately 1×10^6 brown adipocytes differentiated over 8 days with or without LPS 100 ng/mL, according to differentiation protocol, using DNeasy Blood and Tissue Mini Kit (#69504 Qiagen, UK) in accordance with the manufacturer's instructions. RNase treatment was performed to eliminate possible RNA contamination. DNA was eluted with 100 μ L AE buffer and quantified using a spectrophotometer (Nanodrop ND-1000, Labtech). 10 ng of DNA was used to determine relative amounts of mitochondrial DNA copy number through qRT-PCR in an ABI Prism7500 thermo cycler (Life Technologies) with use of SYBR Green JumpStart Taq ReadyMix (#S4438 Sigma-Aldrich, UK). Mitochondrial (mtND1) and nuclear (RIP140) gene primers in table below were used to determine relative amounts of mitochondrial DNA. Each sample was measured in duplicate. The mitochondrial number was calculated based on the following formula: $\text{mtDNA copy number} = 2^{\Delta\text{CT}}$, where $\Delta\text{Ct} = \text{mtND1} - \text{RIP140}$

Gene		
ND1	Forward	5' –ATTTATCTCAACCCTAGCAGAAACAAA- 3'
	Reverse	5' – AAACCCTGATACTAATTCTGATTCTCCTT - 3'
RIP140	Forward	5' –GAACCTGGGCTTTTGAATGG- 3'
	Reverse	5' –GTTTTGGTCAGTCTTGGAGAGTCTT- 3'

5.2.2 Reactive Oxygen Species (ROS) Assay

Immortalised pre-brown adipocytes were seeded onto gelatin-coated 96-well black opaque cell culture plates at a density of 10,000 cells/well. Cells were grown and differentiated in phenol-free media (DMEM/F-12, #11039047 Gibco) according to the standard protocol and differentiation was carried out with or without LPS (100 or 1000 ng/mL, E. Coli O55:B5, Sigma, L6529). A fluorescence assay was used to indicate ROS levels within the live cells, by using non-fluorescent H2DCFDA, which is converted to highly fluorescent 2',7'-dichlorofluorescein (DCF) upon cleavage of the acetate groups by intracellular esterases and oxidation. Adherent cells were washed with 1x HBSS buffer (#14065056 Gibco) and incubated with diluted H2DCFDA stain to final concentration 60 μ M in HBSS (# D399, Invitrogen, H2DCFDA were dissolved in ethanol) for 20 minutes at 37 °C. Dye Solution was removed, cells were washed with 1x HBSS buffer and maintained in 1x HBSS buffer in the presence and absence of H₂O₂ (75 μ M). Fluorescence was read with a PheraStar FS microplate reader (BMG Labtech) at 485/535 nm excitation/emission immediately and every 10 minutes up to one hour with cells were maintained at 37 °C. For background correction, cells with no DCF and were used. Fluorescence measurements for each treatment group were plotted as an indication of ROS levels. Both DCF stain concentration, incubation time and H₂O₂ concentration were optimized prior to experiment.

5.2.3 Endogenous Antioxidant Activity Assays (SOD Assay & Catalase Assay)

The activity of endogenous antioxidants superoxide dismutase (SOD) and catalase was assessed with a colorimetric method, using OxiSelect™ Superoxide Dismutase Activity Assay (STA-340) and OxiSelect™ Catalase Activity Assay (STA-341) Kits (Cell Biolabs). Following brown adipocyte differentiation with or without LPS (100 or 1000 ng/mL, E. Coli O55:B5, Sigma, L6529) according to the standard protocol, 1.2 x 10⁶ adherent cells were washed 3 times with ice-cold PBS, harvested with a cell

scraper in 1 mL of cold Lysis buffer (10 mM Tris, pH 7.5, 150 mM NaCl, 0.1 mM EDTA). Samples were then homogenised, centrifuged and stored at -80°C until assayed. All assays were performed within 1 month of sample collection and were conducted according to manufacturer's instructions. Absorbance was read using a PheraStar FS microplate reader (BMG Labtech) at 490 nm for SOD activity and at 520 nm for catalase activity.

SOD activity was calculated based on optical density as illustrated in the following formula: SOD activity (inhibition %) = $(OD_{\text{blank}} - OD_{\text{sample}}) / OD_{\text{blank}} \times 100$

The concentration of active Catalase was determined by interpolation of a catalase standard curve (ranging from 0 – 1600 Units/mL) where plate reader analysis software (PheraStar FS) was used with a 4 parameter logistic curve fitting program to calculate a second order polynomial regression for each sample, and Catalase activity in Units/mL value for each sample were collected.

5.2.4 ATP Assay

Immortalised brown pre-adipocytes were seeded onto gelatin-coated 96-well white opaque cell culture plates at a density of 10,000 cells/well. Cells were grown and differentiated according to the standard protocol and the differentiation carried out with or without LPS (100 or 1000 ng/mL, E. Coli O55:B5, Sigma, L6529). Bioluminescent determination of ATP abundance was conducted using EnzyLight™ ATP Assay Kit (BioAssay Systems, EATP-100) following the manufacturer's instructions for adherent cells. Luminescence was read using a PheraStar FS microplate reader (BMG Labtech), and ATP concentrations determined based on interpolation of a standard curve of known ATP concentrations ranging from 0 – 30 µM.

5.3 Results

5.3.1 LPS Administration Up-Regulated Oxidative Stress

Oxidative stress was assessed via fluorescence measurement of DCF dye as representative of total levels of reactive oxygen species (ROS). LPS markedly increased total ROS which rose by up to 50 % when exposed to oxidative agent Hydrogen peroxide (H_2O_2), while the basal levels were unaltered (Figure 5.3.1.1). H_2O_2 causes a high stress condition which leads to a great increase in ROS production (643,644); as LPS-treated cells were less able to cope with H_2O_2 -induced stress, ROS production was significantly higher in these cells compared to control cells. This increase in ROS under stress may indicate suppression of the capacity of endogenous antioxidant systems in cells differentiated with LPS.

The expression of primary antioxidant enzymes, which neutralise or prevent the formation of free radicals, including Glutathione peroxidase (Gpx1, Gpx2), catalase (CAT), and superoxide dismutase (SOD) was investigated. In addition to peroxiredoxins (PRDX3) which neutralize small amounts of peroxides; these enzymes use their interior active site cysteine residues to reduce target molecules (645). As expected, Catalase showed a marked decrease with LPS treatment, both in terms of mRNA transcript levels (27 % with LPS 100 ng/mL, 69 % LPS 1000 ng/mL ($P < 0.001$); Figure 5.3.1.2, B) and a striking decrease in activity (92 % with LPS 100 ng/mL ($P < 0.0001$), 99 % LPS 1000 ng/mL ($P < 0.0001$); Figure 5.3.1.1, B). The activity of endogenous antioxidant superoxide dismutase (SOD) was significantly impaired with LPS treatment (27 % with LPS 100 ng/mL ($P < 0.01$), 48 % LPS 1000 ng/mL ($P < 0.0001$); Figure 5.3.1.1, B), while LPS treatment resulted in no change in SOD2 mRNA transcript levels (Figure 5.3.1.2, A).

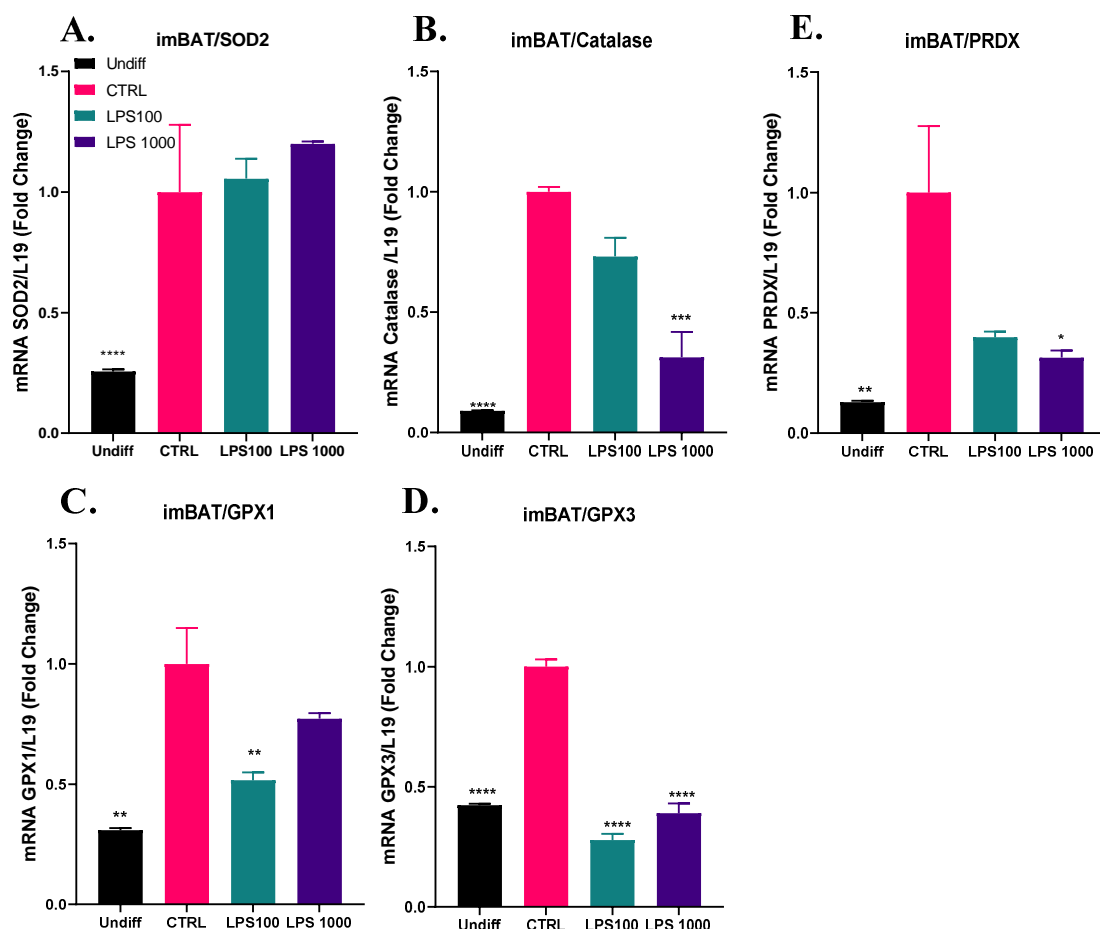


Figure 5.3.1.2 Effect of LPS on Brown Adipocyte Antioxidants Enzymes.

ImBAT cells were differentiated with/without LPS (100 ng/mL or 1000 ng/mL). mRNA expression levels of (A) SOD2 (n=3), (B) Catalase (n=3), (C) GPX1 (n=3), (D) GPX3 (n=3) and (E) PRDX (n=3). Data are expressed as mean \pm standard error of the mean. one-way ANOVA was used for comparisons. *p<0.05, **p<0.01, ***p<0.001, ****p<0.0001 Compared to CTRL. SOD2; Superoxide dismutase 2. Gpx1: glutathione peroxidase 1. Gpx3: glutathione peroxidase 3. PRDX: peroxiredoxin3. CTRL; control

5.3.2 LPS Administration Resulted in Alteration in Mitochondrial Proteostasis

Given that LPS resulted in increased ROS accumulation in response to H₂O₂ and impaired endogenous antioxidant response, the possibility of damage to mitochondrial protein translation was investigated. Abnormal mitochondrial proteostasis occurs as a result of mitonuclear protein imbalance when protein synthesis from mitochondrial DNA (mtDNA) is not matched by protein synthesis from nuclear DNA (nDNA). In this instance LPS led to adverse effects on mitochondrial protein translation, as evidenced by decreased absolute levels of succinate dehydrogenase complex subunit A (SDHA) protein (approximately 1.6-fold decrease, P<0.01) and gene expression

levels (approximately 1.5-fold decrease, $P < 0.05$) (Figure 5.3.2.1, A, C1, C2), when imBAT cells were differentiated with LPS. Also, LPS reduced mRNA expression levels of MtDNA-encoded cytochrome c oxidase subunit 1 (MT-CO1) (approximately 3-fold decrease maximum, $P < 0.01$) (Figure 5.3.2.1, B), however, MT-CO1 protein absolute variations were less obvious (Figure 5.3.2.1, D1, D2). The protein ratio indicated an increase of mitochondrial protein encoded by mitochondrial DNA (MT-CO1) versus nuclear DNA-encoded mitochondrial protein (SDHA), although this increase was not significant (Figure 5.3.2.1, E). As a result, LPS induces mitonuclear protein imbalance which possibly disturbs mitochondrial proteostasis.

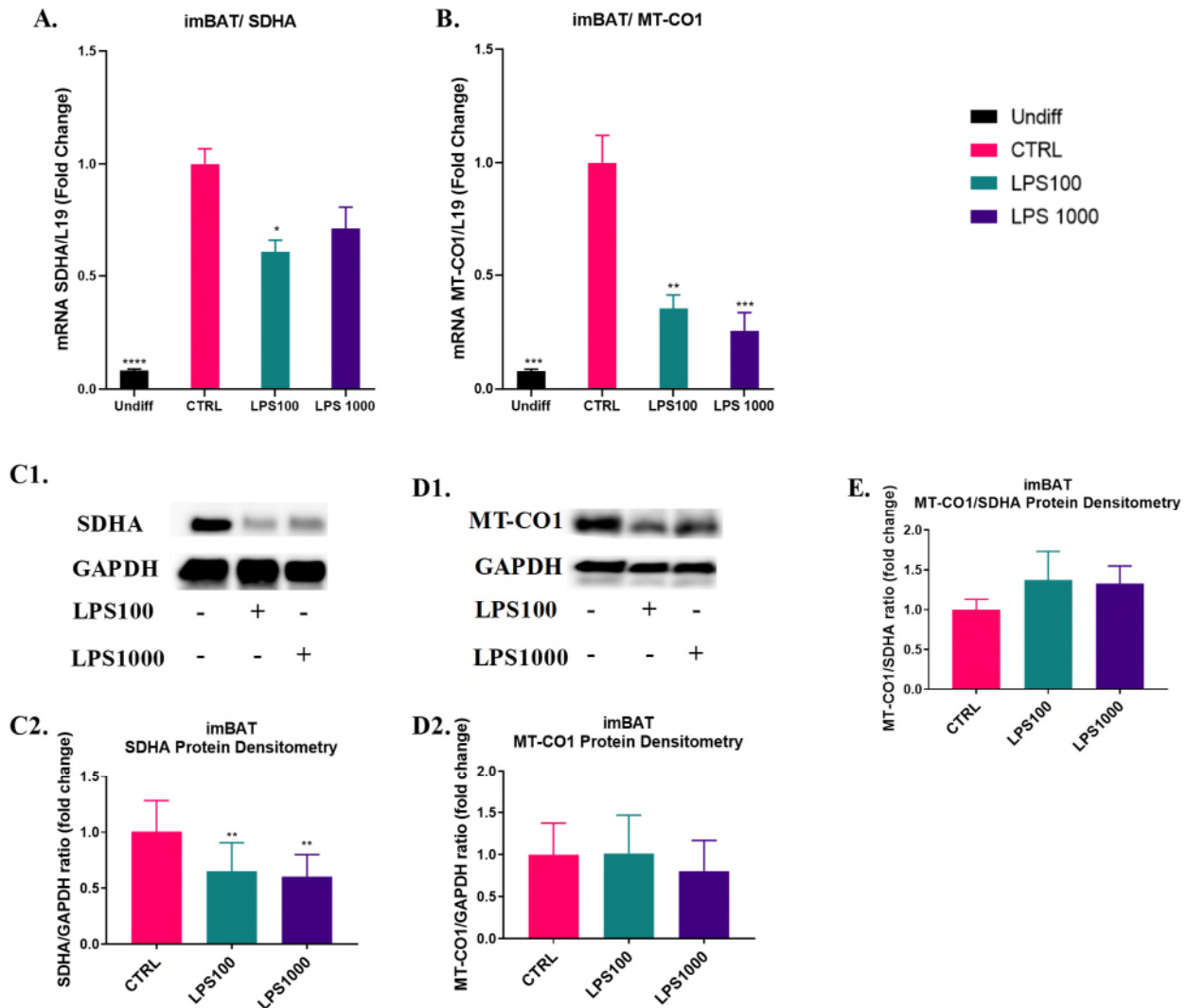


Figure 5.3.2.1 Mitochondrial Protein Abundance (Denoted by Mitochondrial MT-CO1 to Nuclear SDHA Protein Ratio) in imBAT following Differentiation with/without LPS (100 ng/mL, 1000 ng/mL).

mRNA expression levels of (A) SDHA (n=3), (B) MT-CO1 (n=3). Western blot membrane images of (C1) SDHA and loading control GAPDH, (D1) MT-CO1 loading control GAPDH. Densitometry of absolute levels of SDHA (C2) and MT-CO1 (D2). (E) Densitometry of relative levels of mitochondrial MT-CO1 to nuclear SDHA protein. Data are expressed as fold change from control, and bars represent means \pm standard error of the mean. Two-way ANOVA was used for comparisons. **p<0.005, compared to CTRL. CTRL; control. SDHA; Succinate dehydrogenase complex subunit A, MT-CO1; MtDNA-encoded cytochrome c oxidase subunit 1. GAPDH; glyceraldehyde-3-phosphate dehydrogenase.

5.3.3 LPS Administration Resulted in Deterioration in Mitochondrial Dynamics

LPS appears to reduce mitochondrial dynamic indicators evidenced by investigations on both gene expression and protein levels. In this context, the expression of genes associated with mitochondrial fission were reduced, including Dynamin-1-like protein

(DRP1; 3.2-fold decrease; $P<0.001$, Figure 5.3.3.1 A) and Mitochondrial fission 1 (FIS1; 1.8-fold decrease; $P<0.01$ Figure 5.3.3.1 B) when differentiating imBAT cells with LPS. Similarly, genes associated with mitochondrial fusion including Mitofusin 2 (MFN2; 2.4-fold decrease; $P<0.001$, Figure 5.3.3.1 D) and mitochondrial dynamin like GTPase (OPA1; 3-fold decrease; $P<0.05$, Figure 5.3.3.1 C) were reduced when differentiating imBAT cells with LPS.

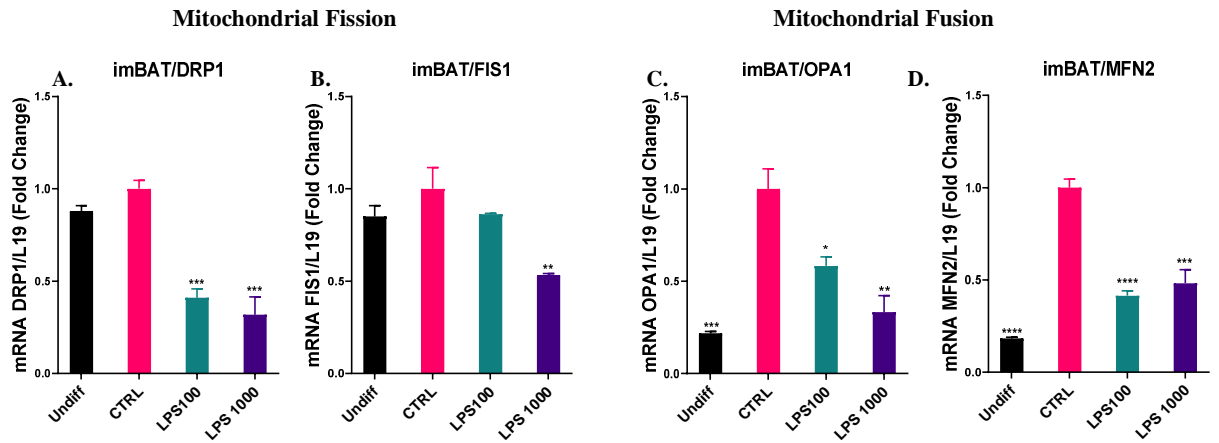
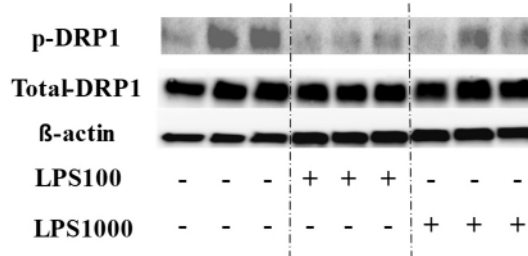


Figure 5.3.3.1 Effect of LPS on Genes Involved in Mitochondrial Dynamics in Brown Adipocytes.

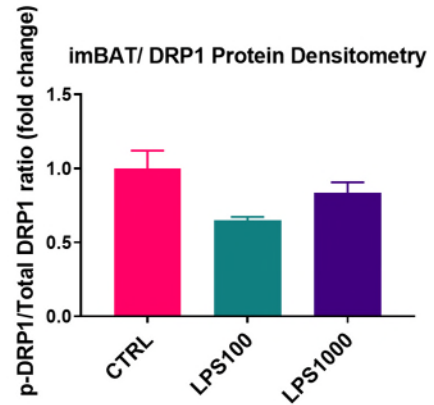
ImBAT cells were differentiated with/without LPS (100 ng/mL or 1000 ng/mL). Mitochondrial fission genes: DRP1 gene expression levels (A) and FIS1 gene expression levels (B). Mitochondrial fusion genes: OPA1 gene expression levels (C) and MFN2 gene expression levels (D). Data are expressed as a mean of fold change from control cells. Bars represent means \pm standard error of the mean. * $p<0.05$, ** $p<0.01$, *** $p<0.001$, **** $p<0.0001$ compared to CTRL. One-way ANOVA was used for comparisons. CTRL; control. MFN2: Mitofusin 2; OPA1: mitochondrial dynamin like GTPase; DRP1: Dynamin-1-like protein; FIS1: Mitochondrial fission 1 protein.

These changes in gene expression were accompanied by alterations in proteins associated with mitochondrial dynamics. Investigations of phosphorylated mitochondrial fission protein p-DRP1 showed a reduction (1.2-fold decrease; Figure 5.3.3.2 A A1) in imBAT cells differentiated with LPS as well as both forms of mitochondrial fusion proteins: OPA1 (long OPA1 (L-OPA1) and short OPA1 s-OPA1) (3.4-fold decrease; $P<0.01$ Figure 5.3.3.2 B2 B3). However, the ratio between L-OPA1/S-OPA1 did not change Figure 5.3.3.2, B1.

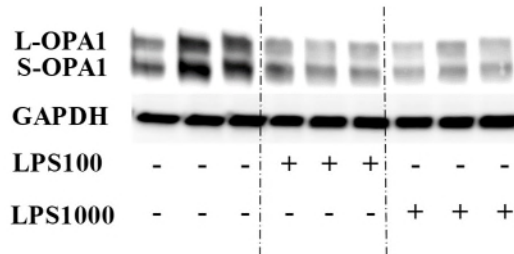
A.



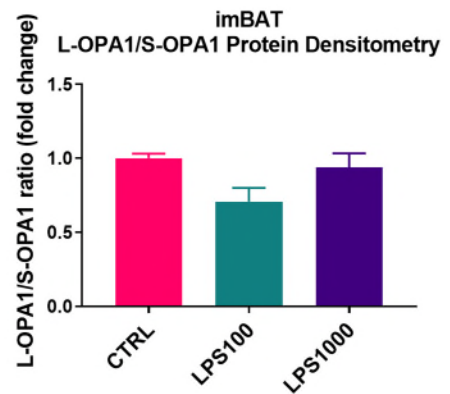
A1.



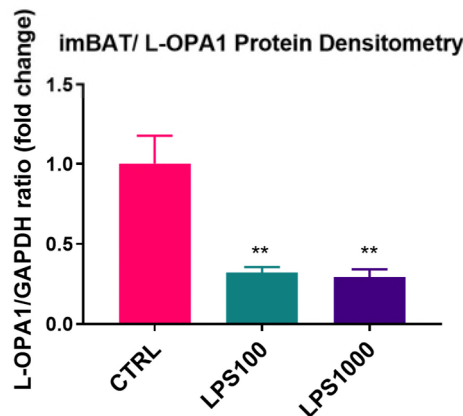
B.



B1.



B2.



B3.

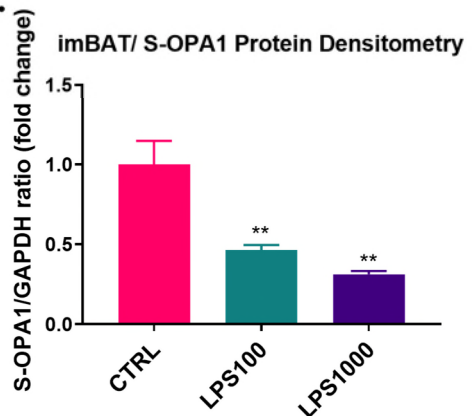


Figure 5.3.3.2 Effect of LPS on Proteins Involved in Mitochondrial Dynamics in imBAT.

ImBAT cells were differentiated with/without LPS (100 ng/mL, 1000 ng/mL). Mitochondrial dynamics-associated protein expression and densitometry including fission protein DRP1 (A, A1) and fusion protein OPA1 (B, B1, B2, B3) in imBAT cells. (A) Image of p-DRP1, total-DRP1 and loading control GAPDH Western blot membranes. (B) Image of L-OPA1, S-OPA1 and loading control GAPDH Western blot membranes. Results are expressed as a mean of fold change from control cells. Bars represent means \pm standard error of the mean. ** $p < 0.01$, compared to CTRL. One-way ANOVA was used for comparisons. CTRL; control. P-DRP1: phosphorylated Dynamin-1-like protein; DRP1: Dynamin-1-like protein; GAPDH: glyceraldehyde-3-phosphate dehydrogenase; OPA1: mitochondrial dynamin like GTPase. L-OPA1: long OPA1; S-OPA1, short OPA1.

5.3.4 LPS Administration Resulted in Alteration in Expression of Genes Associated with Mitochondrial Biogenesis and Oxidative Phosphorylation and Other Important Functions

Following the investigation of LPS on mitochondrial dynamics, the impact of LPS on transcript levels of genes associated with a range of mitochondrial functions (biogenesis, oxidative phosphorylation, uncoupling and general mitochondrial capacity) was investigated in brown adipocytes.

Mitochondrial biogenesis is the process through which mitochondria merge (become larger through fusion) and divide (become smaller through fission) to produce new mitochondria, conserving function and disposing of faulty mitochondrial DNA. Mitochondrial biogenesis is regulated by multiple genes and adequate execution of mitochondrial biogenesis protects mitochondrial DNA quality and function. The expression of genes involved in mitochondrial biogenesis was lower when differentiating the brown adipocytes with LPS compared to control cells. This was the case for tested genes including DNA polymerase gamma (POLG; 1.72-fold decrease; $P<0.01$, Figure 5.3.4.1, A), transcription factor A (TFAM; 4.3-fold decrease; $P<0.001$, Figure 5.3.4.1, B) and nuclear respiratory factor 1 (NRF1; 10-fold decrease; $P<0.0001$, Figure 5.3.4.1, C). Gene expression levels of LPS-treated adipocytes are shown in Figure 5.3.4.1, as fold-change relative to control cells.

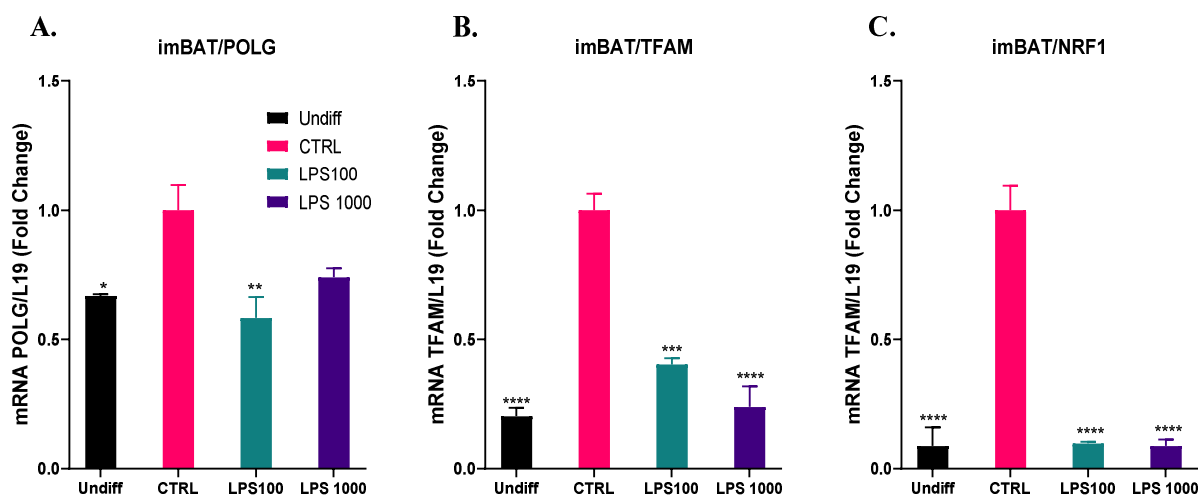


Figure 5.3.4.1 Effect of LPS on Genes Involved in Mitochondrial Biogenesis in Brown Adipocytes.

ImBAT cells were differentiated with/without LPS (100 ng/mL or 1000 ng/mL). (A) POLG gene expression levels. (B) TFAM gene expression levels. (C) NRF1 gene expression levels. Data are expressed as a mean of fold change from control cells. Bars represent means \pm standard error of the mean. * $p < 0.05$, ** $p < 0.01$, *** $p < 0.001$, **** $p < 0.0001$ compared to CTRL. One-way ANOVA was used for comparisons. CTRL; control. POLG; DNA polymerase gamma, catalytic subunit. TFAM; transcription factor A, mitochondrial. NRF1; nuclear respiratory factor 1.

The expression of mRNA levels of genes involved in oxidative phosphorylation (OXPHOS), the primary pathway in mitochondria for energy production in the form of ATP, was investigated. These include oxidase subunit 4 isoform 1 (COX4I1), Cytochrome c, ATP synthase subunit 8 (ATP8) and NADH dehydrogenase subunit 1 (ND1). Differentiating imBAT cells with LPS reduced gene expression of all tested genes with \approx 1.5-fold decrease in COX4I1 ($P < 0.01$, Figure 5.3.4.2, A) and Cytochrome c (Figure 5.3.4.2, B), 6.6-fold decrease in ATP8 ($P < 0.05$, Figure 5.3.4.2, C), and 2-fold decrease ($P < 0.05$) in ND1 (Figure 5.3.4.2, D). This reduction of expression level of these OXPHOS genes when differentiating brown adipocytes with LPS indicates impaired oxidative capacity which is closely linked to insulin actions (646).

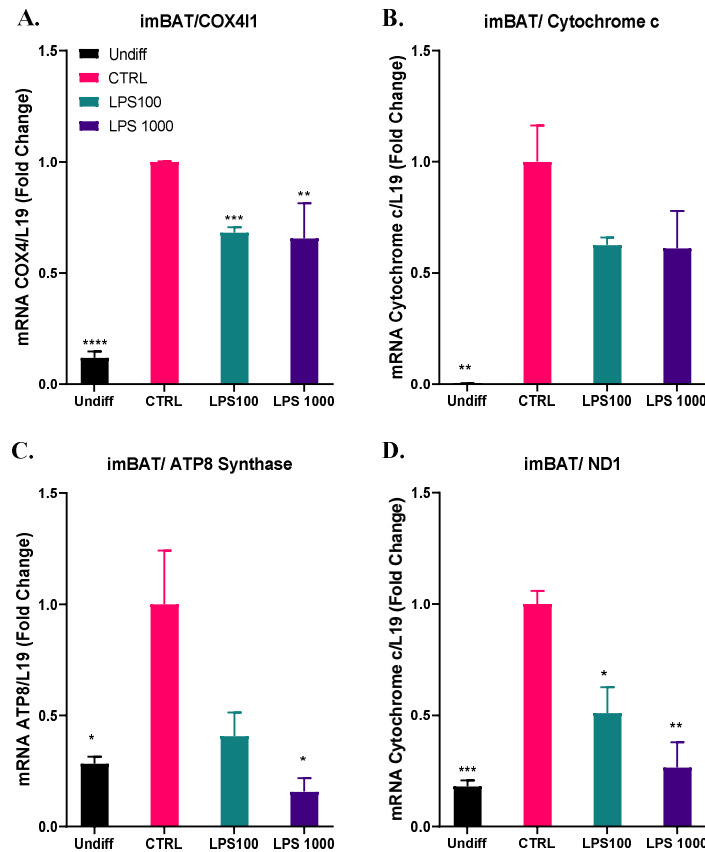


Figure 5.3.4.2 Effect of LPS on Genes Involved in Mitochondrial Oxidative Phosphorylation in Brown Adipocytes.

ImBAT cells were differentiated with/without LPS (100 ng/mL or 1000 ng/mL). (A) COX4I1 gene expression levels. (B) Cytochrome c gene expression levels. (C) ATP8 Synthase gene expression levels. (D) ND1 gene expression levels. Data are expressed as a mean of fold change from control cells. Bars represent means \pm standard error of the mean. * $p < 0.05$, ** $p < 0.01$, *** $p < 0.001$, **** $p < 0.0001$ compared to CTRL. One-way ANOVA was used for comparisons. CTRL; control. COX4I1; oxidase subunit 4 isoform 1. ATP8; ATP synthase subunit 8. ND1; NADH dehydrogenase subunit 1.

In addition, the expression of genes required for other basic mitochondrial functions were investigated. Therefore, the expression of Carnitine palmitoyltransferase 1B (CPT1 β) which mediates mitochondrial fatty acid oxidation, the major contribution for thermogenesis, and citrate synthase (CS), the key enzyme of oxidative metabolism and Krebs Cycle were determined. The expression of both CS and CPT1 β was significantly reduced when imBAT cells were differentiating with LPS with 14-fold decrease for CPT1 β (Figure 5.3.4.3, B) and 3.8-fold decrease for CS (Figure 5.3.4.3, A). This means reduced capacity for oxidative phosphorylation in LPS-treated brown adipocytes.

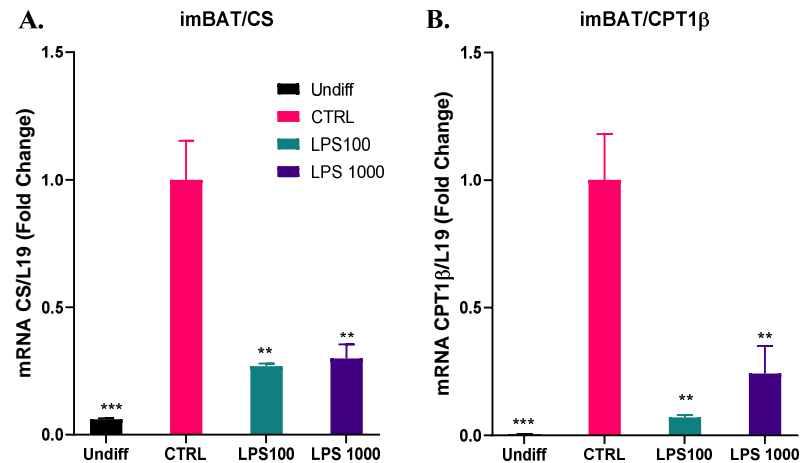


Figure 5.3.4.3 Effect of LPS on Genes Involved in Other Mitochondrial Function in Brown Adipocytes.

ImBAT cells were differentiated with/without LPS (100 ng/mL or 1000 ng/mL). (A) CS gene expression levels. (B) CPT1β gene expression levels. Data are expressed as a mean of fold change from control cells. Bars represent means \pm standard error of the mean. * $p<0.05$, ** $p<0.01$, *** $p<0.001$ compared to CTRL. One-way ANOVA was used for comparisons. CTRL; control. CS: citrate synthase. CPT1β: carnitine palmitoyltransferase 1B

5.3.5 Effect of LPS on Mitochondrial Bioenergetics

A 78 % reduction in mitochondrial copy number was revealed when brown adipocytes were differentiated with LPS ($P<0.05$, Figure 5.3.5.1, C). To understand the implications of differentiating brown adipocytes with LPS on mitochondrial function, a Seahorse extracellular flux analyser was used to measure basal oxygen consumption rate (OCR) in live cells as an indicator of aerobic respiration in live cells. Higher OCR levels indicate that cells are preferentially producing ATP through oxidative phosphorylation, the more efficient form of energy production. Also, using a confocal microscope, live cell imaging was undertaken to assess mitochondrial membrane potential. Prior to imaging, cells were incubated with MitoTracker Green FM (MTG) and MitoTracker Red CMXRos (MTR), which stain mitochondria independent of and dependent on membrane potential, respectively. Relative intensity (MTR/MTG) of these stains was then used as a measure of mitochondrial polarization.

As shown in Figure 5.3.5.1, A1, A2 LPS altered the OCR and led to 44 % overall reduction in basal respiration in imBAT cells ($P<0.0001$). It also decreased CL-induced OCR respiration in these cells (Figure 5.3.5.1,E) Analysing normalized OCR

results following application of mito-stress test chemicals provided information on aspects of mitochondrial function, as described in Figure 5.3.5.1, A1.

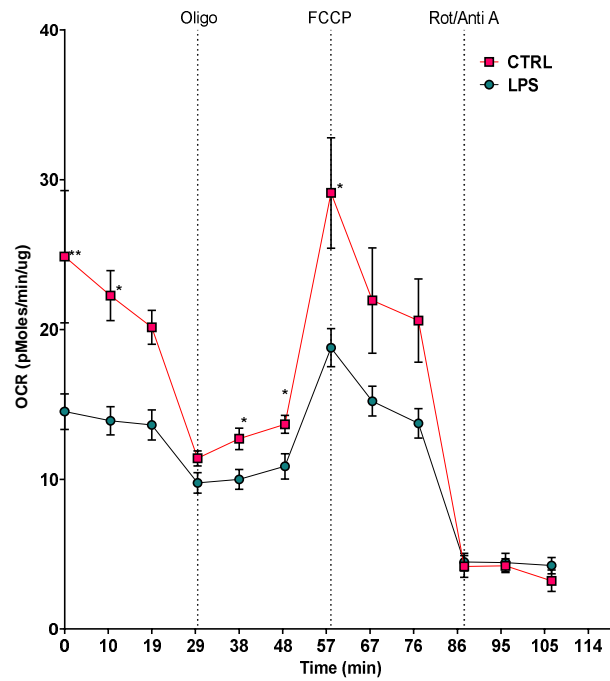
LPS treatment reduced spare respiration capacity, an indicator of long-term cellular survival and function, by 58.9 % relative to control. ATP production (Figure 5.3.5.1, A5) was reduced but without impaired bioenergetic efficiency (data not shown). Interestingly, proton leak (Figure 5.3.5.1,A4) and mitochondrial membrane potential (Figure 5.3.5.1, B1, B2) were reduced by LPS treatment (demonstrated by fading of the MTR signal while the MTG signal remained intense in Figure 5.3.5.1, B1), indicating that reduced mitochondrial uncoupling is not related to mitochondrial efficiency.

A summary of the results obtained on the effect of treatments on mitochondrial dysfunction is provided in Table 5.3.5.1, indicating that LPS induces mitochondrial dysfunction.

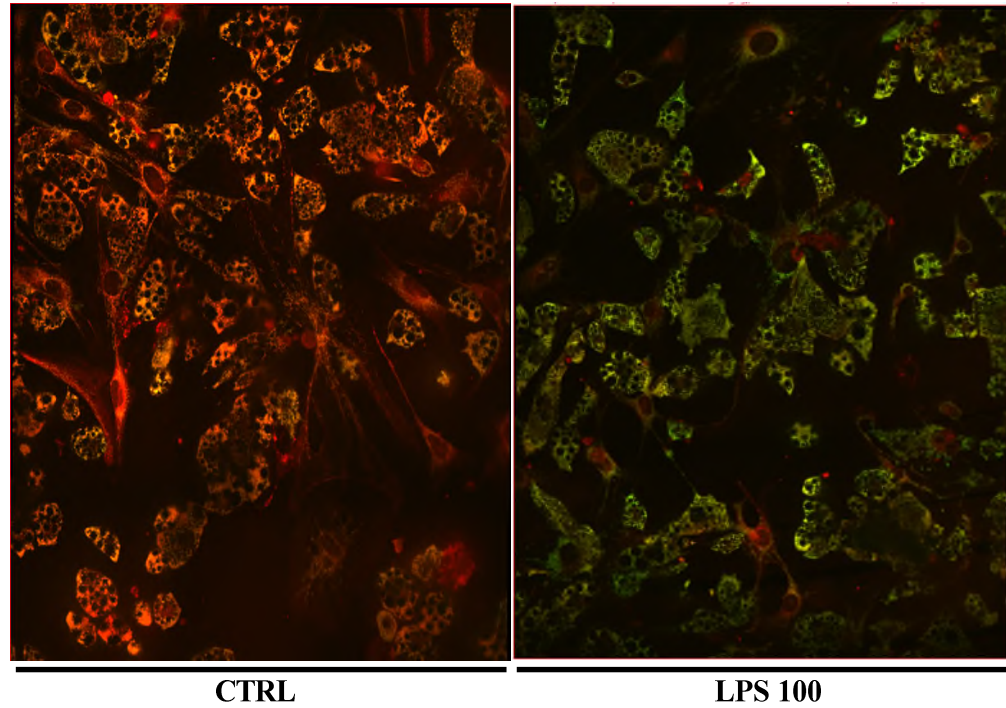
Figure 5.3.5.1 Effect of LPS on Basal Mitochondrial Bioenergetics in Brown Adipocytes.

ImBAT cells were differentiated with/without LPS (100 ng/mL or 1000 ng/mL) (A1) Time-lapse of aerobic capacity as measured by oxygen consumption rate (OCR) during a seahorse mitochondria stress test in which pharmacological inhibitors oligomycin (oligo), carbonyl cyanide p-trifluoromethoxy-phenylhydrazone (FCCP) and a combination of rotenone (Rot) & antimycin A (Anti A) were added sequentially, as indicated. (A2) Basal oxygen consumption rate (OCR), (A3) Spare respiratory capacity (SRC), (A4) proton leak, (A5) ATP-production. (B1). Representative confocal microscopies images of live cells of control (left panel) and LPS-treated brown adipocytes (right panel) brown adipocyte stained with MitoTracker Green FM (125 nM) and MitoTracker Red CMXRos (250 nM). Images are shown at 40x magnification, (B2) mitochondrial membrane potential (MMP; expressed as relative fluorescence signal) calculated through confocal microscopy analysis of fluorescence intensity of MTR/MTG (n=70) and plotted relative to control, (C) mitochondrial DNA copy number in imBAT (D) ATP abundance. (E) Time-lapse of aerobic capacity as measured by oxygen consumption rate (OCR) under CL-treatment. Data represent means \pm standard error of the mean. * $p < 0.05$, ** $p < 0.01$, *** $p < 0.001$ compared to CTRL. Unpaired t test was used for comparisons. One-way ANOVA was used was used for Time-lapse seahorse assay. CTRL; control

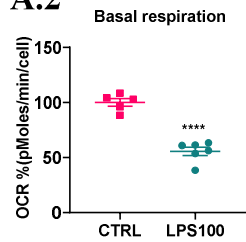
A.1



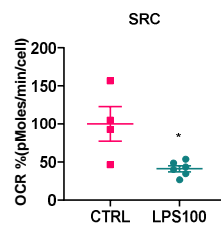
B.1



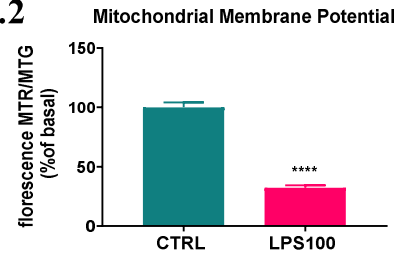
A.2



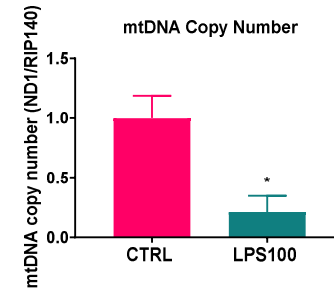
A.3



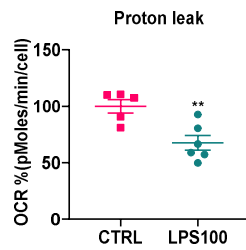
B.2



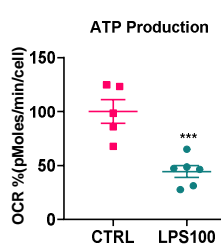
C.



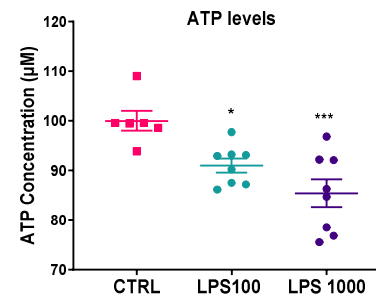
A.4



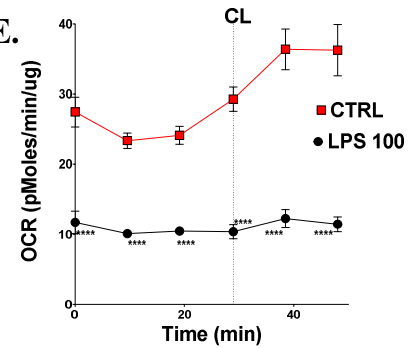
A.5



D.



E.



Function	Description	Result
Basal respiration	An indicator of oxidative phosphorylation and oxygen consumption used to meet cellular ATP demand and resulting from mitochondrial proton leak. Shows energetic demand of the cell under baseline conditions.	44 % reduction in LPS-treated cells relative to control (P<0.0001)
Spare respiratory capacity (SRC)	Indicator of the capability of the cell to respond to an extra energetic demand under stressful conditions as well as how closely the cell is to respiring to its theoretical maximum. In other words, it is the amount of extra ATP that can be produced by oxidative phosphorylation in case of a sudden increase in energy demand. The cell's ability to respond to demand can be an indicator of cell fitness, flexibility, survival and function.	58.9 % reduction in LPS-treated cells relative to control (P<0.05)
Proton leak	Remaining basal respiration not coupled to ATP production. Proton leak can be a sign of mitochondrial damage or can be used as a mechanism to regulate the mitochondrial ATP production. In brown adipocytes, proton leak in the mitochondrial inner membrane dissipate proton motive force as heat because of a high content of mitochondrial UCP1 (up to 8 % of total mitochondrial protein) (647).	32 % reduction in LPS-treated cells relative to control (P<0.001)
ATP production	The decrease in oxygen consumption rate upon injection of the ATP synthase inhibitor oligomycin represents the portion of basal respiration that was being used to drive ATP production. Shows ATP produced by the mitochondria that contributes to meeting the energetic needs of the cell.	55 % reduction in LPS-treated cells relative to control (P<0.001)

Table 5.3.5.1 Summary of Mitochondrial Characteristics following LPS Treatment.

Basal respiration, Spare respiratory capacity, Proton leak and ATP production were all assessed in imBAT cells following differentiation with/without LPS (100 ng/mL).

5.3.6 Effect of LPS on Global Mitochondrial Transcriptome through TLR4

In the previous Chapter, RNA-sequencing was performed to explore a wide range of LPS-effects and identify TLR4 receptor involvement in LPS actions on wild type and TLR4 knockout brown adipocytes. To perform RNA-seq, brown adipocytes were grown and differentiated with/without LPS (100 ng/mL), followed by RNA extraction

and RNA analysis as described earlier (Chapter 4). Gene ontology (GO) analysis was performed by submitting the top 500 up-/down-regulated DEGs to DAVID (at adjusted P-value <0.05). When searching for all GO terms containing the word “mitochondria” in all the GO outcomes (only GO with adjusted P-value <0.05 were considered), nine associated GO terms were defined, all of which were associated with top 500 significantly down regulated DEGs and shown in Table 5.3.6.1. GO:0005739 which refers to mitochondrion cellular component had the highest percentage with 115 significantly repressed genes (23.7 % of total genes in the list). All of these mitochondrial associated GO terms were associated with cellular component terms apart from mitochondrion organization which belongs to biological process terms. In contrast, for analysis of TLR4ko.BAT, only one term (GO:0005739: mitochondrion) appeared in the search and was significantly enriched in response to LPS. It was associated with downregulated DEGs, but to a much lower extent than wt.BAT (Table 5.3.6.1).

Wt.BAT

GO	GO Description	Count DEGs	%DEGs	Adjusted value	P-
GO:0005739	mitochondrion	115	23.711	8.20504E-23	
GO:0005743	mitochondrial inner membrane	45	9.2784	3.28536E-16	
GO:0005759	mitochondrial matrix	18	3.7113	8.46401E-05	
GO:0031966	mitochondrial membrane	10	2.0619	0.01402986	
GO:0042645	mitochondrial nucleoid	7	1.4433	0.014613056	
GO:0005750	mitochondrial respiratory chain complex III	4	0.8247	0.025936507	
GO:0007005	mitochondrion organization	10	2.0619	0.012133365	

TLR4ko.BAT

GO:0005739	mitochondrion	51	14.912	0.001272359	
------------	---------------	----	--------	-------------	--

Table 5.3.6.1 Enriched Gene Ontology Terms Associated with “Mitochondria”.

To further investigate the overall LPS effect on mitochondrial gene expression, mitochondrial gene sets with important aspects of mitochondrial biology were defined by searching for all gene ontology terms containing the word “mitochondria”/ “respiration” on GO-terms outcome (resulted from submitting all top 1000 altered genes together (500up+500down)) and plotting the associated DEGs using the heatmapper online tool (as outlined in Methods of Chapter 4).

The effect of LPS is evident in all figures of wt.BAT including effects on genes associated with mitochondrial respiratory function (Figure 5.3.6.1), mitochondrial biological processes (Figure 5.3.6.2) and mitochondrial membrane associated genes (Figure 5.3.6.3). Conversely, the LPS effect is almost negligible on TLR4ko.BAT which indicates that TLR4 mediates the majority of LPS actions on mitochondrial genes.

Twenty-two genes were included in assessment of mitochondrial respiratory function, and 77.2 % of these genes were significantly downregulated by LPS treatment (Figure 5.3.6.1). FOXRED1, (FAD dependent oxidoreductase domain containing 1), which functions as a chaperone protein required for the function of mitochondrial complex I, was among the genes repressed by LPS (log2FoldChange = -0.67, adjusted P-value <0.05). FOXRED1 was not significantly affected by LPS in TLR4ko.BAT.

Thirty three genes were included in assessment of mitochondrial biological processes, and 93.9 % of these genes were significantly downregulated by LPS treatment (Figure 5.3.6.2). This list included genes vital for mitochondrial function with UCP1, the main thermogenesis factor, at the top of the down regulated genes (log2FoldChange = -5.83, adjusted P-value <0.05), as well as PGC1 α , the master regulator of UCP1 (Ppargc1a, log2FoldChange = -1.49, adjusted P-value <0.05). Chchd10, coiled-coil-helix-coiled-coil-helix domain containing 10, was also reduced by LPS (log2FoldChange = -1.57, adjusted P-value <0.05). Chchd10 encodes a mitochondrial protein that is enriched at cristae junctions in the intermembrane space and plays a role in cristae morphology maintenance and oxidative phosphorylation. Genes that regulate mitochondrial dynamics were also affected, including fusion genes MFN2 (log2FoldChange = -0.51, adjusted P-value <0.05) and OPA1 (log2FoldChange = -0.42, adjusted P-value <0.05). None of these genes were significantly altered by LPS in TLR4ko.BAT.

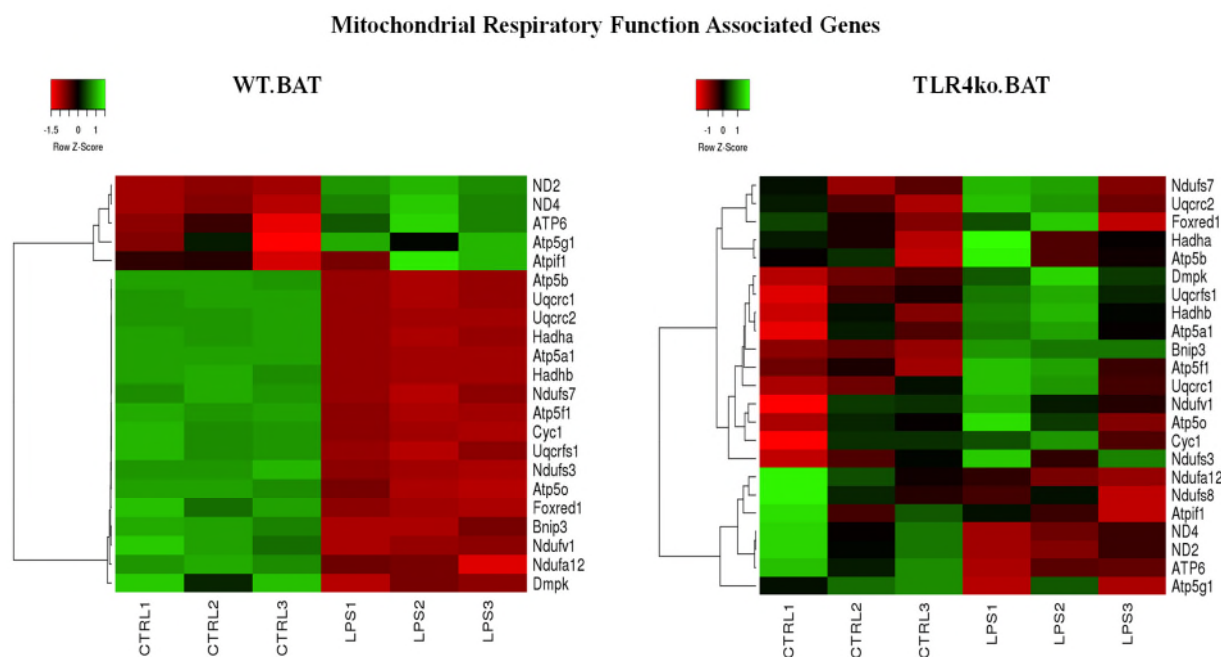


Figure 5.3.6.1 Heatmaps from RNA-Sequencing for Genes Associated with Mitochondrial Respiratory Function in wt.BAT cells (left panel) and TLR4ko.BAT cells (right panel)

Rows represent the different genes and each column represents a sample. For the relative gene expression level of each sample a different colour of the red-green scale is assigned. green represents an expression level above the mean, red colour represents expression below the mean.

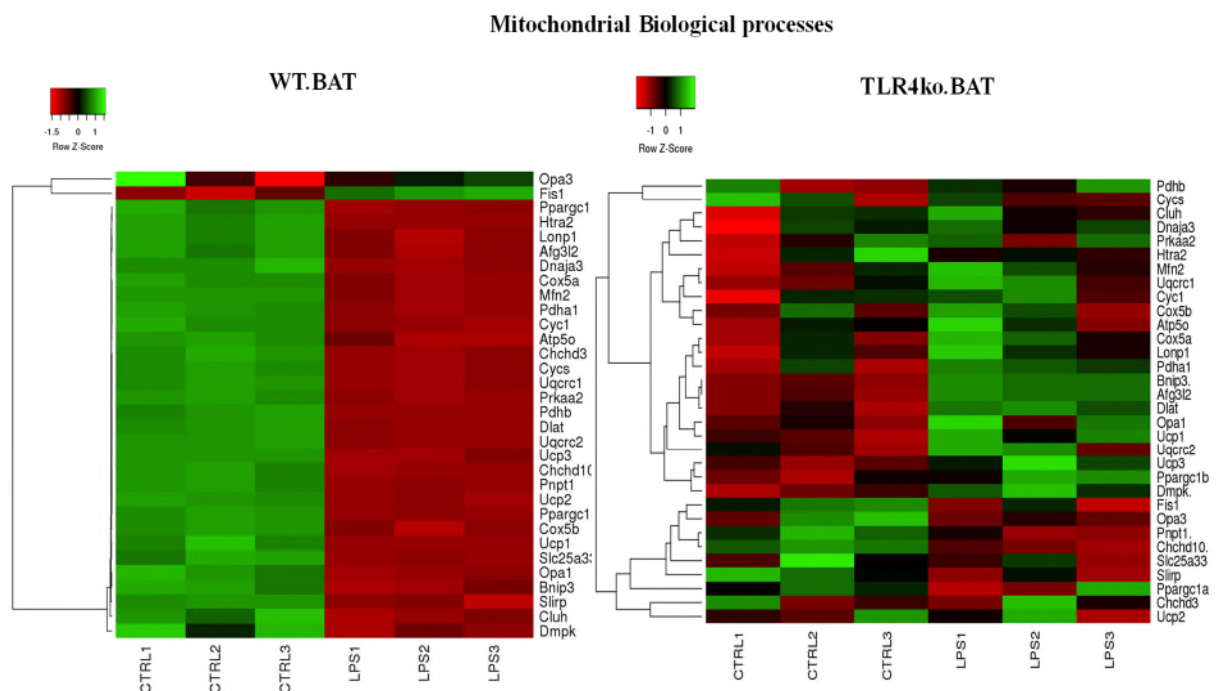


Figure 5.3.6.2 Heatmaps from RNA-Sequencing for Genes Associated with Mitochondrial Biological Processes in wt.BAT cells (left panel) and TLR4ko.BAT cells (right panel)

Rows represent the different genes and each column represents a sample. For the relative gene expression level of each sample a different colour of the red-green scale is assigned. green represents an expression level above the mean, red colour represents expression below the mean.

Eighty-six genes were included in the assessment of mitochondrial membrane function and 82.4 % of these genes were significantly downregulated by LPS treatment as in Figure 5.3.6.3. CYP27A1, cytochrome P450 family 27 subfamily A member 1, encodes a member of the cytochrome P450 superfamily of enzymes, and was inhibited by LPS in wt.BAT cells ($\log_2\text{FoldChange} = -2.88$, adjusted P-value <0.05). CYP27A1 is involved in overall cholesterol homeostasis and its impaired levels by LPS could indicate increased risk of obesity and diabetes complications. Pdk4, pyruvate dehydrogenase kinase 4, which contributes to the regulation of glucose metabolism, was also reduced ($\log_2\text{FoldChange} = -1.98$, adjusted P-value <0.05). LPS did not significantly impact either CYP27A1 or Pdk4 in the absence of TLR4.

Next, oxidative phosphorylation (OXPHOS), the primary role of the mitochondria, was investigated. OXPHOS is the culmination of a series of energy transformations that generate most of the living cell's ATP from food, known as cellular respiration (648). OXPHOS was one of the significantly enriched KEGG pathways associated with downregulated genes Figure 4.3.4.1 in Chapter 4. To understand, in more detail, the effects of LPS on transcriptional regulators of oxidative phosphorylation, the

illustration charts below were plotted using the Pathview online tool (Figure 5.3.6.4, Figure 5.3.6.5).

This current data highlights (Figure 5.3.6.4) that overall genes involved in transcription of ETC complexes were reduced by LPS in wt.BAT. For instance:

- Ubiquinone oxidoreductase subunit A13 (NDUFA13) which is required for complex I assembly and electron transfer activity (log2foldchange = -1.21, adjusted P-value <0.05)
- Succinate dehydrogenase complex flavoprotein subunit A (SDHA) which encodes a major catalytic subunit of succinate-ubiquinone oxidoreductase, complex II (log2foldchange = -0.41, adjusted P-value <0.05)
- Ubiquinol-cytochrome c reductase core protein 2 (UQCRC2) which is part of the ubiquinol-cytochrome c reductase complex (complex III) (log2foldchange = -0.58, adjusted P-value <0.05)
- Cytochrome c oxidase subunit 6A2 (COX6A2) which is the terminal enzyme of the mitochondrial respiratory chain (complex IV), catalyzes the electron transfer from reduced cytochrome c to oxygen (log2foldchange = -1.49, adjusted P-value <0.05).
- ATPase H⁺/K⁺ transporting subunit beta (ATP4B) which belongs to a family of P-type cation-transporting ATPases and is a proton pump that catalyzes the hydrolysis of ATP coupled with the exchange of H(+) and K(+) ions (log2foldchange = -2.17, adjusted P-value <0.05).

In comparison, TLR4ko.BAT cells showed minimal changes in genes associated with ETC complexes in terms of fold change and number of altered genes of each complex (Figure 5.3.6.5)

Rows represent the different genes and each column represents a sample. For the relative gene expression level of each sample a different colour of the red-green scale is assigned. green represents an expression level above the mean, red colour represents expression below the mean.

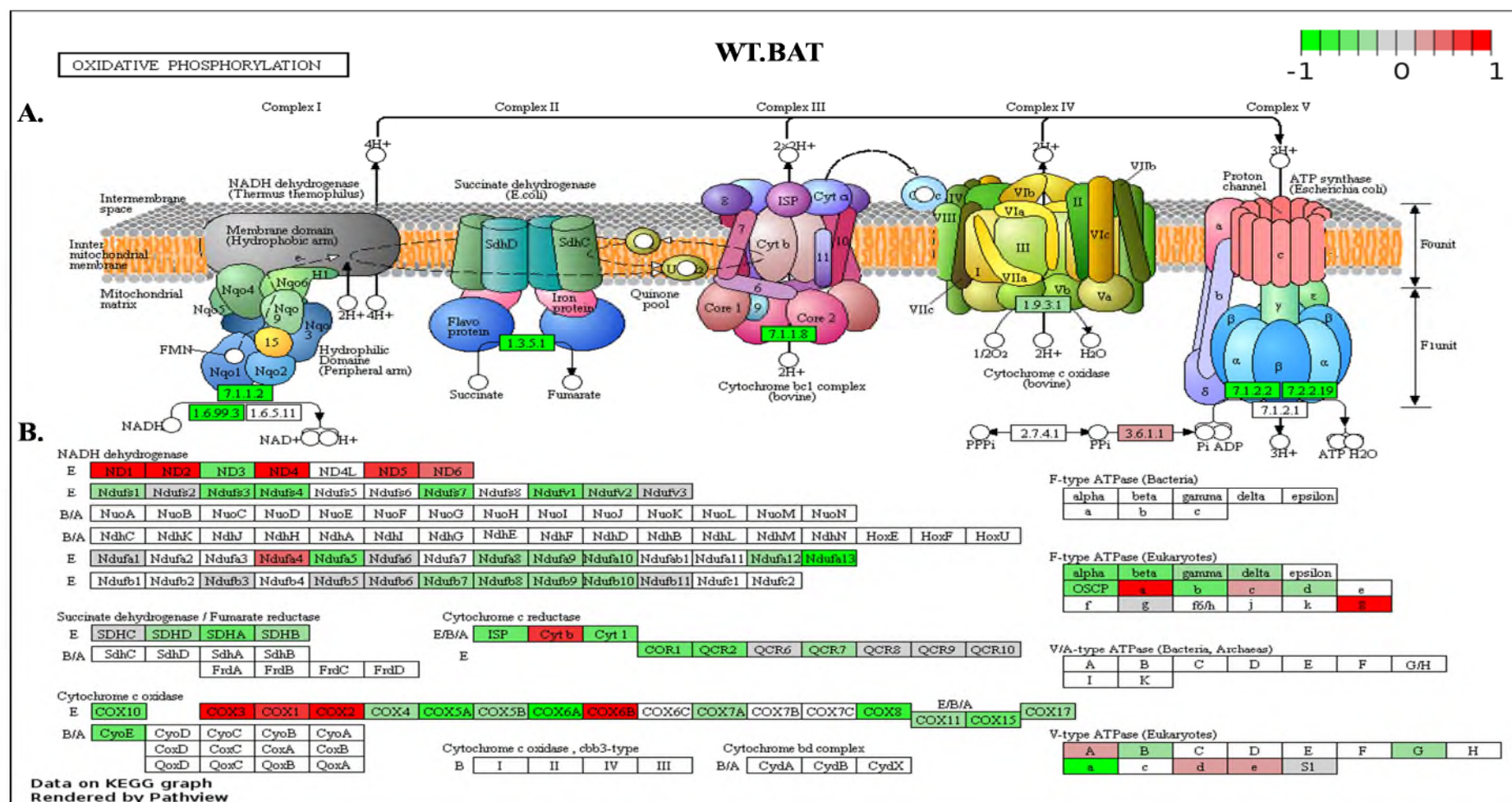


Figure 5.3.6.4 Changes in Oxidative Phosphorylation Gene Expression under LPS Treatment in wt.BAT.

(A.) Schematic diagram of the process of oxidative phosphorylation. Boxes represent EC Numbers (Enzyme Commission: EC; numbers do not specify enzymes, but enzyme-catalysed reactions). Red boxes represent upregulated EC and Green boxes represent downregulated EC. Grey/white boxes represent unchanged EC. 7.1.1.2 NADH: ubiquinone reductase (H^+ -translocating), 1.6.99.3: NADH dehydrogenase, 1.3.5.1: succinate dehydrogenase, 7.1.1.8: quinol-cytochrome-c reductase, 1.9.3.1: cytochrome-c oxidase, 7.1.2.2: H^+ -transporting two-sector ATPase, 7.2.2.19 H^+/K^+ -exchanging ATPase and 3.6.1.1 inorganic diphosphatase. (B.) Different genes involved in various reactions of oxidative phosphorylation, red boxes represent upregulated genes and green boxes represent downregulated genes.

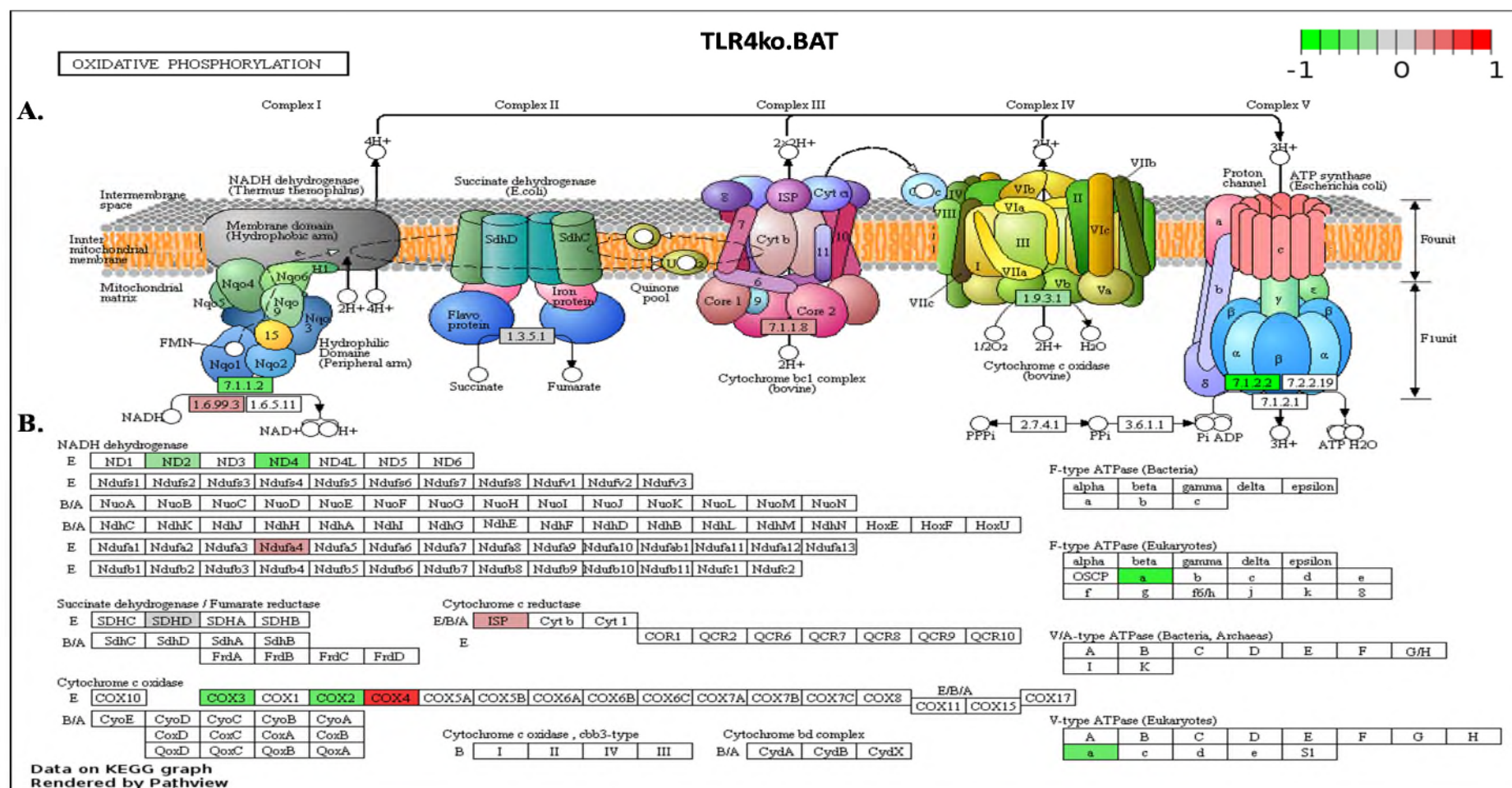


Figure 5.3.6.5 Changes in Oxidative Phosphorylation Gene Expression under LPS Treatment in TLR4ko.BAT.

(A.) Schematic diagram of the process of oxidative phosphorylation. Boxes represent EC Numbers (Enzyme Commission: EC; numbers do not specify enzymes, but enzyme-catalysed reactions). Red boxes represent upregulated EC and Green boxes represent downregulated EC. Grey/white boxes represent unchanged EC. 7.1.1.2 NADH: ubiquinone reductase (H⁺-translocating), 1.6.99.3: NADH dehydrogenase, 7.1.1.8: quinol-cytochrome-c reductase, 1.9.3.1: cytochrome-c oxidase, 7.1.2.2: H⁺-transporting two-sector ATPase, (B.) Different genes involved in various reactions of oxidative phosphorylation, Red boxes represent upregulated genes and Green boxes represent downregulated genes.

Evidently, LPS downregulated ETC complexes in wt.BAT cells which will disturb the electrochemical gradient and eventually lead to less available ATP for the biological functions of the cells. Also, it raises the possibility that reduced levels of ETC complexes can make the complexes become easily saturated with electrons and excess electrons are instead pumped directly to oxygen, generating ROS, especially with accompanied reduction of inter-membrane proteins known as uncoupling proteins (UCPs). That is because UCPs play an important role in lowering this electrochemical gradient, either by utilizing it to produce heat (as in the case of UCP1 in brown adipose tissue which is reduced by LPS as indicated above) or by facilitating proton leak to prevent excess ROS formation (UCP2 and 3) (485,649,650). This is similar to what occurs in the obesity state when there is an excess supply of electrons and low oxygen utilization (high nutrient supply and low energy demand), but it is triggered by LPS alone in this current study. Altogether, these findings indicate that LPS leads to global repression of mitochondrial transcriptome through TLR4.

5.4 Discussion

In this present chapter, it was hypothesized that LPS-TLR4 activation impairs brown adipocyte mitochondrial function in a similar manner to white adipocytes, leading to metabolic cellular dysfunction. This was following observations of LPS acting to attenuate both basal and CL-induced UCP1 levels with a reduction in key brown fat gene expression levels (outlined in previous chapters). Thus, immortalised mouse brown adipocytes were treated with LPS to test the direct effect on mitochondrial function. Several findings were established through these studies, firstly, LPS impairs mitochondrial bioenergetics, secondly, it also diminishes oxidative phosphorylation capacity and finally that LPS induces oxidative stress. These findings demonstrate that increased LPS levels, when delivered *in vitro*, can directly trigger mitochondrial damage and cause dysfunctional bioenergetics. As such, this has the capacity to impair the utilization of readily available lipids as a fuel supply of brown adipose tissue thermogenesis and the capacity to maintain the unique property of brown adipocytes mediated by UCP1 to uncouple oxidative phosphorylation from ATP synthesis to produce heat. This is evidenced by (1) Inhibition of mitochondrial oxidative phosphorylation at transcription levels (2) Reduced bioenergetic efficiency (3) Increased oxidative stress features.

The key outcome of this chapter was that incubation of brown adipocytes with LPS through differentiation led to a reduction in oxidative phosphorylation which the cell would normally be primarily reliant on for energy requirements. In other words, LPS compromises the main mitochondrial function and ATP production. Decreased oxidative phosphorylation pathway capacity was established by being one of the KEGG pathways associated with significantly downregulated genes in unbiased RNA-sequence analysis of wt.BAT cells. The importance of this finding is tied to the fact that decreased expression of genes encoding key enzymes in oxidative metabolism and mitochondrial function are also present in adipose tissue of T2DM patients and “prediabetic” insulin resistant subjects (651,652); along with impaired structure and function of mitochondria (506,646,653–655). LPS dependant decreased expression of genes related to oxidative phosphorylation in wt BAT cells is also in line with obesity associated downregulation of

transcription levels of genes that were involved in oxidative phosphorylation in human white adipose tissue, which suggests that obesity can trigger such effect in BAT (650). Interestingly, deletion of TLR4 completely prevented LPS effects on the oxidative phosphorylation pathway which indicates that TLR4 is the main mediator of all actions of LPS on this pathway. Therefore, the LPS-TLR4 pathway could represent a target to investigate for preventing deleterious LPS effects on mitochondria and ultimately obesity complications.

Secondly, reduced bioenergetic efficiency was evidenced by attenuated basal and CL-stimulated oxygen consumption rate, uncoupled respiration from proton leak, maximal respiration and ATP-coupled respiration. Real-time measurements of oxygen consumption rate were assessed by Seahorse XF-bio analyser in live cells and followed by calculations to measure different aspects of mitochondrial function including spare respiration capacity, ATP production and proton leak. This inadequacy of mitochondrial bioenergetic could be explained by deteriorated mitochondrial membrane potential or uncoupling action. Mitochondrial membrane potential was measured by analysing images obtained by confocal microscopy. This data of reduced bioenergetics efficiency in LPS-treated BAT cells through differentiation can be put in context with previous studies stating that basal oxygen consumption per gram of adipose tissue being found to be higher in lean subjects than in obese subjects (656), and the maximal respiration rates of mitochondria and mitochondrial respiration being negatively correlated with body mass index (BMI) values (657,658), which could ultimately mean LPS triggers these actions on mitochondrial bioenergetic in obesity in adipose tissue.

In addition, in the current study LPS mediated suppression of transcription of mitochondrial biogenesis genes could explain TLR4-mediated LPS downregulation of UCP1 as there was a reduction in mRNA of biogenesis mitochondrial genes including PGC-1 α which coactivates the transcription factor PPAR γ which stimulates the promoters of target genes, such as UCP1 (77,143). However, it has been reported that LPS activation of TLR4 did not lead to changes in mitochondrial biogenesis genes including nuclear respiratory factor 1 (NRF-1) and transcription factor A (TFAM), and two nuclei encoded mitochondrial genes, cytochrome c oxidase subunit IV a (Cox4a) and cytochrome b-c1 complex subunit 6 (Uqcrh) (344). This difference in the effect of LPS effect can be a result

of duration of LPS treatment; previous investigations applied acute LPS treatment on differentiated brown adipocytes for 12–15 hours, while in this study LPS treatment was chronic and the brown adipocytes were differentiated with LPS from day one.

Moreover, in this chapter, application of LPS throughout differentiation of wt.BAT cells resulted in sustained conditions of oxidative stress and down-regulation of antioxidant enzyme transcription in tandem with decreased mitochondrial number. In fact, LPS compromised antioxidant defence systems represented by different antioxidant enzymes and was the underlying cause of reduced capability to cope with oxidative stress induced by H₂O₂ and leading to higher ROS levels compared to control cells. Indeed, LPS-induced oxidative stress as well as LPS-mediated impairment of transcription of mitochondrial biogenesis genes are possibly the reason behind the observed decrease in mitochondrial number. That is because sustained conditions of high mitochondrial oxidative stress and further increased ROS production are known to compromise mitochondrial DNA quality and adversely impact general mitochondrial function and insulin signalling (480,485,659), and in this instance either through defective protein translation, redox signalling or some other unknown mechanism resulted in the metabolic phenotype observed. Further research is required to elucidate this interaction, and specifically the relationship between LPS and brown adipose mitochondria and thermogenesis.

In summary, this study provides direct, a novel mechanism where by increasing weight gain, which changes adipose tissue function, may cause BAT mitochondrial dysfunction due to Gut-derived LPS induced inflammation. Also, LPS mediates downregulation of UCP1 expression with mitochondrial dysfunction including reduced mitochondrial oxidative phosphorylation and mitochondrial biogenesis, leading to suppressed mitochondrial respiration in immortalized brown adipocytes, and may initiate and/or exacerbate the metabolic syndrome. These results suggest that LPS-mediated inflammation in brown adipocytes and lowering LPS levels in circulation (either through diet, pharmacotherapy and/or surgery) may be potential therapeutic targets to modulate BAT function for obesity treatment and prevention, and warrant further investigation.

Chapter 6. Lipopolysaccharide Reduces the Browning Process in Human Adipocytes

6.1 Introduction

Beige (brown-in-white) adipocytes, which have a brown phenotype yet present in WAT, are formed through the browning process which is induced following a response to cold adaptation or other stimuli (93). The formation of beige adipocytes occurs in parallel with increased production of healthy mitochondria, via mitochondrial biogenesis, and constant fusion and fission to maintain their shape, distribution and size in order to function optimally and carry out quality control processes (197,660,661). Transcriptional regulation plays an important role in managing mitochondrial biogenesis and dynamics, with key proteins involved in these processes highly regulated at the transcriptional level (470,481,662,663). Beige phenotype stimulation is an interesting subject because of the widespread prevalence of obesity and its related diseases; it can aid weight loss and reduce morbidity risk by encouraging energy dissipation rather than energy storage. In this context, many studies demonstrate that obese individuals have reduced BAT/ beige compared with their lean counterparts (205–207,664). Studies have detailed that higher content of BAT/beige is correlated with improved insulin sensitivity in both humans and animal models (207,214–216,664,665), with BAT glucose uptake rates highly reduced in obese individuals compared with healthy individuals (213). BAT transplantations have supported this evidence in mice, whereby transplant models that increase BAT mass also improve glucose metabolism, increase insulin sensitivity, and reduce adiposity and body mass (218–221).

Despite these prior studies highlighting that the beige phenotype is reduced in obesity, and that this is associated with many negative health impacts, there is limited understanding as to the mechanism behind it. It is suggested that a combination of high ambient temperature, leptin receptor deficiency, β -adrenergic signalling impairment, and lipase deficiency contribute to chronic inflammation and brown adipocyte death observed in obesity (348). Further studies show inflammatory mediators impact the function of BAT, *e.g.* TNF α inducing insulin resistance, and pro-inflammatory cytokines from macrophages suppressing the thermogenic activity of BAT (313–315,319). Therefore, these aforementioned studies indicate it would be important to consider the direct impact of inflammatory mediators on the beige phenotype. For instance, LPS triggers chronic

inflammation in adipocytes which represents a potential mechanism to impair the browning process as it is prevalent in obese individuals and dysfunctional adipocytes themselves contribute to this inflammation (666). As mentioned earlier, LPS enters the bloodstream in the obese state because of an abnormal permeability of the gut wall, known as 'leaky gut', causing induction of a persistent inflammatory state and secretion of inflammatory cytokines. In fact, consumption of one high fat meal is enough to increase serum LPS (461,464,667,668). Data from the study of mouse adipocytes in the previous chapters of this thesis showed a direct effect of LPS on impairing brown adipocyte function. Furthermore, it has been reported that LPS-induced TLR4 activation prevents WAT browning (669), however this study only investigated cAMP-induced browning with no use of browning agents such as rosiglitazone. In line with this, LPS-binding protein (LBP), which facilitates the binding of LPS to its receptor TLR4, has been identified as a negative regulator of the browning process (429), providing further evidence that the LPS pathway may be responsible for the reduced beige phenotype in obese individuals. These previous investigations into the impact of LPS on adipocyte browning have neglected to assess the direct impact of LPS on the browning capacity of white adipocytes *in vivo* and *in vitro*, especially in humans. Such research will provide information about impairments in the ability of brown adipocytes to provide protection against obesity and disease.

Thus the next step in this thesis was to investigate the effect of LPS on the browning process utilising both *in vitro* and *in vivo* human data. In addition, addressing mitochondrial biogenesis and dynamics at the transcriptional level in response to LPS to provide insight into the impact on beige cells and their mitochondrial health. The specific aims of the study were to:

1. Investigate the difference in expression levels of brown fat genes in lean, overweight and obese cohorts as well as the correlation between the expression of brown fat genes and inflammatory/mitochondrial genes within these cohorts.
2. Study the impact of LPS on the beige genotype in mouse and human white adipocytes following stimulation with a browning agent.

3. Determine the impact of LPS on mitochondrial gene expression in the beige genotype of mouse and human adipocytes, and examine the relationship between serum LPS and both mitochondrial genes and brown fat genes.

6.2 Methods

6.2.1 Ethics and Study Design

Women participants (n=128; BMI: 17.6 – 47.7 kg/m², age: 18-46) undergoing elective, non-emergency abdominal surgeries at University Hospital Coventry and Warwickshire (UHCW), Coventry, UK, were recruited to take part in this study. All participants were non-diabetic, pre-menopausal, Caucasian women; any subjects taking thiazolidinediones or other medication known to affect mitochondrial function were excluded. Adipose tissue biopsies from abdominal subcutaneous (Sc) and omental (Om) fat depots were obtained, alongside serum samples.

This study was approved by the Ethics Committee of the University Hospital Coventry and Warwickshire NHS Trust Research and Development Department, Number SK06/9309. All participants in the study provided written and informed consent in accordance with the Declaration of Helsinki and had adipose tissue collected at University Hospital Coventry and Warwickshire NHS Trust.

6.2.2 Blood Biochemistry and Anthropometry

Biochemical and anthropometric measurements were performed at the time of surgery. Fasted blood samples were collected, aliquoted and stored at -80 °C until assayed. Serum glucose, HbA1c, insulin and lipids were determined at George Eliot Hospital laboratory. Height (cm), weight (kg) and body fat mass data were also collected.

6.2.3 Primary Human Pre-Adipocyte Isolation

Abdominal and subcutaneous adipose tissue was digested with collagenase to isolate pre-adipocyte cells, as previously described (670). Sterile conditions in a category 2 tissue culture room were used and to minimise lysis of fat the procedure was carried out as soon possible after collecting the adipose tissue (within 1 hour). Between 3 cm³ and 10 cm³ of WAT was placed in a 50 mL centrifuge tube containing 10 mL collagenase (mL, Worthington, UK), pre-warmed to 37 °C. The WAT was cut with sterile scissors until the fat pieces were no bigger than 2 mm in diameter. The centrifuge tube was placed in a rack

in a shaking water bath at 37 °C for 30 minutes and shaken vigorously by hand at 10 minute intervals to form a smooth lipid and collagenase mixture. This mixture was filtered through sterile cotton mesh into a sterile 50 mL centrifuge tube and centrifuged at 2000 rpm for 5 minutes. The supernatant was discarded then the pellet containing preadipocytes was resuspended in 5 mL lysis buffer, incubated at room temperature for 5 minutes and then centrifuged at 2000 rpm for 5 minutes. The supernatant was discarded and the remaining pellet was resuspended in 5 mL primary adipocyte growth media and transferred to a 75 cm² tissue culture flask (T75) (corning, UK) containing 15 mL primary adipocyte growth media that had been pre-incubated in a 37 °C, 5 % CO₂ humidified incubator for 15 minutes. The flask was labelled and stored in a 37 °C, 5 % CO₂ humidified incubator and the media was changed every 48 hours.

6.2.4 Primary Human Pre-Adipocyte Differentiation and Treatment

Isolated human primary preadipocytes were grown until 80 % confluent in culture flasks (T75) (corning, UK) in growth media DMEM/F12 (#11039-021, Gibco, The UK) which contains 10 % FBS (#s1810-500, Biowest), 1 % Penicillin/streptomycin (#10378-016, Invitrogen), 1 % L-Glutamine (#25030-081, Gibco), Fibroblast growth factor-basic (FGF-basic), recombinant human 5 ng/mL (#VXPHG0026, Fisher Scientific), Transferrin 10 ng/mL (#VX0030124SA, Fisher Scientific). This growth media was changed every other day.

At 80 % confluency, cells were washed with sterile phosphate buffered saline (PBS) pre-warmed to 37 °C and incubated with 5 mL 0.05 % trypsin – EDTA (#25300-062, Life Technologies) for 5 minutes. Cells were then seeded on to gelatin-coated 12-well plates (Corning) at 4000 cells/cm² with 2 mL primary adipocyte growth media in each well. Growth media was changed every 48 hours until 100 % confluence. Two days post confluence, cells were treated with differentiation media for 6 days with media change every other day. LPS (100 ng/mL, E. Coli O55:B5, Sigma#L6529) was added to the relevant wells at this step. The differentiation media DMEM/F12 (#11039-021, Gibco, The UK) was supplemented by 3 % FBS (#s1810-500, Biowest), 1 % Penicillin/streptomycin (#10378-016, Invitrogen), 5 µg/mL insulin (#I2643, SIGMA-ALDRICH, UK), 1 nM Triiodo-L-thyronine (#T6397, SIGMA-ALDRICH, UK), 2 µM

rosiglitazone (#71740, Cayman Chemical, Cambridge, UK), 0.25 mM 3-Isobutyl-1-methylxanthine (#I5879, SIGMA-ALDRICH, UK), 500 nM Dexamethasone (#D4902, SIGMA-ALDRICH, UK), 1.7 mM Pantothenate (#P5155, Sigma-Aldrich, UK), 3.3 mM Biotin (#B4639, Sigma-Aldrich, UK).

Cells were then treated with nutrition media for 8 days with media change every other day. LPS continued to be added to the relevant wells at this step. The nutrition media DMEM/F12 (#11039-021, Gibco, The UK) was supplemented by 3 % FBS (#s1810-500, Biowest), 500 nM Dexamethasone (#D4902, SIGMA-ALDRICH, UK), 1.7 mM Pantothenate (#P5155, Sigma-Aldrich, UK), 3.3 mM Biotin (#B4639, Sigma-Aldrich, UK). No Penicillin/streptomycin were added at this step. 2 μ M rosiglitazone (#71740, Cayman Chemical, Cambridge, UK) was added only to the relevant wells and removed completely 72 hours prior to harvesting.

6.2.5 RNA Isolation

For adipose tissue, 100 mg of frozen tissue was homogenised in 1 mL TRI Reagent® (#T9424 Sigma-Aldrich, UK). For cell culture, cells were washed with PBS and lysed in 1 mL of TRI Reagent. Samples were then processed for RNA extraction and quantification followed by cDNA Synthesis and qRT-PCR as described in methods section (Chapter 2).

6.2.6 Statistical Analysis

Statistical analyses were performed using the SPSS 21.0 software and GraphPad Prism 7.04. Data were examined for normality according to the D'Agostino & Pearson normality test. Visual inspection of the data histograms, normal Q-Qplots and box plots was examined, with skewness and kurtosis z-values accepted at (-1.96-1.96) (Carmer,1998; Cramer& Howitt,2004, Doane &Seward, 2011). Comparisons of cohorts with different BMIs were performed via one-way ANOVA (if parametric) or Kruskal–Wallis test (if non-parametric) followed by Tukey's (if parametric) or Dunn's (if non-parametric) multiple comparisons test to define significant differences between individual groups. For Pearson correlation analyses, data were log-transformed prior to analysis if non-

parametric. Two-way ANOVA, followed by Tukey's multiple comparison test, was performed for all comparisons between different cell culture treatments. P-values of <0.05 were considered statistically significant. Data are reported as mean \pm standard deviation (SD) with statistical differences compared to control indicated with * $p<0.05$, ** $p<0.01$, *** $p<0.001$, **** $p<0.0001$ unless otherwise specified.

6.3 Results

6.3.1 Anthropometric and Metabolic Variables for Study Participants

Clinical, anthropometric and biochemical data collected for lean (n=44), overweight (n=49) and obese (n=37) cohorts are shown in Table 6.3.1.1.

HDL was significantly decreased in both overweight ($p<0.05$) and obese ($p<0.01$) cohorts compared to lean. Insulin was significantly increased in overweight ($p<0.01$) and obese ($p<0.001$) cohorts compared to lean.

	Lean	Overweight	Obese
n	44	49	37
Age, years	32.1±0.8	31.5±0.1	31.2±1
BMI	22.2±1.9	27.4±1.3***	35.3±4.7*** <i>fff</i>
Glucose (mmol/l)	3.6±0.1	3.7±0.1	3.9±0.1
LDL (mmol/l)	4.6±0.2	4.5±0.2	4.1±0.2
HDL (mmol/l)	1.7±0.1	1.6±0.1*	1.5±0.1**
TGs (mmol/l)	3.1±0.2	3.2±0.1	3.2±0.2
Insulin (pmol/l)	39.79±5	65.36±5.96**	84.56±9.20*** <i>fff</i>

Table 6.3.1.1 Clinical Characteristics of Participants According to Group.

Data are presented as mean ± standard error of the mean, apart from BMI which is presented as mean ± standard deviation. All serum samples were taken in a fasted state. Between group comparisons one-way ANOVA (if parametric distribution) or the Kruskal-Wallis (if not parametric distribution) test were used to test significance: * $p<0.05$, ** $p<0.01$, *** $p<0.001$ for lean vs overweight and lean vs obese, *f* $p<0.05$, *ff* $p<0.01$, *fff* $p<0.001$ for overweight vs obese. BMI: body mass index, TGs: triglycerides. LDL: low-density lipoproteins. HDL: High-density lipoprotein.

6.3.2 BMI Correlation with BAT Genes

To investigate whether there was a relationship between BMI and the beige phenotype, the expression levels of key brown fat genes cell death-inducing DFFA-like effector A (CIDEA), ELOVL fatty acid elongase 3 (ELOVL3), perilipin 5 (PLIN5) and Solute Carrier Family 27 Member 2 (SLC27A2) were determined in both subcutaneous and

omental adipose tissue samples from subjects with a range of BMIs. UCP1, the main thermogenic marker, was not detectable in these samples. This might be due to a generally low expression of UCP1 in WAT. A strong negative correlation between BMI and brown fat genes was observed (Figure 6.3.2.1), with a maximum r value of -0.446 ($P < 0.0001$). In addition, brown fat gene expression was significantly decreased in obese compared to lean subjects, and there was a significant decrease between overweight and obese subjects in both subcutaneous and omental tissue samples for ELOVL3 ($FC = -1.65$ ($P < 0.05$), $FC = -1.52$ ($P < 0.01$), respectively). This decrease can be seen in Figure 6.3.2.2 below

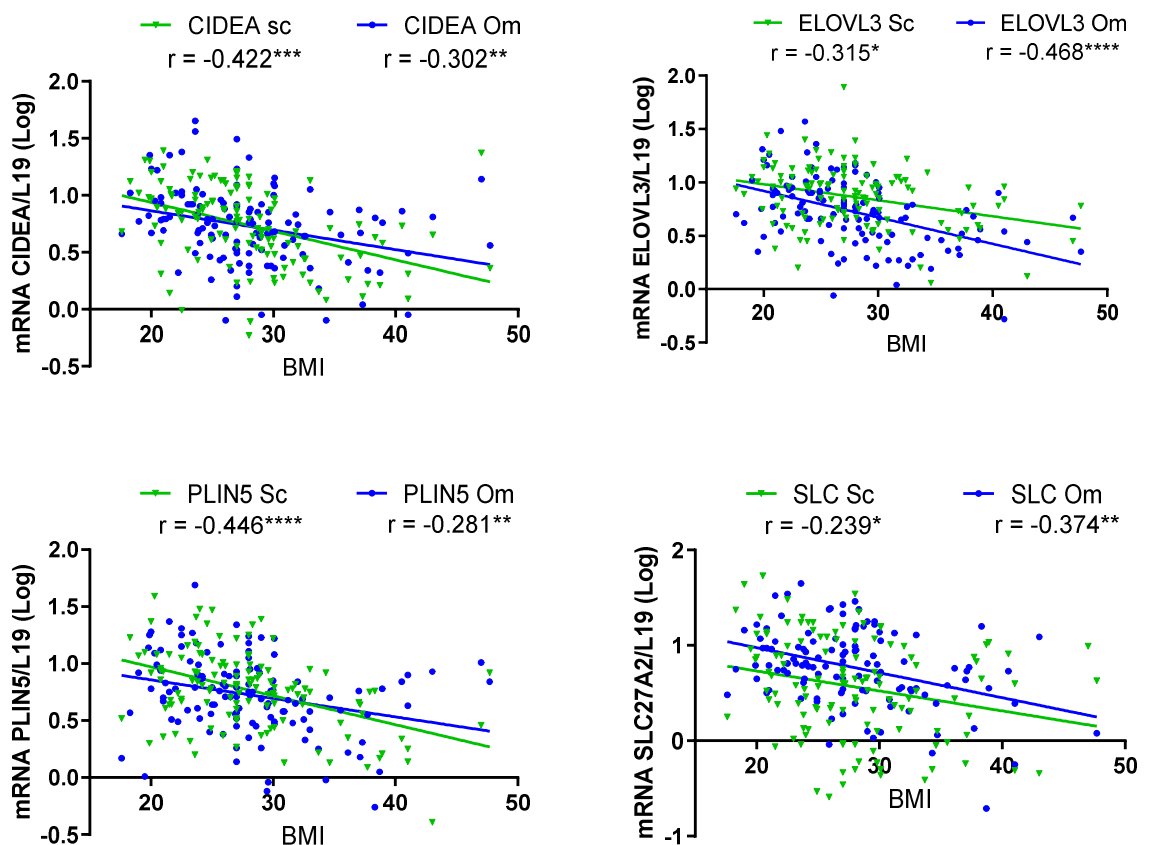


Figure 6.3.2.1 BMI Correlates with Reduced Brown Adipose Tissue Genes.

The expression of key brown fat genes: CIDEA, ELOVL3, PLIN5 and SLC27A2 was measured in subcutaneous (Sc) and omental (Om) fat depots by RT-PCR using L19 as a housekeeping gene. Correlations were calculated using normalized gene expression values in the entire patient cohort ($n=130$) for Sc or Om tissue samples. All genes had a strong negative correlation with BMI. Linear trend line is shown with Pearson correlation statistic (r) and $*p < 0.05$, $**p < 0.01$, $***p < 0.001$ and $****p < 0.0001$. If non-parametric, variables were log-transformed prior to correlation analysis to improve normality. CIDEA: cell death-inducing DFFA-like effector A, ELOVL3: fatty acid elongase 3, PLIN5: perilipin 5.

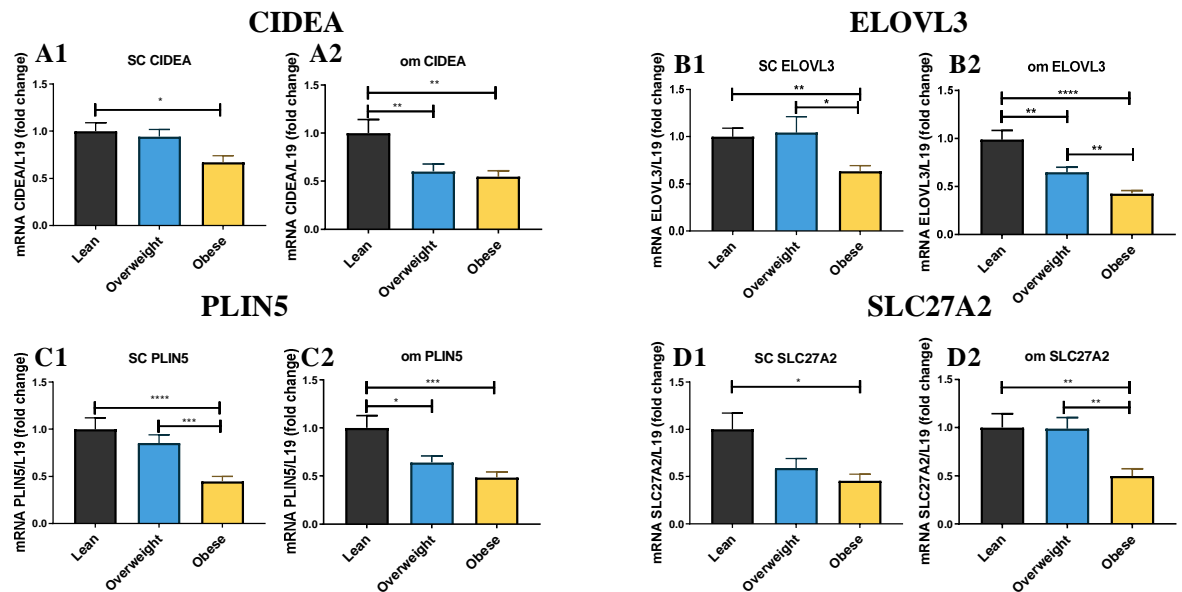


Figure 6.3.2.2 Key Brown Fat Genes are Decreased with BMI.

CIDEA (A1, A2), ELOVL3 (B1, B2), PLIN5 (C1, C2) and SLC27A2 (D1, D2) were measured in lean (n=44), overweight (n=49) and obese (37) participants using RT-PCR with L19 as a housekeeping gene. Data represent mean \pm standard error of the mean. The one-way ANOVA test (if parametric distribution) or the Kruskal-Wallis (if not parametric distribution) test was used to test significance levels: * $p < 0.05$, ** $p < 0.01$, *** $p < 0.001$ compared to lean control. CIDEA: cell death-inducing DFFA-like effector A, ELOVL3: fatty acid elongase 3, PLIN5: perilipin 5.

6.3.3 Inflammatory Markers and the Relation with BMI

To determine if inflammation was increased with BMI, inflammatory markers interleukin 6 (IL6), tumour necrosis factor alpha (TNF α), monocyte chemotactic protein-1 (MCP1) and interleukin 1 beta (IL1 β) were measured in lean, overweight and obese groups in both subcutaneous and omental fat depots (Figure 6.3.3.1). All inflammatory markers were significantly upregulated in obese participants compared to lean, with a maximum 3-fold difference observed with IL1 β .

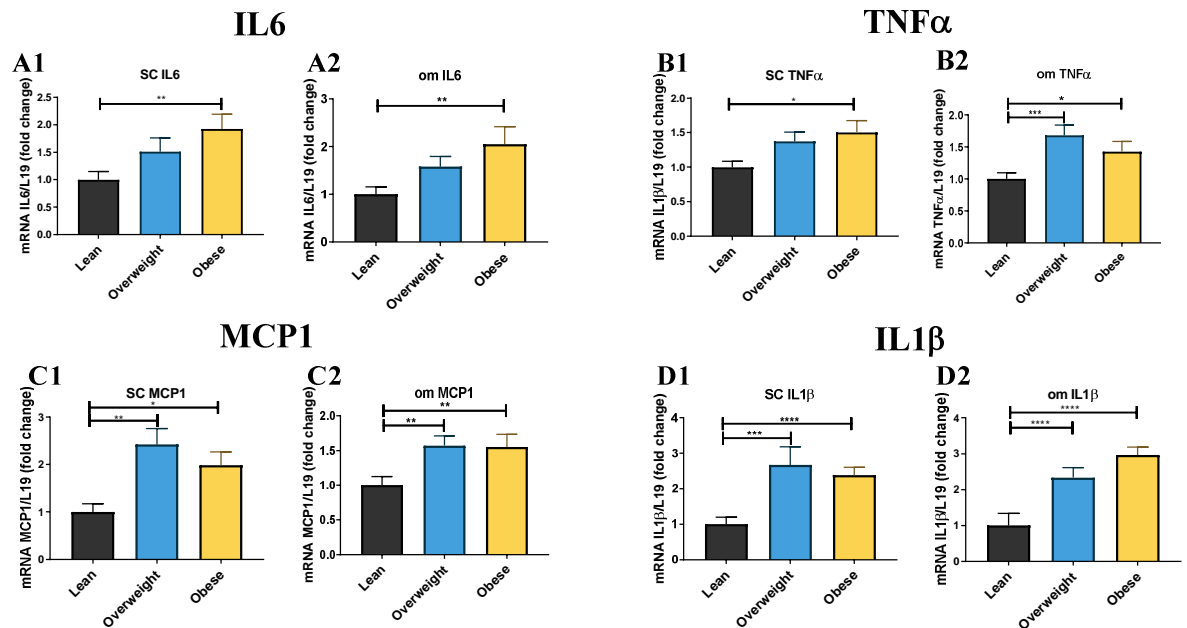


Figure 6.3.3.1 Inflammatory Markers Are Increased with BMI.

Key inflammatory markers IL6 (A1, A2), TNFα (B1, B2), MCP1 (C1, C2) and IL1β (D1, D2) were measured in lean (n=44), overweight (n=49) and obese (37) participants using qRT-PCR with L19 as a housekeeping gene. Data represent mean ± standard error of the mean. The one-way ANOVA (if parametric distribution) or the Kruskal-Wallis (if not parametric distribution) test was used to test significance levels: *p<0.05, **p<0.01, ***p<0.001 compared to lean control. IL6: interleukin 6, TNFα: tumour necrosis factor alpha, MCP1: monocyte chemotactic protein-1, IL1β interleukin 1 beta.

6.3.4 Inflammatory Genes Correlate with Reduced BAT Genes

As the expression of both BAT-associated genes was shown to decrease with increasing BMI, while inflammatory genes were shown to increase with increasing BMI, the direct relationship between the two was investigated. The Pearson correlation test was carried out to determine any significant correlations. This highlighted that there was a strong negative correlation between the BAT and inflammatory genes in omental adipose tissue, with a less apparent negative correlation present in subcutaneous adipose tissue (Table 6.3.4.1).

		IL6		MCP1		TNF α		IL1 β	
		Pearson's r	P value	Pearson's r	P value	Pearson's r	P value	Pearson's r	P value
CIDEA	Sc	-0.01	0.91	0.01	0.93	-0.05	0.55	0.03	0.78
	Om	-0.33 ***	2.00E-04	-0.31 ***	6.00E-04	-0.12	0.21	-0.40 ****	7.25E-06
ELOVL3	Sc	-0.23 **	0.01	-0.16	0.08	-0.06	0.52	-0.13	0.17
	Om	-0.33 ***	2.00E-04	-0.30 ***	7.00E-04	-0.05	0.62	-0.35 ***	1.00E-04
PLIN5	Sc	-0.20 *	0.03	-0.05	0.58	-0.26 **	3.00E-03	-0.16	0.08
	Om	-0.26 **	3.00E-03	-0.22 *	0.02	-0.17	0.05	-0.23 *	0.01
SLC27A2	Sc	0.07	0.47	0.004	0.96	-0.10	0.28	0.10	0.28
	Om	-0.13	0.19	-0.12	0.19	0.01	0.91	-0.29 **	1.00E-03

Table 6.3.4.1 Correlation of Inflammatory Genes with BAT Genes.

The correlation of inflammatory genes IL6, MCP1, TNF α and IL1 β with brown adipose tissue (BAT) genes CIDEA, ELOVL3, PLIN5 and SLC27A2 was assessed using the Pearson Correlation test. If non-parametric, variables were log-transformed prior to correlation analysis to improve normality. Significant correlations are highlighted, *p<0.05, **p<0.01, ***p<0.001 and **** p<0.0001. CIDEA: cell death-inducing DFFA-like effector A, ELOVL3: fatty acid elongase 3, PLIN5: perilipin 5. IL6: interleukin 6, TNF α : tumour necrosis factor alpha, MCP1: monocyte chemotactic protein-1, IL1 β interleukin 1 beta.

6.3.5 BAT Genes Correlation with Mitochondrial Dynamic and Biogenesis Genes

To investigate if BAT genes are associated with mitochondrial genes, the correlation between BAT genes (CIDEA, ELOVL3, PLIN5 and SLC27A2) and genes related to mitochondrial dynamics, biogenesis and other important mitochondrial functions were investigated.

BAT genes were positively correlated with some mitochondrial dynamics, biogenesis, oxidative phosphorylation and oxidative metabolism genes (Table 6.3.5.1). MFN2, the fusion gene, had the largest positive correlation with all BAT genes in omental and subcutaneous tissue (maximum r =0.64 (P<0.0001)). In addition, both CIDEA and

ELOVL3 were positively correlated with fission and fusion genes (Table 6.3.5.1). Biogenesis genes were only positively correlated with ELOVL3 in omental tissue apart from PGC1 α which was correlated with SLC27A2 (Table 6.3.5.2). Both COX4 and citrate synthase, key enzymes of oxidative phosphorylation and oxidative metabolism and Krebs Cycle, consequently, were positively correlated with all BAT-genes in omental and subcutaneous tissue (Table 6.3.5.3).

		Fission				Fusion			
		FIS 1		DRP1		MFN 2		OPA1	
		Pearson's r	P value	Pearson's r	P value	Pearson's r	P value	Pearson's r	P value
CIDEA	Sc	0.33***	2.55E-04	0.18*	0.04	0.39***	9.60E-06	0.16	0.09
	Om	0.08	0.38	0.19*	0.03	0.38***	2.14E-05	0.17	0.05
ELOVL3	Sc	0.47***	3.31E-08	0.31***	5.40E-04	0.55***	3.11E-11	0.32***	2.67E-04
	Om	0.10	0.25	0.28**	2.10E-03	0.43***	8.57E-07	0.31***	4.49E-04
PLIN5	Sc	0.20*	0.03	0.09	0.34	0.64***	1.90E-15	0.07	0.43
	Om	0.01	0.95	-0.02	0.78	0.32***	3.33E-04	-0.04	0.70
SLC27A2	Sc	0.07	0.46	0.02	0.78	0.10	0.26	0.07	0.45
	Om	0.05	0.60	0.14	0.13	0.05	0.60	0.13	0.16

Table 6.3.5.1 Correlation of BAT Genes with Mitochondrial Dynamics Genes.

The correlation of brown adipose tissue (BAT) genes (CIDEA, ELOVL3, PLIN5 and SLC27A2) with mitochondrial fission (FIS1, DRP1) and fusion genes (MFN2, OPA1) was assessed using the Pearson correlation test. If non-parametric, variables were log-transformed prior to correlation analysis to improve normality. Significant correlations are highlighted, *p<0.05, **p<0.01, ***p<0.001 and ****p<0.0001. CIDEA: cell death-inducing DFFA-like effector A, ELOVL3: fatty acid elongase 3, PLIN5: perilipin 5, FIS1: mitochondrial fission 1, DRP1: dynamin-related protein 1, MFN2: mitofusin 2. OPA1: mitochondrial dynamin like GTPase.

		Biogenesis					
		PGC1 α		Nrf1		TFAM	
		Pearson's r	P value	Pearson's r	P value	Pearson's r	P value
CIDEA	Sc	-0.05	0.59	0.05	0.62	0.06	0.53
	Om	0.10	0.27	0.12	0.19	0.13	0.16
ELOVL3	Sc	0.01	0.92	0.12	0.19	0.20*	0.03
	Om	0.19*	0.04	0.29***	9.85E-04	0.19*	0.04
PLIN5	Sc	-0.12	0.19	0.06	0.55	-0.06	0.49
	Om	-0.02	0.86	0.09	0.31	-0.05	0.57
SLC27A2	Sc	0.28**	2.00E-03	0.07	0.42	0.03	0.74
	Om	0.41****	3.61E-06	0.11	0.26	0.08	0.42

Table 6.3.5.2 Correlation of BAT Genes with Mitochondrial Biogenesis Genes.

The correlation of brown adipose tissue (BAT) genes (CIDEA, ELOVL3, PLIN5 and SLC27A2) with mitochondrial biogenesis genes was assessed using the Pearson correlation test. If non-parametric, variables were log-transformed prior to correlation analysis to improve normality. Significant correlations are highlighted, *p<0.05, **p<0.01, ***p<0.001. CIDEA: cell death-inducing DFFA-like effector A, ELOVL3: fatty acid elongase 3, PLIN5: perilipin 5, PGC1 α : peroxisome proliferator-activated receptor gamma coactivator 1-alpha, NRF1: nuclear respiratory factor 1, TFAM: mitochondrial transcription factor A.

		Cox4		SOD2		CS	
		Pearson's r	P value	Pearson's r	P value	Pearson's r	P value
CIDEA	Sc	0.37****	2.82E-05	0.23*	0.01	0.31***	4.95E-04
	Om	0.50****	4.56E-09	-0.20*	0.03	0.65****	7.65E-16
ELOVL3	Sc	0.48****	1.40E-08	0.17	0.06	0.52****	4.40E-10
	Om	0.46****	9.27E-08	-0.09	0.31	0.65****	1.41E-15
PLIN5	Sc	0.51****	1.23E-09	0.17	0.07	0.27**	2.22E-03
	Om	0.30***	7.17E-04	-0.19*	0.03	0.40****	4.67E-06
SLC27A2	Sc	0.01	0.91	0.17	0.06	0.30***	7.74E-04
	Om	0.30***	8.78E-04	-0.01	0.92	0.56****	3.98E-11

Table 6.3.5.3 Correlation of BAT Genes with Mitochondrial Genes.

The correlation of brown adipose tissue (BAT) genes (CIDEA, ELOVL3, PLIN5 and SLC27A2) with reactive oxygen species clearance gene (SOD2), oxidative phosphorylation gene 4 (Cox4) and the key enzyme of oxidative metabolism and Krebs Cycle genes (CS) was assessed using the Pearson correlation test. If non-parametric, variables were log-transformed prior to correlation analysis to improve normality. Significant correlations are highlighted, *p<0.05, **p<0.01, ***p<0.001. CIDEA: cell death-inducing DFFA-like effector A, ELOVL3: fatty acid elongase 3, PLIN5: perilipin 5, SOD2: superoxide dismutase 2. COX4: cytochrome c oxidase subunit. CS: citrate synthase.

6.3.6 Inflammatory Genes Correlate with Mitochondrial Genes

To investigate if mitochondrial genes were associated with inflammatory genes, the correlation between inflammatory genes (IL6, MCP1, TNF α , IL1 β) and mitochondrial fission (FIS1, DRP1), fusion (MFN2, OPA1), biogenesis (PGC1 α , NRF1, TFAM), reactive oxygen species clearance (SOD2), oxidative phosphorylation (Cox4) and the key enzyme of oxidative metabolism and Krebs Cycle gene (CS) were investigated. It was identified that the inflammatory genes were positively correlated with fission (FIS1) (Table 6.3.6.1), whilst they were negatively correlated with fusion gene (MFN2) (Table 6.3.6.1), biogenesis (Table 6.3.6.2), oxidative phosphorylation and oxidative metabolism genes (Table 6.3.6.3).

In general, there was no correlation between inflammatory genes and mitochondrial biogenesis genes, however, NRF1 showed significant positive correlation with inflammatory genes in subcutaneous samples (Table 6.3.6.2). Similarly, SOD2 showed a

significant positive correlation with inflammatory genes in subcutaneous samples (Table 6.3.6.3). This positive correlation might be part of a protective mechanism against increased inflammation.

		Fission				Fusion			
		FIS 1		DRP1		MFN2		OPA1	
		Pearson's r	P value	Pearson's r	P value	Pearson's r	P value	Pearson's r	P value
IL6	Sc	-0.01	0.94	0.04	0.69	-0.21*	0.02	0.18*	0.05
	Om	0.03	0.78	0.01	0.91	-0.34***	1.20E-04	0.03	0.77
MCP1	Sc	-0.08	0.39	-0.04	0.69	-0.24**	6.00E-03	0.00	0.97
	Om	0.04	0.62	0.00	1.00	-0.36***	3.16E-05	0.00	1.00
IL1 β	Sc	0.20*	0.03	0.01	0.92	-0.22*	0.01	0.08	0.36
	Om	0.31***	4.40E-04	0.07	0.47	-0.44****	3.67E-07	-0.05	0.58
TNF α	Sc	0.33**	1.52E-04	0.23*	0.01	-1.88*	0.04	0.19*	0.03
	Om	0.37****	2.03E-05	0.33***	1.38E-04	-0.11	0.24	0.345**	7.70E-05

Table 6.3.6.1 Correlation of Inflammatory Genes with Mitochondrial Dynamics Genes.

The correlation of inflammatory genes (IL6, MCP1, TNF α , IL1 β) with mitochondrial fission (FIS1, DRP1) and fusion genes (MFN2, OPA1) was assessed using the Pearson correlation test. If non-parametric, variables were log-transformed prior to correlation analysis to improve normality. Significant correlations are highlighted, *p<0.05, **p<0.01, ***p<0.001. IL6: interleukin 6, TNF α : tumour necrosis factor alpha, MCP1: monocyte chemotactic protein-1, IL1 β interleukin 1 beta, FIS1: mitochondrial fission 1, DRP1: dynamin-related protein 1, MFN2: mitofusin 2. OPA1: mitochondrial dynamin like GTPase.

		biogenesis					
		PGC1 α		Nrf1		TFAM	
		Pearson's r	P value	Pearson's r	P value	Pearson's r	P value
IL6	Sc	-0.06	0.48	0.18*	0.04	0.16	0.08
	Om	0.18*	0.05	0.02	0.87	-0.02	0.79
MCP1	Sc	0.00	0.99	0.20*	0.03	0.00	0.97
	Om	0.10	0.28	0.07	0.43	-0.02	0.83
IL1 β	Sc	0.02	0.80	0.24**	6.00E-03	0.10	0.29
	Om	0.05	0.62	0.05	0.61	0.06	0.54
TNF α	Sc	0.08	0.40	0.40****	4.69E-06	0.26**	4.00E-03
	Om	0.02	0.81	0.52****	4.47E-10	0.44****	2.87E-07

Table 6.3.6.2 Correlation of Inflammatory Genes with Mitochondrial Biogenesis Genes.

The correlation of inflammatory genes (IL6, MCP1, TNF α , IL1 β) with mitochondrial biogenesis genes was assessed using the Pearson correlation test. If non-parametric, variables were log-transformed prior to correlation analysis to improve normality. Significant correlations are highlighted, *p<0.05, **p<0.01, ***p<0.001 and ****p<0.0001. IL6: interleukin 6, TNF α : tumour necrosis factor alpha, MCP1: monocyte chemotactic protein-1, IL1 β interleukin 1 beta, PGC1 α : peroxisome proliferator-activated receptor gamma coactivator 1-alpha, NRF1: nuclear respiratory factor 1, TFAM: mitochondrial transcription factor A.

		Cox4		SOD2		CS	
		Pearson's r	P value	Pearson's r	P value	Pearson's r	P value
IL6	Sc	-0.07	0.42	0.63****	6.59E-15	-0.06	0.48
	Om	-0.21*	0.02	0.65****	1.36E-16	-0.22*	0.02
MCP1	Sc	-0.15	0.10	0.13	0.14	0.00	0.99
	Om	-0.30***	4.92E-04	0.54**	6.75E-11	-0.20*	0.02
IL1 β	Sc	-0.10	0.28	0.54****	4.23E-11	0.02	0.80
	Om	-0.36****	4.17E-05	0.053	0.56	-0.25**	7.00E-03
TNF α	Sc	-0.12	0.19	0.18*	0.05	-0.08	0.40
	Om	-0.06	0.49	0.079	0.38	0.12	0.18

Table 6.3.6.3 Correlation of Inflammatory Genes with Mitochondrial Genes.

The correlation of inflammatory genes (IL6, MCP1, TNF α , IL1 β) with reactive oxygen species clearance gene (SOD2), oxidative phosphorylation gene (4 Cox4) and the key enzyme of oxidative metabolism and Krebs Cycle genes (CS) was assessed using the Pearson correlation test. If non-parametric, variables were log-transformed prior to correlation analysis to improve normality. Significant correlations are highlighted, *p<0.05, **p<0.01, ***p<0.001, ****p<0.0001. IL6: interleukin 6, TNF α : tumour necrosis factor alpha, MCP1: monocyte chemotactic protein-1, IL1 β interleukin 1 beta, SOD2: superoxide dismutase 2. COX4: cytochrome c oxidase subunit. CS: citrate synthase.

6.3.7 LPS Induces Inflammation in Mouse Adipocytes and Primary Human Adipocytes

Following the correlation of inflammatory genes with BAT genes from *in vivo* adipose tissue samples, the direct impact of LPS (an inducer of inflammation) on *in vitro* mouse adipocytes and primary human adipocytes was investigated.

Mouse cells were treated with 100 ng/mL or 1000 ng/mL LPS, and/or 2 μ M rosiglitazone to induce browning, 10 μ M CL to induce UCP1 expression in order to mimic the beige phenotype, or combinations of these. Similarly, human cells were treated with 100 ng/mL LPS, 2 μ M rosiglitazone to induce browning, 10 μ M isoproterenol to induce UCP1 expression in order to investigate the beige phenotype, or combinations of these.

Following treatment, the gene expression of adipocyte protein 2 (aP2) was measured. Given that aP2 gene expression levels did not significantly change between different

treatments, it was accepted that treatments had not impacted differentiation in all tested cells which include mouse sWAT immortalized cell line (Figure 6.3.7.1, A), and mouse primary sWAT (Figure 6.3.7.1, B) and human primary adipocytes from lean (Figure 6.3.7.2, A1, A2) and obese (Figure 6.3.7.2, B1, B2).

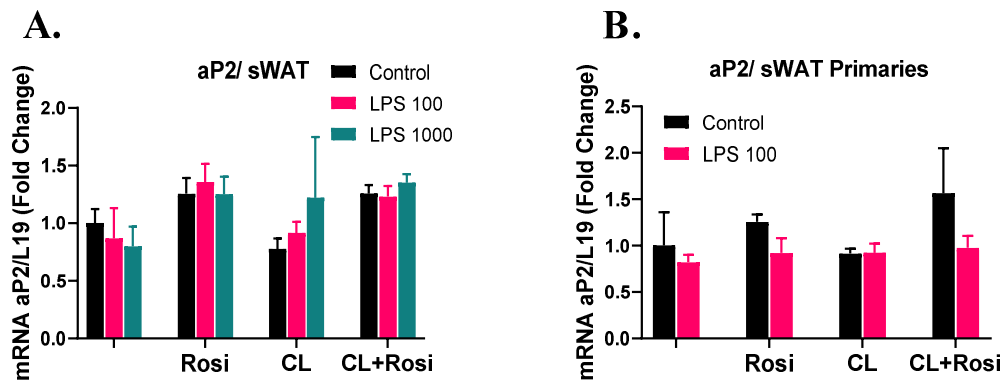


Figure 6.3.7.1 Effect of Inflammatory and Adipocyte Browning Treatments on Mouse Adipocyte Differentiation.

Immortalized white sWAT (A, n=3) and primary white sWAT (B, n=3) primary human adipocyte cells were grown and differentiated with/without 2 μ M rosiglitazone (Rosi) to promote browning, 100 ng/mL lipopolysaccharide (Lps100), or a combination of the two and treated with/without UCP1 inducer, 10 μ M CL. Adipocyte Protein 2 (aP2) gene expression was measured as a marker of differentiation using q-rt-PCR using L19 as a housekeeping control. Data represent mean \pm standard error of the mean. The two-way ANOVA test was used to test significance levels, no significant differences were determined.

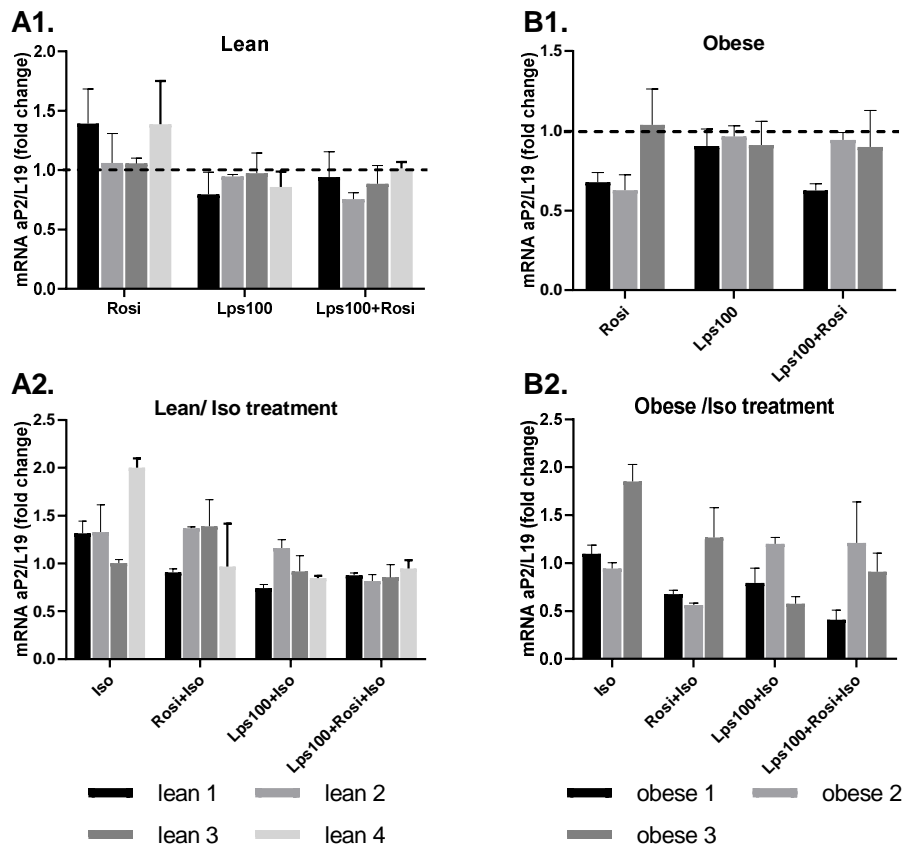


Figure 6.3.7.2 Effect of Inflammatory and Adipocyte Browning Treatments on Primary Human Adipocyte Differentiation.

Lean (A1/A2, n=4) and obese (B1/B2, n=3) primary human adipocyte cells were grown and differentiated with/without 2 μ M rosiglitazone (Rosi), 100 ng/mL lipopolysaccharide (Lps100), or a combination of the two and treated on the day of the experiment with UCP1 inducer, 10 μ M isoproterenol (Iso) (A2/B2) or vehicle (A1, B1). Adipocyte Protein 2 (aP2) gene expression was measured as a marker of differentiation. Data represent mean \pm standard error of the mean. The two-way ANOVA test was used to test significance levels; no significant differences were determined.

As expected, inflammatory genes IL6 and MCP1 were significantly upregulated with LPS treatment, with a maximum 15-fold increase ($P < 0.0001$) observed in human primary adipocytes (Figure 6.3.7.4). The maximum fold increase observed in immortalized mice primaries was 60 ($P < 0.0001$) (Figure 6.3.7.3, A). In addition, rosiglitazone, the browning stimulator, reduced the inflammatory response – more clearly for MCP1 in human cells (Figure 6.3.7.4, B1, B2) and IL6 in the mouse cell line (Figure 6.3.7.3, A). For mouse primary adipocyte cultures both IL6 and MCP1 were reduced in response to LPS with rosiglitazone treatment (Figure 6.3.7.3, B, B1). In fact, rosiglitazone is one of the thiazolidinedione class of PPAR- γ ligands which has established anti-inflammatory activity through its ability to antagonize nuclear factor κ B (NF κ B) and AP1 signalling pathways (671,672). The cellular targets of this anti-inflammatory PPAR function are not only inflammatory cells of the immune system but also resident and structural cells of the adipose tissue that play significant roles during inflammation (673). Thus, this observed anti-inflammatory role for rosiglitazone when used with LPS in differentiating brown adipocytes is in agreement with findings in other cell types. However, it is not clear how long an anti-inflammatory response would be maintained after withdrawal of the rosiglitazone. Therefore, an alternative explanation is that beige adipocytes are less responsive to inflammation than white adipocytes. This may be a more acceptable explanation because the rosiglitazone as a browning inducer changes the transcription to brown fat genes program.

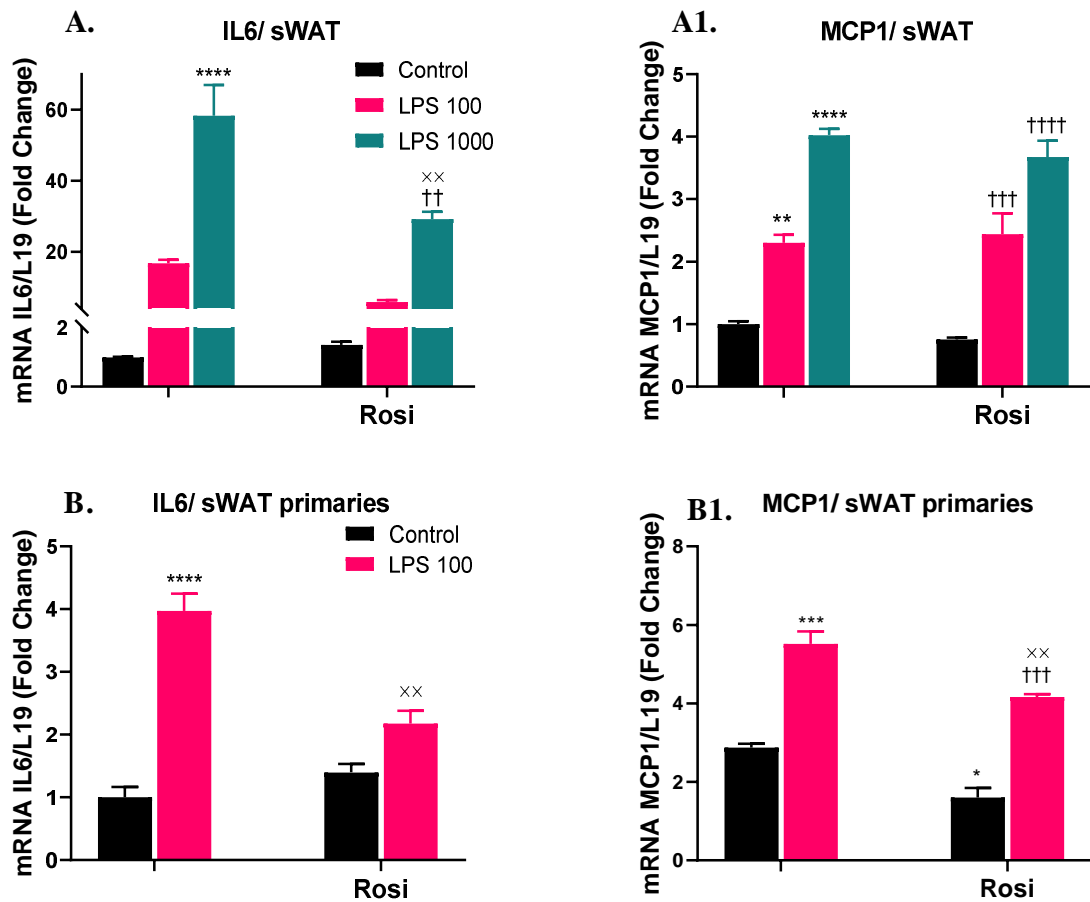


Figure 6.3.7.3 Effect of Inflammatory and Adipocyte Browning Treatments on Mouse Adipocyte Inflammation.

Immortalized white sWAT (A, n=3) and primary white sWAT (B, n=3) adipocytes were grown and differentiated with/without 2 μ M rosiglitazone (Rosi) for 'beiging' effect, 100 ng/mL or 1000 ng/mL lipopolysaccharide (Lps100, LPS1000), or a combination of the two. Inflammatory genes interleukin 6 (IL6) and monocyte chemotactic protein-1 (MCP1) are measured using q-rt-PCR using L19 as a housekeeping control. Data represent mean \pm standard error of the mean. The two-way ANOVA test was used to test significance levels, ** p <0.01, *** p <0.001, **** p <0.0001 compared to control, †† p <0.01, ††† p <0.001 compared to Rosi treatment. \times p <0.05, $\times\times$ p <0.01, $\times\times\times$ p <0.001 and $\times\times\times\times$ p <0.0001 compared to LPS treatment

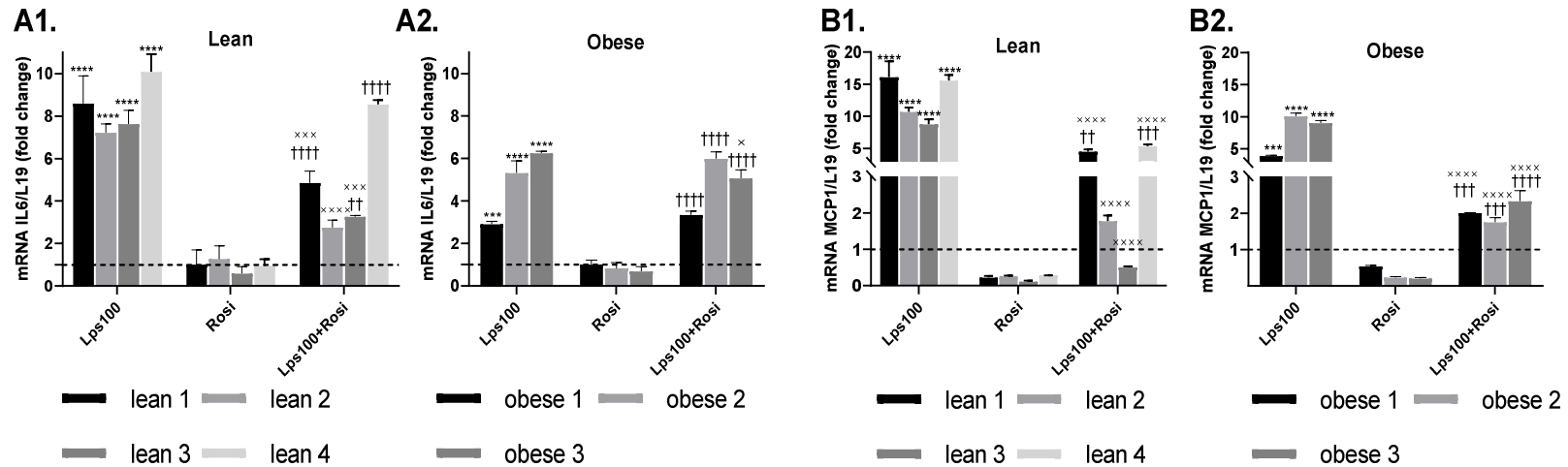


Figure 6.3.7.4 Effect of Inflammatory and Adipocyte Browning Treatments on Primary Human Adipocyte Inflammation.

Lean (A1/B1, n=4) and obese (A2/B2, n=3) primary human adipocyte cells were grown and differentiated with/without 2 μ M rosiglitazone (Rosi), 100 ng/mL lipopolysaccharide (Lps100), or a combination of the two. Inflammatory genes interleukin 6 (IL6), monocyte chemotactic protein-1 (MCP1) were measured by RT-PCR using L19 as a housekeeping control. Data represent mean \pm standard error of the mean. The two-way ANOVA test was used to test significance levels; *p<0.05, **p<0.01, ***p<0.001 compared to control, † p<0.05, †† p<0.01, ††† p<0.001 and †††† p<0.0001 compared to Rosi treatment. × p<0.05, ×× p<0.01, ××× p<0.001 and ×××× p<0.0001 compared to LPS treatment

6.3.8 LPS Effects on Adipocyte Browning

As the expression of inflammatory genes correlated with BAT genes, and LPS was noted to upregulate the inflammatory genes, the direct impact of LPS on BAT gene expression was next investigated. Firstly, the impact of LPS on brown fat genes was investigated in mouse white adipocytes using two cell models, immortalized and primary cultures. Secondly, the lean and obese primary human adipocytes were studied. White adipocytes were grown and differentiated with/without 2 μ M rosiglitazone (to promote the beige phenotype), 100 ng/mL LPS (and 1000 ng/mL for immortalized cells), or a combination of the two.

In the mouse adipocyte models, LPS treatment greatly reduced the expression of BAT genes in beige (Rosi-treated) adipocytes. This included CIDEA, ELOVL3 and PLIN5 in immortalized sWAT (Figure 6.3.8.1, A) and primary cultures (Figure 6.3.8.1, B), compared to browned cells. rosiglitazone treatment markedly upregulated all BAT genes by a maximum of 10-fold for immortalized sWAT, and 200-fold for primary sWAT. However, this was significantly reduced when LPS was included in the treatment (Figure 6.3.8.1).

In human primary adipocytes LPS treatment reduced the expression of the BAT genes CIDEA, PLIN5 and SLC compared to control. rosiglitazone treatment significantly upregulated all BAT genes by a maximum of 18-fold. Similar to mouse adipocytes, this was significantly reduced when LPS was included in the treatment (Figure 6.3.8.2). The data showed that generally, the cells from lean patients show a greater browning response than those from obese while LPS effect was less obvious in obese cells. This was particularly clear for SLC and ELOVL3 in obese cells where the browning response was minimal or absent. It is possible that obese cells already have reduced browning capacity and therefore are less impacted by LPS.

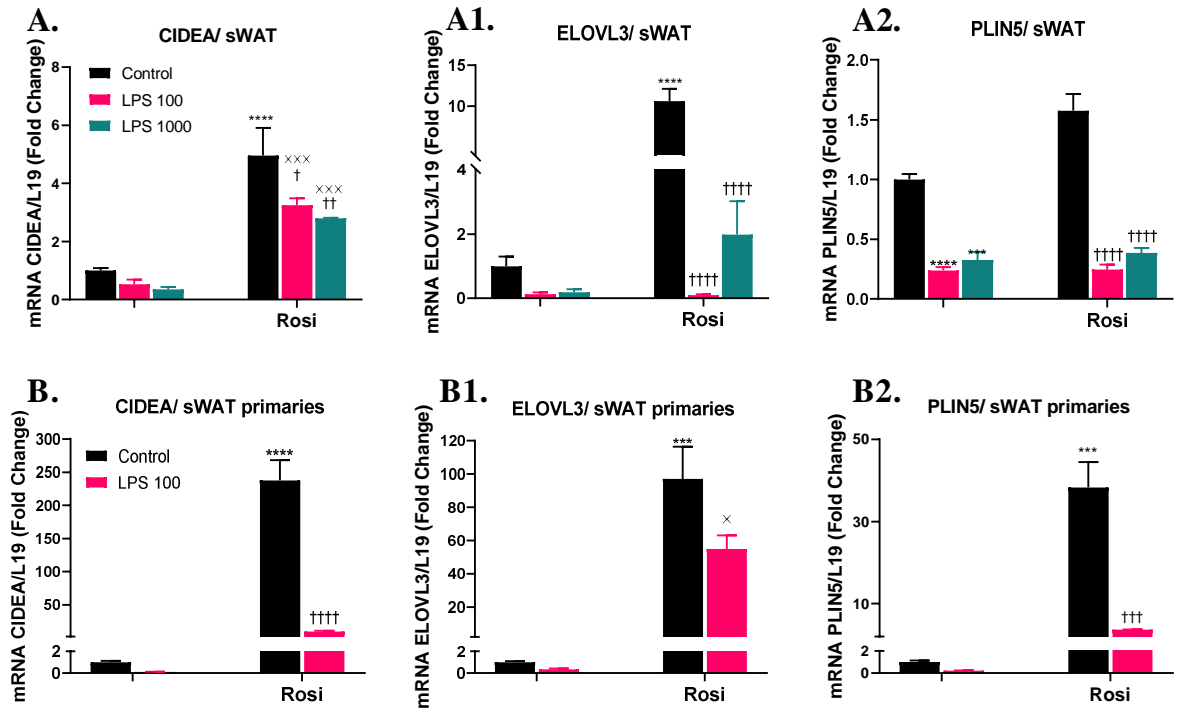


Figure 6.3.8.1 Impact of LPS on Mouse Adipocyte Browning.

Immortalized white sWAT (A/A1/A2, n=3) and primary white adipocytes sWAT (B/B1/B2, n=3) were grown and differentiated with/without 2 μ M rosiglitazone (Rosi) -for beiging effect-, 100 ng/mL or 1000 ng/mL lipopolysaccharide (Lps100 or Lps1000), or a combination of the two. Browning genes: cell death-inducing DFFA-like effector A (CIDEA), ELOVL fatty acid elongase 3 (ELOVL3), perilipin 5 (PLIN5) and Solute Carrier Family 27 Member 2 (SLC27A2) were analysed using q-RT-PCR with L19 as a housekeeping control. Data represent mean \pm standard error of the mean. The two-way ANOVA test was used to test significance levels; ***p<0.001, ****p<0.0001 compared to control, † p<0.05, †† p<0.01, ††† p<0.001, †††† p<0.0001 compared to Rosi treatment. × p<0.05, ××× p<0.001 compared to LPS treatment

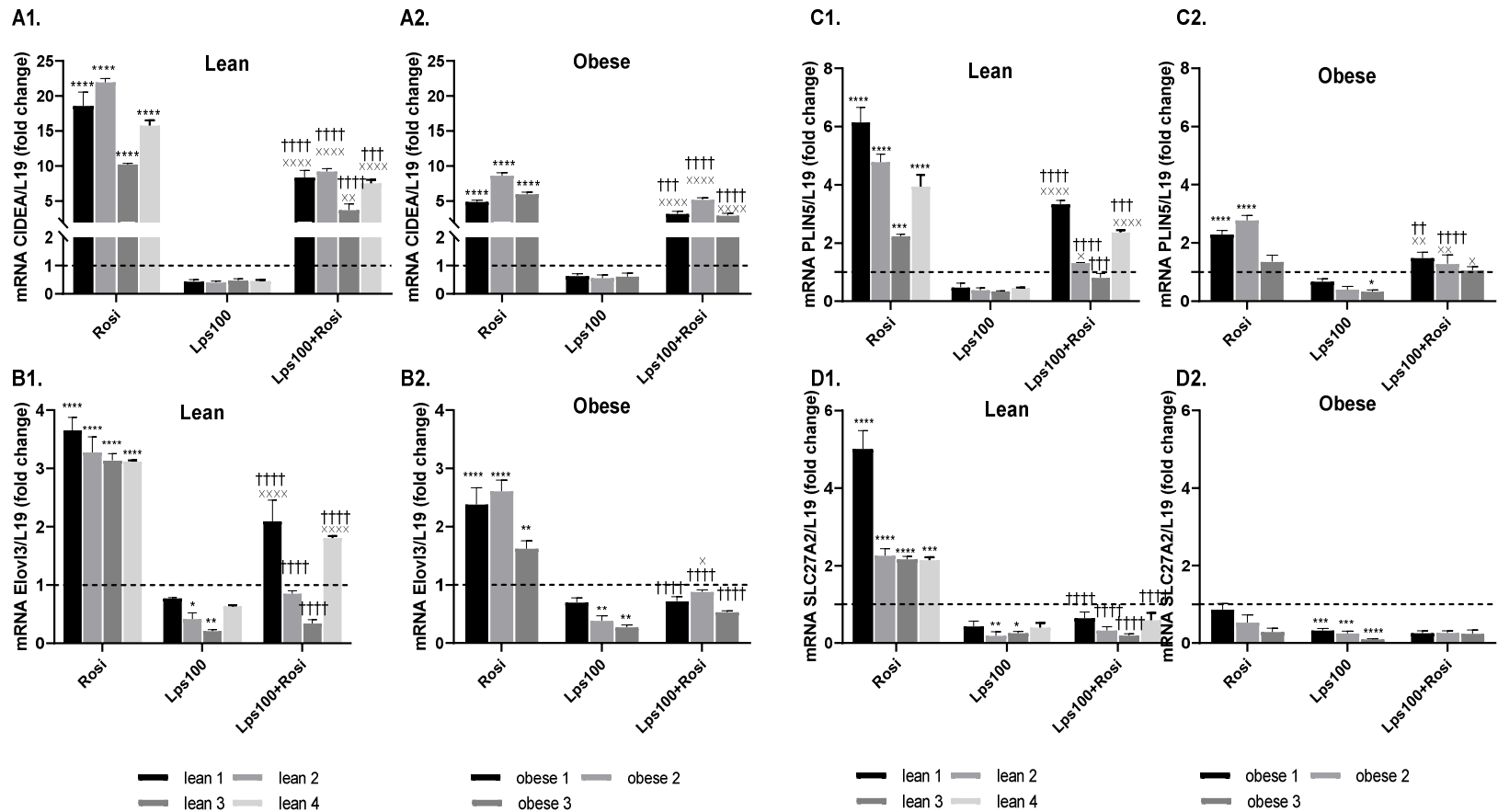


Figure 6.3.8.2 Impact of LPS on Human Primary Adipocyte Browning.

Lean (A1/B1/C1/D1) and obese (A2/B2/C2/D2) primary human adipocytes were differentiated with/without 2 μ M rosiglitazone (Rosi), 100 ng/mL lipopolysaccharide (LPS100) or a combination of the two. Browning genes cell death-inducing DFFA-like effector A (CIDEA), ELOVL fatty acid elongase 3 (ELOVL3), perilipin 5 (PLIN5) and Solute Carrier Family 27 Member 2 (SLC27A2) were analysed using qRT-PCR with L19 as a housekeeping control. Data represent mean \pm standard error of the mean. The two-way ANOVA test was used to test significance levels; * p <0.05, ** p <0.01, *** p <0.001 compared to control, † p <0.05, †† p <0.01, ††† p <0.001 compared to Rosi treatment. \times p <0.05, $\times\times\times$ p <0.0001 compared to LPS treatment.

6.3.9 LPS Effects on Thermogenesis-Associated Genes in Beige Cells

As it was observed that LPS reduced the level of genes involved in the browning of adipocytes, the impact of LPS on the ability of beige cells to function correctly was next investigated by measuring the gene expression of UCP1 and PGC1 α . UCP1 is the main thermogenic marker and distinguishes brown and beige adipocytes from white adipocytes, and PGC1 α is its master regulator.

Mouse white adipocytes from both an immortalized cell line and primary adipocyte cultures were used during this study. Also, primary human adipocytes from lean and obese subjects were studied. Both mouse and human adipocytes were differentiated to activate beige adipocytes and stimulated to induce an adrenergic response, which should induce UCP1 and PGC1 α expression if the cells are functioning correctly. As such, on day eight mouse cells were fully differentiated and treated with/without 10 μ M CL; similarly, human cells were fully differentiated on day 14 and were treated with/without 10 μ M isoproterenol (Iso).

CL treatment in mouse cell models and Iso treatment in human adipocytes increased the expression of both UCP1 and PGC1 α ; in mouse immortalized cells (Figure 6.3.9.1, A1, A2) and primary cultures (Figure 6.3.9.1, B1, B2) and in human cells from lean (Figure 6.3.9.2, A1, B1) and obese (Figure 6.3.9.2, A2, B2). However, LPS treatment reduced the expression of both genes in the presence and absence of rosiglitazone, indicating that LPS reduces the browning effect and therefore the capacity of adipocytes to respond to an adrenergic stimulus (Figure 6.3.9.2). Similar to the previously tested brown fat genes, it seems that lean cells are generally more responsive to the browning treatment compared with obese cells (Figure 6.3.9.1).

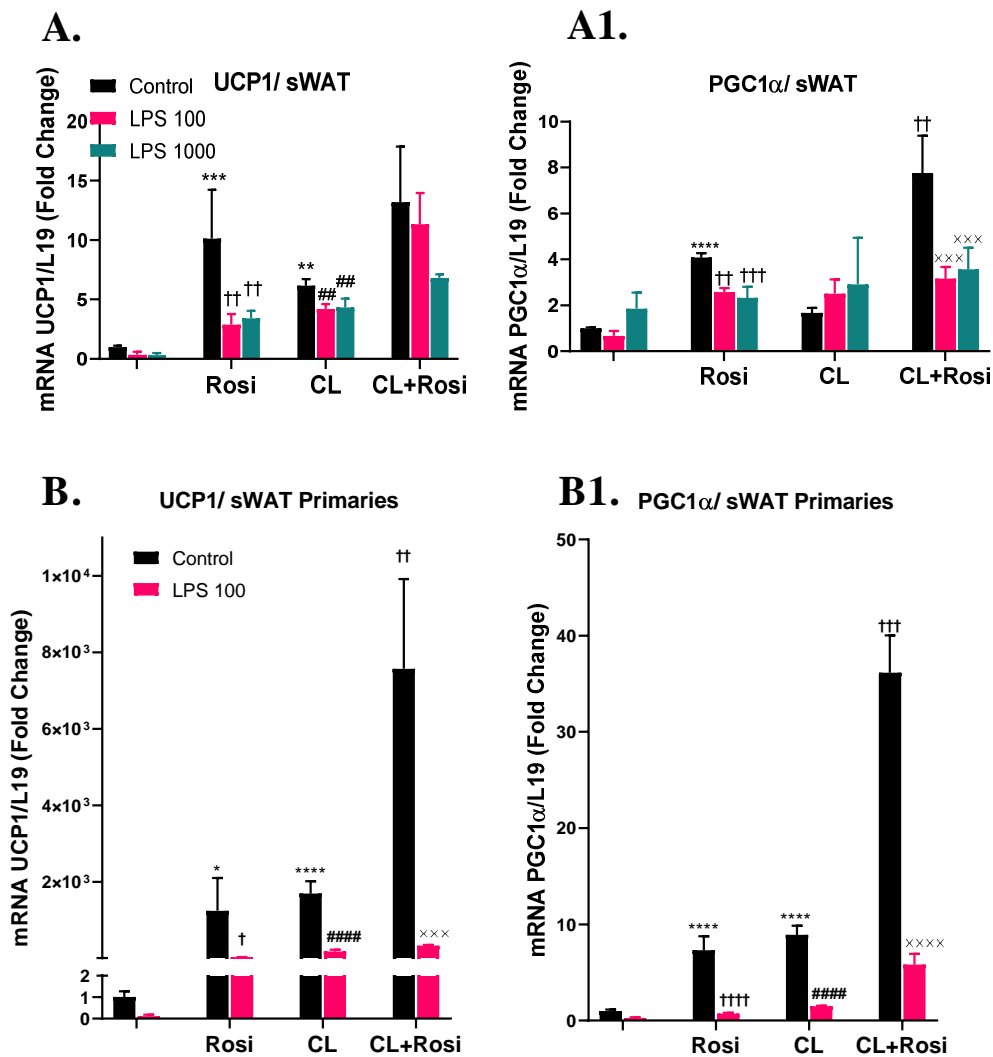


Figure 6.3.9.1 Impact of LPS on Beige Mouse Adipocyte Function.

Immortalized white sWAT (A/A1, n=3) and primary white adipocytes sWAT (B/B1, n=3) were grown and differentiated with/without 2 μ M rosiglitazone (Rosi) to induce beige effects, 100 ng/mL or 1000 ng/mL lipopolysaccharide (Lps100), (Lps1000) or a combination of the two. Differentiated cells were treated with/without CL (10 μ M) at day 8. Main BAT genes Uncoupling Protein 1 (UCP1) and Peroxisome proliferator-activated receptor gamma coactivator 1-alpha (PGC1 α) were analysed using qRT-PCR with L19 as a housekeeping control. Data represent mean \pm standard error of the mean. The two-way ANOVA test was used to test significance levels; *p<0.05, **p<0.01, ***p<0.001 compared to control, † p<0.05, †† p<0.01, ††† p<0.001 compared to Rosi treatment. # compared to CL, × compared to Rosi+CL.

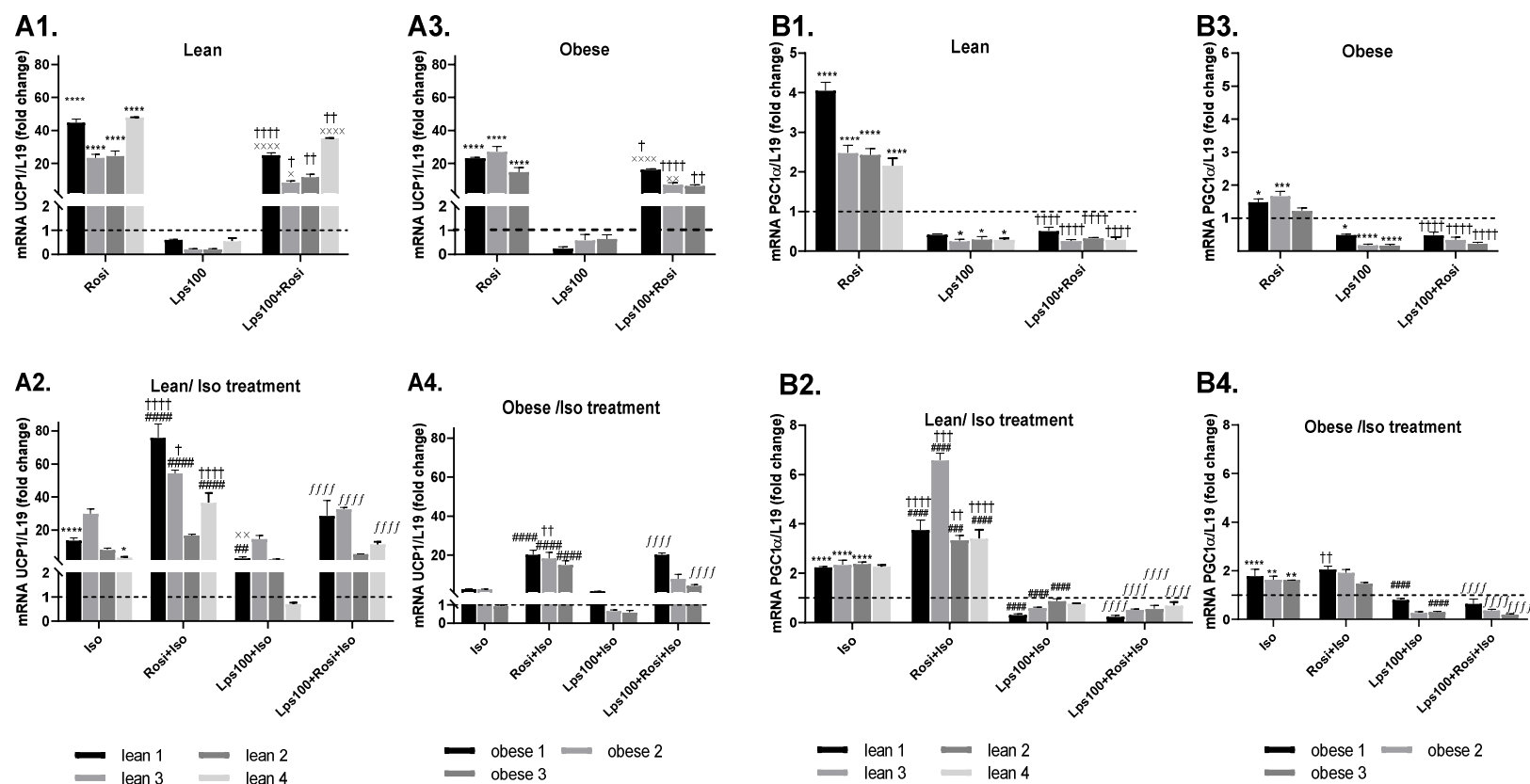


Figure 6.3.9.2 Impact of LPS on Beige Adipocyte Function.

Lean (A1/A2/B1/B2) and obese (A3/A4/B3/B4) primary human adipocytes were differentiated with/without 2 μ M rosiglitazone (Rosi), 100 ng/mL lipopolysaccharide (LPS100) or a combination of the two. When fully differentiated, cells were treated with/without 10 μ M isoproterenol (Iso) on day 14. Main BAT genes Uncoupling Protein 1 (UCP1) and Peroxisome proliferator-activated receptor gamma coactivator 1-alpha (PGC1 α) were analysed using qRT-PCR with L19 as a housekeeping control. Data represent mean \pm standard error of the mean. The two-way ANOVA test was used to test significance levels; * p <0.05, ** p <0.01, *** p <0.001 compared to control, † p <0.05, †† p <0.01, ††† p <0.001 compared to Rosi treatment, \times p <0.05, $\times\times\times$ p <0.0001 compared to LPS, ## p <0.01, ### p <0.001 and #### p <0.0001 compared to Iso treatment. ffff p <0.001 compared to Rosi+Iso treatment.

6.3.10 LPS Effect on Mitochondrial Function of Mouse Beige Adipocytes

After observing that treatment with LPS reduced UCP1 gene expression, as the main thermogenic marker in beige adipocytes (Rosi-treated), a Seahorse extracellular flux analyser was used to measure basal oxygen consumption rate (OCR) as an indicator of the rate of aerobic respiration. This was used to investigate the functional consequences of LPS treatment. Also, given that obesity represents a chronic stress to adipocytes, it became necessary to understand the functional implications of LPS treatment when adipocyte mitochondria are under stress. Therefore, a Seahorse Mito Stress Test was performed after differentiating both white (control) and beige (Rosi-treated) adipocytes with LPS treatment.

As expected, OCR of beige adipocytes was higher than OCR of white adipocytes (Figure 6.3.10.1, A). Also, as shown in Figure 6.3.10.1, LPS treatment reduced basal OCR in both types of adipocytes: white (control) and beige (Rosi-treated) (Figure 6.3.10.1, A1). Similarly, spare respiratory capacity (SRC) was reduced with LPS treatment (Figure 6.3.10.1, A2). When using CL to induce an adrenergic response, there was also significant reduction in OCR in both types of adipocytes (Figure 6.3.10.1, B)

Overall, this data provides evidence of a negative influence of chronic LPS treatment on the browning capacity of white adipocytes.

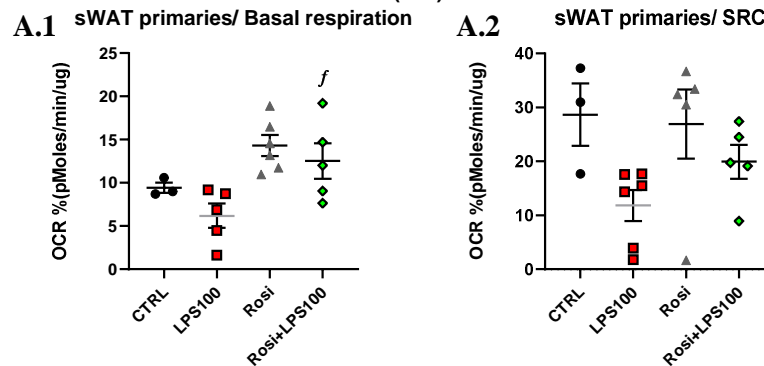
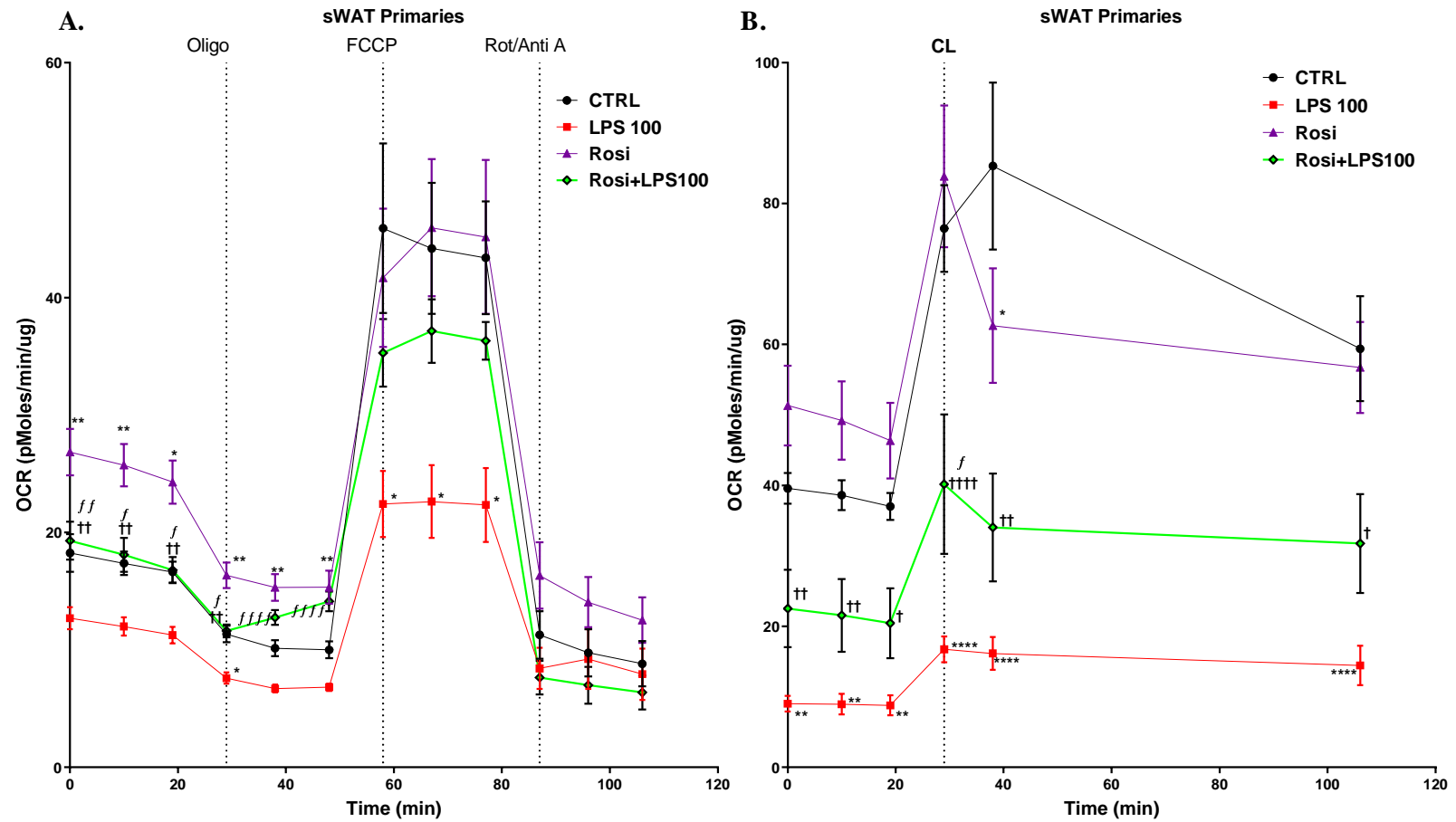


Figure 6.3.10.1 Effect of LPS on Aerobic Capacity Under Stress or Adrenergic Stimulus.

Time-lapse of aerobic capacity as measured by oxygen consumption rate (OCR) during (A) a Seahorse mitochondria stress test or (B) CL, adrenergic stimulus performed after differentiated cells with/without 2 μ M rosiglitazone (Rosi) -for being effect-, 100 ng/mL lipopolysaccharide (LPS100) or a combination of the two. Values were normalised to protein content of each experimental well to account for inter-well cell number variability. Basal Mitochondrial Bioenergetics were calculated including: (A1) Basal oxygen consumption rate (OCR) and (A2) Spare respiratory capacity (SRC). Error bars represent SEM. The two-way ANOVA test was used to test significance levels; * $p < 0.05$, ** $p < 0.01$, *** $p < 0.001$, **** $p < 0.0001$ compared to control, †† $p < 0.01$, ††† $p < 0.001$ and †††† $p < 0.0001$ compared to Rosi treatment. f $p < 0.05$, ff $p < 0.01$ and $ffff$ $p < 0.0001$. CTRL: Control.

6.3.11 LPS Effect on Expression of Genes Associated with Mitochondrial Dynamics

To further understand the impact of LPS on beige adipocyte biology, the effect on mitochondria-associated gene expression was assessed with a focus on genes required for fission and fusion events in both mouse and human adipocytes.

Fission genes dynamin-related protein 1 (DRP1) and mitochondrial fission 1 (FIS1), as well as fusion genes mitofusin 2 (MFN2) and mitochondrial dynamin like GTPase (OPA1) were analysed in mouse cells from two models including immortalized white adipocytes and primary cultures, and primary human adipocytes from lean and obese subjects following differentiation with rosiglitazone, LPS or a combination of the two.

Higher levels of mitochondrial dynamic-related gene expression were measured in beige adipocytes compared with white adipocytes. This increase can be seen in both Figure 6.3.11.1 and Figure 6.3.11.2 upon rosiglitazone treatment in mouse and lean human cells. The increase was less clear in human primary adipocytes derived from obese subjects. This observation in mitochondrial dynamic related genes following rosiglitazone is in line with recent findings that rosiglitazone ameliorates adipogenesis in 3T3 cells under oxidative stress conditions by improving mitochondrial biogenesis, dynamics and respiration (674).

In mouse cells, LPS significantly reduced the expression of all mitochondrial dynamic genes in beige adipocytes (rosiglitazone-treated) from both models, suggesting that LPS reduces the ability of the adipocytes to maintain healthy mitochondria following a browning stimulus (Figure 6.3.11.1).

Similarly, in human cells LPS significantly reduced the expression of all mitochondrial dynamic genes in both the presence and absence of rosiglitazone, further supporting that LPS reduces the ability of the adipocytes to maintain healthy mitochondria and undergo browning (Figure 6.3.11.2). Furthermore, once again it is clear that the lean fat-derived adipocytes were more sensitive to the effects of rosiglitazone compared to those derived from obese individuals.

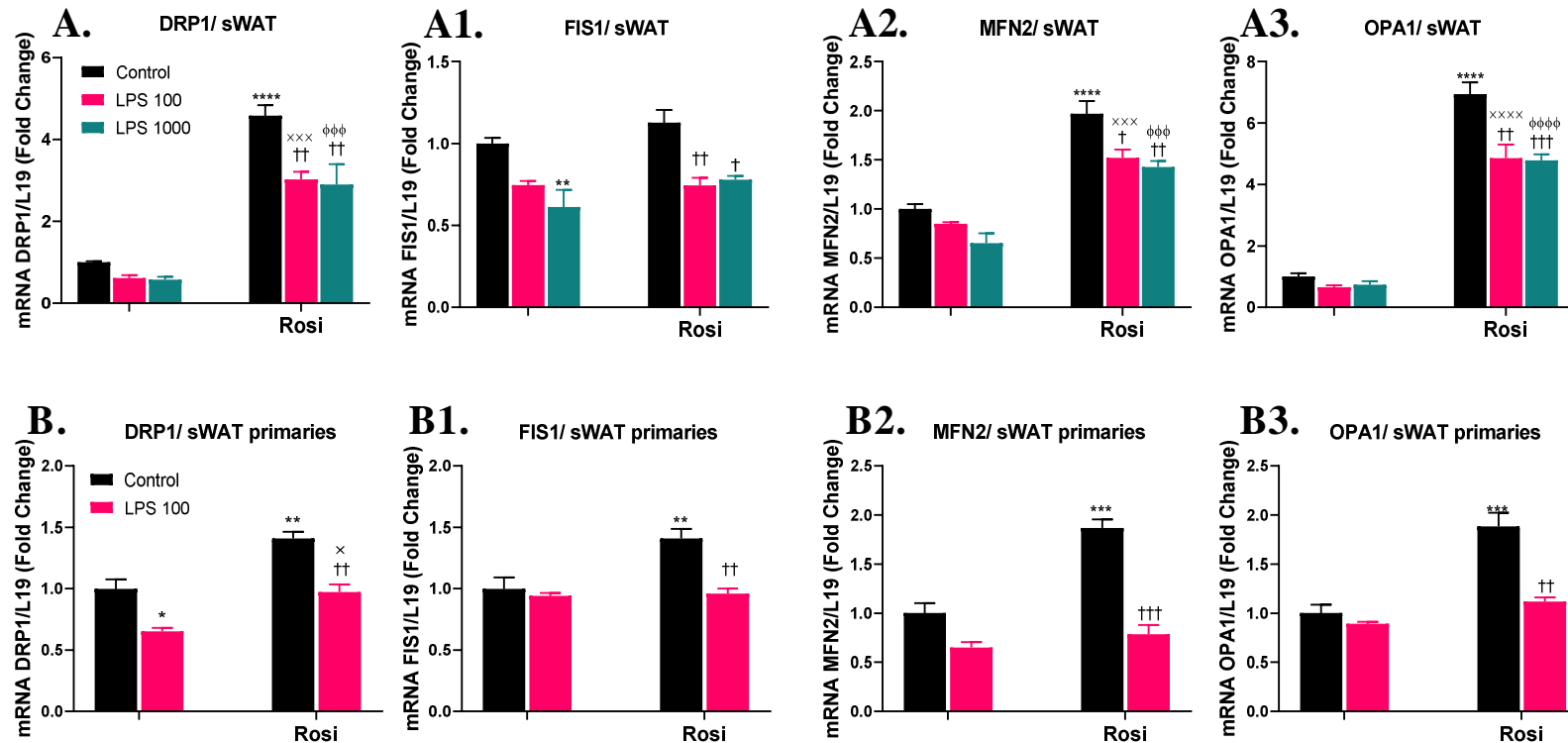


Figure 6.3.11.1 Impact of LPS on the Expression of Genes Associated with Mitochondrial Dynamics in Mouse Adipocytes.

Immortalized white sWAT (A/A1/A2/A3, n=3) and primary white adipocytes sWAT (B/B1/B2/B3, n=3) were grown and differentiated with/without 2 μ M rosiglitazone (Rosi) -for beiging effect-, 100 ng/mL or 1000 ng/mL lipopolysaccharide (Lps100), (Lps1000) or a combination of the two. Mitochondrial fission genes dynamin-related protein 1 (DRP1) (A,B) and mitochondrial fission 1 (FIS1) (A1,B1), as well as fusion genes mitofusin 2 (MFN2) (A2,B2) and mitochondrial dynamin like GTPase (OPA1) (A3,B3) were analysed by RT-PCR, with L19 as a housekeeping control. Data represent mean \pm standard error of the mean. The two-way ANOVA test was used to test significance levels; * p <0.05, ** p <0.01, *** p <0.001, **** p <0.0001 compared to control, † p <0.05, †† p <0.01, ††† p <0.001 compared to Rosi treatment. \times p <0.05, $\times\times$ p <0.001, and $\times\times\times$ p <0.0001 compared to LPS100, $\phi\phi\phi$ p <0.001, $\phi\phi\phi\phi$ p <0.0001 compared to LPS1000.

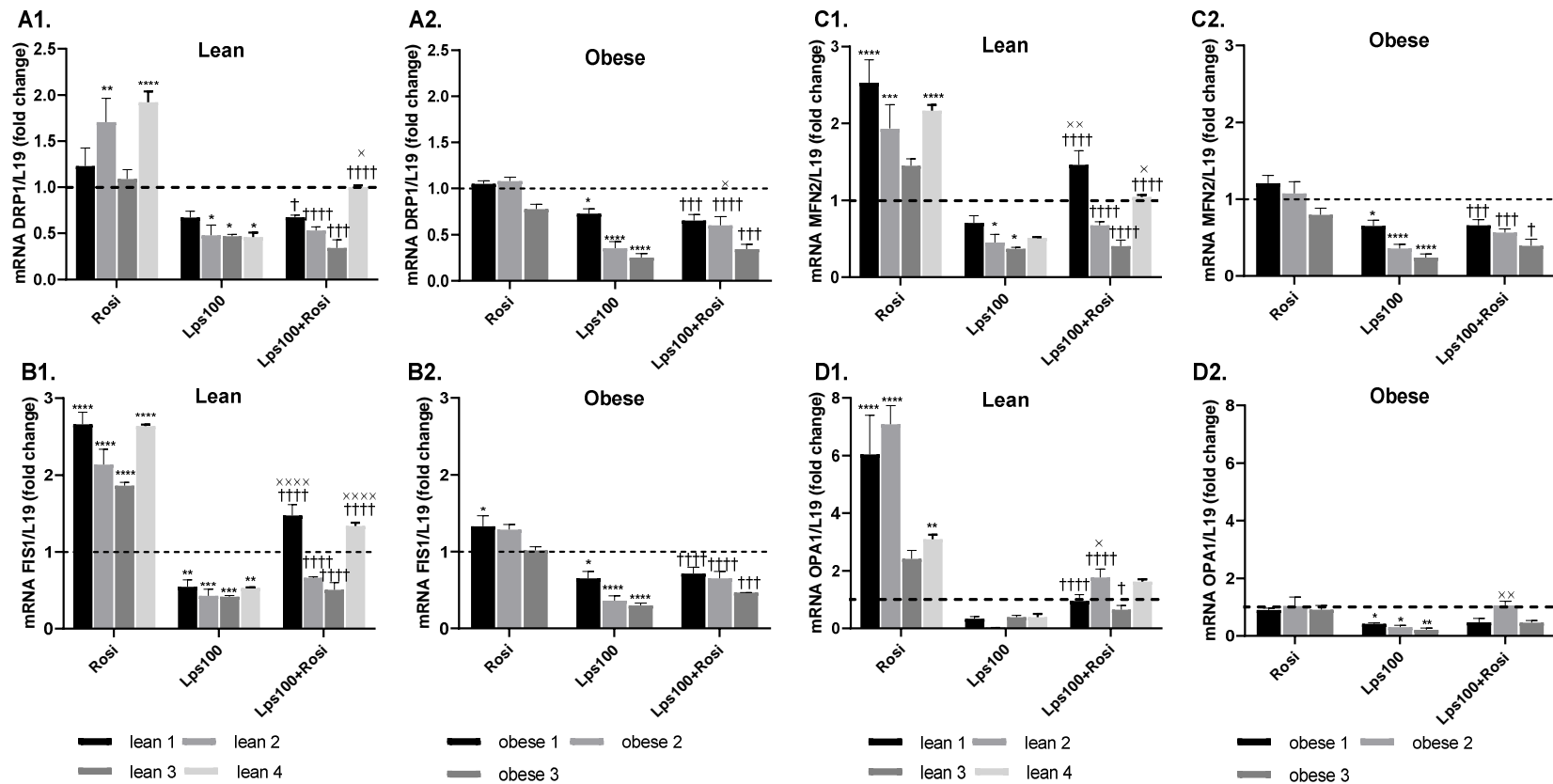


Figure 6.3.11.2 Impact of LPS on the Expression of Genes Associated with Mitochondrial Dynamics in Human Adipocytes.

Following differentiation of lean (A1/B1/C1/D1, n=4) and obese (A2/B2/C2/D2, n=3) primary human adipocytes with 2 μ M rosiglitazone (Rosi), 100 ng/mL lipopolysaccharide (Lps100) or a combination of the two, mitochondrial fission genes dynamin-related protein 1 (DRP1) and mitochondrial fission 1 (FIS1), as well as fusion genes mitofusin 2 (MFN2) and mitochondrial dynamin like GTPase (OPA1) were analysed via RT-PCR, with L19 as a housekeeping control. Data represent mean \pm standard error of the mean. The two-way ANOVA test was used to test significance levels.; *p<0.05, **p<0.01, ***p<0.001 compared to control, † p<0.05, †† p<0.01, ††† p<0.001 compared to Rosi treatment. × p<0.05, ×× p<0.01, and ×××× p<0.0001 compared to LPS.

6.3.12 LPS Effect on the Expression of Mitochondrial Biogenesis Genes

Mitochondrial biogenesis genes DNA polymerase gamma (POLG), nuclear respiratory factor 1 (NRF1) and mitochondrial transcription factor A (TFAM) were analysed by qRT-PCR following the differentiation of mouse immortalized and primary adipocyte cultures as well as primary human adipocytes in the presence of rosiglitazone, LPS or a combination of the two.

Rosiglitazone, the browning stimulus, appeared to upregulate these genes, most evident in lean human cells. This is in agreement with documented improved insulin sensitivity with rosiglitazone, accompanied by dramatically increased mitochondrial biogenesis and remodelling, including shape and size in the white adipocytes of obese mice (134–136,675). However, none of these studies were conducted in human cells.

LPS treatment mainly reduced expression of POLG in both mouse models in the absence and present of rosiglitazone, suggesting that LPS negatively impacts POLG in the production of new mitochondria in adipocytes (Figure 6.3.12.1, A, B). There was no clear effect of LPS treatment on NRF1 and TFAM in mouse cells (Figure 6.3.12.1, A1, B1, A2, B2)..

In human cells, LPS treatment reduced expression of all genes both in the presence and absence of rosiglitazone, suggesting that LPS negatively impacts the production of new mitochondria in adipocytes (Figure 6.3.12.2). As seen in the above investigated genes, the effect of LPS was clearer in cells from lean subjects.

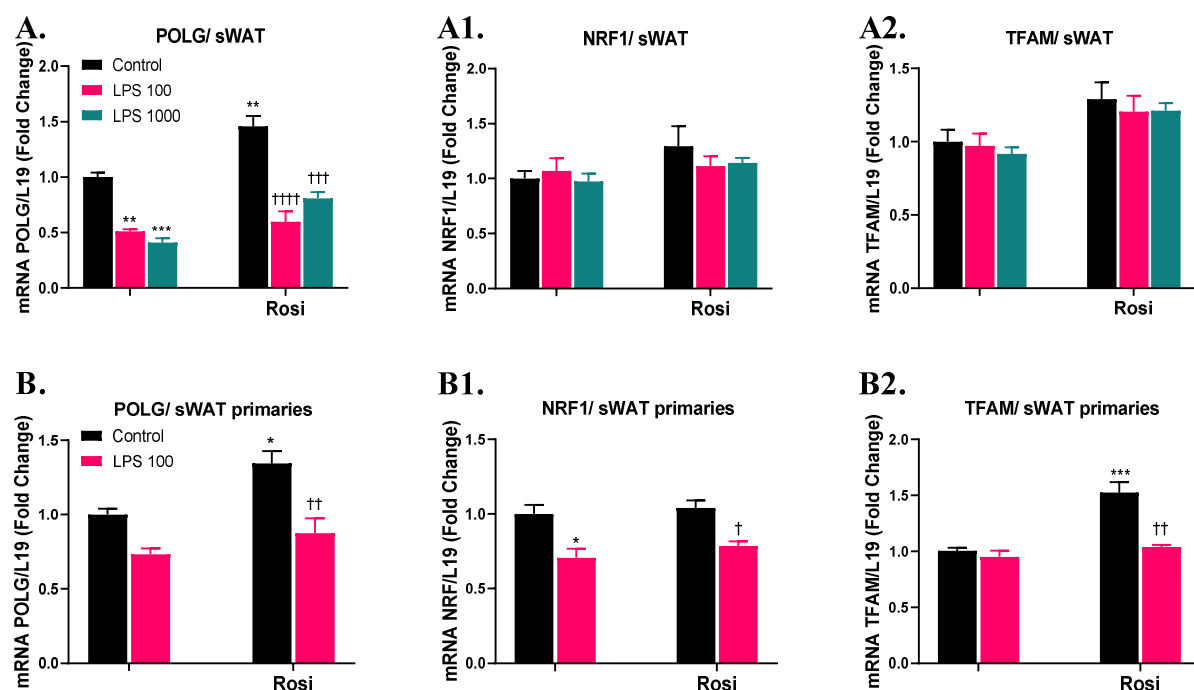


Figure 6.3.12.1 The Impact of LPS on the Expression of Mitochondrial Biogenesis Genes in Mouse Adipocytes.

Immortalized white sWAT (A/A1/A2/A3, n=3) and primary white adipocytes sWAT (B/B1/B2/B3, n=3) were grown and differentiated with/without 2 μ M rosiglitazone (Rosi) -for beiging effect-, 100 ng/mL or 1000 ng/mL lipopolysaccharide (Lps100), (Lps1000) or a combination of the two. Mitochondrial biogenesis genes DNA polymerase gamma (POLG), nuclear respiratory factor 1 (NRF1) and mitochondrial transcription factor A (TFAM) were measured using RT-PCR with L19 as a housekeeping control. Data represent mean \pm standard error of the mean. The two-way ANOVA test was used to test significance levels; * p <0.05, ** p <0.01, *** p <0.001 compared to control, † p <0.05, †† p <0.01, ††† p <0.001 compared to Rosi treatment.

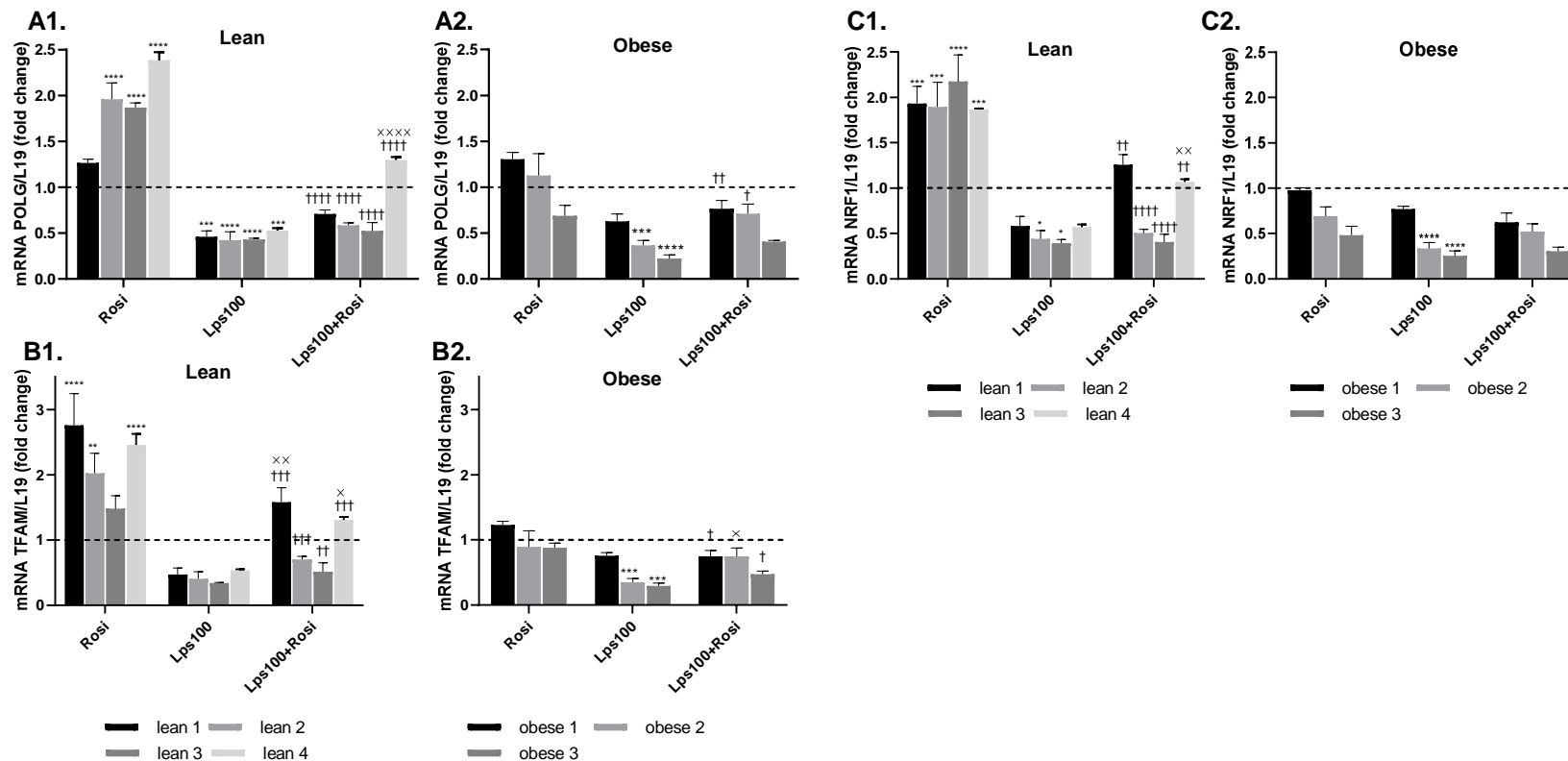


Figure 6.3.12.2 The Impact of LPS on the Expression of Mitochondrial Biogenesis Gene Expression.

Primary human adipocytes were differentiated with/without rosiglitazone (Rosi), 100 ng/mL lipopolysaccharide, or a combination of the two. Mitochondrial biogenesis genes DNA polymerase gamma (POLG), nuclear respiratory factor 1 (NRF1) and mitochondrial transcription factor A (TFAM) were measured using qRT-PCR with L19 as a housekeeping control. Data represent mean \pm standard error of the mean. The two-way ANOVA test was used to test significance levels; * p <0.05, ** p <0.01, *** p <0.001 compared to control, † p <0.05, †† p <0.01, ††† p <0.001 compared to Rosi treatment. \times p <0.05, $\times\times$ p <0.01 compared to LPS.

6.3.13 LPS Effect on Other Important Mitochondrial Genes

To understand the impact of LPS on mitochondrial efficiency, the genes involved in oxidative phosphorylation - cytochrome c oxidase subunit 4 (COX4), Citrate synthase (CS) and carnitine palmitoyltransferase 1b (CPT1 β), were investigated. In addition, genes involved in the clearance of reactive oxygen species: catalase (CAT) and superoxide dismutase 2 (SOD2), were analysed via qRT-PCR following treatment of mouse immortalized sWAT, mouse primary sWAT or lean and obese primary human adipocytes with rosiglitazone, LPS or a combination of the two.

First, significantly higher levels of CS, CPT1 β and COX4 expression were measured in beige adipocytes compared to white adipocytes. This can be attributed to the fact that beige adipocytes have more mitochondria than white adipocytes, hence higher gene expression required for basic mitochondrial functions. This increase can be seen in both Figure 6.3.13.1 and Figure 6.3.13.2 upon rosiglitazone-treatment in mouse cell lines, mouse primary adipocytes and human primary adipocytes originated from lean subjects. The increase was less clear in human primary adipocytes prepared from obese subjects, which supports a decreased browning capacity in these cells.

In addition, gene expression levels of CS, CPT1 β and COX4 were significantly blunted following LPS treatment in mouse beige (rosiglitazone -treated) adipocytes from two models; immortalised cell line and primary cells (Figure 6.3.13.1). Similarly, human beige (rosiglitazone-treated) adipocytes from lean and obese subjects showed a significant decline in expression of all these genes due to being differentiated with LPS (Figure 6.3.13.2). This data further supports that LPS negatively impacts the fundamental role of beige adipocytes in adaptive thermogenesis through acting to damage their mitochondrial function.

However, LPS effects on white adipocytes were less pronounced in all adipocytes from either humans or mice. For instance, in mouse cells, under LPS treatment both CS and COX4 transcription levels were decreased, albeit not significantly (Figure 6.3.13.1), and CPT1 β transcription levels were not affected (Figure 6.3.13.1). In human cells, LPS significantly reduced COX4 expression levels from both obese and lean subjects (Figure

6.3.13.2, B1, B2). The reduction in CS gene expression levels were not significant (Figure 6.3.13.2, A1, A2), and no change was observed for CPT1 β (Figure 6.3.13.2, C1, C2).

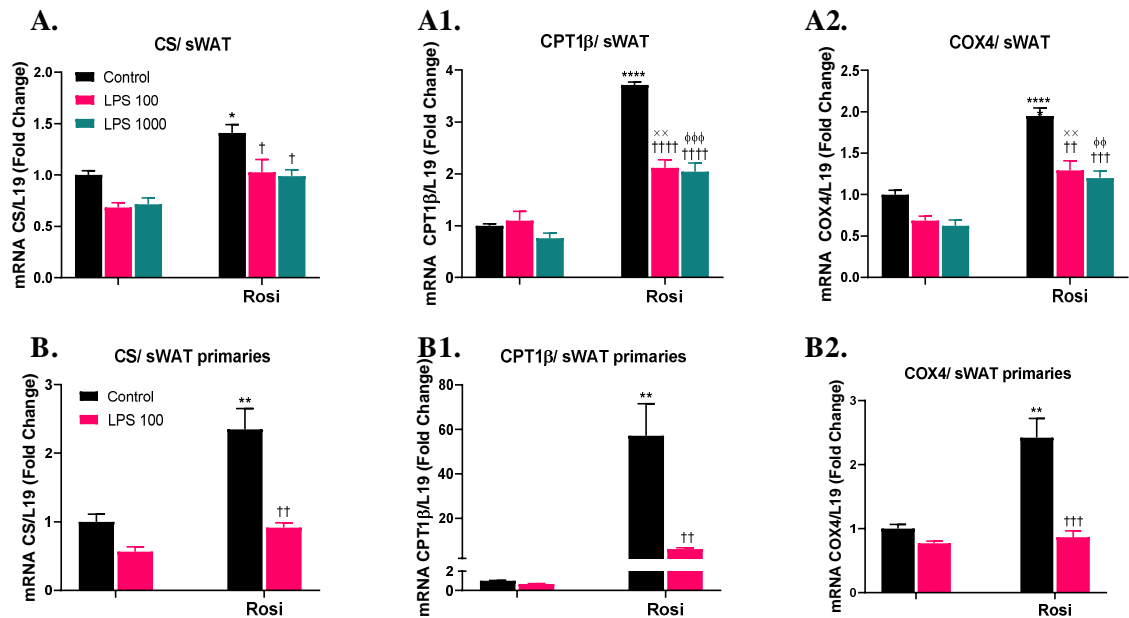


Figure 6.3.13.1 The Impact of LPS on Important Mitochondrial Genes in Mouse Cells.

Immortalized white sWAT (A/A1/A2, n=3) and primary white adipocytes sWAT (B/B1/B2, n=3) were grown and differentiated with/without 2 μ M rosiglitazone (Rosi) -for beiging effect-, 100 ng/mL or 1000 ng/mL lipopolysaccharide (Lps100), (Lps1000) or a combination of the two. Mitochondrial genes Citrate synthase (CS), cytochrome c oxidase subunit 4 (COX4) and carnitine palmitoyltransferase 1b (CPT1 β) were measured using qRT-PCR with L19 as a housekeeping control. Data represent mean \pm standard error of the mean. The two-way ANOVA test was used to test significance levels; * p <0.05, ** p <0.01, *** p <0.001 compared to control, \dagger p <0.05, $\dagger\dagger$ p <0.01, $\dagger\dagger\dagger$ p <0.001 compared to Rosi treatment. $\times\times$ p <0.01 compared to LPS100, $\phi\phi$ p <0.01, $\phi\phi\phi$ p <0.001 compared to LPS1000.

Reactive oxygen species (ROS) are natural by-products of cellular oxidative metabolism and play important roles in obesity stress. Mitochondria are widely recognized as a source of reactive oxygen species (ROS) and over-production of ROS leads to an overwhelmed antioxidant system and oxidative stress. Therefore, regulation of ROS levels via the integration of ROS production and consumption by mitochondrial antioxidant pathways is necessary to maintain mitochondrial and cellular health. Both SOD2 and CAT function as part of the reactive oxygen species clearance system. Hence, their gene expression levels in beige adipocytes were investigated.

Activity of the endogenous antioxidant CAT was significantly impaired with LPS treatment in beige adipocytes from mice in both tested mouse cell models, including the immortalized cell line and primary adipocytes (Figure 6.3.13.3), and from lean human adipose samples (Figure 6.3.13.4). The reduction in CAT expression with LPS treatment was less clear in obese cells (Figure 6.3.13.4, A2). In addition, beige adipocytes showed a significant augmentation in transcription of CAT compared to white adipocytes (Figure 6.3.13.4). White adipocytes also exhibited significantly lower levels of CAT for mouse (Figure 6.3.13.3, A1) and lean human cells (Figure 6.3.13.4, A1), but not obese cells (Figure 6.3.13.4, A2).

Conversely, endogenous antioxidant superoxide dismutase 2 (SOD2) showed a variable response. Beige adipocytes from the immortalized cell line showed a slight increase in response to LPS, significant for the higher dose (LPS1000) (Figure 6.3.13.3, A2). Beige adipocytes from mouse primary adipocytes were not affected by LPS. Human adipocytes from lean subjects treated with LPS exhibited a marked increase in SOD2 in terms of mRNA transcript levels in response to LPS, and obese cells showed similar but minimal response (Figure 6.3.13.4). Also, only beige adipocytes from mouse primary adipocytes increased levels of SOD2 compared to white cells, while there was either no observed effect or levels were reduced in beige cells for the other tested cell models. In white adipocytes, LPS led to a significant enhancement of SOD2 transcription in both mouse (Figure 6.3.13.3, A2, B2) and human cells (Figure 6.3.13.4, B1, B2).

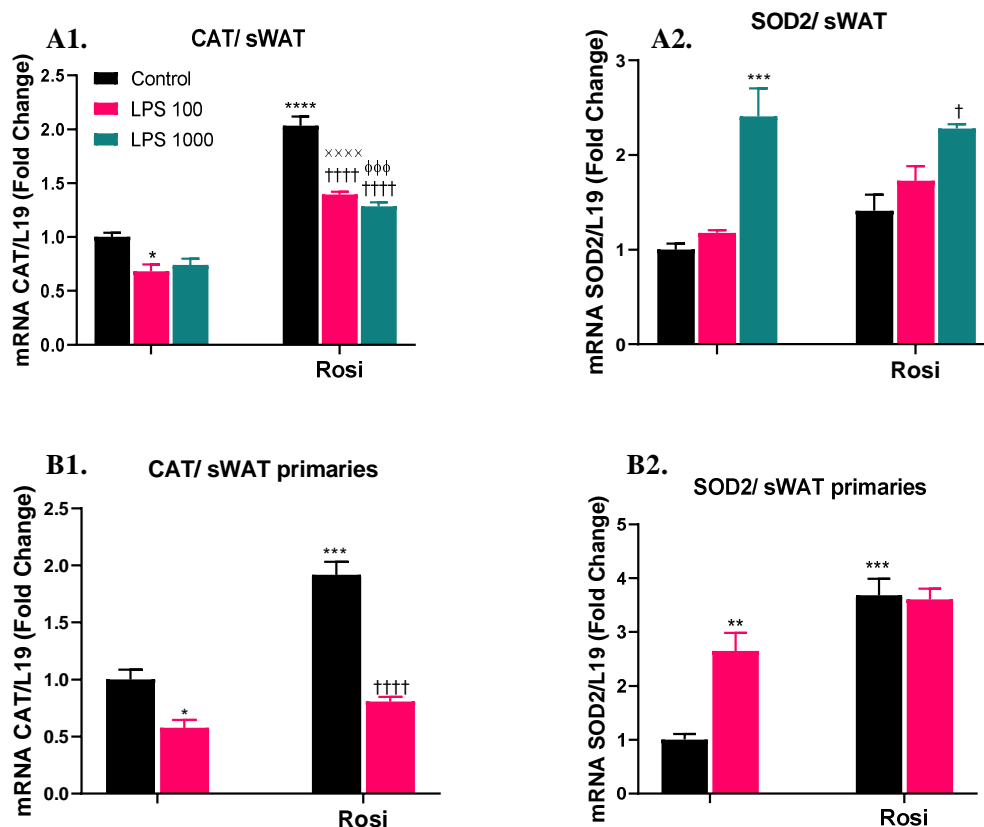


Figure 6.3.13.3 The Impact of LPS on Reactive Oxygen Species Clearance Genes in Mouse White Adipocytes.

Immortalized white sWAT (A/A1/A2, n=3) and primary white adipocytes sWAT (B/B1/B2, n=3) were grown and differentiated with/without 2 μ M rosiglitazone (Rosi) -for beiging effect-, 100 ng/mL or 1000 ng/mL lipopolysaccharide (Lps100), (Lps1000) or a combination of the two. Mitochondrial Reactive oxygen species clearance genes Catalase (CAT), and Superoxide dismutase 2 (SOD2) were measured using qRT-PCR with L19 as a housekeeping control. Data represent mean \pm standard error of the mean. The two-way ANOVA test was used to test significance levels; * p <0.05, ** p <0.01, *** p <0.001 compared to control, † p <0.05, †† p <0.01, ††† p <0.001 compared to Rosi treatment. ×××× p <0.0001 compared to LPS100, φφφ p <0.001 compared to LPS1000.

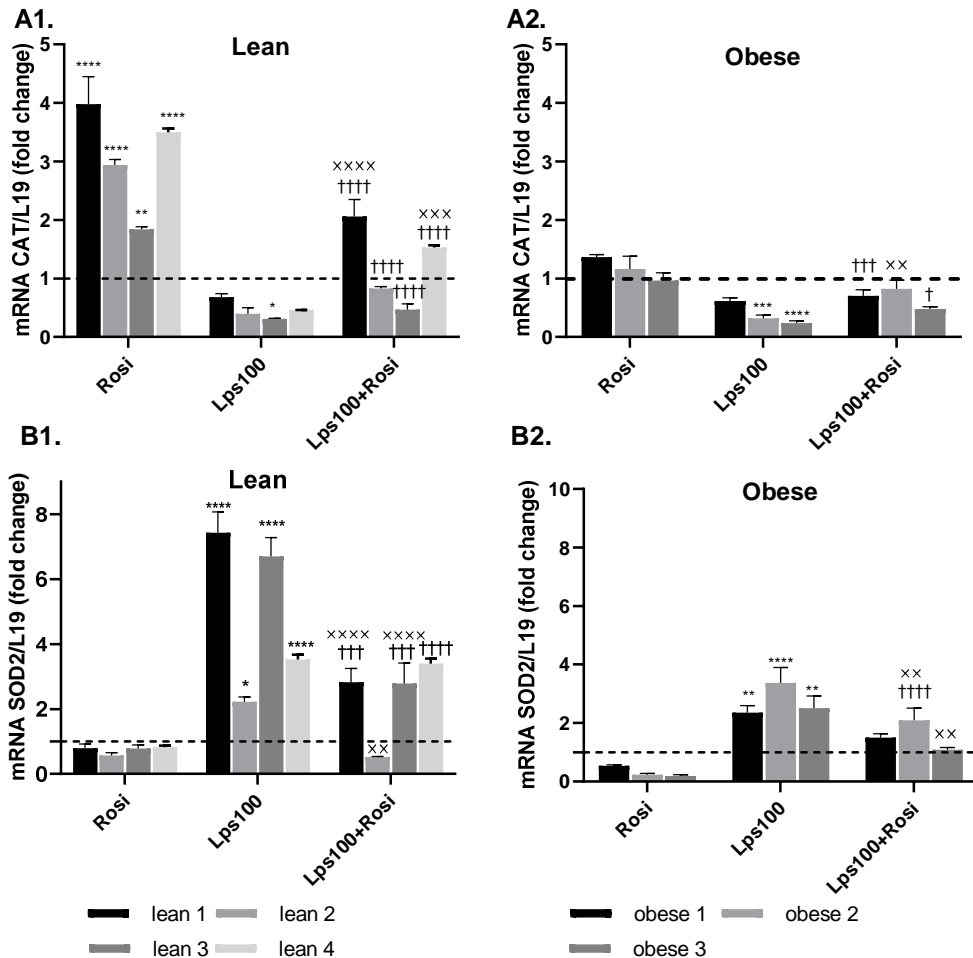


Figure 6.3.13.4 The Impact of LPS on Reactive Oxygen Species Clearance Genes in Human Cells.

Primary human adipocytes were differentiated with/without rosiglitazone (Rosi), 100 ng/mL lipopolysaccharide, or a combination of the two. Mitochondrial reactive oxygen species clearance genes Catalase (CAT), and Superoxide dismutase 2 (SOD2) were measured using qRT-PCR with L19 as a housekeeping control. Data represent mean \pm standard error of the mean. The two-way ANOVA test was used to test significance levels; * $p < 0.05$, ** $p < 0.01$, *** $p < 0.001$ compared to control, † $p < 0.05$, †† $p < 0.01$, ††† $p < 0.001$ compared to Rosi treatment. × $p < 0.05$, ×× $p < 0.01$ and ××× $p < 0.001$ compared to LPS.

6.3.14 Is Serum LPS Negatively Correlated with BAT and Mitochondrial Dynamic/Biogenesis Genes?

Following the findings that revealed the negative impact of LPS on the browning process and mitochondrial function *in vitro*, the next step was an attempt to investigate whether these effects were also represented *in vivo*. The measurement of serum LPS levels was planned for clinical samples as well as determining its relationship with BAT genes and mitochondrial dynamic and biogenesis genes. However, the Endolisa kit and DL-Develop General Lipopolysaccharides (LPS) ELISA Kit (DL-LPS-GE, DL-Develop, China) have failed to detect LPS levels in these samples. At the time of

writing this thesis, the work is still ongoing with Alice Murphy at NTU to measure these LPS levels and continue this study.

6.4 Discussion

This study aimed to investigate the impact of LPS on adipocyte browning both *in vitro* and *in vivo*. To explore this, RNA was extracted from immortalized sWAT and primary sWAT adipocyte cultures from mice. Also, RNA was extracted from human lean, overweight and obese adipose tissue and from cultured primary human adipocytes. Gene expression of inflammatory, BAT and mitochondrial genes was analysed to assess the impact of LPS on the browning process. The results from these investigations support that LPS directly impacts the browning process in adipocytes, as evidenced by: (1) LPS treatment significantly reduced beige -associated gene expression in primary adipocytes; (2) LPS treatment significantly reduced the signalling of beige cells; (3) LPS treatment significantly reduced the expression of genes associated with mitochondrial dynamics, biogenesis and oxidative phosphorylation in primary adipocytes.

The relationship between BMI and BAT gene expression in WAT was investigated in a human cohort, observing a strong negative correlation between the two. Also, a positive correlation was seen between BMI and inflammatory genes. This is in line with recognised impairment of BAT function in obese humans compared to lean, where BAT activity in response to cold and insulin are severely blunted in obesity (213,676). It has also been reported that overweight people have lower BAT activity, and the activity is (re)gained after weight loss (101,677). Furthermore, these correlations are consistent with earlier described findings in men, where BMI and percentage of body fat had significant negative correlations with BAT activity and UCP1 levels upon exposure to cold (52,206). Similarly, negative correlation was observed in the expression of CIDEA with increased BMI in obese subcutaneous tissues (664,678).

In addition, this current study demonstrated a strong negative correlation between the BAT and inflammatory genes in omental adipose tissue, with a less apparent negative correlation present in subcutaneous adipose tissue. In fact, higher expression of inflammatory markers was documented in the adipose tissue of obese patients compared with lean subjects, and this expression was reduced after weight loss (679–681). However, the relationship between inflammatory markers and BAT genes in humans has not been described in the literature prior to this current study. There is

evidence that inflammatory processes occurring in the adipose tissue environment can modify their beige plasticity, impair the capacity of browning in these depots and favour the local release of damaging signals (205,213,336,368,429,502). LPS is a known mediator of inflammation in white adipose tissue and as such could trigger the reduction in beige phenotype in the obese state, where systemic LPS levels are known to be high (446,682,683).

In order to study the browning process, cells were treated with rosiglitazone as browning agent. Rosiglitazone is a peroxisome proliferator-activated receptor (PPAR γ) activator and known browning agent. PPAR γ agonists increase UCP1 mRNA and protein levels in mouse white adipocytes with increased norepinephrine induced thermogenesis and mitochondrial function (134,135,198,675,684,685), increase UCP1 content and/or multilocularization in WAT *in vivo* (136,685,686), and increase UCP1 mRNA in human adipocytes (137,687,688). Thus, in this study rosiglitazone was used as a valid approach to induce the browning process. As expected, treatment with the browning agent rosiglitazone on both mouse and human adipocytes led to the induction of BAT genes in white cultures which is an indication of conversion of white to brown-like phenotype or beige adipocytes. Also, a novel finding was that key BAT gene expression in beige adipocytes (rosiglitazone-treated) was significantly reduced with LPS treatment including UCP1, CIDEA, PLIN5 and ELOVL3 in mouse and human cells. Furthermore, the impact of LPS on the responsiveness of beige cells to an adrenergic stimulus similar to cold exposure was determined. CL316243 or isoproterenol, which induce thermogenesis features, were used to test the effect of LPS on acquisition of the brown genotype in response to an adrenergic stimulus. Isoproterenol- or CL-treated beige cells showed reduced to no capacity to induce UCP1 transcription in response to adrenergic stimulus when differentiated with LPS treatment. This indicates that LPS reduces adipocyte browning as well as the ability of beige adipocytes to respond to an adrenergic stimulus by inducing non-shivering thermogenesis. This is in line with previous studies in mice (356,669), however this result is the first to demonstrate the ability of LPS to directly inhibit browning (stimulated by rosiglitazone) in both mouse and human adipocytes. This highlights the potent effects of LPS to suppress the induction of browning process which would be relevant to conditions of elevated LPS such as obesity. It provides evidence that counteracting LPS actions represents a therapeutic target to aid activation of WAT-

browning which will benefit weight loss. In addition, the effect of LPS on the browning capacity was more pronounced in adipocytes from lean subjects than obese. This has not been identified before, but is likely due to obese subjects expressing lower levels of each BAT gene which has been demonstrated both in our studies and in previous reports (50,310,684). This is important, as it suggests that obese subjects may be less susceptible to potential browning treatments that are currently being studied (689).

Our studies indicated that LPS significantly reduces the expression of genes associated with mitochondrial dynamics, biogenesis and oxidative phosphorylation in beige adipocytes from both mice and humans. Healthy mitochondria utilise oxidative phosphorylation as the more efficient form of energy production, relying on mitochondrial biogenesis and a balance of fission and fusion in order to do this (660,690). The reduction in expression of genes controlling mitochondrial dynamics, biogenesis and oxidative phosphorylation with LPS treatment in this study highlights a potential mechanism for the role of LPS in the development of T2DM in obese patients. During obesity, LPS is able to cross from the gut to the circulation due to increased permeability of the gut wall (691). This raises the possibility that once LPS reaches the adipose tissue, it not only reduces both the number and function of beige adipocytes, but also directly compromises mitochondrial health. Studies have shown that reduced mitochondrial health induces metabolic stress, causes an accumulation of ROS and promotes pro-inflammatory cytokine production (692). These processes are known to impair insulin signalling and, over time, induce insulin resistance leading to development of type 2 diabetes (693). As such, these results further support previous reports that suggested LPS could contribute to the development of insulin resistance type 2 diabetes in obese patients (446,694–699), albeit through a different mechanism where not only can LPS increase an inflammatory response it can also act as an inhibitor of cellular browning. In addition, similar to BAT gene expression, LPS had a more pronounced impact on adipocytes from lean subjects compared to obese. This may have arisen as systemic LPS levels are increased in obese subjects, and therefore these adipocytes may already have been exposed to the insult *in vivo*. As such, treatment with rosiglitazone had a reduced impact on BAT and mitochondrial genes in adipocytes from obese subjects, and further treatment with LPS resulted in less of a change in expression than was seen in cells from lean subjects.

In conclusion, the findings in this study indicate that LPS may play a key role in both the browning of adipocytes and the pathogenesis of type 2 diabetes. As such, targeting LPS may be a viable option to prevent the development of type 2 diabetes via increasing the number of beige adipocytes, improving the function of beige cells, and improving mitochondrial health and efficiency.

**Chapter 7. TUG-891 Reverses Lipopolysaccharide
Mediated Biological and Mitochondrial Alterations in
Brown Adipocytes**

7.1 Introduction

Strategies that target the inflammatory state may have the potential to reverse adipose tissue dysfunction and prevent progression of metabolic diseases. Suppression of inflammation using pharmacological agents, with reduction of pro-inflammatory cytokines and macrophage infiltration in WAT, improves AKT-phosphorylation in response to insulin along with improved body weight and fat mass (511–514). The evidence of beneficial effects from pharmacological agents on insulin response in BAT by reversing inflammation is less established. Additionally, there is also evidence that dietary intervention can cause anti-inflammatory activity, which leads to enhanced insulin sensitivity.

Fatty acids (FA) are an example of dietary constituents that act as inflammation modulators. Importantly, Omega-3 fatty acids (ω 3-FAs: n-3 polyunsaturated fatty acids (n-3PUFAs)) have anti-inflammatory effects and may significantly impact chronic inflammatory diseases including obesity related disorders (533). An ω 3-enriched diet, in non-obesogenic non-inflammatory conditions, leads to synthesis of oxylipins which have an anti-inflammatory response in both WAT and BAT with a macrophage modulation effect, but with no influence on inflammatory cytokine secretion (518). FFAs are active stimulators for members of the rhodopsin-like family of G protein-coupled receptors (GPCRs) including GPR40, GPR41, GPR43, GPR84, and GPR120 (519,520).

GPR120 is of special interest because it is highly expressed in both BAT and WAT as well as its documented anti-inflammatory properties. In fact, TUG-891, GPR120 agonism, has been reported in macrophages and white adipose tissue to exert potent anti-inflammatory effects with activated ERK phosphorylation. In addition, GW9508, a non-selective agonist of GPR120, significantly inhibits the ability of LPS to stimulate inflammatory responses in macrophages. Thus, GW9508 inhibited LPS-stimulated phosphorylation of IKK β and JNK, prevented I κ B degradation, and inhibited secretion of pro-inflammatory cytokines (TNF α and IL6) (528). However, the consequences of GPR120 activation in BAT on inflammatory signalling has not been fully understood. Moreover, Christian and co-workers have shown previously reported that GPR120 positively impacts metabolic health by stimulating mitochondrial respiration in brown fat via intracellular Ca²⁺ release which results in

mitochondrial depolarization and fragmentation(524). This occurs along with mitochondrial UCP1 activation, which may act synergistically with mitochondrial fragmentation to increase respiration. GPR120 activation by the agonist TUG-891 upregulates fat combustion in BAT thereby reducing fat mass, while GPR120 deficiency diminishes expression of genes involved in nutrient metabolism (524). Moreover, GPR120 deficiency leads to obesity, glucose intolerance, and hepatic steatosis in mice fed a high-fat diet (526). Importantly, GPR120 mediates the anti-inflammatory and insulin sensitizing effects of ω 3-FAs by inhibition of inflammatory pathways and cytokine secretion in adipocytes and macrophages (528,532). A role for GPR120 in BAT activation and WAT browning in response to cold via FGF21 secretion has also been confirmed (527).

Collectively, TUG-891 has effects on BAT mitochondrial function and overall metabolic health and represents a candidate to investigate its capacity to counteract LPS-induced dysfunction of mitochondria and brown adipocytes. Therefore, the objectives of this chapter were to:

1. Provide evidence to target GPR120 in human brown/ beige adipocytes.
2. Determine the effects of TUG-891 on brown adipocyte biology.
3. Assess whether there are protective effects of TUG-891 against LPS actions on both brown adipocyte alterations and mitochondrial dysfunction.
4. Identify possible pathways through which TUG-891 acts to provide cellular protection in brown adipocytes.

7.2 Methods

Brown pre-adipocyte (imBAT/Primaries/Spheroids) were differentiated into mature adipocytes over 8-10 days with or without LPS 100 ng/ml or 1000 ng/ml (100 ng/ml if not otherwise indicated), with or without TUG-891 (10 μ M) according to the differentiation protocol detailed in the general methods section (Chapter 2). RNA and protein were harvested for qRT-PCR and Western Blotting to look at changes in levels of key markers of brown fat, inflammatory and mitochondria. Cells were analysed for glucose uptake to study insulin response in the presence and absent of LPS, TUG-891 and their combinations. Brown adipocyte were also studied with a Seahorse XF Analyser to determine the impact of LPS, TUG-891 and their combinations on mitochondrial function. Live cell imaging using a spinning disk confocal microscope was conducted to assess how mitochondrial membrane potential is affected by using MitoTracker Green FM (MTG) and MitoTracker Red CMXRos (MTR). Conditioned media was collected for Proteome Profiler Array assay and ELISA assays. Proteome Profiler Array assay was used to investigate how TUG-891 could alter the response to LPS in terms of cytokines secretion. ELISA assays were used to confirm secretion of selected highly secreted cytokines including BAFF, CXCL16, CXCL5 and MMP3.

7.3 Results

7.3.1 GPR120 Is Expressed in Human Brown/Beige Adipocytes

GPR120 is recognized as a brown-fat-associated gene in mice. In humans, it is however not so clear if it is expressed and has the same role as a brown-fat-associated gene. Therefore, it was of interest to investigate whether there is correlation with other human brown fat genes to elucidate this. In addition, GPR120 correlations with inflammatory genes were explored to identify the relationship between transcription of GPR120 and inflammatory markers as this has not been done before in humans.

Positive correlations were observed between GPR120 and three of the four investigated brown fat genes in subcutaneous WAT (Table 7.3.1.1). This included positive correlation with PLIN5 ($P<0.01$), ELOVL3 ($P<0.0001$) and SLC27A2 ($P<0.01$). However, in omental WAT, only ELOVL3 positively correlated with GPR120 gene expression ($P<0.05$). This could be due to omental tissue being less susceptible to browning compared to scWAT and therefore displaying a reduced correlation with the brown phenotype (700).

		CIDEA		PLIN5		ELOVL3		SLC27A2	
		Pearson's r	P value	Pearson's r	P value	Pearson's r	P value	Pearson's r	P value
GPR120	Sc	0.13	0.15	0.29**	1.00 E-03	0.55****	2.893 5E-11	-0.26**	3.70 E-03
	Om	0.12	0.19	0.10	0.25	0.22*	0.02	-0.10	0.30

Table 7.3.1.1 GPR120 Gene Expression Correlation with Brown Fat Genes.

The correlation of brown adipose tissue (BAT) genes (CIDEA, ELOVL3, PLIN5 and SLC27A2) with GPR120 was assessed using the Pearson correlation test. If non-parametric, variables were log-transformed prior to correlation analysis to improve normality. Significant correlations are highlighted, * $p<0.05$, ** $p<0.01$ and **** $p<0.0001$. CIDEA: cell death-inducing DFFA-like effector A, ELOVL3: fatty acid elongase 3, PLIN5: perilipin 5, GPR120: G protein-coupled receptor 120.

Interestingly, negative correlations were observed between GPR120 and inflammatory genes IL6 ($P<0.05$) and MCP1 ($P<0.05$) in subcutaneous WAT (Table 7.3.1.2). This is in agreement with previous findings highlighting that GPR120 is down-regulated in obesity (an inflammatory state) and after a fatty meal (701). It also supports GPR120 as a brown fat marker as it positively correlates with brown fat genes and it negatively correlates with inflammatory genes.

		IL6		MCP1		TNF α		IL1 β	
		Pearson's r	P value	Pearson's r	P value	Pearson's r	P value	Pearson's r	P value
GPR120	Sc	-0.20*	0.03	-0.20*	0.03	0.16	0.07	-0.10	0.28
	Om	-0.06	0.48	-0.20*	0.03	0.07	0.46	0.17	0.07

Table 7.3.1.2 GPR120 Gene Expression Correlation with Inflammatory Genes.

The correlation of genes (IL6, MCP1, TNF α , IL1 β) with GPR120 was assessed using the Pearson correlation test. If non-parametric, variables were log-transformed prior to correlation analysis to improve normality. Significant correlations are highlighted, * $p < 0.05$, ** $p < 0.01$ and *** $p < 0.0001$. IL6: interleukin 6, TNF α : tumour necrosis factor alpha, MCP1: monocyte chemotactic protein-1, IL1 β interleukin 1 beta, GPR120: G protein-coupled receptor 120.

In order to determine how an inflammatory state impacts GPR120 expression, both human and mouse primary adipocytes were treated with LPS. This caused a significant reduction in GPR120 expression ($P < 0.01$), with beige adipocytes being more affected than white (Figure 7.3.1.1), and lean more affected than obese (Figure 7.3.1.2). As a result, LPS appeared to play a direct role in reducing GPR120 gene expression. This further supports GPR120 as a brown marker and at least at the transcriptional level, it is under browning program control.

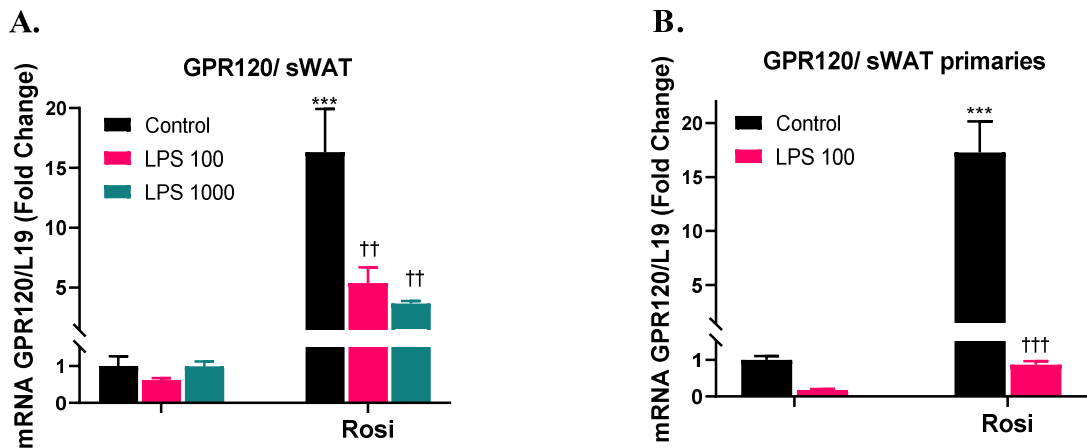


Figure 7.3.1.1 Impact of LPS on GPR120 Gene Expression in Beige Mouse Adipocytes.

Immortalized white sWAT (A2, n=3) and primary white adipocytes sWAT (B, n=3) were grown and differentiated with/without 2 μ M rosiglitazone (Rosi) -for beiging effect-, 100 ng/ml or 1000 ng/ml lipopolysaccharide (Lps100 or Lps1000), or a combination of the two. GPR120 was analysed using q-RT-PCR with L19 as a housekeeping control. *** $p < 0.001$ compared to control, †† $p < 0.01$ and ††† $p < 0.001$ compared to Rosi treatment.

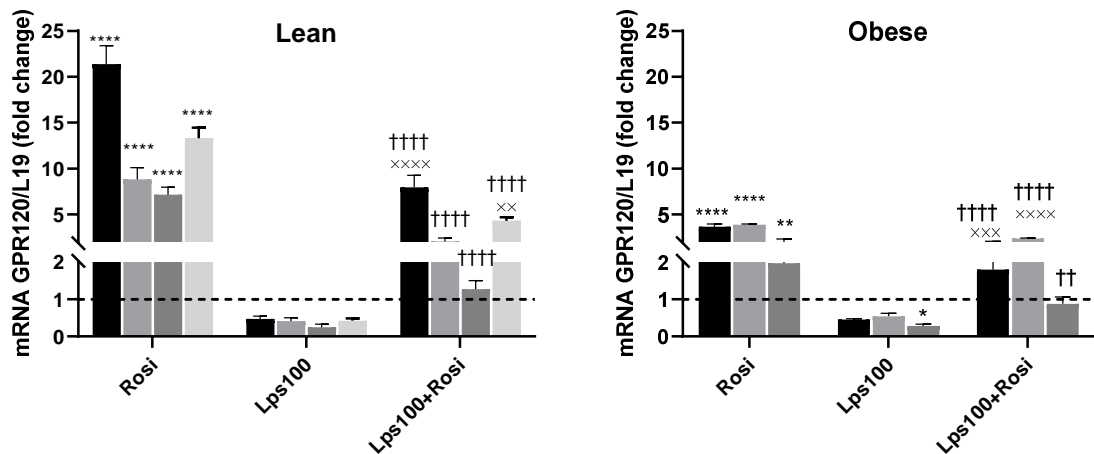


Figure 7.3.1.2 Impact of LPS on GPR120 Gene Expression of Human Primary Adipocytes.

Lean (left paned) and obese (right paned) primary human adipocytes were differentiated with/without 2 μ M rosiglitazone (Rosi), 100 ng/ml lipopolysaccharide (LPS100) or a combination of the two. GPR120 was analysed using qRT-PCR with L19 as a housekeeping control. Data represent mean \pm standard error of the mean. The two-way ANOVA test was used to test significance levels; * p <0.05, ** p <0.01, **** p <0.0001 compared to control, †† p <0.01 and †††† p <0.0001 compared to Rosi treatment. ×× p <0.01, ××× p <0.001 and ×××× p <0.0001 compared to LPS treatment.

7.3.2 Brown Adipocyte Differentiation in the Presence of TUG-891 and/or LPS

Before studying the effect of TUG-891 on brown adipocyte biology, the impact of chronic presence of TUG-891 and/or LPS on differentiation of brown adipocytes of different models including 2D, 3D was explored. Using spheroids as a 3D model provides valuable information about brown adipocyte responses in a closer environment to their physiological state.

Prior to the application of induction media, imBAT cells and primary brown adipocytes showed a flat and more compact shape (Figure 7.3.2.2; A1, B1) while spheroids when sectioned and stained with H&E staining showed no lipid droplets (Figure 7.3.2.2; C1), suggesting all cells were not differentiated. Around day 4 lipid droplets started to develop and become larger and more numerous with the progression of differentiation. On day 8, all the cells were considered fully differentiated, including cells differentiated in the presence of TUG-891, LPS or combination of the two. This was judged based on both morphology and induction of aP2. This suggests that the treatments do not impact differentiation.

Photographs were taken of imBAT adipocytes (Figure 7.3.2.2; A2, A3,A4, A5) to show lipid accumulation using Oil Red-O staining demonstrating successful

differentiation of cells under the different treatments used. Similarly, further digital images (Figure 7.3.2.2; B2, B3,B4, B5) also show differentiated primary brown adipocytes with each treatment. Due to the limited number of cells obtained for primary BAT culture, it was not possible to plate additional wells to perform Oil Red-O staining as a comparator for all treatment regimens each day. Despite this, the images clearly show fully differentiated brown adipocytes under the different treatments. Finally, the spheroid cell model also shows differentiated brown adipocytes full of lipid droplets with H&E staining (Figure 7.3.2.2; C2, C3,C4, C5). Similarly, the induction of the adipocyte marker aP2 confirmed that imBAT, primaries and spheroids efficiently differentiate in the presence of each treatment (Figure 7.3.2.1).

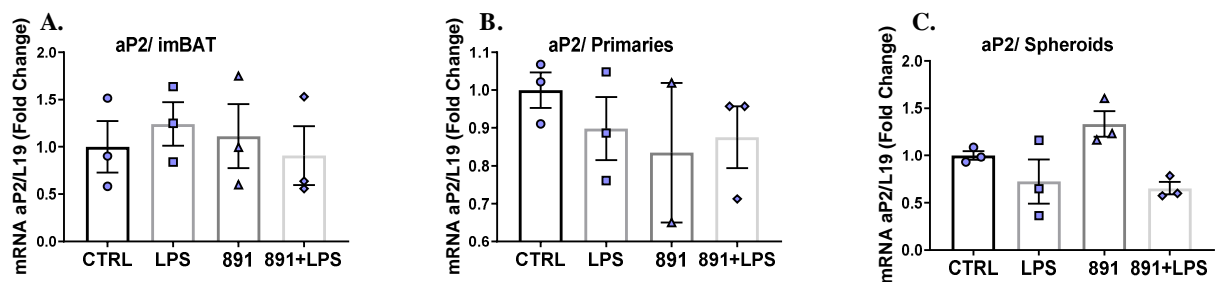


Figure 7.3.2.1 aP2 Expression in Brown Adipocytes.

ImBAT, primaries, spheroids were differentiated with/without LPS (100 ng/ml), 891 (10 μ M) or combination of 891 and LPS. aP2 gene expression levels in imBAT (A), primaries (B) and spheroids (C). Results are expressed as a fold change from control cells. Bars represent means \pm standard error of the mean. Two-way ANOVA was used for comparisons. CTRL; control. aP2: fatty acid binding protein 4, 891:TUG-891.

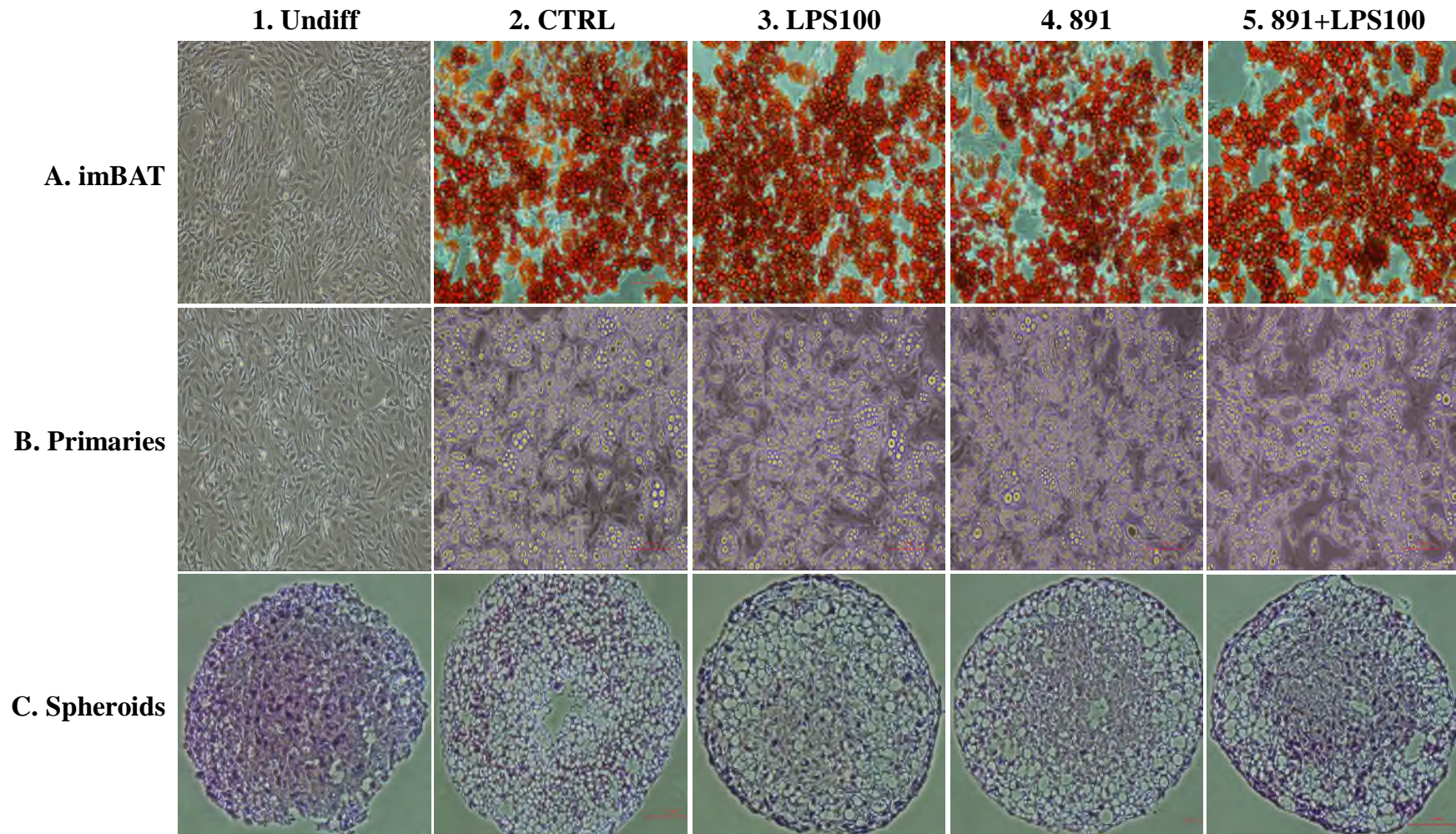


Figure 7.3.2.2 Morphology of Brown Adipocytes Differentiated in the Absence and Presence of TUG-891 and/or LPS.

Pictures of undifferentiated imBAT (A1), primaries (B1), spheroids (C1). Control (A2, B2, C3), LPS treated (100 ng/ml) (A3, B3, C3), TUG-891 treated (A4, B4, C4), TUG-891+LPS (100 ng/ml) (A5, B5, C5) differentiated brown adipocytes of imBAT, primaries, spheroids for each treatment. 20x magnification. imBAT were stained with Oil Red O. Spheroids were stained with H&E. CTRL: Control, 891: TUG-891.

7.3.3 TUG-891 Administration to Brown Adipocytes Reduces LPS-Induced Insulin Resistance

To test the hypothesis that TUG-891 has a positive role on brown adipocyte biology and could reverse brown adipocyte insulin resistance, induced via LPS, the first step was to establish whether *in vitro* TUG-891 administration could directly reverse insulin resistance in imBAT cells. As shown in Figure 7.3.3.1, both doses of LPS (100 ng/mL and 1000 ng/mL) induced insulin resistance in imBAT cells evidenced by significant reductions in uptake of radio-labelled glucose following an acute dose of insulin (100 nM) compared with control adipocytes (FC=-2.94, $P<0.0001$, FC=-3.01, $P<0.0001$). Conversely, culturing cells with TUG-891 enhanced insulin sensitivity as labelled glucose uptake rate was doubled compared to control adipocytes (FC=1.85, $P<0.0001$). In addition, cells treated with a combination of LPS and TUG-891 led to partial reversal of LPS-induced insulin resistance at both doses of LPS. Notably, the capability of TUG-891 to restore insulin sensitivity was higher with the lower LPS dose (100 ng/mL: FC=2.28, $P<0.001$) compared to higher dose (1000 ng/mL) (Figure 7.3.3.1, D)

This functional observation of LPS-induced insulin resistance was accompanied by reduced phosphorylation of the Serine/Threonine Kinase AKT in response to insulin treatment, a key step in the insulin signalling cascade (FC=-2.63, $P<0.01$, Figure 7.3.3.1; E1, E2). Treating imBAT cells with a combination of TUG-891 and LPS resulted in increased phosphorylation of AKT after an acute dose of insulin (100 nM) compared to LPS-treated cells alone (FC= 2.17, $P<0.05$). The higher dose of LPS (1000 ng/mL) resulted in undetectable p-AKT, which was restored to detectable levels by treatment in the presence of TUG-891.

Gene expression of solute carrier family 2 (facilitated glucose transporter), member 4 (GLUT4) was investigated as this is the insulin-regulated glucose transporter. Differentiating different models of brown adipocytes (imBAT, primaries, spheroids) with LPS (100 ng/mL) reduced GLUT4 gene expression levels by maximum of 97 % ($P<0.0001$). TUG-891 partially restored decreased GLUT4 by LPS treatment in all three tested cells models (2.25-fold increase in imBAT ($P<0.05$), 2-fold increase in

primaries and 10-fold increase in spheroids ($P<0.05$)) (Figure 7.3.3.1, A1, B1, C1). Solute carrier family 2 (facilitated glucose transporter), member 1 (GLUT1) catalyses the transport of glucose across the plasma membrane under basal conditions. Unlike the consistent changes observed for GLUT4, GLUT1 expression varied across the different cell models. LPS alone decreased GLUT1 gene expression in imBAT cells, whereas it increased GLUT1 gene expression in both spheroids and primaries. Also, TUG-891 alone did not alter GLUT1 gene expression in imBAT but increased GLUT1 in both spheroids and primaries. Although there is a lack of a consistent response of GLUT1 to LPS and TUG-891 treated separately, a combination of LPS and TUG-891 significantly increased GLUT1 gene expression levels compared to LPS treatment alone in all tested cell models (1.75-fold increase in imBAT ($P<0.05$), 2.6-fold increase in primaries ($P<0.05$) and 3-fold increase in spheroids ($P<0.05$)).(Figure 7.3.3.1 A2, B2, C2).

Thus, differentiating brown adipocytes with TUG-891 alleviated impaired insulin signalling and adipocyte glucose uptake induced by LPS, with stronger effects in reversing the lower LPS lower dose.

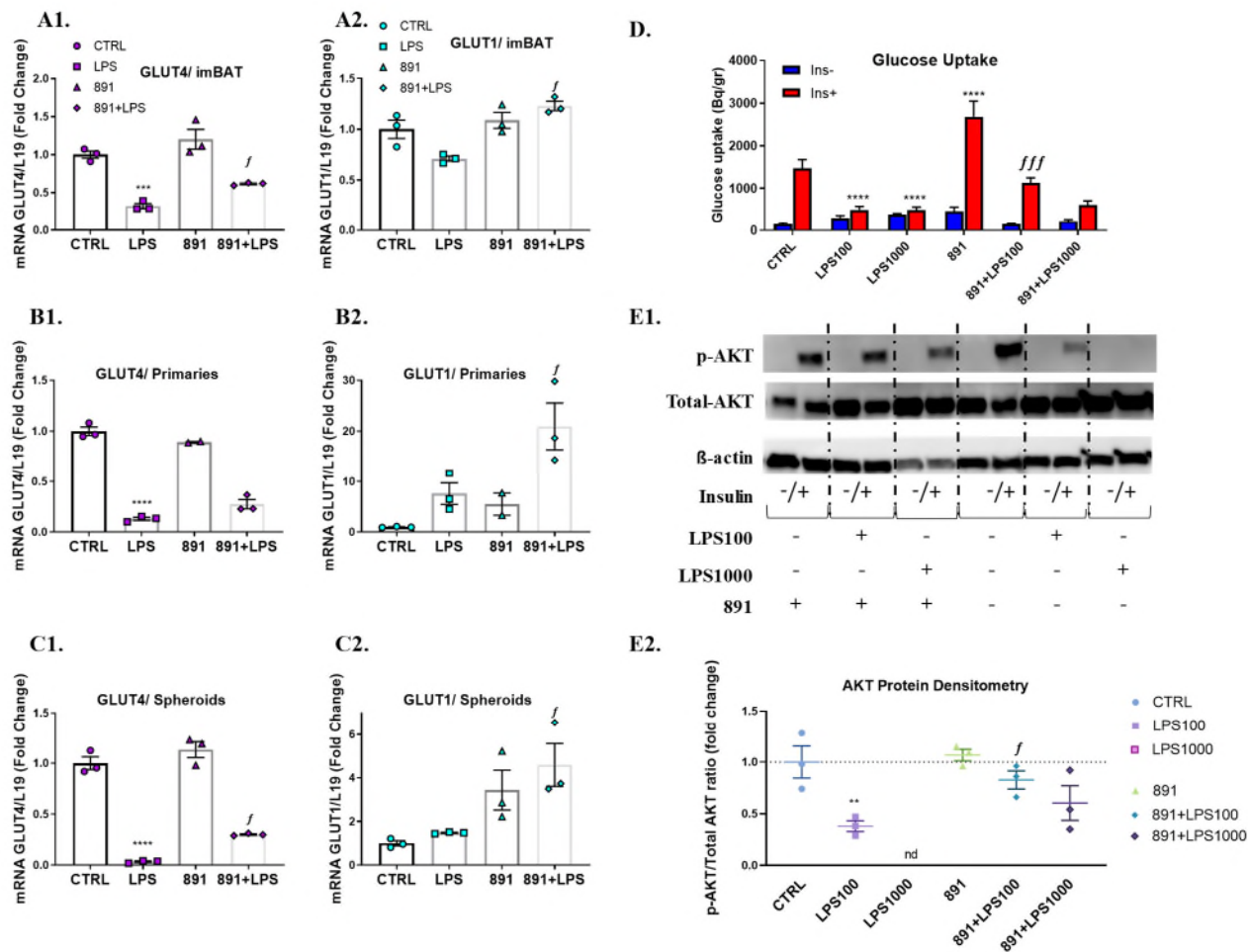


Figure 7.3.3.1 Effect of TUG-891 (891) on Brown Adipocyte Insulin Sensitivity.

ImBAT, primaries and spheroids were differentiated with/without LPS (100 ng/ml, 1000 ng/ml), 891 or combination of 891 and LPS. (A1, B1, C1) GLUT4 gene expression levels in imBAT, primaries, spheroids respectively. (A2, B2, C2) GLUT1 gene expression levels in imBAT, primaries, spheroids respectively. (D) Glucose uptake of 2-DG and (E1, E2) AKT protein expression and densitometry in imBAT following acute dose of insulin (100 nM). (E1) Image of AKT and loading control β -actin Western blot membranes. For protein densitometry and gene expression, results are expressed as fold change relative to control cells. For glucose uptake normalised counts per minute to total protein content are shown. Bars represent means \pm standard error of the mean. * $p < 0.05$, ** $p < 0.01$, *** $p < 0.001$, **** $p < 0.0001$ compared to CTRL. *f* $p < 0.05$, *ff* $p < 0.01$, *fff* $p < 0.001$ compared to LPS. Two-way ANOVA was used for comparisons. GLUT4; solute carrier family 2 (facilitated glucose transporter), member 4, GLUT1; solute carrier family 2 (facilitated glucose transporter), member 1. AKT; Serine/Threonine Kinase. CTRL; control. 2-DG; 2-Deoxyglucose. 891: TUG-891

7.3.4 TUG-891 Administration to Brown Adipocytes Reduces LPS-Induced Inflammation

It has been demonstrated that GPR120 agonists have anti-inflammatory effects (528,533). In order to investigate the consequences of GPR120 activation on inflammatory signalling in BAT, inflammatory markers were studied following

GPR120 and LPS treatment in this study. As expected, differentiating brown adipocytes in the presence of LPS induced the expression of inflammatory markers including IL6 and MCP1 in imBAT (IL6: FC=67.24 , P<0.0001, Figure 7.3.4.1, A1) (MCP1: FC=4.36, P<0.0001, Figure 7.3.4.1, A2), primary brown adipocytes (IL6: FC=10.9, P<0.0001, Figure 7.3.4.1, B1) (MCP1: FC=86.44, P<0.0001, Figure 7.3.4.1, B2) and brown adipocyte spheroids (IL6: FC=214.15, P<0.0001, Figure 7.3.4.1, C1) (MCP1: FC=59.8, P<0.0001, Figure 7.3.4.1, C2). This was accompanied by the phosphorylation of NFκB in primaries (Figure 7.3.4.1, B3, B4) and c-Jun in imBAT cells (FC=1.62, P<0.0001, Figure 7.3.4.1, A3, A4) upon LPS treatment for only 30 minutes. Unfortunately, phosphorylated NFκB was not detectable in imBAT, while phosphorylated c-Jun was not detectable in primaries.

Co-administration of TUG-891 with LPS significantly reduced LPS-induction of inflammatory gene expression of both IL6 and MCP1 in imBAT (IL6: FC=-1.81, P<0.0001, Figure 7.3.4.1, A1) (MCP1: FC=-1.47, P<0.01, Figure 7.3.4.1, A2), primaries (IL6: FC=-1.42, P<0.05, Figure 7.3.4.1, B1) (MCP1: FC=-1.41, P<0.05, Figure 7.3.4.1, B2) and spheroids (IL6: FC=-2.73, P<0.0001, Figure 7.3.4.1, C1) (MCP1: FC=-3.46, P<0.0001, Figure 7.3.4.1, C2). In line with this, TUG-891 reduced the phosphorylation of NFκB in primaries (Figure 7.3.4.1, B3, B4) and c-Jun in imBAT upon LPS treatment (FC=-1.26, P<0.05, Figure 7.3.4.1, A3, A4).

Ultimately, these results suggest that TUG-891 activation of GPR120 has anti-inflammatory effects that oppose LPS actions at JNK/IKKβ level in all tested brown adipocytes models.

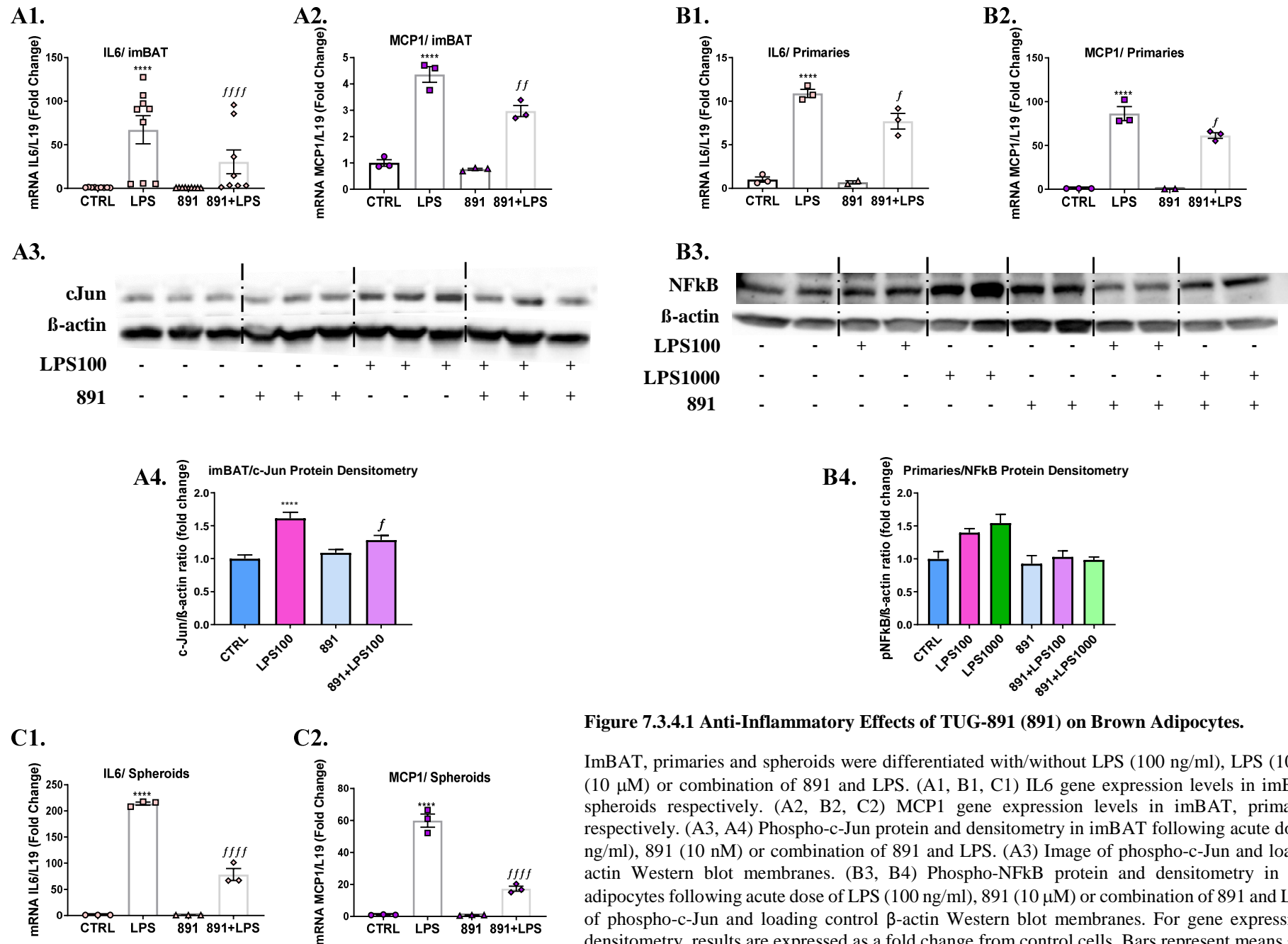


Figure 7.3.4.1 Anti-Inflammatory Effects of TUG-891 (891) on Brown Adipocytes.

ImBAT, primaries and spheroids were differentiated with/without LPS (100 ng/ml), LPS (1000 ng/ml), 891 (10 μ M) or combination of 891 and LPS. (A1, B1, C1) IL6 gene expression levels in imBAT, primaries, spheroids respectively. (A2, B2, C2) MCP1 gene expression levels in imBAT, primaries, spheroids respectively. (A3, A4) Phospho-c-Jun protein and densitometry in imBAT following acute dose of LPS (100 ng/ml), 891 (10 nM) or combination of 891 and LPS. (A3) Image of phospho-c-Jun and loading control β -actin Western blot membranes. (B3, B4) Phospho-NF κ B protein and densitometry in primary brown adipocytes following acute dose of LPS (100 ng/ml), 891 (10 μ M) or combination of 891 and LPS. (B3) Image of phospho-c-Jun and loading control β -actin Western blot membranes. For gene expression and protein densitometry, results are expressed as a fold change from control cells. Bars represent means \pm standard error of the mean. * p <0.05, ** p <0.01, *** p <0.001, **** p <0.0001 compared to CTRL. f p <0.05, ff p <0.01, fff p <0.001 compared to LPS. Two-way ANOVA was used for comparisons. CTRL; control. NF κ B; nuclear factor κ B or RelA (p65), c-Jun; transcription factor activator protein-1 Ser73.

7.3.5 TUG-891 Administration to Brown Adipocytes Enhances UCP1 Expression

After observing the positive effects of TUG-891 on opposing LPS actions including insulin resistance and inflammation, the next step was to investigate any potential effect on features of thermogenesis, the main characteristic of brown adipocytes. Therefore, modifications of UCP1 gene expression and protein levels when differentiating cells were treated with TUG-891 were explored. Strikingly, TUG-891 significantly promoted UCP1 gene expression in imBAT (FC=1.76, $P<0.05$, Figure 7.3.5.1; A), primaries (FC=6.67, $P<0.05$, Figure 7.3.5.1; B).and spheroids (FC=1.81, $P<0.001$, Figure 7.3.5.1; C). This is also in line with an increase in UCP1 protein levels in imBAT cells when differentiated with TUG-891 (FC=1.51, $P<0.05$, Figure 7.3.5.1; D, E). Also, immunohistochemical staining of UCP1 in spheroids was increased with TUG-891 treatment (Figure 7.3.5.1; B2 vs B4). Thus, TUG-891 appears to enhance the expression of UCP1, the main thermogenesis protein, in brown adipocytes.

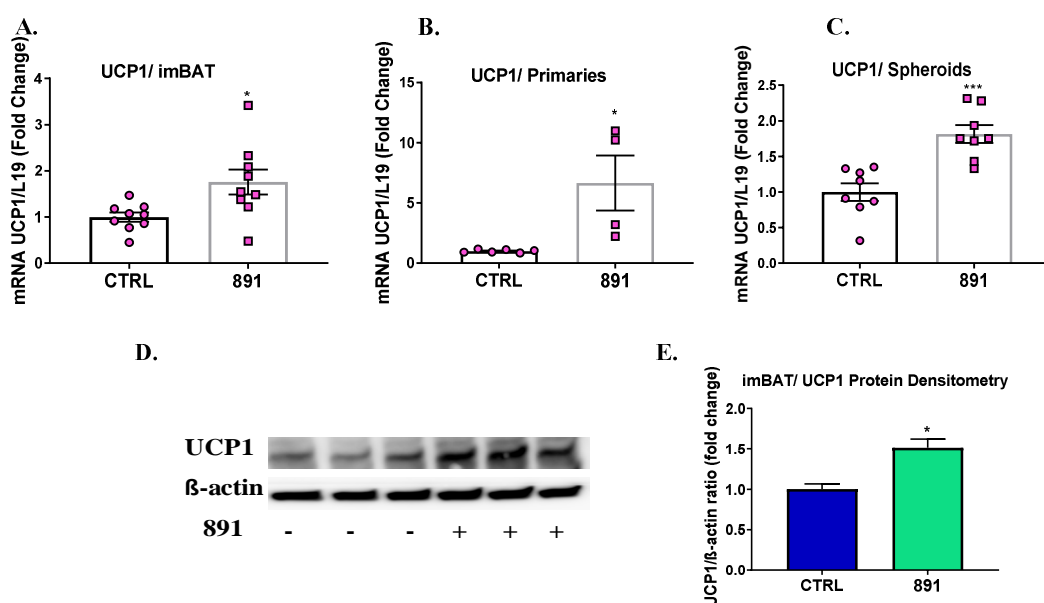


Figure 7.3.5.1 Effects of TUG-891 (891) on UCP1 in Brown Adipocytes.

ImBAT, primaries and spheroids were differentiated with/without 891 (10 μ M). (A, B, C) UCP1 gene expression levels in imBAT, primaries, spheroids respectively. (D, E) UCP1 protein expression and densitometry in imBAT. (D) Image of UCP1 and loading control β -actin Western blot membranes. For gene expression and protein densitometry, results are expressed as a fold change from control cells. Bars represent means \pm standard error of the mean. * $p<0.05$, ** $p<0.01$, *** $p<0.001$ compared to CTRL. Unpaired T-Test was used for comparisons. CTRL; control. UCP1; uncoupling protein 1. 891:TUG-891.

This new positive effect of TUG-891 on UCP1 induction in brown adipocytes was further investigated to demonstrate whether it has any influence on reversing UCP1-reduction upon LPS treatment in these brown adipocytes *in vitro*. Hence, imBAT, primaries and spheroids were differentiated with/without LPS (100 ng/ml), TUG-891 (10 μ M) or combinations of TUG-891 and LPS. Interestingly, TUG-891 partially reversed LPS-dependent reduction of UCP1 gene expression levels as it led to notable increase when used in combination with LPS. This was the case for all tested models of adipocytes including imBAT (FC=4.75, $P<0.05$, Figure 7.3.5.2; A) primaries (FC=15, $P<0.05$, Figure 7.3.5.2; B) and spheroids (FC=3.4, $P<0.0001$, Figure 7.3.5.2; C), (Figure 7.3.5.3; B3 vs B5).

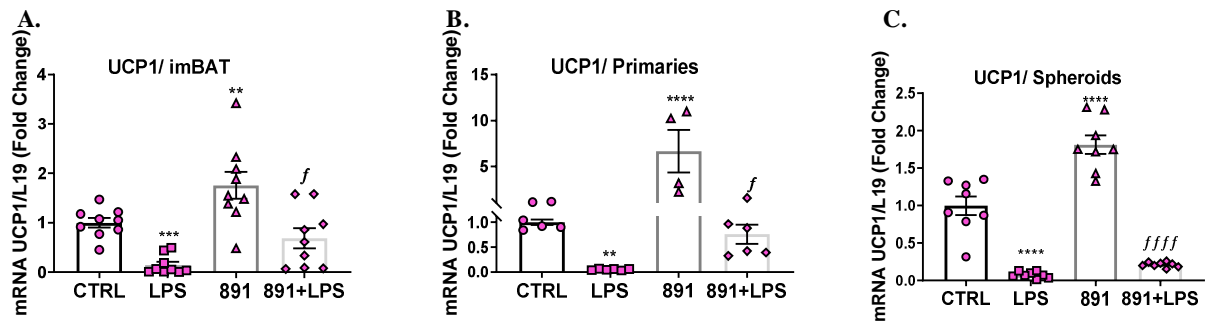


Figure 7.3.5.2 Effects of TUG-891 (891) on UCP1 Gene Expression in LPS-Treated Brown Adipocytes.

ImBAT, primaries, spheroids were differentiated with/without LPS (100 ng/ml), 891 (10 μ M) or combination of 891 and LPS. (A, B, C) UCP1 gene expression levels in imBAT, primaries and spheroids respectively. Results are expressed as a fold change from control cells. Bars represent means \pm standard error of the mean. * $p<0.05$, ** $p<0.01$, *** $p<0.001$ **** $p<0.0001$ compared to CTRL. f $p<0.05$, ff $p<0.01$, fff $p<0.001$, ffff $p<0.0001$ compared to LPS. Two-way ANOVA was used for comparisons. CTRL; control. UCP1; uncoupling protein 1. 891:TUG-891

UCP1 immunostaining of spheroids, in Figure 7.3.5.3, revealed that in the differentiating spheroid model, TUG-891 protected the cells from reduced UCP1 levels occurring upon LPS treatment. The brown colour is the UCP1 stain and the darker the colour, the more UCP1 inside the cells. Co-treatment of TUG-891 with LPS treatment resulted in cells with increased UCP1 compared to LPS treated cells (Figure 7.3.5.4). The upper panel of (Figure 7.3.5.3; A1, A2, A3, A4, A5) shows that there was no staining in the absence of anti-UCP1 antibody indicating that the staining is specific for the anti-UCP1 antibody. Overall, TUG-891 not only increases UCP1 expression in brown adipocytes, but also reduces the deleterious effects of LPS and considerably increases UCP1 levels.

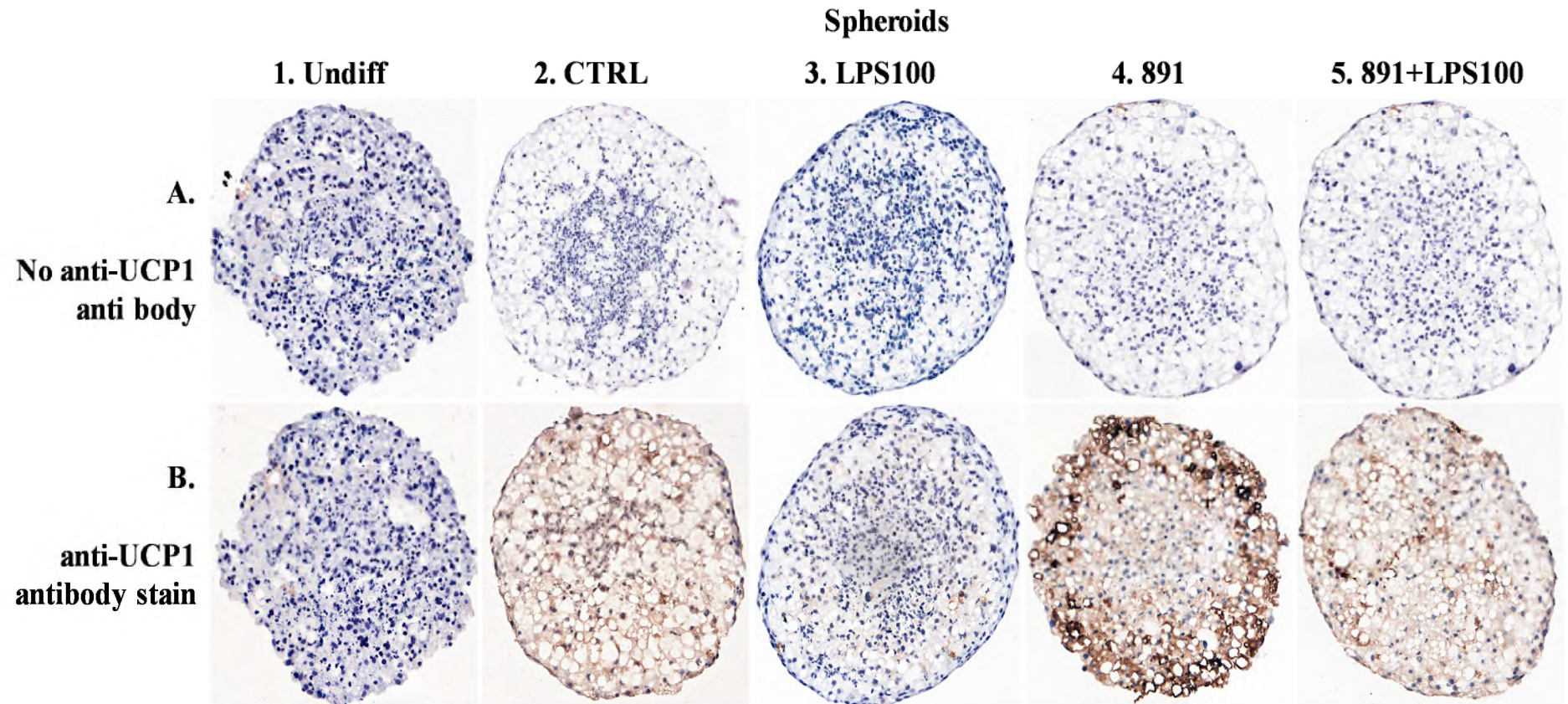


Figure 7.3.5.3 UCP1 Staining, in Murine Brown Adipocyte Spheroids by Immunohistochemistry.

Sectioned spheroids were incubated without (A1, A2, A3, A4, A5)/with (B1, B2, B3, B4, B5) UCP1-primary antibody and staining was detected using an HRP/DAB detection kit. Sections were counterstained using haematoxylin. Pictures taken with a 40x magnification. B4 appears more stained compared to B2 which indicate 891 increased UCP1 levels in brown adipocyte spheroids. B5 appears more stained compared to B3 which indicates the combination of 891 with LPS protected brown adipocyte spheroids from LPS-reduced UCP1.

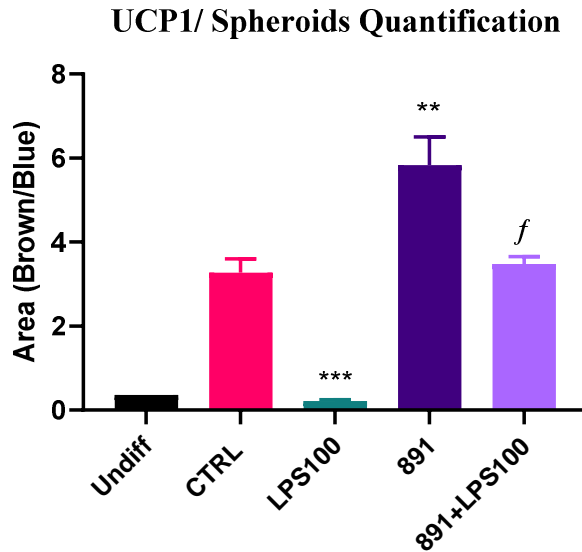


Figure 7.3.5.4 UCP1 Staining Quantification, in Mouse Brown Adipocytes Spheroids By Immunohistochemistry.

At least 3 stained spheroids at dilution 1:1000 for UCP1 antibody were quantified. Data are expressed as mean \pm standard error of the mean. Unpaired t test was used for comparisons. *** $p < 0.001$ compared to CTRL. *f* $p < 0.05$ compared to LPS. Two-way ANOVA was used for comparisons. CTRL; control. UCP1; uncoupling protein 1, 891:TUG-891.

7.3.6 TUG-891 Administration to Brown Adipocytes Enhances Brown Fat Gene Expression

Following the findings that TUG-891 increased UCP1, the main thermogenic protein in brown adipocytes, other key brown fat genes markers were explored. These included CIDEA, PLIN5, and ELOVL3. TUG-891 increased CIDEA gene expression levels in imBAT cells by 33 % (Figure 7.3.6.1, A1) and spheroids by 20.4 % (Figure 7.3.6.1, A2), while it did not have an effect in primaries (Figure 7.3.6.1, A3). However, the observed increase in CIDEA gene expression with TUG-891 was not statistically significant in any of the three models. PLIN5 gene expression levels significantly increased with TUG-891 treatment in imBAT cells (FC=1.23, $P < 0.05$ Figure 7.3.6.1; A2) and primaries (FC=1.94, $P < 0.01$ Figure 7.3.6.1; B2), however the increase in spheroids was not statistically significant (Figure 7.3.6.1; C2). ELOVL3 gene expression levels significantly increased with TUG-891 treatment in imBAT (FC=2.38, $P < 0.0001$ Figure 7.3.6.1; A3), primaries (FC=3.01, $P < 0.001$ Figure 7.3.6.1; B3) and spheroids (FC=5.09, $P < 0.0001$ Figure 7.3.6.1; C3).

Generally, the combination of TUG-891 and LPS enhanced CIDEA gene expression in brown adipocytes compared with LPS-treated cells as there was 65 % increase in imBAT cells (Figure 7.3.6.1; A1), 147 % increase in primaries (Figure 7.3.6.1, B1), and 521 % increase in spheroids (Figure 7.3.6.1; C1). However, this increase was only statistically significant in primaries ($P<0.01$). In parallel, PLIN5 gene expression levels were restored when differentiating the brown adipocytes with TUG-891 and LPS compared to LPS alone as there was 77.4 % increase in imBAT cells ($P<0.05$, Figure 7.3.6.1; A2), 131 % increase in primaries ($P<0.05$, Figure 7.3.6.1; B2), 937 % increase in spheroids ($P<0.05$, Figure 7.3.6.1; C2). In line with restoration of CIDEA and PLIN5, ELOVL3 gene expression levels was restored when differentiating the brown adipocytes with TUG-891 and LPS compared to LPS alone as there was 523 % increase in imBAT ($P<0.001$, Figure 7.3.6.1; A3), 283 % increase in primaries ($P<0.05$, Figure 7.3.6.1; B3), 4586 % increase in spheroids ($P<0.001$ Figure 7.3.6.1; C3).

From these findings, TUG-891 appears to enhance expression of brown fat genes including (PINL5 and ELOVL3) and partially reverse the deleterious effects of LPS on the reduction of CIDEA, PLIN5 and ELOVL3 in brown adipocytes. It is noteworthy that the percentage restoration due to TUG-891 was always higher in the spheroid model. As this model provides a 3D culture environment closer to the physiological status, it supports the potential for TUG-891 to have a potent brown fat gene-inducing action *in vivo*.

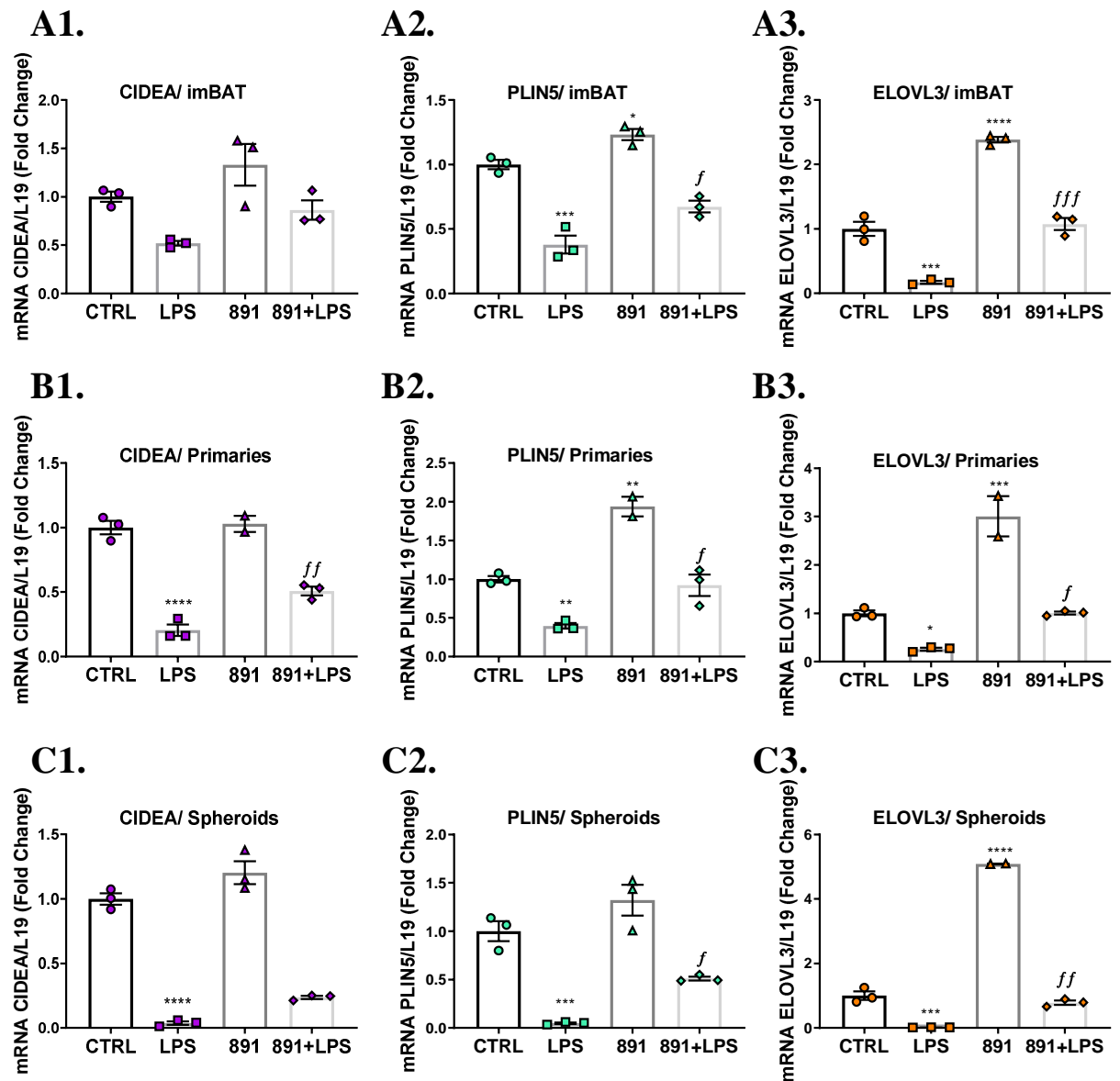


Figure 7.3.6.1 Effect of TUG-891 (891) on Brown Fat Genes in Brown Adipocytes.

ImBAT cells, primaries and spheroids were differentiated with/without LPS (100 ng/ml), 891 or combination of 891 and LPS. (A1, B1, C1) CIDEA gene expression levels in imBAT cells, primaries, and spheroids, respectively. (A2, B2, C2) PLIN5 gene expression levels in imBAT cells, primaries, and spheroids, respectively. (A3, B3, C3) ELOVL3 gene expression levels in imBAT cells, primaries, and spheroids, respectively. Results are expressed as a fold change from control cells. Bars represent means \pm standard error of the mean. * $p < 0.05$, ** $p < 0.01$, *** $p < 0.001$, **** $p < 0.0001$ compared to CTRL. *f* $p < 0.05$, *ff* $p < 0.01$ compared to LPS. Two-way ANOVA was used for comparisons. CTRL; control. CIDEA; cell death inducing DFFA like effector a. PLIN5; perilipin 5. ELOVL3; elongation of very long chain fatty acids protein 3, 891:TUG-891.

Gene expression analysis for GPR120, itself a brown fat maker and the receptor for TUG-891, revealed a significant increase with TUG-891 treatment in primaries (200 %, $P < 0.0001$, Figure 7.3.6.2, B), however no increase was detected in imBAT cells or spheroids (Figure 7.3.6.2, A, C). Nevertheless, GPR120 gene expression levels were

restored when differentiating the brown adipocytes with TUG-891 and LPS compared to LPS alone in spheroids (733 %, $P<0.05$) (Figure 7.3.6.2; C).

It is possible that the increased GPR120 levels contribute to the positive effects of TUG-891 on UCP1 and other brown fat genes. However, a larger number of samples is needed to confirm this conclusion.

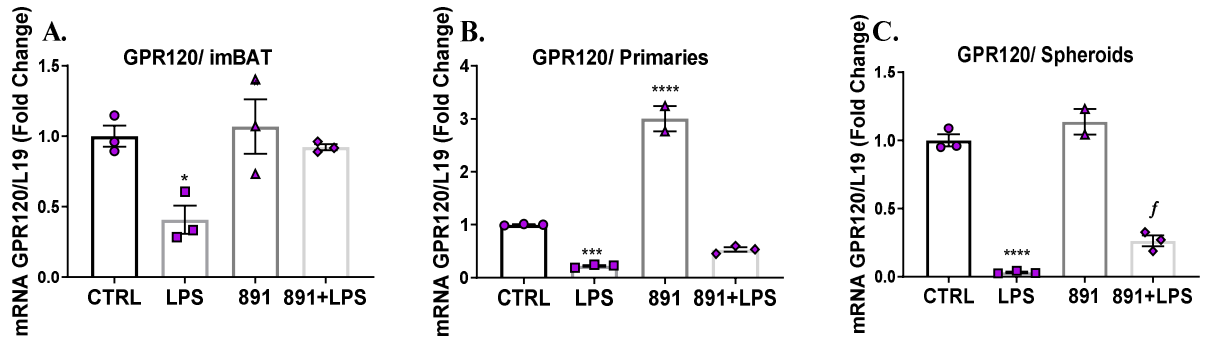


Figure 7.3.6.2 Effect of TUG-891 (891) on GPR120 Gene Expression in Brown Adipocytes.

ImBAT cells, primaries and spheroids were differentiated with/without LPS (100 ng/ml), 891 or combination of 891 and LPS. (A, B, C) GPR120 gene expression levels in imBAT cells, primaries, and spheroids, respectively. Results are expressed as a fold change from control cells. Bars represent means \pm standard error of the mean. * $p<0.05$, ** $p<0.01$, *** $p<0.001$, **** $p<0.0001$ compared to CTRL. *f* $p<0.05$ compared to LPS. Two-way ANOVA was used for comparisons. CTRL; control. GPR120; free fatty acid receptor 4, 891:TUG-891.

7.3.7 Effect of TUG-891 Administration to Brown Adipocytes on Reactive Oxygen Species Clearance

Next, oxidative stress processes were explored via measurement of antioxidant enzymes levels as an indicator including catalase (CAT) and superoxide dismutase 2 (SOD2) gene expression.

SOD2 showed a marked increase in terms of mRNA transcript levels when differentiating imBAT cells, primaries and spheroids with LPS. A combination of TUG-891 and LPS treatment during the differentiation of brown adipocytes resulted in similar levels of SOD2 expression to LPS alone (Figure 7.3.7.1; A2, B2, C2). However, the mRNA expression of the antioxidant catalase was significantly impaired with LPS treatment during differentiation of imBAT cells, primaries and spheroids (Figure 7.3.7.1; A1, B1, C1), and TUG-891 seems to restore catalase gene expression and reverse LPS actions on catalase levels imBAT cells (FC=1.60, Figure 7.3.7.1; A1),

primaries (FC=1.47, $P<0.05$, Figure 7.3.7.1; B1) and spheroids (FC=2.58, $P<0.05$, Figure 7.3.7.1; C1).

Collectively, TUG-891 protected the anti-oxidant role of catalase which was impaired when LPS is present which would influence mitochondrial function.

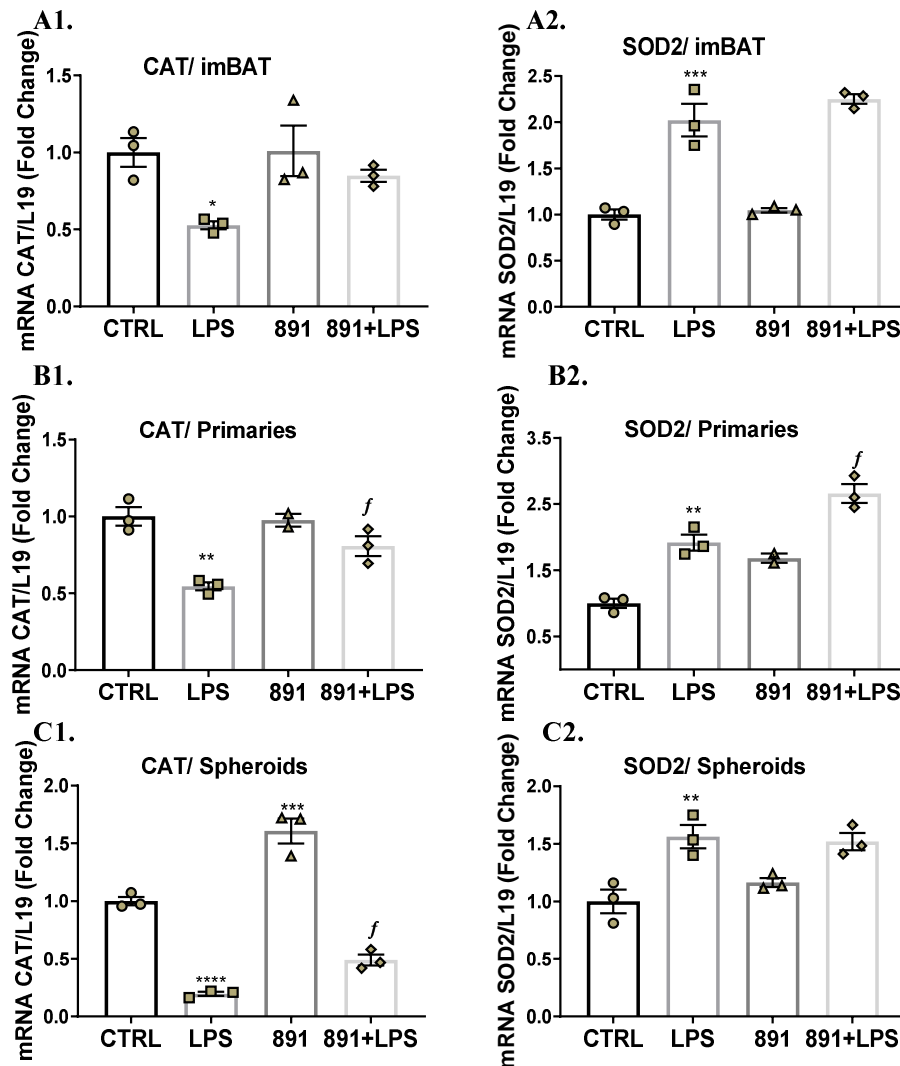


Figure 7.3.7.1 Effect of TUG-891 (891) on Catalase (CAT) and Superoxide Dismutase 2 (SOD2) in Brown Adipocytes.

ImBAT cells, primaries and spheroids were differentiated with/without LPS (100 ng/ml), 891 or combination of 891 and LPS. (A1, B1, C1) CAT gene expression levels in imBAT cells, primaries, and spheroids, respectively. (A2, B2, C2) SOD2 gene expression levels in imBAT cells, primaries, and spheroids, respectively. Results are expressed as a fold change from control cells. Bars represent means \pm standard error of the mean. * $p<0.05$, ** $p<0.01$, *** $p<0.001$, **** $p<0.0001$ compared to CTRL. ^f $p<0.05$ compared to LPS. Two-way ANOVA was used for comparisons. CTRL; control, 891: TUG-891.

7.3.8 Effect of TUG-891 Administration on the Expression of Genes Involved in Mitochondrial Biogenesis, and Protein Depletion

In order to determine the impact of LPS on mitochondrial biogenesis, gene expression of PPAR γ coactivator 1 α (PGC1 α), DNA polymerase γ (POLG), transcription factor A (TFAM) and nuclear respiratory factor 1 (NRF1) were measured across each cell type. LPS treatment reduced expression of every gene measured in each cell type, with a maximum decrease of -89 % ($P < 0.001$) observed in expression levels of PGC1 α in spheroid model as shown in Figure 7.3.8.1 as fold-change of control cells.

Differentiating imBAT, primaries and spheroids with a combination of LPS and TUG-891 blunted the repression induced by LPS on genes involved in mitochondrial biogenesis. This is evidenced by an increase in mitochondrial biogenesis gene expression levels in cells treated with combination of LPS and TUG-891 compared to LPS by a 213 % maximum increase in PGC1 α ($P < 0.01$), 108 % maximum increase in POLG ($P < 0.0001$), 117 % maximum increase in TFAM ($P < 0.001$) and 64 % maximum increase in NRF1 ($P < 0.01$). The increase was statistically significant in imBAT cells when investigating PGC1 α (Figure 7.3.8.1; A1) and POLG (Figure 7.3.8.1, A2), in primaries when investigating POLG (Figure 7.3.8.1, B2), and in spheroids when investigating POLG (Figure 7.3.8.1, C1), TFAM (Figure 7.3.8.1, C3), NRF1 (Figure 7.3.8.1, C4).

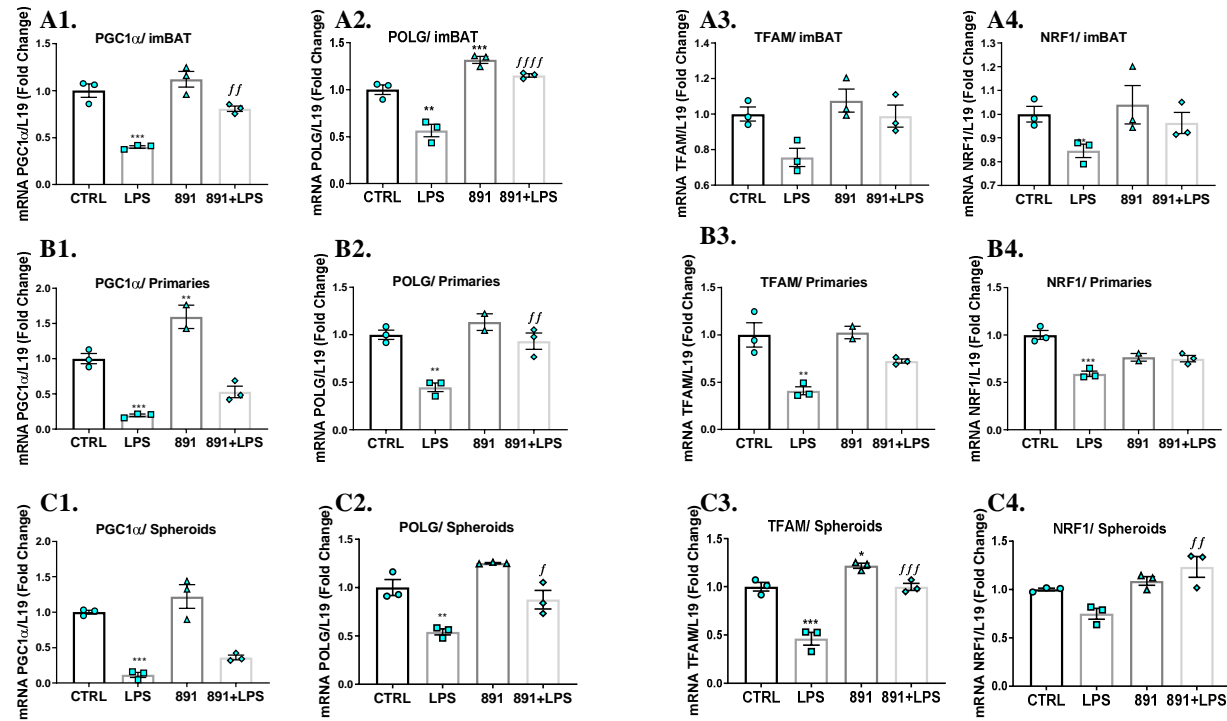


Figure 7.3.8.1 Effect of TUG-891 (891) on Genes Involved in Mitochondrial Biogenesis in Brown Adipocytes.

ImBAT cells, primaries and spheroids were differentiated with/without LPS (100 ng/ml), 891(10 μ M) or combination of 891 and LPS. (A1, B1, C1) PGC1 α gene expression levels in imBAT cells, primaries, and spheroids, respectively. (A2, B2, C2) POLG gene expression levels in imBAT cells, primaries, and spheroids, respectively. (A3, B3, C3) TFAM gene expression levels in imBAT cells, primaries, and spheroids, respectively. (A4, B4, C4) NRF1 gene expression levels in imBAT cells, primaries, and spheroids, respectively. Results are expressed as a fold change from control cells. Bars represent means \pm standard error of the mean. * p <0.05, ** p <0.01, *** p <0.001, **** p <0.0001 compared to CTRL. f p <0.05, ff p <0.01, fff p <0.001, $ffff$ p <0.0001 compared to LPS. Two-way ANOVA was used for comparisons. CTRL; control. PGC1 α ; PPARG coactivator 1 alpha. POLG; DNA polymerase gamma, catalytic subunit. TFAM; transcription factor A, mitochondrial. NRF1; nuclear respiratory factor 1, 891:TUG-891.

In addition, adverse effects on mitochondrial protein translation were observed when differentiating imBAT cells were treated with LPS. Succinate dehydrogenase complex subunit A (SDHA) protein levels were decreased when imBAT cells were differentiated with LPS. However, LPS effects on MtDNA-encoded cytochrome c oxidase subunit 1 (MT-CO1) protein levels were less obvious. The ratio indicated evidence of an increase of mitochondrial protein encoded in mitochondrial DNA (MT-CO1) versus nuclear DNA-encoded mitochondrial protein (SDHA), albeit none significant (Figure 7.3.8.2, C).

Differentiating imBAT cells treated with a combination of LPS and TUG-891 lessened effects observed with LPS alone on SDHA levels (Figure 7.3.8.2, A1, A2). but did not affect MT-CO1 (Figure 7.3.8.2, B1, B2). Also, when using a combination of LPS and TUG-891, compared to LPS alone. Mitochondrial protein encoded in mitochondrial DNA (MT-CO1) increased compared to nuclear DNA-encoded mitochondrial protein (SDHA). However, further investigations using a larger number of samples are needed to confirm these results.

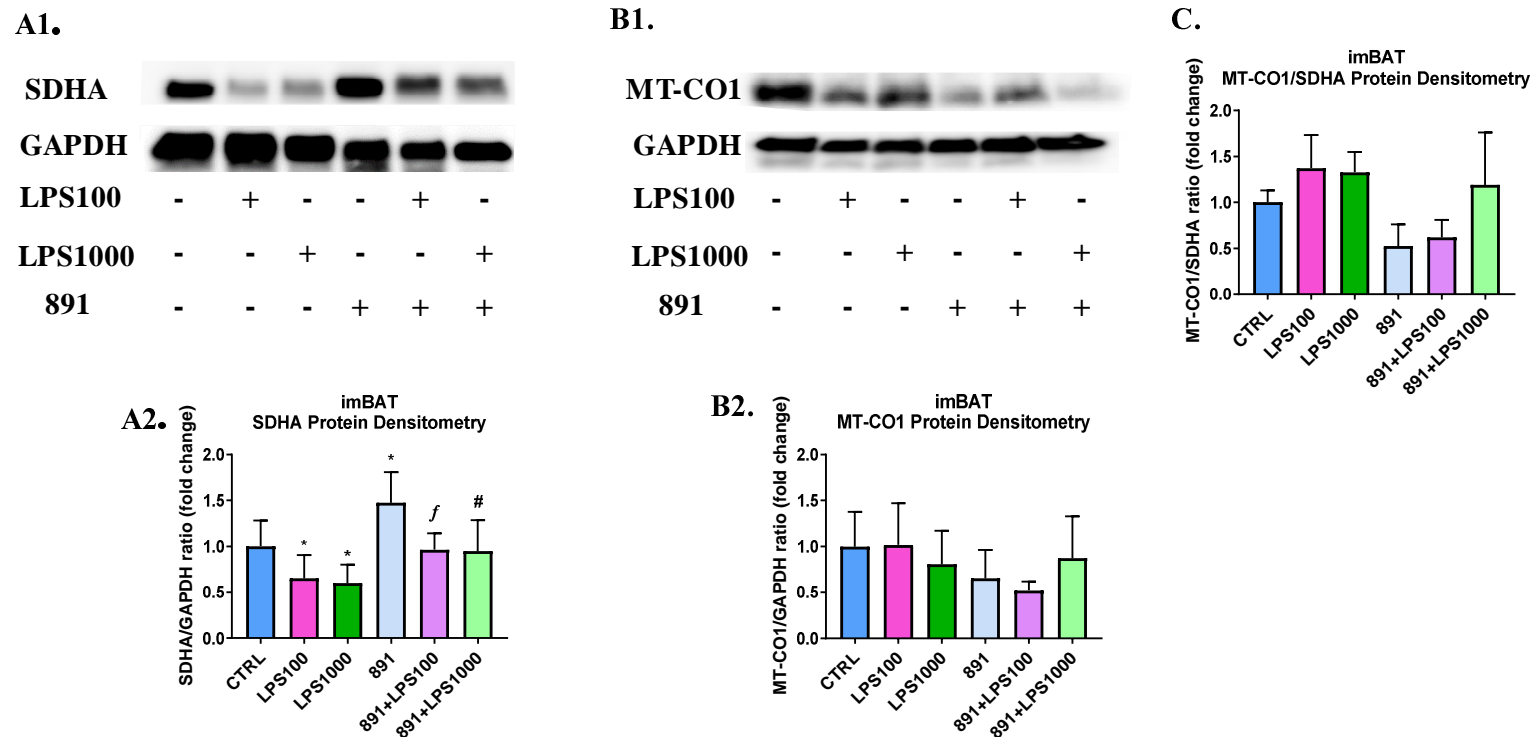


Figure 7.3.8.2 Mitochondrial Protein Abundance (Denoted by Mitochondrial MT-CO1 to Nuclear SDHA Protein Ratio) in imBAT Cells following Differentiation with/without LPS (100 ng/ml, 1000 ng/ml), 891(10 μ M) or combination of 891 and LPS.

Image of SDHA and loading control GAPDH (A1), MT-CO1 and loading control GAPDH (B1) Western blot membranes. Densitometry of absolute levels of SDHA (A2) and MT-CO1 (B2). (C) Densitometry of relative levels of mitochondrial MT-CO1 to nuclear SDHA protein. Data are expressed as fold change from control, and bars represent means \pm standard error of the mean. Linear mixed model was fitted so that random effects can be included since samples were loaded on different gels. * $p < 0.05$, compared to CTRL. f $p < 0.05$, compared to LPS 100. # $p < 0.05$, compared to LPS 1000. CTRL; control. SDHA; Succinate dehydrogenase complex subunit A, MT-CO1; MtDNA-encoded cytochrome c oxidase subunit 1. GAPDH; glyceraldehyde-3-phosphate dehydrogenase, 891:TUG-891.

7.3.9 Effect of TUG-891 Administration on Mitochondrial Dynamics

LPS appears to reduce indicators of mitochondrial dynamics evidenced by investigations on both gene expression and protein levels. In this context, mitochondrial fission genes including Dynamin-1-like protein (DRP1) and Mitochondrial fission 1 protein (FIS1) had reduced expression when differentiating imBAT cells, primaries and spheroids in the presence of LPS. Similarly, mitochondrial fusion genes including both Mitofusin 2 (MFN2) and mitochondrial dynamin like GTPase (OPA1) had reduced expression levels when differentiating imBAT cells, primaries and spheroids with LPS (Figure 7.3.9.1).

Differentiating brown adipocytes with TUG-891 increased expression of Drp1 compared to control cells by 34 % ($P<0.05$) in imBAT cells, 112 % in primaries without being statistically significant and 7396 % ($P<0.0001$) in spheroids. TUG-891 also significantly recovered reduced DRP1 levels by LPS as the data indicated an increase in DRP1 in combination of LPS and TUG-891 compared to LPS treatment alone by 42.8 % ($P<0.05$) increase in imBAT cells, 254.6 % ($P<0.05$) in primaries and 10455 % ($P<0.001$) in spheroids (Figure 7.3.9.1; A, B, C). In line with this observed TUG-891 effect on DPR1, differentiating brown adipocytes with combinations of LPS and TUG-891 resulted in a reduction of the LPS effect and restoration of other gene expression levels involved in both fission and fusion. This included recovered FIS1-levels from the decrease induced by LPS as the data indicated 36.5 % ($P<0.05$) increase in imBAT cells, 203 % ($P<0.0001$) in primaries and 273.8 % (without being significant) in spheroids (Figure 7.3.9.1; A, B, C). Similarly, mitochondrial fusion gene expression of MFN2 and OPA1 was recovered from the effect of LPS by TUG-891 co-administration as the data showed 52.9 %, and 147 % increase of MFN2 and OPA1 respectively in imBAT cells, 39.4 % and 142.5 % of MNF2 and OPA1 respectively in primaries, and 90.6 % and 97 % of MFN2 and OPA1 respectively in spheroids. The restoration was significant for MFN2 in imBAT ($P<0.01$) and for OPA1 in imBAT ($P<0.001$) and in primary cells ($P<0.01$) (Figure 7.3.9.1; A, B, C).

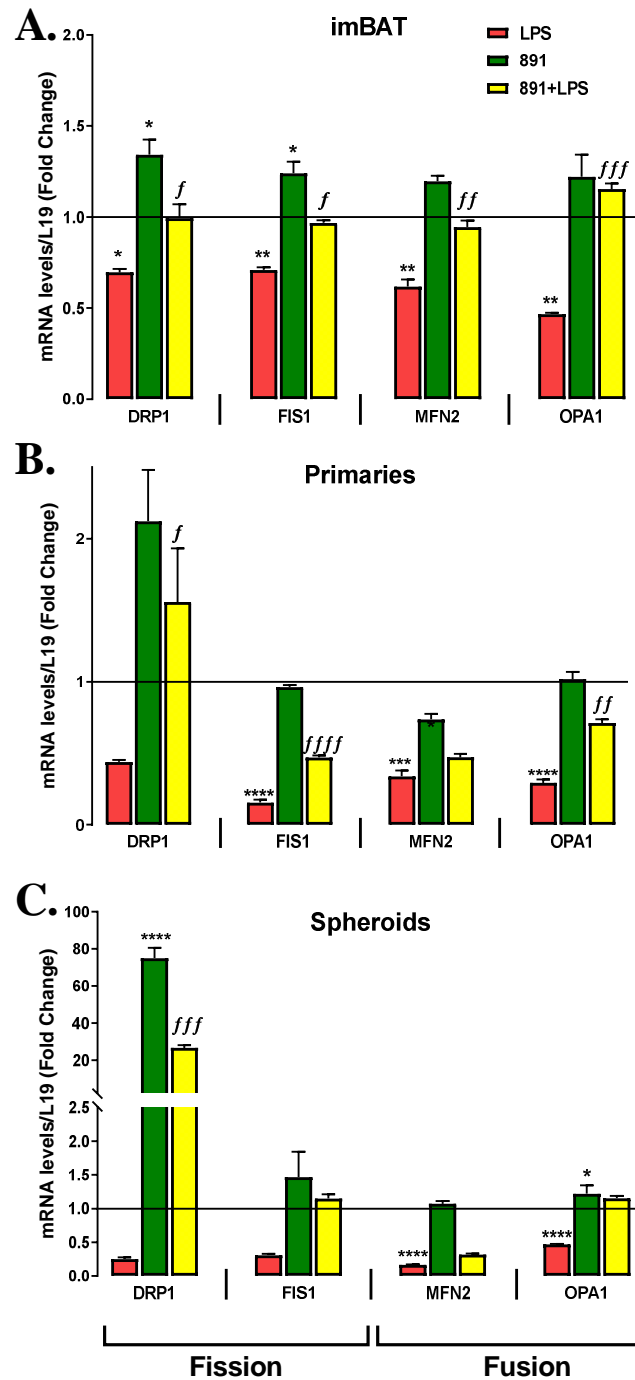


Figure 7.3.9.1 Effect of TUG-891 (891) on Genes Involved in Mitochondrial Dynamics in Brown Adipocytes.

ImBAT cells, primaries and spheroids were differentiated with/without LPS (100 ng/ml), 891(10 μ M) or combination of 891 and LPS. Gene expression levels of mitochondrial fission genes: DRP1, FIS1, and mitochondrial fusion genes MFN2, OPA1 in imBAT (A), primaries (B) and spheroids (C). Results are expressed as a fold change from control cells (n=3 for each treatment). Bars represent means \pm standard error of the mean. *p<0.05, **p<0.01, *** p<0.001, **** p<0.0001 compared to CTRL. ^f p<0.05, ^{ff} p<0.01, ^{fff} p<0.001, compared to LPS. Two-way ANOVA was used for comparisons. CTRL; control. MFN2: Mitofusin 2; OPA1: mitochondrial dynamin like GTPase; DRP1: Dynamin-1-like protein; FIS1: Mitochondrial fission 1 protein, 891:TUG-891.

These changes in gene expression were accompanied by alterations in the protein levels of factors that control mitochondrial dynamics. Investigation of phosphorylated mitochondrial fission protein p-DRP1 showed a reduction in imBAT cells differentiated with LPS (Figure 7.3.9.2; A, A1) as well as both forms of mitochondrial fusion protein OPA1 (long OPA1 (L-OPA1) and short OPA1 s-OPA1). However, the ratio between L-OPA1/S-OPA1 did not change (Figure 7.3.9.2; B, B1, B2, B3).

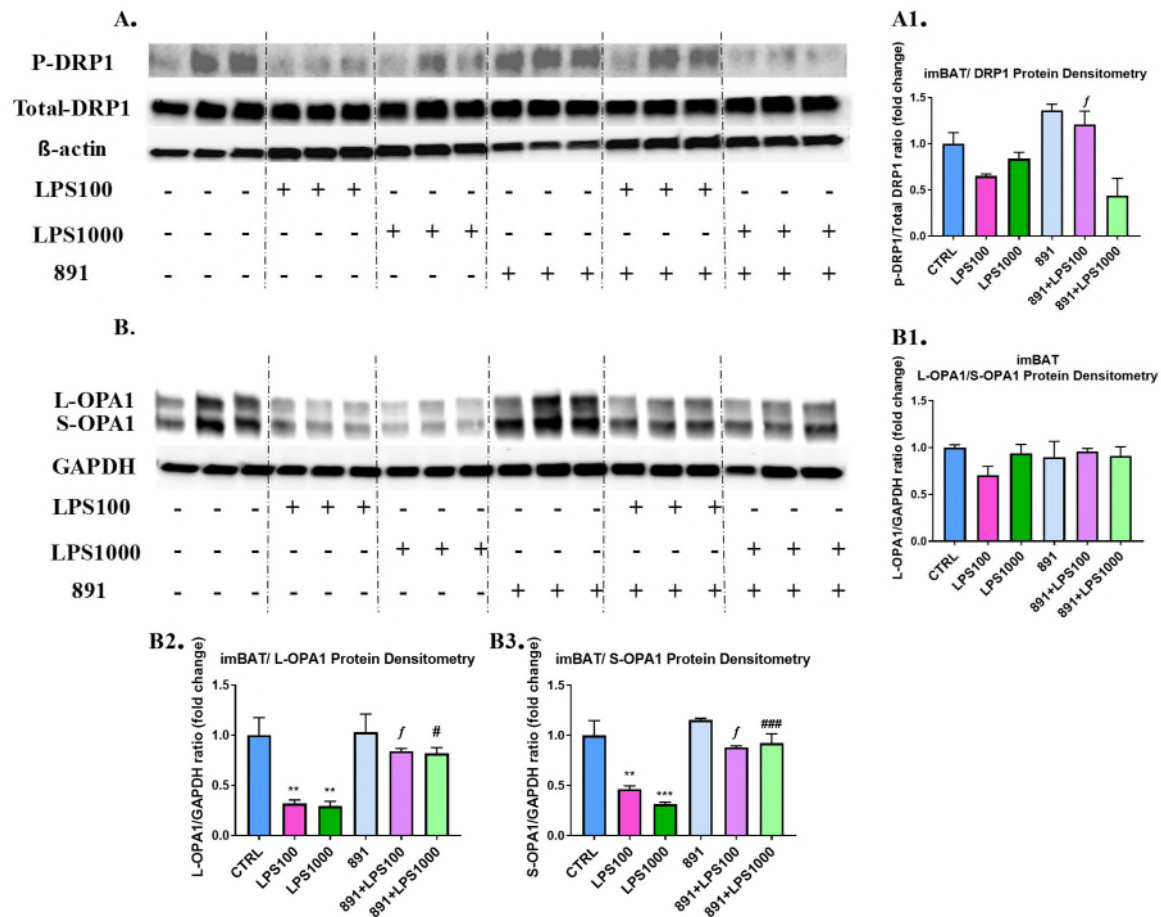


Figure 7.3.9.2 Effect of TUG-891 (891) on Protein Involved in Mitochondrial Dynamics in imBAT Cells.

ImBAT cells were differentiated with/without LPS (100 ng/ml, 1000 ng/ml), 891(10 μ M) or combination of 891 and LPS. Protein expression and densitometry including fission protein DRP1 (A, A1) and fusion protein OPA1 (B, B1, B2, B3) in imBAT cells. (A) Image of p-DRP1, total-DRP1 and loading control GAPDH Western blot membranes. (B) Image of L-OPA1, S-OPA1 and loading control GAPDH Western blot membranes. Results are expressed as a fold change from control cells. Bars represent means \pm standard error of the mean. * p <0.05, ** p <0.01, *** p <0.001 compared to CTRL. f p <0.05 compared to LPS 100, # p <0.05, ## p <0.01, ### p <0.001. Two-way ANOVA was used for comparisons. CTRL; control. P-DRP1: phosphorylated Dynamin-1-like protein; DRP1: Dynamin-1-like protein; GAPDH: glyceraldehyde-3-phosphate dehydrogenase; OPA1: mitochondrial dynamin like GTPase. L-OPA1: long OPA1; S-OPA1, short OPA1.

When differentiating imBAT cells with TUG-891 and LPS in combination, TUG-891 restored p-DRP1 protein levels with the lower dose of LPS. However, it failed to reverse the effect on p-DRP1 with LPS at the higher dose (Figure 7.3.9.2; A, A1).

Both L-OPA1 and S-OPA1 protein levels were significantly restored when differentiating imBAT cells with TUG-891 and LPS in combination compared to LPS alone. However, the L-OPA1/S-OPA1 ratio was not affected by LPS and TUG-891 treatments (Figure 7.3.9.2; A, A1).

7.3.10 Effect of TUG-891 Administration on Other Mitochondrial Functions

Following findings of TUG-891 protective effects against LPS in brown adipocytes with regard to mitochondrial dynamics and biogenesis, indicators that reflect other mitochondrial functions were investigated. This included mRNA gene expression of Cytochrome c oxidase subunit 4 isoform 1 (COX4I1) which is involved in oxidative phosphorylation, carnitine palmitoyltransferase 1B (CPT1 β) which mediates mitochondrial fatty acid oxidation, the major contributor for thermogenesis, citrate synthase (CS), the key enzyme of oxidative metabolism and the Krebs Cycle, and PPARG Related Coactivator 1 (PRC) which is a functional relative of PPAR-gamma coactivator 1.

Each one of CS, CPT1 β , COX4I1 gene expression level was significantly reduced with differentiating imBAT cells, primaries and spheroids with LPS (Figure 7.3.10.1). The greater changes were in spheroids in CS (maximum FC= -9.9, $P<0.0001$, Figure 7.3.10.1) and CPT1 β (maximum FC=-16.5, $P<0.001$, Figure 7.3.10.1).

Differentiating these different brown adipocyte models with combinations of LPS and TUG- TUG-891 reversed LPS-dependent effects to different extents on CS, CPT1 β , COX4I1 gene expression level (Figure 7.3.10.1). In this context, combined TUG-891 and LPS treatment recovered CS levels by 40.7 % in imBAT cells ($P<0.05$), 106 % in primaries ($P<0.05$) and 180.3 % ($P<0.01$) in spheroids (Figure 7.3.10.1; A1, A2, A3), compared to LPS alone. Similarly, CPT1 β levels recovered from the LPS effect with using combination of TUG-891 and LPS by 115 % in imBAT cells ($P<0.05$), 184.5 % in primaries ($P<0.01$) and 499 % in spheroids (Figure 7.3.10.1; B1, B2, B3). Finally, COX4I1 levels were partially restored from the LPS effect using a

combination of TUG-891 and LPS with a 47.6 % increase in imBAT cells, 54.4 % in primaries ($P<0.05$) and 114.4 % in spheroids ($P<0.05$) (Figure 7.3.10.1; D1, D2, D3).

In addition, TUG-891 increased CPT1 β gene expression levels in imBAT and spheroids compared to control cells (Figure 7.3.10.1; A2). In contrast, PRC levels did not seem to be affected by either LPS, TUG-891 or their combinations except reduction in PRC levels with TUG-891 treatment in imBAT cells which was not significant (Figure 7.3.10.1; C1, C2, C3).

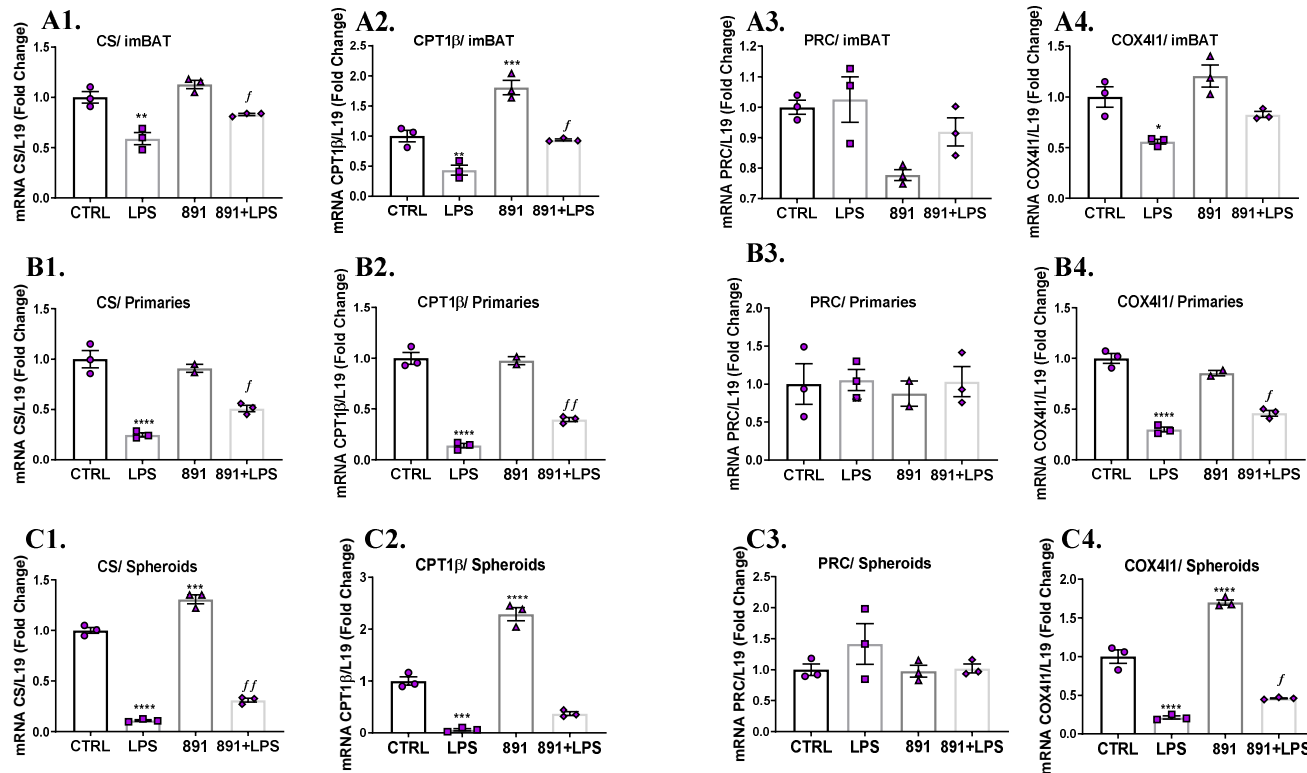


Figure 7.3.10.1 Effect of TUG-891 (891) on Genes Involved in Key Mitochondrial Functions in Brown Adipocytes.

ImBAT cells, primaries and spheroids were differentiated with/without LPS (100 ng/ml), 891(10 μ M) or combination of 891 and LPS. CS gene expression levels (A1, B1, C1) in imBAT cells, primaries, and spheroids, respectively, and CPT1 β gene expression levels (A2, B2, C2) in imBAT cells, primaries, and spheroids, respectively. (A3, B3, C3) PRC gene expression levels in imBAT cells, primaries, and spheroids, respectively and (A4, B4, C4) COX4I1 gene expression levels in imBAT cells, primaries, and spheroids, respectively. Results are expressed as a fold change from control cells. Bars represent means \pm standard error of the mean. * p <0.05, ** p <0.01, *** p <0.001, **** p <0.0001 compared to CTRL. f p <0.05, ff p <0.01, compared to LPS. Two-way ANOVA was used for comparisons. CTRL; control. CS: citrate synthase (CS). CPT1 β : carnitine palmitoyltransferase 1B. PRC: PPARG Related Coactivator 1. COX4I1: Cytochrome c oxidase subunit 4 isoform 1. 891:TUG-891

7.3.11 TUG-891 Administration Prevented the Inhibitory Action of LPS

To understand the functional implications of differentiating brown adipocytes in the presence of TUG-891 on mitochondrial function, a Seahorse extracellular flux analyzer was used to measure basal oxygen consumption rate (OCR) as an indicator of aerobic respiration in live cells. Also, using a confocal microscope, live cell imaging was undertaken to assess mitochondrial membrane potential. Prior to imaging, cells were incubated with MitoTracker Green FM (MTG) and MitoTracker Red CMXRos (MTR), which stain mitochondria independent of and dependent on membrane potential, respectively. Relative intensity (MTR/MTG) of these stains was then used as a measure of mitochondrial polarization.

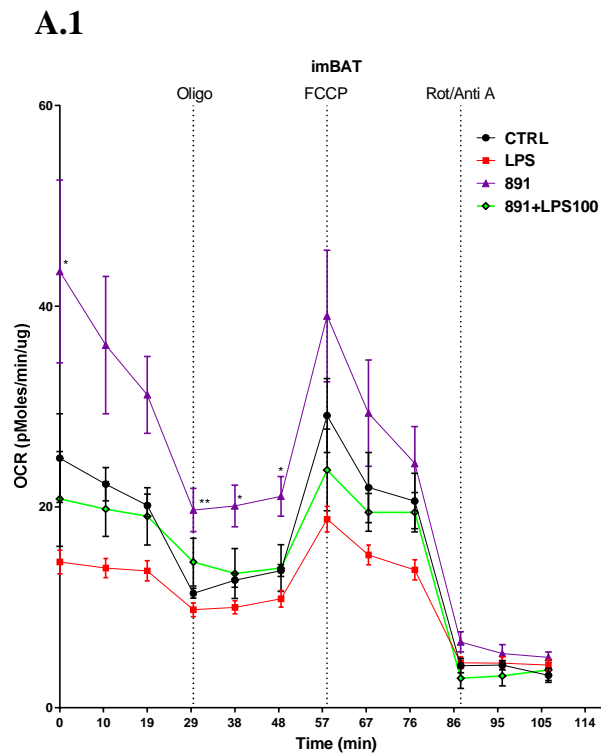
As shown in Figure 7.3.11.1, LPS altered OCR and reduced basal respiration in both imBAT cells (FC=-1.81, $P<0.01$, Figure 7.3.11.1; A3) and primaries (FC=-1.18, without being significant, Figure 7.3.11.1; B3). ATP production was reduced in imBAT cells (FC=-2.25, $P<0.01$, Figure 7.3.11.1; A3) and primaries (FC=-1.23, without being significant, Figure 7.3.11.1; B3) but without impaired bioenergetic efficiency (data not shown). Interestingly, LPS treatment reduced both proton leak (Figure 7.3.11.1; A5, B5) and mitochondrial membrane potential (demonstrated by fading of the MTR signal while the MTG signal remained intense in Figure 7.3.11.2), indicating reduced mitochondrial uncoupling is not related to mitochondrial efficiency.

Differentiating brown adipocytes with TUG-891 increased OCR and basal respiration in both imBAT cells (FC=1.31, $P<0.05$, Figure 7.3.11.1; A) and primaries (FC=1.38, without being significant, Figure 7.3.11.1; B), while ATP production was not affected (Figure 7.3.11.1; A3, B3), and no effect on bioenergetic efficiency was observed (data not shown). Proton leak was higher with TUG-891 compared to control imBAT cells, while it was decreased in primary cells (Figure 7.3.11.1; A5, B5). In addition, the effect of TUG-891 on MTR signal was limited with a tendency to be increased compared to control cells (Figure 7.3.11.1). Thus, long-term TUG-891 treatment increased respiration with no obvious effect on different measured respiration parameters.

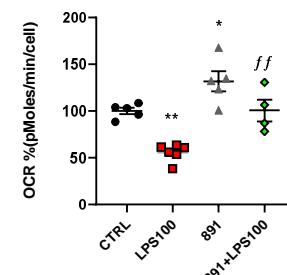
TUG-891 treatment partially protected the cells from the reductions in OCR and basal respiration caused by LPS in both imBAT (FC=1.81, $P<0.01$, Figure 7.3.11.1; A) and primaries (FC= 1.70, $P<0.01$, Figure 7.3.11.1; B). ATP production was higher when differentiating brown adipocytes were treated with TUG-891 and LPS in combination compared to LPS alone in imBAT cells (FC=1.98, $P<0.05$, Figure 7.3.11.1; A3) primaries (FC= 2.18, $P<0.001$, Figure 7.3.11.1; B3), but without effects on bioenergetic efficiency (data not shown). Proton leak was higher with LPS and TUG-891 in combination compared to LPS treatment in imBAT cells. In addition, this combination of both LPS and TUG-891 reversed fading of the MTR signal, indicative of reversing the LPS-dependent mitochondrial depolarization effect (Figure 7.3.11.1), which could explain the TUG-891-dependent increase in respiration and opposing LPS effects on respiration. The findings of effects of combinations of LPS and TUG-891 on different respiration parameters is summarised in Table 7.3.11.1.

Figure 7.3.11.1 Effect of TUG-891 on Aerobic Capacity under Stress and Mitochondrial Bioenergetics.

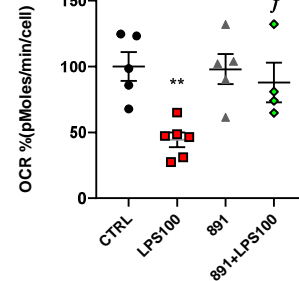
Time-lapse of aerobic capacity measured by oxygen consumption rate (OCR) during a Seahorse mitochondria stress test performed on (A1) ImBAT cells/ (B1) primaries which were differentiated with/without LPS (100 ng/ml), 891 (10 μ M) or combination of 891 and LPS. Pharmacological inhibitors oligomycin (oligo), carbonyl cyanide p-trifluoromethoxy-phenylhydrazone (FCCP) and a combination of rotenone (R) & antimycin A (A) were added sequentially, as indicated. Basal respiration rate for on (A2) ImBAT cells/ (B2) primaries. ATP abundance for (A3) ImBAT cells/ (B3) primaries. Spare respiratory capacity for (A4) ImBAT cells/ (B4) primaries. Proton leak for (A4) ImBAT cells/ (B4) primaries. OCR values were normalised to protein content for ImBAT cells and to cell number for primaries of each experimental group to account for inter-well cell number variability. Mitochondrial Bioenergetics values express fold change from control mean. Means are shown with Error bars represent standard error of the mean. * $p < 0.05$, ** $p < 0.01$, *** $p < 0.001$, **** $p < 0.0001$ compared to CTRL. *f* $p < 0.05$, *ff* $p < 0.01$, *fff* $p < 0.001$ compared to LPS. Two-way ANOVA was used for comparisons. CTRL; control. SRC: Spare respiratory capacity, 891:TUG-891.



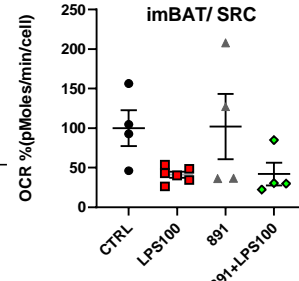
A.2 imBAT/ Basal respiration



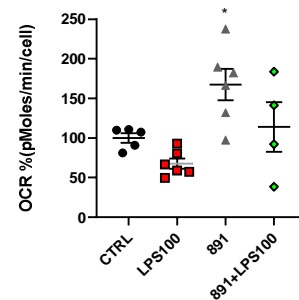
A.3 imBAT/ ATP Production



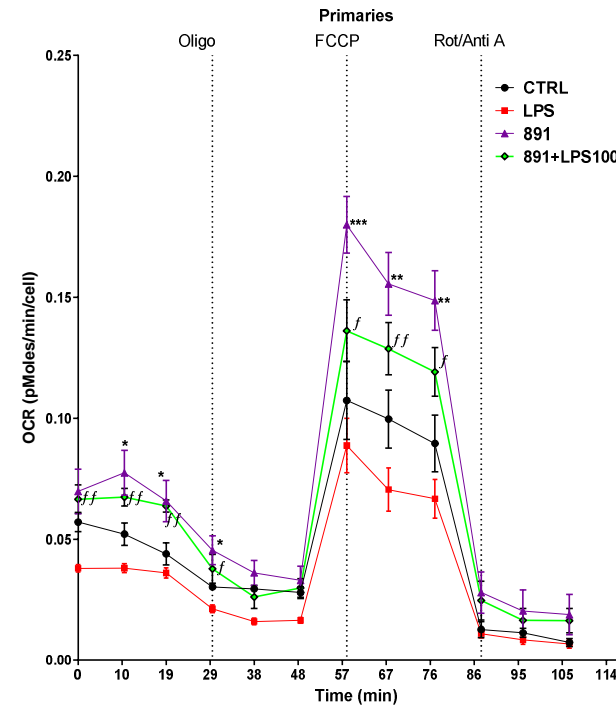
A.4 imBAT/ SRC



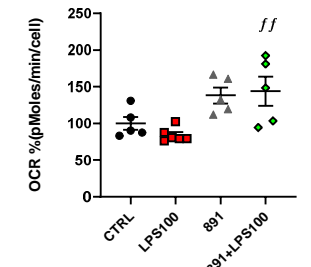
A.5 imBAT/ Proton leak



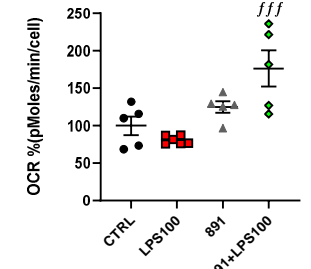
B.1



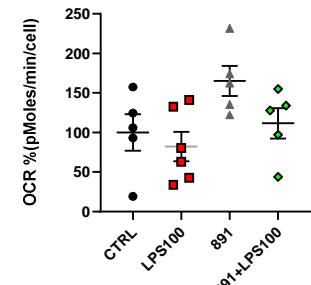
B.2 primaries/ Basal respiration



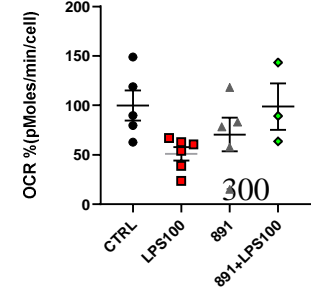
B.3 primaries/ ATP Production



B.4 primaries/ SRC



B.5 primaries/ Proton leak



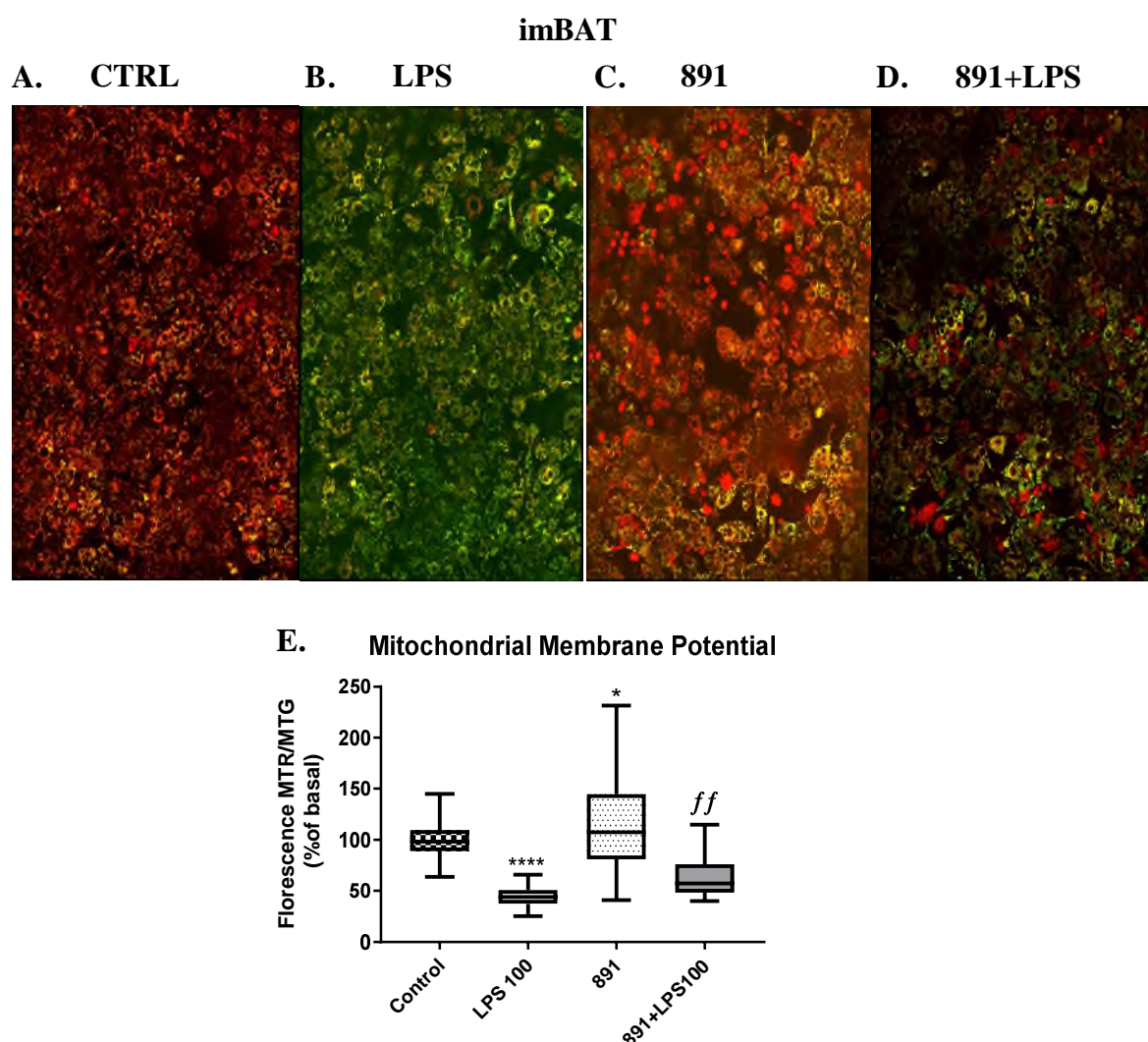


Figure 7.3.11.2 Confocal Microscopies of Differentiated imBAT Cells without (A)/with LPS (100 ng/ml) (B), 891(10 μ M) (C) or Combination of 891 and LPS (D).

Representative images are shown at 40x magnification, stitched images of 9 different places of each sample. live Brown adipocytes stained with Mitotracker Green FM (125 nM) and Mitotracker Red CMXros (250 nM). And (E) plotted relative to control. Means are shown with Error bars represent standard error of the mean. * $p < 0.05$, **** $p < 0.0001$ compared to CTRL. ff $p < 0.001$ compared to LPS. Two-way ANOVA was used for comparisons. CTRL; control.

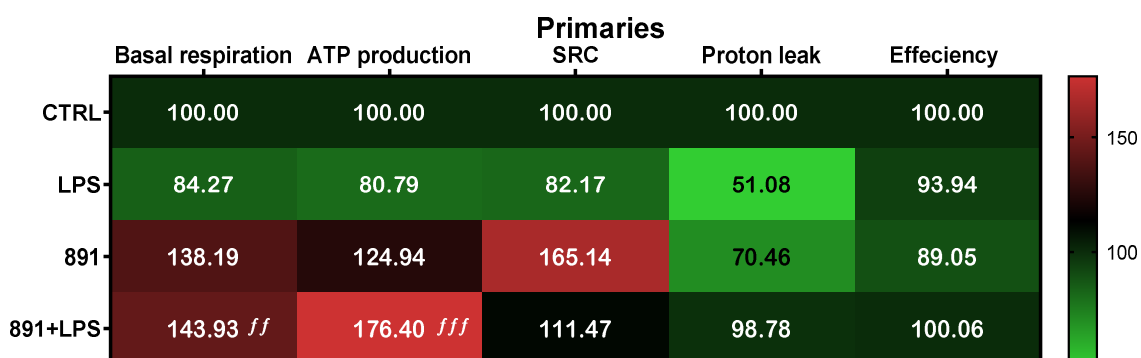
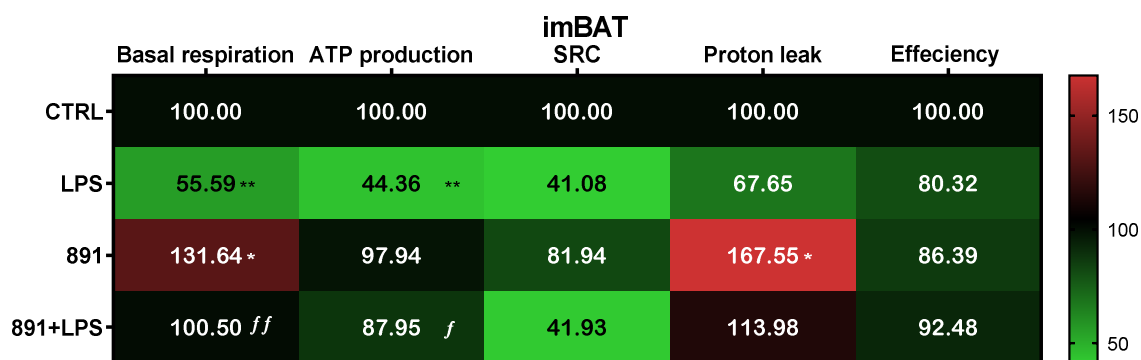


Table 7.3.11.1 Effect of TUG-891 on Mitochondrial Function.

Basal respiration, ATP production, spare respiratory capacity (SRC), proton leak and mitochondrial efficiency ratio was measured differentiated with/without LPS (100 ng/ml), 891(10 μ M) or combination of 891 and LPS. Results are displayed as percentage relative to control values as a heatmap where red cells indicate an increase and green or black cells indicate lower or similar values to control, respectively. * $p < 0.05$, ** $p < 0.01$, *** $p < 0.001$, **** $p < 0.0001$ compared to CTRL. *f* $p < 0.05$, *ff* $p < 0.01$, *fff* $p < 0.001$ compared to LPS. Two-way ANOVA was used for comparisons. CTRL; control.

These results on OCR need additional confirmation to examine TUG-891 effects on reversing LPS damaging actions on different parameters of respiration.

7.3.12 LPS-Induced Secretion of Cytokines by Brown Adipocytes is Inhibited by TUG-891

From Chapter 4 in this thesis, Proteome Cytokines Array investigations of differentiated brown adipocytes led to identification of upregulated secreted cytokines with LPS treatment. This included angiogenesis-related factors (e.g. CXCL1/KC, MMP3, CXCL16), different members of ECM fibrous proteins and integrin signalling pathways (e.g. VCAM-1, Endostatin, MMP3), and the typical response to exposure to an inflammatory agent such as LPS (e.g IL6, IL23a, Eotaxin, CXCL1/KC and CD14) (Figure 7.3.12.1).

TUG-891 interestingly, reduced the basal levels of almost all secreted cytokines by mature adipocytes including those involved in immune and inflammatory responses such as CCL6/C10, CCL12/MCP-5, IL-4, IL-7, LIF, CXCL5 (LIX), M-CSF, GMP-140/ CD62P. This provides further evidence of the potent role of TUG-891 as an anti-inflammatory factor even at the basal level.

In addition, differentiating cells treated with a combination of LPS and TUG-891 led to reduced secretion of many cytokines by both imBAT cells and primaries (Figure 7.3.12.1). The reduction was most noticeable for CXCL16, Proliferin, CXCL10/IP-10 (which are angiogenesis-related factors), VCAM-1, Endostatin (which are involved in ECM fibrous proteins and integrin signalling pathways), and IL-23, CD14, Lipocalin-2/NGAL (which have immune and inflammatory roles).

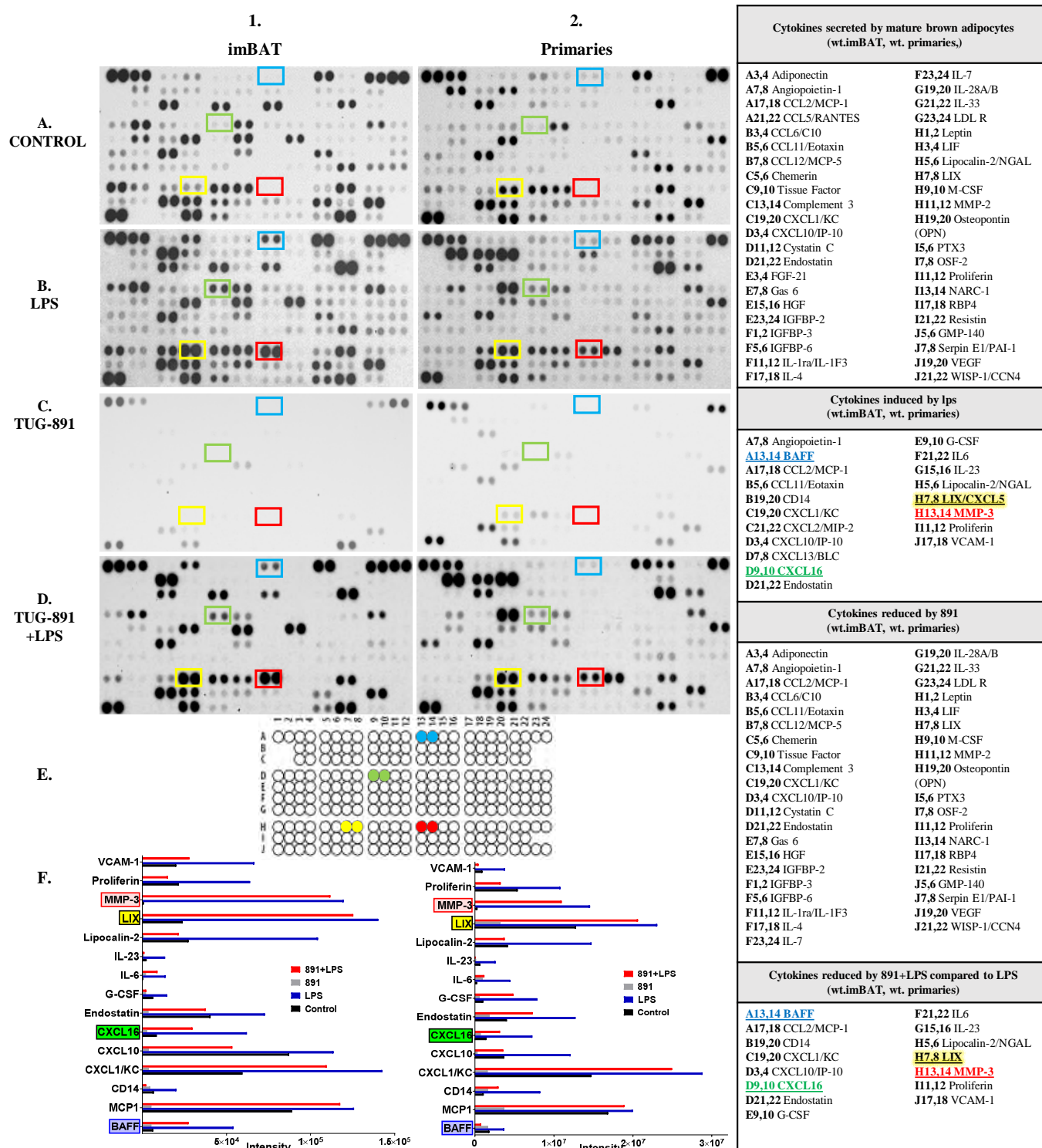


Figure 7.3.12.1 Media Cytokine Array for Brown Adipocytes (both 1.imBAT cells and 2.primaries).

ImBAT cells/ primaries were differentiated with/without LPS (100 ng/ml), 891 (10 μ M) or combination of 891 and LPS. A1, A2 shows immunoblots for imBAT cells and Primaries, respectively. B1, B2 shows LPS effect immunoblots for imBAT cells and Primaries respectively. C1, C2 shows 891 effect immunoblots for imBAT cells and Primaries, respectively. D1, D2 shows LPS and 891 combination effect immunoblots for imBAT cells and Primaries, respectively. E. shows the distribution of cytokines in the blots. F1, F2 shows densitometry of the cytokines induced by LPS and they show control, LPS, 891, LPS and 891 combination effect in imBAT cells and primaries, respectively. Top right table represent secreted cytokines by mature adipocytes, followed by induced cytokines by LPS treatment. Then by induced cytokines by 891-treatment and finally 891 effect against LPS cytokines induction.

The four cytokines followed up earlier in chapter 4 (BAFF, CXCL16, LIX and MMP3) were also further investigated. Secretion levels were measured by ELISA (Figure 7.3.12.2) and gene expression levels by qRT-PCR (Figure 7.3.12.3) in order to establish whether TUG-891 has further effects in opposing LPS.

BAFF, CXCL16, LIX and MMP3 concentrations in conditioned media were decreased when a combination of LPS and TUG-891 was used in differentiating imBAT, with 62 % decrease in BAFF ($P < 0.01$, Figure 7.3.12.2; A1), 49.8 % decrease in LIX ($P < 0.01$, Figure 7.3.12.2; A2), 61.6 % decrease in CXCL16 ($P < 0.0001$, Figure 7.3.12.2; A3) and 79.5 % decrease in MMP3 ($P < 0.0001$, Figure 7.3.12.2; A4) compared to LPS alone. In parallel, these results were reproducible in primaries in response to being differentiated with a combination of LPS and TUG-891 with a 67.5 % decrease in BAFF ($P < 0.01$, Figure 7.3.12.2; B1), 55.2 % decrease in LIX ($P < 0.01$, Figure 7.3.12.2; B2), 71.1 % decrease in CXCL16 ($P < 0.0001$, Figure 7.3.12.2; B3) and 57.4 % decrease in MMP3 compared to LPS alone ($P < 0.0001$, Figure 7.3.12.2; B4). Further confirmation was obtained when observing the response of spheroids to a combination of LPS and TUG-891 compared to LPS alone, with 56.4 % decrease in BAFF ($P < 0.05$, Figure 7.3.12.2; C1), 63.6 % decrease in LIX ($P < 0.01$, Figure 7.3.12.2; C2), 78.2 % decrease in CXCL16 (Figure 7.3.12.2; C3, $P < 0.0001$) and 60.7 % decrease in MMP3 ($P < 0.0001$, Figure 7.3.12.2; C4).

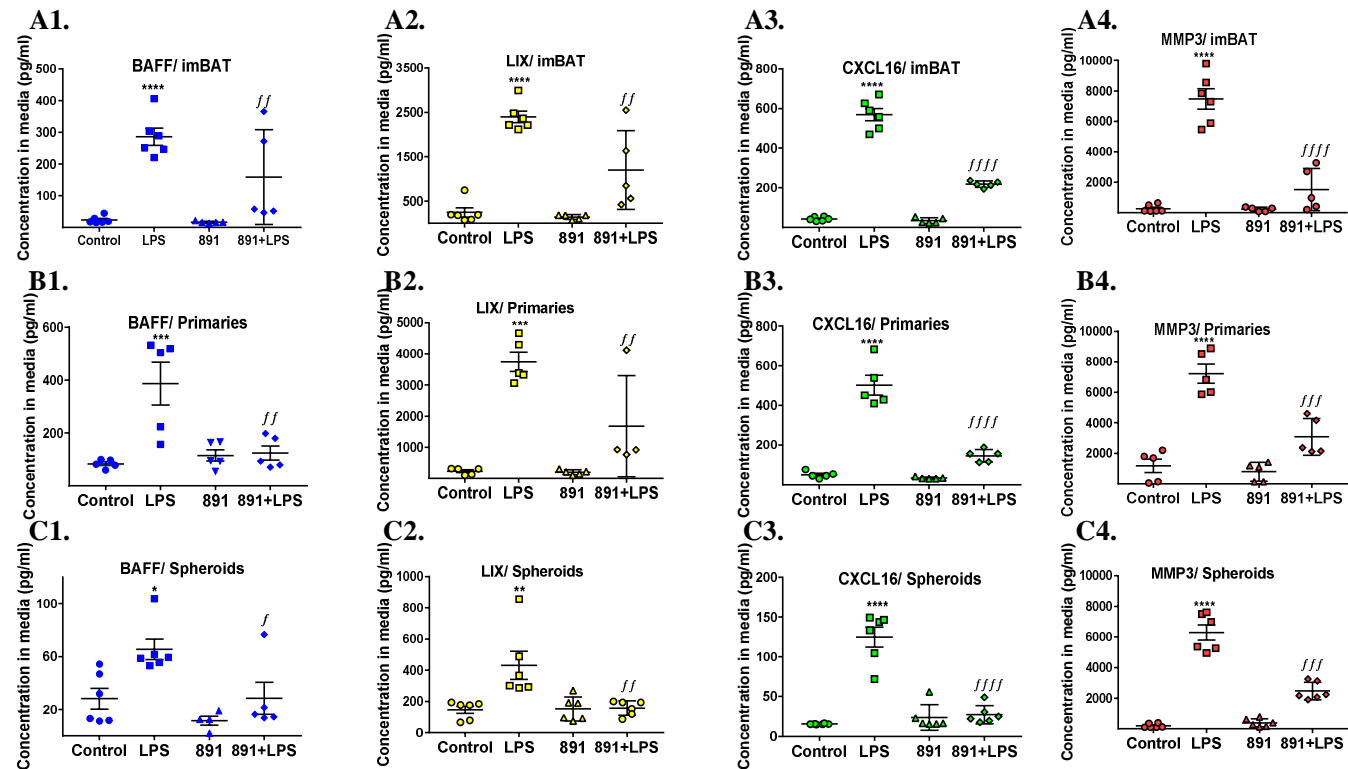


Figure 7.3.12.2 Selected Cytokines Measured by ELISA in Media of imBAT Cells.

ImBAT cells/ primaries or spheroids were differentiated with/without LPS (100 ng/ml), 891(10 μ M) or combination of 891 and LPS. BAFF (A1. in imBAT cells, B1. in primaries, C1 in spheroids), LIX (A2. in imBAT cells, B2. in primaries C2 in spheroids), CXCL16 (A3. in imBAT cells, B3. in primaries, C3 in spheroids), MMP3 (A4. in imBAT cells, B4. in primaries, C4. in spheroids). ELISA imBAT cells, Primaries and spheroids data represent the mean of three (total n=6 each treatment), two experiments (total n=5 each treatment), two experiments (total n=6 each treatment), respectively. Error bars represent standard error of the mean. Two-way ANOVA was used for comparisons. * $p < 0.05$, ** $p < 0.01$, *** $p < 0.001$ **** $p < 0.0001$ compared to control. *f* $p < 0.05$, *ff* $p < 0.01$, *fff* $p < 0.001$, *ffff* $p < 0.0001$ compared to LPS. BAFF: B-cell activating factor, CXCL16: C-X-C motif chemokine ligand 16, LIX (CXCL5): chemokine (C-X-C motif) ligand 5. MMP3: matrix metalloproteinase 3.

This reduction in conditioned media concentrations of these tested cytokines was accompanied by significant downregulation of gene expression detected by qRT-PCR analysis. In this context, differentiating imBAT with a combination of LPS and TUG-891 caused a decrease in gene expression levels of BAFF by 3.6 % (Figure 7.3.12.3; A1), LIX by 95.5 % ($P<0.01$, Figure 7.3.12.3; A3), CXCL16 by 24.8 % ($P<0.01$, Figure 7.3.12.3; A2) and MMP3 by 10 % (Figure 7.3.12.3; A4) compared to LPS alone. Similarly, reductions in gene expression levels were also observed in differentiating primaries exposed to a combination of LPS and TUG-891 with 27.3 % decrease in BAFF ($P<0.01$, Figure 7.3.12.3; B1), 34.9 % decrease in LIX ($P<0.01$, Figure 7.3.12.3; B3), 27.3 % decrease in CXCL16 ($P<0.01$, Figure 7.3.12.3; B2) and 27.6 % decrease in MMP3 ($P<0.001$, Figure 7.3.12.3; B4), compared to LPS alone. Consistently, differentiated spheroids with a combination of LPS and TUG-891 compared to LPS had lower gene expression of BAFF with 55.5 % decrease ($P<0.01$, Figure 7.3.12.3; C1), LIX with 59.1 % decrease ($P<0.01$, Figure 7.3.12.3; C3), CXCL16 with 47.3 % decrease ($P<0.01$, Figure 7.3.12.3; C3) and MMP3 with 87.5 % decrease, compared to LPS alone ($P<0.01$, Figure 7.3.12.3; C4). This effect of TUG-891 on reducing LPS actions, and decreasing gene expression levels of BAFF, CXCL16, LIX and MMP3, was statistically significant except for BAFF in imBAT cells (Figure 7.3.12.3; A1).

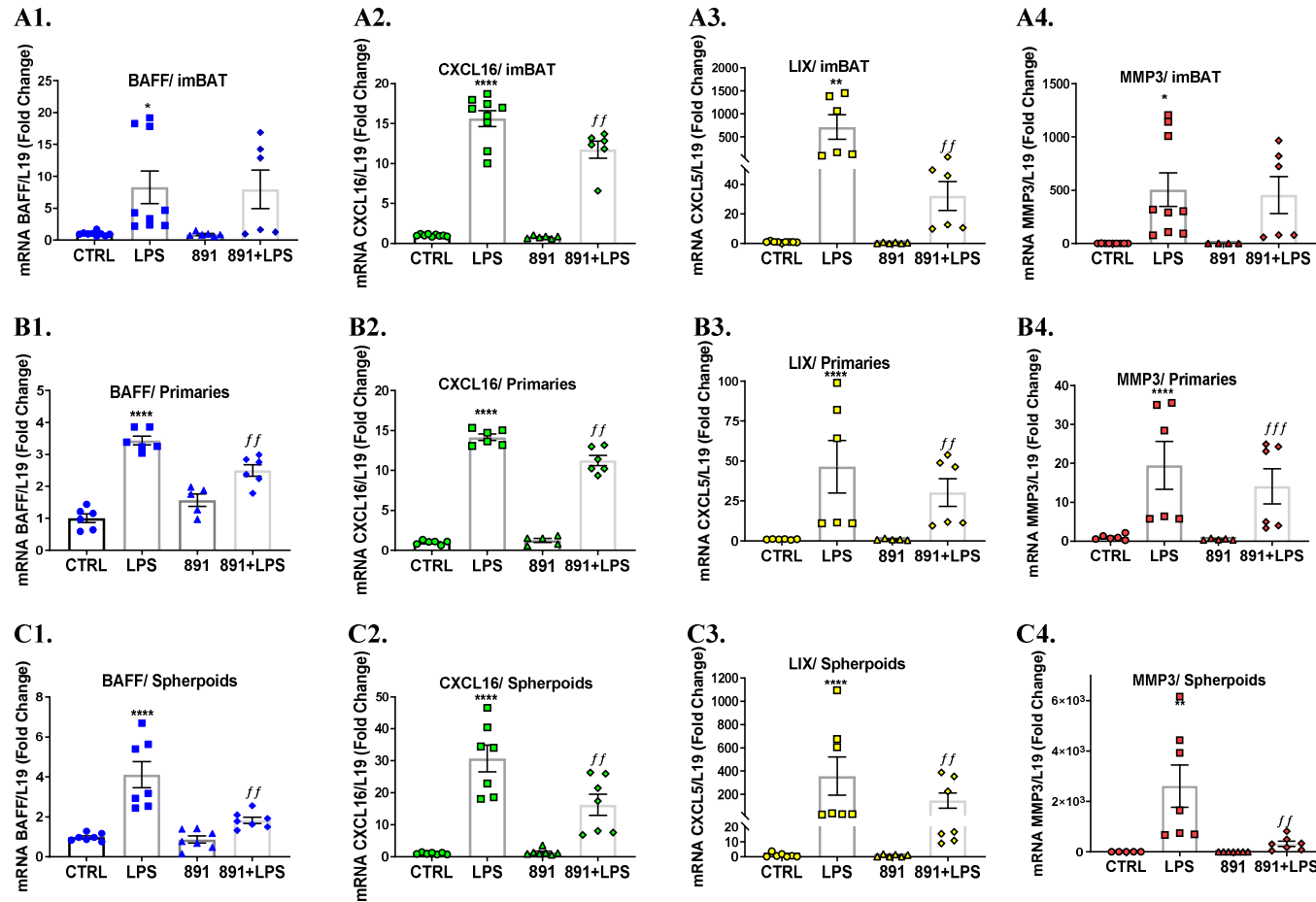


Figure 7.3.12.3 Selected Cytokines Gene Expression in imBAT Cells.

ImBAT/ primaries or spheroids were differentiated with/without LPS (100 ng/ml), 891(10 mM) or combination of 891 and LPS. BAFF (A1. in imBAT, B1. in primaries and C1 in spheroids), CXCL16 (A2. in imBAT, B2. in primaries and C2 in spheroids), LIX (A3. in imBAT, B3. in primaries, C3 in spheroids), MMP3 (A4. in imBAT, B4. in primaries, C4 in spheroids). q-RT PCR imBAT, Primaries and spheroids data represent the mean of three (total n=9 each treatment), two experiments (total n=6 each treatment), two experiments (total n=6/7 each treatment). Error bars represent standard error of the mean. *P < 0.05, ** P < 0.01, ***P < 0.001 compared to control. *f* p<0.05, *ff* p<0.01, *fff* p<0.001, *ffff* p<0.0001 compared to LPS. Two-ways ANOVA was used for comparisons. BAFF: B-cell activating factor, CXCL16: C-X-C motif chemokine ligand 16, LIX (CXCL5): chemokine (C-X-C motif) ligand 5. MMP3: matrix metalloproteinase 3, 891:TUG-891.

Overall, it was observed that the brown adipocytes secreted BAFF, CXCL16, LIX and MMP3 into conditioned media when induced by LPS. The addition of TUG-891 to the LPS treatment reduced the level of secretion of these factors. This was consistent across the three brown adipocyte models to great extent with decreased gene expression of these cytokines when TUG-891 was used alongside LPS instead of LPS alone. This is an indication that secretion of BAFF, CXCL16, LIX and MMP3 from brown adipocytes is likely to be regulated at the gene expression level.

7.4 Discussion

The purpose of this study was to evaluate any therapeutic potential and mechanisms of action of TUG-891, GPR120 agonist, against LPS-effects on brown adipocyte biology and mitochondrial dysfunction. To establish this, TUG-891 actions were comprehensively evaluated using three *in vitro* models of brown adipocytes. The central novel outcome from this chapter was that TUG-891 enhanced brown adipocyte features and opposed the effects of LPS on inflammatory markers and mitochondrial function. This was evidenced by the association of TUG-891 with induction of UCP1, the main thermogenic protein, at both the gene expression and protein levels and it was able to reverse the downregulation of UCP1 by LPS. Furthermore, TUG-891 reversed the action of LPS on inflammation and oxidative stress in tandem with mitochondrial protein depletion and dramatic alterations in biogenesis and dynamics of mitochondria.

The therapeutic potential of the GPR120 agonist TUG-891 was explored. TUG-891 is a more selective and potent agonist for GPR120 than previously used ligands such as α -linolenic acid, GW9508, and NCG21 (702,703). Brown adipocytes differentiated with TUG-891 exhibited increased UCP1 expression at both the gene and protein level in 2D and 3D cellular models. Furthermore, other key brown fat genes, mainly ELOVL3 and PLIN5 were increased with TUG-891 treatment, indicating augmented brown adipocyte activity. These novel results are in line with previous studies that observed positive effects of GPR120 activation on the brown fat phenotype. For instance, stimulation with GW9508, a non-selective GPR120 agonist, upregulated thermogenic genes such as ELOVL3, Dio2 and others in BAT of mice, without changing body weight and food intake (527). In addition, this chapter highlighted TUG-891 was capable of reducing or completely preventing deleterious effects of LPS on key brown adipocytes markers involved in thermogenesis. Its thermogenic protective effects included recovered UCP1, CIDEA, ELOVL3 and PLIN5 gene expression along with clear UCP1 restoration when immunohistochemical stain was used in spheroids.

Furthermore, TUG-891 clearly enhanced the uptake of glucose by brown adipocytes without a major effect on AKT, GLUT1 or GLUT4, which could indicate another mechanism might be involved in this enhanced response to insulin *in vitro*. However,

in cells treated with LPS, TUG-891 improved the insulin response by reversing the LPS-dependent inhibition of AKT and GLUT4. This is an indication that the mechanism underlying improved insulin sensitivity with TUG-891 in LPS treated cells is via the AKT pathway and GLUT4. These insulin sensitizing effects following GPR120 activation were previously described in primary white adipose tissue, 3T3-L1 adipocytes and macrophages through GLUT4 (528,533,704). Also, it was previously reported that ω 3-FAs supplementation with high fat diet (HFD) improved glucose tolerance in WT animals compared to both WT and GPR120ko-animals on HFD alone, whilst ω 3-FAs supplementation did not have an effect in the GPR120ko animals. In light of this current data, it can be speculated that GPR120 activation by ω 3-FAs in these WT animals opposed LPS induced glucose intolerance caused by the HFD and led to this improvement in insulin response (528,533). These studies investigated the insulin response to TUG-891 *in vivo*, and as such this chapter is the first to show this response in isolated brown adipocytes. Collectively, this chapter combined with previous research highlight that activation of GPR120 by TUG-891 inhibits LPS-mediated insulin resistance. It is therefore possible that a wide range of diseases mediated by any number of pathways affected by LPS can be targeted via GPR120 agonists.

Interestingly, this chapter demonstrated that TUG-891 has potent anti-inflammatory effects in brown adipocytes. As expected, it reduced LPS-upregulated gene expression of inflammatory cytokines including IL6 and MCP1. Also, the reduced levels of the phosphorylated forms of both NF κ B and c-Jun protein levels in response to LPS were restored by TUG-891. Strikingly, the expected anti-inflammatory effects of TUG-891 were further supported by the data of proteome cytokines array investigations; TUG-891 not only reduced mature adipocyte basal secretion levels of almost all cytokines involved in immune and inflammatory responses, but also lowered LPS-dependent secretion of many cytokines. Consistently, all the novel cytokines (BAFF, CXCL16, LIX and MMP3) further analysed and demonstrated that concentrations in conditioned media and at the gene expression level were more similar to control cells when using TUG-891 with LPS than using LPS alone. This is in line with the reported effects of docosahexaenoic acid (DHA), an ω -3-FA and agonist GPR120, which abolishes LPS-mediated phosphorylation and activation of I κ B kinase (IKK) and c-Jun N-terminal kinase (JNK) in macrophages; upon GPR120 knockdown, DHA has no effect (533).

This chapter shows that TUG-891 plays an important role in the control of inflammation and subsequent cytokine secretion and raises the possibility that many inflammatory disease states (including obesity, diabetes, cancer and cardiovascular disease) could potentially be attenuated by targeting GPR120 via TUG-891. This is important because low doses of ω 3-FAs are largely clinically ineffective, even in the context of combination therapy (533). Should fish oils prove impractical as therapeutic agents, the identification of the synthetic mimetic TUG-891 as a potent GPR120 ligand by the current study suggests that it could provide the same and greater anti-inflammatory effects, which could be further explored to obtain clinical benefits.

To further elucidate the effects of TUG-891 on brown adipocyte function and the consequence of long term activation of its receptor GPR120, oxygen consumption and mitochondrial activity was assessed. TUG-891 not only induced increased O₂ consumption in brown adipocytes as reported before (524) but also relieved the inhibition of O₂ consumption caused by LPS which has not been reported before this chapter. This is also in line with increased O₂ consumption in mice upon stimulation with GW9508, a non-selective GPR120 agonist (527). This new positive effect of TUG-891 identified by this chapter on the O₂ consumption rate when co-administered with LPS could be due to direct activation of mitochondrial UCP1 in the chronic treatment in addition to activation of GPR120. From previous findings in other cell types; similar to oleate and other long-chain fatty acids (LCFAs), TUG-891 relieves the natural inhibition of UCP1 by GDP (705–707), thereby leading to increased UCP1 activity and uncoupled mitochondrial respiration.

To investigate the mechanism through which TUG-891 signalling could increase brown adipocyte respiration and reverse LPS effects, mitochondrial functions were analysed. Chronic TUG-891 treatment increased mitochondrial membrane potential (MMP) resulting in mitochondrial polarization. Mitochondrial function is directly linked to mitochondrial polarization state. Intact mitochondria are polarized, i.e. they sustain a highly charged membrane potential for full functionality (708,709). Mitochondria were co-stained with the MMP-sensitive MitoTracker CMXRos (MTR) and the MMP-insensitive MitoTracker Green (MTG) (710), and the relative ratio of MTR/MTG was used as a measure of mitochondrial depolarization. TUG-891 stimulation resulted in an increase in the MTR/MTG ratio in LPS-treated brown

adipocytes, which is indicative of enhanced mitochondrial polarization. TUG-891 also improved mitochondrial dynamics including fission and fusion and biogenesis which were reduced by LPS. These results suggest that TUG-891 signalling could recover decreased metabolic activity of brown adipocytes, due to LPS, by stimulation of mitochondrial function.

This study has some limitations, namely, an *in vitro* study design which, though selected because it would minimise interference of confounders, does not necessarily reflect the phenomenon as it would occur *in vivo*. It is noteworthy that the spheroid model used is more representative of the *in vivo* state. However, further research is required to elucidate this interaction, and specifically the relationship between LPS, TUG-891 and brown adipose biology and mitochondria.

In conclusion, this study provides direct, novel evidence, that TUG-891, an agonist of the free FA receptor GPR120, is linked with improved brown adipocyte metabolism, direct stimulation of BAT activity, and insulin sensitizing effects through reversing of gut-derived LPS effects. Its action in this context was mainly through inhibiting LPS-dependent inflammation, which resulted in improved brown adipose thermogenesis indicators and alleviated mitochondrial dysfunction. Further studies are needed to investigate the safety of TUG-891 and the potential of increased BAT activity in humans. Thus it can be anticipated that TUG-891 is a promising therapeutic strategy to increase BAT activity and oppose low grade inflammation, thereby reducing obesity and associated disorders.

Chapter 8. Final Conclusions

The current predictions indicate that the rate of obesity pandemic is going to continue to grow (711). Obesity is associated with various metabolic pathologies and underlie the majority of common causes of illness and death; including T2DM, cancer and cardiovascular disease (712,713). Therefore, the findings of this thesis are valuable for in-depth understanding of the biology of obesity to effectively develop novel treatment strategies and prevention measures. This thesis explored the alterations in characteristic aspects of thermogenesis in murine and human adipocytes following chronic activation by an inflammatory stimulus, LPS, and a treatment considered to reduce inflammation, TUG-891. The *in vitro* and *in vivo* studies in this thesis allowed further understanding of brown adipocyte biology in inflammatory conditions beyond detecting changes in selected markers or solely using one model of adipocytes as in previous studies (344,356). Further experimental research also highlighted the effect of LPS on the browning process of human white adipocytes as well as adipose tissue. In addition, the protective effects of TUG-891 against mitochondrial dysfunction and the suppression of thermogenesis features caused by inflammation were investigated, as well as identifying a potential molecular pathway through which TUG-891 may act. This has direct relevance to the current obesity pandemic (711,714–716) as impaired adipose tissue thermogenesis appears to play a main role in developing obesity (50,52,205,310,323,717).

Reviewing previous studies have highlighted that increased LPS in adiposity may increase pro-inflammatory cytokines in WAT and contribute to the pathogenic risk of obesity associated metabolic disorders (446,447,458–462). So far, few studies have investigated LPS-induced inflammation in BAT, the specialised tissue in energy expenditure, in contrast to WAT, which stores energy. Although there is evidence that LPS-mediated inflammation may negatively impact gene expression of UCP1, the main thermogenic protein, alongside other brown adipocyte genes and mitochondrial respiration in brown adipocytes as well as WAT browning (344,669). However, the chronic effect of LPS on various models of brown adipocytes themselves, the detailed role of TLR4 or the wide spectrum of LPS effects were not addressed before. No study to date has investigated the direct influence of LPS on the browning process of white adipocytes, the induction of UCP1 in WAT, or the associated impact on the production of mitochondria, especially in human adipocytes and tissues (429,669). Also, in humans, these studies were limited in number or looked at mixed gender populations

(429,669). Chapters 3-6 of this thesis therefore shed light on the broader effects of LPS on brown adipocytes and their mitochondria along with the role of TLR4 in mediating LPS actions, highlighting novel factors which may be targeted in order to reduce the inflammation-induced brown adipocyte dysfunction.

Previous reports showed that anti-inflammatory modulators could play an essential role in reducing inflammation-induced brown adipocyte dysfunction, thus promoting metabolic health in obesity and associated disorders (718). However, these studies have not addressed how anti-inflammatory modulators may influence brown adipocyte function. GPR120 was determined as being of particular interest due to its role in controlling brown fat adipogenesis, thermogenesis, stimulating mitochondrial respiration, browning of WAT and improving metabolic health (163,524). As such, GPR120 activation by TUG-891 was investigated in Chapter 7 as a strategy to combat the consequences of inflammation in brown adipocytes. To perform the investigations for this thesis, models of mouse and human cell culture as well as *in vivo* human tissue samples were studied using different analytical laboratory practices.

The initial studies in this thesis investigated the effects of activation of the LPS-TLR4 pathway on thermogenesis related features of brown adipocytes during their differentiation. These studies carried out in 2D cell lines are in accord with prior studies, noting the work presented here also investigated the effects of LPS in 3D spheroids model, as well as TLR4ko.BAT cells. This thesis is the first to study the chronic effect of LPS in 3D spheroids which more closely resemble the complexity of adipose tissue than 2D culture. Thus, 3D spheroids, created by scaffold-free method, are able to illustrate the mechanisms of metabolic disease on a more realistic level (719). These spheroid results confirmed the response to LPS observed in 2D cell culture, providing further evidence that this process is likely to occur *in vivo*. In addition, using murine TLR4ko.BAT cells enabled the exploration of LPS signalling in the absence of the TLR4 receptor in brown adipocytes, which has not been done before. Overall, the data provides direct evidence for TLR4-mediated detrimental downregulation in key brown fat genes involved in thermogenesis under chronic LPS treatment, with striking elimination of LPS actions with TLR4-deletion. As such, modulating TLR4-mediated response to LPS represents an important aspect to study in order to reduce obesity and its associated disorders.

Since it was evident in Chapter 3 that LPS activated the TLR4 pathway and inflammation in brown adipocytes, Chapter 4 of this thesis investigated further the broad extent of LPS effects and how LPS affected pro and anti-inflammatory adipokines release. Brown adipocyte responses to LPS were explored, utilising a comprehensive unbiased RNA-sequence analysis combined with protein secretome assay in order to evaluate the activity of brown adipocytes in the context of inflammation. This approach revealed the capability of brown adipocytes to express and secrete many factors, which has not been reported before this current thesis. Also, a number of novel BAT adipokines were observed to be released in response to LPS, including BAFF, CXCL5, CXCL16 and MMP3. These four cytokines displayed high response to LPS which suggest a prominent role in brown adipocyte dysfunction. Use of the TLR4ko.BAT cells suggested that the induction of these cytokines was mostly mediated by TLR4 pathway. Also, the analysis of the data showed that the development of LPS-induced inflammation can lead to fibrosis and whitening of brown adipocytes with a broad-spectrum of affected pathways including upregulation of ECM components and downregulation of thermogenesis as well as aspects of mitochondrial function. These findings underscore how brown adipocytes themselves act as a secretory endocrine system and are components of the immune response, linking metabolism and immunity by driving systemic chronic inflammation. The identified novel secreted factors may participate in altering insulin signalling and other metabolic processes seen in obesity. As such, these cytokines represent prospective biomarkers to evaluate BAT activity as well as novel therapeutic targets to reduce brown adipocyte dysfunction in conditions that involve increased LPS such as obesity. Hence, interventions in LPS-activated pathways harbour the potential to provide novel strategies to increase BAT activity as a therapeutic target for obesity. However, further studies are required to address the role of these cytokines in brown adipocyte dysfunction as well as the crosstalk with other hormone and insulin signalling pathways. This can be achieved by treating brown adipocytes with each of the identified cytokines and monitoring the changes in brown adipocyte biology. Additional investigations are also invaluable to validate using any of these novel cytokines as indicator of brown adipocytes health in adiposity and related disorders.

In addition, the analysis carried out in Chapter 4 highlighted that various pathways involved in regulating mitochondrial function were disrupted in brown adipocytes

treated with LPS. Given the instrumental role of mitochondria in BAT thermogenesis and metabolic homeostasis (473,654,720–723), this was investigated in more depth in Chapter 5. The effects of pro-inflammatory mediators on mitochondrial function have been studied in various cell types including white adipocytes (724–726), however the relationship in brown adipocytes has up until now remained largely unknown. As such, a number of techniques including ROS assays, Seahorse analysis, confocal imaging and RNA-sequence were used to study the metabolic and dynamic events that occur in brown adipose mitochondria following their differentiation with LPS. Here, this thesis shows for the first time that in brown adipocytes, LPS plays a pivotal role in contributing to mitochondrial dysfunction. This was demonstrated by chronic LPS treatment reducing the ability of mitochondria to compensate for stress, as shown by increased ROS production and downregulation of antioxidant function. In addition, decreased mitochondrial membrane potential, proton leak, and impaired mitochondrial dynamics were observed in cells differentiated with LPS. RNA-sequence analysis revealed that TLR4 appears to mediate most of the LPS-induced mitochondrial dysfunction, at least at a transcriptional level. This is the first time this has been described in brown adipocytes, supporting previous studies that demonstrate the crosstalk between LPS-induced inflammation and mitochondria in brown adipocytes. Collectively, the findings outlined in this chapter highlight the TLR4 pathway as a link between increased LPS levels and impaired functionality of mitochondria in brown adipose tissue, with potential implications for systemic lipid toxicity and metabolic disease. Further investigations into pathways involved in this crosstalk may allow the development of new pharmacological interventions, which could consequently improve cellular and general health in obesity.

As the conducted research in prior chapters in this thesis identified the potent effects of LPS on brown adipocyte biology and mitochondrial function, further analysis was undertaken in chapter 6 to examine the impact of LPS on the browning capacity of white adipocytes and physiologic functions of beige adipocytes. The direct impact of LPS on the production of beige cells and their mitochondrial health was evaluated, utilising *in vitro* mouse and both *in vivo* and *in vitro* human cells from lean and obese primary adipocytes. Expression levels of genes encoding key brown fat markers, mitochondrial fission and fusion, antioxidant defences, and mitochondrial biogenesis were studied. The data showed for the first time in human adipocytes that LPS

perturbed mitochondrial health, exacerbated in conditions of weight gain, which reduced the browning capacity of white adipocytes and the production of functional beige adipocytes. In parallel, human tissue samples from obese subjects, which are known to have increased LPS, displayed reduced expression of BAT markers compared to their lean counterparts. These results are the first to identify a correlation between BAT genes and inflammatory genes across a range of BMIs. This correlation supports the literature speculation that inflammatory genes may be associated with brown gene expression (310,664). These new findings suggest that the previously seen impact of weight loss in enhancing browning of adipocytes is mediated by significantly reduced levels of circulating LPS (208–211,447,727,728). Future investigations into thermogenesis, bioenergetic capacity and ROS production as well as characterisation of adipose tissue morphology on an individual basis, would allow us to examine how closely the gene expression analyses reflect browning capacity and mitochondrial function. It is also important to underline that the adipocytes from obese individuals possessed a lower browning capacity and mitochondrial functionality than those from lean individuals. A possible reason for this could be the increased level of inflammation in obese individuals (662,729). This finding has implications in the search for therapies that induce browning in the adipose tissue of obese individuals, as agents that are known to induce browning in lean individuals may not have the same effect in obese individuals. Also, as the cohort in this thesis included overweight and obese participants, it also permitted for the characterisation of changes of both key brown fat genes and mitochondrial genes during the progression of obesity. However, future studies should investigate this further. Causation research involving longitudinal studies which incorporate participants with a range of BMIs are required to understand how early impairment of browning capacity may develop with weight gain. Moreover, a study considering participants from all BMI weight categories over a longer period of time would indicate whether a decreased browning capacity precedes weight gain and enhances a tendency for gaining weight, or if it is a symptom related to over-nutrition.

This thesis generated murine and human data outlined in Chapter 3-6, revealing the strong negative impact of LPS on brown adipocytes and therefore its potential effect on the progression of obesity. As such, Chapter 7 of this thesis sought to examine specific pharmaceutical agents to ameliorate LPS-induced brown adipocyte

dysfunction. Such pharmaceutical agents may provide substantial clinical benefits given outlook that the alarming rates of obesity are not going to drop. Recent evidence from rodent studies has implicated agonism of the free fatty acid receptor GPR120 in improved metabolic health outcomes through weight loss, improved glucose tolerance, improved mitochondrial function and decreased inflammation (524,526). This thesis is the first to show evidence that in human WAT samples a cross-talk between transcriptional regulation of GPR120 and inflammatory genes, highlighting the relevance of GPR120 as an anti-inflammatory mediator to maintain metabolic homeostasis in humans. Further to this, *in vitro* analysis revealed that GPR120 was downregulated following chronic LPS treatment, suggesting that GPR120 is a beige and BAT specific gene regulated in a similar manner to other brown fat markers such as UCP1. Given these results, the effect of GPR120 agonism, TUG-891, on improving brown adipocyte function by reversing LPS actions was explored in different models of brown adipocytes. The use of TUG-891 throughout differentiation of murine brown adipocytes lessened LPS-induced damage on key features of healthy brown adipocytes, in addition to improving insulin responses and mitochondrial function. Furthermore, the use of TUG-891 to activate GPR120 reversed the secretion of the novel cytokines identified in Chapter 4, in response to chronic LPS treatment. This demonstrates the potential of TUG-891 as a promising therapeutic strategy to prevent LPS-mediated brown adipocyte dysfunction. In order to investigate this further, the role of GPR120 within the mechanism of TUG-891 protection against LPS should be explored with the use of GPR120koBAT cells. In addition, the beneficial mechanism of TUG-891 should be confirmed in humans.

Final Summary

In conclusion, this thesis has provided a better understanding of LPS-induced inflammation on brown adipocyte dysfunction and the browning process, as well as insights into protective effects of anti-inflammatory mediators. This thesis identified novel data, providing evidence for:

1. The suppressive effect of LPS on the thermogenic activity of murine brown adipocytes which appears to operate via TLR-4 mechanism
2. The new pathways activated by LPS that contribute to dysfunction of brown adipocytes and novel LPS-induced secreted cytokines of murine brown adipocytes

3. The LPS-induced mitochondrial dysfunction in murine brown adipocytes mostly mediated via LPS-TLR4 pathway on at least transcriptional level
4. The LPS-dependent inhibition of the browning process and production of beige adipocytes in murine as well as human primary white adipocytes and human WAT
5. TUG-891 therapeutic benefit to mitigate LPS induced BAT dysfunction

As such, the aims set out at the beginning of this thesis have been accomplished and contributions have been made to new areas within the fields of metabolism, adipocyte tissue research and immunology. Collectively, the results suggest that LPS is a potent inhibitor of physiological brown and beige adipocyte function and that targeting LPS may be a viable option to prevent the development of metabolic diseases. In addition, TUG-891 was identified as a potential therapeutic strategy to reverse the effects of LPS. These findings can guide subsequent investigations to develop novel therapeutic strategies to ameliorate LPS induced adipocyte dysfunction, and support to ease the medical and socio-economic burden of human obesity and its complications.

Appendix

Supplementary Table 2.1 Primer Sequences

Primer sequences for mouse genes

Gene	Primer sequence		Product length (bp)
<i>aP2</i>	Forward	5'- ACACCGAGATTTCTTCAAAGTG -3'	88
	Reverse	5'- CCATCTAGGGTTATGATGCTCTTCA -3'	
<i>UCP1</i>	Forward	5'- TACCCAAGCGTACCAAGCTG -3'	97
	Reverse	5'- ACCCGAGTCGCAGAAAAGAA -3'	
<i>CIDEA</i>	Forward	5'- CACGCATTTTCATGATCTTGGA -3'	74
	Reverse	5'- GTTGCTTGCAGACTGGGACAT -3'	
<i>PLIN5</i>	Forward	5'- ATGTCCGGTGATCAGACAGC-3'	82
	Reverse	5'- CCACCACTCGATTCACCACA-3'	
<i>ELOVL3</i>	Forward	5'- GGATGACGCCGTAGTCAGAT-3'	217
	Reverse	5'- GACAGAATGGACGCCAAAGT-3'	
<i>GPR120</i>	Forward	5'- CCCCTCTGCATCTTGTTC -3'	102
	Reverse	5'- GATTTCTCCTATGCGGTTGG -3'	
<i>TLR4</i>	Forward	5'- TCTGGGGAGGCACATCTTCT-3'	110
	Reverse	5'- AGGTCCAAGTTGCCGTTTCT-3'	
<i>MCPI</i>	Forward	5'-CCAATGAGTAGGCTGGAGAGC-3'	119
	Reverse	5'- ACCCATTCCTTCTTGGGGTC-3'	
<i>IL6</i>	Forward	5'-CTCTGGGAAATCGTGGAAAT-3'	134
	Reverse	5'-CCAGTTTGGTAGCATCCATC-3'	
<i>L19</i>	Forward	5'-GAGCACATCCACAAGCTGAA-3'	95
	Reverse	5'-TTTCGTGCTTCCTTGGTCTT-3'	
<i>PGC1α</i>	Forward	5'- GATGGCACGCAGCCCTAT -3'	70
	Reverse	5'- CTCGACACGGAGAGTTAAAGGAA -3'	
<i>Cytochrome c</i>	Forward	5' - CAGCTACCCATGGTCTCATCGT - 3'	70
	Reverse	5' - CTGGAAACCCCTCCGAATG - 3'	
<i>ND1</i>	Forward	5' –ATTTATCTCAACCCTAGCAGAAACAAA- 3'	79
	Reverse	5' – AAACCCTGATACTAATTCTGATTCTCCTT - 3'	
<i>COX4</i>	Forward	5' –CAGCGGTGGCAGAATGTTG- 3'	71
	Reverse	5' –ACACCGAAGTAGAAATGGCTCTCTT- 3'	

<i>ATP8 synthase</i>	Forward Reverse	5' – CAATTATCTCATCAATAATTACCCTATTTATCTTA- 3' 5' –GGTTGTTAGTGATTTTGGTGAAGGT- 3'	98
<i>TFAM</i>	Forward Reverse	5' – CAATTATCTCATCAATAATTACCCTATTTATCTTA- 3' 5' –CCTTTTTTTTCTGCTTCTGGTAGCT- 3'	93
<i>NRF1</i>	Forward Reverse	5' – CGT TTG CTT CGG AAA CTC AGA- 3' 5' –CAA TCG CTT GCT GTC CCA C- 3'	67
<i>PGC1β</i>	Forward Reverse	5' – TGCGGAGACACAGATGAAGA- 3' 5' – GGCTTGTATGGAGGTGTGGT- 3'	182
<i>PRC</i>	Forward Reverse	5' – GGCCCAGCACAGGAAGTAGTC- 3' 5' – CAAGAAAGGAGGCGGAGAGAA- 3'	77
<i>CPT1β</i>	Forward Reverse	5' – ACCACATCCGCCAAGCA- 3' 5' – TTCCTCAGCTGTCTGTCTTGGA- 3'	69
<i>Catalase</i>	Forward Reverse	5' – GCTGAGAAGCCTAAGAACGCAAT- 3' 5' – CCCTTCGCAGCCATGTG- 3'	65
<i>SOD2</i>	Forward Reverse	5' –GAACAATCTCAACGCCACCG- 3' 5' –GCTGAAGAGCGACCTGAGTT- 3'	80
<i>RIP140</i>	Forward Reverse	5' – GAACCTGGGCTTTTGAATGG- 3' 5' – GTTTTGGTCAGTCTTGGAGAGTCTT- 3'	116
<i>GPX3</i>	Forward Reverse	5' -CCGGGGACAAGAGAAGTCTA-3' 5' -TCGATGGTGAGGGCTCCATA-3'	81
<i>PRDX3</i>	Forward Reverse	5' -TCTGCCCAAGGAAAGTCAGC-3' 5' -TAAAATAGGGCGCGTGCTGG-3'	79
<i>soluble Sod1</i>	Forward Reverse	5' -TCCACGTCCATCAGTATGGG-3' 5' -AACATGCCTCTCTTCATCCGC-3'	110
<i>DRP1</i>	Forward Reverse	5' -TCACACCAAAAACAAGCTTTACAC-3' 5' -GGATTGGCTCAGGGCTTACC-3'	100
<i>CS</i>	Forward Reverse	5' -CAACCCGGCTCTTGGGAG-3' 5' -TTCGTGGAAGAAGCACTGGC-3'	76
<i>OPA1</i>	Forward Reverse	5' -TCAGCTGGCAGAAGATCTCA-3' 5' -TGAGCAGGATTTTGACACAGTCT-3'	106
<i>MFN2</i>	Forward Reverse	5' -CCTACATCCAAGAGAGCGCC-3' 5' -GACCTGCTCTTCCGTGGTAA-3'	83
<i>FIS1</i>	Forward Reverse	5' -CAAAGAGGAACAGCGGGACT-3' 5' -ACAGCCCTCGCACATACTTT-3'	95
<i>POLG</i>	Forward	5' -GAGCCCCACTGTAGAATCCG-3'	94

	Reverse	5'-TTGCTGCTTCCCCTGTTCAA-3'	
<i>ND6</i>	Forward	5'-GGATTGGGGTAGCGGCAATA-3'	72
	Reverse	5'-CCGCAAACAAAGATCACCCA-3'	
<i>SDHA</i>	Forward	5'-TGC GGCTTTCAC TTCTCTGT-3'	93
	Reverse	5'-TTCATGATCCACCACTGGGT-3'	
<i>MT-COI</i>	Forward	5'-GACTTGCAACCCTACACGGA-3'	97
	Reverse	5'-CCGGTTAGACCACCAACTGT-3'	
<i>GPX1</i>	Forward	5'-GTGCAATCAGTTCGGACACCA-3'	77
	Reverse	5'-CACCAGGTCGGACGTACTTG-3'	
<i>BAFF</i> (<i>Tnfsf13b</i>)	Forward	5'-CCCAAACACTGCCCAACAA-3'	88
	Reverse	5'-CCCGAGGAATTGCAAGCTGA-3'	
<i>MMP3</i>	Forward	5'-TTCCAGGTGTTGACTCAAGGG-3'	83
	Reverse	5'-TTCCAAGTGC GAAGATCCAC-3'	
<i>CXCL16</i>	Forward	5'-CCAGATACCGCAGGGTACTT-3'	91
	Reverse	5'-GGACTGCAACTGGAACCTGATA-3'	
<i>CXCL5(LIX)</i>	Forward	5'-GCGTTGTGTTTGCTTAACCG-3'	110
	Reverse	5'-GTTTAGCTATGACTTCCACCGT-3'	
<i>GLUT4</i>	Forward	5'- CTATTCAACCAGCATCTTCGAG -3'	140
	Reverse	5'- CTACTAAGAGCACCGAGACC -3'	
<i>GLUT1</i>	Forward	5'- GACGGGCCGCCTCATGTTGG -3'	110
	Reverse	5'- GCTCTCCGTAGCGGTGGTTCC -3'	

Primer sequences for Human genes

Gene	Primer sequence		Product length (bp)
<i>L19</i>	Forward Reverse	5'- GCGGAAGGGTACAGCCAA-3' 5'- GCAGCCGCGCAGAAA-3'	77
<i>UCP1</i>	Forward Reverse	5'- GTGTGCCCAACTGTGCAATG-3' 5'- CCAGGATCCAAGTCGCAAGA-3'	95
<i>CIDEA</i>	Forward Reverse	5'- CATGTATGAGATGTACTCCGTGTC-3' 5'- GAGTAGGACAGGAACCGCAG-3'	90
<i>PLIN5</i>	Forward Reverse	5'- GTGGATCACTTCCTGCCCAT-3' 5'- CTCCTCTGATCCTCCACCGA-3'	95
<i>ELOVL3</i>	Forward Reverse	5'- AAGGAACGCAAGGGCTTCAA-3' 5'- TGCCCCCAGGATACTGAAGA-3'	81
<i>SLC27A2</i>	Forward Reverse	5'- AAGGCCCGGTTTCTAAGAA-3' 5'- TTAAAGCCCTCCTCCACCAG-3'	90
<i>aP2</i>	Forward Reverse	5'- TGTTGCAGAAATGGGATGGAAA-3' 5'- CAACGTTCCCTTGGCTTATGCT-3'	134
<i>MCPI</i>	Forward Reverse	5'-CAGCAGCAAGTGTCCCAAAG-3' 5'-GAATCCTGAACCCACTTCTGCTT-3'	93
<i>IL6</i>	Forward Reverse	5'- AGTAGTGAGGAACAAGCCAGA-3' 5'- GTCAGGGGTGGTTATTGCATC-3'	102
<i>TNFα</i>	Forward Reverse	5'- GCTGCACTTTGGAGTGATCG-3' 5'- GTCACTCGGGGTTCGAGAAG-3'	109
<i>IL1β</i>	Forward Reverse	5'- CGCCAGTGAAATGATGGCT-3' 5'- GAGGGCAGAGGTCCAGGTC-3'	110
<i>GPR120 A2</i>	Forward Reverse	5'- CCAAAATTTTACAGATCACAAAGGC-3' 5'- ATCTGGTGGCTCTCCGAGT-3'	76
<i>CS</i>	Forward Reverse	5'- CAGGGTATCAGCCGAACCA -3' 5'- TTGCTGCAACACAAGGTAGC-3'	85
<i>CPT1β</i>	Forward Reverse	5'- AGGAGCCCTCTCATGGTGAA-3' 5'- TGGCGTGGATGATGTTTCCC-3'	103
<i>PGC1α</i>	Forward Reverse	5'- TGAAGAGCGCCGTGTGATT-3' 5'- CAGTTCTGTCCGTGTTGTGTCA-3'	61

<i>FIS1</i>	Forward Reverse	5'- AAGACGTAATCCCGCTGTTCC-3' 5'- TGACATCCGTAAAGGCATCG-3'	78
<i>DRP1</i>	Forward Reverse	5'- TGTCTTCTTCGTAAAAGGTTGCC-3' 5'- ACAAGCATCAGCAAAGTCTGG-3'	108
<i>MFN2</i>	Forward Reverse	5'- GCAGCTTGTCATCAGCTACAC-3' 5'- ATGAGCAAAGGTCCCAGACAG-3'	76
<i>OPA1</i>	Forward Reverse	5'- AGGGAACAGCTCTGAAAGCAT-3' 5'- TCACTTGGTGTGCCTTTAGCA-3'	104
<i>NRF1</i>	Forward Reverse	5'- TGGTCATCTCACCTCCCTGT-3' 5'- GAATGCCAACCACGGTCA-3'	102
<i>TFAM</i>	Forward Reverse	5'- ACCCATATTTAAAGCTCAGAACCC-3' 5'- CCAACGCTGGGCAATTCTTC-3'	70
<i>COX4I1</i>	Forward Reverse	5'- ACCTCTGTGTGTGTACGAGC-3' 5'- ACGCCGATCCATATAAGCTGG-3'	78
<i>catalase</i>	Forward Reverse	5'- CTTCGACCCAAGCAACATGC-3' 5'- CGGTGAGTGTGAGGATAGGC-3'	90
<i>SOD2</i>	Forward Reverse	5'- CGTCACCGAGGAGAAGTACC-3' 5'- TTCAGTGCAGGCTGAAGAGC-3'	78
<i>POLG</i>	Forward Reverse	5'- GCCTTGCAGATCACCAACCT-3' 5'- TGGGGCAAGTCATTGAGACC-3'	71

Supplementary Table 4.1: RNA Integrity Number (RIN) and 28s/18s rRNA Ratio of the Samples Used in RNA-sequence Analysis

Sample ID	RIN	28s/18s rRNA ratio
wt.BAT CTRL1	8.10	1.3
wt.BAT CTRL2	7.90	1.2
wt.BAT CTRL3	7.60	1.3
wt.BAT LPS1	9.20	1.3
wt.BAT LPS2	9.10	1.5
wt.BAT LPS3	9.20	1.4
TLR4ko.BAT CTRL1	9.10	1.7
TLR4ko.BAT CTRL2	9	1.7
TLR4ko.BAT CTRL3	9.40	1.6
TLR4ko.BAT LPS1	9.20	2.1
TLR4ko.BAT LPS2	8.50	1.7
TLR4ko.BAT LPS3	9.20	2.1

Supplementary Table 4.2 wt.BAT Top 50 Up-Regulated and Down-Regulated Genes in Response to LPS

Symbol	EnsemblID	Full Gene Title	log2FoldChange	Padj
Cxcl5	ENSMUSG000000029371	chemokine (C-X-C motif) ligand 5(Cxcl5)	10.26	4.21E-109
Mmp3	ENSMUSG000000043613	matrix metalloproteinase 3(Mmp3)	8.62	5.25E-12
Saa3	ENSMUSG000000040026	serum amyloid A 3(Saa3)	8.00	0
Lgi2	ENSMUSG000000039252	leucine-rich repeat LGI family, member 2(Lgi2)	7.72	0
Mmp9	ENSMUSG000000017737	matrix metalloproteinase 9(Mmp9)	7.55	4.45E-09
Nat8	ENSMUSG000000030004	N-acetyltransferase 8 (GCN5-related)(Nat8)	7.53	1.81E-08
Serpib2	ENSMUSG000000062345	serine (or cysteine) peptidase inhibitor, clade B, member 2(Serpib2)	7.52	1.79E-39
Serpina3i	ENSMUSG000000079014	serine (or cysteine) peptidase inhibitor, clade A, member 3I(Serpina3i)	7.45	3.62E-17
Nos2	ENSMUSG000000020826	nitric oxide synthase 2, inducible(Nos2)	7.23	3.94E-36
Spon1	ENSMUSG000000038156	spondin 1, (f-spondin) extracellular matrix protein(Spon1)	7.18	6.91E-80
Npy1r	ENSMUSG000000036437	neuropeptide Y receptor Y1(Npy1r)	6.78	2.13E-22
Nat8f5	ENSMUSG000000079494	N-acetyltransferase 8 (GCN5-related) family member 5(Nat8f5)	6.66	4.25E-06
Chl1	ENSMUSG000000030077	cell adhesion molecule L1-like(Chl1)	6.53	8.58E-06
Tnfrsf11	ENSMUSG000000022015	tumor necrosis factor (ligand) superfamily, member 11(Tnfrsf11)	6.35	1.18E-48
Csmd1	ENSMUSG000000060924	CUB and Sushi multiple domains 1(Csmd1)	6.19	6.6E-39
Clstn2	ENSMUSG000000032452	calyculin 2(Clstn2)	6.16	0.000055
Lcn2	ENSMUSG000000026822	lipocalin 2(Lcn2)	6.15	0
Camp	ENSMUSG000000038357	cathelicidin antimicrobial peptide(Camp)	6.12	1.26E-07
Nat8f3	ENSMUSG000000051262	N-acetyltransferase 8 (GCN5-related) family member 3(Nat8f3)	6.07	9.95E-11
Slpi	ENSMUSG000000017002	secretory leukocyte peptidase inhibitor(Slpi)	6.05	8.27E-10
Ecscr	ENSMUSG000000073599	endothelial cell surface expressed chemotaxis and apoptosis regulator(Ecscr)	5.99	0.0000248
Gm11476	ENSMUSG000000085596	predicted gene 11476(Gm11476)	5.94	0.0000297
Pi16	ENSMUSG000000024011	peptidase inhibitor 16(Pi16)	5.92	0.000035
Fndc1	ENSMUSG000000071984	fibronectin type III domain containing 1(Fndc1)	5.91	3.11E-201
Adamts3	ENSMUSG000000043635	a disintegrin-like and metalloproteinase (reprolysin type) with thrombospondin type 1 motif, 3(Adamts3)	5.89	4.66E-10
Dcn	ENSMUSG000000019929	decorin(Dcn)	5.89	0

Cxcl1	ENSMUSG00000029380	chemokine (C-X-C motif) ligand 1(Cxcl1)	5.72	0
Cd38	ENSMUSG00000029084	CD38 antigen(Cd38)	5.69	4.94E-06
Wfdc17	ENSMUSG00000069792	WAP four-disulfide core domain 17(Wfdc17)	5.69	0.0000815
Il12a	ENSMUSG00000027776	interleukin 12a(Il12a)	5.66	0.0005639
Mgam	ENSMUSG00000068587	maltase-glucoamylase(Mgam)	5.62	6.38E-09
Nlrp2	ENSMUSG00000035177	NLR family, pyrin domain containing 2(Nlrp2)	5.59	0.0010793
Bdkrb1	ENSMUSG00000041347	bradykinin receptor, beta 1(Bdkrb1)	5.53	0.2474558
Gm16998	ENSMUSG00000097069	predicted gene, 16998(Gm16998)	5.46	0.0014086
Clec2g	ENSMUSG00000000248	C-type lectin domain family 2, member g(Clec2g)	5.37	4.88E-08
A2m	ENSMUSG00000030111	alpha-2-macroglobulin(A2m)	5.20	2.46E-07
Serpina3g	ENSMUSG00000041481	Serine protease inhibitor A3G	5.13	1.31E-38
Lif	ENSMUSG00000034394	leukemia inhibitory factor(Lif)	5.09	6.26E-42
Adamdec1	ENSMUSG00000022057	ADAM-like, decysin 1(Adamdec1)	5.05	0.0000706
Ccl11	ENSMUSG00000020676	chemokine (C-C motif) ligand 11(Ccl11)	5.00	5.5E-17
Galnt16	ENSMUSG00000021130	UDP-N-acetyl-alpha-D-galactosamine:polypeptide acetylgalactosaminyltransferase 16(Galnt16)	N- 4.98	1.55E-29
Spns2	ENSMUSG00000040447	spinster homolog 2(Spns2)	4.89	9.92E-48
Vstm2a	ENSMUSG00000048834	V-set and transmembrane domain containing 2A(Vstm2a)	4.78	6.37E-77
Mctp2	ENSMUSG00000032776	multiple C2 domains, transmembrane 2(Mctp2)	4.77	4.04E-29
4931431B13Rik	ENSMUSG000000108354	RIKEN cDNA 4931431B13 gene(4931431B13Rik)	4.73	5.54E-29
Cyp7b1	ENSMUSG00000039519	cytochrome P450, family 7, subfamily b, polypeptide 1(Cyp7b1)	4.70	1.28E-58
Cd55	ENSMUSG00000026399	CD55 molecule, decay accelerating factor for complement(Cd55)	4.68	0.0004955
Clec14a	ENSMUSG00000045930	C-type lectin domain family 14, member a(Clec14a)	4.63	1.08E-08
Agtr1a	ENSMUSG00000049115	angiotensin II receptor, type 1a(Agtr1a)	4.62	3.32E-48
Ccr12	ENSMUSG00000043953	chemokine (C-C motif) receptor-like 2(Ccr12)	-3.16	1.82E-19
Esm1	ENSMUSG00000042379	endothelial cell-specific molecule 1(Esm1)	-3.19	9.96E-06
Tnr	ENSMUSG00000015829	tenascin R(Tnr)	-3.20	0.0138428
Mpeg1	ENSMUSG00000046805	macrophage expressed gene 1(Mpeg1)	-3.26	0
Mmd2	ENSMUSG00000039533	monocyte to macrophage differentiation-associated 2(Mmd2)	-3.26	0.0002624
Phf11a	ENSMUSG00000044703	PHD finger protein 11A(Phf11a)	-3.28	3.12E-39

Misp	ENSMUSG00000035852	mitotic spindle positioning(Misp)	-3.29	6.31E-13
Trim66	ENSMUSG00000031026	tripartite motif-containing 66(Trim66)	-3.29	5.66E-44
Slc22a12	ENSMUSG00000061742	solute carrier family 22 (organic anion/cation transporter), member 12(Slc22a12)	-3.32	8.96E-09
1700047G03Rik	ENSMUSG00000099349	RIKEN cDNA 1700047G03 gene(1700047G03Rik)	-3.36	0.0416131
Rgs9bp	ENSMUSG00000056043	regulator of G-protein signalling 9 binding protein(Rgs9bp)	-3.37	0.0354142
Lmo7	ENSMUSG00000033060	LIM domain only 7(Lmo7)	-3.39	6.09E-11
Coro6	ENSMUSG00000020836	coronin 6(Coro6)	-3.41	5.47E-23
Ifit2	ENSMUSG00000045932	interferon-induced protein with tetratricopeptide repeats 2(Ifit2)	-3.45	0
Acot11	ENSMUSG00000034853	acyl-CoA thioesterase 11(Acot11)	-3.62	1.99E-43
Heatr9	ENSMUSG00000018925	HEAT repeat containing 9(Heatr9)	-3.64	0.0004891
Kif19a	ENSMUSG00000010021	kinesin family member 19A(Kif19a)	-3.73	0.0174269
Gm17757	ENSMUSG00000099241	GTPase, very large interferon inducible 1 pseudogene(Gm17757)	-3.79	0.0102869
Gm11967	ENSMUSG00000084819	predicted gene 11967(Gm11967)	-3.80	0.0015263
Gabbr2	ENSMUSG00000039809	gamma-aminobutyric acid (GABA) B receptor, 2(Gabbr2)	-3.81	9.55E-08
Gm5431	ENSMUSG00000058163	predicted gene 5431(Gm5431)	-3.82	3.64E-41
Pstpip1	ENSMUSG00000032322	proline-serine-threonine phosphatase-interacting protein 1(Pstpip1)	-3.95	0.0055912
Gm13293	ENSMUSG00000086006	predicted gene 13293(Gm13293)	-3.99	0.0063796
Shisa8	ENSMUSG00000096883	shisa family member 8(Shisa8)	-4.01	3.97E-06
Serpib9f	ENSMUSG00000038327	serine (or cysteine) peptidase inhibitor, clade B, member 9f(Serpib9f)	-4.07	0.0038369
Lncenc1	ENSMUSG00000078952	long non-coding RNA, embryonic stem cells expressed 1(Lncenc1)	-4.08	0.0215485
Aspg	ENSMUSG00000037686	asparaginase(Aspg)	-4.12	0
Cbfa2t3	ENSMUSG00000006362	core-binding factor, runt domain, alpha subunit 2, translocated to, 3 (human)(Cbfa2t3)	-4.21	0.0150364
Pou3f1	ENSMUSG00000090125	POU domain, class 3, transcription factor 1(Pou3f1)	-4.21	0.0156682
Rn7sk	ENSMUSG00000065037	RNA, 7SK, nuclear(Rn7sk)	-4.33	7.26E-33
Slc22a14	ENSMUSG00000070280	solute carrier family 22 (organic cation transporter), member 14(Slc22a14)	-4.37	0.010842
Ifi209	ENSMUSG00000043263	interferon activated gene 209(Ifi209)	-4.46	1.82E-209
AA467197	ENSMUSG00000033213	expressed sequence AA467197(AA467197)	-4.50	0.0062224
Tgtp1	ENSMUSG00000078922	T cell specific GTPase 1(Tgtp1)	-4.51	2.26E-190
2310015D24Rik	ENSMUSG00000099411	RIKEN cDNA 2310015D24 gene(2310015D24Rik)	-4.78	2.91E-06

Pycard	ENSMUSG00000030793	PYD and CARD domain containing(Pycard)	-4.89	0.0015631
Ptch2	ENSMUSG00000028681	patched 2(Ptch2)	-4.94	1.93E-22
Ptpn22	ENSMUSG00000027843	protein tyrosine phosphatase, non-receptor type 22 (lymphoid)(Ptpn22)	-5.11	0.0055038
Slc40a1	ENSMUSG00000025993	solute carrier family 40 (iron-regulated transporter), member 1(Slc40a1)	-5.11	1.52E-48
Akr1b7	ENSMUSG00000052131	aldo-keto reductase family 1, member B7(Akr1b7)	-5.16	0.002958
Slco4a1	ENSMUSG00000038963	solute carrier organic anion transporter family, member 4a1(Slco4a1)	-5.19	0.2736572
Cngb3	ENSMUSG00000056494	cyclic nucleotide gated channel beta 3(Cngb3)	-5.19	2.06E-16
Hspa1a	ENSMUSG000000091971	heat shock protein 1A(Hspa1a)	-5.37	0
Nptx1	ENSMUSG00000025582	neuronal pentraxin 1(Nptx1)	-5.52	3.65E-06
Itgbl1	ENSMUSG00000032925	integrin, beta-like 1(Itgbl1)	-5.68	0.0000621
Ucp1	ENSMUSG00000031710	uncoupling protein 1 (mitochondrial, proton carrier)(Ucp1)	-5.83	3.35E-69
Rpph1	ENSMUSG00000092837	ribonuclease P RNA component H1(Rpph1)	-6.39	2.75E-06
Depp1	ENSMUSG00000048489	RIKEN cDNA 8430408G22 gene(8430408G22Rik)	-6.58	5.86E-09
Hamp2	ENSMUSG00000056978	hepcidin antimicrobial peptide 2(Hamp2)	-6.66	3.51E-06
Rmrp	ENSMUSG00000088088	RNA component of mitochondrial RNAase P(Rmrp)	-8.66	3.49E-12

Supplementary Table 4.3 TLR4ko.BAT Top 50 Up-Regulated and Down-Regulated Genes in Response to LPS

Symbol	EnsemblID	Full Gene Title	log2FoldChange	Padj
Smtnl2	ENSMUSG000000045667	smoothelin-like 2(Smtnl2)	1.10	0.000477625
Reep1	ENSMUSG000000052852	receptor accessory protein 1(Reep1)	0.96	0.0086887
Eno2	ENSMUSG000000004267	enolase 2, gamma neuronal(Eno2)	0.95	2.24871E-25
Nos2	ENSMUSG000000020826	nitric oxide synthase 2, inducible(Nos2)	0.93	7.39376E-35
Nptx1	ENSMUSG000000025582	neuronal pentraxin 1(Nptx1)	0.91	0.001556311
Fads6	ENSMUSG000000044788	fatty acid desaturase domain family, member 6(Fads6)	0.89	0.005687121
Cda	ENSMUSG000000028755	cytidine deaminase(Cda)	0.84	0.007741615
Sema3g	ENSMUSG000000021904	sema domain, immunoglobulin domain (Ig), short basic domain, secreted, (semaphorin) 3G(Sema3g)	0.83	7.35075E-40
Ddit4	ENSMUSG000000020108	DNA-damage-inducible transcript 4(Ddit4)	0.81	1.54453E-05
Depp1	ENSMUSG000000048489	RIKEN cDNA 8430408G22 gene(8430408G22Rik)	0.81	6.06471E-06
Peg10	ENSMUSG000000092035	paternally expressed 10(Peg10)	0.78	5.13538E-09
Ptgs2	ENSMUSG000000032487	prostaglandin-endoperoxide synthase 2(Ptgs2)	0.77	1.12308E-14
Wt1	ENSMUSG000000016458	Wilms tumor 1 homolog(Wt1)	0.76	0.036492313
Ankrd37	ENSMUSG000000050914	ankyrin repeat domain 37(Ankrd37)	0.76	0.000756988
Prelid2	ENSMUSG000000056671	PRELI domain containing 2(Prelid2)	0.75	0.014083621
Kcne4	ENSMUSG000000047330	potassium voltage-gated channel, Isk-related subfamily, gene 4(Kcne4)	0.75	0.001186705
Cacna1g	ENSMUSG000000020866	calcium channel, voltage-dependent, T type, alpha 1G subunit(Cacna1g)	0.75	0.01136443
Ndrp1	ENSMUSG000000005125	N-myc downstream regulated gene 1(Ndrp1)	0.73	1.09619E-40
Cox4i2	ENSMUSG000000009876	cytochrome c oxidase subunit IV isoform 2(Cox4i2)	0.72	0.002871741
Ier3	ENSMUSG000000003541	immediate early response 3(Ier3)	0.72	6.96494E-18
Asap3	ENSMUSG000000036995	ArfGAP with SH3 domain, ankyrin repeat and PH domain 3(Asap3)	0.72	0.001244513
Egl3	ENSMUSG000000035105	egl-9 family hypoxia-inducible factor 3(Egl3)	0.68	2.99036E-74
Selenbp2	ENSMUSG000000068877	selenium binding protein 2(Selenbp2)	0.68	0.001053065
Tppp	ENSMUSG000000021573	tubulin polymerization promoting protein(Tppp)	0.66	0.021491241
Pafah1b3	ENSMUSG000000005447	platelet-activating factor acetylhydrolase, isoform 1b, subunit 3(Pafah1b3)	0.66	0.007736998
Kcnb1	ENSMUSG000000050556	potassium voltage gated channel, Shab-related subfamily, member 1(Kcnb1)	0.64	1.36837E-09

Smad7	ENSMUSG00000025880	SMAD family member 7(Smad7)	0.64	1.69268E-07
Selenbp1	ENSMUSG00000068874	selenium binding protein 1(Selenbp1)	0.63	2.42532E-30
Ptp4a3	ENSMUSG00000059895	protein tyrosine phosphatase 4a3(Ptp4a3)	0.63	1.81658E-15
Slc25a34	ENSMUSG00000040740	solute carrier family 25, member 34(Slc25a34)	0.63	1.3725E-14
Nt5e	ENSMUSG00000032420	5' nucleotidase, ecto(Nt5e)	0.62	3.17624E-07
Ano1	ENSMUSG00000031075	anoctamin 1, calcium activated chloride channel(Ano1)	0.62	9.92744E-07
H2-Q7	ENSMUSG00000060550	histocompatibility 2, Q region locus 7(H2-Q7)	0.61	0.024665881
Rcor2	ENSMUSG00000024968	REST corepressor 2(Rcor2)	0.60	0.000139115
Ffar4	ENSMUSG00000054200	free fatty acid receptor 4(Ffar4)	0.58	1.9457E-11
Ablim2	ENSMUSG00000029095	actin-binding LIM protein 2(Ablim2)	0.58	0.000618033
Rassf6	ENSMUSG00000029370	Ras association (RalGDS/AF-6) domain family member 6(Rassf6)	0.56	0.040743571
Fndc1	ENSMUSG00000071984	fibronectin type III domain containing 1(Fndc1)	0.55	5.45979E-14
Gja1	ENSMUSG00000050953	gap junction protein, alpha 1(Gja1)	0.54	1.04827E-08
0610040F04Rik	ENSMUSG00000087341	RIKEN cDNA 0610040F04 gene(0610040F04Rik)	0.54	0.000228934
Epm2a	ENSMUSG00000055493	epilepsy, progressive myoclonic epilepsy, type 2 gene alpha(Epm2a)	0.53	0.030847481
Nxph4	ENSMUSG00000040258	neurexophilin 4(Nxph4)	0.52	0.001588004
Uaca	ENSMUSG00000034485	uveal autoantigen with coiled-coil domains and ankyrin repeats(Uaca)	0.52	1.36993E-05
Aatk	ENSMUSG00000025375	apoptosis-associated tyrosine kinase(Aatk)	0.52	0.029953321
Ak4	ENSMUSG00000028527	adenylate kinase 4(Ak4)	0.51	1.00772E-13
Ppp1r3c	ENSMUSG00000067279	protein phosphatase 1, regulatory (inhibitor) subunit 3C(Ppp1r3c)	0.51	2.68786E-10
Aspg	ENSMUSG00000037686	asparaginase(Aspg)	0.50	3.45579E-07
Ntsr2	ENSMUSG00000020591	neurotensin receptor 2(Ntsr2)	0.50	0.033676204
Loxl2	ENSMUSG00000034205	lysyl oxidase-like 2(Loxl2)	0.50	5.22934E-23
Abcc4	ENSMUSG00000032849	ATP-binding cassette, sub-family C (CFTR/MRP), member 4(Abcc4)	-0.36	3.28334E-06
Ifi202b	ENSMUSG00000026535	interferon activated gene 202B(Ifi202b)	-0.37	6.29452E-09
1810014B01Rik	ENSMUSG00000097412	#N/A	-0.37	1.20912E-16
Hcar2	ENSMUSG00000045502	hydroxycarboxylic acid receptor 2(Hcar2)	-0.37	0.045408051
Pthr2	ENSMUSG00000072582	peptidyl-tRNA hydrolase 2(Pthr2)	-0.37	0.013705007
Pdia3	ENSMUSG00000027248	protein disulfide isomerase associated 3(Pdia3)	-0.38	3.14675E-22
ND2	ENSMUSG00000064345	NADH dehydrogenase subunit 2(ND2)	-0.39	0.010720021

Spp1	ENSMUSG00000029304	secreted phosphoprotein 1(Spp1)	-0.40	0.000148989
Samd9l	ENSMUSG00000047735	sterile alpha motif domain containing 9-like(Samd9l)	-0.40	1.1278E-07
Car6	ENSMUSG00000028972	carbonic anhydrase 6(Car6)	-0.40	0.033816653
Calhm6	ENSMUSG00000046031	family with sequence similarity 26, member F(Fam26f)	-0.40	0.031519832
Xaf1	ENSMUSG00000040483	XIAP associated factor 1(Xaf1)	-0.43	4.23955E-05
Irgm2	ENSMUSG00000069874	immunity-related GTPase family M member 2(Irgm2)	-0.43	3.74228E-09
ND4	ENSMUSG00000064363	NADH dehydrogenase subunit 4(ND4)	-0.43	0.021622309
Ccl9	ENSMUSG00000019122	chemokine (C-C motif) ligand 9(Ccl9)	-0.44	3.0759E-07
Nucb2	ENSMUSG00000030659	nucleobindin 2(Nucb2)	-0.45	8.1322E-10
Ifit3	ENSMUSG00000074896	interferon-induced protein with tetratricopeptide repeats 3(Ifit3)	-0.47	1.95739E-10
Dhx58	ENSMUSG00000017830	DEXH (Asp-Glu-X-His) box polypeptide 58(Dhx58)	-0.47	3.77128E-05
Ifit1	ENSMUSG00000034459	interferon-induced protein with tetratricopeptide repeats 1(Ifit1)	-0.48	4.3021E-14
Gbp11	ENSMUSG00000092021	guanylate binding protein 11(Gbp11)	-0.49	0.000139115
Ly6e	ENSMUSG00000022587	lymphocyte antigen 6 complex, locus E(Ly6e)	-0.49	7.14391E-27
Ifitm3	ENSMUSG00000025492	interferon induced transmembrane protein 3(Ifitm3)	-0.50	6.06067E-05
Oasl2	ENSMUSG00000029561	2'-5' oligoadenylate synthetase-like 2(Oasl2)	-0.50	2.99381E-13
Irf7	ENSMUSG00000025498	interferon regulatory factor 7(Irf7)	-0.50	1.91164E-10
Phf11d	ENSMUSG00000068245	PHD finger protein 11D(Phf11d)	-0.51	1.07439E-06
Sfxn2	ENSMUSG00000025036	sideroflexin 2(Sfxn2)	-0.51	0.002871741
Rsad2	ENSMUSG00000020641	radical S-adenosyl methionine domain containing 2(Rsad2)	-0.52	0.018073136
Gbp3	ENSMUSG00000028268	guanylate binding protein 3(Gbp3)	-0.52	1.33548E-09
Ifi44	ENSMUSG00000028037	interferon-induced protein 44(Ifi44)	-0.52	1.3925E-06
Igtp	ENSMUSG00000078853	interferon gamma induced GTPase(Igtp)	-0.53	1.66093E-08
COX2	ENSMUSG00000064354	cytochrome c oxidase subunit II(COX2)	-0.54	0.002135606
Zbp1	ENSMUSG00000027514	Z-DNA binding protein 1(Zbp1)	-0.54	5.07275E-08
Plscr2	ENSMUSG00000032372	phospholipid scramblase 2(Plscr2)	-0.55	0.001727827
COX3	ENSMUSG00000064358	cytochrome c oxidase subunit III(COX3)	-0.57	0.008277581
Iigp1	ENSMUSG00000054072	interferon inducible GTPase 1(Iigp1)	-0.57	9.17617E-16
Gm4951	ENSMUSG00000073555	predicted gene 4951(Gm4951)	-0.57	9.79837E-05
Hmga2	ENSMUSG00000056758	high mobility group AT-hook 2(Hmga2)	-0.58	0.000559895

Derl3	ENSMUSG00000009092	Der1-like domain family, member 3(Derl3)	-0.58	1.52356E-06
Fam166a	ENSMUSG00000026969	family with sequence similarity 166, member A(Fam166a)	-0.58	0.029139402
Tmem88	ENSMUSG00000045377	transmembrane protein 88(Tmem88)	-0.59	0.00619638
Ifit3b	ENSMUSG00000062488	interferon-induced protein with tetratricopeptide repeats 3B(Ifit3b)	-0.63	5.7009E-10
Rtp4	ENSMUSG00000033355	receptor transporter protein 4(Rtp4)	-0.64	8.23142E-17
Apol9a	ENSMUSG00000057346	apolipoprotein L 9a(Apol9a)	-0.70	0.000558274
Cxcl9	ENSMUSG00000029417	chemokine (C-X-C motif) ligand 9(Cxcl9)	-0.71	2.19361E-15
ATP6	ENSMUSG00000064357	ATP synthase F0 subunit 6(ATP6)	-0.71	2.90293E-06
F5	ENSMUSG00000026579	coagulation factor V(F5)	-0.75	0.027231346
Mgp	ENSMUSG00000030218	matrix Gla protein(Mgp)	-0.81	0.01522529
Sp110	ENSMUSG00000070034	Sp110 nuclear body protein(Sp110)	-0.82	0.021313948
Apol9b	ENSMUSG00000068246	apolipoprotein L 9b(Apol9b)	-0.89	2.99946E-05
Cd74	ENSMUSG00000024610	CD74 antigen (invariant polypeptide of major histocompatibility complex, class II antigen-associated)(Cd74)	-1.09	0.001525062

Supplementary Table 4.4 GO Enrichment Analyses Summarized Using REVIGO
Derived from Up-Regulated Genes in wt.BAT

WT.BATBP GO associated TOP 500 UP REGULATED

term ID	description	frequency	pin?	log ₁₀ p-value	uniqueness	dispensability
GO:0001666	response to hypoxia	0.049 %		-3.8570	0.81	0.00
GO:0006024	glycosaminoglycan biosynthetic process	0.559 %		-3.1035	0.95	0.00
GO:0007155	cell adhesion	0.544 %		-11.5702	0.85	0.00
GO:0033627	cell adhesion mediated by integrin	0.013 %	✖	-1.5165	0.87	0.73
GO:0010811	positive regulation of cell-substrate adhesion	0.021 %	✖	-2.8983	0.64	0.89
GO:0034446	substrate adhesion-dependent cell spreading	0.018 %	✖	-1.5008	0.60	0.88
GO:0007160	cell-matrix adhesion	0.051 %	✖	-3.0964	0.84	0.81
GO:0030198	extracellular matrix organization	0.060 %		-7.8268	0.83	0.00
GO:0030199	collagen fibril organization	0.009 %	✖	-5.8665	0.83	0.88
GO:0001525	angiogenesis	0.096 %		-6.3830	0.63	0.06
GO:0045766	positive regulation of angiogenesis	0.023 %	✖	-2.1740	0.50	0.88
GO:0016525	negative regulation of angiogenesis	0.020 %	✖	-1.4923	0.58	0.90
GO:0001568	blood vessel development	0.136 %	✖	-4.0438	0.64	0.96
GO:0055114	oxidation-reduction process	15.060 %		-2.7715	0.87	0.09
GO:0030335	positive regulation of cell migration	0.076 %		-6.3307	0.59	0.13
GO:0014911	positive regulation of smooth muscle cell migration	0.003 %	✖	-2.2565	0.64	0.82
GO:0060326	cell chemotaxis	0.060 %	✖	-3.0964	0.58	0.80
GO:0006935	chemotaxis	0.475 %	✖	-2.2475	0.63	0.83
GO:0016477	cell migration	0.293 %	✖	-3.8069	0.76	0.77
GO:0031623	receptor internalization	0.016 %		-1.5008	0.85	0.17
GO:0055072	iron ion homeostasis	0.141 %		-1.4239	0.85	0.18
GO:0071347	cellular response to interleukin-1	0.014 %		-3.7305	0.69	0.22
GO:0071356	cellular response to tumor necrosis factor	0.029 %	✖	-3.1018	0.68	0.79
GO:0034612	response to tumor necrosis factor	0.032 %	✖	-1.5730	0.70	0.82
GO:0019221	cytokine-mediated signaling pathway	0.093 %	✖	-1.5667	0.56	0.89
GO:0070208	protein heterotrimerization	0.003 %		-2.0563	0.91	0.27
GO:0042060	wound healing	0.094 %		-3.7328	0.82	0.40
GO:0034383	low-density lipoprotein particle clearance	0.004 %		-2.4873	0.71	0.46
GO:0042493	response to drug	0.266 %		-1.5016	0.73	0.46
GO:0010575	positive regulation of vascular endothelial growth factor production	0.005 %		-1.6365	0.60	0.47
GO:0043589	skin morphogenesis	0.002 %		-1.9719	0.72	0.48
GO:0007568	aging	0.088 %		-1.8923	0.74	0.50
GO:0031100	animal organ regeneration	0.005 %		-2.0811	0.71	0.51
GO:0051897	positive regulation of protein kinase B signaling	0.016 %		-1.3258	0.60	0.51
GO:0071549	cellular response to dexamethasone stimulus	0.003 %		-1.6233	0.71	0.52
GO:0051384	response to glucocorticoid	0.012 %	✖	-1.4313	0.72	0.93
GO:0001649	osteoblast differentiation	0.040 %		-1.9025	0.66	0.53
GO:0050731	positive regulation of peptidyl-tyrosine phosphorylation	0.032 %		-3.9914	0.70	0.54
GO:0070374	positive regulation of ERK1 and ERK2 cascade	0.034 %	✖	-2.0116	0.55	0.76
GO:0010886	positive regulation of cholesterol storage	0.002 %		-1.4914	0.74	0.54
GO:0010886	positive regulation of cholesterol storage	0.002 %		-1.4914	0.74	0.54
GO:0001503	ossification	0.074 %		-3.0414	0.73	0.55
GO:0045444	fat cell differentiation	0.042 %		-1.3013	0.72	0.57
GO:0010466	negative regulation of peptidase activity	0.170 %		-2.2663	0.78	0.58
GO:0008284	positive regulation of cell proliferation	0.151 %		-5.4672	0.64	0.60
GO:0048146	positive regulation of fibroblast proliferation	0.009 %	✖	-1.7173	0.68	0.73
GO:0008285	negative regulation of cell proliferation	0.128 %	✖	-3.3125	0.72	0.87
GO:0050679	positive regulation of epithelial cell proliferation	0.028 %	✖	-1.9285	0.67	0.78
GO:0034097	response to cytokine	0.136 %		-3.0306	0.70	0.60
GO:0001501	skeletal system development	0.107 %		-1.5388	0.67	0.63
GO:0009612	response to mechanical stimulus	0.035 %		-3.8416	0.78	0.66
GO:0032496	response to lipopolysaccharide	0.043 %		-1.4643	0.69	0.67
GO:0035987	endodermal cell differentiation	0.011 %		-3.1391	0.66	0.68

WT.BAT CC GO associated TOP 500 UP REGULATED

term ID	description	frequency	pin?	log ₁₀ p-value	uniqueness	dispensability
GO:0005576	extracellular region	2.375 %		-41.5258	0.93	0.00
GO:0005581	collagen trimer	0.071 %		-13.6968	0.89	0.00
GO:0005925	focal adhesion	0.109 %		-5.9469	0.93	0.00
GO:0009986	cell surface	0.241 %		-14.2388	0.89	0.00
GO:0016020	membrane	61.592 %		-5.0680	0.97	0.00
GO:0031012	extracellular matrix	0.275 %		-36.1959	0.61	0.00
GO:1903561	extracellular vesicle	0.686 %	pin?	-2.4462	0.44	0.99
GO:0070062	extracellular exosome	0.682 %	pin?	-26.5003	0.44	0.84
GO:0005615	extracellular space	0.538 %	pin?	-32.5834	0.60	0.77
GO:0045121	membrane raft	0.076 %		-2.3596	0.93	0.00
GO:0030175	filopodium	0.020 %		-2.0453	0.89	0.04
GO:0042383	sarcolemma	0.024 %		-2.4950	0.87	0.04
GO:0043025	neuronal cell body	0.073 %		-1.4234	0.89	0.05
GO:0005783	endoplasmic reticulum	1.332 %		-7.6840	0.65	0.06
GO:0005794	Golgi apparatus	0.969 %	pin?	-2.4050	0.66	0.78
GO:0014069	postsynaptic density	0.030 %		-1.9134	0.80	0.20
GO:0005811	lipid particle	0.055 %		-2.4203	0.78	0.22
GO:0042470	melanosome	0.016 %		-1.9299	0.72	0.28
GO:0048471	perinuclear region of cytoplasm	0.135 %		-3.0146	0.80	0.33
GO:0043234	protein complex	6.419 %		-2.2244	0.90	0.34
GO:0015629	actin cytoskeleton	0.402 %		-1.3320	0.76	0.36
GO:0005886	plasma membrane	10.510 %		-1.3392	0.85	0.36
GO:0005796	Golgi lumen	0.003 %		-1.6748	0.74	0.47
GO:0005588	collagen type V trimer	0.001 %		-1.6384	0.62	0.49
GO:0043231	intracellular membrane-bounded organelle	13.760 %		-1.6682	0.68	0.53
GO:0005788	endoplasmic reticulum lumen	0.027 %		-3.6364	0.72	0.55
GO:0072562	blood microparticle	0.032 %		-3.8729	0.65	0.61
GO:0005578	proteinaceous extracellular matrix	0.177 %		-34.4498	0.59	0.70
GO:0005604	basement membrane	0.041 %	pin?	-15.4330	0.59	0.83
GO:0005605	basal lamina	0.005 %	pin?	-2.7592	0.63	0.87

WT.BAT MF GO associated TOP 500 UP REGULATED

term ID	description	frequency	pin?	log ₁₀ p-value	uniqueness	dispensability
GO:0004222	metalloendopeptidase activity	0.616 %		-1.3795	0.92	0.00
GO:0004896	cytokine receptor activity	0.031 %		-2.9138	0.89	0.00
GO:0005201	extracellular matrix structural constituent	0.028 %		-6.9835	0.92	0.00
GO:0008201	heparin binding	0.029 %		-10.1223	0.85	0.00
GO:0016504	peptidase activator activity	0.009 %		-3.2141	0.76	0.00
GO:0030414	peptidase inhibitor activity	0.143 %	pin?	-2.3260	0.74	0.82
GO:0004867	serine-type endopeptidase inhibitor activity	0.068 %	pin?	-2.3260	0.74	0.94
GO:0042056	chemoattractant activity	0.005 %		-1.8113	0.92	0.00
GO:0050840	extracellular matrix binding	0.011 %		-5.5321	0.88	0.03
GO:0005178	integrin binding	0.017 %		-6.0353	0.62	0.03
GO:0016491	oxidoreductase activity	12.783 %		-3.2209	0.93	0.04
GO:0005515	protein binding	4.410 %		-2.3152	0.87	0.05
GO:0005509	calcium ion binding	0.967 %		-6.4131	0.84	0.11
GO:0005539	glycosaminoglycan binding	0.107 %		-2.0807	0.86	0.19
GO:0048407	platelet-derived growth factor binding	0.002 %		-4.5594	0.70	0.31
GO:0001968	fibronectin binding	0.004 %		-1.5471	0.70	0.32
GO:0043394	proteoglycan binding	0.011 %		-1.5264	0.67	0.34
GO:0005102	receptor binding	0.420 %		-2.0722	0.64	0.42
GO:0002020	protease binding	0.019 %		-2.0392	0.68	0.43
GO:0019838	growth factor binding	0.034 %		-1.5942	0.67	0.44
GO:0005044	scavenger receptor activity	0.041 %		-2.0209	0.89	0.44
GO:0046872	metal ion binding	15.425 %		-1.3905	0.83	0.48
GO:0008009	chemokine activity	0.016 %		-1.3860	0.64	0.63
GO:0008047	enzyme activator activity	0.308 %		-1.3239	0.77	0.63
GO:0005518	collagen binding	0.016 %		-4.5652	0.66	0.68
GO:0008083	growth factor activity	0.069 %		-2.2753	0.62	0.68

Supplementary Table 4.5 GO Enrichment Analyses Summarized Using REVIGO

Derived from Down-Regulated Genes in wt.BAT

WT.BATBP GO associated DOWN 500 REGULATED

term ID	description	frequency	pin?	log ₁₀ p-value	uniqueness	dispensability
GO:0002376	immune system process	0.600 %		-12.9393	0.94	0.00
GO:0006810	transport	17.616 %		-1.9571	0.95	0.00
GO:0007623	circadian rhythm	0.057 %		-1.6987	0.94	0.00
GO:0008152	metabolic process	75.387 %		-4.6308	0.98	0.00
GO:0035458	cellular response to interferon-beta	0.003 %		-21.2620	0.70	0.00
GO:0048511	rhythmic process	0.077 %		-1.6965	0.94	0.00
GO:0006099	tricarboxylic acid cycle	0.469 %		-12.3382	0.70	0.02
GO:0006102	isocitrate metabolic process	0.022 %	⚡	-3.1403	0.76	0.77
GO:0006096	glycolytic process	0.545 %	⚡	-4.5817	0.60	0.73
GO:0006754	ATP biosynthetic process	0.432 %	⚡	-1.8209	0.71	0.81
GO:0045071	negative regulation of viral genome replication	0.008 %		-8.7545	0.91	0.02
GO:0007005	mitochondrion organization	0.418 %		-1.9160	0.92	0.03
GO:0019941	modification-dependent protein catabolic process	0.612 %		-1.6929	0.84	0.06
GO:0005975	carbohydrate metabolic process	5.260 %		-4.5867	0.90	0.07
GO:0048661	positive regulation of smooth muscle cell proliferation	0.008 %		-1.9217	0.86	0.14
GO:0006629	lipid metabolic process	3.522 %		-2.2200	0.82	0.18
GO:0051607	defense response to virus	0.098 %		-19.3143	0.64	0.21
GO:0042832	defense response to protozoan	0.004 %	⚡	-3.0926	0.69	0.71
GO:0045087	innate immune response	0.148 %	⚡	-6.0862	0.67	0.76
GO:0009615	response to virus	0.117 %	⚡	-17.2581	0.73	0.85
GO:0006734	NADH metabolic process	0.007 %		-6.0650	0.76	0.21
GO:0006006	glucose metabolic process	0.430 %		-3.9788	0.71	0.30
GO:0006094	gluconeogenesis	0.262 %	⚡	-2.4416	0.72	0.88
GO:0055114	oxidation-reduction process	15.060 %		-6.5935	0.82	0.30
GO:0006103	2-oxoglutarate metabolic process	0.020 %		-2.2334	0.79	0.32
GO:0001666	response to hypoxia	0.049 %		-2.1561	0.75	0.40
GO:0045821	positive regulation of glycolytic process	0.002 %		-1.6882	0.67	0.47
GO:0006952	defense response	0.568 %		-2.4941	0.72	0.49
GO:0035457	cellular response to interferon-alpha	0.002 %		-1.9086	0.70	0.63
GO:0035455	response to interferon-alpha	0.003 %		-1.9086	0.71	0.63
GO:0071346	cellular response to interferon-gamma	0.011 %		-2.3751	0.61	0.69
GO:0034341	response to interferon-gamma	0.015 %	⚡	-1.6340	0.61	0.74

WT.BAT CC GO associated DOWN 500 REGULATED


term ID	description	frequency	pin?	log ₁₀ p-value	uniqueness	dispensability
GO:0005739	mitochondrion	2.156 %		-22.0857	0.47	0.00
GO:0005913	cell-cell adhesion junction	0.028 %		-1.3110	0.91	0.00
GO:0016020	membrane	61.592 %		-7.8539	0.96	0.00
GO:0070469	respiratory chain	0.296 %		-2.8065	0.89	0.00
GO:0043209	myelin sheath	0.049 %		-20.4724	0.84	0.05
GO:0000502	proteasome complex	0.389 %		-1.7515	0.72	0.14
GO:0005811	lipid particle	0.055 %		-1.7515	0.65	0.23
GO:0005737	cytoplasm	26.017 %		-8.6180	0.68	0.26
GO:0070062	extracellular exosome	0.682 %		-7.8013	0.47	0.38
GO:0031410	cytoplasmic vesicle	0.729 %	⚡	-2.1168	0.47	0.86
GO:0031012	extracellular matrix	0.275 %	⚡	-1.5358	0.80	0.79
GO:0005743	mitochondrial inner membrane	0.623 %		-15.4828	0.38	0.40
GO:0031966	mitochondrial membrane	0.817 %	⚡	-1.8529	0.37	0.94
GO:0005750	mitochondrial respiratory chain complex III	0.025 %	⚡	-1.5861	0.45	0.75
GO:0005759	mitochondrial matrix	0.336 %	⚡	-4.0726	0.41	0.81
GO:0005783	endoplasmic reticulum	1.332 %		-4.0052	0.45	0.44
GO:0005789	endoplasmic reticulum membrane	0.761 %	⚡	-3.7852	0.43	0.75
GO:0005829	cytosol	2.553 %		-7.3645	0.53	0.48
GO:0016529	sarcoplasmic reticulum	0.017 %		-1.4040	0.56	0.53
GO:0005634	nucleus	8.965 %		-6.1891	0.45	0.55
GO:0020005	symbiont-containing vacuole membrane	0.000 %		-3.2518	0.61	0.57
GO:0042645	mitochondrial nucleoid	0.037 %		-1.8353	0.46	0.67

WT.BAT MF GO associated DOWN 500 REGULATED

term ID	description	frequency	pin?	log ₁₀ p-value	uniqueness	dispensability
GO:0003725	double-stranded RNA binding	0.084 %		-5.2807	0.76	0.00
GO:0003824	catalytic activity	65.827 %		-4.0061	0.97	0.00
GO:0003924	GTPase activity	1.135 %		-4.1805	0.90	0.00
GO:0030374	ligand-dependent nuclear receptor transcription coactivator activity	0.011 %		-1.6074	0.91	0.00
GO:0001730	2'-5'-oligoadenylate synthetase activity	0.001 %		-3.4895	0.90	0.02
GO:0042288	MHC class I protein binding	0.002 %		-2.6400	0.79	0.03
GO:0016616	oxidoreductase activity, acting on the CH-OH group of donors, NAD or NADP as acceptor	1.451 %		-2.1622	0.90	0.03
GO:0016491	oxidoreductase activity	12.783 %		-4.6696	0.91	0.05
GO:0005515	protein binding	4.410 %		-3.7011	0.83	0.05
GO:0000287	magnesium ion binding	1.785 %		-1.5987	0.81	0.07
GO:0051287	NAD binding	0.956 %		-3.9208	0.74	0.09
GO:0003950	NAD+ ADP-ribosyltransferase activity	0.033 %		-2.1436	0.89	0.12
GO:0003690	double-stranded DNA binding	0.508 %		-2.0700	0.76	0.20
GO:0001047	core promoter binding	0.045 %		-1.6237	0.78	0.28
GO:0005525	GTP binding	1.783 %		-3.7033	0.70	0.29
GO:0003723	RNA binding	5.283 %		-2.0200	0.73	0.30
GO:0043531	ADP binding	0.183 %		-2.6939	0.74	0.30
GO:0031625	ubiquitin protein ligase binding	0.107 %		-2.6190	0.76	0.34
GO:0044822	poly(A) RNA binding	0.168 %		-2.6743	0.76	0.41
GO:0031072	heat shock protein binding	0.091 %		-1.8300	0.76	0.43
GO:0042802	identical protein binding	0.400 %		-1.3141	0.75	0.48
GO:0005524	ATP binding	14.125 %		-7.5834	0.66	0.52
GO:0000166	nucleotide binding	20.185 %	⚡	-5.7235	0.68	0.72

Supplementary Table 4.6 GO Enrichment Analyses Summarized Using REVIGO
Derived from Up-Regulated Genes in TLR4ko.BAT


TLR4 KO.BAT BP GO associated UP 500 REGULATED

term ID	description	frequency	pin?	log ₁₀ p-value	uniqueness	dispensability
GO:0001666	response to hypoxia	0.049 %		-5.0066	0.65	0.00
GO:0071456	<i>cellular response to hypoxia</i>	0.022 %		-4.3098	0.63	0.94
GO:0006096	glycolytic process	0.545 %		-12.4101	0.52	0.00
GO:0008152	metabolic process	75.387 %		-2.7194	0.96	0.00
GO:0001568	blood vessel development	0.136 %		-1.6184	0.79	0.07
GO:0005975	carbohydrate metabolic process	5.260 %		-5.1643	0.82	0.07
GO:0030199	collagen fibril organization	0.009 %		-3.0942	0.76	0.13
GO:0016477	cell migration	0.293 %		-1.8639	0.73	0.17
GO:0055114	oxidation-reduction process	15.060 %		-3.6253	0.73	0.22
GO:0018401	peptidyl-proline hydroxylation to 4-hydroxy-L-proline	0.001 %		-1.8449	0.71	0.27
GO:0030388	fructose 1,6-bisphosphate metabolic process	0.014 %		-1.3579	0.77	0.37
GO:0071260	cellular response to mechanical stimulus	0.011 %		-1.4035	0.68	0.61
GO:0006094	gluconeogenesis	0.262 %		-1.9246	0.60	0.65
GO:0005977	glycogen metabolic process	0.166 %		-3.0942	0.59	0.67

TLR4 KO.BAT CC GO associated UP 500 REGULATED

term ID	description	frequency	pin?	log ₁₀ p-value	uniqueness	dispensability
GO:0005576	extracellular region	2.375 %		-6.0482	0.86	0.00
GO:0005581	collagen trimer	0.071 %		-6.6799	0.82	0.00
GO:0005829	cytosol	2.553 %		-5.8416	0.69	0.00
GO:0016020	membrane	61.592 %		-3.4306	0.94	0.00
GO:0031012	extracellular matrix	0.275 %		-10.7100	0.49	0.00
GO:0070062	<i>extracellular exosome</i>	0.682 %		-8.8069	0.44	0.79
GO:0005615	<i>extracellular space</i>	0.538 %		-6.9706	0.48	0.84
GO:0043209	myelin sheath	0.049 %		-2.3362	0.82	0.05
GO:0043005	neuron projection	0.190 %		-1.8001	0.81	0.06
GO:0005737	cytoplasm	26.017 %		-7.4001	0.77	0.26
GO:0000015	phosphopyruvate hydratase complex	0.070 %		-1.3253	0.82	0.33
GO:0005739	mitochondrion	2.156 %		-2.0361	0.65	0.48
GO:0005578	proteinaceous extracellular matrix	0.177 %		-8.6326	0.48	0.70
GO:0005604	<i>basement membrane</i>	0.041 %		-4.1555	0.50	0.83

TLR4 KO.BAT MF GO associated UP 500 REGULATED

term ID	description	frequency	pin?	log ₁₀ p-value	uniqueness	dispensability
GO:0003824	catalytic activity	65.827 %		-2.4838	0.93	0.00
GO:0005201	extracellular matrix structural constituent	0.028 %		-3.1445	0.81	0.00
GO:0031418	L-ascorbic acid binding	0.062 %		-2.7079	0.61	0.00
GO:0005536	<i>glucose binding</i>	0.025 %		-1.3246	0.63	0.87
GO:0051213	dioxygenase activity	0.494 %		-6.5901	0.80	0.00
GO:0016491	oxidoreductase activity	12.783 %		-3.8125	0.83	0.04
GO:0005515	protein binding	4.410 %		-1.7794	0.76	0.05
GO:0042802	identical protein binding	0.400 %		-1.4357	0.62	0.06
GO:0046872	metal ion binding	15.425 %		-2.4608	0.75	0.16
GO:0048407	platelet-derived growth factor binding	0.002 %		-1.3246	0.66	0.37
GO:0046982	protein heterodimerization activity	0.280 %		-1.3568	0.63	0.52

Supplementary Table 4.7 GO Enrichment Analyses Summarized Using REVIGO

Derived from Down-Regulated Genes in TLR4ko.BAT

TLR4 KO.BAT BP GO associated DOWN 500 REGULATED

term ID	description	frequency	pin?	log ₁₀ p-value	uniqueness	dispensability
GO:0002376	immune system process	0.600 %		-8.4921	0.91	0.00
GO:0006457	protein folding	0.903 %		-5.0000	0.88	0.00
GO:0006810	transport	17.616 %		-1.4962	0.90	0.00
GO:0009615	response to virus	0.117 %		-11.1675	0.65	0.00
GO:0051607	defense response to virus	0.098 %	no	-8.3098	0.55	0.85
GO:0045071	negative regulation of viral genome replication	0.008 %		-3.8928	0.84	0.02
GO:0018279	protein N-linked glycosylation via asparagine	0.015 %		-3.9586	0.79	0.02
GO:0061077	chaperone-mediated protein folding	0.043 %		-1.7541	0.89	0.03
GO:0006629	lipid metabolic process	3.522 %		-1.8367	0.81	0.13
GO:0006641	triglyceride metabolic process	0.038 %		-1.4093	0.82	0.14
GO:0035458	cellular response to interferon-beta	0.003 %		-10.0292	0.54	0.21
GO:0045087	innate immune response	0.148 %		-5.5575	0.59	0.28
GO:0006412	translation	5.686 %		-2.5890	0.79	0.29
GO:0055114	oxidation-reduction process	15.060 %		-1.5796	0.81	0.30
GO:0034976	response to endoplasmic reticulum stress	0.100 %		-4.8633	0.58	0.44
GO:0043066	negative regulation of apoptotic process	0.173 %		-2.6677	0.77	0.50
GO:0006986	response to unfolded protein	0.037 %		-5.4034	0.48	0.51
GO:0030968	endoplasmic reticulum unfolded protein response	0.027 %	no	-4.7190	0.39	0.94
GO:0030433	ER-associated ubiquitin-dependent protein catabolic process	0.049 %		-4.9830	0.37	0.60
GO:0036503	ERAD pathway	0.053 %	no	-2.4269	0.38	0.91
GO:0030970	retrograde protein transport, ER to cytosol	0.011 %	no	-4.5768	0.40	0.90
GO:0035456	response to interferon-beta	0.004 %		-2.9183	0.55	0.64
GO:0035455	response to interferon-alpha	0.003 %		-2.4269	0.55	0.64

TLR4 KO.BAT CC GO associated DOWN 500 REGULATED

term ID	description	frequency	pin?	log ₁₀ p-value	uniqueness	dispensability
GO:0005783	endoplasmic reticulum	1.332 %		-37.9066	0.37	0.00
GO:0000139	Golgi membrane	0.403 %	no	-3.2284	0.38	0.71
GO:0030176	integral component of endoplasmic reticulum membrane	0.140 %	no	-4.0017	0.39	0.84
GO:0005794	Golgi apparatus	0.969 %	no	-3.4157	0.38	0.78
GO:0005789	endoplasmic reticulum membrane	0.761 %	no	-19.5850	0.33	0.75
GO:0005925	focal adhesion	0.109 %		-7.7328	0.90	0.00
GO:0005913	cell-cell adherens junction	0.028 %	no	-2.0016	0.90	0.87
GO:0016020	membrane	61.592 %		-19.2503	0.98	0.00
GO:0043209	myelin sheath	0.049 %		-1.8323	0.87	0.05
GO:0009986	cell surface	0.241 %		-2.6470	0.86	0.06
GO:0005811	lipid particle	0.055 %		-2.0157	0.64	0.22
GO:0005737	cytoplasm	26.017 %		-4.1355	0.69	0.23
GO:0031116	endoplasmic reticulum-Golgi intermediate compartment membrane	0.008 %		-4.0246	0.57	0.26
GO:0005793	endoplasmic reticulum-Golgi intermediate compartment	0.026 %		-9.6364	0.60	0.29
GO:0048471	perinuclear region of cytoplasm	0.135 %		-1.8321	0.60	0.33
GO:0070062	extracellular exosome	0.682 %		-15.9626	0.52	0.36
GO:0031012	extracellular matrix	0.275 %	no	-3.6459	0.88	0.79
GO:0034663	endoplasmic reticulum chaperone complex	0.003 %		-11.8894	0.49	0.47
GO:0005840	ribosome	4.198 %		-3.4342	0.40	0.48
GO:0030529	intracellular ribonucleoprotein complex	5.291 %	no	-2.8169	0.60	0.91
GO:0005790	smooth endoplasmic reticulum	0.005 %		-10.5157	0.51	0.49
GO:0036513	Derlin-1 retrotranslocation complex	0.005 %		-3.3947	0.47	0.49
GO:0000839	Hrd1p ubiquitin ligase ERAD-L complex	0.005 %		-2.0263	0.47	0.49
GO:0005739	mitochondrion	2.156 %		-2.8954	0.47	0.52
GO:0005829	cytosol	2.553 %		-3.0315	0.52	0.53
GO:0005778	peroxisomal membrane	0.086 %		-1.7630	0.52	0.53
GO:0022625	cytosolic large ribosomal subunit	0.092 %		-2.0357	0.48	0.55
GO:0015935	small ribosomal subunit	0.551 %	no	-1.8695	0.43	0.73
GO:0022627	cytosolic small ribosomal subunit	0.078 %	no	-1.7630	0.48	0.89
GO:0005788	endoplasmic reticulum lumen	0.027 %		-11.1785	0.43	0.55
GO:0043231	intracellular membrane-bounded organelle	13.760 %		-2.9606	0.46	0.57
GO:0005730	nucleolus	0.664 %		-2.2398	0.48	0.57
GO:0005791	rough endoplasmic reticulum	0.039 %		-3.4225	0.45	0.57
GO:0020005	symbiont-containing vacuole membrane	0.000 %		-2.4909	0.65	0.57
GO:0008250	oligosaccharyltransferase complex	0.023 %		-5.0453	0.43	0.57
GO:0042470	melanosome	0.016 %		-8.3089	0.58	0.62
GO:0005770	late endosome	0.074 %		-1.8109	0.44	0.69

TLR4 KO.BAT MF GO associated DOWN 500 REGULATED

term ID	description	frequency	pin?	log ₁₀ p-value	uniqueness	dispensability
GO:0003735	structural constituent of ribosome	2.679 %		-2.4725	0.86	0.00
GO:0004579	dolichyl-diphosphooligosaccharide-protein glycotransferase activity	0.016 %		-4.5317	0.84	0.00
GO:0044822	poly(A) RNA binding	0.168 %		-12.7570	0.71	0.00
GO:0016853	isomerase activity	2.691 %		-1.4604	0.84	0.02
GO:0051787	misfolded protein binding	0.007 %		-5.0159	0.68	0.03
GO:0003924	GTPase activity	1.135 %		-1.4185	0.84	0.04
GO:0016491	oxidoreductase activity	12.783 %		-1.8484	0.85	0.05
GO:0005515	protein binding	4.410 %		-2.2047	0.80	0.05
GO:0001047	core promoter binding	0.045 %		-2.5092	0.75	0.17
GO:0003723	RNA binding	5.283 %		-2.3636	0.72	0.26
GO:0098641	cadherin binding involved in cell-cell adhesion	0.004 %		-1.4061	0.68	0.30
GO:0051082	unfolded protein binding	0.486 %		-4.1284	0.64	0.40
GO:0003725	double-stranded RNA binding	0.084 %		-3.5214	0.71	0.41
GO:0019899	enzyme binding	0.618 %		-3.5784	0.64	0.57

Supplementary Table 4.8 Significantly Enriched KEGG Pathways Associated with Top Up-Regulated Genes and Corresponding P-values in wt.BAT

Enrichment FDR	Mapped DEGs	Total genes	%	Functional Category
1.67E-08	36	79	45.57	EGFR tyrosine kinase inhibitor resistance
5.13E-08	34	75	45.33	Glioma
9.03E-19	88	198	44.44	Focal adhesion
2.15E-05	22	50	44.00	N-Glycan biosynthesis
1.93E-09	44	101	43.56	AGE-RAGE signalling pathway in diabetic complications
2.45E-07	33	76	43.42	Chronic myeloid leukemia
2.45E-07	33	76	43.42	Pertussis
4.18E-07	32	74	43.24	Bacterial invasion of epithelial cells
1.99E-06	29	68	42.65	Renal cell carcinoma
2.45E-07	35	83	42.17	ECM-receptor interaction
1.31E-10	54	129	41.86	Ribosome
2.23E-06	30	72	41.67	Adherens junction
9.52E-15	81	199	40.70	Proteoglycans in cancer
1.46E-09	52	129	40.31	Relaxin signalling pathway
6.73E-06	29	72	40.28	Melanoma
3.77E-12	71	180	39.44	Axon guidance
1.58E-05	28	71	39.44	P53 signalling pathway
1.09E-06	36	92	39.13	Small cell lung cancer
1.16E-07	43	110	39.09	TNF signalling pathway
3.63E-07	40	103	38.83	Amoebiasis
2.01E-09	55	142	38.73	Fluid shear stress and atherosclerosis
1.65E-05	29	75	38.67	Pancreatic cancer
4.63E-08	47	122	38.52	Sphingolipid signalling pathway
6.20E-09	54	142	38.03	MicroRNAs in cancer
9.99E-07	39	103	37.86	Chagas disease (American trypanosomiasis)
1.65E-07	46	123	37.40	Lysosome
4.08E-06	36	97	37.11	Prostate cancer
2.30E-05	31	84	36.90	ErbB signalling pathway
6.96E-07	44	121	36.36	Neurotrophin signalling pathway

3.00E-05	33	93	35.48	TGF-beta signalling pathway
8.46E-11	81	231	35.06	Ras signalling pathway
2.64E-06	43	123	34.96	Osteoclast differentiation
6.66E-16	123	353	34.84	PI3K-Akt signalling pathway
6.64E-10	75	216	34.72	Regulation of actin cytoskeleton
1.93E-09	72	209	34.45	Rap1 signalling pathway
1.15E-10	84	245	34.29	Human cytomegalovirus infection
1.25E-07	58	170	34.12	Hepatocellular carcinoma
8.96E-07	53	159	33.33	Wnt signalling pathway
8.88E-07	54	163	33.13	Hepatitis B
4.53E-11	97	294	32.99	MAPK signalling pathway
9.03E-19	173	532	32.52	Pathways in cancer
3.38E-06	52	162	32.10	Protein processing in endoplasmic reticulum
6.46E-06	54	174	31.03	Cellular senescence
3.17E-06	62	205	30.24	Kaposi sarcoma-associated herpesvirus infection
3.38E-06	65	219	29.68	Viral carcinogenesis
1.58E-05	58	197	29.44	Chemokine signalling pathway
6.73E-06	66	228	28.95	Human immunodeficiency virus 1 infection
9.88E-06	67	235	28.51	Human T-cell leukemia virus 1 infection
1.83E-06	94	348	27.01	Human papillomavirus infection
1.06E-06	281	1301	21.60	Metabolic pathways

Supplementary Table 4.9 Significantly Enriched KEGG Pathways Associated with Top Down-Regulated Genes and Corresponding P-values in wt.BAT

Enrichment FDR	Mapped DEGs	Total genes	%	Functional Category
9.76E-22	96	227	42.29	Thermogenesis
4.07E-14	58	131	44.27	Oxidative phosphorylation
8.16E-14	295	1301	22.67	Metabolic pathways
1.02E-13	72	189	38.10	Huntington disease
6.18E-13	58	140	41.43	Parkinson disease
8.99E-13	52	119	43.70	Carbon metabolism
7.93E-12	58	148	39.19	Non-alcoholic fatty liver disease (NAFLD)
2.13E-10	22	32	68.75	Citrate cycle (TCA cycle)
2.63E-10	23	35	65.71	DNA replication
5.15E-10	50	130	38.46	Spliceosome
5.15E-10	60	171	35.09	Alzheimer disease
1.82E-08	24	44	54.55	Aminoacyl-tRNA biosynthesis
1.19E-05	29	77	37.66	Biosynthesis of amino acids
7.77E-05	33	101	32.67	Glucagon signalling pathway
1.08E-03	35	123	28.46	Cell cycle
1.52E-03	43	165	26.06	RNA transport
1.68E-03	42	161	26.09	Influenza A
1.70E-03	14	33	42.42	Base excision repair
1.78E-03	10	19	52.63	2-Oxocarboxylic acid metabolism
2.27E-03	34	124	27.42	AMPK signalling pathway
2.62E-03	18	51	35.29	Fanconi anemia pathway
2.62E-03	48	197	24.37	NOD-like receptor signalling pathway
2.83E-03	14	35	40.00	Fructose and mannose metabolism
3.36E-03	25	84	29.76	PPAR signalling pathway
3.36E-03	25	84	29.76	Peroxisome
4.56E-03	35	135	25.93	Purine metabolism
4.58E-03	15	41	36.59	Homologous recombination
4.98E-03	24	82	29.27	RNA degradation
4.98E-03	40	162	24.69	Protein processing in endoplasmic reticulum
5.00E-03	16	46	34.78	Proteasome
5.00E-03	10	22	45.45	Mismatch repair
5.16E-03	20	64	31.25	Central carbon metabolism in cancer
6.67E-03	33	129	25.58	Autophagy
8.37E-03	49	216	22.69	Epstein-Barr virus infection
1.20E-02	14	41	34.15	Ferroptosis
1.26E-02	32	129	24.81	Ribosome
1.63E-02	13	38	34.21	Pyruvate metabolism
1.65E-02	37	158	23.42	Hepatitis C
1.80E-02	11	30	36.67	Glyoxylate and dicarboxylate metabolism
2.25E-02	17	58	29.31	Lysine degradation
2.31E-02	25	98	25.51	Phosphatidylinositol signalling system

2.33E-02	15	49	30.61	Cysteine and methionine metabolism
2.50E-02	28	115	24.35	Oocyte meiosis
2.50E-02	32	136	23.53	Apoptosis
2.50E-02	32	136	23.53	Apelin signalling pathway
2.50E-02	28	115	24.35	Thyroid hormone signaling pathway
2.58E-02	15	50	30.00	Fatty acid degradation
3.35E-02	18	66	27.27	Glycolysis / Gluconeogenesis
3.81E-02	16	57	28.07	Fatty acid metabolism
4.14E-02	26	109	23.85	Insulin resistance

Supplementary Table 4.10 Significantly Enriched KEGG Pathways Associated with Top Up-regulated Genes and Corresponding P-values in TLR4ko.BAT

Enrichment FDR	Genes in list	Total genes	%	Functional Category
8.19E-15	17	66	25.76	Glycolysis / Gluconeogenesis
4.80E-14	19	103	18.45	HIF-1 signalling pathway
1.04E-09	16	119	13.45	Carbon metabolism
4.01E-09	51	1301	3.92	Metabolic pathways
2.36E-08	9	33	27.27	Starch and sucrose metabolism
3.37E-07	8	32	25.00	Galactose metabolism
3.37E-07	11	77	14.29	Biosynthesis of amino acids
5.87E-07	8	35	22.86	Fructose and mannose metabolism
5.87E-07	11	83	13.25	ECM-receptor interaction
5.66E-06	9	64	14.06	Central carbon metabolism in cancer
2.92E-05	10	101	9.90	Glucagon signalling pathway
2.92E-05	10	101	9.90	AGE-RAGE signalling pathway in diabetic complications
7.26E-05	6	32	18.75	Pentose phosphate pathway
7.44E-05	9	90	10.00	Protein digestion and absorption
2.09E-04	10	129	7.75	Relaxin signalling pathway
3.09E-04	9	109	8.26	Insulin resistance
5.53E-04	8	92	8.70	Small cell lung cancer
1.16E-03	8	103	7.77	Amoebiasis
1.35E-03	11	198	5.56	Focal adhesion
1.54E-03	15	348	4.31	Human papillomavirus infection
1.71E-03	15	353	4.25	PI3K-Akt signalling pathway
2.34E-03	19	532	3.57	Pathways in cancer
2.37E-03	7	90	7.78	IL-17 signalling pathway
3.10E-03	8	124	6.45	AMPK signalling pathway
4.51E-03	5	49	10.20	Amino sugar and nucleotide sugar metabolism
4.76E-03	5	50	10.00	Arginine and proline metabolism
5.58E-03	8	138	5.80	Insulin signalling pathway
7.08E-03	6	82	7.32	RNA degradation
1.11E-02	2	5	40.00	Neomycin, kanamycin and gentamicin biosynthesis
1.64E-02	5	68	7.35	Renal cell carcinoma
2.39E-02	7	142	4.93	MicroRNAs in cancer
2.39E-02	7	142	4.93	Fluid shear stress and atherosclerosis
2.40E-02	4	48	8.33	Type II diabetes mellitus
2.40E-02	5	76	6.58	Pertussis
2.46E-02	6	110	5.45	TNF signalling pathway
2.46E-02	5	78	6.41	Salmonella infection
2.81E-02	5	81	6.17	Rheumatoid arthritis

Supplementary Table 4.11 Significantly Enriched KEGG Pathways Associated with Top Down-Regulated Genes and Corresponding P-values in TLR4ko.BAT

Enrichment FDR	Genes in list	Total genes	%	Functional Category
3.06E-31	38	162	23.46	Protein processing in endoplasmic reticulum
1.52E-06	14	129	10.85	Ribosome
1.76E-04	6	27	22.22	Protein export
1.95E-04	9	80	11.25	Antigen processing and presentation
3.39E-04	12	161	7.45	Influenza A
1.10E-03	7	61	11.48	Cytosolic DNA-sensing pathway
1.10E-03	11	158	6.96	Hepatitis C
1.54E-03	12	197	6.09	NOD-like receptor signalling pathway
1.62E-03	10	142	7.04	Measles
1.85E-03	39	1301	3.00	Metabolic pathways
5.33E-03	7	84	8.33	PPAR signalling pathway
5.43E-03	5	41	12.20	Ferroptosis
5.43E-03	9	142	6.34	Fluid shear stress and atherosclerosis
5.79E-03	6	64	9.38	Glutathione metabolism
1.17E-02	5	50	10.00	N-Glycan biosynthesis
1.88E-02	9	176	5.11	Necroptosis
1.88E-02	5	57	8.77	Legionellosis
2.14E-02	10	216	4.63	Epstein-Barr virus infection
2.25E-02	5	61	8.20	Glycerolipid metabolism
2.25E-02	7	119	5.88	Carbon metabolism
2.28E-02	3	19	15.79	Steroid biosynthesis
3.11E-02	5	68	7.35	RIG-I-like receptor signalling pathway
3.32E-02	7	131	5.34	Oxidative phosphorylation
4.49E-02	8	175	4.57	Tuberculosis
4.59E-02	14	418	3.35	Herpes simplex virus 1 infection
4.64E-02	6	109	5.50	Insulin resistance
4.64E-02	2	9	22.22	Vitamin B6 metabolism

References

1. Rosen ED, Spiegelman BM. Adipocytes as regulators of energy balance and glucose homeostasis. *Nature*. 2006 Dec 13;444(7121):847–53.
2. Nedergaard J, Cannon B. The Changed Metabolic World with Human Brown Adipose Tissue: Therapeutic Visions. *Cell Metab*. 2010;11(4):268–72.
3. Deshmukh AS, Peijs L, Beaudry JL, Jespersen NZ, Nielsen CH, Ma T, et al. Proteomics-Based Comparative Mapping of the Secretomes of Human Brown and White Adipocytes Reveals EPDR1 as a Novel Adokine. *Cell Metab*. 2019;30(5):963-975.e7.
4. Harms M, Seale P. Brown and beige fat: Development, function and therapeutic potential. *Nat Med*. 2013;19(10):1252–63.
5. Van Vleet ES, Candileri S, McNeillie J, Reinhardt SB, Conkright ME, Zwiessler A. Neutral lipid components of eleven species of Caribbean sharks. *Comp Biochem Physiol -- Part B Biochem*. 1984;79(4):549–54.
6. McKay RM, McKay JP, Avery L, Graff JM. *C. elegans*: A Model for Exploring the Genetics of Fat Storage. *Dev Cell*. 2003 Jan;4(1):131–42.
7. Mescher AL. Adipose Tissue. In: MorphJunqueira's Basic Histology : Text & Atlas. 15th ed. Indiana: McGraw-Hill Education; 2019. p. 101–4.
8. Berry DC, Stenesen D, Zeve D, Graff JM. The developmental origins of adipose tissue. *Development*. 2013;140:3939–49.
9. Lo KAA, Sun L. Turning WAT into BAT: a review on regulators controlling the browning of white adipocytes. *Biosci Rep*. 2013;33(5):711–9.
10. Scherer PE. Adipose tissue: From lipid storage compartment to endocrine organ. *Diabetes*. 2006;55(6):1537–45.
11. Cinti S. The Adipose Organ. In: Fantuzzi G, Braunschweig C, editors. *Adipose Tissue and Adipokines in Health and Disease*. Totowa, NJ: Humana Press; 2014. p. 3–19.
12. Musi N, Guardado-Mendoza R. Adipose Tissue as an Endocrine Organ. *Cell Endocrinol Heal Dis*. 2014;33(1):229–37.
13. Deng T, Lyon CJ, Bergin S, Caligiuri MA, Hsueh WA. Obesity, Inflammation, and Cancer. Vol. 11, *Annual Review of Pathology: Mechanisms of Disease*. 2016. 421–449 p.
14. Kwon H, Pessin JE. Adipokines mediate inflammation and insulin resistance.

- Front Endocrinol (Lausanne). 2013;4(JUN):1–13.
15. Ouchi N, Parker JL, Lugus JJ, Walsh K. Adipokines in inflammation and metabolic disease. *Nat Rev Immunol*. 2011 Feb 21;11(2):85–97.
 16. MacDougald OA, Burant CF. The Rapidly Expanding Family of Adipokines. *Cell Metab*. 2007;6(3):159–61.
 17. Rega-Kaun G, Kaun C, Wojta J. More than a simple storage organ: Adipose tissue as a source of adipokines involved in cardiovascular disease. *Thromb Haemost*. 2013;110(4):641–50.
 18. Pellegrinelli V, Peirce VJ, Howard L, Virtue S, Türei D, Senzacqua M, et al. Adipocyte-secreted BMP8b mediates adrenergic-induced remodeling of the neuro-vascular network in adipose tissue. *Nat Commun*. 2018;9(1):1–18.
 19. Jung UJ, Choi MS. Obesity and its metabolic complications: The role of adipokines and the relationship between obesity, inflammation, insulin resistance, dyslipidemia and nonalcoholic fatty liver disease. *Int J Mol Sci*. 2014;15(4):6184–223.
 20. Poissonnet CM, Burdi AR, Garn SM. The chronology of adipose tissue appearance and distribution in the human fetus. *Early Hum Dev*. 1984;10(1–2):1–11.
 21. Fischer-Posovszky P, Roos J, Zoller V, Wabitsch M. White adipose tissue development and function in children and adolescents: Preclinical models. In: Freemark M, editor. *Pediatric Obesity: Etiology, Pathogenesis and Treatment*. 2nd ed. Cham, Switzerland: Springer International Publishing; 2018. p. 81–93.
 22. Symonds ME. Brown Adipose Tissue Growth and Development. *Scientifica (Cairo)*. 2013;2013:1–14.
 23. Billon N, Monteiro MC, Dani C. Developmental origin of adipocytes: new insights into a pending question. *Biol Cell*. 2008;100(10):563–75.
 24. Chamberlain G, Fox J, Ashton B, Middleton J. Concise Review: Mesenchymal Stem Cells: Their Phenotype, Differentiation Capacity, Immunological Features, and Potential for Homing. *Stem Cells*. 2007;25(11):2739–49.
 25. Seale P, Bjork B, Yang W, Kajimura S, Chin S, Kuang S, et al. PRDM16 controls a brown fat/skeletal muscle switch. *Nature*. 2008 Aug;454(7207):961–7.
 26. Jeffery E, Wing A, Holtrup B, Sebo Z, Kaplan JL, Saavedra-Peña R, et al. The Adipose Tissue Microenvironment Regulates Depot-Specific Adipogenesis in

- Obesity. *Cell Metab.* 2016 Jul;24(1):142–50.
27. Shan T, Liang X, Bi P, Zhang P, Liu W, Kuang S. Distinct populations of adipogenic and myogenic Myf5-lineage progenitors in white adipose tissues. *J Lipid Res.* 2013;54(8):2214–24.
 28. Sanchez-Gurmaches J, Hung C-M, Guertin DA. Emerging Complexities in Adipocyte Origins and Identity. *Trends Cell Biol.* 2016 May;26(5):313–26.
 29. Rosenwald M, Perdikari A, Rüllicke T, Wolfrum C. Bi-directional interconversion of brite and white adipocytes. *Nat Cell Biol.* 2013;15(6):659–67.
 30. Petrovic N, Walden TB, Shabalina IG, Timmons JA, Cannon B, Nedergaard J. Chronic peroxisome proliferator-activated receptor γ (PPAR γ) activation of epididymally derived white adipocyte cultures reveals a population of thermogenically competent, UCP1-containing adipocytes molecularly distinct from classic brown adipocytes. *J Biol Chem.* 2010;285(10):7153–64.
 31. Wu J, Khandekar M, Nuutila P, Schaart G, Huang K, Tu H, et al. Beige Adipocytes are a Distinct Type of Thermogenic Fat Cell in Mouse and Human. *Cell.* 2012;150(2):366–76.
 32. Lee Y-H, Petkova AP, Mottillo EP, Granneman JG. In Vivo Identification of Bipotential Adipocyte Progenitors Recruited by β 3-Adrenoceptor Activation and High-Fat Feeding. *Cell Metab.* 2012 Apr;15(4):480–91.
 33. Crossno JT, Majka SM, Grazia T, Gill RG, Klemm DJ. Rosiglitazone promotes development of a novel adipocyte population from bone marrow-derived circulating progenitor cells. *J Clin Invest.* 2006;116(12):3220–8.
 34. Himms-Hagen J, Melnyk A, Zingaretti MC, Ceresi E, Barbatelli G, Cinti S. Multilocular fat cells in WAT of CL-316243-treated rats derive directly from white adipocytes. *Am J Physiol - Cell Physiol.* 2000;279(3 48-3):670–81.
 35. Garcia RA, Roemmich JN, Claycombe KJ. Evaluation of markers of beige adipocytes in white adipose tissue of the mouse. *Nutr Metab.* 2016;13(1):1–14.
 36. Wang W, Seale P. Control of brown and beige fat development. *Nat Rev Mol Cell Biol.* 2016 Nov 24;17(11):691–702.
 37. Sarjeant K, Stephens JM. Adipogenesis. *Cold Spring Harb Perspect Biol.* 2012 Sep 1;4(9):a008417–a008417.
 38. Tran K Van, Gealekman O, Frontini A, Zingaretti MC, Morroni M, Giordano A, et al. The Vascular Endothelium of the Adipose Tissue Gives Rise to Both

- White and Brown Fat Cells. *Cell Metab.* 2012 Feb;15(2):222–9.
39. Berry R, Rodeheffer MS. Characterization of the adipocyte cellular lineage in vivo. *Nat Cell Biol.* 2013;15(3):302–8.
 40. Min SY, Kady J, Nam M, Rojas-Rodriguez R, Berkenwald A, Kim JH, et al. Human “brite/beige” adipocytes develop from capillary networks, and their implantation improves metabolic homeostasis in mice. *Nat Med.* 2016 Mar 25;22(3):312–8.
 41. Min SY, Desai A, Yang Z, Sharma A, DeSouza T, Genga RMJ, et al. Diverse repertoire of human adipocyte subtypes develops from transcriptionally distinct mesenchymal progenitor cells. *Proc Natl Acad Sci U S A.* 2019;116(36):17970–9.
 42. Jespersen NZ, Larsen TJ, Peijs L, Dugaard S, Homøe P, Loft A, et al. A classical brown adipose tissue mRNA signature partly overlaps with brite in the supraclavicular region of adult humans. *Cell Metab.* 2013;17(5):798–805.
 43. Seale P. Transcriptional control of brown adipocyte development and thermogenesis. *Int J Obes.* 2010;34:S17–22.
 44. Kajimura S, Seale P, Kubota K, Lunsford E, Frangioni J V, Gygi SP, et al. Initiation of myoblast/brown fat switch through a PRDM16-C/EBP- β transcriptional complex. *Nature.* 2009;460(7259):1154–8.
 45. Tran K Van, Brown EL, DeSouza T, Jespersen NZ, Nandrup-Bus C, Yang Q, et al. Human thermogenic adipocyte regulation by the long noncoding RNA LINC00473. *Nat Metab.* 2020;2(5):397–412.
 46. Farmer SR. Transcriptional control of adipocyte formation. *Cell Metab.* 2006 Oct;4(4):263–73.
 47. de Jong JMA, Larsson O, Cannon B, Nedergaard J. A stringent validation of mouse adipose tissue identity markers. *Am J Physiol - Endocrinol Metab.* 2015;308(12):E1085–105.
 48. Lee P, Greenfield JR, Ho KKY, Fulham MJ. A critical appraisal of the prevalence and metabolic significance of brown adipose tissue in adult humans. *Am J Physiol - Endocrinol Metab.* 2010;299(4):601–6.
 49. Wang Q, Zhang M, Xu M, Gu W, Xi Y, Qi L, et al. Brown adipose tissue activation is inversely related to central obesity and metabolic parameters in adult human. *PLoS One.* 2015;10(4):1–13.
 50. Cypess AM, Lehman S, Williams G, Tal I, Rodman D, Goldfine AB, et al.

- Identification and Importance of Brown Adipose Tissue in Adult Humans. *N Engl J Med*. 2009 Apr 9;360(15):1509–17.
51. Saito M, Okamatsu-Ogura Y, Matsushita M, Watanabe K, Yoneshiro T, Nio-Kobayashi J, et al. High incidence of metabolically active brown adipose tissue in healthy adult humans: Effects of cold exposure and adiposity. *Diabetes*. 2009;58(7):1526–31.
 52. van Marken Lichtenbelt WD, Vanhomerig JW, Smulders NM, Drossaerts JMAFL, Kemerink GJ, Bouvy ND, et al. Cold-Activated Brown Adipose Tissue in Healthy Men. *N Engl J Med*. 2009 Apr 9;360(15):1500–8.
 53. Virtanen KA, Lidell ME, Orava J, Heglind M, Westergren R, Niemi T, et al. Functional Brown Adipose Tissue in Healthy Adults. *N Engl J Med*. 2009 Apr 9;360(15):1518–25.
 54. Zingaretti MC, Crosta F, Vitali A, Guerrieri M, Frontini A, Cannon B, et al. The presence of UCP1 demonstrates that metabolically active adipose tissue in the neck of adult humans truly represents brown adipose tissue. *FASEB J*. 2009;23(9):3113–20.
 55. Sacks H, Symonds ME. Anatomical locations of human brown adipose tissue: Functional relevance and implications in obesity and type 2 diabetes. *Diabetes*. 2013;62(6):1783–90.
 56. Holstila M, Virtanen KA, Grönroos TJ, Laine J, Lepomäki V, Saunavaara J, et al. Measurement of brown adipose tissue mass using a novel dual-echo magnetic resonance imaging approach: A validation study. *Metabolism*. 2013;62(8):1189–98.
 57. Cypess AM, White AP, Vernochet C, Schulz TJ, Xue R, Sass CA, et al. Anatomical localization, gene expression profiling and functional characterization of adult human neck brown fat. *Nat Med*. 2013;19(5):635–9.
 58. Bjørndal B, Burri L, Staalesen V, Skorve J, Berge RK. Different adipose depots: Their role in the development of metabolic syndrome and mitochondrial response to hypolipidemic agents. *J Obes*. 2011;2011.
 59. Karpe F, Pinnick KE. Biology of upper-body and lower-body adipose tissue—link to whole-body phenotypes. *Nat Rev Endocrinol*. 2014;11(2):90–100.
 60. Grzybek M, Palladini A, Alexaki VI, Surma MA, Simons K, Chavakis T, et al. Comprehensive and quantitative analysis of white and brown adipose tissue by shotgun lipidomics. *Mol Metab*. 2019;22(January):12–20.

61. Gesta S, Tseng YH, Kahn CR. Developmental Origin of Fat: Tracking Obesity to Its Source. *Cell*. 2007;131(2):242–56.
62. Neeland IJ, Ayers CR, Rohatgi AK, Turer AT, Berry JD, Das SR, et al. Associations of visceral and abdominal subcutaneous adipose tissue with markers of cardiac and metabolic risk in obese adults. *Obesity*. 2013 May;21(9):n/a-n/a.
63. Gallagher D, Kuznia P, Heshka S, Albu J, Heymsfield SB, Goodpaster B, et al. Adipose tissue in muscle: a novel depot similar in size to visceral adipose tissue. *Am J Clin Nutr*. 2005 Apr 1;81(4):903–10.
64. Shen W, Chen J, Punyanitya M, Shapses S, Heshka S, Heymsfield SB. MRI-measured bone marrow adipose tissue is inversely related to DXA-measured bone mineral in Caucasian women. *Osteoporos Int*. 2007;18(5):641–7.
65. Pinnick KE, Collins SC, Londos C, Gauguier D, Clark A, Fielding BA. Pancreatic ectopic fat is characterized by adipocyte infiltration and altered lipid composition. *Obesity*. 2008;16(3):522–30.
66. Schoettl T, Fischer IP, Ussar S. Heterogeneity of adipose tissue in development and metabolic function. *J Exp Biol*. 2018 Mar 7;221(Suppl 1):jeb162958.
67. Christian M. In Vitro Models for Study of Brown Adipocyte Biology. In: Pfeifer A., Klingenspor M. HS, editor. *Brown Adipose Tissue Handbook of Experimental Pharmacology*. vol 251. Cham: Springer; 2018. p. 85–96.
68. Peirce V, Pellegrinelli V, Vidal-Puig A. Adipose Structure (White, Brown, Beige). In: *Metabolic Syndrome*. Cham: Springer International Publishing; 2016. p. 369–96.
69. Jung SM, Sanchez-Gurmaches J, Guertin DA. Brown Adipose Tissue Development and Metabolism. In: Pfeifer A., Klingenspor M. HS, editor. *Brown Adipose Tissue Handbook of Experimental Pharmacology*. vol 251. Cham: Springer; 2018. p. 3–36.
70. Collins S, Yehuda-Shnaidman E, Wang H. Positive and negative control of Ucp1 gene transcription and the role of β -adrenergic signaling networks. *Int J Obes*. 2010;34:S28–33.
71. Bartness TJ, Song CK. Sympathetic and sensory innervation of white adipose tissue. *J Lipid Res*. 2007;48(8):1655–72.
72. Kai Sun PES. Adipose Tissue Dysfunction: A Multistep Process. In: Cle´ment, Karine Cle, Christen Yves SBM, editor. *Novel Insights into Adipose Cell*

- Functions (Research and Perspectives in Endocrine Interactions). Springer-Verlag Berlin Heidelberg; 2010. p. 67–76.
73. Martinez-Santibañez, WonCho K, Lumeng CN. Imaging White Adipose Tissue With Confocal Microscopy. *Methods Enzym.* 2014;537:17–30.
 74. Skurk T, Alberti-Huber C, Herder C, Hauner H. Relationship between adipocyte size and adipokine expression and secretion. *J Clin Endocrinol Metab.* 2007;92(3):1023–33.
 75. CANNON B, NEDERGAARD J. Brown Adipose Tissue: Function and Physiological Significance. *Physiol Rev.* 2004 Jan;84(1):277–359.
 76. Szablewski L. Introductory Chapter: Adipose Tissue. In: *Adipose Tissue - An Update. the Edited.* Warsaw: IntechOpen; 2019.
 77. Tiraby C, Tavernier G, Lefort C, Larrouy D, Bouillaud F, Ricquier D, et al. Acquirement of brown fat cell features by human white adipocytes. *J Biol Chem.* 2003;278(35):33370–6.
 78. Miller JM, Oligino T, Pazdera M, López AJ, Hoshizaki DK. Identification of fat-cell enhancer regions in *Drosophila melanogaster*. *Insect Mol Biol.* 2002;11(1):67–77.
 79. Booth A, Magnuson A, Fouts J, Foster MT. Adipose tissue: an endocrine organ playing a role in metabolic regulation. *Horm Mol Biol Clin Investig.* 2016 Jan 1;26(1):25–42.
 80. Villarroya F, Cereijo R, Villarroya J, Giralt M. Brown adipose tissue as a secretory organ. *Nat Rev Endocrinol.* 2017;13(1):26–35.
 81. Olefsky JM, Glass CK. Macrophages, Inflammation, and Insulin Resistance. *Annu Rev Physiol.* 2010;72:219–46.
 82. Tchkonina T, Thomou T, Zhu Y, Karagiannides I, Pothoulakis C, Jensen MD, et al. Mechanisms and Metabolic Implications of Regional Differences among Fat Depots. *Cell Metab.* 2013 May;17(5):644–56.
 83. Hardy OT, Czech MP, Corvera S. What causes the insulin resistance underlying obesity? *Curr Opin Endocrinol Diabetes Obes.* 2012 Apr;19(2):81–7.
 84. Lovren F, Teoh H, Verma S. Obesity and Atherosclerosis: Mechanistic Insights. *Can J Cardiol.* 2015;31(2):177–83.
 85. Trayhurn P. THERMOGENESIS. In: *Encyclopedia of Food Sciences and Nutrition.* Elsevier; 2003. p. 5762–7.
 86. Silva JE. Thermogenic Mechanisms and Their Hormonal Regulation. *Physiol*

- Rev. 2006 Apr;86(2):435–64.
87. Himms-Hagen J. Does Brown Adipose Tissue (BAT) Have a Role in the Physiology or Treatment of Human Obesity? *Rev Endocr Metab Disord*. 2001;2(4):395–401.
 88. Rosenbaum M, Leibel RL. Adaptive thermogenesis in humans. *Int J Obes*. 2010;34(0 1):S47–55.
 89. Westerterp KR. Diet induced thermogenesis. *Nutr Metab (Lond)*. 2004 Aug 18;1(1):5.
 90. Feldmann HM, Golozoubova V, Cannon B, Nedergaard J. UCP1 Ablation Induces Obesity and Abolishes Diet-Induced Thermogenesis in Mice Exempt from Thermal Stress by Living at Thermoneutrality. *Cell Metab*. 2009;9(2):203–9.
 91. Aldiss P, Betts J, Sale C, Pope M, Budge H, Symonds ME. Exercise-induced ‘browning’ of adipose tissues. *Metabolism*. 2018;81:63–70.
 92. Berry DC, Jiang Y, Graff JM. Mouse strains to study cold-inducible beige progenitors and beige adipocyte formation and function. *Nat Commun*. 2016;7.
 93. Wu J, Cohen P, Spiegelman BM. Adaptive thermogenesis in adipocytes: Is beige the new brown? *Genes Dev*. 2013 Feb 1;27(3):234–50.
 94. Frontini A, Vitali A, Perugini J, Murano I, Romiti C, Ricquier D, et al. White-to-brown transdifferentiation of omental adipocytes in patients affected by pheochromocytoma. *Biochim Biophys Acta - Mol Cell Biol Lipids*. 2013;1831(5):950–9.
 95. Rosenwald M, Wolfrum C. The origin and definition of brite versus white and classical brown adipocytes. *Adipocyte*. 2014;3(1):4–9.
 96. Ricquier D. Uncoupling protein 1 of brown adipocytes, the only uncoupler: A historical perspective. *Front Endocrinol (Lausanne)*. 2011;2(DEC):1–7.
 97. Brondani L de A, Assmann TS, Duarte GCK, Gross JL, Canani LH, Crispim D. The role of the uncoupling protein 1 (UCP1) on the development of obesity and type 2 diabetes mellitus. *Arq Bras Endocrinol Metabol*. 2012;56(4):215–25.
 98. Divakaruni AS, Brand MD. The regulation and physiology of mitochondrial proton leak. *Physiology (Bethesda)*. 2011;26(3):192–205.
 99. Martin Jastroch, Ajit S. Divakaruni, Shona Mookerjee, Jason R. Treberg and MDB, Treberg JR, Martin D. Mitochondrial proton and electron leaks oxygen consumption and pH data. *Essays Biochem* . 2010;53–67.

100. Vargas-Castillo A, Fuentes-Romero R, Rodriguez-Lopez LA, Torres N, Tovar AR. Understanding the Biology of Thermogenic Fat: Is Browning A New Approach to the Treatment of Obesity? *Arch Med Res.* 2017;48(5):401–13.
101. Nedergaard J, Cannon B. Brown adipose tissue as a heat-producing thermoeffector. In: Romanovsky AA, editor. *Handbook of Clinical Neurology.* 1st ed. Amsterdam: Elsevier B.V.; 2018. p. 137–52.
102. Klingenspor M. Cold-Induced Recruitment of Brown Adipose Tissue Thermogenesis. *Exp Physiol.* 2003 Jan;88(1):141–8.
103. Dalgaard LT, Pedersen O. Uncoupling proteins: Functional characteristics and role in the pathogenesis of obesity and Type II diabetes. *Diabetologia.* 2001;44(8):946–65.
104. Liu X, Cervantes C, Liu F. Common and distinct regulation of human and mouse brown and beige adipose tissues: a promising therapeutic target for obesity. *Protein Cell.* 2017;8(6):446–54.
105. Collins S. β -Adrenoceptor signaling networks in adipocytes for recruiting stored fat and energy expenditure. *Front Endocrinol (Lausanne).* 2012;3(JAN):1–7.
106. Bachman ES, Dhillon H, Zhang CY, Cinti S, Bianco AC, Kobilka BK, et al. β AR signaling required for diet-induced thermogenesis and obesity resistance. *Science (80-).* 2002;297(5582):843–5.
107. Palou A, Bonet ML. Controlling lipogenesis and thermogenesis and the use of ergogenic aids for weight control. In: C.J.K. Henry, editor. *Novel Food Ingredients for Weight Control.* Cambridge: Woodhead Publishing Limited; 2007. p. 58–103.
108. Zhao J, Unelius L, Bengtsson T, Cannon B, Nedergaard J. Coexisting β -adrenoceptor subtypes: Significance for thermogenic process in brown fat cells. *Am J Physiol - Cell Physiol.* 1994;267(4 37-4):969–79.
109. Robidoux J, Martin TL, Collins S. β -Adrenergic Receptors And Regulation Of Energy Expenditure: A Family Affair. *Annu Rev Pharmacol Toxicol.* 2004 Feb 10;44(1):297–323.
110. Barbatelli G, Murano I, Madsen L, Hao Q, Jimenez M, Kristiansen K, et al. The emergence of cold-induced brown adipocytes in mouse white fat depots is determined predominantly by white to brown adipocyte transdifferentiation. *Am J Physiol - Endocrinol Metab.* 2010;298(6):1244–53.

111. Arch JRS. Challenges in β 3-adrenoceptor agonist drug development. *Ther Adv Endocrinol Metab.* 2011;2(2):59–64.
112. Calderon-Dominguez M, Mir JF, Fucho R, Weber M, Serra D, Herrero L. Fatty acid metabolism and the basis of brown adipose tissue function. *Adipocyte.* 2016;5(2):98–118.
113. Deiliulis JA, Liu LF, Belury MA, Rim JS, Shin S, Lee K. B3-Adrenergic Signaling Acutely Down Regulates Adipose Triglyceride Lipase in Brown Adipocytes. *Lipids.* 2010;45(6):479–89.
114. Bartelt A, Merkel M, Heeren J. A new, powerful player in lipoprotein metabolism: Brown adipose tissue. *J Mol Med.* 2012;90(8):887–93.
115. Rim JS, Xue B, Gawronska-Kozak B, Kozak LP. Sequestration of thermogenic transcription factors in the cytoplasm during development of brown adipose tissue. *J Biol Chem.* 2004;279(24):25916–26.
116. Shin S, El-Sabbagh AS, Lukas BE, Tanneberger SJ, Jiang Y. Adipose stem cells in obesity: challenges and opportunities. *Biosci Rep.* 2020 Jun 26;40(6):1–15.
117. Rosen ED. C/EBP α induces adipogenesis through PPAR γ : a unified pathway. *Genes Dev.* 2002 Jan 1;16(1):22–6.
118. Lin J, Wu P-H, Tarr PT, Lindenberg KS, St-Pierre J, Zhang C, et al. Defects in Adaptive Energy Metabolism with CNS-Linked Hyperactivity in PGC-1 α Null Mice. *Cell.* 2004 Oct;119(1):121–35.
119. Uldry M, Yang W, St-Pierre J, Lin J, Seale P, Spiegelman BM. Complementary action of the PGC-1 coactivators in mitochondrial biogenesis and brown fat differentiation. *Cell Metab.* 2006 May;3(5):333–41.
120. Seale P, Conroe HM, Estall J, Kajimura S, Frontini A, Ishibashi J, et al. Prdm16 determines the thermogenic program of subcutaneous white adipose tissue in mice. *J Clin Invest.* 2011 Jan 4;121(1):96–105.
121. Song T, Kuang S. Adipocyte dedifferentiation in health and diseases. *Clin Sci.* 2019;133(20):2107–19.
122. Dixon TM, Daniel KW, Farmer SR, Collins S. CCAAT/enhancer-binding protein α is required for transcription of the β 3-adrenergic receptor gene during adipogenesis. *J Biol Chem.* 2001;276(1):722–8.
123. Lefterova MI, Lazar MA. New developments in adipogenesis. *Trends Endocrinol Metab.* 2009 Apr;20(3):107–14.
124. Darlington GJ, Ross SE, MacDougald OA. The role of C/EBP genes in

- adipocyte differentiation. *J Biol Chem*. 1998;273(46):30057–60.
125. Karamanlidis G, Karamitri A, Docherty K, Hazlerigg DG, Lomax MA. C/EBP β reprograms white 3T3-L1 preadipocytes to a brown adipocyte pattern of gene expression. *J Biol Chem*. 2007;282(34):24660–9.
 126. Zhang JW, Klemm DJ, Vinson C, Lane MD. Role of CREB in Transcriptional Regulation of CCAAT/Enhancer-binding Protein β Gene during Adipogenesis. *J Biol Chem*. 2004;279(6):4471–8.
 127. Villarroya F, Peyrou M, Giralt M. Transcriptional regulation of the uncoupling protein-1 gene. *Biochimie*. 2017;134:86–92.
 128. Tang QQ, Grønborg M, Huang H, Kim JW, Otto TC, Pandey A, et al. Sequential phosphorylation of CCAAT enhancer-binding protein β by MAPK and glycogen synthase kinase 3 β is required for adipogenesis. *Proc Natl Acad Sci U S A*. 2005;102(28):9766–71.
 129. Bonet ML, Oliver P, Palou A. Pharmacological and nutritional agents promoting browning of white adipose tissue. *Biochim Biophys Acta - Mol Cell Biol Lipids*. 2013;1831(5):969–85.
 130. Thonberg H, Fredriksson JM, Nedergaard J, Cannon B. A novel pathway for adrenergic stimulation of cAMP-response-element-binding protein (CREB) phosphorylation: Mediation via α 1-adrenoceptors and protein kinase C activation. *Biochem J*. 2002;364(1):73–9.
 131. Floyd ZE, Stephens JM. Controlling a master switch of adipocyte development and insulin sensitivity: Covalent modifications of PPAR γ . *Biochim Biophys Acta - Mol Basis Dis*. 2012 Jul;1822(7):1090–5.
 132. Gray SL, Dalla Nora E, Backlund EC, Manieri M, Virtue S, Noland RC, et al. Decreased brown adipocyte recruitment and thermogenic capacity in mice with impaired peroxisome proliferator-activated receptor (P465L PPAR γ) function. *Endocrinology*. 2006;147(12):5708–14.
 133. Tontonoz P, Spiegelman BM. Fat and Beyond: The Diverse Biology of PPAR γ . *Annu Rev Biochem*. 2008;77(1):289–312.
 134. Pardo R, Enguix N, Lasheras J, Feliu JE, Kralli A, Villena JA. Rosiglitazone-induced mitochondrial biogenesis in white adipose tissue is independent of peroxisome proliferator-activated receptor γ coactivator-1 α . *PLoS One*. 2011;6(11).
 135. Wilson-Fritch L, Burkart A, Bell G, Mendelson K, Leszyk J, Nicoloso S, et al.

- Mitochondrial Biogenesis and Remodeling during Adipogenesis and in Response to the Insulin Sensitizer Rosiglitazone. *Mol Cell Biol*. 2003 Feb 1;23(3):1085–94.
136. Koh YJ, Park BH, Park JH, Han J, Lee IK, Park JW, et al. Activation of PPAR γ induces profound multilocularization of adipocytes in adult mouse white adipose tissues. *Exp Mol Med*. 2009;41(12):880–95.
 137. Pisani DF, Djedaini M, Beranger GE, Elabd C, Scheideler M, Ailhaud G, et al. Differentiation of human adipose-derived stem cells into “brite” (brown-in-white) adipocytes. *Front Endocrinol (Lausanne)*. 2011;2(NOV):1–9.
 138. Herzig S, Long F, Jhala US, Hedrick S, Quinn R, Bauer A, et al. CREB regulates hepatic gluconeogenesis through the coactivator PGC-1. *Nature*. 2001 Sep;413(6852):179–83.
 139. Lin J, Handschin C, Spiegelman BM. Metabolic control through the PGC-1 family of transcription coactivators. *Cell Metab*. 2005;1(6):361–70.
 140. Puigserver P, Spiegelman BM. Peroxisome Proliferator-Activated Receptor- γ Coactivator 1 α (PGC-1 α): Transcriptional Coactivator and Metabolic Regulator. *Endocr Rev*. 2003 Feb 1;24(1):78–90.
 141. Picard F, Géhin M, Annicotte J-S, Rocchi S, Champy M, O’Malley BW, et al. SRC-1 and TIF2 Control Energy Balance between White and Brown Adipose Tissues. *Cell*. 2002 Dec;111(7):931–41.
 142. Boström P, Wu J, Jedrychowski MP, Korde A, Ye L, Lo JC, et al. A PGC1- α -dependent myokine that drives brown-fat-like development of white fat and thermogenesis. *Nature*. 2012 Jan 11;481(7382):463–8.
 143. Puigserver P, Wu Z, Park CW, Graves R, Wright M, Spiegelman BM. A Cold-Inducible Coactivator of Nuclear Receptors Linked to Adaptive Thermogenesis. *Cell*. 1998 Mar;92(6):829–39.
 144. Hallberg M, Morganstein DL, Kiskinis E, Shah K, Kralli A, Dilworth SM, et al. A Functional Interaction between RIP140 and PGC-1 α Regulates the Expression of the Lipid Droplet Protein CIDEA. *Mol Cell Biol*. 2008;28(22):6785–95.
 145. Seale P, Kajimura S, Yang W, Chin S, Rohas LM, Uldry M, et al. Transcriptional Control of Brown Fat Determination by PRDM16. *Cell Metab*. 2007 Jul;6(1):38–54.
 146. Kajimura S, Seale P, Tomaru T, Erdjument-Bromage H, Cooper MP, Ruas JL,

- et al. Regulation of the brown and white fat gene programs through a PRDM16/CtBP transcriptional complex. *Genes Dev.* 2008 May 15;22(10):1397–409.
147. Lee Y, Jung Y, Choi D. Recent advance in brown adipose physiology and its therapeutic potential. *Exp Mol Med.* 2014 Feb 21;46(2):e78–e78.
 148. Dempersmier J, Sambeat A, Gulyaeva O, Paul SM, Hudak CSS, Raposo HF, et al. Cold-Inducible Zfp516 Activates UCP1 Transcription to Promote Browning of White Fat and Development of Brown Fat. *Mol Cell.* 2015 Jan;57(2):235–46.
 149. Duteil D, Tosic M, Lausecker F, Nenseth HZ, Müller JM, Urban S, et al. Lsd1 Ablation Triggers Metabolic Reprogramming of Brown Adipose Tissue. *Cell Rep.* 2016 Oct;17(4):1008–21.
 150. Sambeat A, Gulyaeva O, Dempersmier J, Tharp KM, Stahl A, Paul SM, et al. LSD1 Interacts with Zfp516 to Promote UCP1 Transcription and Brown Fat Program. *Cell Rep.* 2016 Jun;15(11):2536–49.
 151. Chartoumpekis D V., Habeos IG, Ziros PG, Psyrogiannis AI, Kyriazopoulou VE, Papavassiliou AG. Brown Adipose Tissue Responds to Cold and Adrenergic Stimulation by Induction of FGF21. *Mol Med.* 2011 Jul 25;17(7–8):736–40.
 152. Kharitononkov A, Shiyanova TL, Koester A, Ford AM, Micanovic R, Galbreath EJ, et al. FGF-21 as a novel metabolic regulator. *J Clin Invest.* 2005 Jun 1;115(6):1627–35.
 153. Hondares E, Iglesias R, Giralt A, Gonzalez FJ, Giralt M, Mampel T, et al. Thermogenic activation induces FGF21 expression and release in brown adipose tissue. *J Biol Chem.* 2011;286(15):12983–90.
 154. Fisher FM, Kleiner S, Douris N, Fox EC, Mepani RJ, Verdeguer F, et al. FGF21 regulates PGC-1 and browning of white adipose tissues in adaptive thermogenesis. *Genes Dev.* 2012 Feb 1;26(3):271–81.
 155. Villarroya F. Irisin, Turning Up the Heat. *Cell Metab.* 2012 Mar;15(3):277–8.
 156. Whittle AJ, Carobbio S, Martins L, Slawik M, Hondares E, Vázquez MJ, et al. BMP8B Increases Brown Adipose Tissue Thermogenesis through Both Central and Peripheral Actions. *Cell.* 2012 May;149(4):871–85.
 157. Chainani-Wu N, Weidner G, Purnell DM, Frenda S, Merritt-Worden T, Kemp C, et al. Relation of B-Type Natriuretic Peptide Levels to Body Mass Index

- After Comprehensive Lifestyle Changes. *Am J Cardiol.* 2010 Jun;105(11):1570–6.
158. CANNON B, HOUSTEK J, NEDERGAARD J. Brown Adipose Tissue: More Than an Effector of Thermogenesis? *a. Ann N Y Acad Sci.* 1998 Sep;856(1 MOLECULAR MEC):171–87.
 159. Glatz JFC, Luiken JJFP, Bonen A. Membrane Fatty Acid Transporters as Regulators of Lipid Metabolism: Implications for Metabolic Disease. *Physiol Rev.* 2010 Jan;90(1):367–417.
 160. Yamamoto T, Yamamoto A, Watanabe M, Matsuo T, Yamazaki N, Kataoka M, et al. Classification of FABP isoforms and tissues based on quantitative evaluation of transcript levels of these isoforms in various rat tissues. *Biotechnol Lett.* 2009;31(11):1695–701.
 161. Furuhashi M, Saitoh S, Shimamoto K, Miura T. Fatty Acid-Binding Protein 4 (FABP4): Pathophysiological Insights and Potent Clinical Biomarker of Metabolic and Cardiovascular Diseases. *Clin Med Insights Cardiol.* 2014 Jan 2;8s3:CMC.S17067.
 162. Christian M. Transcriptional fingerprinting of “browning” white fat identifies NRG4 as a novel adipokine. *Adipocyte.* 2015;4(1):50–4.
 163. Rosell M, Kaforou M, Frontini A, Okolo A, Chan Y-W, Nikolopoulou E, et al. Brown and white adipose tissues: intrinsic differences in gene expression and response to cold exposure in mice. *Am J Physiol Endocrinol Meta.* 2014;306(8):E945–64.
 164. Jakobsson A, Jørgensen JA, Jacobsson A. Differential regulation of fatty acid elongation enzymes in brown adipocytes implies a unique role for Elovl3 during increased fatty acid oxidation. *Am J Physiol - Endocrinol Metab.* 2005;289(4 52-4).
 165. Tvrdik P, Asadit A, Kozak LP, Nedergaard J, Cannon B, Jacobsson A. Cig30, a mouse member of a novel membrane protein gene family, is involved in the recruitment of brown adipose tissue. *J Biol Chem.* 1997;272(50):31738–46.
 166. Zach-Avec D, Brolinson A, Fisher RM, Carneheim C, Csikasz RI, Bertrand-Michel J, et al. Ablation of the very-long-chain fatty acid elongase ELOVL3 in mice leads to constrained lipid storage and resistance to diet-induced obesity. *FASEB J.* 2010;24(11):4366–77.
 167. Inohara N, Koseki T, Chen S, Wu X, Núñez G. CIDE, a novel family of cell

- death activators with homology to the 45 kDa subunit of the DNA fragmentation factor. *EMBO J.* 1998;17(9):2526–33.
168. Zhou Z, Toh SY, Chen Z, Guo K, Ng CP, Ponniah S, et al. Cidea-deficient mice have lean phenotype and are resistant to obesity. *Nat Genet.* 2003;35(1):49–56.
 169. Nordström EA, Rydén M, Backlund EC, Dahlman I, Kaaman M, Blomqvist L, et al. A human-specific role of cell death-inducing DFFA (DNA fragmentation factor- α)-like effector A (CIDEA) in adipocyte lipolysis and obesity. *Diabetes.* 2005;54(6):1726–34.
 170. Shimizu T, Yokotani K. Acute cold exposure-induced down-regulation of CIDEA, cell death-inducing DNA fragmentation factor- α -like effector A, in rat interscapular brown adipose tissue by sympathetically activated β 3-adrenoreceptors. *Biochem Biophys Res Commun.* 2009;387(2):294–9.
 171. Gummesson A, Jernås M, Svensson PA, Larsson I, Glad CAM, Schéle E, et al. Relations of adipose tissue CIDEA gene expression to basal metabolic rate, energy restriction, and obesity: Population-based and dietary intervention studies. *J Clin Endocrinol Metab.* 2007;92(12):4759–65.
 172. Moraes RC, Blondet A, Birkenkamp-Demtroeder K, Tirard J, Orntoft TF, Gertler A, et al. Study of the Alteration of Gene Expression in Adipose Tissue of Diet-Induced Obese Mice by Microarray and Reverse Transcription-Polymerase Chain Reaction Analyses. *Endocrinology.* 2003;144(11):4773–82.
 173. Dahlman I, Linder K, Nordström EA, Andersson I, Lidén J, Verdich C, et al. Changes in adipose tissue gene expression with energy-restricted diets in obese women. *Am J Clin Nutr.* 2005;81(6):1275–85.
 174. Dahlman I, Kaaman M, Jiao H, Kere J, Laakso M, Arner P. The CIDEA gene V115F polymorphism is associated with obesity in Swedish subjects. *Diabetes.* 2005;54(10):3032–4.
 175. Sztalryd C, Brasaemle DL. The perilipin family of lipid droplet proteins: Gatekeepers of intracellular lipolysis. *Biochim Biophys Acta - Mol Cell Biol Lipids.* 2017;1862(10):1221–32.
 176. Bickel PE, Tansey JT, Welte MA. PAT proteins, an ancient family of lipid droplet proteins that regulate cellular lipid stores. *Biochim Biophys Acta - Mol Cell Biol Lipids.* 2009 Jun;1791(6):419–40.
 177. Sztalryd C, Kimmel AR. Perilipins: Lipid droplet coat proteins adapted for tissue-specific energy storage and utilization, and lipid cytoprotection.

- Biochimie. 2014 Jan;96:96–101.
178. Carr RM, Ahima RS. Pathophysiology of lipid droplet proteins in liver diseases. *Exp Cell Res*. 2016 Jan;340(2):187–92.
 179. Granneman JG, Moore HPH, Mottillo EP, Zhu Z, Zhou L. Interactions of Perilipin-5 (Plin5) with adipose triglyceride lipase. *J Biol Chem*. 2011;286(7):5126–35.
 180. Gallardo-Montejano VI, Saxena G, Kusminski CM, Yang C, McAfee JL, Hahner L, et al. Nuclear Perilipin 5 integrates lipid droplet lipolysis with PGC-1 α /SIRT1-dependent transcriptional regulation of mitochondrial function. *Nat Commun*. 2016;7:1–14.
 181. Wolins NE, Quaynor BK, Skinner JR, Tzekov A, Croce MA, Gropler MC, et al. OXPAT/PAT-1 is a PPAR-induced lipid droplet protein that promotes fatty acid utilization. *Diabetes*. 2006;55(12):3418–28.
 182. Najt CP, Khan SA, Heden TD, Witthuhn BA, Perez M, Heier JL, et al. Lipid Droplet-Derived Monounsaturated Fatty Acids Traffic via PLIN5 to Allosterically Activate SIRT1. *Mol Cell*. 2020;77(4):810-824.e8.
 183. Perera RJ, Marcusson EG, Koo S, Kang X, Kim Y, White N, et al. Identification of novel PPAR γ target genes in primary human adipocytes. *Gene*. 2006;369(1–2):90–9.
 184. Leonardsson G, Steel JH, Christian M, Pocock V, Milligan S, Bell J, et al. Nuclear receptor corepressor RIP140 regulates fat accumulation. *Proc Natl Acad Sci U S A*. 2004;101(22):8437–42.
 185. Ali AT, Hochfeld WE, Myburgh R, Pepper MS. Adipocyte and adipogenesis. *Eur J Cell Biol*. 2013;92(6–7):229–36.
 186. Wang Y, Hudak C, Sul HS. Role of preadipocyte factor 1 in adipocyte differentiation. *Clin Lipidol*. 2010;5(1):109–15.
 187. Obregon M-J. Thyroid Hormone and Adipocyte Differentiation. *Thyroid*. 2008 Feb;18(2):185–95.
 188. Klemm DJ, Leitner JW, Watson P, Nesterova A, Reusch JEB, Goalstone ML, et al. Insulin-induced adipocyte differentiation: Activation of CREB rescues adipogenesis from the arrest caused by inhibition of prenylation. *J Biol Chem*. 2001;276(30):28430–5.
 189. Moustaid N, Lasnier F, Hainque B, Quignard-Boulange A, Pairault J. Analysis of gene expression during adipogenesis in 3T3-F442A preadipocytes: Insulin

- and dexamethasone control. *J Cell Biochem.* 1990;42(4):243–54.
190. Chapman AB, Knight DM, Dieckmann BS, Ringold GM. Analysis of gene expression during differentiation of adipogenic cells in culture and hormonal control of the developmental program. *J Biol Chem.* 1984;259(24):15548–55.
 191. Essayan DM. Cyclic nucleotide phosphodiesterases. *J Allergy Clin Immunol.* 2001;108(5):671–80.
 192. Styner M, Sen B, Xie Z, Case N, Rubin J. Indomethacin promotes adipogenesis of mesenchymal stem cells through a cyclooxygenase independent mechanism. *J Cell Biochem.* 2010 Nov 1;111(4):1042–50.
 193. Lehmann JM, Moore LB, Smith-Oliver TA, Wilkison WO, Willson TM, Kliewer SA. An antidiabetic thiazolidinedione is a high affinity ligand for peroxisome proliferator-activated receptor γ (PPAR γ). Vol. 270, *Journal of Biological Chemistry.* 1995. p. 12953–6.
 194. Gburcik V, Cawthorn WP, Nedergaard J, Timmons JA, Cannon B. An essential role for *tbx15* in the differentiation of brown and “brite” but not white adipocytes. *Am J Physiol - Endocrinol Metab.* 2012;303(8):1053–60.
 195. Ikeda K, Maretich P, Kajimura S. The Common and Distinct Features of Brown and Beige Adipocytes. *Trends Endocrinol Metab.* 2018 Mar;29(3):191–200.
 196. Mund RA, Frishman WH. Brown adipose tissue thermogenesis: $\beta 3$ adrenoreceptors as a potential target for the treatment of obesity in humans. *Cardiol Rev.* 2013;21(6):265–9.
 197. Beranger GE, Karbiener M, Barquissau V, Pisani DF, Scheideler M, Langin D, et al. In vitro brown and “brite”/“beige” adipogenesis: Human cellular models and molecular aspects. *Biochim Biophys Acta - Mol Cell Biol Lipids.* 2013;1831(5):905–14.
 198. Sell H, Berger JP, Samson P, Castriota G, Lalonde J, Deshaies Y, et al. Peroxisome proliferator-activated receptor γ agonism increases the capacity for sympathetically mediated thermogenesis in lean and *ob/ob* mice. *Endocrinology.* 2004;145(8):3925–34.
 199. Ghorbani M, Shafiee Ardestani M, Gigloo SH, Cohan RA, Inanlou DN, Ghorbani P. Anti Diabetic effect of CL 316,243 (A $\beta 3$ -Adrenergic Agonist) by Down Regulation of Tumour Necrosis Factor (TNF- α) Expression. *PLoS One.* 2012;7(10):7–11.
 200. De Souza CJ, Hirshman MF, Horton ES. CL-316,243, a $\beta 3$ -specific

- adrenoceptor agonist, enhances insulin-stimulated glucose disposal in nonobese rats. *Diabetes*. 1997;46(8):1257–63.
201. Czech MP. Mechanisms of insulin resistance related to white, beige, and brown adipocytes. *Mol Metab*. 2020;34(January):27–42.
 202. World Health Organization [WHO]. Obesity and overweight. 2020;April.
 203. Weir CB, Jan A. BMI Classification Percentile And Cut Off Points. *StatPearls*. 2020.
 204. McNelis JC, Olefsky JM. Macrophages, Immunity, and Metabolic Disease. *Immunity*. 2014;41(1):36–48.
 205. Leitner BP, Huang S, Brychta RJ, Duckworth CJ, Baskin AS, McGehee S, et al. Mapping of human brown adipose tissue in lean and obese young men. *Proc Natl Acad Sci U S A*. 2017 Aug 8;114(32):8649–54.
 206. Vijgen GHEJ, Bouvy ND, Teule GJJ, Brans B, Schrauwen P, van Marken Lichtenbelt WD. Brown adipose tissue in morbidly obese subjects. *PLoS One*. 2011;6(2):2–7.
 207. Matsushita M, Yoneshiro T, Aita S, Kameya T, Sugie H, Saito M. Impact of brown adipose tissue on body fatness and glucose metabolism in healthy humans. *Int J Obes*. 2014;38(6):812–7.
 208. Vijgen GHEJ, Bouvy ND, Teule GJJ, Brans B, Hoeks J, Schrauwen P, et al. Increase in brown adipose tissue activity after weight loss in morbidly obese subjects. *J Clin Endocrinol Metab*. 2012;97(7):1229–33.
 209. Adami GF, Carbone F, Montecucco F, Camerini G, Cordera R. Adipose Tissue Composition in Obesity and After Bariatric Surgery. *Obes Surg*. 2019;29(9):3030–8.
 210. Dadson P, Hannukainen JC, Din MU, Lahesmaa M, Kalliokoski KK, Iozzo P, et al. Brown adipose tissue lipid metabolism in morbid obesity: Effect of bariatric surgery-induced weight loss. *Diabetes, Obes Metab*. 2018;20(5):1280–8.
 211. Hankir MK, Seyfried F. Do Bariatric Surgeries Enhance Brown/Beige Adipose Tissue Thermogenesis? *Front Endocrinol (Lausanne)*. 2020;11(April):1–11.
 212. Sakamoto T, Nitta T, Maruno K, Yeh YS, Kuwata H, Tomita K, et al. Macrophage infiltration into obese adipose tissues suppresses the induction of UCP1 level in mice. *Am J Physiol - Endocrinol Metab*. 2016;310(8):E676–87.
 213. Rissanen A, Orava J, Nuutila P, Noponen T, Parkkola R, Viljanen T, et al.

- Blunted Metabolic Responses to Cold and Insulin Stimulation in Brown Adipose Tissue of Obese Humans. *Obes (Silver Spring)*. 2013;21(11):2279–87.
214. Koksharova E, Ustyuzhanin D, Philippov Y, Mayorov A, Shestakova M, Shariya M, et al. The Relationship Between Brown Adipose Tissue Content in Supraclavicular Fat Depots and Insulin Sensitivity in Patients with Type 2 Diabetes Mellitus and Prediabetes. *Diabetes Technol Ther*. 2017;19(2):96–102.
 215. Chondronikola M, Volpi E, Børsheim E, Porter C, Annamalai P, Enerbäck S, et al. Brown Adipose Tissue Improves Whole-Body Glucose Homeostasis and Insulin Sensitivity in Humans. *Diabetes*. 2014 Dec 1;63(12):4089–99.
 216. Wu C, Cheng W, Sun Y, Dang Y, Gong F, Zhu H, et al. Activating brown adipose tissue for weight loss and lowering of blood glucose levels: A microPET study using obese and diabetic model mice. *PLoS One*. 2014 Dec;9(12):1–14.
 217. Entringer S, Rasmussen J, Cooper DM, Ikenoue S, Waffarn F, Wadhwa PD, et al. Association between supraclavicular brown adipose tissue composition at birth and adiposity gain from birth to 6 months of age. *Pediatr Res*. 2017;82(6):1017–21.
 218. Shankar K, Kumar D, Gupta S, Varshney S, Rajan S, Srivastava A, et al. Role of brown adipose tissue in modulating adipose tissue inflammation and insulin resistance in high-fat diet fed mice. *Eur J Pharmacol*. 2019;854(February):354–64.
 219. Stanford KI, Middelbeek RJW, Townsend KL, An D, Nygaard EB, Hitchcox KM, et al. Brown adipose tissue regulates glucose homeostasis and insulin sensitivity. *J Clin Invest*. 2013 Jan 2;123(1):215–23.
 220. Liu X, Wang S, You Y, Meng M, Zheng Z, Dong M, et al. Brown Adipose Tissue Transplantation Reverses Obesity in Ob / Ob Mice. *Endocrinology*. 2015 Jul;156(July):2461–9.
 221. Xiaomeng L, Zongji Z, Xiaoming Z, Minghui M, Lan L, Yanyan S, et al. Brown adipose tissue transplantation improves whole-body energy metabolism. *Cell Res*. 2013;23:851–4.
 222. Bråkenhielm E, Cao R, Gao B, Angelin B, Cannon B, Parini P, et al. Angiogenesis Inhibitor, TNP-470, Prevents Diet-Induced and Genetic Obesity in Mice. *Circ Res*. 2004 Jun 25;94(12):1579–88.
 223. Cao Y. Angiogenesis modulates adipogenesis and obesity. *J Clin Invest*. 2007

Sep 4;117(9):2362–8.

- 224. Folkman J. Angiogenesis in cancer, vascular, rheumatoid and other disease. *Nat Med.* 1995 Jan;1(1):27–30.
- 225. Pellegrinelli V, Carobbio S, Vidal-Puig A. Adipose tissue plasticity: how fat depots respond differently to pathophysiological cues. *Diabetologia.* 2016;59(6):1075–88.
- 226. Tinahones FJ, Coín-Aragüez L, Mayas MD, Garcia-Fuentes E, Hurtado-Del-Pozo C, Vendrell J, et al. Obesity-associated insulin resistance is correlated to adipose tissue vascular endothelial growth factors and metalloproteinase levels. *BMC Physiol.* 2012;12(1):4.
- 227. Choe SS, Huh JY, Hwang IJ, Kim JI, Kim JB. Adipose tissue remodeling: Its role in energy metabolism and metabolic disorders. *Front Endocrinol (Lausanne).* 2016;7(APR):1–16.
- 228. Wang QA, Tao C, Gupta RK, Scherer PE. Tracking adipogenesis during white adipose tissue development, expansion and regeneration. *Nat Med.* 2013;19(10):1338–44.
- 229. Joe AWB, Lin Y, Even Y, Vogl AW, Rossi FMV. Depot-specific differences in adipogenic progenitor abundance and proliferative response to high-fat diet. *Stem Cells.* 2009;27(10):2563–70.
- 230. Hammarstedt A, Gogg S, Hedjazifar S, Nerstedt A, Smith U. Impaired adipogenesis and dysfunctional adipose tissue in human hypertrophic obesity. *Physiol Rev.* 2018;98(4):1911–41.
- 231. Salans LB, Cushman SW, Weismann RE. Studies of human adipose tissue. Adipose cell size and number in nonobese and obese patients. *J Clin Invest.* 1973;52(4):929–41.
- 232. Bukowiecki L, Lupien J, Follea N. Mechanism of enhanced lipolysis in adipose tissue of exercise-trained rats. *Am J Physiol - Endocrinol Metab.* 1980;2(6).
- 233. Ye J. Mechanisms of insulin resistance in obesity. *Front Med.* 2013 Mar 9;7(1):14–24.
- 234. Collier B, Dossett LA, May AK, Diaz JJ. Glucose control and the inflammatory response. *Nutr Clin Pract.* 2008;23(1):3–15.
- 235. van Diepen JA, Berbée JFP, Havekes LM, Rensen PCN. Interactions between inflammation and lipid metabolism: Relevance for efficacy of anti-inflammatory drugs in the treatment of atherosclerosis. *Atherosclerosis.*

2013;228(2):306–15.

- 236. Schedlowski M, Engler H, Grigoleit JS. Endotoxin-induced experimental systemic inflammation in humans: A model to disentangle immune-to-brain communication. *Brain Behav Immun*. 2014;35:1–8.
- 237. Trayhurn P, Wang B, Wood IS. Hypoxia in adipose tissue: A basis for the dysregulation of tissue function in obesity? *Br J Nutr*. 2008;100(2):227–35.
- 238. Rupnick MA, Panigrahy D, Zhang CY, Dallabrida SM, Lowell BB, Langer R, et al. Adipose tissue mass can be regulated through the vasculature. *Proc Natl Acad Sci U S A*. 2002;99(16):10730–5.
- 239. Cohen P, Spiegelman BM. Brown and beige fat: Molecular parts of a thermogenic machine. *Diabetes*. 2015;64(7):2346–51.
- 240. Xue Y, Petrovic N, Cao R, Larsson O, Lim S, Chen S, et al. Hypoxia-Independent Angiogenesis in Adipose Tissues during Cold Acclimation. *Cell Metab*. 2009;9(1):99–109.
- 241. Lim S, Honek J, Xue Y, Seki T, Cao Z, Andersson P, et al. Cold-induced activation of brown adipose tissue and adipose angiogenesis in mice. *Nat Protoc*. 2012;7(3):606–15.
- 242. Sun K, Kusminski CM, Luby-Phelps K, Spurgin SB, An YA, Wang QA, et al. Brown adipose tissue derived VEGF-A modulates cold tolerance and energy expenditure. *Mol Metab*. 2014;3(4):474–83.
- 243. Nisoli E, Clementi E, Tonello C, Sciorati C, Briscini L, Carruba MO. Effects of nitric oxide on proliferation and differentiation of rat brown adipocytes in primary cultures. *Br J Pharmacol*. 1998;125(4):888–94.
- 244. Mahdavian K, Chess D, Wu Y, Shirihai O, Aprahamian TR. Autocrine effect of vascular endothelial growth factor-A is essential for mitochondrial function in brown adipocytes. *Metabolism*. 2016 Jan;65(1):26–35.
- 245. Shimizu I, Aprahamian T, Kikuchi R, Shimizu A, Papanicolaou KN, MacLauchlan S, et al. Vascular rarefaction mediates whitening of brown fat in obesity. *J Clin Invest*. 2014 May 1;124(5):2099–112.
- 246. Friederich-Persson M, Nguyen Dinh Cat A, Persson P, Montezano AC, Touyz RM. Brown Adipose Tissue Regulates Small Artery Function Through NADPH Oxidase 4-Derived Hydrogen Peroxide and Redox-Sensitive Protein Kinase G-1. *Arterioscler Thromb Vasc Biol*. 2017;37(3):455–65.
- 247. N. F, K. C-M, H. C, M. D, L. L, K.S. O, et al. Heterozygous embryonic lethality

- induced by targeted inactivation of the VEGF gene. *Nature*. 1996;380(6573):439–42.
248. Dvorak HF, Brown LF, Detmar M, Dvorak AM. Vascular permeability factor/vascular endothelial growth factor, microvascular hyperpermeability, and angiogenesis. *Am J Pathol*. 1995;146(5):1029–39.
 249. Carmeliet P, Ng YS, Nuyens D, Theilmeier G, Brusselmans K, Cornelissen I, et al. Impaired myocardial angiogenesis and ischemic cardiomyopathy in mice lacking the vascular endothelial growth factor isoforms VEGF164 and VEGF188. *Nat Med*. 1999;5(5):495–502.
 250. Makino Y, Kanopka A, Wilson WJ, Tanaka H, Poellinger L. Inhibitory PAS domain protein (IPAS) is a hypoxia-inducible splicing variant of the hypoxia-inducible factor-3 α locus. *J Biol Chem*. 2002;277(36):32405–8.
 251. Huang LE, Bindra RS, Glazer PM, Harris AL. Hypoxia-induced genetic instability - A calculated mechanism underlying tumor progression. *J Mol Med*. 2007;85(2):139–48.
 252. Ryan HE. HIF-1 α is required for solid tumor formation and embryonic vascularization. *EMBO J*. 1998 Jun 1;17(11):3005–15.
 253. Gealekman O, Burkart A, Chouinard M, Nicoloso SM, Straubhaar J, Corvera S. Enhanced angiogenesis in obesity and in response to PPAR γ activators through adipocyte VEGF and ANGPTL4 production. *Am J Physiol - Endocrinol Metab*. 2008;295(5):1056–65.
 254. Wree A, Mayer A, Westphal S, Beilfuss A, Canbay A, Schick RR, et al. Adipokine expression in brown and white adipocytes in response to hypoxia. *J Endocrinol Invest*. 2012;35(5):522–7.
 255. Elias I, Franckhauser S, Bosch F. New insights into adipose tissue VEGF-A actions in the control of obesity and insulin resistance. *Adipocyte*. 2013;2(2):109–12.
 256. Elias I, Franckhauser S, Ferré T, Vilà L, Tafuro S, Muñoz S, et al. Adipose tissue overexpression of vascular endothelial growth factor protects against diet-induced obesity and insulin resistance. *Diabetes*. 2012;61(7):1801–13.
 257. Sung HK, Doh KO, Son JE, Park JG, Bae Y, Choi S, et al. Adipose vascular endothelial growth factor regulates metabolic homeostasis through angiogenesis. *Cell Metab*. 2013;17(1):61–72.
 258. Michailidou Z, Turban S, Miller E, Zou X, Schrader J, Ratcliffe PJ, et al.

- Increased angiogenesis protects against adipose hypoxia and fibrosis in metabolic disease-resistant 11 β -hydroxysteroid dehydrogenase type 1 (HSD1)-deficient mice. *J Biol Chem*. 2012;287(6):4188–97.
259. Halberg N, Khan T, Trujillo ME, Wernstedt-Asterholm I, Attie AD, Sherwani S, et al. Hypoxia-Inducible Factor 1 α Induces Fibrosis and Insulin Resistance in White Adipose Tissue. *Mol Cell Biol*. 2009;29(16):4467–83.
 260. Hosogai N, Fukuhara A, Oshima K, Miyata Y, Tanaka S, Segawa K, et al. Adipose tissue hypoxia in obesity and its impact on adipocytokine dysregulation. *Diabetes*. 2007;56(4):901–11.
 261. Rausch ME, Weisberg S, Vardhana P, Tortoriello D V. Obesity in C57BL/6J mice is characterized by adipose tissue hypoxia and cytotoxic T-cell infiltration. *Int J Obes*. 2008;32(3):451–63.
 262. Mazzatti D, Lim FL, O'Hara A, Wood IS, Trayhurn P. A microarray analysis of the hypoxia-induced modulation of gene expression in human adipocytes. *Arch Physiol Biochem*. 2012;118(3):112–20.
 263. Pasarica M, Sereda OR, Redman LM, Albarado DC, Hymel DT, Roan LE, et al. Reduced adipose tissue oxygenation in human obesity evidence for rarefaction, macrophage chemotaxis, and inflammation without an angiogenic response. *Diabetes*. 2009;58(3):718–25.
 264. Goossens GH, Bizzarri A, Venteclef N, Essers Y, Cleutjens JP, Konings E, et al. Increased adipose tissue oxygen tension in obese compared with lean men is accompanied by insulin resistance, impaired adipose tissue capillarization, and inflammation. *Circulation*. 2011;124(1):67–76.
 265. Karpe F, Fielding BA, Ilic V, Macdonald IA, Summers LKM, Frayn KN. Impaired Postprandial Adipose Tissue Blood Flow Response Is Related to Aspects of Insulin Sensitivity. *Diabetes*. 2002 Aug 1;51(8):2467–73.
 266. Ruiz-Ojeda, Méndez-Gutiérrez, Aguilera, Plaza-Díaz. Extracellular Matrix Remodeling of Adipose Tissue in Obesity and Metabolic Diseases. *Int J Mol Sci*. 2019 Oct 2;20(19):4888.
 267. Sun K, Park J, Gupta OT, Holland WL, Auerbach P, Zhang N, et al. Endotrophin triggers adipose tissue fibrosis and metabolic dysfunction. *Nat Commun*. 2014;5(2014):3485.
 268. Lawler HM, Underkofler CM, Kern PA, Erickson C, Bredbeck B, Rasouli N. Adipose tissue hypoxia, inflammation, and fibrosis in obese insulin-sensitive

- and obese insulin-resistant subjects. *J Clin Endocrinol Metab.* 2016;101(4):1422–8.
269. Nakajima I, Yamaguchi T, Ozutsumi K, Aso H. Adipose tissue extracellular matrix: Newly organized by adipocytes during differentiation. *Differentiation.* 1998;63(4):193–200.
 270. Mori S, Kiuchi S, Ouchi A, Hase T, Murase T. Characteristic expression of extracellular matrix in subcutaneous adipose tissue development and adipogenesis; Comparison with visceral adipose tissue. *Int J Biol Sci.* 2014;10(8):825–33.
 271. Lin D, Chun T-H, Kang L. Adipose extracellular matrix remodelling in obesity and insulin resistance. *Biochem Pharmacol.* 2016 Nov;119(3):8–16.
 272. Spencer M, Unal R, Zhu B, Rasouli N, McGehee RE, Peterson CA, et al. Adipose tissue extracellular matrix and vascular abnormalities in obesity and insulin resistance. *J Clin Endocrinol Metab.* 2011;96(12):1990–8.
 273. Divoux A, Tordjman J, Lacasa D, Veyrie N, Hugol D, Aissat A, et al. Fibrosis in human adipose tissue: Composition, distribution, and link with lipid metabolism and fat mass loss. *Diabetes.* 2010;59(11):2817–25.
 274. Sun K, Tordjman J, Clément K, Scherer PE. Fibrosis and Adipose Tissue Dysfunction. *Cell Metab.* 2013 Oct;18(4):470–7.
 275. Cescon M, Gattazzo F, Chen P, Bonaldo P. Collagen VI at a glance. *J Cell Sci.* 2015 Oct 1;128(19):3525–31.
 276. Khan T, Muise ES, Iyengar P, Wang Z V., Chandalia M, Abate N, et al. Metabolic Dysregulation and Adipose Tissue Fibrosis: Role of Collagen VI. *Mol Cell Biol.* 2009;29(6):1575–91.
 277. Villarroya J, Cereijo R, Giralt M, Villarroya F. Secretory proteome of brown adipocytes in response to cAMP-mediated thermogenic activation. *Front Physiol.* 2019;10(FEB):1–8.
 278. Varma V, Yao-Borengasser A, Bodles AM, Rasouli N, Phanavanh B, Nolen GT, et al. Thrombospondin-1 Is an Adipokine Associated With Obesity, Adipose Inflammation, and Insulin Resistance. *Diabetes.* 2008 Feb 1;57(2):432–9.
 279. Matsuo Y, Tanaka M, Yamakage H, Sasaki Y, Muranaka K, Hata H, et al. Thrombospondin 1 as a novel biological marker of obesity and metabolic syndrome. *Metabolism.* 2015 Nov;64(11):1490–9.

280. Inoue M, Jiang Y, Barnes RH, Tokunaga M, Martinez-Santibañez G, Geletka L, et al. Thrombospondin 1 mediates high-fat diet-induced muscle fibrosis and insulin resistance in male mice. *Endocrinology*. 2013;154(12):4548–59.
281. Li Y, Tong X, Rumala C, Clemons K, Wang S. Thrombospondin1 deficiency reduces obesity-associated inflammation and improves insulin sensitivity in a diet-induced obese mouse model. *PLoS One*. 2011;6(10).
282. Matsugi K, Hosooka T, Nomura K, Ogawa W. Thrombospondin 1 suppresses insulin signaling in C2C12 myotubes. *Kobe J Med Sci*. 2016;62(1):E13–8.
283. Hynes RO. Integrins: Bidirectional, Allosteric Signaling Machines. *Cell*. 2002 Sep;110(6):673–87.
284. Meakin PJ, Morrison VL, Sneddon CC, Savinko T, Uotila L, Jalicy SM, et al. Mice lacking beta2-integrin function remain glucose tolerant in spite of insulin resistance, neutrophil infiltration and inflammation. *PLoS One*. 2015;10(9):1–15.
285. Kang L, Ayala JE, Lee-Young RS, Zhang Z, James FD, Neuffer PD, et al. Diet-induced muscle insulin resistance is associated with extracellular matrix remodeling and interaction with integrin $\alpha 2\beta 1$ in mice. *Diabetes*. 2011;60(2):416–26.
286. Naor D, Sionov RV, Ish-Shalom D. CD44: Structure, function, and association with the malignant process. *Adv Cancer Res*. 1997;71(February 1997):241–319.
287. Kang HS, Liao G, DeGraff LM, Gerrish K, Bortner CD, Garantzotis S, et al. CD44 Plays a Critical Role in Regulating Diet-Induced Adipose Inflammation, Hepatic Steatosis, and Insulin Resistance. *PLoS One*. 2013;8(3).
288. Kodama K, Horikoshi M, Toda K, Yamada S, Hara K, Irie J, et al. Expression-based genome-wide association study links the receptor CD44 in adipose tissue with type 2 diabetes. *Proc Natl Acad Sci U S A*. 2012;109(18):7049–54.
289. Bonnans C, Chou J, Werb Z. Remodelling the extracellular matrix in development and disease. *Nat Rev Mol Cell Biol*. 2014;15(12):786–801.
290. Chavey C, Mari B, Monthouel MN, Bonnafous S, Anglard P, Van Obberghen E, et al. Matrix metalloproteinases are differentially expressed in adipose tissue during obesity and modulate adipocyte differentiation. *J Biol Chem*. 2003;278(14):11888–96.
291. Caolo V, Swennen G, Chalaris A, Wagenaar A, Verbruggen S, Rose-John S, et al. ADAM10 and ADAM17 have opposite roles during sprouting angiogenesis.

- Angiogenesis. 2015;18(1):13–22.
292. Moest H, Frei AP, Bhattacharya I, Geiger M, Wollscheid B, Wolfrum C. Malfunctioning of adipocytes in obesity is linked to quantitative surfaceome changes. *Biochim Biophys Acta - Mol Cell Biol Lipids*. 2013;1831(7):1208–16.
 293. Strissel KJ, Stancheva Z, Miyoshi H, Perfield JW, DeFuria J, Jick Z, et al. Adipocyte death, adipose tissue remodeling, and obesity complications. *Diabetes*. 2007;56(12):2910–8.
 294. Kahn SE. The relative contributions of insulin resistance and beta-cell dysfunction to the pathophysiology of Type 2 diabetes. *Diabetologia*. 2003;46(1):3–19.
 295. Butler AE, Janson J, Bonner-Weir S, Ritzel R, Rizza RA, Butler PC. β -Cell Deficit and Increased β -Cell Apoptosis in Humans With Type 2 Diabetes. *Diabetes*. 2003 Jan 1;52(1):102–10.
 296. Kahn BB, Flier JS. Obesity and insulin resistance. *J Clin Invest*. 2000 Aug 15;106(4):473–81.
 297. Rhodes CJ. Type 2 diabetes - A matter of β -cell life and death? *Science* (80-). 2005;307(5708):380–4.
 298. Dennedy MC, Vidal-Puig A. Review Article: An Adipocentric View of the Metabolic Syndrome and Cardiovascular Disease. *Curr Cardiovasc Risk Rep*. 2014;8(3):1–9.
 299. Frayn KN, Shadid S, Hamrani R, Humphreys SM, Clark ML, Fielding BA, et al. Regulation of fatty acid movement in human adipose tissue in the postabsorptive-to-postprandial transition. *Am J Physiol - Endocrinol Metab*. 1994;266(3 29-3).
 300. Christianson JL, Nicoloso S, Straubhaar J, Czech MP. Stearoyl-CoA desaturase 2 is required for peroxisome proliferator-activated receptor γ expression and adipogenesis in cultured 3T3-L1 cells. *J Biol Chem*. 2008;283(5):2906–16.
 301. Itani SI, Ruderman NB, Schmieder F, Boden G. Lipid-induced insulin resistance in human muscle is associated with changes in diacylglycerol, protein kinase C, and I κ B- α . *Diabetes*. 2002;51(7):2005–11.
 302. Hotamisligil GS. Inflammation and metabolic disorders. *Nature*. 2006 Dec 13;444(7121):860–7.
 303. Glass CK, Olefsky JM. Inflammation and lipid signaling in the etiology of

- insulin resistance. *Cell Metab.* 2012;15(5):635–45.
304. Prieur X, Mok CYL, Velagapudi VR, Núñez V, Fuentes L, Montaner D, et al. Differential lipid partitioning between adipocytes and tissue macrophages modulates macrophage lipotoxicity and M2/M1 polarization in obese mice. *Diabetes.* 2011;60(3):797–809.
 305. Langin D. Recruitment of brown fat and conversion of white into brown adipocytes: Strategies to fight the metabolic complications of obesity? *Biochim Biophys Acta - Mol Cell Biol Lipids.* 2010;1801(3):372–6.
 306. Shao M, Wang QA, Song A, Vishvanath L, Busbuso NC, Scherer PE, et al. Cellular origins of beige fat cells revisited. *Diabetes.* 2019;68(10):1874–85.
 307. Maurer S, Harms M, Boucher J. The colorful versatility of adipocytes: white-to-brown transdifferentiation and its therapeutic potential in man. *FEBS J.* 2020 Jul 22;febs.15470.
 308. Lizcano F. The beige adipocyte as a therapy for metabolic diseases. *Int J Mol Sci.* 2019;20(20).
 309. Yoneshiro T, Aita S, Matsushita M, Kameya T, Nakada K, Kawai Y, et al. Brown adipose tissue, whole-body energy expenditure, and thermogenesis in healthy adult men. *Obesity.* 2011;19(1):13–6.
 310. Nascimento EBM, Sparks LM, Divoux A, van Gisbergen MW, Broeders EPM, Jørgensen JA, et al. Genetic Markers of Brown Adipose Tissue Identity and In Vitro Brown Adipose Tissue Activity in Humans. *Obesity.* 2018;26(1):135–40.
 311. McArdle MA, Finucane OM, Connaughton RM, McMorrow AM, Roche HM. Mechanisms of obesity-induced inflammation and insulin resistance: Insights into the emerging role of nutritional strategies. *Front Endocrinol (Lausanne).* 2013;4(MAY):1–23.
 312. Roberts-Toler C, O'Neill BT, Cypess AM. Diet-induced obesity causes insulin resistance in mouse brown adipose tissue. *Obesity.* 2015;23(9):1765–70.
 313. Valverde AM, Teruel T, Navarro P, Benito M, Lorenzo M. Tumor necrosis factor- α causes insulin receptor substrate-2-mediated insulin resistance and inhibits insulin-induced adipogenesis in fetal brown adipocytes. *Endocrinology.* 1998 Mar;139(3):1229–38.
 314. Lorenzo M, Fernández-Veledo S, Vila-Bedmar R, Garcia-Guerra L, De Alvaro C, Nieto-Vazquez I. Insulin resistance induced by tumor necrosis factor- α in myocytes and brown adipocytes¹². *J Anim Sci.* 2008 Apr 1;86(suppl_14):E94–

315. Nieto-Vazquez I, Fernández-Veledo S, Krämer DK, Vila-Bedmar R, Garcia-Guerra L, Lorenzo M. Insulin resistance associated to obesity: The link TNF- α . *Arch Physiol Biochem*. 2008;114(3):183–94.
316. Albert V, Svensson K, Shimobayashi M, Colombi M, Muñoz S, Jimenez V, et al. mTORC 2 sustains thermogenesis via Akt-induced glucose uptake and glycolysis in brown adipose tissue . *EMBO Mol Med*. 2016;8(3):232–46.
317. Martinez N, Cheng CY, Ketheesan N, Cullen A, Tang Y, Lum J, et al. mTORC2/Akt activation in adipocytes is required for adipose tissue inflammation in tuberculosis. *EBioMedicine*. 2019;45:314–27.
318. Saltiel AR, Olefsky JM. Inflammatory linking obesity and metabolic disease and metabolic disease. *J Clin Invest*. 2017;127(1):1–4.
319. Sakamoto T, Takahashi N, Sawaragi Y, Naknukool S, Yu R, Goto T, et al. Inflammation induced by RAW macrophages suppresses UCP1 mRNA induction via ERK activation in 10T1/2 adipocytes. *Am J Physiol Physiol*. 2013;304(8):C729–38.
320. Goto T, Naknukool S, Yoshitake R, Hanafusa Y, Tokiwa S, Li Y, et al. Proinflammatory cytokine interleukin-1 β suppresses cold-induced thermogenesis in adipocytes. *Cytokine*. 2016;77:107–14.
321. Rebiger L, Lenzen S, Mehmeti I. Susceptibility of brown adipocytes to pro-inflammatory cytokine toxicity and reactive oxygen species. *Biosci Rep*. 2016;36(2):1–11.
322. García M del C, Pazos P, Lima L, Diéguez C. Regulation of energy expenditure and brown/beige thermogenic activity by interleukins: New roles for old actors. *Int J Mol Sci*. 2018;19(9).
323. van den Berg SM, van Dam AD, Rensen PCN, de Winther MPJ, Lutgens E. Immune modulation of brown(ing) adipose tissue in obesity. *Endocr Rev*. 2017;38(1):46–68.
324. Thomas D, Apovian C. Macrophage functions in lean and obese adipose tissue. *Metabolism*. 2017 Jul;72(5):120–43.
325. Reitman ML. How Does Fat Transition from White to Beige? *Cell Metab*. 2017;26(1):14–6.
326. Finlin BS, Zhu B, Confides AL, Westgate PM, Harfmann BD, Dupont-Versteegden EE, et al. Mast cells promote seasonal white adipose beiging in

- humans. *Diabetes*. 2017;66(5):1237–46.
327. Brestoff JR, Artis D. Immune Regulation of Metabolic Homeostasis in Health and Disease. *Cell*. 2015 Mar;161(1):146–60.
 328. Brestoff JR, Kim BS, Saenz SA, Stine RR, Monticelli LA, Sonnenberg GF, et al. Group 2 innate lymphoid cells promote beiging of white adipose tissue and limit obesity. *Nature*. 2015 Mar 22;519(7542):242–6.
 329. Lee SE, Kang SG, Choi MJ, Jung SB, Ryu MJ, Chung HK, et al. Growth Differentiation Factor 15 Mediates Systemic Glucose Regulatory Action of T-Helper Type 2 Cytokines. *Diabetes*. 2017;66(11):2774–88.
 330. Chung K-J, Chatzigeorgiou A, Economopoulou M, Garcia-Martin R, Alexaki VI, Mitroulis I, et al. A self-sustained loop of inflammation-driven inhibition of beige adipogenesis in obesity. *Nat Immunol*. 2017 Jun 17;18(6):654–64.
 331. Campderrós L, Moure R, Cairó M, Gavalda-Navarro A, Quesada-López T, Cereijo R, et al. Brown Adipocytes Secrete GDF15 in Response to Thermogenic Activation. *Obesity*. 2019;27(10):1606–16.
 332. Hui X, Gu P, Zhang J, Nie T, Pan Y, Wu D, et al. Adiponectin Enhances Cold-Induced Browning of Subcutaneous Adipose Tissue via Promoting M2 Macrophage Proliferation. *Cell Metab*. 2015;22(2):279–90.
 333. Lv Y, Zhang SY, Liang X, Zhang H, Xu Z, Liu B, et al. Adrenomedullin 2 enhances beiging in white adipose tissue directly in an adipocyte-autonomous manner and indirectly through activation of M2 macrophages. *J Biol Chem*. 2016;291(45):23390–402.
 334. Rao RR, Long JZ, White JP, Svensson KJ, Lou J, Lokurkar I, et al. Meteorin-like is a hormone that regulates immune-adipose interactions to increase beige fat thermogenesis. *Cell*. 2014 Jun;157(6):1279–91.
 335. Zhang X, Wang X, Yin H, Zhang L, Feng A, Zhang QX, et al. Functional Inactivation of Mast Cells Enhances Subcutaneous Adipose Tissue Browning in Mice. *Cell Rep*. 2019;28(3):792-803.e4.
 336. Villarroya F, Cereijo R, Gavalda-Navarro A, Villarroya J, Giralt M. Inflammation of brown/beige adipose tissues in obesity and metabolic disease. *J Intern Med*. 2018;284(5):492–504.
 337. Odegaard JI, Kahn CR. Mechanisms of macrophage activation in obesity-induced insulin resistance. *Nat Clin Pr Endocrinol Metab*. 2008;4(11):619–26.
 338. Tilg H, Moschen AR. Inflammatory mechanisms in the regulation of insulin

- resistance. *Mol Med*. 2008;14(3–4):222–31.
339. Chawla A, Nguyen KD, Goh YPS. Macrophage-mediated inflammation in metabolic disease. *Nat Rev Immunol*. 2011 Nov 10;11(11):738–49.
 340. McGregor RA, Kwon EY, Shin SK, Jung UJ, Kim E, Park JHY, et al. Time-course microarrays reveal modulation of developmental, lipid metabolism and immune gene networks in intrascapular brown adipose tissue during the development of diet-induced obesity. *Int J Obes*. 2013;37(12):1524–31.
 341. Alcalá M, Calderon-Dominguez M, Bustos E, Ramos P, Casals N, Serra D, et al. Increased inflammation, oxidative stress and mitochondrial respiration in brown adipose tissue from obese mice. *Sci Rep*. 2017;7(1):1–12.
 342. Fitzgibbons TP, Kogan S, Aouadi M, Hendricks GM, Straubhaar J, Czech MP. Similarity of mouse perivascular and brown adipose tissues and their resistance to diet-induced inflammation. *Am J Physiol - Hear Circ Physiol*. 2011;301(4).
 343. Dowal L, Parameswaran P, Phat S, Akella S, Majumdar ID, Ranjan J, et al. Intrinsic Properties of Brown and White Adipocytes Have Differential Effects on Macrophage Inflammatory Responses. *Mediators Inflamm*. 2017;2017(10).
 344. Bae J, Ricciardi CJ, Esposito D, Komarnytsky S, Hu P, Curry BJ, et al. Activation of pattern recognition receptors in brown adipocytes induces inflammation and suppresses uncoupling protein 1 expression and mitochondrial respiration. *AJP Cell Physiol*. 2014;306(10):C918–30.
 345. Xu H, Barnes GT, Yang Q, Tan G, Yang D, Chou CJ, et al. Chronic inflammation in fat plays a crucial role in the development of obesity-related insulin resistance. *J Clin Invest*. 2003 Dec 15;112(12):1821–30.
 346. Cinti S, Mitchell G, Barbatelli G, Murano I, Ceresi E, Faloia E, et al. Adipocyte death defines macrophage localization and function in adipose tissue of obese mice and humans. *J Lipid Res*. 2005;46(11):2347–55.
 347. Brun P, Castagliuolo I, Di Leo V, Buda A, Pinzani M, Palù G, et al. Increased intestinal permeability in obese mice: New evidence in the pathogenesis of nonalcoholic steatohepatitis. *Am J Physiol - Gastrointest Liver Physiol*. 2007;292(2):518–25.
 348. Kotzbeck P, Giordano A, Mondini E, Murano I, Severi I, Venema W, et al. Brown adipose tissue whitening leads to brown adipocyte death and adipose tissue inflammation. *J Lipid Res*. 2018;59(5):784–94.
 349. Wolf Y, Boura-Halfon S, Cortese N, Haimon Z, Sar Shalom H, Kuperman Y,

- et al. Brown-adipose-tissue macrophages control tissue innervation and homeostatic energy expenditure. *Nat Immunol.* 2017;18(6):665–74.
350. Weisberg SP, Leibel RL, Anthony W, Jr F, Weisberg SP, Hunter D, et al. CCR2 modulates inflammatory and metabolic effects of high-fat feeding Find the latest version : CCR2 modulates inflammatory and metabolic effects of high-fat feeding. *J Clin Invest.* 2006;116(1):115–24.
 351. Harte AL, Tripathi G, Piya MK, Barber TM, Clapham JC, Al-Daghri N, et al. NFκB as a potent regulator of inflammation in human adipose tissue, influenced by depot, adiposity, T2DM status, and TNFα. *Obesity.* 2013;21(11):2322–30.
 352. Weisberg SP, Leibel RL, Anthony W, Jr F, Weisberg SP, Mccann D, et al. Obesity is associated with macrophage accumulation in adipose tissue Find the latest version : Obesity is associated with. *J Clin Invest.* 2003;112(12):1796–808.
 353. Polyák Á, Winkler Z, Kuti D, Ferenczi S, Kovács KJ. Brown adipose tissue in obesity: Fractalkine-receptor dependent immune cell recruitment affects metabolic-related gene expression. Vol. 1861, *Biochimica et Biophysica Acta - Molecular and Cell Biology of Lipids.* Elsevier B.V.; 2016. 1614–1622 p.
 354. Martins FF, Bargut TCL, Aguila MB, Mandarim-de-Lacerda CA. Thermogenesis, fatty acid synthesis with oxidation, and inflammation in the brown adipose tissue of ob/ob (–/–) mice. *Ann Anat.* 2017;210:44–51.
 355. Nøhr MK, Bobba N, Richelsen B, Lund S, Pedersen SB. Inflammation downregulates UCP1 expression in brown adipocytes potentially via SIRT1 and DBC1 interaction. *Int J Mol Sci.* 2017;18(5).
 356. Okla M, Zaher W, Alfayez M, Chung S. Inhibitory Effects of Toll-Like Receptor 4, NLRP3 Inflammasome, and Interleukin-1β on White Adipocyte Browning. *Inflammation.* 2018;41(2):626–42.
 357. Kwok KHM, Lam KSL, Xu A. Heterogeneity of white adipose tissue: Molecular basis and clinical implications. *Exp Mol Med.* 2016;48(3):e215-12.
 358. Sidossis L, Kajimura S. Brown and beige fat in humans: Thermogenic adipocytes that control energy and glucose homeostasis. *J Clin Invest.* 2015;125(2):478–86.
 359. Bruun JM, Lihn AS, Pedersen SB, Richelsen B. Monocyte chemoattractant protein-1 release is higher in visceral than subcutaneous human adipose tissue (AT): Implication of macrophages resident in the AT. *J Clin Endocrinol Metab.*

2005;90(4):2282–9.

360. Harman-Boehm I, Blüher M, Redel H, Sion-Vardy N, Ovadia S, Avinoach E, et al. Macrophage infiltration into omental versus subcutaneous fat across different populations: Effect of regional adiposity and the comorbidities of obesity. *J Clin Endocrinol Metab.* 2007;92(6):2240–7.
361. Alvehus M, Burén J, Sjöström M, Goedecke J, Olsson T. The human visceral fat depot has a unique inflammatory profile. *Obesity.* 2010;18(5):879–83.
362. Fried SK, Bunkin DA, Greenberg AS. Omental and subcutaneous adipose tissues of obese subjects release interleukin-6: Depot difference and regulation by glucocorticoid. *J Clin Endocrinol Metab.* 1998;83(3):847–50.
363. Donath MY, Shoelson SE. Type 2 diabetes as an inflammatory disease. *Nat Rev Immunol.* 2011;11(2):98–107.
364. Votruba SB, Mattison RS, Dumesic DA, Koutsari C, Jensen MD. Meal fatty acid uptake in visceral fat in women. *Diabetes.* 2007;56(10):2589–97.
365. McQuaid SE, Humphreys SM, Hodson L, Fielding BA, Karpe F, Frayn KN. Femoral adipose tissue may accumulate the fat that has been recycled as VLDL and nonesterified fatty acids. *Diabetes.* 2010;59(10):2465–73.
366. Parker VER, Savage DB, O’Rahilly S, Semple RK. Mechanistic insights into insulin resistance in the genetic era. *Diabet Med.* 2011;28(12):1476–86.
367. Gandotra S, Le Dour C, Bottomley W, Cervera P, Giral P, Reznik Y, et al. Perilipin deficiency and autosomal dominant partial lipodystrophy. *N Engl J Med.* 2011;364(8):740–8.
368. Estève D, Boulet N, Volat F, Zakaroff-Girard A, Ledoux S, Coupaye M, et al. Human White and Brite Adipogenesis is Supported by MSCA1 and is Impaired by Immune Cells. *Stem Cells.* 2015 Apr;33(4):1277–91.
369. Müller TD, Lee SJ, Jastroch M, Kabra D, Stemmer K, Aichler M, et al. p62 Links β -adrenergic input to mitochondrial function and thermogenesis. *J Clin Invest.* 2013 Jan 2;123(1):469–78.
370. Costa C, Incio J, Soares R. Angiogenesis and chronic inflammation: Cause or consequence? *Angiogenesis.* 2007;10(3):149–66.
371. Fiedler U, Reiss Y, Scharpfenecker M, Grunow V, Koidl S, Thurston G, et al. Angiopoietin-2 sensitizes endothelial cells to TNF- α and has a crucial role in the induction of inflammation. *Nat Med.* 2006;12(2):235–9.
372. Funa K, Uramoto H. Regulatory mechanisms for the expression and activity of

- platelet-derived growth factor receptor. *Acta Biochim Pol.* 2003;50(3):647–58.
373. Ribatti D, Crivellato E. Immune cells and angiogenesis. *J Cell Mol Med.* 2009;13(9 A):2822–33.
 374. Crewe C, An YA, Scherer PE. The ominous triad of adipose tissue dysfunction: inflammation, fibrosis, and impaired angiogenesis. *J Clin Invest.* 2017 Jan 3;127(1):74–82.
 375. Ley K. Pathways and bottlenecks in the web of inflammatory adhesion molecules and chemoattractants. *Immunol Res.* 2001;24(1):87–95.
 376. Rondinone CM. Adipocyte-derived hormones, cytokines, and mediators. *Endocrine.* 2006;29(1):81–90.
 377. Vaisse C, Halaas JL, Horvath CM, Darnell JE, Stoffel M, Friedman JM. Leptin activation of Stat3 in the hypothalamus of wild-type and ob/ob mice but not db/db mice. *Nat Genet.* 1996 Sep;14(1):95–7.
 378. Münzberg H, Flier JS, Bjørbæk C. Region-specific leptin resistance within the hypothalamus of diet-induced obese mice. *Endocrinology.* 2004;145(11):4880–9.
 379. Myers MG, Leibel RL, Seeley RJ, Schwartz MW. Obesity and leptin resistance: Distinguishing cause from effect. *Trends Endocrinol Metab.* 2010;21(11):643–51.
 380. Scherer PE, Williams S, Fogliano M, Baldini G, Lodish HF. A novel serum protein similar to C1q, produced exclusively in adipocytes. *J Biol Chem.* 1995;270(45):26746–9.
 381. Yamauchi T, Kamon J, Minokoshi Y, Ito Y, Waki H, Uchida S, et al. Adiponectin stimulates glucose utilization and fatty-acid oxidation by activating AMP-activated protein kinase. *Nat Med.* 2002;8(11):1288–95.
 382. Berg AH, Combs TP, Du X, Brownlee M, Scherer PE. The adipocyte-secreted protein Acrp30 enhances hepatic insulin action. *Nat Med.* 2001;7(8):947–53.
 383. De Rosa A, Ludovica Monaco M, Capasso M, Forestieri P, Pilone V, Nardelli C, et al. Adiponectin oligomers as potential indicators of adipose tissue improvement in obese subjects. *Eur J Endocrinol.* 2013;169(1):37–43.
 384. Gunawardana SC, Piston DW. Reversal of type 1 diabetes in mice by brown adipose tissue transplant. *Diabetes.* 2012;61(3):674–82.
 385. Berbeé JFP, Boon MR, Khedoe PPSJ, Bartelt A, Schlein C, Worthmann A, et al. Brown fat activation reduces hypercholesterolaemia and protects from

- atherosclerosis development. *Nat Commun.* 2015;6.
386. Braga M, Reddy ST, Vergnes L, Pervin S, Grijalva V, Stout D, et al. Follistatin promotes adipocyte differentiation, browning, and energy metabolism. *J Lipid Res.* 2014;55(3):375–84.
 387. Svensson KJ, Long JZ, Jedrychowski MP, Cohen P, Lo JC, Serag S, et al. A Secreted Slit2 Fragment Regulates Adipose Tissue Thermogenesis and Metabolic Function. *Cell Metab.* 2016 Mar;23(3):454–66.
 388. Cereijo R, Gavaldà-Navarro A, Cairó M, Quesada-López T, Villarroya J, Morón-Ros S, et al. CXCL14, a Brown Adipokine that Mediates Brown-Fat-to-Macrophage Communication in Thermogenic Adaptation. *Cell Metab.* 2018;28(5):750-763.e6.
 389. Virtue S, Feldmann H, Christian M, Tan CY, Masoodi M, Dale M, et al. A new role for lipocalin prostaglandin D synthase in the regulation of brown adipose tissue substrate utilization. *Diabetes.* 2012;61(12):3139–47.
 390. Giralt M, Gavaldà-Navarro A, Villarroya F. Fibroblast growth factor-21, energy balance and obesity. *Mol Cell Endocrinol.* 2015;418:66–73.
 391. Véniant MM, Sivits G, Helmering J, Komorowski R, Lee J, Fan W, et al. Pharmacologic Effects of FGF21 Are Independent of the “Browning” of White Adipose Tissue. *Cell Metab.* 2015;21(5):731–8.
 392. Hara T, Tanegashima K. Pleiotropic functions of the CXC-type chemokine CXCL14 in mammals. *J Biochem.* 2012;151(5):469–76.
 393. Hara T, Nakayama Y. Chapter 5 CXCL14 and Insulin Action. *Vitam Horm.* 2009;80(C):107–23.
 394. Tanaka R, Miwa Y, Mou K, Tomikawa M, Eguchi N, Urade Y, et al. Knockout of the l-pgds gene aggravates obesity and atherosclerosis in mice. *Biochem Biophys Res Commun.* 2009;378(4):851–6.
 395. Macia L, Tsai VWW, Nguyen AD, Johnen H, Kuffner T, Shi YC, et al. Macrophage inhibitory cytokine 1 (MIC-1/GDF15) decreases food intake, body weight and improves glucose tolerance in mice on normal & obesogenic diets. *PLoS One.* 2012;7(4):1–8.
 396. Chrysovergis K, Wang X, Kosak J, Lee SH, Kim JS, Foley JF, et al. NAG-1/GDF-15 prevents obesity by increasing thermogenesis, lipolysis and oxidative metabolism. *Int J Obes.* 2014;38(12):1555–64.
 397. Hansen IR, Jansson KM, Cannon B, Nedergaard J. Contrasting effects of cold

- acclimation versus obesogenic diets on chemerin gene expression in brown and white adipose tissues. *Biochim Biophys Acta - Mol Cell Biol Lipids*. 2014;1841(12):1691–9.
398. Klepac K, Kilić A, Gnad T, Brown LM, Herrmann B, Wilderman A, et al. The G q signalling pathway inhibits brown and beige adipose tissue. *Nat Commun*. 2016;7.
 399. Steculorum SM, Ruud J, Karakasilioti I, Backes H, Engström Ruud L, Timper K, et al. AgRP Neurons Control Systemic Insulin Sensitivity via Myostatin Expression in Brown Adipose Tissue. *Cell*. 2016;165(1):125–38.
 400. Lehrke M, Becker A, Greif M, Stark R, Laubender RP, Von Ziegler F, et al. Chemerin is associated with markers of inflammation and components of the metabolic syndrome but does not predict coronary atherosclerosis. *Eur J Endocrinol*. 2009;161(2):339–44.
 401. Rourke JL, Muruganandan S, Dranse HJ, McMullen NM, Sinal CJ. Gpr1 is an active chemerin receptor influencing glucose homeostasis in obese mice. *J Endocrinol*. 2014;222(2):201–15.
 402. Mattern A, Zellmann T, Beck-Sickinger AG. Processing, signaling, and physiological function of chemerin. *IUBMB Life*. 2014;66(1):19–26.
 403. Böhm F, Pernow J. The importance of endothelin-1 for vascular dysfunction in cardiovascular disease. *Cardiovasc Res*. 2007;76(1):8–18.
 404. Kowalczyk A, Kleniewska P, Kolodziejczyk M, Skibska B, Goraca A. The role of endothelin-1 and endothelin receptor antagonists in inflammatory response and sepsis. *Arch Immunol Ther Exp (Warsz)*. 2015;63(1):41–52.
 405. Eriksson AKS, Van Harmelen V, Stenson BM, Åström G, Wåhlén K, Laurencikiene J, et al. Endothelin-1 stimulates human adipocyte lipolysis through the ET A receptor. *Int J Obes*. 2009;33(1):67–74.
 406. Braga M, Pervin S, Norris K, Bhasin S, Singh R. Inhibition of in vitro and in vivo brown fat differentiation program by myostatin. *Obesity*. 2013 Jun;21(6):1180–8.
 407. Koncarevic A, Kajimura S, Cornwall-Brady M, Andreucci A, Pullen A, Sako D, et al. A novel therapeutic approach to treating obesity through modulation of TGFβ signaling. *Endocrinology*. 2012;153(7):3133–46.
 408. Pervin S, Singh V, Tucker A, Collazo J, Singh R. Modulation of transforming growth factor-β/follistatin signaling and white adipose browning: therapeutic

- implications for obesity related disorders. *Horm Mol Biol Clin Investig.* 2017 Jan 28;31(2).
409. Fournier B, Murray B, Gutzwiller S, Marcaletti S, Marcellin D, Bergling S, et al. Blockade of the Activin Receptor IIB Activates Functional Brown Adipogenesis and Thermogenesis by Inducing Mitochondrial Oxidative Metabolism. *Mol Cell Biol.* 2012;32(14):2871–9.
 410. Zhang C, McFarlane C, Lokireddy S, Masuda S, Ge X, Gluckman PD, et al. Inhibition of myostatin protects against diet-induced obesity by enhancing fatty acid oxidation and promoting a brown adipose phenotype in mice. *Diabetologia.* 2012;55(1):183–93.
 411. Dong J, Dong Y, Dong Y, Chen F, Mitch WE, Zhang L. Inhibition of myostatin in mice improves insulin sensitivity via irisin-mediated cross talk between muscle and adipose tissues. *Int J Obes.* 2016;40(3):434–42.
 412. Yamashita H, Sato Y, Kizaki T, Oh-ishi S, Nagasawa J ichi, Ohno H. Basic fibroblast growth factor (bFGF) contributes to the enlargement of brown adipose tissue during cold acclimation. *Pflügers Arch Eur J Physiol.* 1994;428(3–4):352–6.
 413. Lorenzo M, Valverde AM, Teruel T, Benito M. IGF-I is a mitogen involved in differentiation-related gene expression in fetal rat brown adipocytes. *J Cell Biol.* 1993;123(6 I):1567–75.
 414. Burysek L, Houstek J. B-Adrenergic stimulation of interleukin-1 α and interleukin-6 expression in mouse brown adipocytes. *FEBS Lett.* 1997;411(1):83–6.
 415. Spadaro O, Camell CD, Bosurgi L, Nguyen KY, Youm YH, Rothlin C V., et al. IGF1 Shapes Macrophage Activation in Response to Immunometabolic Challenge. *Cell Rep.* 2017;19(2):225–34.
 416. Chang HR, Kim HJ, Xu X, Ferrante AW. Macrophage and adipocyte IGF1 maintain adipose tissue homeostasis during metabolic stresses. *Obesity.* 2016 Jan;24(1):172–83.
 417. Egecioglu E, Anesten F, Schéle E, Palsdottir V. Interleukin-6 is important for regulation of core body temperature during long-term cold exposure in mice. *Biomed Reports.* 2018;9(3):206–12.
 418. Mauer J, Chaurasia B, Goldau J, Vogt MC, Ruud J, Nguyen KD, et al. Signaling by IL-6 promotes alternative activation of macrophages to limit endotoxemia

- and obesity-associated resistance to insulin. *Nat Immunol.* 2014;15(5):423–30.
419. DeFuria J, Belkina AC, Jagannathan-Bogdan M, Snyder-Cappione J, Carr JD, Nersesova YR, et al. B cells promote inflammation in obesity and type 2 diabetes through regulation of T-cell function and an inflammatory cytokine profile. *Proc Natl Acad Sci U S A.* 2013;110(13):5133–8.
 420. Pal M, Febbraio MA, Whitham M. From cytokine to myokine: the emerging role of interleukin-6 in metabolic regulation. *Immunol Cell Biol.* 2014 Apr 11;92(4):331–9.
 421. Bastard JP, Jardel C, Bruckert E, Blondy P, Capeau J, Laville M, et al. Elevated levels of interleukin 6 are reduced in serum and subcutaneous adipose tissue of obese women after weight loss. *J Clin Endocrinol Metab.* 2000;85(9):3338–42.
 422. Priceman SJ, Kujawski M, Shen S, Cherryholmes GA, Lee H, Zhang C, et al. Regulation of adipose tissue T cell subsets by Stat3 is crucial for diet-induced obesity and insulin resistance. *Proc Natl Acad Sci U S A.* 2013;110(32):13079–84.
 423. Han J, Meng Q, Shen L, Wu G. Interleukin-6 induces fat loss in cancer cachexia by promoting white adipose tissue lipolysis and browning. *Lipids Health Dis.* 2018;17(1):1–8.
 424. Simon MC, Bilan S, Nowotny B, Dickhaus T, Burkart V, Schloot NC. Fatty acids modulate cytokine and chemokine secretion of stimulated human whole blood cultures in diabetes. *Clin Exp Immunol.* 2013;172(3):383–93.
 425. Bulua AC, Simon A, Maddipati R, Pelletier M, Park H, Kim KY, et al. Mitochondrial reactive oxygen species promote production of proinflammatory cytokines and are elevated in TNFR1-associated periodic syndrome (TRAPS). *J Exp Med.* 2011;208(3):519–33.
 426. Sears DD, Kim JJ. TLR4 and insulin resistance. *Gastroenterol Res Pract.* 2010;2010.
 427. Valladares A, Roncero C, Benito M, Porras A. TNF- α inhibits UCP-1 expression in brown adipocytes via ERKs - Opposite effect of p38MAPK. *FEBS Lett.* 2001;493(1):6–11.
 428. Suárez-Zamorano N, Fabbiano S, Chevalier C, Stojanović O, Colin DJ, Stevanović A, et al. Microbiota depletion promotes browning of white adipose tissue and reduces obesity. *Nat Med.* 2015 Dec 16;21(12):1497–501.
 429. Gavaldà-Navarro A, Moreno-Navarrete JM, Quesada-López T, Cairó M, Giralt

- M, Fernández-Real JM, et al. Lipopolysaccharide-binding protein is a negative regulator of adipose tissue browning in mice and humans. *Diabetologia*. 2016;59(10):2208–18.
430. Gregor MF, Hotamisligil GS. Inflammatory mechanisms in obesity. *Annu Rev Immunol*. 2011;29:415–45.
 431. Lee CC, Avalos AM, Ploegh HL. Accessory molecules for Toll-like receptors and their function. *Nat Rev Immunol*. 2012;12(3):168–79.
 432. Jin C, Henao-Mejia J, Flavell RA. Innate Immune Receptors: Key Regulators of Metabolic Disease Progression. *Cell Metab*. 2013 Jun;17(6):873–82.
 433. Jin C, Flavell RA. Innate sensors of pathogen and stress: Linking inflammation to obesity. *J Allergy Clin Immunol*. 2013 Aug;132(2):287–94.
 434. O'Neill L a J, Bowie AG. The family of five: TIR-domain-containing adaptors in Toll-like receptor signalling. *Nat Rev Immunol*. 2007;7(5):353–64.
 435. Kawai T, Akira S. TLR signaling. *Cell Death Differ*. 2006;13:816–825.
 436. Shi H, Kokoeva M V, Inouye K, Tzameli I, Yin H, Flier JS. TLR4 links innate immunity and fatty acid – induced insulin resistance. *J Clin Invest*. 2006;116(11):3015–25.
 437. Brikos C, O'Neill LAJ. Signalling of toll-like receptors. *Handb Exp Pharmacol*. 2008;183:21–50.
 438. Hu E, Kim JB, Sarraf P, Spiegelman BM. Inhibition of Adipogenesis Through MAP Kinase-Mediated Phosphorylation of PPAR. *Science* (80-). 1996 Dec 20;274(5295):2100–3.
 439. Gray JP, Burns KA, Leas TL, Perdew GH, Vanden Heuvel JP. Regulation of peroxisome proliferator-activated receptor α by protein kinase C. *Biochemistry*. 2005;44(30):10313–21.
 440. Kumari M, Wang X, Lantier L, Lyubetskaya A, Eguchi J, Kang S, et al. IRF3 promotes adipose inflammation and insulin resistance and represses browning. *J Clin Invest*. 2016;126(8):2839–54.
 441. Olefsky JM. IKK ϵ : A Bridge between Obesity and Inflammation. *Cell*. 2009;138(5):834–6.
 442. Lumeng CN, Saltiel AR. Inflammatory links between obesity and metabolic disease. *J Clin Invest*. 2011;121(6):2111–7.
 443. Chiang S, Bazuine M, Lumeng CN, Geletka LM, White NM, Ma J, et al. The protein kinase IKK ϵ regulates energy expenditure, insulin sensitivity and

- chronic inflammation in obese mice. *Cell*. 2010;138(5):961–75.
444. Taddonio MA, Dolgachev V, Bosmann M, Ward PA, Su G, Wang SC, et al. Influence of Lipopolysaccharide-Binding Protein on Pulmonary Inflammation in Gram-Negative Pneumonia. *Shock*. 2015 Jun;43(6):612–9.
 445. Pahwa R, Devaraj S, Jialal I. The effect of the accessory proteins, soluble CD14 and lipopolysaccharide-binding protein on Toll-like receptor 4 activity in human monocytes and adipocytes. *Int J Obes*. 2016;40(November 2015):1–5.
 446. Creely SJ, McTernan PG, Kusminski CM, Fisher ff. M, Da Silva NF, Khanolkar M, et al. Lipopolysaccharide activates an innate immune system response in human adipose tissue in obesity and type 2 diabetes. *Am J Physiol Metab*. 2007 Mar;292(3):E740–7.
 447. Trøseid M, Nestvold TK, Rudi K, Thoresen H, Nielsen EW, Lappegård KT. Plasma lipopolysaccharide is closely associated with glycemic control and abdominal obesity: Evidence from bariatric surgery. *Diabetes Care*. 2013;36(11):3627–32.
 448. Beutler B, Rietschel ET. Innate immune sensing and its roots: the story of endotoxin. *Nat Rev Immunol*. 2003;3(2):169–76.
 449. Wikoff WR, Anfora AT, Liu J, Schultz PG, Lesley SA, Peters EC, et al. Metabolomics analysis reveals large effects of gut microflora on mammalian blood metabolites. *Proc Natl Acad Sci U S A*. 2009;106(10):3698–703.
 450. Sokol H, Pigneur B, Watterlot L, Lakhdari O, Bermúdez-Humarán LG, Gratadoux J-J, et al. *Faecalibacterium prausnitzii* is an anti-inflammatory commensal bacterium identified by gut microbiota analysis of Crohn disease patients. *Proc Natl Acad Sci U S A*. 2008;105(43):16731–6.
 451. Rousseaux C, Thuru X, Gelot A, Barnich N, Neut C, Dubuquoy L, et al. *Lactobacillus acidophilus* modulates intestinal pain and induces opioid and cannabinoid receptors. *Nat Med*. 2007;13(1):35–7.
 452. Pizzorno J. Toxins From the Gut. *Integr Med A Clin J*. 2014;13(6):8-11 4p.
 453. Yanez J, Vicente V, Alcaraz M, Castillo J, Benavente- O, Canteras M, et al. Fecal Water Genotoxicity Is Predictive of Tumor- Preventive Activities by Inulin-Like Oligofructoses, Probiotics (*Lactobacillus rhamnosus* and *Bifidobacterium lactis*), and Their Synbiotic Combination. *Nutr Cancer*. 2004;49(2):144–55.
 454. Cani PD, Amar J, Iglesias MA, Poggi M, Knauf C, Bastelica D, et al. Metabolic

- Endotoxemia Initiates Obesity and Insulin Resistance. *Diabetes*. 2007;56(July):1761–72.
455. LeBlanc JG, Milani C, de Giori GS, Sesma F, van Sinderen D, Ventura M. Bacteria as vitamin suppliers to their host: A gut microbiota perspective. *Curr Opin Biotechnol*. 2013;24(2):160–8.
 456. Conlon MA, Bird AR. The impact of diet and lifestyle on gut microbiota and human health. *Nutrients*. 2015;7:17–44.
 457. Caesar R, Tremaroli V, Kovatcheva-Datchary P, Cani PD, Bäckhed F. Crosstalk between gut microbiota and dietary lipids aggravates WAT inflammation through TLR signaling. *Cell Metab*. 2015;22(4):658–68.
 458. Dixon AN, Valsamakis G, Hanif MW, Field A, Boutsiadis A, Harte A, et al. Effect of the orlistat on serum endotoxin lipopolysaccharide and adipocytokines in South Asian individuals with impaired glucose tolerance. *Int J Clin Pract*. 2008 Jun 4;62(7):1124–9.
 459. Miller MA, McTernan PG, Harte AL, Silva NF da, Strazzullo P, Alberti KGMM, et al. Ethnic and sex differences in circulating endotoxin levels: A novel marker of atherosclerotic and cardiovascular risk in a British multi-ethnic population. *Atherosclerosis*. 2009;203(2):494–502.
 460. A. R. Baker, A. L. Harte, N. Howell, D. C. Pritlove, A. M. Ranasinghe NF da S, Youssef EM, Khunti K, Davies MJ, Bonser RS, Kumar S, et al. Epicardial Adipose Tissue as a Source of Nuclear Factor- κ B and c-Jun N-Terminal Kinase Mediated Inflammation in Patients with Coronary Artery Disease. *J Clin Endocrinol Metab*. 2009;94(1):261–7.
 461. Harte AL, Varma MC, Tripathi G, Mcgee KC, Al-Daghri NM, Al-Attas OS, et al. High fat intake leads to acute postprandial exposure to circulating endotoxin in type 2 diabetic subjects. *Diabetes Care*. 2012;35(2):375–82.
 462. Harte AL, da Silva NF, Creely SJ, McGee KC, Billyard T, Youssef-Elabd EM, et al. Elevated endotoxin levels in non-alcoholic fatty liver disease. *J Inflamm (Lond)*. 2010;7(15):2–10.
 463. Nøhr MK, Dudele A, Poulsen MM, Ebbesen LH, Radko Y, Christensen LP, et al. LPS-enhanced glucose-stimulated insulin secretion is normalized by resveratrol. *PLoS One*. 2016;11(1):1–15.
 464. Cani PD, Bibiloni R, Knauf C, Neyrinck AM, Delzenne NM, Waget A, et al. Changes in Gut Microbiota Control Metabolic Endotoxemia-Induced

- Inflammation in High-Fat Diet–Induced Obesity and Diabetes in Mice. *Diabetes*. 2008 Jun;57(June):1470–1481.
465. Cho I, Yamanishi S, Cox L, Methe BA, Zavadil J, Li K, et al. Antibiotics in early life alter the murine colonic microbiome and adiposity. *Nature*. 2012;488(7413):621–6.
 466. Mogensen TH. Pathogen recognition and inflammatory signaling in innate immune defenses. *Clin Microbiol Rev*. 2009;22(2):240–73.
 467. Montero Vega MT, de Andrés Martín A. The significance of toll-like receptors in human diseases. *Allergol Immunopathol (Madr)*. 2009;37(5):252–63.
 468. Putti R, Sica R, Migliaccio V, Lionetti L. Diet impact on Mitochondrial Bioenergetics and Dynamics. *Front Physiol*. 2015;6(MAR):1–7.
 469. Westermann B. Mitochondrial fusion and fission in cell life and death. *Nat Rev Mol Cell Biol*. 2010;11(12):872–84.
 470. Alberts B, Johnson A, Lewis J et al, Alberts Bruce, Johnson Alexander, Lewis Julian, Raff Martin, Roberts Keith WP. The Mitochondrion. In: ALberts B, editor. *Molecular Biology of the Cell*. 4th editio. New York: Garland Science; 2002. p. NBK21054.
 471. Yin F, Cadenas E. Mitochondria: The Cellular Hub of the Dynamic Coordinated Network. *Antioxidants Redox Signal*. 2015;22(12):961–4.
 472. Brand MD, Nicholls DG. Assessing mitochondrial dysfunction in cells. *Biochem J*. 2011;435(2):297–312.
 473. Lee JH, Park A, Oh KJ, Lee SC, Kim WK, Bae KH. The role of adipose tissue mitochondria: Regulation of mitochondrial function for the treatment of metabolic diseases. *Int J Mol Sci*. 2019;20(19).
 474. Detmer SA, Chan DC. Functions and dysfunctions of mitochondrial dynamics. *Nat Rev Mol Cell Biol*. 2007;8(11):870–9.
 475. Westermann B. Molecular machinery of mitochondrial fusion and fission. *J Biol Chem*. 2008;283(20):13501–5.
 476. Jheng H-F, Tsai P-J, Guo S-M, Kuo L-H, Chang C-S, Su I-J, et al. Mitochondrial Fission Contributes to Mitochondrial Dysfunction and Insulin Resistance in Skeletal Muscle. *Mol Cell Biol*. 2012;32(2):309–19.
 477. Gao AW, Houtkooper RH. Mitochondrial fission: Firing up mitochondria in brown adipose tissue. *EMBO J*. 2014;33(5):401–2.
 478. Wikstrom JD, Mahdavian K, Liesa M, Sereda SB, Si Y, Las G, et al. Hormone-

- induced mitochondrial fission is utilized by brown adipocytes as an amplification pathway for energy expenditure. *EMBO J.* 2014;33(5):418–36.
479. Archer SL. Mitochondrial dynamics - Mitochondrial fission and fusion in human diseases. *N Engl J Med.* 2013;369(23):2236–51.
 480. Liesa M, Shirihai OS. Mitochondrial Dynamics in the Regulation of Nutrient Utilization and Energy Expenditure. *Cell Metab.* 2013 Apr;17(4):491–506.
 481. Jornayvaz FR, Shulman GI. Regulation of mitochondrial biogenesis. *Essays Biochem.* 2010;47:69–84.
 482. Scarpulla RC. Transcriptional paradigms in mammalian mitochondrial biogenesis and function. *Physiol Rev.* 2008;88(2):611–38.
 483. Wu Z, Puigserver P, Andersson U, Zhang C, Adelmant G, Mootha V, et al. Mechanisms Controlling Mitochondrial Biogenesis and Respiration through the Thermogenic Coactivator PGC-1. *Cell.* 1999 Jul;98(1):115–24.
 484. Duncan JG, Fong JL, Medeiros DM, Finck BN, Kelly DP. Insulin-resistant heart exhibits a mitochondrial biogenic response driven by the peroxisome proliferator-activated receptor- α /PGC-1 α gene regulatory pathway. *Circulation.* 2007;115(7):909–17.
 485. Kim J, Wei Y, Sowers JR. Role of Mitochondrial Dysfunction in Insulin Resistance. *Circ Res.* 2008 Feb 29;102(4):401–14.
 486. Brehm A, Krssak M, Schmid AI, Nowotny P, Waldhäusl W, Roden M. Increased lipid availability impairs insulin-stimulated ATP synthesis in human skeletal muscle. *Diabetes.* 2006;55(1):136–40.
 487. Zorzano A, Liesa M, Palacín M. Role of mitochondrial dynamics proteins in the pathophysiology of obesity and type 2 diabetes. *Int J Biochem Cell Biol.* 2009;41(10):1846–54.
 488. Heinonen S, Buzkova J, Muniandy M, Kaksonen R, Ollikainen M, Ismail K, et al. Impaired mitochondrial biogenesis in adipose tissue in acquired obesity. *Diabetes.* 2015;64(9):3135–45.
 489. Keuper M, Sachs S, Walheim E, Berti L, Raedle B, Tews D, et al. Activated macrophages control human adipocyte mitochondrial bioenergetics via secreted factors. *Mol Metab.* 2017;6(10):1226–39.
 490. Hahn WS, Kuzmich J, Burrill JS, Donoghue MA, Foncea R, Jensen MD, et al. Proinflammatory cytokines differentially regulate adipocyte mitochondrial metabolism, oxidative stress, and dynamics. *Am J Physiol - Endocrinol Metab.*

2014;306(9):1033–45.

491. Schenk S, Saberi M, Olefsky JM. Personal perspective Insulin sensitivity : modulation by nutrients and inflammation. *Department Med Div Endocrinol Metab.* 2008;118(9):2992–3002.
492. Savage DB, Petersen KF, Shulman GI. Disordered lipid metabolism and the pathogenesis of insulin resistance. *Physiol Rev.* 2007;87(2):507–20.
493. Gao Z, Zhang X, Zuberi A, Hwang D, Quon MJ, Lefevre M, et al. Inhibition of insulin sensitivity by free fatty acids requires activation of multiple serine kinases in 3T3-L1 adipocytes. *Mol Endocrinol.* 2004;18(8):2024–34.
494. Yu C, Chen Y, Cline GW, Zhang D, Zong H, Wang Y, et al. Mechanism by which fatty acids inhibit insulin activation of insulin receptor substrate-1 (IRS-1)-associated phosphatidylinositol 3-kinase activity in muscle. *J Biol Chem.* 2002;277(52):50230–6.
495. Westwick JK, Bielawska AE, Dbaiibo G, Hannun YA, Brenner DA. Ceramide activates the stress-activated protein kinases. *J Biol Chem.* 1995;270(39):22689–92.
496. Gurung P, Lukens JR, Kanneganti T-D. Mitochondria: diversity in the regulation of the NLRP3 inflammasome. *Trends Mol Med.* 2015 Mar;21(3):193–201.
497. Woo CY, Jang JE, Lee SE, Koh EH, Lee KU. Mitochondrial dysfunction in adipocytes as a primary cause of adipose tissue inflammation. *Diabetes Metab J.* 2019;43(3):247–56.
498. Dahlman I, Forsgren M, Sjögren A, Nordström EA, Kaaman M, Näslund E, et al. Downregulation of electron transport chain genes in visceral adipose tissue in type 2 diabetes independent of obesity and possibly involving tumor necrosis factor- α . *Diabetes.* 2006;55(6):1792–9.
499. de-Lima-Júnior JC, Souza GF, Moura-Assis A, Gaspar RS, Gaspar JM, Rocha AL, et al. Abnormal brown adipose tissue mitochondrial structure and function in IL10 deficiency. *EBioMedicine.* 2019;39:436–47.
500. Matsuda M, Shimomura I. Increased oxidative stress in obesity: Implications for metabolic syndrome, diabetes, hypertension, dyslipidemia, atherosclerosis, and cancer. *Obes Res Clin Pract.* 2013;7(5):e330–41.
501. Bondia-Pons I, Ryan L, Martinez JA. Oxidative stress and inflammation interactions in human obesity. *J Physiol Biochem.* 2012;68(4):701–11.

502. Fernández-Sánchez A, Madrigal-Santillán E, Bautista M, Esquivel-Soto J, Morales-González Á, Esquivel-Chirino C, et al. Inflammation, oxidative stress, and obesity. *Int J Mol Sci.* 2011;12(5):3117–32.
503. Patti ME, Corvera S. The role of mitochondria in the pathogenesis of type 2 diabetes. *Endocr Rev.* 2010;31(3):364–95.
504. Frohnert BI, Bernlohr DA. Protein Carbonylation, Mitochondrial Dysfunction, and Insulin Resistance. *Adv Nutr.* 2013;4(2):157–63.
505. Evans JL, Maddux BA, Goldfine ID. The Molecular Basis for Oxidative Stress-Induced Insulin Resistance. *Antioxid Redox Signal.* 2005 Jul;7(7–8):1040–52.
506. Morino K, Petersen KF, Dufour S, Befroy D, Frattini J, Shatzkes N, et al. Reduced mitochondrial density and increased IRS-1 serine phosphorylation in muscle of insulin-resistant offspring of type 2 diabetic parents. *J Clin Invest.* 2005;115(12):3587–93.
507. Nishikawa T, Araki E. Impact of mitochondrial ROS production in the pathogenesis of diabetes mellitus and its complications. *Antioxidants Redox Signal.* 2007;9(3):343–53.
508. Chouchani ET, Kazak L, Jedrychowski MP, Lu GZ, Erickson BK, Szpyt J, et al. Mitochondrial ROS regulate thermogenic energy expenditure and sulfenylation of UCP1. *Nature.* 2016 Apr 30;532(7597):112–6.
509. Vernochet C, Damilano F, Mourier A, Bezy O, Mori MA, Smyth G, et al. Adipose tissue mitochondrial dysfunction triggers a lipodystrophic syndrome with insulin resistance, hepatosteatosis, and cardiovascular complications. *FASEB J.* 2014;28(10):4408–19.
510. Vazquez-Prieto MA, Bettaieb A, Haj FG, Fraga CG, Oteiza PI. (–)-Epicatechin prevents TNF α -induced activation of signaling cascades involved in inflammation and insulin sensitivity in 3T3-L1 adipocytes. *Arch Biochem Biophys.* 2012 Nov;527(2):113–8.
511. Chen C, Zhang W, Shi H, Zhuo Y, Yang G, Zhang A, et al. A novel benzenediamine derivative FC98 reduces insulin resistance in high fat diet-induced obese mice by suppression of metaflammation. *Eur J Pharmacol.* 2015;761:298–308.
512. Yuan M, Konstantopoulos N, Lee J, Hansen L, Li ZW, Karin M, et al. Reversal of obesity- and diet-induced insulin resistance with salicylates or targeted disruption of Ikk β . *Science (80-).* 2001;293(5535):1673–7.

513. Larsen CM, Faulenbach M, Vaag A, Vølund A, Ehses JA, Seifert B, et al. Interleukin-1-receptor antagonist in type 2 diabetes mellitus. *N Engl J Med.* 2007;356(15):1517–26.
514. Sanchez-Zamora Y, Terrazas LI, Vilches-Flores A, Leal E, Juárez I, Whitacre C, et al. Macrophage migration inhibitory factor is a therapeutic target in treatment of non-insulin-dependent diabetes mellitus. *FASEB J.* 2010;24(7):2583–90.
515. Li J, Feng B, Nie Y, Jiao P, Lin X, Huang M, et al. Sucrose nonfermenting-related kinase regulates both adipose inflammation and energy homeostasis in mice and humans. *Diabetes.* 2018;67(3):400–11.
516. Li J, An R, Liu S, Xu H. Deregulation of PP2A-Akt Interaction Contributes to Sucrose Non-Fermenting Related Kinase (SNRK) Deficiency Induced Insulin Resistance in Adipose Tissue (P21-071-19). *Curr Dev Nutr.* 2019 Jun 1;3(Supplement_1):26–35.
517. Brendle C, Stefan N, Stef I, Ripkens S, Soekler M, la Fougère C, et al. Impact of diverse chemotherapeutic agents and external factors on activation of brown adipose tissue in a large patient collective. *Sci Rep.* 2019;9(1):1–8.
518. Song Z, Revelo X, Shao W, Tian L, Zeng K, Lei H, et al. Dietary Curcumin Intervention Targets Mouse White Adipose Tissue Inflammation and Brown Adipose Tissue UCP1 Expression. *Obesity.* 2018;26(3):547–58.
519. Hirasawa A, Hara T, Katsuma S, Adachi T, Tsujimoto G. Free fatty acid receptors and drug discovery. *Biol Pharm Bull.* 2008;31(10):1847–51.
520. Yonezawa T, Kurata R, Yoshida K, Murayama MA, Cui X, Hasegawa A. Free Fatty Acids-Sensing G Protein-Coupled Receptors in Drug Targeting and Therapeutics. *Curr Med Chem.* 2013;20(31):3855–71.
521. Ulven T. Short-chain free fatty acid receptors FFA2/GPR43 and FFA3/GPR41 as new potential therapeutic targets. *Front Endocrinol.* 2012;3(October):111.
522. Hirasawa A, Tsumaya K, Awaji T, Katsuma S, Adachi T, Yamada M, et al. Free fatty acids regulate gut incretin glucagon-like peptide-1 secretion through GPR120. *Nat Med.* 2005;11(1):90–4.
523. Katsuma S, Hatae N, Yano T, Ruike Y, Kimura M, Hirasawa A, et al. Free fatty acids inhibit serum deprivation-induced apoptosis through GPR120 in a murine enteroendocrine cell line STC-1. *J Biol Chem.* 2005;280(20):19507–15.
524. Schilperoort M, Dam AD, Hoeke G, Shabalina IG, Okolo A, Hanyaloglu AC,

- et al. The GPR 120 agonist TUG -891 promotes metabolic health by stimulating mitochondrial respiration in brown fat . *EMBO Mol Med*. 2018;10(3):1–18.
525. Quesada-López T, Gavalda-Navarro A, Morón-Ros S, Campderrós L, Iglesias R, Giralt M, et al. GPR120 controls neonatal brown adipose tissue thermogenic induction. *Am J Physiol Endocrinol Metab*. 2019;317(5):E742–50.
 526. Caiazzo R, Hul W Van, Gaal L Van, Horber F, Balkau B, Pigeire M, et al. Dysfunction of lipid sensor GPR120 leads to obesity in both mouse and human . *Nature*. 2012;483:350–4.
 527. Quesada-López T, Cereijo R, Turatsinze J, Planavila A, Cairó M, Gavalda-Navarro A, et al. The lipid sensor GPR120 promotes brown fat activation and FGF21 release from adipocytes. *Nat Commun*. 2016 Dec 17;7(1):13479.
 528. Oh DY, Talukdar S, Bae EJ, Imamura T, Morinaga H, Fan W, et al. GPR120 Is an Omega-3 Fatty Acid Receptor Mediating Potent Anti-inflammatory and Insulin-Sensitizing Effects. *Cell*. 2010 Sep;142(5):687–98.
 529. Gotoh C, Hong YH, Iga T, Hishikawa D, Suzuki Y, Song SH, et al. The regulation of adipogenesis through GPR120. *Biochem Biophys Res Commun*. 2007;354(2):591–7.
 530. Song T, Zhou Y, Peng J, Tao YX, Yang Y, Xu T, et al. GPR120 promotes adipogenesis through intracellular calcium and extracellular signal-regulated kinase 1/2 signal pathway. *Mol Cell Endocrinol*. 2016;434:1–13.
 531. Zhang D, Leung PS. Potential roles of GPR120 and its agonists in the management of diabetes. *Drug Des Devel Ther*. 2014;8:1013–27.
 532. Oh DY, Walenta E, Akiyama TE, Lagakos WS, Lackey D, Pessentheiner AR, et al. A Gpr120-selective agonist improves insulin resistance and chronic inflammation in obese mice. *Nat Med*. 2014 Aug 6;20(8):942–7.
 533. Talukdar S, Olefsky JM, Osborn O. Targeting GPR120 and other fatty acid-sensing GPCRs ameliorates insulin resistance and inflammatory diseases. *Trends Pharmacol Sci*. 2011 Sep;32(9):543–50.
 534. Colson C, Ghandour RA, Dufies O, Rekima S, Loubat A, Munro P, et al. Diet supplementation in ω 3 polyunsaturated fatty acid favors an anti-inflammatory basal environment in mouse adipose tissue. *Nutrients*. 2019;11(2):1–17.
 535. Trayhurn P. Hypoxia and adipose tissue function and dysfunction in obesity. *Physiol Rev*. 2013;93(1):1–21.

536. Hasan AU, Ohmori K, Konishi K, Igarashi J, Hashimoto T, Kamitori K, et al. Eicosapentaenoic acid upregulates VEGF-A through both GPR120 and PPAR γ mediated pathways in 3T3-L1 adipocytes. *Mol Cell Endocrinol.* 2015;406:10–8.
537. Hoshino K, Takeuchi O, Kawai T, Sanjo H, Ogawa T, Takeda Y, et al. Cutting edge: Toll-like receptor 4 (TLR4)-deficient mice are hyporesponsive to lipopolysaccharide: evidence for TLR4 as the Lps gene product. *J Immunol.* 1999;162(7):3749–52.
538. Irshad Z, Dimitri F, Christian M, Zammit VA. Diacylglycerol acyltransferase 2 links glucose utilization to fatty acid oxidation in the brown adipocytes. *J Lipid Res.* 2017 Jan;58(1):15–30.
539. Cannon B, Nedergaard J. Cultures of Adipose Precursor Cells from Brown Adipose Tissue and of Clonal Brown-Adipocyte- Like Cell Lines. In: *Adipose Tissue Protocols.* New Jersey: Humana Press; 2001. p. 213–24.
540. Rasouli N, Kern PA. Adipocytokines and the metabolic complications of obesity. *J Clin Endocrinol Metab.* 2008;93(11 SUPPL. 1):64–73.
541. Sun S, Ji Y, Kersten S, Qi L. Mechanisms of Inflammatory Responses in Obese Adipose Tissue. *Annu Rev Nutr.* 2012 Aug 21;32(1):261–86.
542. Villarroya F, Cereijo R, Villarroya J, Gavalda-Navarro A, Giralt M. Toward an Understanding of How Immune Cells Control Brown and Beige Adipobiology. *Cell Metab.* 2018;27(5):954–61.
543. Kawai T, Akira S. The roles of TLRs, RLRs and NLRs in pathogen recognition. *Int Immunol.* 2009;21(4):317–37.
544. Hotamisligil GS, Erbay E. Nutrient sensing and inflammation in metabolic diseases. *Nat Rev Immunol.* 2008 Dec;8(12):923–34.
545. Davis JE, Braucher DR, Walker-Daniels J, Spurlock ME. Absence of Tlr2 protects against high-fat diet-induced inflammation and results in greater insulin-stimulated glucose transport in cultured adipocytes. *J Nutr Biochem.* 2011;22(2):136–41.
546. Himes RW, Smith CW. Tlr2 is critical for diet-induced metabolic syndrome in a murine model . *FASEB J.* 2010;24(3):731–9.
547. Kuo LH, Tsai PJ, Jiang MJ, Chuang YL, Yu L, Lai KTA, et al. Toll-like receptor 2 deficiency improves insulin sensitivity and hepatic insulin signalling in the mouse. *Diabetologia.* 2011;54(1):168–79.

548. Ehse JA, Meier DT, Wueest S, Rytka J, Boller S, Wielinga PY, et al. Toll-like receptor 2-deficient mice are protected from insulin resistance and beta cell dysfunction induced by a high-fat diet. *Diabetologia*. 2010;53(8):1795–806.
549. Könner AC, Brüning JC. Toll-like receptors: Linking inflammation to metabolism. *Trends Endocrinol Metab*. 2011;22(1):16–23.
550. Fischer H, Ellström P, Ekström K, Gustafsson L, Gustafsson M, Svanborg C. Ceramide as a TLR4 agonist; a putative signalling intermediate between sphingolipid receptors for microbial ligands and TLR4. *Cell Microbiol*. 2007;9(5):1239–51.
551. Li L, Chen L, Hu L, Liu Y, Sun HY, Tang J, et al. Nuclear factor high-mobility group box1 mediating the activation of toll-like receptor 4 signaling in hepatocytes in the early stage of nonalcoholic fatty liver disease in mice. *Hepatology*. 2011;54(5):1620–30.
552. Nicholson JK, Holmes E, Kinross J, Burcelin R, Gibson G, Jia W, et al. Host-gut microbiota metabolic interactions. *Science* (80-). 2012;336(6086):1262–7.
553. Song MJ, Kim KH, Yoon JM, Kim JB. Activation of Toll-like receptor 4 is associated with insulin resistance in adipocytes. *Biochem Biophys Res Commun*. 2006;346(3):739–45.
554. Fusaru AM, Stănciulescu CE, Şurlin V, Taisescu C, Bold A, Pop OT, et al. Role of innate immune receptors TLR2 and TLR4 as mediators of the inflammatory reaction in human visceral adipose tissue. *Rom J Morphol Embryol*. 2012;53(3 SUPPL.):693–701.
555. Huang RL, Yuan Y, Zou GM, Liu G, Tu J, Li Q. LPS-stimulated inflammatory environment inhibits BMP-2-induced osteoblastic differentiation through crosstalk between TLR4/MyD88/NF- κ B and BMP/Smad signaling. *Stem Cells Dev*. 2014;23(3):277–89.
556. Pierre N, Deldicque L, Barbé C, Naslain D, Cani PD, Francaux M. Toll-Like Receptor 4 Knockout Mice Are Protected against Endoplasmic Reticulum Stress Induced by a High-Fat Diet. *PLoS One*. 2013;8(5):1–11.
557. Devaraj S, Hemarajata P, Versalovic J. The Human Gut Microbiome and Body Metabolism: Implications for Obesity and Diabetes. *Clin Chem*. 2013 Apr 1;59(4):617–28.
558. Cani P, Delzenne N. The Role of the Gut Microbiota in Energy Metabolism and Metabolic Disease. *Curr Pharm Des*. 2009;15(13):1546–58.

559. Erridge C, Attina T, Spickett CM, Webb DJ. A high-fat meal induces low-grade endotoxemia: Evidence of a novel mechanism of postprandial inflammation. *Am J Clin Nutr.* 2007;86(5):1286–92.
560. Chadt A, Al-Hasani H. Glucose transporters in adipose tissue, liver, and skeletal muscle in metabolic health and disease. *Pflugers Arch Eur J Physiol.* 2020;
561. Richard D, Picard F. Brown fat biology and thermogenesis. *Front Biosci.* 2011;16(1):1233.
562. Kiskinis E, Chatzeli L, Curry E, Kaforou M, Frontini A, Cinti S, et al. RIP140 represses the “brown-in-white” adipocyte program including a futile cycle of triacylglycerol breakdown and synthesis. *Mol Endocrinol.* 2014;28(3):344–56.
563. Nedergaard J, Cannon B. How brown is brown fat? It depends where you look. *Nat Med.* 2013;19(5):540–1.
564. Kamei N, Tobe K, Suzuki R, Ohsugi M, Watanabe T, Kubota N, et al. Overexpression of monocyte chemoattractant protein-1 in adipose tissues causes macrophage recruitment and insulin resistance. *J Biol Chem.* 2006;281(36):26602–14.
565. Kanda H, Tateya S, Tamori Y, Kotani K, Hiasa K, Kitazawa R, et al. MCP-1 contributes to macrophage infiltration into adipose tissue, insulin resistance, and hepatic steatosis in obesity¹. Kanda H, Tateya S, Tamori Y, Kotani K, Hiasa K, Kitazawa R, Kitazawa S, Miyachi H, Maeda S, Egashira K, others. MCP-1 contributes to m. *J Clin Invest.* 2006;116(6):1494.
566. Emanuelli B, Peraldi P, Filloux C, Sawka-Verhelle D, Hilton D, Van Obberghen E. SOCS-3 is an insulin-induced negative regulator of insulin signaling. *J Biol Chem.* 2000;275(21):15985–91.
567. Kristiansen OP, Mandrup-Poulsen T. Interleukin-6 and Diabetes: The Good, the Bad, or the Indifferent? *Diabetes.* 2005 Dec 1;54(Supplement 2):S114–24.
568. Bost F, Aouadi M, Caron L, Binétruy B. The role of MAPKs in adipocyte differentiation and obesity. *Biochimie.* 2005;87(1 SPEC. ISS.):51–6.
569. Taniguchi CM, Emanuelli B, Kahn CR. Critical nodes in signalling pathways: Insights into insulin action. *Nat Rev Mol Cell Biol.* 2006;7(2):85–96.
570. Fessler M, Rudel L, Brown M. Toll-like receptor signaling links dietary fatty acids to the metabolic syndrome. *Natl Inst Heal.* 2011;20(5):379–85.
571. Davis JE, Gabler NK, Walker-Daniels J, Spurlock ME. Tlr-4 deficiency selectively protects against obesity induced by diets high in saturated fat.

- Obesity. 2008;16(6):1248–55.
572. Kim F, Pham M, Luttrell I, Bannerman DD, Tupper J, Thaler J, et al. Toll-like receptor-4 mediates vascular inflammation and insulin resistance in diet-induced obesity. *Circ Res*. 2007;100(11):1589–96.
 573. Saberi M, Woods N, de Luca C, Schenk S, Lu JC, Bandyopadhyay G, et al. Hematopoietic Cell-Specific Deletion of Toll-like Receptor 4 Ameliorates Hepatic and Adipose Tissue Insulin Resistance in High-Fat-Fed Mice. *Cell Metab*. 2009 Nov;10(5):419–29.
 574. Poggi M, Bastelica D, Gual P, Iglesias MA, Gremeaux T, Knauf C, et al. C3H/HeJ mice carrying a toll-like receptor 4 mutation are protected against the development of insulin resistance in white adipose tissue in response to a high-fat diet. *Diabetologia*. 2007;50(6):1267–76.
 575. Zhang Y, Castellani LW, Sinal CJ, Gonzalez FJ, Edwards PA. Peroxisome proliferator-activated receptor- γ coactivator 1 α (PGC-1 α) regulates triglyceride metabolism by activation of the nuclear receptor FXR. *Genes Dev*. 2004;18(2):157–69.
 576. Mazzucotelli A, Viguerie N, Tiraby C, Mairal A, Klimcakova E, Lepin E, et al. Control the Expression of Glycerol Kinase and Metabolism Genes Independently of PPAR α Activation in. *Diabetes*. 2007;56(October):2467–75.
 577. Silva JE, Larsen PR. Potential of brown adipose tissue type II thyroxine 5'-deiodinase as a local and systemic source of triiodothyronine in rats. *J Clin Invest*. 1985;76(6):2296–305.
 578. Zhu Z, Spicer EG, Gavini CK, Goudjo-Ako AJ, Novak CM, Shi H. Enhanced sympathetic activity in mice with brown adipose tissue transplantation (transBATation). *Physiol Behav*. 2014 Feb;125(1):21–9.
 579. Villarroya F, Giralt M. The beneficial effects of brown fat transplantation: Further evidence of an endocrine role of brown adipose tissue. *Endocrinology*. 2015;156(7):2368–70.
 580. Seale P. Transcriptional regulatory circuits controlling brown fat development and activation. *Diabetes*. 2015;64(7):2369–75.
 581. Mohan V, Das A, Sagi I. Emerging roles of ECM remodeling processes in cancer. *Semin Cancer Biol*. 2019 Sep;(July):0–1.
 582. Kim S-H, Turnbull J, Guimond S. Extracellular matrix and cell signalling: the dynamic cooperation of integrin, proteoglycan and growth factor receptor. *J*

Endocrinol. 2011 May;209(2):139–51.

583. Lee HJ, Jang M, Kim H, Kwak W, Park WC, Hwang JY, et al. Comparative Transcriptome Analysis of Adipose Tissues Reveals that ECM-Receptor Interaction Is Involved in the Depot-Specific Adipogenesis in Cattle. *PLoS One*. 2013;8(6).
584. Yeo CR, Agrawal M, Hoon S, Shabbir A, Shrivastava MK, Huang S, et al. SGBS cells as a model of human adipocyte browning: A comprehensive comparative study with primary human white subcutaneous adipocytes. *Sci Rep*. 2017;7(1):1–12.
585. Lee MJ, Wu Y, Fried SK. Adipose tissue remodeling in pathophysiology of obesity. *Curr Opin Clin Nutr Metab Care*. 2010;13(4):371–6.
586. Sun K, Kusminski CM, Scherer PE. Adipose tissue remodeling and obesity. *J Clin Invest*. 2011 Jun 1;121(6):2094–101.
587. Luo T, Nocon A, Fry J, Sherban A, Rui X, Jiang B, et al. AMPK activation by metformin suppresses abnormal extracellular matrix remodeling in adipose tissue and ameliorates insulin resistance in obesity. *Diabetes*. 2016;65(8):2295–310.
588. Craft CS, Pietka TA, Schappe T, Coleman T, Combs MD, Klein S, et al. The extracellular matrix protein MAGP1 supports thermogenesis and protects against obesity and diabetes through regulation of TGF- β . *Diabetes*. 2014;63(6):1920–32.
589. Li Y, Wang X, Wang F, You L, Xu P, Cao Y, et al. Identification of intracellular peptides associated with thermogenesis in human brown adipocytes. *J Cell Physiol*. 2019;234(5):7104–14.
590. Lee MH, Goralczyk AG, Kriszt R, Ang XM, Badowski C, Li Y, et al. ECM microenvironment unlocks brown adipogenic potential of adult human bone marrow-derived MSCs. *Sci Rep*. 2016;6(May 2015):1–16.
591. Huang DW, Sherman BT, Lempicki RA. Systematic and integrative analysis of large gene lists using DAVID bioinformatics resources. *Nat Protoc*. 2009;4(1):44–57.
592. Supek F, Bošnjak M, Škunca N, Šmuc T. Revigo summarizes and visualizes long lists of gene ontology terms. *PLoS One*. 2011;6(7).
593. Babicki S, Arndt D, Marcu A, Liang Y, Grant JR, Maciejewski A, et al. Heatmapper: web-enabled heat mapping for all. *Nucleic Acids Res*.

- 2016;44(W1):W147–53.
594. Ge SX, Jung D. ShinyGO: a graphical enrichment tool for animals and plants. *bioRxiv*. 2018;(315150):2.
 595. Luo W, Pant G, Bhavnasi YK, Blanchard SG, Brouwer C. Pathview Web: User friendly pathway visualization and data integration. *Nucleic Acids Res*. 2017;45(W1):W501–8.
 596. Ott C, Jacobs K, Haucke E, Navarrete Santos A, Grune T, Simm A. Role of advanced glycation end products in cellular signaling. *Redox Biol*. 2014;2(1):411–29.
 597. Asadipooya K, Uy EM. Advanced Glycation End Products (AGEs), Receptor for AGEs, Diabetes, and Bone: Review of the Literature. *J Endocr Soc*. 2019 Oct 1;3(10):1799–818.
 598. Barberá MJ, Schlüter A, Pedraza N, Iglesias R, Villarroya F, Giralt M. Peroxisome proliferator-activated receptor α activates transcription of the brown fat uncoupling protein-1 gene. A link between regulation of the thermogenic and lipid oxidation pathways in the brown fat cell. *J Biol Chem*. 2001;276(2):1486–93.
 599. Hondares E, Rosell M, Díaz-Delfín J, Olmos Y, Monsalve M, Iglesias R, et al. Peroxisome proliferator-activated receptor α (PPAR α) induces PPAR γ coactivator 1 α (PGC-1 α) gene expression and contributes to thermogenic activation of brown fat: Involvement of PRDM16. *J Biol Chem*. 2011;286(50):43112–22.
 600. Braissant O, Foulle F, Scotto C, Dauça M, Wahli W. Differential expression of peroxisome proliferator-activated receptors (PPARs): tissue distribution of PPAR-alpha, -beta, and -gamma in the adult rat. *Endocrinology*. 1996 Jan;137(1):354–66.
 601. Westerberg R, Månsson JE, Golozoubova V, Shabalina IG, Backlund EC, Tvrdik P, et al. ELOVL3 is an important component for early onset of lipid recruitment in brown adipose tissue. *J Biol Chem*. 2006;281(8):4958–68.
 602. Jia Z, Pei Z, Maignel D, Toomer CJ, Watkins PA. The fatty acid transport protein (FATP) family: Very long chain acyl-CoA synthetases or solute carriers? *J Mol Neurosci*. 2007;33(1):25–31.
 603. Hirai T, Fukui Y, Motojima K. PPAR α agonists positively and negatively regulate the expression of several nutrient/drug transporters in mouse small

- intestine. *Biol Pharm Bull.* 2007;30(11):2185–90.
604. Cao W, Daniel KW, Robidoux J, Puigserver P, Medvedev A V., Bai X, et al. p38 Mitogen-Activated Protein Kinase Is the Central Regulator of Cyclic AMP-Dependent Transcription of the Brown Fat Uncoupling Protein 1 Gene. *Mol Cell Biol.* 2004;24(7):3057–67.
 605. Tseng Y, Kokkotou E, Schulz TJ, Huang TL, Winnay JN, Taniguchi CM, et al. New role of bone morphogenetic protein 7 in brown adipogenesis and energy expenditure. *Nature.* 2008 Aug;454(7207):1000–4.
 606. Fernandez-Marcos PJ, Auwerx J. Regulation of PGC-1 α , a nodal regulator of mitochondrial biogenesis. *Am J Clin Nutr.* 2011 Apr 1;93(4):884S-890S.
 607. Cao W, Medvedev A V., Daniel KW, Collins S. β -adrenergic activation of p38 MAP kinase in adipocytes: cAMP induction of the uncoupling protein 1 (UCP1) gene requires p38 map kinase. *J Biol Chem.* 2001;276(29):27077–82.
 608. Matesanz N, Nikolic I, Leiva M, Pulgarín-Alfaro M, Santamans AM, Bernardo E, et al. P38A Blocks Brown Adipose Tissue Thermogenesis Through P38 Δ Inhibition. *PLoS Biol.* 2018;16(7):1–29.
 609. Viengchareun S, Zennaro MC, Talleg LP Le, Lombes M. Brown adipocytes are novel sites of expression and regulation of adiponectin and resistin. *FEBS Lett.* 2002;532(3):345–50.
 610. Fu Z, Yao F, Abou-Samra AB, Zhang R. Lipasin, thermoregulated in brown fat, is a novel but atypical member of the angiopoietin-like protein family. *Biochem Biophys Res Commun.* 2013;430(3):1126–31.
 611. Zhang R, Abou-Samra AB. Emerging roles of Lipasin as a critical lipid regulator. *Biochem Biophys Res Commun.* 2013;432(3):401–5.
 612. Mysore R, Liebisch G, Zhou Y, Olkkonen VM, Nidhina Haridas PA. Angiopoietin-like 8 (Angptl8) controls adipocyte lipolysis and phospholipid composition. *Chem Phys Lipids.* 2017;207:246–52.
 613. Dallabrida SM, Zurakowski D, Shih SC, Smith LE, Folkman J, Moulton KS, et al. Adipose tissue growth and regression are regulated by angiopoietin-1. *Biochem Biophys Res Commun.* 2003;311(3):563–71.
 614. Abella V, Scotece M, Conde J, Gómez R, Lois A, Pino J, et al. The potential of lipocalin-2/NGAL as biomarker for inflammatory and metabolic diseases. *Biomarkers.* 2015;20(8):565–71.
 615. Moschen AR, Adolph TE, Gerner RR, Wieser V, Tilg H. Lipocalin-2: A Master

- Mediator of Intestinal and Metabolic Inflammation. *Trends Endocrinol Metab.* 2017;28(5):388–97.
616. Rosell M, Hondares E, Iwamoto S, Gonzalez FJ, Wabitsch M, Staels B, et al. Peroxisome proliferator-activated receptors- α and - γ and cAMP-mediated pathways, control retinol-binding protein-4 gene expression in brown adipose tissue. *Endocrinology.* 2012;153(3):1162–73.
 617. Lee M-WM, Lee M-WM, Oh K-J. Adipose Tissue-Derived Signatures for Obesity and Type 2 Diabetes: Adipokines, Batokines and MicroRNAs. Vol. 8, *Journal of Clinical Medicine.* 2019. 854 p.
 618. Park J, Kim M, Sun K, An YA, Gu X, Scherer PE. VEGF-A - Expressing adipose tissue shows rapid beiging and enhanced survival after transplantation and confers IL-4-independent metabolic improvements. *Diabetes.* 2017;66(6):1479–90.
 619. Bagchi M, Kim LA, Boucher J, Walshe TE, Kahn CR, D'Amore PA. Vascular endothelial growth factor is important for brown adipose tissue development and maintenance. *FASEB J.* 2013;27(8):3257–71.
 620. Sun K, Asterholm IW, Kusminski CM, Bueno AC, Wang Z V., Pollard JW, et al. Dichotomous effects of VEGF-A on adipose tissue dysfunction. *Proc Natl Acad Sci.* 2012;109(15):5874–9.
 621. Shimizu I, Walsh K. The Whitening of Brown Fat and Its Implications for Weight Management in Obesity. *Curr Obes Rep.* 2015;4(2):224–9.
 622. Lee M, Odegaard JI, Mukundan L, Qiu Y, Molofsky AB, Nussbaum JC, et al. Activated Type 2 Innate Lymphoid Cells Regulate Beige Fat Biogenesis. *Cell.* 2015 Jan;160(1–2):74–87.
 623. van der Burg JMM, Bacos K, Wood NI, Lindqvist A, Wierup N, Woodman B, et al. Increased metabolism in the R6/2 mouse model of Huntington's disease. *Neurobiol Dis.* 2008;29(1):41–51.
 624. Wang W, Meng X, Yang C, Fang D, Wang X, An J, et al. Brown adipose tissue activation in a rat model of Parkinson's disease. *Am J Physiol Metab.* 2017 Dec 1;313(6):E731–6.
 625. McCourt AC, Jakobsson L, Larsson S, Holm C, Piel S, Elmér E, et al. White adipose tissue browning in the R6/2 mouse model of Huntington's disease. *PLoS One.* 2016;11(8):1–23.
 626. Ma WT, Gao F, Gu K, Chen DK. The role of monocytes and macrophages in

- autoimmune diseases: A comprehensive review. *Front Immunol*. 2019;10(MAY):1–24.
627. Thompson N, Isenberg DA, Jury EC, Ciurtin C. Exploring BAFF: Its expression, receptors and contribution to the immunopathogenesis of Sjögren's syndrome. *Rheumatol (United Kingdom)*. 2016;55(9):1548–55.
 628. Kawasaki K, Abe M, Tada F, Tokumoto Y, Chen S, Miyake T, et al. Blockade of B-cell-activating factor signaling enhances hepatic steatosis induced by a high-fat diet and improves insulin sensitivity. *Lab Investig*. 2013;93(3):311–21.
 629. Hamada M, Abe M, Miyake T, Kawasaki K, Tada F, Furukawa S, et al. B cell-activating factor controls the production of adipokines and induces insulin resistance. *Obesity*. 2011;19(10):1915–22.
 630. Matsumura Y, Iwasawa A, Toshihiro Kobayashi, Toshiaki Kamachi TO, Masahiro K. Health Beneficial Effects of Food Factors Can Be Applicable to Humans? *J Clin Biochem Nutr*. 2013;52(3):186–92.
 631. Kim DH, Do MS. BAFF knockout improves systemic inflammation via regulating adipose tissue distribution in high-fat diet-induced obesity. *Exp Mol Med*. 2015;47(1):e129-11.
 632. Kim YH, Choi BH, Cheon HG, Do MS. B cell activation factor (BAFF) is a novel adipokine that links obesity and inflammation. *Exp Mol Med*. 2009;41(3):208–16.
 633. Ma KL, Wu Y, Zhang Y, Wang GH, Hu ZB, Ruan XZ. Activation of the CXCL16/CXCR6 pathway promotes lipid deposition in fatty livers of apolipoprotein e knockout mice and HepG2 cells. *Am J Transl Res*. 2018;10(6):1802–16.
 634. Kurki E, Shi J, Martonen E, Finckenberg P, Mervaala E. Distinct effects of calorie restriction on adipose tissue cytokine and angiogenesis profiles in obese and lean mice. *Nutr Metab*. 2012;9(1):1.
 635. Bruemmer D. Targeting angiogenesis as treatment for obesity. *Arterioscler Thromb Vasc Biol*. 2012;32(2):161–2.
 636. Cutchins A, Harmon DB, Kirby JL, Doran AC, Oldham SN, Skafien M, et al. Inhibitor of differentiation-3 mediates high fat diet-induced visceral fat expansion. *Arterioscler Thromb Vasc Biol*. 2012;32(2):317–24.
 637. Cao Y. Adipose tissue angiogenesis as a therapeutic target for obesity and metabolic diseases. *Nat Rev Drug Discov*. 2010;9(2):107–15.

638. Li M, Qian M, Xu J. Vascular Endothelial Regulation of Obesity-Associated Insulin Resistance. *Front Cardiovasc Med*. 2017;4(August):1–9.
639. Zhao Y, Zhang X, Zhao H, Wang J, Zhang Q. CXCL5 secreted from adipose tissue-derived stem cells promotes cancer cell proliferation. *Oncol Lett*. 2018;15(2):1403–10.
640. Nunemaker CS, Chung HG, Verrilli GM, Corbin KL, Upadhye A, Sharma PR. Increased serum CXCL1 and CXCL5 are linked to obesity, hyperglycemia, and impaired islet function. *J Endocrinol*. 2014 Aug;222(2):267–76.
641. Chavey C, Lazennec G, Lagarrigue S, Clapé C, Teyssier J, Annicotte J, et al. CXCL5 is an adipose tissue derived factor that links obesity to insulin resistance. *Cell*. 2010;9(4):339–49.
642. Maquoi E, Munaut C, Colige A, Collen D, Roger Lijnen H. Modulation of adipose tissue expression of murine MMP and their TIMP with obesity. *Diabetes*. 2002;51(4):1093–101.
643. Chernyak B V., Izyumov DS, Lyamzaev KG, Pashkovskaya AA, Pletjushkina OY, Antonenko YN, et al. Production of reactive oxygen species in mitochondria of HeLa cells under oxidative stress. *Biochim Biophys Acta - Bioenerg*. 2006 May;1757(5–6):525–34.
644. Oparka M, Walczak J, Malinska D, van Oppen LMPE, Szczepanowska J, Koopman WJH, et al. Quantifying ROS levels using CM-H 2 DCFDA and HyPer. *Methods*. 2016;109:3–11.
645. Ruiz-Ojeda FJ, Olza J, Gil Á, Aguilera CM. Oxidative Stress and Inflammation in Obesity and Metabolic Syndrome. In: Marti del Moral A, Aguilera CM, editors. *Obesity-Oxidative Stress and Dietary Antioxidants*. Elsevier; 2018. p. 1–15.
646. Petersen KF, Befroy D, Dufour S, Dziura J, Ariyan C, Rothman DL, et al. Mitochondrial dysfunction in the elderly: Possible role in insulin resistance. *Science (80-)*. 2003;300(5622):1140–2.
647. Oelkrug R, Kutschke M, Meyer CW, Heldmaier G, Jastroch M. Uncoupling protein 1 decreases superoxide production in brown adipose tissue mitochondria. *J Biol Chem*. 2010;285(29):21961–8.
648. Alberts B, Johnson A, Lewis J et al. The Mitochondrion. In: ALberts B, editor. *Molecular Biology of the Cell* 4th edition. 4th ed. New York: Garland Science, c2002.; 2002. p. NBK26894.

649. Kozak LP. Genetic variation in brown fat activity and body weight regulation in mice: Lessons for human studies. *Biochim Biophys Acta - Mol Basis Dis.* 2014 Mar;1842(3):370–6.
650. Arsenijevic D, Onuma H, Pecqueur C, Raimbault S, Manning BS, Miroux B, et al. Disruption of the uncoupling protein-2 gene in mice reveals a role in immunity and reactive oxygen species production. *Nat Genet.* 2000;26(4):435–9.
651. Patti ME, Butte AJ, Crunkhorn S, Cusi K, Berria R, Kashyap S, et al. Coordinated reduction of genes of oxidative metabolism in humans with insulin resistance and diabetes: Potential role of PGC1 and NRF1. *Proc Natl Acad Sci U S A.* 2003;100(14):8466–71.
652. Daly MJ, Patterson N, Mesirov JP, Golub TR, Tamayo P, Spiegelman B. PGC-1 α -responsive genes involved in oxidative phosphorylation are coordinately downregulated in human diabetes. *Nat Genet.* 2003;34(3):267–73.
653. Schrauwen-Hinderling VB, Kooi ME, Hesselink MKC, Jeneson JAL, Backes WH, Van Echteld CJA, et al. Impaired in vivo mitochondrial function but similar intramyocellular lipid content in patients with type 2 diabetes mellitus and BMI-matched control subjects. *Diabetologia.* 2007;50(1):113–20.
654. Petersen KF, Dufour S, Befroy D, Garcia R, Shulman GI. Impaired Mitochondrial Activity in the Insulin-Resistant Offspring of Patients with Type 2 Diabetes. *N Engl J Med.* 2004 Feb 12;350(7):664–71.
655. Kelley DE, He J, Menshikova E V., Ritov VB. Dysfunction of mitochondria in human skeletal muscle in type 2 diabetes. *Diabetes.* 2002;51(10):2944–50.
656. Hallgren P, Sjöström L., Hedlund H, Lundell L, Olbe L. Influence of age, fat cell weight, and obesity on O₂ consumption of human adipose tissue. *Am J Physiol - Endocrinol Metab.* 1989;256(4).
657. Xiao YX, Lanza IR, Swain JM, Sarr MG, Nair KS, Jensen MD. Adipocyte mitochondrial function is reduced in human obesity independent of fat cell size. *J Clin Endocrinol Metab.* 2014;99(2):209–16.
658. Fischer B, Schöttl T, Schempp C, Fromme T, Hauner H, Klingenspor M, et al. Inverse relationship between body mass index and mitochondrial oxidative phosphorylation capacity in human subcutaneous adipocytes. *Am J Physiol - Endocrinol Metab.* 2015;309(4):E380–7.
659. Wang T, Si Y, Shirihai OS, Si H, Schultz V, Corkey RF, et al. Respiration in

- Adipocytes is Inhibited by Reactive Oxygen Species. *Obesity*. 2010 Aug 24;18(8):1493–502.
660. Tilokani L, Nagashima S, Paupe V, Prudent J. Mitochondrial dynamics: overview of molecular mechanisms. Garone C, Minczuk M, editors. *Essays Biochem*. 2018 Jul 20;62(3):341–60.
 661. Mahdaviani K, Benador IY, Su S, Gharakhanian RA, Stiles L, Trudeau KM, et al. Mfn2 deletion in brown adipose tissue protects from insulin resistance and impairs thermogenesis. *EMBO Rep*. 2017;18(7):1123–38.
 662. Pearce SF, Rebelo-Guiomar P, D'Souza AR, Powell CA, Van Haute L, Minczuk M. Regulation of Mammalian Mitochondrial Gene Expression: Recent Advances. *Trends Biochem Sci*. 2017;42(8):625–39.
 663. Ferree A, Shirihai O. Mitochondrial Dynamics: The Intersection of Form and Function. In: *Physiology & behavior*. 2012. p. 13–40.
 664. Al-Amrani A, AbdelKarim M, ALZabin M, Alzoghaibi M. Low expression of brown and beige fat genes in subcutaneous tissues in obese patients. *Arch Med Sci*. 2019;15(5):1113–22.
 665. Merlin J, Evans BA, Dehvari N, Sato M, Bengtsson T, Hutchinson DS. Could burning fat start with a brite spark? Pharmacological and nutritional ways to promote thermogenesis. *Mol Nutr Food Res*. 2016;60(1):18–42.
 666. Xiao L, Yang X, Lin Y, Li S, Jiang J, Qian S, et al. Large adipocytes function as antigen-presenting cells to activate CD4 + T cells via upregulating MHCII in obesity. *Int J Obes*. 2016;40(1):112–20.
 667. Ahmad R, Rah B, Bastola D, Dhawan P, Singh AB. Obesity-induces Organ and Tissue Specific Tight Junction Restructuring and Barrier Deregulation by Claudin Switching /631/80/79/1987 /692/699/1702/393 /96/63 /14/19 /82/29 /64/60 /141 article. *Sci Rep*. 2017 Dec;7(1):1–16.
 668. Ott B, Skurk T, Hastreiter L, Lagkouvardos I, Fischer S, Büttner J, et al. Effect of caloric restriction on gut permeability, inflammation markers, and fecal microbiota in obese women. *Sci Rep*. 2017;7(1):1–10.
 669. Okla M, Wang W, Kang I, Pashaj A, Carr T, Chung S. Activation of Toll-like receptor 4 (TLR4) attenuates adaptive thermogenesis via endoplasmic reticulum stress. *J Biol Chem*. 2015;290(44):26476–90.
 670. McTernan P, Anwar A, Eggo M, Barnett A, Stewart P, Kumar S. Gender differences in the regulation of P450 aromatase expression and activity in

- human adipose tissue. *Int J Obes*. 2000 Jul 25;24(7):875–81.
671. Daynes RA, Jones DC. Emerging roles of PPARs in inflammation and immunity. *Nat Rev Immunol*. 2002;2(10):748–59.
 672. Ialenti A, Grassia G, Di Meglio P, Maffia P, Di Rosa M, Ianaro A. Mechanism of the anti-inflammatory effect of thiazolidinediones: Relationship with the glucocorticoid pathway. *Mol Pharmacol*. 2005;67(5):1620–8.
 673. Wahli W, Michalik L. PPARs at the crossroads of lipid signaling and inflammation. *Trends Endocrinol Metab*. 2012;23(7):351–63.
 674. Fernando R, Wardelmann K, Deubel S, Kehm R, Jung T, Mariotti M, et al. Low steady-state oxidative stress inhibits adipogenesis by altering mitochondrial dynamics and decreasing cellular respiration. *Redox Biol*. 2020;32(January):101507.
 675. Wilson-Fritch L, Nicoloso S, Chouinard M, Lazar MA, Chui PC, Leszyk J, et al. Mitochondrial remodeling in adipose tissue associated with obesity and treatment with rosiglitazone. *J Clin Invest*. 2004 Nov 1;114(9):1281–9.
 676. Carey AL, Formosa MF, Van Every B, Bertovic D, Eikelis N, Lambert GW, et al. Ephedrine activates brown adipose tissue in lean but not obese humans. *Diabetologia*. 2013;56(1):147–55.
 677. Fischer AW, Csikasz RI, von Essen G, Cannon B, Nedergaard J. No insulating effect of obesity. *Am J Physiol Metab*. 2016 Jul 1;311(1):E202–13.
 678. Feldo M, Kocki J, Łukasik S, Bogucki J, Feldo J, Terlecki P, et al. CIDE-A gene expression in patients with abdominal obesity and LDL hyperlipoproteinemia qualified for surgical revascularization in chronic limb ischemia. *Pol Prz Chir Polish J Surg*. 2013;85(11):644–8.
 679. Clément K, Viguerie N, Poitou C, Carette C, Pelloux Vé, Curat CA, et al. Weight loss regulates inflammation-related genes in white adipose tissue of obese subjects. *FASEB J*. 2004 Nov;18(14):1657–69.
 680. Fain JN, Madan AK, Hiler ML, Cheema P, Bahouth SW. Comparison of the release of adipokines by adipose tissue, adipose tissue matrix, and adipocytes from visceral and subcutaneous abdominal adipose tissues of obese humans. *Endocrinology*. 2004;145(5):2273–82.
 681. Clément K, Viguerie N, Poitou C, Carette C, Pelloux Vé, Curat CA, et al. Weight loss regulates inflammation-related genes in white adipose tissue of obese subjects. *FASEB J*. 2004;18(14):1657–69.

682. Rainone V, Schneider L, Saulle I, Ricci C, Biasin M, Al-Daghri NM, et al. Upregulation of Inflammasome activity and increased gut permeability are associated with obesity in children and adolescents. *Int J Obes.* 2016;40(6):1026–33.
683. Moreno-Navarrete JM, Ortega F, Serino M, Luche E, Waget A, Pardo G, et al. Circulating lipopolysaccharide-binding protein (LBP) as a marker of obesity-related insulin resistance. *Int J Obes.* 2012;36(11):1442–9.
684. Carey AL, Vorlander C, Reddy-Luthmoodoo M, Natoli AK, Formosa MF, Bertovic DA, et al. Reduced UCP-1 content in in vitro differentiated beige/ brite adipocytes derived from preadipocytes of human subcutaneous white adipose tissues in obesity. *PLoS One.* 2014;9(3).
685. Vernochet C, Peres SB, Davis KE, McDonald ME, Qiang L, Wang H, et al. C/EBP α and the Corepressors CtBP1 and CtBP2 Regulate Repression of Select Visceral White Adipose Genes during Induction of the Brown Phenotype in White Adipocytes by Peroxisome Proliferator-Activated Receptor γ Agonists. *Mol Cell Biol.* 2009;29(17):4714–28.
686. Fukui Y, Masui SI, Osada S, Umesono K, Motojima K. A new thiazolidinedione, NC-2100, which is a weak PPAR- γ activator, exhibits potent antidiabetic effects and induces uncoupling protein 1 in white adipose tissue of KKAY obese mice. *Diabetes.* 2000;49(5):759–67.
687. Digby JE, Montague CT, Sewter CP, Sanders L, Wilkison WO, O’Rahilly S, et al. Thiazolidinedione exposure increases the expression of uncoupling protein 1 in cultured human preadipocytes. *Diabetes.* 1998;47(1):138–41.
688. Bogacka I, Xie H, Bray GA, Smith SR. Pioglitazone induces mitochondrial biogenesis in human subcutaneous adipose tissue in vivo. *Diabetes.* 2005;54(5):1392–9.
689. Kuryłowicz A, Puzianowska-Kuźnicka M. Induction of adipose tissue browning as a strategy to combat obesity. *Int J Mol Sci.* 2020;21(17):1–28.
690. Bulthuis EP, Adjobo-Hermans MJW, Willems PHGM, Koopman WJH. Mitochondrial Morphofunction in Mammalian Cells. *Antioxid Redox Signal.* 2019 Jun 20;30(18):2066–109.
691. Sato T, Kotake D, Hiratsuka M, Hirasawa N. Enhancement of Inflammatory Protein Expression and Nuclear Factor Kb (NF-Kb) Activity by Trichostatin A (TSA) in OP9 Preadipocytes. Sigmund B, editor. *PLoS One.* 2013 Mar

26;8(3):e59702.

692. de Mello AH, Costa AB, Engel JDG, Rezin GT. Mitochondrial dysfunction in obesity. *Life Sci.* 2018 Jan;192:26–32.
693. Bhatti JS, Bhatti GK, Reddy PH. Mitochondrial dysfunction and oxidative stress in metabolic disorders — A step towards mitochondria based therapeutic strategies. *Biochim Biophys Acta - Mol Basis Dis.* 2017 May;1863(5):1066–77.
694. Jialal I, Kaur H, Devaraj S. Toll-like receptor status in obesity and metabolic syndrome: A translational perspective. *J Clin Endocrinol Metab.* 2014;99(1):39–48.
695. Gupta S, Maratha A, Siednienko J, Natarajan A, Gajanayake T, Hoashi S, et al. Analysis of inflammatory cytokine and TLR expression levels in Type 2 Diabetes with complications. *Sci Rep.* 2017;7(1):1–10.
696. Carvalho BM, Guadagnini D, Tsukumo DML, Schenka AA, Latuf-Filho P, Vassallo J, et al. Modulation of gut microbiota by antibiotics improves insulin signalling in high-fat fed mice. *Diabetologia.* 2012;55(10):2823–34.
697. Rempel JD, Packiasamy J, Dean HJ, McGavock J, Janke A, Collister M, et al. Preliminary analysis of immune activation in early onset type 2 diabetes. *Int J Circumpolar Health.* 2013;72(SUPPL.1):1–8.
698. Dasu MR, Devaraj S, Park S, Jialal I. Increased Toll-Like Receptor (TLR) activation and TLR ligands in recently diagnosed type 2 diabetic subjects. *Diabetes Care.* 2010;33(4):861–8.
699. Jialal I, Huet BA, Kaur H, Chien A, Devaraj S. Increased toll-like receptor activity in patients with metabolic syndrome. *Diabetes Care.* 2012;35(4):900–4.
700. Cheng Y, Jiang L, Keipert S, Zhang S, Hauser A, Graf E, et al. Prediction of Adipose Browning Capacity by Systematic Integration of Transcriptional Profiles. *Cell Rep.* 2018;23(10):3112–25.
701. Rodriguez-Pacheco F, Garcia-Serrano S, Garcia-Escobar E, Gutierrez-Repiso C, Garcia-Arnes J, Valdes S, et al. Effects of obesity/fatty acids on the expression of GPR120. *Mol Nutr Food Res.* 2014;58(9):1852–60.
702. Hudson BD, Shimpukade B, Mackenzie AE, Butcher AJ, Padiani JD, Christiansen E, et al. The pharmacology of TUG-891, a potent and selective agonist of the free fatty acid receptor 4 (FFA4/GPR120), demonstrates both

- potential opportunity and possible challenges to therapeutic agonism. *Mol Pharmacol*. 2013;84(5):710–25.
703. Shimpukade B, Hudson BD, Hovgaard CK, Milligan G, Ulven T. Discovery of a Potent and Selective GPR120 Agonist. *J Med Chem*. 2012 May 10;55(9):4511–5.
 704. Christiansen E, Watterson KR, Stocker CJ, Sokol E, Jenkins L, Simon K, et al. Activity of dietary fatty acids on FFA1 and FFA4 and characterisation of pinolenic acid as a dual FFA1/FFA4 agonist with potential effect against metabolic diseases. *Br J Nutr*. 2015 Jun 14;113(11):1677–88.
 705. Matthias A, Ohlson KBE, Fredriksson JM, Jacobsson A, Nedergaard J, Cannon B. Thermogenic responses in brown fat cells are fully UCP1-dependent. UCP2 or UCP3 do not substitute for UCP1 in adrenergically or fatty acid-induced thermogenesis. *J Biol Chem*. 2000;275(33):25073–81.
 706. Shabalina IG, Jacobsson A, Cannon B, Nedergaard J. Native UCP1 displays simple competitive kinetics between the regulators purine nucleotides and fatty acids. *J Biol Chem*. 2004;279(37):38236–48.
 707. Fedorenko A, Lishko P V., Kirichok Y. Mechanism of fatty-acid-dependent UCP1 uncoupling in brown fat mitochondria. *Cell*. 2012;151(2):400–13.
 708. Zorova LD, Popkov VA, Plotnikov EY, Silachev DN, Pevzner IB, Jankauskas SS, et al. Mitochondrial membrane potential. *Anal Biochem*. 2018;552:50–9.
 709. Kroemer G, Galluzzi L, Brenner C. Mitochondrial membrane permeabilization in cell death. *Physiol Rev*. 2007;87(1):99–163.
 710. Pendergrass W, Wolf N, Pool M. Efficacy of MitoTracker GreenTM and CMXRosamine to measure changes in mitochondrial membrane potentials in living cells and tissues. *Cytom Part A*. 2004;61(2):162–9.
 711. Klim M, Marsh T, Brown M. Modelling Future Trends in Obesity and the Impact on Health. In: *Foresight Tackling Obesities: Future Choices*. 2007. p. 1–72.
 712. Bhaskaran K, Douglas I, Forbes H, Dos-Santos-Silva I, Leon DA, Smeeth L. Body-mass index and risk of 22 specific cancers: A population-based cohort study of 5·24 million UK adults. *Lancet*. 2014;384(9945):755–65.
 713. Schuster D. Obesity and the development of type 2 diabetes: the effects of fatty tissue inflammation. *Diabetes, Metab Syndr Obes Targets Ther*. 2010;253.
 714. Baker C. Obesity Statistics: Briefing Paper 3336. House Commons Libr.

- 2019;(3336):1–18.
715. Misra A, Khurana L. Obesity and the metabolic syndrome in developing countries. *J Clin Endocrinol Metab*. 2008;93(11 SUPPL. 1):9–30.
 716. Popkin BM, Adair LiS, Ng SW. NOW AND THEN: The Global Nutrition Transition: The Pandemic of Obesity in Developing Countries. *Nutrients*. 2017;58(1):1–10.
 717. Alexaki VI, Chavakis T. The role of innate immunity in the regulation of brown and beige adipogenesis. *Rev Endocr Metab Disord*. 2016;17(1):41–9.
 718. Connaughton RM, McMorrow AM, McGillicuddy FC, Lithander FE, Roche HM. Impact of anti-inflammatory nutrients on obesity-associated metabolic-inflammation from childhood through to adulthood. *Proc Nutr Soc*. 2016;75(2):115–24.
 719. Klingelhutz AJ, Gourronc FA, Chaly A, Wadkins DA, Burand AJ, Markan KR, et al. Scaffold-free generation of uniform adipose spheroids for metabolism research and drug discovery. *Sci Rep*. 2018;8(1):1–13.
 720. Zorzano A, Liesa M, Palacín M. Role of mitochondrial dynamics proteins in the pathophysiology of obesity and type 2 diabetes. *Int J Biochem Cell Biol*. 2009;41(10):1846–54.
 721. Rovira-Llopis S, Bañuls C, Diaz-Morales N, Hernandez-Mijares A, Rocha M, Victor VM. Mitochondrial dynamics in type 2 diabetes: Pathophysiological implications. *Redox Biol*. 2017;11(January):637–45.
 722. Choo HJ, Kim JH, Kwon OB, Lee CS, Mun JY, Han SS, et al. Mitochondria are impaired in the adipocytes of type 2 diabetic mice. *Diabetologia*. 2006;49(4):784–91.
 723. Porporato PE, Filigheddu N, Pedro JMBS, Kroemer G, Galluzzi L. Mitochondrial metabolism and cancer. *Cell Res*. 2018;28(3):265–80.
 724. Hahn WS, Kuzmicic J, Burrill JS, Donoghue MA, Foncea R, Jensen MD, et al. Proinflammatory cytokines differentially regulate adipocyte mitochondrial metabolism, oxidative stress, and dynamics. *Am J Physiol - Endocrinol Metab*. 2014;306(9):1033–45.
 725. Bakar MHA, Sarmidi MR, Kai CK, Huri HZ, Yaakob H. Amelioration of Mitochondrial Dysfunction-Induced Insulin Resistance in Differentiated 3T3-L1 Adipocytes via Inhibition of NF- κ B Pathways. *Int J Mol Sci*. 2014;15(12):22227–57.

- 726. van Horssen J, van Schaik P, Witte M. Inflammation and mitochondrial dysfunction: A vicious circle in neurodegenerative disorders? *Neurosci Lett*. 2019;710:132931.
- 727. Chen Y, Yang J, Nie X, Song Z, Gu Y. Effects of Bariatric Surgery on Change of Brown Adipocyte Tissue and Energy Metabolism in Obese Mice. *Obes Surg*. 2018;28(3):820–30.
- 728. Yang PJ, Lee WJ, Tseng PH, Lee PH, Lin MT, Yang WS. Bariatric surgery decreased the serum level of an endotoxin-Associated marker: Lipopolysaccharide-binding protein. *Surg Obes Relat Dis*. 2014;10(6):1182–7.
- 729. van Marken Lichtenbelt WD, Schrauwen P. Implications of nonshivering thermogenesis for energy balance regulation in humans. Vol. 301, *American Journal of Physiology - Regulatory Integrative and Comparative Physiology*. Am J Physiol Regul Integr Comp Physiol; 2011.